PROCEEDINGS OF THE INTERNATIONAL GEOTECHNICAL CONFERENCE

GEOTECHNICAL CHALLENGES IN MEGACITIES

Volume 3

2010 MOSCOW

7-10 June 2010
Moscow, Russia

PROCEEDINGS
OF THE INTERNATIONAL GEOTECHNICAL CONFERENCE

GEOTECHNICAL CHALLENGES IN MEGACITIES

Moscow, 7-10 June 2010

Volume 3

Edited by V.P. Petrukhin, V.M. Ulitsky,
I.V. Kolybin, M.B. Lisyuk, M.L. Kholmyansky

Moscow
2010

Proceedings of the International geotechnical conference "Geotechnical challenges in megacities".

In 1st volume of the Proceedings the lectures presented by the authors in English and Russian are published.

In 2nd and 3rd volumes of the Proceedings the papers presented by the authors in English are published.

In 4th and 5th volumes of the Proceedings the papers presented by the authors in Russian are published.

The responsibility for content and editing is placed upon the authors of the papers of this volume.

Published by: GRF
190005, 4 Izmaylovsky prosp., St. Petersburg, Russia

ISBN 978-5-9902005-2-4

Printed in printing house 'MST', Russia, St. Petersburg

Table of contents

Volume 3

Session 2a
Effect of new buildings and constructions on underground structures

Effect of new underground structures on existing buildings and networks

Session 3a
Geofailures & risk assessment

Improved soils

Geological risks in urban planning

Session 3b
Preservation of hydrogeological situation

Geoecological problems

Session 2a

Effect of new buildings and constructions on underground structures

Effect of new underground structures on existing buildings and networks

Effect of new buildings and constructions on underground structures

Analysis of the impact of newly constructed buildings on underground structures

A.Dabska, P.Popielski
Warsaw University of Technology, Warsaw, Poland

A.B.Fadeev
Saint-Petersburg State University of Architecture and Civil Engineering, Saint-Petersburg, Russia

E.V.Gorodnova
Petersburg State Transport University, Saint-Petersburg, Russia

ABSTRACT: This article discusses issues resulting from the application of additional loads on stress-deformation condition existing in the ground. It presents results of numerical analysis of the impact of new buildings on underground structures in examples of buildings implemented in Poland (metro tunnels and stations in Warsaw) and Russia (municipal interceptors in Saint Petersburg). Numerical analysis based on finite elements methods was used for the calculations, which allows drawing conclusions on the safety of the structures.

1. INTRODUCTION

The centers of big cities are densely developed urban areas usually comprising historical buildings of high architectural value. The construction of a new building in such conditions always implicates problems related to the application of additional loads on the stress-deformation condition which already exists in the ground. Additional stresses and deformations brought about by new buildings affect not only the existing buildings but also underground engineering structures (metro tunnels and stations), municipal infrastructure (intercepting sewers), and other structures potentially susceptible to displacements and located in complicated geological conditions. In such cases, when designing the foundation of a building where trench steening, foundation plate and other structural elements have to work together, numerical analysis is the only method of determining the interaction between the new and existing structures.

Advance estimation of the values of additional stresses and expected displacements is necessary to guarantee the safety of underground structures. To this end, complicated geotechnical problems have to be solved, and these are typically analyzed by finite elements methods.

Such numerical analysis is a very difficult task conditioned by many factors. The calculation quality depends on correct and precise digitization of the calculation scheme, and on the adopted geotechnical parameters of the soil. The foundation works together with subsoil at a large depth which often exceeds the depth of bores made as part of geology determination. Experimental research shows that parameters of higher value can be expected from deeper soil layers as a result of greater influence of consolidation and more intensive effective stresses. Deformations become slighter with depth increasing below the foundation level. For the so-called “small deformations”, the modulus of elasticity values are greater than those for the large deformations range, and the parameter determining the rigidity of soil mass (responsible for soil settlements) is very strongly dependent on the current deformation state of the soil [5].

Usually, given the lack of a sufficient number of parameters to apply advanced soil models, designers decide to use calculations based on the Coulomb–Mohr or Drucker–Prager criterion assuming a constant value of the modulus of deformation/elasticity (E = const.).

The modulus of elasticity for small deformations can be determined by geophysical methods such as microseismic prospecting or by examining the deformation-stress relation in a triaxial compression apparatus with a precise measurement (piezoelectrical elements) of small deformations. Unfortunately, these are very rarely used in engineering determination of geology. Therefore, on the basis of the small deformations theory [1], modifications of the values of parameters for deep ground layers are sometimes used in numerical calculations for deep foundations.

This article presents results of numerical analysis of the influence of new buildings on underground structures in examples of buildings constructed in Poland (Warsaw) and Russia (Saint Petersburg).

2. STRUCTURES IMPLEMENTED IN POLAND

2.1. Method of analysis

Numerical analyses for the structures described below were done using the HYDRO-GEO software which is now under development at the Warsaw University of Technology [3]. On the account of the available material parameters, the elastic-plastic soil model was adopted on the basis of the Coulomb-Mohr plasticity criterion. The calculations were performed as a two-dimensional task in the plain state of strain. The model was digitized using six-node isoparametric triangular elements of second-order shape function. The analysis was done in the so-called effective stresses.

2.2. Numerical analysis of the construction of Dworzec Gdański A17 metro station and a multi-storey building

Numerical analysis of the construction of Dworzec Gdański A17 metro station and a multi-storey building to be subsequently erected over the station was conducted. Its aim was to identify the optimal type of foundation for the station, in which settlements of the building would be uniform and minimal.

The full length of the station is 156 m, and its width in the inside diameter of cavity walls - 20 m. The bottom of the excavation is situated at the ordinate of 16÷14 m below the ground level. The excavation walls are protected by 80 cm thick and 21 m long cavity walls, located at the depth of 6÷8 m below the foundation plate. It was assumed at the construction design stage that a 10-storey building would be constructed over the A17 station in the future. That structure would rest on piles in the central part of the metro station and in the cavity walls. With the view to design a foundation which would guarantee minimal and uniform settlement of the metro station, analysis of several foundation options was conducted. The options differed by quantities and depths of cavity walls, and by thickness of foundation plates.

For the needs of these assumptions, cavity walls of locally extended diameters (T-shaped sections) were planned to be used in selected station axes, thus becoming integral parts of the structure, Fig. 1 and 2.

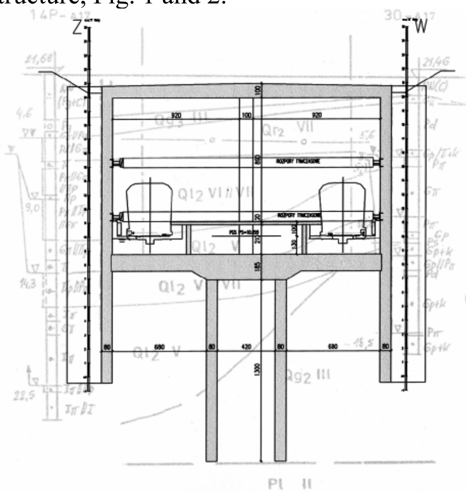

Figure 1. Scheme of foundation type adopted for Dworzec Gdański A17 metro station

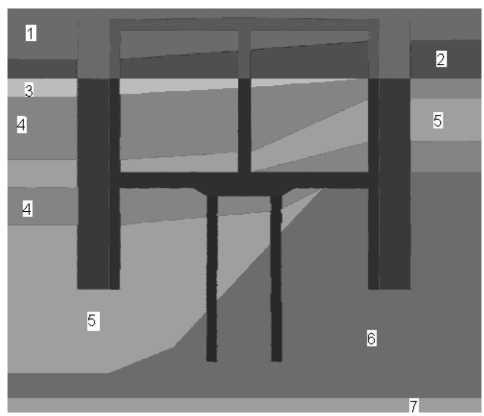

Figure 2. Scheme of material zones adopted for calculation purposes for Dworzec Gdański A17 metro station

The walls design accounted for the fact that the station was constructed by the under-floored method taking into account the high level of underground waters. The cavity walls which protected the excavation in the initial phase were ultimately to become part of the station structure. The floor slab was designed as a full one, with thickness varying from 80 to 100 cm, supported by piles and cavity walls. In the implementation phase, the walls were spaced in two levels by tubular struts ϕ 711 mm. The 20 cm thick platform slab was based on two ferroconcrete walls. The bottom foundation plate was designed as a 120 cm thick one without expansion joints. Under the foundation plate, thickened by additional 65 cm in its central part, a foundation case was constructed in the form of two series of 80 cm thick foundation barrettes with spacing in axes of 500 cm. The barrettes were located at the depth of 13 m below the downside of the thickened bottom plate (185 cm thick). The bottom plate was protected from underground waters by heavy sealing. The upside of the bottom plate was positioned at the ordinate of 12,7 m below the ground level. The piles making up the construction supporting the floor slab were located in the central axis of the station.

Table 1. presents the identified geotechnical layers [6] along proposed characteristic values of their physical and mechanical parameters [7]. In addition, a hybrid concrete-soil material was specified and used for numerical illustration of the local extension of the construction walls within the section in question.

The statistical calculations showed that the level of underground waters at the external side of the cavity walls should be lowered to 7,0 m below the ground level and held unchanged by the time of the station completion in as-built state. The pressure admitted to work on the foundation plate after it acquired its full strength and before the as-built state would be implemented was 30 kPa.

The numerical modeling was carried out in six stages reflecting the construction process:

Stage I – Initial stresses resulting from the weight of soil layers were calculated,

Stage II – The implementation of cavity walls was modeled, followed by the implementation of the excavation which involved elements being taken out to the adopted ordinate of the downside of the foundation plate; the floor slab was left in place and straining beams were added,

Stage III – The implementation of the foundation plate was modeled by adding concrete elements, where the load was generated by the dead weight of the plate (bulk density of concrete was adopted at γ=25 kN/m^3),

Stage IV – New elements were added: piles were erected and uplift pressure load was accounted for,

Stage V – Loads from the remaining station structure elements were imposed,

Stage VI – Loads from the 10-storey building were imposed in the form of forces working on the piles and cavity walls.

After the completion of the metro station, a backward analysis was conducted in order to verify the material parameters adopted for the calculations. This process was carried out on the basis of the existing displacement monitoring. The initial soil parameters were adopted as in geological documentation [6] and the report „Analysis of settlements of Dworzec Gdański metro station structure" [4]. In successive approximations, the modulus of elasticity values for selected soil layers were being modified by the time the numerical calculations showed plate displacements consistent with those obtained in „in situ" measurements. The modifying of the numerical model was in this way conducted. The so-called "small deformations" theory was the basis for increasing the modulus of elasticity values in successive approximations. For those deformations the modulus of elasticity values are greater than those for the large deformations range, e.g. [5]. The obtained results have been compared in Table 1 below. A change in rigidity only occurred in materials 4, 5, 6 and 7 located in the zone of small deformations, i.e. below 10^{-4}.

Table 1. Verification of material parameters (modulus of elasticity) – table of results

Item	Name of material	Modulus of elasticity E [MPa]		
		Geotechnical opinion	Comparative method	Backward analysis
1	Windrow	40	40	40
2	Fine and silty sands	60	60	60
3	Fine and silty sands under water	60	60	60
4	Silts, fine and dusty sands	53	100	179
5	Clays	30	60	107
6	Sandy clays	47	80	143
7	Pliocene clays	26	150	210

The Geotechnical opinion column of Table 1 presents values found in the geology determination, the Comparative method column contains values used by the authors of report [4, 2] on the basis of their experience in the implementation of similar projects, and the third column contains values obtained as a result of backward analysis [8, 2]. Comparative calculations for individual concepts of implementation of the station foundation were performed using material parameters obtained by backward analysis. The calculations have confirmed that the option actually adopted for implementation was the best solution.

2.3. The construction of a pedestrian subway in the area of Dworzec Gdański A17 metro station

An analysis of the construction of a pedestrian subway in the area of Dworzec Gdański A17 metro station was carried out in order to determine parameters of the cavity walls applied in the construction of that subway and its influence on the existing metro station and tunnels. In this example, the value of displacements of metro rails should not exceed the admissible values of displacements caused by the constant train traffic.

The material parameters verified earlier in the calculations concerning Dworzec Gdański A17 metro station were used for this analysis, and the target station foundation scheme as discussed in p. 2.2 was adopted.

Structure-wise, the planned underpass is a rectangular tunnel of 9 m in width in the inside diameter of cavity walls.

Several calculation variants were done for the calculation section in the area of tunnel routes, accounting for various lengths of cavity walls. Their lengths determined the impact of the planned subway on the metro tunnels located nearby. The subway is designed to be implemented in the technology of cavity walls that will subsequently serve as walls of the structure. The distance between the cavity wall of the planned subway and the station structure is 1 m. The following thickness values were adopted for the calculations: 80 cm for cavity walls, 80 cm and 100 cm for tunnel roof, and 100 cm for the downside plate. The subway is to be implemented by the under-floored method.

The other numerical models, differing by the adopted structural solutions, concerned the same hydro-geological section as in p.2.2, located in the part of the station over which a 10-storey tower block would be constructed. The level of underground water was determined on the basis of field observations of the movement.

The modeling was carried out in seven stages recreating the implementation process of the station structure in stages I-V (as in p.2.2), and that of the pedestrian subway in stages VI and VII:

Stage VI – the implementation of cavity walls of the subway was modeled, followed by that of its roof slab,

Stage VII – the roof slab was left in place, and the excavation was executed (under-floored method) by taking out elements to the adopted ordinate of the downside of the foundation plate, the implementation of the foundation plate was modeled by adding concrete elements (the load was generated by the dead weight of the plate where γ=25 kN/m^3).

The scheme of material zones in the area of the A17 station is presented in Figure 3.

Figure 4 presents results of the numerical analysis in the form of displacement isolines drawn every 0,001 m, against outlines of the material zones.

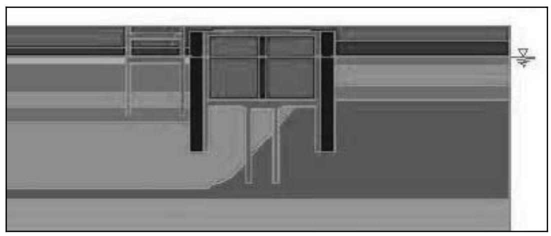

Figure 3. Scheme of material zones adopted for calculation purposes for Dworzec Gdański A17 metro station

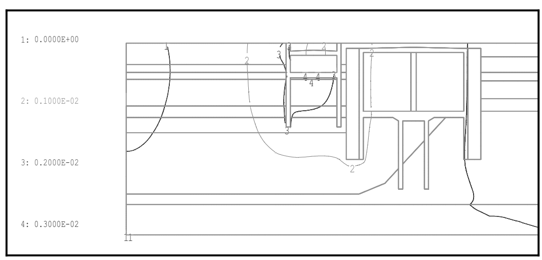

Figure 4. Displacement isolines drawn every 0,001 m against outlines of the material zones for planned pedestrian subway in the area of Dworzec Gdański A17 metro station.

On the basis of the calculations, the depth at which the downside of the cavity walls will be located was adopted at 16 m below the ground level.

2.4. The construction of a car park directly above Wilanowska A7 metro station

The impact of constructing a car park directly above Wilanowska A7 metro station was analyzed, and the value of displacements of metro rails was monitored in order to avoid any breaks in the movement of trains.

The garage was designed in the monolythic ferroconcrete technology with light steel elements (roof) and a one-storey metal structure placed directly over the metro station. The calculations accounted for the mating of the foundation plate, piles groups and the case (technical tier) located directly over metro tunnels.

The geological structure of the soil identified in the determination process was used in the model. The values of material parameters were adopted as in geological documentation and in the standard [7]. For materials located at large depths, the E values (modulus of elasticity) were increased (from 2 to 4 times against the geology determination results). This modification was introduced in connection with a correlation identified in the process of verification of results of other calculations, and displacement values found in the area of the analyzed structures were used. The parameters of individual materials deposited in the analyzed section are presented in Table 2.

Table 2. Material parameters in the section

Item	Name of soil	ν	E MPa	γ kN/m^3	c kPa	φ °
1	Fine and silty sands	0,30	70	19,0	0	35
2	Sandy clays, clayey sands	0,30	40	22,0	25	19
3	Sandy clays, clayey sands	0,30	47	22,5	35	23
4	Fine sands over water	0,30	70	19,0	0	35
5	Fine sands under water*	0,30	100	19,0	0	35
6	Sandy clays, clayey sands*	0,25	170	19,0	0	36
7	Sandy clays, clayey sands, deep layers*	0,25	255	19,0	0	36

* increased modulus of elasticity (E) values – description in text

Numbers of the materials presented in the Tables correspond to the numbering in Figures 2, 3 and 5. The calculation process reproduced the history of stresses in the ground, included changes caused by the prior implementation of metro tunnels, and modeled the garage construction. The calculations were carried out in seven stages. The scheme adopted for the final stage is presented in Figure 5.

Figure 6 illustrates vertical displacements drawn every 0,001 m. at the last calculation stage.

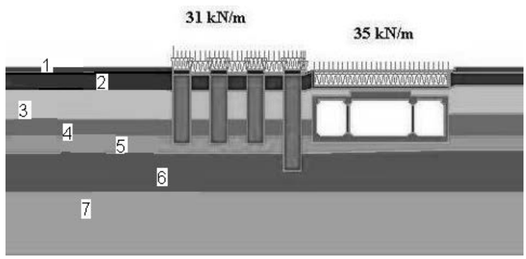

Figure 5. Final stages of FEM calculations for Wilanowska A7 metro station

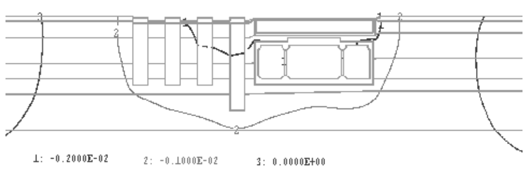

Figure 6. Vertical displacement at the last stage of calculations, determined every 0,001 m

Monitoring of displacements in the subgrade was conducted during the implementation process. Conformity of the measurements and the calculation results was very high. That conformity was obtained by way of increasing the values of geotechnical parameters of the soil at large depths against the values presented in the documentation [6]. This modification was introduced in connection with a correlation identified in the process of verification by backward analysis of results of other calculations done for similar geological conditions.

3. STRUCTURES IMPLEMENTED IN RUSSIA

3.1. Method of analysis

To estimate additional loads applied to the tunnel casings, calculations of stress fields were executed using finite elements methods in two software applications: Geomechanics and PLAXIS [9], arriving at parallel results. Due to the extensive length of the buildings, the calculations were performed as a two-dimensional task [10, 11].

The following principles permitting safe operation of the tunnels were adopted in order to analyze the foundation of multi-storey residential buildings constructed over the routes of intercepting sewers:

1. Not exceeding permissible loads (considering the factors of safety) from additional loads acting on the tunnel lining,
2. Not allowing the permissible dynamic loads to be exceeded,
3. Not allowing any damage to the tunnel lining at the „0” works stage.

3.2. Three-storey apartment house with an underground floor at Deputatskaya street

While constructing a three-storey apartment house with an underground floor at Deputatskaya street, the safety of two interceptor tunnels located directly under the building had to be secured.

The building has a foundation plate placed at 2,5 m below the ground level. One sewer, of cross-section area 1900x1830 mm, was situated at the depth of 25 m, and another, of cross-section area 3160x2450 mm, at the depth of 40 m (Fig. 7). Stresses at the foundation level transmitted to the soil equaled 72 kPa.

There are light Quaternary sediments in the upper part of the soil, and below – a layer of hard Proterozoic formations of large depth (layer 8) and high modulus of deformation (Table 3). Therefore, regarding the geological conditions in the soil, both sewers were located in the layer of Proterozoic carrying clays.

Table 3. Basic soil parameters at Deputatskaya street

Item	Soil	E, kPa	ν	γ kN/m^3	c kPa	φ °
1	Fill soil	1000	0.30	17.0	1	15
2	Fine sand	11000	0.30	19.4	2	26
3	Clayey sand	5000	0.35	18.2	6	7
4	Clayey sand	6500	0.35	19.0	8	9
5	Sandy clay	20000	0.30	21.8	40	26
6	Sandy clay	30000	0.30	22.8	70	30
7	Clayey sand	45000	0.42	20.7	104	15
8	Clayey sand	100000	0.42	21.2	310	27

The calculations were carried out in 3 stages:

Stage I – Initial stresses resulting from the weight of soil layers were calculated,

Stage II – The implementation of the excavation for the building foundation to the depth of 2,5 m was modeled,

Stage III – The load from the planned building was applied.

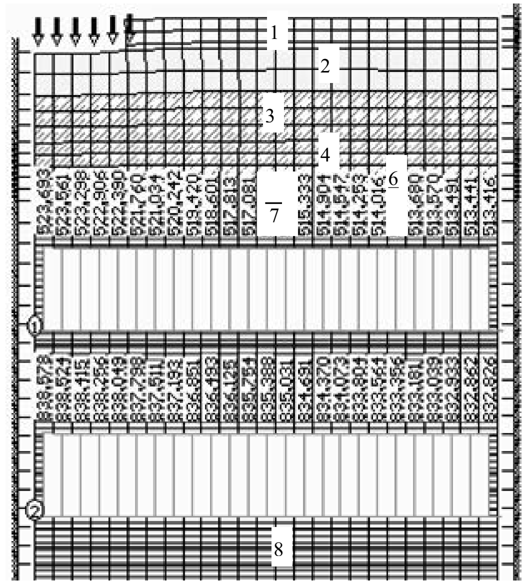

Figure 7. «Geomechanics» calculation scheme for geotechnical conditions at Deputatskaya street

The initial stresses occurring in the soil at the depth of the upper part of the tunnel ordinate equaled 512,45 kPa, and at its foundation ordinate – 830,46 kPa. After the foundation of the planned building was modeled, stresses at the tunnel foundation ordinate reached 838,6 kPa, i.e. it increased by 1,0 %.

The additional vertical stresses which occurred in relation to the building foundation corresponded to the stresses which would have occurred if the tunnel had been located at an ordinate lower by 0,5 m from the actual one. The 1% increase in the stresses is twentyfold lower than the safety reserve adopted for the tunnel strength calculations.

3.3. Multi-storey building with an underground garage in Sverdlovskaya naberezhnaya

During the construction of a multi-storey building with an underground garage in Sverdlovskaya embankment, it was imperative to guarantee the safety of the main intercepting sewer of the northern part of the city, presented as two parallel tunnels of cross-section area 4030x2780 mm, located 64 m under the building.

The designed building is a 14-18-storey residential complex with underground car parks. Some parts of it have a combined foundation in the form of a ribbed plate resting on ferroconcrete piles drilled in casing of diameter Ø 560/670 mm and length L=29 m. The piles footing is set in a layer of glacial silt (IL=0,6, E=18500 kPa). The pressure transmitted to the plate reaches 130 kPa.

The main interceptor suer runs in a Proterozoic formations layer. The basic soil parameters adopted for the calculations are presented in Table 4.

Table 4. Basic soil parameters in Sverdlovskaya nabierezhnaya

No.	Soil	γ, kN/m^3	E, kPa	ν	c kPa	ϕ °
1	Fill soil	17	1000	0,3	1	15
2	Silt	19,5	7000	0,35	10	18
2a	Sandy clay	19,5	7000	0,30	6	33
2b	Silty sand	20,7	28000	0,35	7	7
3	Clayey sand	16,9	4000	0,35	9	18
4	Sandy clay	19,3	7000	0,35	7	7
5	Clayey sand	16,9	4000	0,35	7	7
6	Clayey sand	16,9	4000	0,35	10	18
7	Sandy clay	19,5	18500	0,30	6	37
8	Fine sand	21,3	48000	0,35	10	18
9	Sandy clay	19,5	30000	0,40	140	22

When the construction process started, the value of stresses at the depth at which the casing of the first interceptor line was located reached 679,67 kPa, and after the building was completed - 758,78 kPa. Calculations showed that the stresses increased by 11%, and it should be noted that the calculated displacement of the tunnel casing equaled s = 0,16 mm.

For the second interceptor line, the initial pressure at the level of its casing was 681,55 kPa. After the structure was founded, the stresses in the soil grew to 764,66 kPa, i.e. by 12%. Calculations showed that the vertical displacement of the tunnel casing equaled s = 0,23 mm.

The scheme adopted for the calculations is presented in Figure 8.

The calculations showed that the planned building was safe with regard to further failsafe operation of the intercepting sewers.

Both structures have been built and have not had any negative impact on the sewers' operation. The registered building settlement values fall within permissible limits.

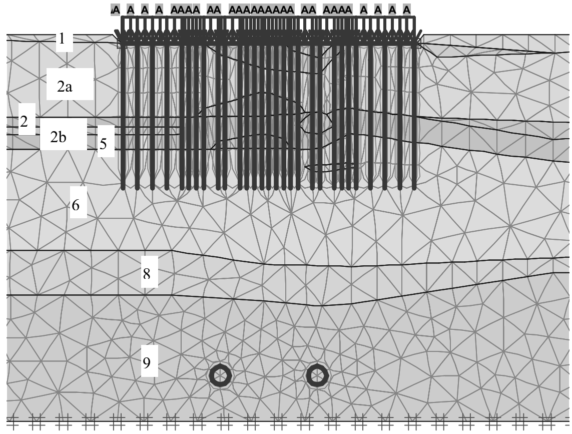

Figure 8. PLAXIS calculation scheme for geotechnical conditions at Sverdlovskaya naberegnaya street.

4. CONCLUSIONS

The following conclusions ensue from the numerical calculations that have been carried out under this project:

- The calculations have confirmed the soundness of the adopted structural solutions applied in the examples discussed above. They have showed that the impacts of the new buildings on the metro tunnels and stations and the intercepting sewers fall within permissible limits.
- Designing and implementing building structures in difficult conditions (complex geological conditions, proximity of existing buildings, deep excavations etc.) cannot be based on typical parameter estimations and standard statistical calculation methods.
- Analysis of deep foundations and their surrounding soils is a task conditioned by numerous factors, such as the technical condition of the existing neighboring structures, geological conditions in the soil, the way of determining ground parameters etc.
- The proper protection of the structure and its further failsafe operation will be conditioned by values of additional displacements which can occur as a result of additional loads, and by possible changes in the work scheme of the structure.

- The foundation works together with soil at large depths (usually much exceeding the depth of geology determination procedures). Tests show that higher values of geotechnical parameters can be expected from deeper layers, mainly as a result of a greater impact of pre-consolidation.
- As for practical issues in building foundation, results of numerical calculations should be verified against the values of measured dislocations.
- Backward analysis carried out on the basis of displacement monitoring results admits of specification of modified (increased) soil parameters.
- At the stage of problem analysis one should necessarily verify the results of soil parameters tests and adopt correct values for calculations.
- Parameters of deeply deposited materials determined by backward analysis may be even several times higher than those adopted on the basis of regular tests and standards.
- Non-standard calculation methods (numerical modeling) impose extension of the monitoring network and using modern soil testing methods.
- Backward analysis performed on the basis of existing displacement monitoring results permits verification of soil parameters, as well as of the schemes and construction implementation stages adopted for calculation purposes.

5. REFERENCES

1. Barański M., Dąbska A., Popielski P., Szczepański T.; *Numerical model verification on the basis of the measurements and investigation carried out during the objects realization*, Proceedings of the International Geotechnical Conference: "Development of Urban Areas and Geotechnical Engineering", Volume 1; St Petersburg 2008; ISBN 978-5-9900771-4-0
2. Chmielewski A., Dąbrowski H., Popielski P., Stankiewicz G., Zalewski P., 2004. *Numerical models of the foundation structure of Dworzec Gdański A17 metro station* (in Polish). Conference on: „Numerical methods for design and analysis of hydrotechnical structures". Korbielów.
3. Dłużewski J. M., 1997. *„HYDRO-GEO" – finite 2elements method software for geotechnics, hydrotechnics and environmental engineering* (in Polish). Warszawa: Oficyna Wydawnicza PW.
4. Dłużewski J.M., Grabowski Z., Siemińska-Lewandowska A., 2001. S*etting analysis for Dworzec Gdański station structure* (in Polish). Geotechnika – Janusz Dłużewski. Warszawa.
5. Georgiannou V.N., Rampello S., Silvestri F., 1991. *Static and dynamic measurements of undrained stiffness on natural overconsolidated clays*. Proc. 10th Firence, Vol. 1, pp. 91 – 95.
6. Geology Institute, 1998. *Evaluation of geology determination status for the Warsaw metro route at sections A16÷A18 for design and implementation purposes* (in Polish). Warszawa.
7. PN-81/B-03020. *Construction grounds. Direct foundation of a structure. Static calculation and design* (in Polish).
8. Popielski P., 2003. *Numerical models for analysis of soil displacements following the construction of a pedestrian subway connecting Dworzec Gdański A17 metro station, Warszawa Gdańska railway station and Żoliborz district. Determination of its impact on displacements of 22metro tunnels and Dworzec Gdański A17 metro station. Phase 1* (in Polish). KIP Biuro projektów konstrukcji Budowlanych Sp. z o.o. Warszawa.
9. СНиП 2.06.09-84. *Тоннели гидротехнические*.
10. СНиП 2.06.09-84. *Туннели гидротехнические*.
11. Фадеев А.Б., 1987. *Метод конечных элементов в геомеханике*. - М.: Недра.
12. Мангушев Р.А., Городнова Е.В., 2005. О расчетном обосновании нового строительства на подземные инженерные коммуникации в условиях слабых грунтов Санкт-Петербурга. *Тр. междунар. научно-практ. семинара „Актуальные проблемы проектирования и стр-ва в условиях городской застройки",* Пермь, pp. 110-11

Microtunneling beneath the City of Albany, California

S.J. Gambino, S.A. Gentzler
URS Corporation, Oakland, California

R.W. Leptien, R. Cunningham
City of Albany, California

ABSTRACT: URS provided alternatives analysis, detailed design, cost estimating, geotechnical services, and construction management support for the Curtis-Neilson-Santa Fe Storm Drain Project, located in Albany, California. All together, over 1,400 feet of 30-inch pipeline was installed at depths of up to 26 feet. The project eliminated chronic flooding in a residential area of the City south of Marin Avenue.
Slurry Earth-Pressure-Balance microtunneling techniques were employed during the tunnelling operation so that settlements were minimized, and to prevent damage to other utility lines or foundations of nearby houses, some of which were less than 20 feet away. The project involved the excavation of multiple jacking/receiving pits in order to carry out the microtunneling operation. The total construction cost was approximately $3.5 M.

1. PROJECT SETTING

The San Francisco Bay Area lies on the shores San Francisco Bay and San Pablo Bay in Northern California. The Bay Area greater metropolitan area is one of the largest in the United States (7,000 square miles), with approximately 7 million people. The Bay Area metropolitan region encompasses nine counties (including Alameda and Contra Costa Counties) and over 100 cities (including San Francisco, Oakland, and San Jose). After New York City, San Francisco has the second highest population density of any major American city. The urban infrastructure consists of a complex network of roads, highways, railroads, bridges, tunnels and commuter rail systems.

Albany is a small city of 1.7 square miles (see Figure 1) and close to 17,000 residents, located on the eastern shoreline of the San Francisco Bay, directly east of the Golden Gate Bridge. Albany was named in honour of the birthplace of the City's first mayor, Frank Roberts. The great earthquake and fire of 1906 resulted in a large migration of families from San Francisco to the East Bay. During World War II, the Federal Government built a housing project called “Codornices Village” to accommodate the thousands of workers at the Richmond shipyards, which were eventually converted to family student housing for those attending the University of California at Berkeley.

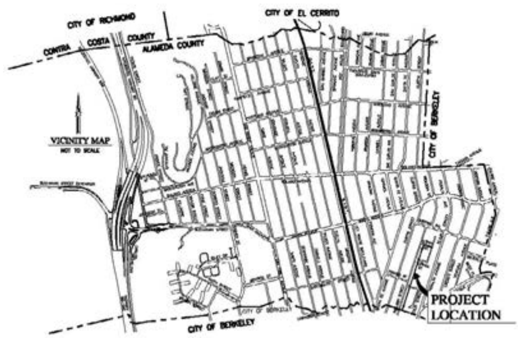

Figure 1. Project location.

This project eliminated chronic flooding in a residential area of the City south of Marin Avenue. The rainfall catchment area involved a relatively small (15 acre) portion of the Village and Codornices Creek watersheds. Except for Codornices Creek, the drainage system is entirely contained within underground pipes and culverts. Many sections of the existing system are on private property, located between or under existing houses and foundations. The drainage system segment immediately downstream from the intersection of Neilson and Albany Terrace Streets was identified as the most deficient area needing improvement in the form of a new storm drain.

The project area is bounded between the two low-lying areas of Albany Terrace to the north (El. 88 feet) and Codornices Creek to the south (El. 82 feet). In between, the terrain rises gently until reaching a maximum elevation of 103 feet at the intersection of Neilson and Terrace Streets. Slopes in the area vary between 3 and 6%, being steeper towards the northern portion of the project. Land use along the new storm drain is predominantly residential. All of the buildings along Neilson Street are one- and two-story residential family houses. Roadways in the project area are covered with a 6-inch layer of asphalt concrete (AC) with an underlying aggregate base layer of the same thickness. Overhead utilities that run along the east side of Neilson Street include telephone, street light, and electrical lines.

2. PROJECT ALIGNMENT

The existing system consisted of a series of clay pipes of diameters from 8 inches to 18 inches, with a 10-inch PVC insert in the pipe between Curtis Street and Neilson Street. The approximate alignment of the new storm drain as designed by URS Corporation of Oakland, California is shown on Figure 2. The upstream end of the alignment begins at the intersection of Albany Terrace and Neilson Streets (tying into the existing drop inlet) then continues south in a straight line along Neilson Street from Albany Terrace Street to Codornices Creek, providing a direct storm drain connection to Codornices Creek.

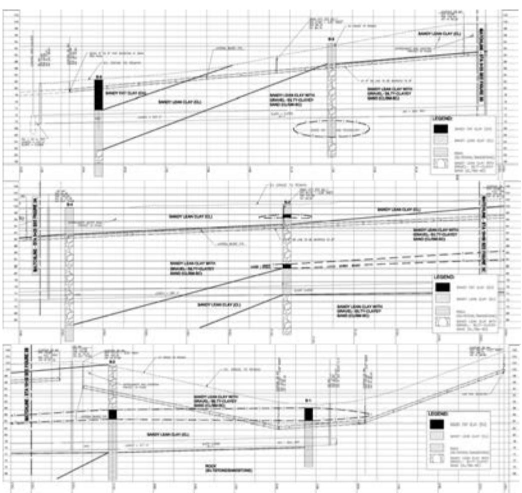

Figure 2. Subsurface profile along alignment.

The new storm drain crosses beneath numerous existing underground utilities, including water lines, sewer lines, drain lines, and gas lines. The majority of the existing underground utilities are located above the crown of the new storm drain. The new storm drain also parallels an existing sanitary sewer line that was replaced by pipe bursting as part of this contract.

The selected alternative involved microtunneling, thereby avoiding placement of pipe between existing homes and in streets already crowded with utilities. The crown of the new storm drain is about 9.5 to 24 feet beneath the existing ground surface, with the greatest amount of cover near the central portions of the alignment and the least amount of cover at the upstream and downstream ends. The new line was installed at a constant slope of 0.5%, dropping approximately 7 feet in elevation over the 1400-foot length of the pipeline. Other noteworthy features of the project include the following:

- Length of pipe is 1,417 linear feet (LF)
- 30-inch inner diameter pipeline
- Neighbourhood is residential
- Houses spaced 50 feet on the west side
- Houses spaced 44 feet on the east side
- Street width is in the order of 25 feet
- House setback typically less than 20 ft
- Pipe depth to invert is 8 ft to 26 ft

3. REGIONAL AND LOCAL GEOLOGY

The project site is located physiographically in the San Francisco Bay block of the northern Coast Ranges (see Figure 3) and tectonically within the Coast Ranges seismotectonic province, a region characterized by a moderate to high level of seismicity. The Coast Ranges are a north-northwest-to northwest-trending series of mountains and intervening valleys extending for 960 kilometres from the Oregon border, south to the Santa Ynez River near Santa Barbara.

The site is underlain by the upper Holocene alluvial fan deposits (less than 10,000 years old) that overlay Pleistocene alluvial fan deposits (less than 500,000 years old). The Holocene and Pleistocene deposits are composed of alluvial materials that are derived from erosion of the Berkeley Hills. These sediments were deposited in a subsiding bay environment. This subsidence is thought to have begun, geologically, fairly recently and is dated as less than 500,000 years ago. The alluvial sediments consist primarily of stiff to hard sandy clay with minor sand, silt, and gravel.

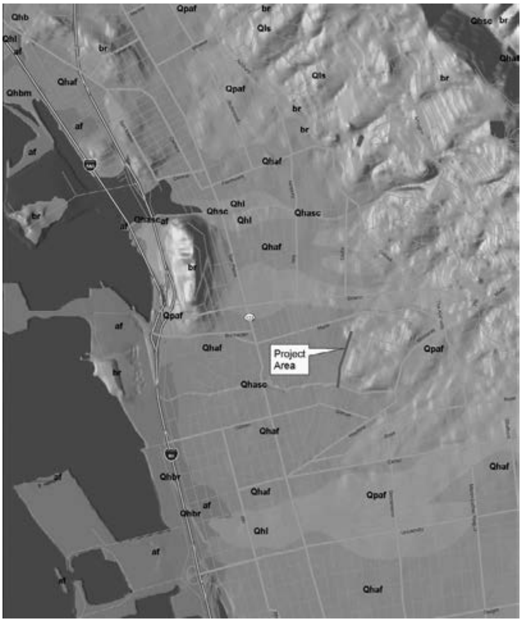

Figure 3. Regional geologic map.

4. SUBSURFACE INVESTIGATIONS

A site-specific subsurface investigation was conducted for this project. A total of six exploratory borings (Borings B-1 through B-6) were completed between March 15 and March 16, 2007. The exploratory borings were completed to depths of about 18 to 40 feet.

Sandstone and claystone/siltstone was encountered in one boring drilled at the site during the subsurface investigation. After reviewing the published data within the region, the bedrock of the site was classified as Franciscan Formation bedrock (dated as 200 to 65 million years old) underlying the alluvial fan deposits at depth.

A series of soil borings, spaced approximately 200 to 400 feet on-centres, were also performed in April and May of 1964 in connection with the construction of aerial structures for the Bay Area Rapid Transit (BART) system's Berkeley-Richmond line. The BART borings were advanced to depths ranging from 50 to 80 feet using a rotary drill rig with a 6-inch diameter borehole. In general, the borings encountered stiff to hard silty and sandy clays with gravel with occasional layers of medium dense to dense clayey sand and gravel.

5. MICROTUNNELING CONSIDERATIONS

The storm drain was constructed in three drives. One drive (from approximately Station 00+00 to 05+35) extended along Neilson Street from near the intersection with Codornices Creek to the intersection with Francis Street. Another drive (from approximately Station 05+35 to 11+00) continued along Neilson Street from the intersection with Francis Street to the intersection with Terrace Street. A third drive (from Station 11+00 to 14+17) continued along Neilson Street from the intersection with Terrace Street to the intersection with Albany Terrace Street.

The subsurface strata along the alignment tend to follow the gentle slope of the terrain, dipping to the south. The new alignment encountered the interface between the upper sandy lean clay and the underlying layer which exhibits substantial gravel and sand contents. The depth to groundwater ranged from 4 to 14 feet below the ground surface. Mixed face conditions, a condition where differing soil types are encountered in a tunnel heading at the same time, were encountered where gravely zones exist within the clay matrix.

A summary of the microtunneling drives is presented in Table 1. Ground conditions at the tunnelling zone for the various drives are summarized in Table 2. Empirical methods (Peck, 1969; Cording and Hansmire, 1975) were used for estimating surface settlement magnitudes due to tunnelling by the study of observed settlements on past projects. Typically, the settlement pattern that develops above a soft ground tunnel is a trough-shaped depression resembling an inverted normal probability (bell-shaped) curve with the maximum settlement occurring above the tunnel centreline as conceptually illustrated in Figure 4.

Table 1. Summary of microtunneling drives

Drive	Stations	Length (Feet)	Cover (Feet)
1	0+00 - 5+35	535	9 – 23
2	5+35 - 11+00	565	21 – 23
3	11+00 - 14+17	317	6 – 21

Table 2. Ground conditions at tunnelling zone

Drive	Stations	Ground Conditions
1	0+00 - 5+35	Raveling to Firm
2	5+35 - 11+00	Raveling to Firm
3	11+00 - 14+17	Firm

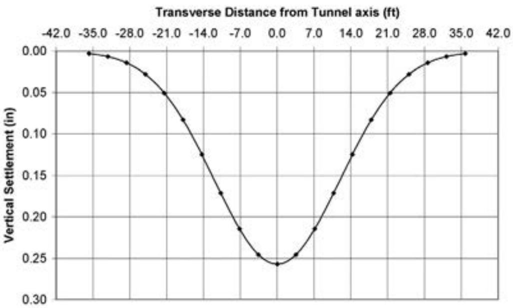

Figure 4. Typical settlement trough geometry.

6. SHAFT EXCAVATIONS

Four storm drain manholes were constructed along the new alignment. These manhole excavations were used as jacking and/or receiving pits during construction. The approximate depth of the base of the manholes below the existing ground surface ranged from about 9 to 26 feet. Before and after photographs at one particular location are shown in Figures 5 and 6, respectively.

Figure 5. Photograph during shaft construction.

Figure 6. Photograph after project completion.

The Contractor was responsible for selecting, designing, and installing appropriate excavation support systems for all shaft excavations. The braced pile and plate shoring systems were designed by J. M. Turner Engineering, Inc. of Santa Rosa, California to accommodate a maximum excavation depth of 30 feet. The structural elements of the excavation support system were designed to limit deflections of the excavation to a maximum of 1 inch at the top of the excavation. In order to avoid damage to existing utilities when the support system was removed, the Contractor was given the option that the supports may be left in place as long as the upper 5 feet are removed.

The Contractor was also required to select, design, and implement adequate groundwater control for all shaft excavations. Drawdown of the groundwater level outside of the excavations was not allowed. Large drawdown of the groundwater level can result in the compression of the underlying soil deposits leading to potential widespread ground surface settlements. Due to the presence of existing settlement-sensitive utilities and buildings, conventional dewatering methods utilizing deep pumping wells were prohibited for this project.

Streets could be partially shut down per the City, but not so that it prevented access to individual homes. The traffic control plan is shown in Figure 7. Streets could be partially blocked, but two-way access for emergency vehicles had to stay open each way from the point of blockage.

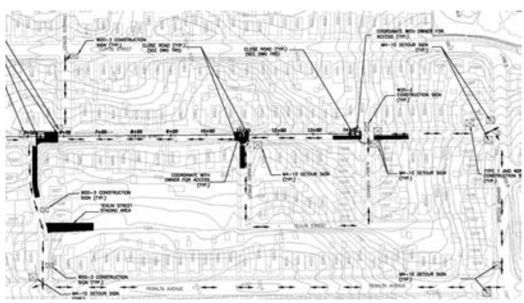

Figure 7. Traffic control plan.

7. MACHINE CONSIDERATIONS

Because of the limited amount of cover above the crown of the storm drain at some locations, it was important to closely monitor and control the pressure applied to the tunnel face and other microtunneling controls to avoid formation of sinkholes, excessive ground settlement, ground heave, or fracturing of the ground and resultant slurry discharge onto public streets and private properties.

The slurry earth-pressure-balance microtunnel boring machine (MTBM) used for this project was specified to have the following requirements:

- Remotely controlled
- Articulated, steerable, closed-face
- Laser guidance system
- Lubrication injection system
- Automated spoil transportation system
- Seals to withstand 25 feet of head
- Ability to back-flush the slurry lines

The final carrier pipe for the new storm drain was installed using pipe jacking methods. The jacking pipe was designed for the maximum axial jacking forces to be exerted on the pipe, as well as the earth loads due to the full overburden pressure. Because the critical loading condition is likely to be the stresses imposed on the pipe during installation, the Contractor was responsible for final design of the jacking pipes. Unacceptable eccentric stresses could be induced in the pipe during jacking if the ends are not within the tolerance for squareness. The pipe was fabricated by Hanson Pipe & Precast of Sacramento, California.

8. CONSTRUCTION PERIOD

Bids were received in the spring of 2008 with the low bid being awarded to Ranger pipelines, Inc. of San Francisco, California. Approximately 2 months out of an overall 8-month construction schedule were allocated for microtunneling. The microtunneling subcontractor was Nada Pacific Corporation of Caruthers, California, who employed an Akkerman Model SL34 MTBM. Various commercially available MTBM models are shown in Figure 8.

Figure 8. MTBM sizes and models (from Akkerman).

The field observation work performed by URS during shaft backfill and compaction included field density and laboratory compaction testing. Field density tests were conducted between November 5, 2008 and February 10, 2009 to ensure that the backfill had been compacted to the specified level, as determined by ASTM D2922. Compaction characteristics of the soil were attained using ASTM D1557, and the results of the laboratory testing are presented in Table 3.

Table 3. Results of Laboratory Compaction Tests

Material Description	Maximum Dry Density (pcf)	Optimum Moisture Content (%)
Brown gravelly silty sand, Recycled aggregate base from Treasure Island, Used in trenches	133.5	6.5
Grayish brown gravelly sand, Recycled aggregate base from Aman Environmental	124.0	9.0

The typical tunnelling rate was on the order of 30 to 40 ft/day. Project completion was certified in the spring of 2009 and the new storm drain system performed exceptionally well during the heavy rains in the fall of 2009. The City's mission statement emphasizes the need for responding to the needs of the community, and providing a safe, healthy environment now and in the future. This project eliminated the chronic flooding that had affected this particular residential area in the City.

9. REFERENCES

Cording, E.J., & W.H. Hansmire, 1975. Displacements Around Soft Ground Tunnels, *Session IV, Tunnels in Soil, 5th Pan-American Congress on Soil Mechanics and Foundation Engineering*, Buenos Aires, pp. 571-632.

Peck, R.B. 1969. *Deep Excavations and Tunnelling in Soft Ground, Proceedings, 7th International Conference on Soil Mechanics and Foundation Engineering*, State of the Art Volume, pp. 225-293.

Earth Forces Applied to an Underground Structure due to Earthquake

N. Kodama
Waseda Institute for Advanced Study, Waseda University, Tokyo, Japan

K. Komiya
Chiba Institute of Technology, Chiba, Japan

ABSTRACT: Model shaking tests were performed in a laboratory to investigate dynamic earth forces applied to an underground structure due to earthquake. The horizontal displacement and the applied earth forces to the underground structure in sandy ground obtained from the model tests. The earth force profiles depended on various factors such as physical properties of the soil, the depth of ground, the mass of the structure, seismic wave properties, etc. Finite element analyses using the Mohr-Coulomb type elasto-viscoplastic model were conducted to simulate the model tests. The earth forces associated with the soil density, the soil depth and the mass of the structure were discussed based on the comparison between the numerical results and the laboratory data.

1. INTRODUCTION

Earth force or earth pressure during earthquake have been causing numerous ill effects on many buildings and utility infrastructures. In order to overcome the earth forces, many seismic design methods have been developed in engineering since early time, for example Mononobe-Okabe earth pressure theory (Mononobe & Matsuo 1929). In modern time, seismic technologies like seismic isolation systems have been developed in the building and the civil engineering. Because of the complex boundary conditions of seismic problems, the use of the Finite Element Method is one of the popular methods to investigate the seismic response of structures. In general, the results of Finite Element analyses are closely linked to the dynamic interaction between the soil and the structure.

In the soil-structure dynamic interaction problems, the earth pressure applied to the structure, the displacement of the structure and the soil deformation are the main concerns. The soil-structure interaction is often modelled by soil-springs to apply external forces, as shown in Figure 1 (e.g. Japan Road Association 2002), to introduce traction and to force displacements at the boundaries. However, when the soil deforms largely or fractures, its behaviour depends on soil properties and the stress history. Therefore, in order to understand the soil-structure interaction mechanism, the nonlinear pressure-displacement behaviour caused by the motion needs to be investigated associated with soil properties.

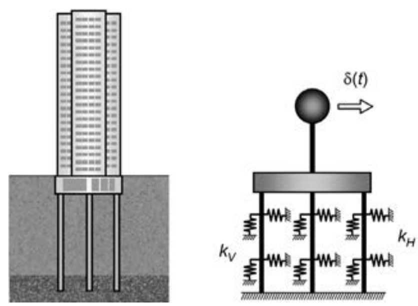

Figure 1. Typical example of numerical model for dynamic seismic verification

The authors have provided that the model test results of the nonlinear relationship between the applied earth pressure and the relative displacement of the underground structure (Komiya et al. 2008). And the authors also indicated that the elasto-viscoplastic model with Mohr-Coulomb yield criteria is adequate for simulations of the relationship (Kodama et al. 2009).

In this study, model shaking tests were performed in a laboratory to investigate the relationship between the horizontal displacement and the applied earth forces of the underground structure in sandy ground. The earth forces associated with the soil density, the soil depth and the mass of the structure are discussed based on the comparison between the results of the model tests and Finite Element analyses.

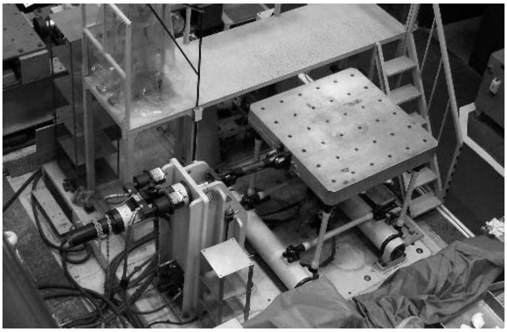

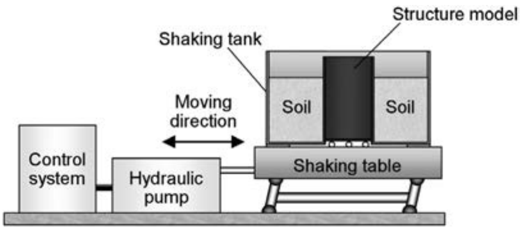

Figure 2. Laboratory shaking test apparatus

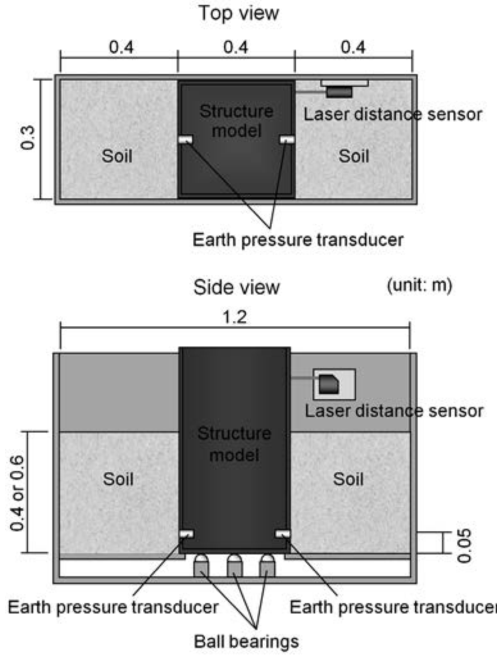

Figure 3. Shaking tank details

2. MODEL SHAKING TEST

2.1. Outline of laboratory shaking test

Laboratory shaking tests were carried out to investigate a dynamic interaction between soil and a structure. A schematic diagram of the laboratory shaking test apparatus is shown in Figure 2 (Komiya et al. 2008, Kodama et al. 2009). The shaking of the tank was allowed in only one horizontal direction as shown in Figure 2.

In the shaking tank, a hollow rectangular structure model made of steel with 0.4 m width, 0.3 m depth and 0.8 m height was placed in its centre. Then at the both sides of the structure model, rectangular parallelepiped model grounds of 0.4 m width, 0.3 m depth and 0.4 m or 0.6 m height were made as shown in Figure 3. The mass of the structure model was adjusted to 50 kg, 75 kg or 100kg. On the interface between the bottom face of the structure model and the inner surface of the tank, ball bearings were installed as shown in the side view of Figure 3, by those lateral force transmitted through the interface was cut off. The soil grounds were made by tamping to bridge the gaps between the structure model and the tank. When the tank was shaking, therefore, only the lateral forces coming from the soil grounds acted upon the structure model except for bearing vertical support forces.

Table 1. Parameters of the test cases

Parameters	Cases			
	A	B	C	D
Frequency f (Hz)	5.0			
Amplitude a (mm)	7.0			
Structure mass m (kg)	50		75	100
Soil depth d (m)	0.4		0.6	0.4
Soil density ρ (g/cm^3)	1.27	1.49	1.51	1.48
Water content w(%)	8.7	11.0	8.9	9.6

The earth force applying to the structure model was measured by two pressure transducers located on the surface of the structure model as shown in Figure 3. The relative displacement between the structure model and the tank was measured by a laser distance sensor attached to the tank. Shaking sinusoidal wave was set to frequency 5 Hz and displacement amplitude 7.0 mm.

Soil ground used in the test was made of wet Toyoura Sand. The parameter details of the three test cases are shown in Table 1. The water content of the sand was approximately 10%. The mass density of the ground was measured to be 1.27 g/cm^3 in Case A, and around 1.50 g/cm^3 in other three cases.

2.2. Laboratory shaking test results

The relations between the applied earth pressure and the relative displacement of the structure model against the shaking tank are shown in Figure 4.

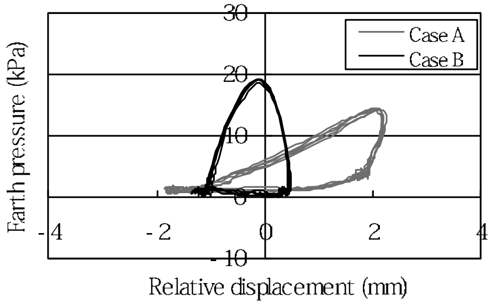

(a) Comparison between Case A (ρ =1.27) and Case B (ρ =1.49)

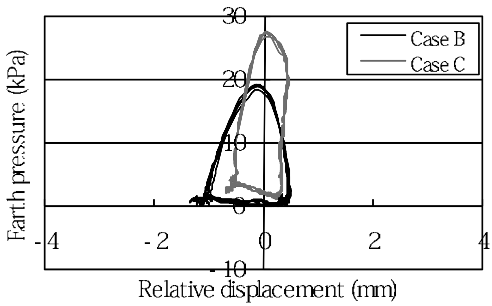

(b) Comparison between Case B (d = 0.4 m) and Case C (d = 0.6 m)

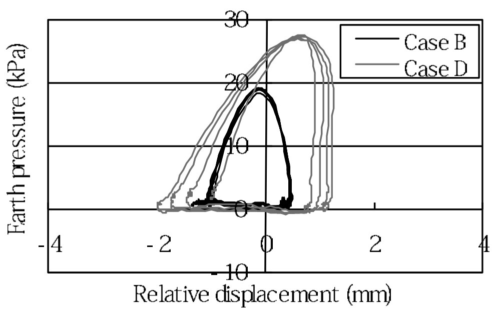

(c) Comparison between Case B (m = 50kg) and Case D (m = 100kg)

Figure 4. Comparison of the experimental earth pressure-displacement relations with different soil densities, soil depths and structure mass

Figure 4 (a) shows the pressure-displacement (hysteresis) curves obtained by the tests in Case A and Case B. It was found that a larger applied earth pressure to the structure was generated in dense sand (Case B: ρ = 1.51 g/cm^3) than in lose sand (Case A: ρ=1.27 g/cm^3). A large compressibility of the soil resulted a large relative displacement of the structure in the lose sand.

Figure 4 (b) shows the hysteresis curves obtained from two tests in different depths (Case B: d = 0.4 m, Case C: d = 0.6 m). Larger maximum applied earth pressure was obtained in thick soil bed (Case C).

The generated confining pressure in the soil due to loading increased with increasing density or depth of the soil. In the tests, the applied earth pressure corresponding to the confining pressure was applied to the structure. Therefore the large applied earth pressure developed in the dense soil or in the thick soil bed.

Figure 4 (c) compares the results of two tests that carried out with different masses of the structure (Case B: m = 50 kg, Case D: m = 100 kg). The pressure-displacement hysteresis loop was expanded in Case D due to an increase in the inertial force of the structure.

3. NUMERICAL SIMULATION

Finite element analyses were carried out to confirm the effects of various parameters associated with the pressure-displacement loops of the model tests, such as soil density, soil depth and mass of the structure, to the generated earth pressure.

In this paper, two dimensional finite element analyses were carried out to simulate the model shaking test described in the previous section. The finite element model used in the calculation is shown in Figure 5. The soil and the structure are modelled by two-dimensional plane-strain elements. Sinusoidal acceleration boundary condition was applied to the leftmost and the rightmost nodes of the soil elements. The elements for soil were modelled by elasto-viscoplastic materials with Mohr-Coulomb yield criteria. Mohr-Coulomb yield criteria can consider the internal friction, which is often observed in soil materials. The structure elements were modelled by elastic material behaviour. Viscoplastic strain velocity $\dot{\varepsilon}_{vp}$ is calculated by Eq. 1 (Owen and Hinton 1980).

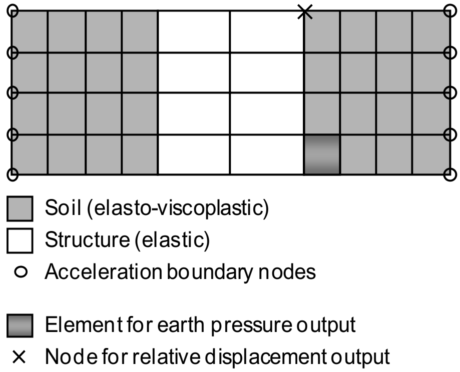

Figure 5. Finite Element model of the shaking tank

Table 2. Material parameters for Finite Element Analysis

Parameter	Soil	Structure
Elastic modulus E (Pa)	A) 2.0E+6 B) 8.0E+6 C) 1.8E+7 D) 8.0E+6	2.1E+11
Poisson's ratio ν	0.35	0.3
Soil density ρ (g/cm^3)	A) 1.27 B) 1.49 C) 1.51 D) 1.48	1.042*
Cohesion c (kPa)	0.1	—
Friction angle ϕ' (deg)	34.0	—
Fluidity parameter γ	0.005	—

* (Structure mass) / (Structure elements volume)

$$\dot{\varepsilon}_{vp} = \gamma \frac{F - F_0}{F_0} \frac{\partial \mathbf{F}}{\partial \boldsymbol{\sigma}} \tag{1}$$

where γ is the fluidity parameter, F is the equivalent stress, $F_0 = c \cos\phi'$ is the uniaxial yield stress, $\mathbf{F}$ is the yield surface function and $\boldsymbol{\sigma}$ is the stress vector. Material parameters for numerical simulation are shown in Table 2. The equation of motion was solved by an explicit direct time integration with a time step 1.0E–6 sec.

Figure 6 shows the hysteresis curves obtained by numerical simulations. The contradistinction of Figure 6 (a), (b) and (c) corresponds to of Figure 4 (a), (b) and (c), respectively. The results of numerical analyses are in accord with the experimental data.

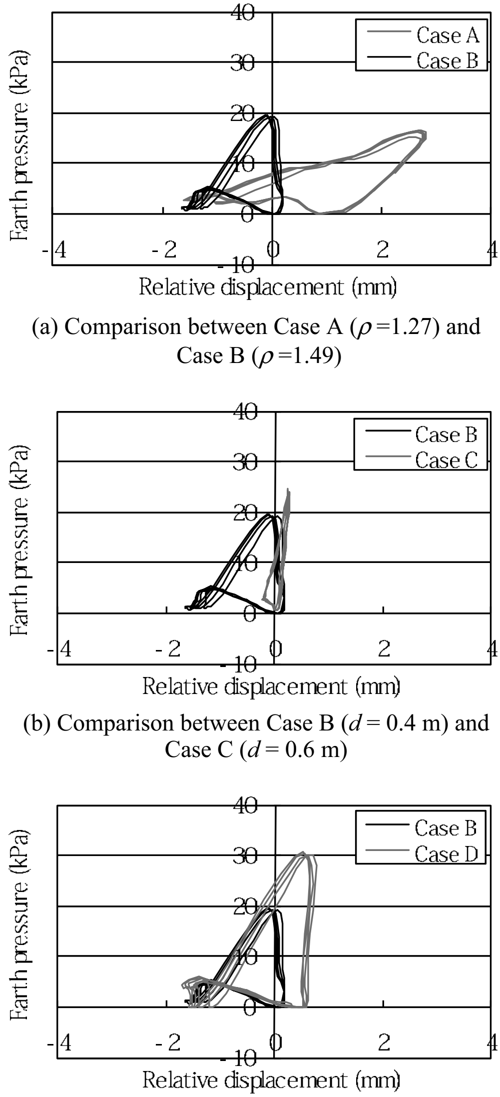

(a) Comparison between Case A (ρ=1.27) and Case B (ρ=1.49)

(b) Comparison between Case B (d = 0.4 m) and Case C (d = 0.6 m)

(c) Comparison between Case B (m = 50kg) and Case D (m = 100kg)

Figure 6. Comparison of the simulated earth pressure-displacement relations with different soil densities, soil depths and structure mass

4. CONCLUSIONS

In this paper, laboratory model shaking tests and finite element analysis were performed to investigate dynamic earth forces applied to an underground structure due to earthquake. The results obtained by the model tests and the numerical analyses were as follows.

- A larger applied earth pressure to the underground structure was generated in

dense soil or in thick soil bed because the generated confining pressure increased with increasing density or depth of the soil.
- In lose sand, a large displacement of the underground structure was caused by a large compressibility of the soil.
- The applied earth pressure-relative displacement hysteresis loop was expanded with increasing mass of the underground structure due to an increase in the inertial force of the underground structure.

5. ACKNOWLEDGEMENTS

The authors would like to acknowledge the financial support from the Grant-in-Aid for Scientific Research (C) (No.19560548) of the Japan's Ministry of Education, Culture, Sports, Science and Technology.

6. REFERENCES

Japan Road Association 2002. *Specifications for highway bridges, Part V Seismic design*. Tokyo: Japan Road Association.

Kodama, N., Komiya, K. & Morozumi, T. 2009. Numerical simulation of soil-tunnel dynamic interaction, *Proceedings of the 2nd International Conference on Computational Methods in Tunnelling*, Bochum, Germany, September 9-11, 2009, pp.71-76.

Komiya, K., Kodama, N. & Shikata, K. 2008. Model experiments on dynamic soil-structure interaction. *Proceedings of the International Geotechnical Conference on Development of Urban Areas and Geotechnical Engineering*, St. Petersburg, Russia, June 16-17, 2008, pp.245-248.

Mononobe, N. & Matsuo, H. 1929. On the determination of earth pressure during earthquakes. *Proceedings of the World Engineering Conference*, Vol. 9, pp.177-185.

Owen, D.R.J. & Hinton, E. 1980. *Finite elements in plasticity*. Swansea: Pineridge Press.

Feasibility study for tunnel-building interaction by using the analytic solution for a circular tunnel in an elastic-plastic half space

S.A. Massinas
OMIKRON KAPPA CONSULTING Ltd, Department of Rural & Surveying Engineering, National Technical University of Athens, Athens, Greece

M.G. Sakellariou
Department of Rural & Surveying Engineering, National Technical University of Athens, Athens, Greece

ABSTRACT: The presentation of the closed-form solution for the problem of the plastic zone and stress distribution around a circular tunnel in an elastic-plastic half space, derived using bipolar coordinates, as well as its implementation in practical examples such as the feasibility study of a tunnel-building interaction, is the main scope of this paper. By assuming a uniformly applied surface loading, the whole semi-infinite space is under uniform pressure, while the plastic zone formation around the circular tunnel is controlled by the applied internal support pressure. The plastic behavior of the half space is described by the Mohr-Coulomb yield criterion and the soil is assumed to be homogeneous and isotropic with earth pressure coefficient K_o equal to unity. In order to study, in a preliminary phase, the tunnel-building interaction problem, this innovative analytic solution is used.

1. INTRODUCTION

Only a few publications describe analytic solutions for tunnelling problems having elastic behaviour and they all concern the stress disturbance of either an equilibrated semi-infinite or an infinite elastic solid due to the presence of a circular cavity (Mindlin, 1939; Muir Wood, 1975; Pender, 1980; Verruijt & Booker, 1996; Verruijt, 1998; Strack, 2002). For the case of elastic-plastic behaviour, the problem of the plastic zone distribution around a circular tunnel has been analyzed by many authors, but only for infinite space (Bray, 1967a, 1967b; Kachanov, 1971; Detournay & John, 1988) which is the case of a very deep tunnel. However the stress disturbance of an elastic-plastic semi-infinite space, pierced by a circular tunnel and bounded by a loaded upper surface, has not yet been analyzed.

A closed from solution of the problem is presented for cohesive-frictional homogeneous isotropic soil with K_o=1.0 (Massinas & Sakellariou, 2009). By using the derived closed form solution the building-tunnel interaction problem has been analyzed in a preliminary phase (feasibility study).

2. ANALYTIC SOLUTION

In the present study, the tunnel is considered to be a horizontal cylindrical cavity of radius r_i with its axis parallel to the z-axis of a rectangular coordinate system x, y, z. The surrounding soil has only an upper boundary, x-axis (the plane y=0), which represents the surface. Such a solid is characterized as a semi-infinite space. The positive direction of y-axis (vertically downward) bisects the circular tunnel and the half-plane (see Fig. 1). A uniform pressure Po acts in the upper boundary (y=0). It is assumed that the earth pressure coefficient K_o is equal to unity, thus vertical stresses are equal to the horizontal stresses. Moreover, the whole half-space is under uniform pressure, thus no gravitational forces are acting (case of zero body force). Finally, it is mentioned that a tension positive notation is used throughout this paper.

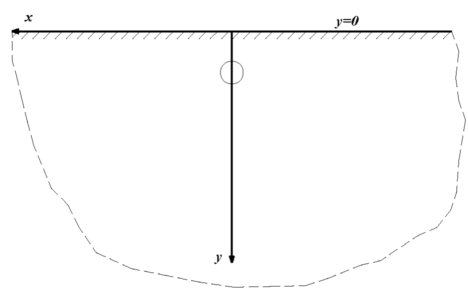

Figure 1. Geometry of the problem

Initially before the tunnel excavation, where an internal uniform pressure P_o acts on the tunnel's periphery, the whole half-space is under uniform stress state P_o. When the excavation of the tunnel begins, the internal pressure decreases from its in situ value P_o ($P_i<P_o$), causing elastic stress distribution around the circular cavity. As the internal pressure decreases further to a critical value P_{cr} (a value connected with soil's cohesion and friction) initial yielding occurs at the tunnel wall. After initial yielding at the cavity wall, a plastic zone of unknown shape (to be calculated in the present study) forms around the tunnel and an elastic-plastic interface is created, with further decrease of the internal pressure.

2.1. Bipolar curvilinear coordinate system

Considering the boundaries of the problem (straight and circular), the mathematical analysis will be simplified by using a proper curvilinear coordinate system (α,β) such as the bipolar coordinate system, which is obtained through the conformal transformation of the type

$$x + iy = i\kappa \coth\frac{\alpha+i\beta}{2}, \tag{1}$$

in which $i=\sqrt{-1}$, κ=distance from the origin to a pole.

This kind of system was first applied in two dimensional elasticity by G. B. Jeffery (1921), who gave the general solution of the elasticity equations in plane strain and plane stress conditions, in bipolar coordinates for the case of zero body force. Solving Equation (1) for x, y the following stands

$$x=\frac{\kappa\sin\beta}{\cosh\alpha-\cos\beta}, \tag{2a}$$

$$y=\frac{\kappa\sinh\alpha}{\cosh\alpha-\cos\beta}, \tag{2b}$$

The general scheme of bipolar coordinates is shown in Fig. 2. If the two poles of the system is O_1 and O_2 at the points $(0,\kappa)$ and $(0,-\kappa)$ respectively and M any point in the plane and if distances (O_1M), (O_2M) are of lengths l_1, l_2 and are inclined at angles θ_2, θ_1 to x-axis, then $\alpha=\log(l_2/l_1)$ and $\beta=\theta_1-\theta_2$.

The curves α=const are a set of coaxial circles having the poles O_1, O_2 for limiting points. The circles corresponding to positive values of α lie below x-axis (along with the direction of positive y-axis) while those corresponding to negative values above. The centers of these circles lie on the y-axis at distances $d=\kappa\coth\alpha$ and they have radii $r=\kappa\,\mathrm{csch}\,\alpha$. The radical circle $\alpha=0$ gives the x-axis. This and a circle $\alpha=\alpha_i=const$ (positive) represent the boundaries of the problem.

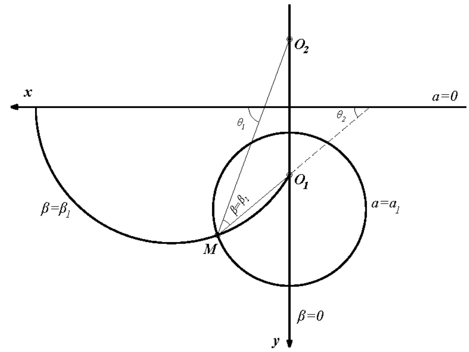

Figure 2. Principle of bipolar coordinate system

The curves $\beta=const$ are circular arcs passing through the poles and cutting the first set of circles orthogonally. β is the angle included between the radius l_1 and l_2. On the right-hand side of the y-axis β is negative and on the left-hand side positive, while on the y-axis β=0, except on the segment (O_1O_2) where $\beta=\pm\pi$. At infinity α=0, β=0 and at the poles O_2, O_1, $\alpha=-\infty$ and $+\infty$ respectively.

The components of stress in bipolar coordinate system were given by Jeffery (1921) as

$$\kappa\sigma_\alpha=\begin{Bmatrix}(\cosh\alpha-\cos\beta)\dfrac{\partial^2}{\partial\beta^2}- \\ -\sinh\alpha\dfrac{\partial}{\partial\alpha}- \\ -\sin\beta\dfrac{\partial}{\partial\beta}+\cosh\alpha\end{Bmatrix}\left(\frac{\chi}{J}\right) \tag{3a}$$

$$\kappa\sigma_\beta=\begin{Bmatrix}(\cosh\alpha-\cos\beta)\dfrac{\partial^2}{\partial\alpha^2}- \\ -\sinh\alpha\dfrac{\partial}{\partial\alpha}- \\ -\sin\beta\dfrac{\partial}{\partial\beta}+\cos\beta\end{Bmatrix}\left(\frac{\chi}{J}\right) \tag{3b}$$

$$\kappa\tau_{\alpha\beta}=-(\cosh\alpha-\cos\beta)\frac{\partial^2}{\partial\alpha\partial\beta}\left(\frac{\chi}{J}\right) \tag{3c}$$

where $J = \dfrac{\kappa}{\cosh\alpha - \cos\beta}$

2.2. Solution procedure

Let assume that the internal pressure in tunnel's periphery decreases from its in situ value, to P_i ($P_{cr}<P_i<P_o$), causing in such way elastic stress distribution around the circular cavity. Considering the above statement, the following expression for the stress function (as proved by Jeffery, 1921) is adopted

$$\frac{\chi}{J} = B_o\alpha(\cosh\alpha - \cos\beta) + \\ +(A_1\cosh 2\alpha + B_1 + C_1\sinh 2\alpha)\cos\beta \tag{4}$$

Calculating σ_α and σ_β according to equations (3) and applying the boundary conditions, σ_α=-P_i on $\alpha=\alpha_i$, σ_α=-P_o on α=0 and $\tau_{\alpha\beta}$=0 on both boundaries, the constants (B_o, A_1, C_1, B_1) of the stress function are calculated. By differentiating equation (4) according to equations (3) and after algebraic manipulations, the elastic stresses are determined by Massinas & Sakellariou (2009).

As the internal pressure decreases further to a critical value P_{cr}, initial yielding begins to occur on the tunnel periphery ($\alpha=\alpha_i$). At this point, the Mohr-Coulomb yield criterion is satisfied

$$\lambda\sigma_\alpha\text{-}\sigma_\beta=Y \tag{5}$$

where λ=(1+sinφ)/(1-sinφ), Y=2$c$cosφ/(1-sinφ) and c,φ are soil's cohesion and frictional angle respectively. Using the elastic stresses and the yield criterion, the critical internal pressure is calculated (Massinas & Sakellariou, 2009)

$$P_{cr} = \frac{2\kappa^2}{2(\kappa^2 + r_i^2\sin^2\beta) + \kappa^2(\lambda-1)} \cdot \left\{ P_o \frac{\left(\kappa^2 + r_i^2\sin^2\beta\right)}{\kappa^2} - \frac{Y}{2} \right\} \tag{6}$$

where r_i is the tunnel.

After the initial yielding at the cavity wall, a plastic zone forms around the tunnel (plastic region) and an elastic-plastic interface is created with further decrease of the internal pressure $P_i<P_{cr}$. It is obvious that the elastic-plastic interface α_c will be a function of variable β, $\alpha_c=f(\beta)$, associated with the geometric properties of the problem (tunnel radius and depth from surface), the external uniform pressure P_0 as well as the internal tunnel pressure and finally, the soil's cohesion and friction angle. We assume that inside the plastic zone the trajectories of principal stresses coincide with the bipolar coordinates (Grigoriev, 1968) and as a result the shear stress $\tau_{\alpha\beta}$ is taken equal to zero. Thus, the equilibrium equation inside the zone is written in the form

$$(\cosh a - \cos\beta)\frac{\partial\sigma_a}{\partial\alpha} - (\sigma_a - \sigma_\beta)\sinh a = 0 \tag{7}$$

where σ_α and σ_β are the principal normal stresses. By combining the differential equation with the yield criterion and after solving, we obtain the principal normal stresses in the plastic zone

$$\sigma_{\alpha pl} = \frac{Y}{\lambda-1} + A\left(\cosh\alpha - \cos\beta\right)^{-(\lambda-1)} \tag{8a}$$

$$\sigma_{\beta pl} = \frac{Y}{\lambda-1} + \lambda A\left(\cosh\alpha - \cos\beta\right)^{-(\lambda-1)} \tag{8b}$$

For the determination of constant A the continuity of stress components at the elastic/plastic interface is used

$$\sigma_{\alpha el,c} = \sigma_{\alpha pl,c} = \text{-}P_c \tag{9}$$

where P_c is the critical value that limits further extension of the plastic zone and is of the same form as Equation (6), but with r_i replaced by r_c which is the plastic zone radius.

By combining Equations (8a) and (9), the constant A is determined and the final expressions for plastic stresses are derived (Massinas & Sakellariou, 2009).

Finally, by applying $\sigma_{\alpha pl}$,

$$\sigma_{\alpha pl} = \frac{Y}{\lambda-1} - \left(P_c + \frac{Y}{\lambda-1}\right)\left(\frac{r}{r_c}\cdot\frac{d_c - r_c\cos\beta}{d - r\cos\beta}\right)^{\lambda-1} \tag{10}$$

at the cavity wall, the relationship between the internal pressure in the tunnel's periphery and the plastic zone radius r_c is derived (Massinas & Sakellariou, 2009)

$$\left(\frac{r_c}{r_i}\cdot\frac{d_i - r_i\cos\beta}{d_c - r_c\cos\beta}\right)^{1-\lambda} = \\ = \frac{\left[2M_o + \kappa^2(\lambda-1)\right]\cdot\left[Y + P_i(\lambda-1)\right]}{2M_o\left[Y + P_o(\lambda-1)\right]} \tag{11}$$

where $M_o=\kappa^2+r^2_c sin^2\beta$. By using Equation (11) the plastic zone shape can be calculated.

2.3. Solution validation

By using the FLAC program, the results from the computational plane-strain analyses are compared with the results extracted from the closed-from solution. The parameters used in both methods of calculation (FDM and analytic solution), are presented in Table 1. It is evident from the results that the analytic calculation of the plastic zone fits very well with the results from the FDM computational analysis (see Fig. 3).

Table 1. FDM & analytical solution (Massinas et al, 2009)

Analysis	Parameters				
	r_i, m	d_i, m	P_o, kPa	P_i, kPa	c, kPa φ, °
SMC1	5	10	250	50	60 25
SMC2	5	10	250	30	35 21

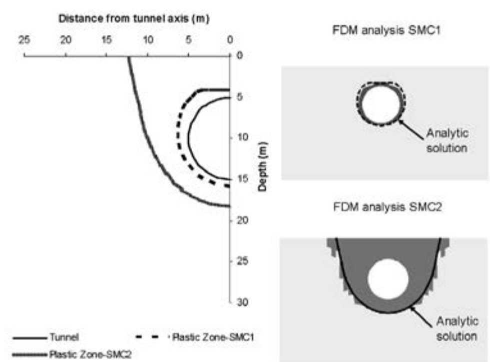

Figure 3. Analytic solution and FDM analysis results: closed-form solution validation (Massinas et al, 2009)

3. FEASIBILTY STUDY FOR TUNNEL-BUILDING INTERACTION

In the present paragraph the problem of the tunnel-building interaction has been examined in a preliminary phase (feasibility study), by using the already presented closed-form solution.

3.1. Introduction of the problem-Geotechnical properties

Assume that a new METRO line, consisted of a 10 m in diameter circular tunnel, is planned to be constructed under a 70-story building. The building reaches a height of 210 m and is founded on a combined pile-raft foundation, with piles of 10 m in length and a raft with a thickness of 4 m. For this kind of building the estimated average pressure (due to building's weight) at the foundation level is B_w=1050 kPa (Sorochan E.A. and Konyukhov D.S, 2005).

The excavation and temporary support of the tunnel is planned to be performed using an earth pressure balance-tunnel boring machine (EPB-TBM): thus temporary support of the tunnel will be provided directly by the EPB-TBM, which is capable of producing pressure with the excavated material and a certain type of foam if needed, in front of the cutter head and around the cavity wall.

The tunnel construction will take place on a bed composed of intercalation of sands of medium fineness, silty sand, grey mucky silty clay and clayey soil layer, with the following general characteristics: γ=20 kN/m^3, cohesion c that varies from 0 to 100 kPa (depend on the soil layer) and friction angle φ=35^o.

The low geotechnical parameters of the soil layers in accordance with the increased weight of the high-rise building determine the "boundaries" of the problem. In order to evaluate the feasibility of a tunnel construction, the proper location (in depth) of the METRO line has to be established and the adequate support pressure has to be calculated. Thus, through parametric analyses the distance of the tunnel from the building's foundation and the appropriate support pressure are calculated, in order to keep the shape of the plastic zone to minimum extension; thus both to reduce the settlement development at the building's foundation level and to ensure the stability of the underground excavation.

3.2. Physical & equivalent model for analytical calculations

For the present feasibility study certain assumptions were taken into consideration. The building is taken into consideration by assuming as an upper boundary of the semi-infinite space its foundation level and applying a uniform surface pressure, infinite in length, equal to building's foundation loading: thus the building's stiffness is neglected. Furthermore, the earth pressure (due to gravity) at the depth of the tunnel is taken into account as additional load, applied uniformly at the upper boundary of the half-space (see Fig. 4).

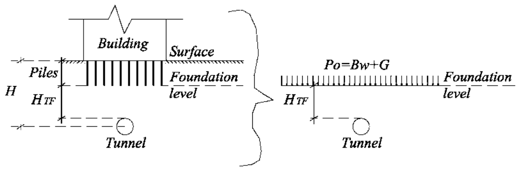

Figure 4. Physical and equivalent model for analytical calculations

Using the closed-form solution of the present study, a quick estimation of the plastic zone shape around the circular tunnel for different tunnel's depths and values of P_i gives a quick estimate of the required EPB-TBM support pressure.

3.3. Analytical calculation results

By using equation (11) different diagrams are constructed showing the plastic zone width at four certain points around the circular tunnel for different values of support pressure: at the crown, 45° from crown, at the sidewalls and below the invert.

For the lower value of the soil's cohesion (c=0 kPa) the plastic zone width is calculated and is presented in the diagram of figure 5, for different values of support pressure. The depth of the centre of the tunnel from the building's foundation level is taken 15 m. Furthermore, the depth of the tunnel's centre from the surface is 25 m: thus for γ=20 kN/m^3 a mean uniform pressure G of 500 kPa is added at the foundation level.

Therefore the total pressure that is uniformly applied at the upper boundary of the half-space (building's foundation level) is consisted of, the building's weight and the earth pressure due to gravity and is given below

$$P_o = B_w + G = 1050\text{ kPa} + 500\text{ kPa} = 1550\text{ kPa} \quad (12)$$

It is evident from the diagram of Fig. 5 that for the lower value of the soil's cohesion and for a support pressure equal to 1 bar, the plastic zone width at the crown is 10 m, thus it propagates up to the foundation level. At the 45° from the crown the plastic zone has a maximum width that exceeds 12 m. At the tunnel's sidewall and invert the plastic zone width is calculated 7 m and 4.5 m respectively.

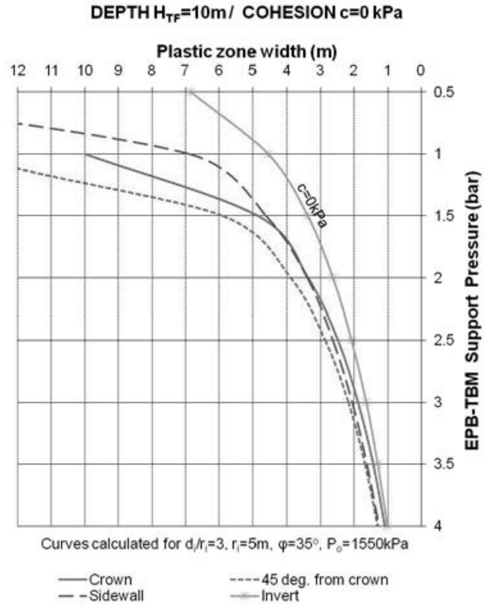

Figure 5. Plastic zone width for P_o=1550 kPa, c=0 kPa & H_{TF}=10 m

It is obvious from the above that in order to keep the shape of the plastic zone to minimum extension (<1 m) a support pressure with mean value greater than 4.5 bar is required from the EPB-TBM.

Moreover, by taking into account the maximum value of soil cohesion (c=100 kPa), the diagram of Fig. 6 is constructed.

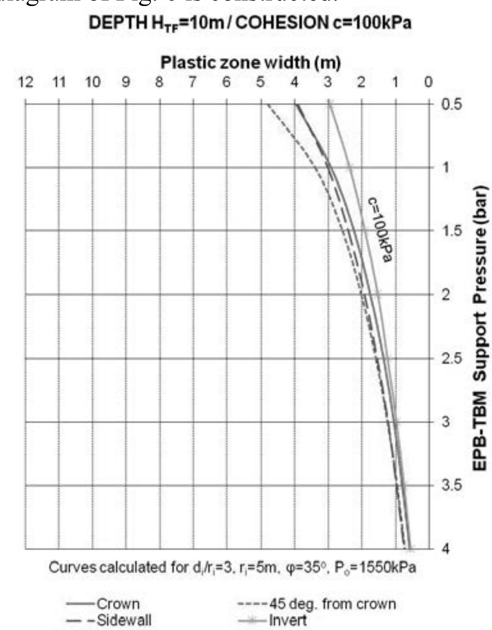

Figure 6. Plastic zone width for P_o=1550 kPa, c=100 kPa & H_{TF}=10 m

In this case for a support pressure of 3 bar the maximum width of the shaped plastic zone does not exceed 1.25 m whereas for support pressure of 3.5 bar the maximum plastic zone width is lower than 1 m. In the diagram of Fig. 7 the above cases (c=0 & 100 kPa) are presented together. Please note that for support pressure of 3 bar in the first case (c=0 kPa) the maximum plastic zone width exceed 2 m.

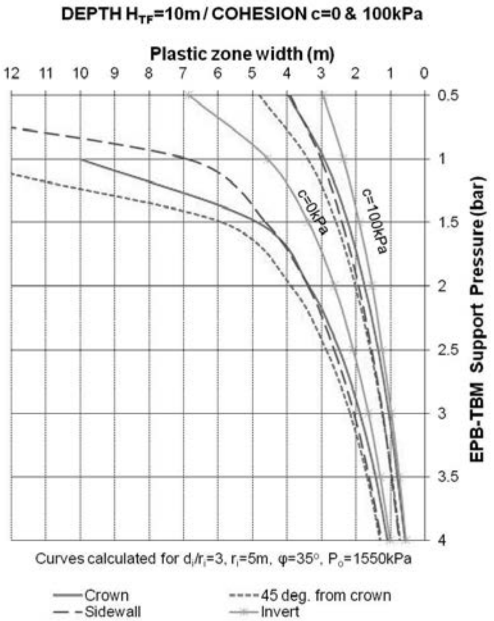

Figure 7. Plastic zone width for P_o=1550 kPa, c=0 & 100 kPa & H_{TF}=10 m

From the diagrams of Fig. 7 is obvious that for small values of support pressure (e.g. 1 bar) the plastic zone shape deviates from absolute circular geometry, whereas for higher values of support pressure (e.g. >3 bar) the plastic zone shape tends to be circular. For the case of c=0 kPa the plastic zone propagates up to the foundation level (for pressure 1 bar).

In order to conclude, for the proper depth of the tunnel and the necessary support pressure to be provided from EPB-TBM a new calculation for the plastic zone is realized by considering the depth of the centre of the tunnel from the building's foundation level at 25 m (35 m from the surface). Considering the new depth of the tunnel, equation (12) takes the following form

$$P_o = B_w + G = 1050 \text{ kPa} + 700 \text{ kPa} = 1750 \text{ kPa} \quad (13)$$

The calculation was made for soil's cohesion equal to 100 kPa (see Fig. 8).

Due to the deeper tunnel alignment the plastic zone shape has a circular geometry (Massinas et al, 2009). For a support pressure of 3 bar & 3.5 bar, provided by the EPB, the maximum width of the plastic zone is calculated 1.25 m and 1 m respectively.

In Table 2 the general results from the above presented calculations are presented.

Table 2. General results of plastic zone calculations

Parameters-Results					
Support pressure (bar)	Soil's cohesion c (kPa)	Tunnel's centre depth from foundation level (m)	Tunnel's centre depth from surface (m)	Plastic zone shape	Max. plastic zone width (m)
>4.5	0	15	25	almost circle	<1.0
3.0	100	15	25	almost circle	1.25
3.5	100	15	25	almost circle	1.0
3.0	100	25	35	circle	1.25
3.5	100	25	35	circle	1.0

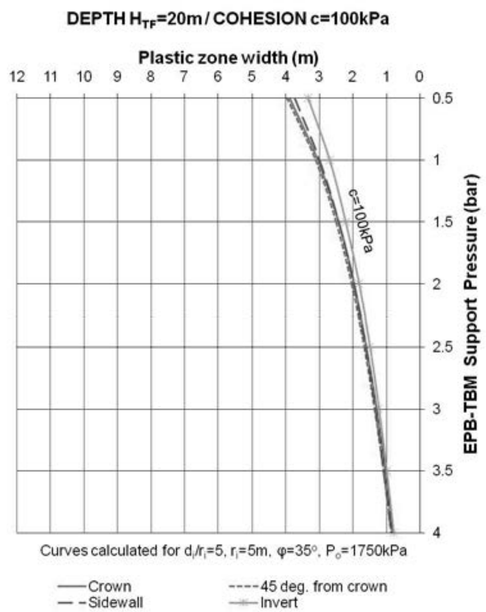

Figure 8. Plastic zone width for P_o=1750 kPa, c=100 kPa & H_{TF}=20 m

3.4. Conclusions

The excavation and temporary support of a circular tunnel under an existing high-rise building and inside a soil with low geotechnical parameters is a problem that is examined in the present paper.

According to the calculation results that are presented synoptically in Table 2 the main parameter that affects the construction of the tunnel are the cohesion of the soil and the depth of the tunnel alignment below the building's foundation level.

These two parameters determine the support pressure that has to be provided from the EPB boring machine in order to keep the shape of the plastic zone to minimum extension; thus both to reduce the settlement development at the building's foundation level and to ensure the stability of the underground excavation.

In the light of the above and taking into consideration that the soil's cohesion varies from 0 to 100 kPa we conclude to the fact that special ground improvement, such as jet grouting, must be provided in the area where the tunnel excavation will take place. With this improvement measure the cohesion of the soil has to be at least 100 kPa at the area of the tunnel excavation, in order for the EPB-TBM to operate with an efficient support pressure (~3.0 bar).

Concerning the longitudinal alignment, the crown of the tunnel is feasible to pass 10 m (H_{TF}) below the foundation level of the building. As it is evident from the calculation results there is no need for a deeper longitudinal alignment. On the contrary, a deeper alignment may cause difficulties in the ground improvement works.

Concluding, for an improved soil with cohesion greater than 100 kPa, only minimum plastic flow will occur around the circular tunnel for a support pressure of ~3.0 bar. Thus minimum settlements will occur at the building's foundation level.

4. REFERENCES

Bray, J. W. 1967a. A study of joined and fractured rock. Part I. Fracture patterns and their failure characteristics. *Rock. Mech. Engng Geol.* Vol. 5, No. 2-3, pp. 117-136.

Bray, J. W. 1967b. A study of joined and fractured rock. Part II. Theory of limiting equilibrium. *Rock. Mech. Engng Geol.* Vol. 5, No. 4, pp. 197-216.

Detournay, E. & John C. M. St 1988. Design charts for a deep circular tunnel under non-uniform loading. *Rock. Mech. Rock Engng,* Vol. 21, No. 2, pp. 119-137.

Grigoriev, O. D. 1968. On plastic equilibrium of an inhomogeneous half-plane when a smooth flat punch is pressed into it. *Prikladnaya Mekhanika,* Vol. 4, No 1, pp 126-128.

Jeffery, G. B. 1921. Plane stress and plane strain in bipolar coordinates. *Phil. Trans. R. Soc. London. Ser. A,* 221, pp. 265-293.

Kachanov, L. M. 1971. *Foundations of the theory of plasticity.* North-Holland Pub. Co.

Mangushev, R. A., Igoshin A. V., Oshurjov N. V. & Fadeev A. B. 2008. Slab-pile foundation for a high-rise building. *Soil Mech. & Found. Engng,* Vol. 45, No. 1, pp. 17-22.

Massinas, S. A. & Sakellariou, M. G. 2009. Closed-form solution for plastic zone formation around a circular tunnel in half-space obeying Mohr-Coulomb criterion. *Géotechnique,* Vol. 59, No. 8, pp. 691-701 (doi:10.1680/geot.8.069).

Mindlin, R. D. 1939. Stress distribution around a tunnel. *ASCE Trans.* 105, pp. 1117-1140.

Muir Wood, A. M. 1975. The circular tunnel in elastic ground. *Géotechnique,* Vol. 25, No. 1, pp. 115-127.

Pender, M. J. 1980. Elastic solutions for a deep circular tunnel. *Géotechnique,* Vol. 30, No. 2, pp. 216-222.

Sorochan, E. A. & Konyukhov D. S. 2005. Anchored-slab foundations for high-rise buildings. *Soil Mech. & Found. Engng,* Vol. 42, No. 4, pp. 127-131.

Strack, O. E. 2002. *Analytic solutions of elastic tunnelling problems.* PhD thesis, Department of Civil Engineering and Geosciences, Delft University.

Ter-Martirosyan, Z. G. 2003. Fundamentals of settlement analysis for high-rise buildings constructed in deep excavations. *Soil Mech. & Found. Engng,* Vol. 40, No. 5, pp. 190-194.

Verruijt, A. 1998. Deformations of an elastic half plane with a circular cavity. *Int. J. Solids Struct.* Vol. 35, No. 21, pp. 2795-2804.

Verruijt, A. & Booker, J. R. 1996. Surface settlements due to deformation of a tunnel in an elastic half plane. *Géotechnique,* Vol. 46, No. 4, pp. 753-756.

Analysis of sources of high sewage pipeline settlement in Vilnius

Zygmunt Meyer
Geotechnical Consulting Office Sp. zo.o., West Pomeranian University of Technology Szczecin, Poland

Mariusz Kowalow
Geotechnical Consulting Office Sp. zo.o, Szczecin, Poland

Niels Knandel
UAB ECE Projektmanagement Vilnius, Vilnius, Lithuania

ABSTRACT: In the town Vilnius a project of errecting a big shopping mall was undertaken. To provide a good communication from the town to the shopping mall a new highway was built up to enable heavy traffic of big trucks. During the errection time a problem occurred of a big settlement of the savage pipeline, placed on this terrain. It turn out, that the pipeline was finally placed along the highway close to the meridian, and at the depth ca. 6 m. In the paper the analysis of the big settlement is given.

1. INTRODUCTION

In the town Vilnius the project of erecting big shopping mall was undertaken. The shopping mall is located at the suburb.

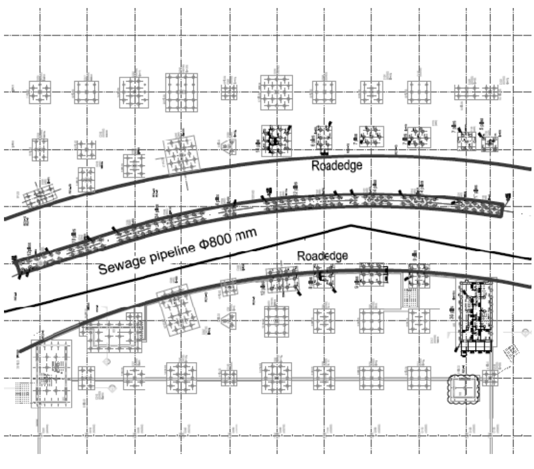

Figure 1. The location of the shopping mall and the pipeline

The Town authority has prepared the plan of urban development. And the location of the shopping centre comes from this plan. According to the urban development plan, the town authority has provided the area with infrastructure objects i.e.: water supply and sewage pipelines, electricity and roads.

A new highway was constructed to link the mall with the town. The highway enables heavy traffic of big trucks.
Earlier, before the shopping mall was erected and the new highway built up, there was placed new savage pipeline made of PCV pipes of a diameter ø 800 mm. The pipeline is located at the depth ca. 6 m under the surface.

The location of the road and the pipeline is given in Figure 1.

The cross – section with dimensions and soil properties is given in Figure 2.

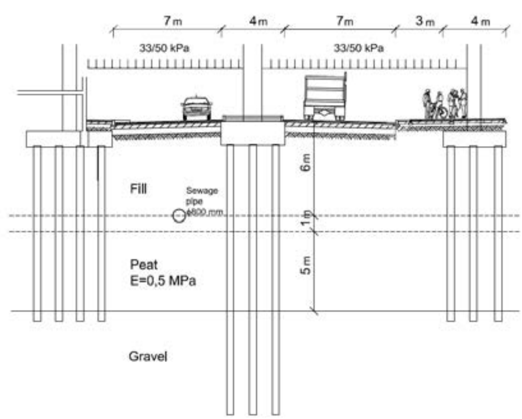

Figure 2. The cross-section of the analysed area

The infrastructure works, especially the sewage pipeline construction required geotechnical investigations. The geotechnical profiles were based upon drillings. The first relieved to the pipe line drillings reached level 6 m bellow terrain. Because of big settlement a new, deeper drillings were undertaken down to 18 m, bellow terrain. Those drillings enabled to conclude that down below the pipeline, there is a peat layer of about 5 m depth, with elasticity modulus M = 0,5 ÷ 0,75 MPa. The peat layer depth varies along the pipeline. Because of existence of the peat layer (organic soil), the first attempt was: to check if the presence of peat produces high pipeline settlement. All possible additional loads were taken into consideration i.e. road traffic and shopping mall foundations.

2. CALCULATIONS OF PEAT LAYER SETTLEMENT

2.1 Peat layer settlement due to road traffic.

The calculations of settlement should be based upon stress distribution within the soil body. As the first step to approximate the settlement stress the distribution according to Boussinesq was applied [1, 4]. Assuming linear elasticity theory we have:

$$\sigma_z(Z) = \frac{3}{2\pi} \cdot \frac{Q \cdot z^3}{(z^2 + y^2 + z^2)^{5/2}}, \tag{1}$$

where

Q	-	is the force [kN],
x, y, z	-	main system of coordinates.

The scheme of Boussinesq approach is given in Figure 3.

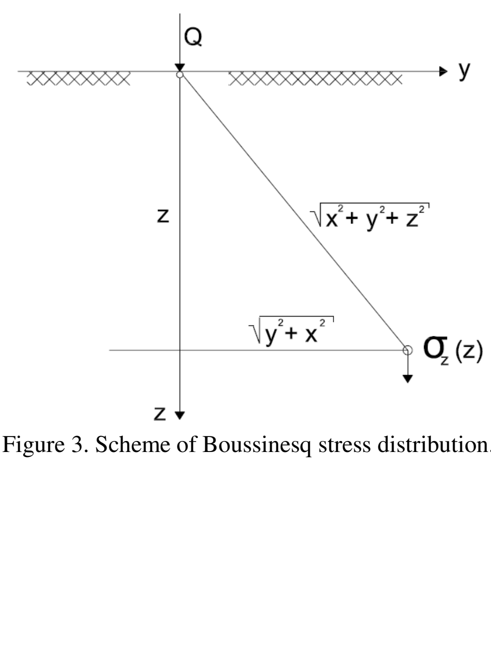

Figure 3. Scheme of Boussinesq stress distribution.

To apply the Boussinesq approach of the stress distribution in soil beneath the road it needs to introduce first the linearly spread load. We have:

$$q = \sigma_0 \cdot B, \tag{2}$$

where:

B	-	the width of the road [m],
σ_0	-	load on the road [kPa].

Including the above assumption we have:

$$\sigma_z(z) = \frac{2 \cdot 3}{2\pi} \cdot \sigma_0 \cdot B \cdot z^3 \int_0^\infty \frac{d\eta}{[z^2 + x^2 + (y-\eta)^2]^{5/2}}, \tag{3}$$

In the above equation the new variable η denotes the place where the load σ_0 is applied.

After calculations it gives:

$$\sigma_z(z) = \frac{2}{\pi} \cdot \frac{q \cdot z^3}{(z^2 + x^2)^2}, \tag{4}$$

Equation 4, allows to calculate the normal stress in the soil at the depth “z” and at a distance “x” from the road axe. This formula was applied for calculations of stress distribution in the peat layer.

The calculations of vertical distribution of stress in the soil were proceeded using dimensions shown in Figure 2 for the both strips of the road. It gives:

- at the upper boundary of peat:

$$\sigma_z^{(1)} = 0{,}65 \cdot \sigma_0 + 0{,}06\,\sigma_0 = 0{,}71\,\sigma_0$$

- at the lower boundary of peat:

$$\sigma_z^{(1)} = 0{,}38 \cdot \sigma_0 + 0{,}11\,\sigma_0 = 0{,}49\,\sigma_0$$

So now we can calculate the settlement of the peat layer under the load coming from the road traffic:

$$S = \frac{\sigma_z^{(1)} + \sigma_z^{(2)}}{2} \cdot \frac{H}{M}, \tag{5}$$

where:

H	-	the depth of the peat layer [m],
M	-	elasticity modulus of the peat.

Earlier raserach Meyer, Bednarek [2] and Meyer, Kowalow [3] suggest that in the case of very soft layer the vertical reduction of stress is very small. It was estimated by Föchlich using so called stress concentration coefficient. So for further calculations following formulae was used

$$S = \frac{\sigma_2^{(1)} \cdot H}{M}, \tag{6}$$

The load coming from the road due to the traffic was taken:

- Case 1: $\sigma_0 = 33$ kPa,
- Case 2: $\sigma_0 = 50$ kPa.

As the result of the calculations it comes
In case 1: s = 23 cm,
In case 2: s = 35 cm.

The resulting settlement is very close to the values coming from field measurements.

2.2 The influence of shopping mall foundations on the pipeline settlement

In the Figure 2 there is also show the location of the foundations of the shopping mall construction.

The foundations are based on piles, coming down to the bearing layer which is the gravel. The dimensions of the foots was calculated in such a way that the maximum settlement does not exceed 3 cm. The calculations of the peat layer settlement, caused by the piles can be adopted using formulae of Baussinesq [1, 4]. This formulae shows also settlement outside the axe of the acting force. We have:

$$S(x) = S(L) \cdot \frac{L}{x}, \tag{7}$$

Where:
L - is the distance from the foot to the pipeline [m],
x - is horizontal coordinate perpendicular to the road axe [m],
S(L) was chosen 3 cm as the maximum allowable foot settlement.

So it gives:

$$S(x) = 3{,}0 \cdot \frac{2\,m}{8{,}5\,m} = 0{,}7\,cm$$

This value is tolerable and can be neglecting while calculating pipeline settlement.

The peat layer settlement caused by piles depends on the skin shear stress at the pile surface. They should not exceed certain values.

Assuming the Baussinesq linear theory of settlement [2] we have the approximate value of the lateral shear of the pile:

$$\tau = \frac{1}{15} \cdot \frac{M}{D} \cdot s \tag{8}$$

Where:
D - is the pile diameter [cm].

Assuming D = 40 cm it gives $\tau = 3{,}0$ kPa. That value can be accepted for the old peats and can produce the aforementioned additional settlement of the peat layer.

2.3 Calculations done using 3 D model.

To confirm the fact that the high settlement of the pipeline is caused by the road traffic the verifying calculations using 3D model were proceeded [4]. The geometry of the model is shown in Figure 1 and 2 and the geological conditions were used the same as in chapter 2.2.

The results of the calculations is shown in Figure 4.

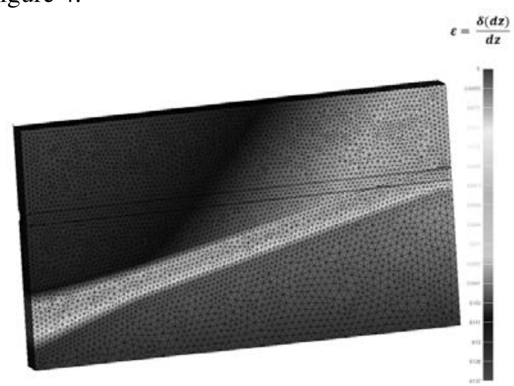

Figure 4. Settlement distribution referred to unit depth of the layer.

The 3D model solution is expressed in term of unit settlement δ(dz) for elementary layer of thickness dz, so it presents value:

$$\varepsilon = \frac{\delta(dz)}{dz}, \tag{9}$$

To calculate the settlement of certain layer it needs to integrate:

$$s = \int_{z_1}^{z_2} \varepsilon(z)dz, \tag{10}$$

In practical cases integration can be replaced by summation of settlement layer by layer. If the thickness of each of them is small, we can obtain result which has accuracy sufficient for practical calculations.

From figure 4 it comes that the high settlement of the pipeline is produced by the load coming from the road traffic and it reached the value obtained earlier in the chapter 2.1.

3. CONCLUSIONS

1. It comes from the experience of the presented paper that the geotechnical investigations they should be referred not only to the current demands but they should cover future investments coming from the urban development plan.
2. More and more often, that new constructions are planned within the existing town infrastructure, so they interfere with the existing buildings.
3. The erected new constructions, in the considered case the new road, they produced additional stresses within the soil body. These stresses create additional settlement, which can be considerably big.
4. In the analysed case of the high settlement of the pipeline the reason was the existence in ground profile, the soft organic peat layer. The additional settlement reached up to 30 cm.
5. The analysis of the high settlement was done using Baussinesq approch. The calculations confirm existence of high settlement. Verifying calculations using 3D model proved that reason of the big settlement is the existence of the soft peat layer.

4. REFERENCES

[1] Bowles J., E., 1996, *Foundation analysis and design*, The McGraw – Hill Co., Inc.,

[2] Meyer Z., Bednarek R., 7-10 June 1999, *Influence of coefficient of stress concentration in Froehlich's Formula upon calculating the settlement of weak layer in stratified soil*, XII Th European Conference On Soil Mechanics And Foundation Engineering, Amsterdam,

[3] Meyer Z., Kowalów M., 23-26 May 2007, *Zmina sposobu wzmacniania gruntów słabych na Ostrowie Grabowskim w oparciu o badania konsolidacji torfów, (In English: "Weak soils reinforcement based upon consolidation analysis"), XXIIIrd* International Conference "Awarie Budowlane" (Structures Failure); Szczecin-Międzyzdroje, Wiłun Z., Zarys Geotechniki, (In Polish: "Introduktion To Geotechnics"), Wkl, Warsaw 1987,

[4] GCO Report - 03.02. 2009, *Final Report - Settlements situation and approximate road and pipe settlement calculation in the road area after executing of bypass works, Building III,* Szczecin.

Effect of new underground structures on existing buildings and networks

Application of Earth Retaining Structure with Soil-cement Mixing Technique for Urban Excavation Project

Y.S.Kim
Korea Institute of Construction Technology, Gyonggi-Do, South Korea

Y.S.Cho
Samsung Construction & Technology, Seoul, South Korea

J.Choo
Korea Institute of Construction Technology, Gyonggi-Do, South Korea

ABSTRACT: In megacities, it is often necessary to perform excavations within narrow spaces in highly congested areas. For an excavation site where the earth retaining structure is extremely close to existing structures, a new earth retaining structure system is proposed which utilizes soil-cement mixture blocks that are comparatively short and large to reinforce the retaining wall.. In order to verify the applicability of earth retaining structures reinforced by soil-cement blocks, the proposed system was applied to an urban excavation project in Seoul and the behavior of the earth retaining structure was analyzed. The result showed that the earth retaining structure with soil-cement mixing technique is applicable for urban excavation sites.

1. INTRODUCTION

Recently, in order to efficiently utilize the limited city areas in megacities, there has been a continuous increase in the need for excavations close to existing structures such as the remodeling of aged infrastructures that encompass huge underground spaces. As a consequence, excavation within exceptionally narrow spaces in highly congested areas is one of the crucial challenges for constructions in megacities.

Conventional earth retaining structures for excavations, however, are not applicable in some cases. For example, if the distance from the retaining wall to the existing structures is less than 5-6m, earth anchors cannot be installed since their minimum required lengths are usually more than the distance to the existing structures. Meanwhile, when the width of the excavation site is more than 30m, it is difficult to construct struts with accurate straightness. Therefore, in cases where structures with a wide underground space need to be constructed in narrow areas, conventional earth retaining systems might not be applicable.

This paper introduces a new earth retaining structure system proposed for sites where the earth retaining wall is exceptionally close to existing structures. In the proposed system, soil-cement reinforcing blocks that are comparatively short and have a large diameter using a soil-cement mixing technique are installed behind the retaining wall to reinforce the wall. The installation of the large diameter soil-cement blocks behind the retaining wall (usually φ = 300-500 mm) enables the reduction of the reinforcing length from that of earth anchors with equal reinforcements

In order to verify the applicability of the earth retaining structure reinforced by soil-cement blocks, the proposed system was applied to an urban excavation project in Seoul. From field measurements and numerical analysis, the behavior of an earth retaining structure with soil-cement reinforcing blocks was analyzed during the excavation procedure up to 10 m. The result showed that the proposed earth retaining structure using the soil-cement mixing technique is applicable at urban excavation sites.

2. DESCRIPTION OF THE PROPOSED EARTH RETAINING STRUCTURE

2.1. General Characteristics

For the reinforcement of an earth retaining structure, the proposed system applies the soil-cement mixing technique of the deep-mixing method for the installation of soil-cement reinforcing blocks similar to the bracing of soil nailing. In the center of the soil-cement reinforcing block, rebar or an anticorrosive FRP rod plays the role of a tensioning material. Cement milk of high compressive strength is simultaneously injected around a 3-layer structure that consists of the rod, cement milk and soil-cement, to ensure the sufficient adhesive strength of the rod (Tateyama and Taniguchi 1993; Mimura et al. 1998).

The soil-cement reinforcing blocks are installed at 300-500 mm diameter centers in the ground at a certain angle. Compared to conventional soil nailing of which the drilling diameter is as small as 100 mm, the soil-cement reinforcing block mobilizes more friction in the ground due to the larger perimeter as illustrated in Fig. 1. Therefore, the proposed earth retaining structure system efficiently constrains the strains caused by the excavation on the wall since there is an enhanced friction resistance between the soil and the reinforcements. Moreover, the large soil-cement reinforcing blocks can significantly reduce the required lengths and the number of reinforcements from those of conventional methods such as earth anchor and soil nailing.

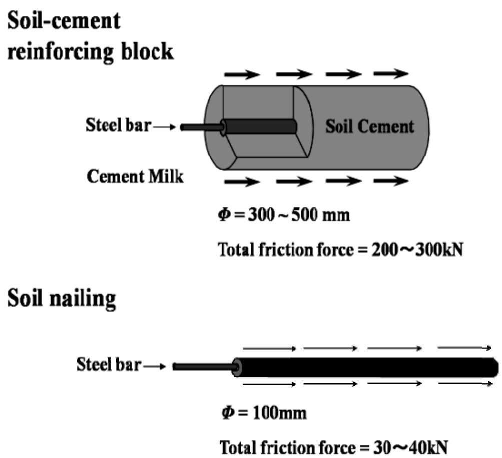

Figure 1. Comparative illustration of the soil-cement mixture reinforcement block and soil nailing

2.2. Construction Procedure

An earth retaining structure reinforced by soil-cement blocks is designed to drive reinforcement at a certain angle upon excavation (Japan Advanced Construction Technology Center, 1997). The application method of the soil-cement mixing retaining system is given as follows. The construction procedure of soil-cement reinforcing block is illustrated in Fig. 2.

① H-pile, S.C.W or steel pile shall be driven in front of the excavation site (this may not be necessary depending on the excavation depth or ground condition).

② Tensioning material (rebar) shall be injected at the center of the mixer.

③ Cement shall be injected by a mixer while boring to form a 300-500 mm large diameter soil-cement block.

④ When the large soil-cement block reaches the target depth, the mixer shall be pulled out by reverse rotating while the mixing speed and cement injection are controlled so as to form cement milk.

⑤ The toe (tensioning material) of the soil-cement block shall be fixed with a bolt and nut using a wale or plate.

⑥ The work sequence of ② – ⑤ shall be repeated while the excavation for the next stage continues.

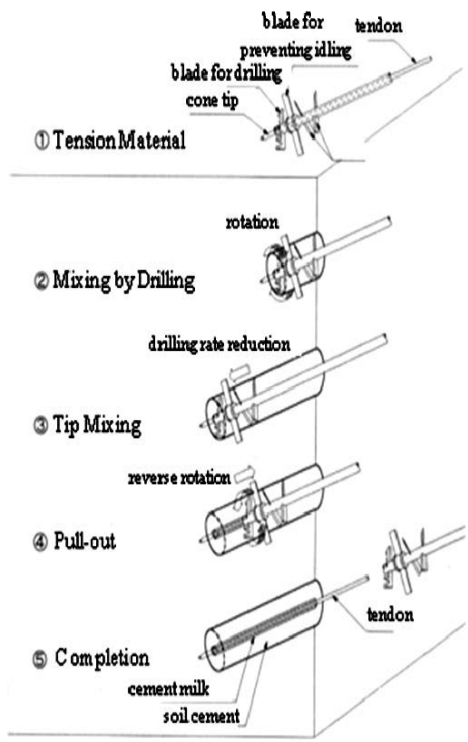

Figure 2. Construction procedure of soil-cement reinforcing block to earth retaining structure

3. FIELD APPLICATION TO AN URBAN EXCAVATION PROJECT IN SEOUL

3.1. Site Description

The proposed earth retaining structure system was applied to an apartment redevelopment project in Seoul. The site was located in a highly congested urban area of northern Seoul. The final excavation depth was 9.8 m, and the groundwater level was about 6 m. The soil layer consisted of fill (0 - 3 m), deposited silty sand (3 - 6.5 m), weathered sand (6.5 - 10.5 m) and weathered rock (10.5 m - bottom). According to a site investigation, the N values of the Standard Penetration Test ranged from 4 to 10 within the deposited silty sand and from 20 to 50 within the weathered sand.

3.2. Strength of soil-cement blocks

Prior to the construction, in order to select an appropriate soil-cement mixing ratio and to confirm the strength of the soil-cement block, a series of unconfined strength tests were performed on soil-cement mixtures with various soil-cement ratios. For each soil-cement ratio, six specimens were tested after curing for 7 and 28 days. Table 1 shows the results of unconfined tests with the average unconfined strengths.

Table 1. Results of unconfined strength tests

Amount of Cement, kg/m^3	Water/cement ratio, %	7-day strength, kPa	28-day strength, kPa
350	60	9,400	12,510
400	60	10,750	12,220
450	60	5,120	9,390

Test results indicated that all the soil-cement mixtures had sufficient strength to be used as reinforcing blocks on this site. Therefore, 350 kg/m^3 was selected as the appropriate amount of cement for soil-cement mixing.

3.3. Application of the soil-cement reinforcing blocks to earth retaining walls

The earth retaining wall of this site was originally designed with earth anchors by Soil-Cement Walls (S.C.W). However, in order to evaluate the behavior of an earth retaining structure with soil-cement reinforcing blocks, the earth anchors in some parts of the walls were changed to soil-cement reinforcing blocks of 400 mm diameter.

The excavation work was carried out through five stages. During each stage, soil-cement reinforcing blocks were installed behind the retaining wall with 20° inclination and 1.35 m spacing, as shown in Fig. 3. Since the short reinforcement length is the major advantage of the proposed earth retaining system, Fig. 4 shows a comparison of the designs between a wall with earth anchors and a wall with soil-cement reinforcing blocks. As indicated in Fig. 4, the application of soil-cement reinforcing blocks shortened the required reinforcing length from 9.62 m to 3.76 m with equal reinforcements. Therefore, it is possible for the proposed earth retaining system to be effectively utilized for urban sites where the construction sites are exceptionally close (e.g. less than 5 m) to existing structures.

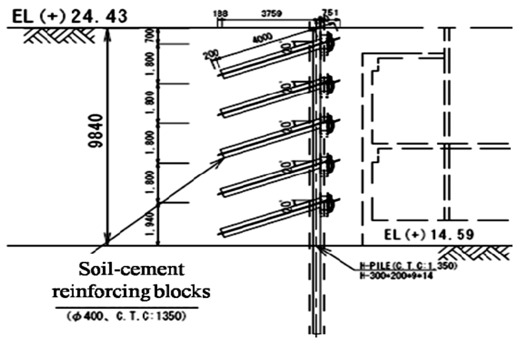

Figure 3. Modified section plan of the excavation after applying soil-cement reinforcing blocks

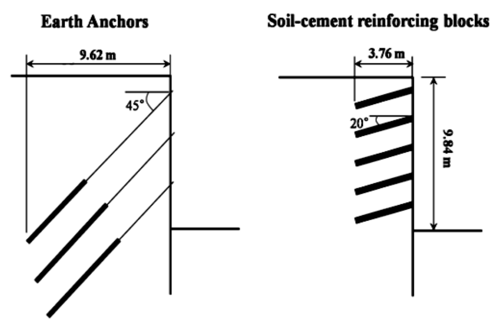

Figure 4. Comparison of the designs between a wall with earth anchors (left) and a wall with soil-cement reinforcing blocks (right) in this site.

4. EVALUATION OF BEHAVIOR OF THE EARTH RETAINING STRUCTURE WITH SOIL-CEMENT REINFORCING BLOCKS

4.1. Field Measurements

Throughout the excavation works, field measurements were carried out in order to evaluate the stability and behavior of the earth retaining structure. Fig. 5 shows the measured lateral displacements of the earth retaining structure during the excavation procedure.

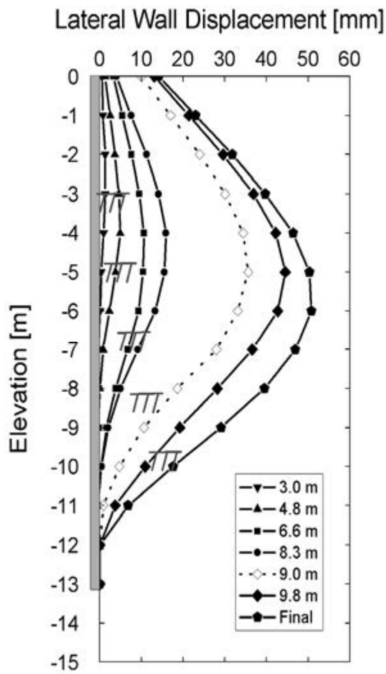

Figure 5. Measured lateral wall displacements for each excavation stage

Up to 8.3 m of excavation (1st to 4th stage), the maximum lateral wall displacement was 15 mm, which is about H/550 (H: excavation depth). Considering that the general requirement for lateral displacement of a retaining wall ranges from H/500 to H/300, the measured lateral displacements are reasonably acceptable. Therefore, it can be concluded that the proposed retaining structure supports lateral earth pressure adequately under a general condition.

After the excavation up to 9.8 m (5th stage), however, the lateral wall displacements suddenly increased up to 45 mm. Considering the previous trend of horizontal displacements, the sudden increase of displacement might be attributed to other factors rather than the stability problem of the retaining structure. In fact, after the dewatering process was carried out at 9.0 m of excavation, it was observed that some soils were washed out with water through the weep holes and that approximately 15 mm of movement had occurred, as shown in Fig. 5. The excessive movements might have occurred after the groundwater flow had loosened the soils at the 3rd and 4th bench and reduced the frictions between the soil and the soil-cement blocks. Therefore, it was concluded that the sudden increase of lateral wall displacement mainly resulted from the dewatering procedure rather than the ground excavation itself. An additional displacement of 5 mm occurred after the final excavation stage due to the grouting that was performed to isolate the water from the wall.

4.2. Numerical Analysis

In parallel with field measurements, numerical analysis was performed to evaluate the behaviour of the retaining structure. A commercial finite element program PLAXIS 8.2 was used for the numerical analysis. Soil layers were modelled by the Mohr-Coulomb model, and the retaining wall and the soil-cement reinforcing blocks were modelled by linear elastic materials. The input parameters of finite element analysis are summarized in Tables 2 and 3.

The construction procedure including ground excavation and installation of the soil-cement blocks was simulated separately in five stages. In the analysis, the length of the soil-cement reinforcing blocks was 4 m and the final depth of excavation was 9.8 m.

Table 2. Input parameter for Mohr-Coulomb models

Soil Type	γ_t, kN/m^3	c' kPa	φ, deg	E, MPa	υ
Fill	17.0	10	35	18	0.30
Deposited Silty Sand	17.0	0	20	10	0.30
Weathered Sand	19.0	15	33	100	0.30
Weathered Rock	20.0	50	37	3000	0.37

Table 3. Input parameter for linear elastic models

Material Type	EA kN/m	EI kNm^2/m	γ_t, kN/m/m	υ
Soil-Cement Wall (S.C.W)	1.23E6	1.97E4	0.48	0.30
Soil-cement block	8.67E5	7.24E3	2.64	0.30

In order to verify the numerical analysis, the lateral wall displacements from field measurements and numerical analysis were compared as shown in Fig. 6. To compare the lateral displacements particularly induced by the excavation process itself, the excessive movement of 15 mm, measured during the dewatering process, was subtracted from the field measurements of the 5th stage (excavation up to 9.8 m).

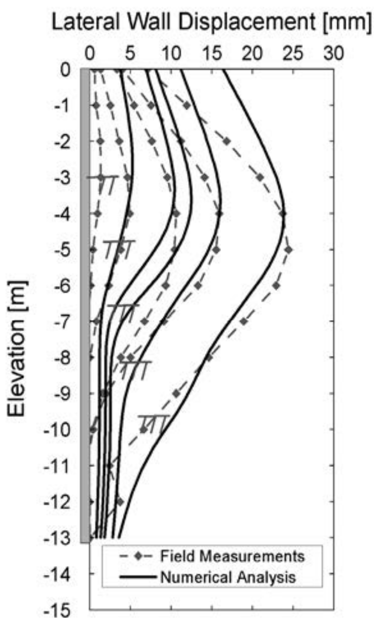

Figure 6. Comparison of lateral wall displacements from field measurements (dashed lines with symbols) and numerical analysis (solid lines)

Up to the 2nd stage (4.8 m) of excavation, the lateral displacements from numerical analysis were slightly larger than the field measurements. This disparity might be ascribed to the simplified soil models in the numerical analysis (i.e. simplification of non-linear soil stiffness at small-strains). However, as the excavation stage progressed and the strain of the ground increased, the results of numerical analysis and field measurements became similar. Therefore, it can be considered that the final results of numerical analysis appropriately simulate the field condition.

Fig. 7 shows the estimated surface settlement of the ground behind the retaining wall as obtained from numerical analysis. The maximum settlement behind the wall was estimated to be 20 mm, which was 0.2%H_c (H_c: final excavation depth), satisfying the general requirement for excavation works in Korea (Ministry of Land, Transport and Maritime Affairs of Korea, 2008). In addition, in terms of differential settlement, the maximum angular distortion was slightly less than 1/500 so it also satisfies the requirement for ordinary structures (Bjerrum, 1963). Based on the criterion suggested for evaluating potential damages to adjacent structures, the angular distortion and horizontal strain induced by this excavation ranges from slight to moderate damages, which is a typical range for shallow foundations, braced cuts and tunnels (Boscardin and Cording, 1989).

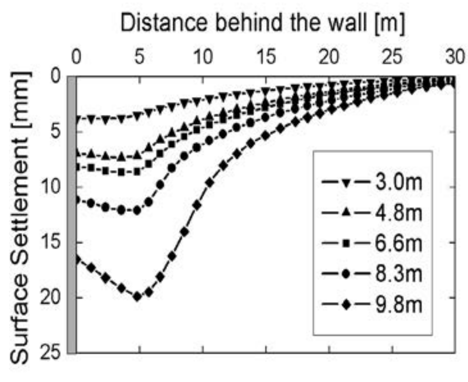

Figure 7. Estimated surface settlement of ground behind the retaining wall from the numerical analysis

Finally, the stability of soil-cement reinforcing blocks was verified by the numerical analysis. Fig. 8 shows the axial force diagrams of the five soil-cement reinforcing blocks after final excavation. From the numerical analysis, the maximum axial force was estimated to be 142.5 kN. Since the tensile yield strength of the steel bar (*φ* 35mm SD300) in the center of the soil-cement reinforcing block is 281.2 kN, the strength of the steel bar is not critical to the stability of the soil-cement reinforcing block.

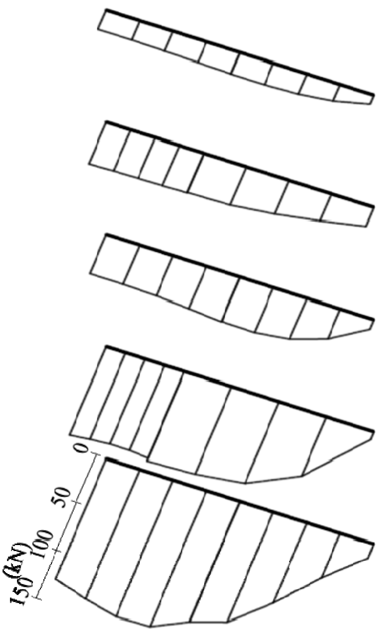

Figure 8. Estimated axial forces of soil-cement reinforcing blocks as obtained from the numerical analysis

5. CONCLUSIONS

This paper has introduced a new earth retaining structure using the soil-cement mixing technique for urban project sites where the retaining wall is exceptionally close to existing structures. The proposed earth retaining structure was applied to an urban excavation project in Seoul and the behavior and the applicability of using an earth retaining wall with soil-cement reinforcing blocks were verified by field measurements and numerical analysis.

Field measurement results indicated that the earth retaining wall with soil-cement reinforcing blocks resisted earth pressure with acceptable horizontal displacements of H/550 (H: excavation depth). However, when the dewatering process was carried out, unexpected ground subsidence subsequently occurred, indicating that the construction process of this system should be improved to consider groundwater conditions.

The behavior of the ground during excavation was investigated by numerical analysis. Behind the retaining wall, the maximum settlement was estimated to be 0.2%H_c (H_c: final excavation depth) and the maximum angular distortion was slightly less than 1/500. These results satisfied the general requirements for urban excavation works.

The stability of soil-cement reinforcing blocks was verified from the numerical analysis results. The yield strength of the tensioning material was considerably larger than the estimated axial force on soil-cement reinforcing blocks. Therefore, the stability of reinforcements was not an important consideration in the proposed earth retaining structure.

In conclusion, the earth retaining structure with a soil-cement mixing technique proposed in this study has the potential to be usefully applied to extremely narrow urban excavation sites, with a similar performance to that of conventional earth retaining systems.

6. ACKNOWLEDGEMENTS

This research was supported by Samsung Corporation and a grant (Grant No. 07-UR-B04) from the High-tech Urban Development Program funded by the Ministry of Land, Transport and Maritime Affairs of Korea.

7. REFERENCES

Bjerrum, L. 1963. Allowable settlement of structures. *Proceding of 3rd European Conference on Soil Mechanics and Foundation Engineering*, Wiesbaden, Vol. 2, pp. 135-137.

Boscardin, M.D. and Cording, E.J. 1989. Building response to excavation-induced settlement. *ASCE Journal of Geotechnical Engineering,* Vol. 115, No. 1, pp. 1-21.

Japan Advanced Construction Technology Center 1997. *Development of a Radish Anchor Method.* Report of ACTC.

Ministry of Land, Transport and Maritime Affairs of Korea. 2008. *Korean Standard Code of practice for Foundations.*

Miura, N., Shen, S.L., Koga, K., and Nakamura, R. 1998. Strength change of the clay in the vicinity of soil cement column. *Journal of Geotechnical Engineering*, JSCE, Vol. 596 (43), pp.209-221.

Tateyama, M. and Taniguchi, Y. 1993. Development of a large diameter reinforced anchor by cement-mixing method. *Report of Japan Railway Technical Research Institute.* Vol.7 pp. 1-8.

Skin resistance factors calibrated from O-cell tested drilled shafts of FHWA database

Jiliang Li and Robert Liang
The University of Akron, Akron, OH USA

ABSTRACT: Skin resistance factors in the current AASHTO specifications for drilled shaft foundation design are not all calibrated using field data. This paper presents a calibration of resistance factors for skin resistance of drilled shafts based on the statistical data of seven O-Cell tested drilled shafts in sands underlain by weak rock layers. Field test data were used to determine the actual measured resistance while the in-situ soil and rock properties and dimensions of drilled shafts were used to calculate the predicted resistance using the SHAFT program consistent with FHWA method. The *Monte Carlo* simulation method was selected to perform the calibration. The skin resistance factors for Strength I limit state were calibrated at a target reliability index of 3.0 and compared with those in literature.

1. HEADING: GENERAL REQUIREMENTS

Load and resistance factor design (LRFD) has been increasingly used for foundation design of bridges in the United States and this design method has become mandatory for all FHWA funded bridge projects. Additionally, LRFD design, considering both uncertainties of load and resistance of a geotechnical system, is recognized as a more rational design approach than allowable stress design (ASD) approach. The main idea of LRFD is to multiply each load component by a larger than unity load factor γ and each nominal resistance component by a smaller than unity resistance factor ϕ to account for the uncertainties in the estimation of the real load and resistance. The implementation of proper load and resistance factors can maintain a compatible reliability index β in each component of a substructure, foundation or superstructure. To achieve this goal, resistance factors need to be updated and calibrated with an adequate number of good quality test data for each design method (Allen et al., (2005); Yang and Liang (2007); Yang et al. (2008); and Liang and Li (2009)). The idea may seem straightforward, but the transition from the traditional ASD to the LRFD in geotechnical engineering has faced great difficulty. One outstanding problem with the resistance factor calibration is that high quality test data is not often available in geotechnical engineering, thus many researchers chose to calibrate resistance factors by fitting LRFD to ASD to maintain a consistent level of reliability with the past practice. The early work by Barker et al. (1991) is one of the good examples. AASHTO LRFD bridge design specifications (AASHTO, 2004) provided resistance factors for design of drilled shafts under axial loads. Even in the latest edition of the AASHTO LRFD Bridge Design Specifications (AASHTO, 2007), a significant number of resistance factors in the foundation design section were still selected based on the calibration with ASD. To improve the implementation of LRFD and achieve compatible reliability with the superstructure design, efforts to calibrate resistance factors from field test data are in great need.

The objective of this study was to develop the skin resistance factor for axially loaded drilled shafts in sand and weak rock collected in the NCHRP Project 24-17 and NCHRP 20-07/Task 183 by Paikowsky et al. (2004). There have been different terminologies used to describe weak rock, such as soft rock and intermediate geomaterials (IGM) or weak rock as used in SHAFT program (Reese et al., 2001). However, there is no unified definition on weak rock. O'Neill and Reese (1999) defined cohesive intermediate geomaterials as rock having unconfined compressive strength from 0.5 to 5MPa (72.5 to 725 psi). However, O'Neill et al. (1996) indicated that the upper limit of 5MPa was selected arbitrarily. Kulhawy and Phoon (1993) provided classifications of rock material strength from different reference sources. From that list, it appears that the rock with unconfined compressive strength from 0.5 to 20MPa (72.5 psi to 2901 psi) can be considered as weak rock. This definition is adopted in the current study.

The total resistance of an axially loaded drilled shaft consists of skin resistance and tip resistance. The recommended design methods for these two components by AASHTO and FHWA are based on O'Neill and Reese's study (1999). Paikowsky et al. (2004) collected 11 drilled shaft load test data in sands.

On the other hand, they calibrated the resistance factor for the total resistance from those tests in which the total load capacity was a combination of skin and tip resistance. From traditional top-down load tests, it is difficult to separate tip and skin resistance from the total measured resistance. In the 2007 AASHTO LRFD Bridge Design Specifications, the recommended skin resistance factor at a reliability index of 3.0 for drilled shafts in IGMs is 0.6, which is based on Paikowsky's study (2004). Liang and Li (2009) further calibrated and updated the total resistance factors for top-down loaded drilled shafts based on FHWA (1999) method.

In this study, the FHWA method based on O'Neill and Reese's work (1999) and Osterberg cell (O-cell) test data were used for the calibration of the skin resistance of drilled shafts in sand and weak rock. As pointed out by Roberts (2006) and illustrated by Yang et al. (2008), the O-cell load tests can measure the skin and tip resistance separately, they can be used to calibrate the resistance factors for skin and tip resistance more rigorously. In this study, the skin resistance factor was further calibrated for drilled shafts in sand and weak rock based on seven NCHRP datasets.

2. OSTERBERG CELL TESTS

The O-Cell test was invented by Dr. Jorj O. Osterberg (1984) and first used in the 1980s. Unlike the conventional top-down load test, the load in this test is applied by a cell, which is pre-installed in the shaft somewhere near the tip. This cell will simultaneously produce an upward force to the upper portion of the shaft and a downward force to the lower portion of the shaft at an equal magnitude, which can be used to estimate the skin resistance and the tip resistance of the shaft separately. Fig. 1 shows the difference between the conventional top down load test and the O-cell load test.

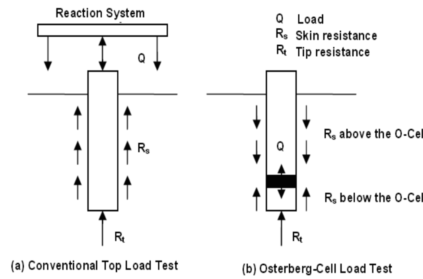

Fig.1. Comparison of conventional top load test and O-cell load test.

In this study, data from seven O-cell tests on drilled shafts in sandy soils and weak rock were collected from NCHRP drilled shaft database. In the database, there are 14 cases of O-Cell tested drilled shaft where 3 drilled shafts in sand-clay-sand layers and 4 cases involving strong rocks with one case without any actual measurement recorded. Therefore the 7 cases (50% of O-Cell tests in the database) of drilled shafts in sand-weak rocks were judged to be useful for the skin resistance factor calibration purpose. The information of these tests was summarized in Table 1.

The load corresponding to a settlement at 5% of the shaft diameter ("0.05D") or plunging load was defined as the nominal capacity, which is recommended by O'Neill and Reese (1999). The selection of this criterion was based on the previous study done by Paikowsky (2004) for calibration consistency, in which seven criteria ("Davisson's, Chin's, Butler and Hoy's, FHWA's "0.05D", Fuller and Hoy's, Brinch-Hansen's 80%, and creep limit method by LOADTEST Inc. were used to estimate the nominal capacity of a drilled shaft based on the O-cell test data(Yang et al., 2008). The statistical analysis showed that the FHWA's "0.05D" method produced the closest and most consistent capacities with the mean value of the capacities determined by seven methods, which has been further confirmed and used by Zhang et al. (2005). However, the skin and tip resistance failure load mobilization originally come from conventional static top-down loading test methods used for LRFD resistance factors calibration (Paikowsky, 2004). In an O-cell test, typically either skin or tip resistance may not reach failure. Sometimes the capacity of the O-Cell itself was small that both skin and tip resistance can not be fully mobilized. Fellenius (2001b) stressed that "it is a sound engineering rule never to interpret the results from a static loading test to obtain an ultimate load larger than the maximum load applied to the pile in the test". In this case, according to Fellenius (2001a), the maximum test load is also the maximum capacity value to use as the "failure load". Further, Gunnink and Kiehne (2002) applied the same technique recommended by Fellenius (2001a and 2001b) in their interpretation of O-Cell tested drilled shaft ultimate failure load capacity. In this paper, the FHWA (1999) and Fellinius (2001a,b) failure load criteria will be applied to load test results for resistance factors calibration.

3. FHWA DESIGN METHOD

The FHWA design method for granular soil and weak rock geomaterials adopted in this study was based on O'Neill and Reese's (1999) report assuming smooth rock sockets surface with closed joints (Reese et al., 2001). Details of this method can be found in the literature, such as O'Neill and Reese's (1999) and Reese et al. (2001). In the Paikowsky (2004) study, however, rough sockets were assumed. The assumption of smooth surface is more commonly used in practice and expected to yield a lower predicted load capacity of drilled shafts. The O-cell data collected in this study were for sandy granular soil with less than 50B/foot and weak rock having a wider range of unconfined compressive strengths than those for IGMs (0.5MPa to 5MPa) defined by O'Neill and Reese (1999). This situation was resulted from limited available data for IGMs, which were not sufficient to conduct a reliability analysis. By expanding the range of weak rock included in the analysis, a reliability analysis became possible. Since O'Neill and Reese's method is limited to the IGMs with an unconfined compressive strength of 0.5 to 5MPa (somewhat arbitrary upper limit as indicated by O'Neill et al. (1996), extrapolations are necessary for estimation of skin resistance of drilled shafts in the rock beyond this range. The extension of this range may increase the variability of the calculated results. However, it also increases the number of datasets, which in turn increase the reliability of the calibrated resistance factors. Since the variability of the calculated results from the wider range is included in the calibrated resistance factors, they are still valid. The extrapolations involve one main parameter in O'Neill and Reese's design method: the β coefficient for calculating skin resistance. The β coefficient for skin resistance in sandy granular soil was used in the following equation:

$$f_{SZ} = K\sigma_z^{'} \tan\phi_c \qquad (1)$$

$$f_{SZ} = \beta\sigma_z^{'} \leq 2.0\text{tsf}(190\text{KPa}) \qquad (2)$$

where f_{sz} is the ultimate load transfer in skin resistance at depth z, and $\sigma^{'}_z$ is the vertical effective stress in soil at depth z, and β_z is the empirical factor that can vary with the depth z.

The β_z coefficient was determined using the following equation (Reese et al., 2001):

$$\beta = 1.5 - 0.135\sqrt{z},\quad 0.25 \leq \beta \leq 1.2 \qquad (3a)$$

$$\beta = N_{60}\left(1.5 - 0.135\sqrt{z}\right)/15,\ \text{for } N_{60} \leq 15 \qquad (3b)$$

where z is depth below ground surface, ft, Equation (3) is non-homogeneous and the value of z must be an appropriate value in English units.

In this study, the following assumptions were also made: (a) the geomaterials are sand and cohesive weak rock, (b) smooth rock sockets, (c) closed joints, (d) if the elastic modulus of the core sample was not available, the suggested relationships by O'Neill et al. (1996), $E_i = 250q_u$, for Argrillaceous geomaterial and Ei =115qu for Calcareous weak rock were adopted, and (e) concrete had slump of 152.4 mm (6 inch minimum recommended from SHAFT) and sand unit weight of 18.86 kN/m^3 (120 lb/ft^3**)** if no information was available.

4. EXAMPLE OF PREDICTED AND MEASURED SKIN RESISTANCE

The drilled shaft database shows the drilled shaft constructions methods and dimensions together with the in-situ soil profiles, elevation, soil descriptions and available parameters that may be used for calculating the nominal predicted skin and tip resistance.

The shaft-soil profiles and parameters used for obtaining the predicted capacity using FHWA (1999) method via SHAFT program (Reese et al., 2001) reported in the database. The calculated skin resistance, tip resistance and total capacity along the drilled shaft depth and the failure load was first tried via FHWA (1999) method, and if not feasible, the maximum measured applied load was considered as "failure load" according to Fellinius (2001a, b) criterion, the measured skin, tip and total resistance are interpreted for statistical analysis and then used for resistance factors calibrations. The O-Cell tested drilled shafts information together with interpreted resistance and predicted resistance are summarized in Table 1.

Table1. Summary of 4.0 ft diameter drilled shafts calculated predicted capacity and interpreted measured skin resistance mobilized through sand and weak rock (all constructed with slurry and casing)

Drilled Shaft ID # (DSID)	Drilled Shaft Full Embed-ded Length (ft)	Measured Skin Resistance Full Length (tons)	Calculated Skin Resistance Full Length (tons)	Measured Unit Skin Full Resistance (tsf)	Calculated Unit Skin Resistance Full Length (tsf)	Bias for Total Skin Resistance along Full Length	Bias For Unit Skin Resistance along Full Length
2347	30.76	1360	124	3.518	0.321	10.968	10.967
3146	35.959	981.4	124	2.172	0.274	7.915	7.915
3147	42.119	2413.5	60	4.560	0.113	40.225	40.225
3150	23	700	190	2.422	0.657	3.684	3.684
3151	36.7	2600	140	5.638	0.304	18.571	18.571
3152	53.7	1400	244	2.075	0.362	5.738	5.738
3153	65.83	1007	72	1.217	0.087	13.986	13.981
MEAN	41.153	1494.557	136.286	3.086	0.303	14.441	14.441
STD	14.443	733.243	64.233	1.563	0.188	12.438	12.438
COV	0.351	0.491	0.471	0.507	0.622	0.861	0.861

Table 2 Statistical characteristics and load factors of live and dead loads (after Paikowsky, et al., 2004).

Load Type	Bias	Coefficient of Variation	Load Factor Used
Dead load	$\lambda_{DL} = 1.05$	COVDL = 0.1	$\gamma_{DL} = 1.25$
Live load	$\lambda_{LL} = 1.15$	COVLL = 0.2	$\gamma_{LL} = 1.75$

Note: Bias is the mean value of the measured/predicted load. COV is the Coefficient of Variation, which is the ratio of the standard deviation over the mean value

5. CALIBRATION OF DRILLED SHAFT SKIN RESISTANCE FACTOR

Several different reliability analysis methods are available to conduct the calibration. Currently two of them have gained the most widely acceptance: first order reliability method (FORM) (Hasofer and Lind, 1974; Ellingwood et. al., 1980; Phoon et al., 1995; Yang, 2006) and *Monte Carlo* method (Allen et al., 2005; Roberts, 2006). In this paper, the *Monte Carlo* method was adopted because it is easy to use especially when dealing with a combination of different load and resistance components with uncertainties and having different types of distributions. The calibration in this study followed the recommended procedures in Transportation Research Circular E-C079 (Allen et al., (2005)).

A limit state function was selected. In this study, only the Strength I limit state was considered and the limit state function can be written as:

$$g = \phi R - \gamma_{LL} LL - \gamma_{DL} DL \qquad (4)$$

Where g is the safety margin; ϕ is the resistance factor, *R* is the nominal resistance,

γ_{LL} and γ_{DL} are the live load and dead factors, and LL and DL are the nominal live and dead loads.

For calibration, the statistical characteristics of load components are necessary. The same parameters used by Paikowsky (2004) were adopted in this study as shown in Table 2. Both live and dead loads were assumed to be normally distributed. This assumption is consistent with Nowak's study (1995).

All the O-cell test data were analyzed to determine the measured values of the skin resistance. In this study, skin resistance was determined from the O-cell load-displacement curve, which is an average skin resistance. Predicted values of skin resistance due to sand and weak rock were calculated using FHWA (1999) O'Neill and Reese's method via SHAFT (Reese et al., 2001).

The bias λ for each drilled shaft was calculated by dividing the measured nominal resistance from the O-Cell data by the corresponding predicted value using SHAFT 5.0 (Reese et al., 2001; O'Neill and Reese, 1999). Statistical analysis on the λ values was then performed. Figures 2 to 3 show the histogram and cumulative distribution function (CDF) curves of the bias values of the total skin and unit skin resistance. Based on the previous study, the bias of resistance was assumed to be log normally distributed. Figures 2 and 3 show that the biases for the skin resistance range from 3.68 to 40.23; therefore, the FHWA method based on O'Neill and Reese's study conservatively underestimated the actual capacities of drilled shafts in sandy soil and weak rock. The reason for this large discrepancy may be attributed to the assumption of smooth sockets, which is commonly used in practice. In reality, sockets may be rough or between rough and smooth. Unfortunately, not enough information was available in the O-Cell test reports to make such an assessment. Note that the mean values and the standard deviation values in Figures 2 and 3 may be used in the calibration for engineering conservativeness. Otherwise, the mean value μ_λ and the standard deviation σ_λ in Figures 2 and 3 can be used to fit the CDF curves following a "fit to tail" strategy recommended by Allen et al. (2005). Detailed procedures to develop the standard normal variables *z* and the CDF plots can be found in Transportation Research Circular E-C079 (Allen et al., (2005)). The "best fit" lognormal distribution parameters used in the calibration were summarized in Tables 3-5.

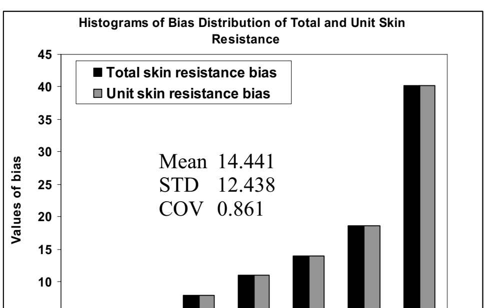

Fig. 2 Histogram of the bias of total and unit skin resistance.

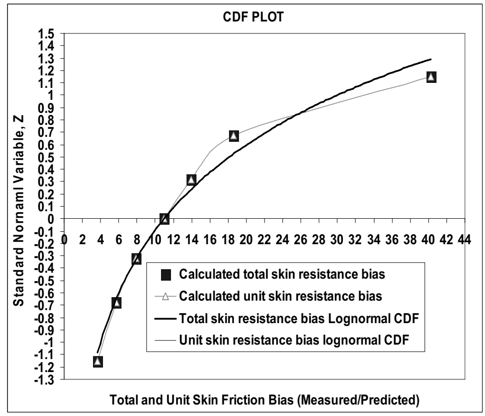

Fig. 3 CDF plot of the bias of total and unit skin resistance.

Table 3. Lognormal distribution parameters for the *Monte Carlo* simulation from measured total skin resistance data

TSR	Total Skin Resistance (tons)
μ_{TSR}	1494.577
σ_{TSR}	733.243
COV_{TSR}	0.491

Table 4. Lognormal distribution parameters for the *Monte Carlo* simulation from measured unit skin resistance data

USR	Unit Skin Resistance (tsf = ton/ft^2)
μ_{USR}	3.086
σ_{USR}	1.563
COV_{USR}	0.507

Table 5. Lognormal distribution parameters used for the *Monte Carlo* simulation from calculated resistance bias λ data for resistance factors calibration

λ	Bias for total and unit skin resistance (tsf) lognormal distribution	"Fit to tail" total and unit skin resistance bias
μ_{λ_R}	14.441	7.265
σ_{λ_R}	12.438	3.438
COV_{λ_R}	0.861	0.473

Prior to the *Monte Carlo* simulation, a target reliability index β_T and a ratio of dead load over live load (DL/LL) must be selected. In this study, the typical reliability index of $\beta_T = 3.0$ (approximately corresponds to the probability of failure $P_f = 0.001$) and the DL/LL ratio of 2.0 were selected. The variation of DL/LL did not influence the calibrated resistance factors.

It is easy to appreciate that depending on the different methods of predicting the skin resistance, there is considerable uncertainty related to the analysis method especially when the soil profile properties are not accurately available. To consider and implement the uncertainty into the reliability-based LRFD design, the *Monte Carlo* simulation method therefore can be employed to investigate the uncertainty effects on resistance factors for the skin resistance and ultimately the drilled shaft load and resistance factors calibration. *Monte Carlo* simulation technique is based on observed load and resistance distribution for analysis and considerations of uncertainties. It can be used to solve complex problems where closed–form solutions are either not possible or extremely difficult and check other solution techniques that require assumptions.

Additional information on *Monte Carlo* simulation details and its applications are available in Ang and Tang (1984), Ayyub and McCuen (1997), etc. For the *Monte Carlo* simulation and calibration of resistance factors, MATLAB will be employed for the reliability analysis based on actual measured drilled shaft static O-cell load test results and predicted nominal resistance.

In a *Monte Carlo* simulation, a large set of randomly generated numbers having a defined probability distribution function (in our case lognormal) is generated. During each trial, a random number is generated from within the probability distribution function for each random variable.

The required number of *Monte Carlo* trials is based upon achieving a particular level of reliability (Harr, 1996; Baecher and Christian, 2003). Each trial in a *Monte Carlo* simulation is assumed to be an independent experiment with a certain probability of success of P. Based upon this assumption, the trials will generate a binomial distribution. When the number of trials, N, is large, the binomial distribution can be approximated as a Gaussian (normal) distribution with a mean of NP and a standard deviation of (NP(1)P))1/2 (Harr, 1996). The level of reliability, or confidence interval, can be set by selecting the level of uncertainty. Based upon this reliability principle, the number of *Monte Carlo* trials required for a confidence level of 90% is approximately 4500 (Harr, 1996). For the results reported in this paper, a *Monte Carlo* simulation with 10,000 trials was conducted.

In the *Monte Carlo* simulation, the program would generate 10,000 groups of random numbers. Each group consisted of 3 random numbers, Za, Zb, Zc (where Zi $= \phi^{-1}(Zi)$ is inverse normal function 0< i = a, b, c<1). The program then calculated random live load, LLrnd, random dead load, DLrnd, and random resistance, Rrnd, by the following equations:

$$LL_{rnd} = LL \cdot \lambda_{LL}\left(1 + z_a \cdot COV_{LL}\right) \tag{5}$$

$$DL_{rnd} = DL \cdot \lambda_{DL} = LL \cdot \frac{DL}{LL} \cdot \lambda_{DL} \cdot \left(1 + z_b \cdot COV_{DL}\right) \tag{6}$$

$$R_{rnd} = \exp\left(\mu_{ln} + z_c \cdot \sigma_{ln}\right) \tag{7}$$

Where

$$\mu_{ln} = LN\left(\mu_{\lambda_R} \cdot \frac{LL \cdot \gamma_{LL} + DL \cdot \gamma_{DL}}{\phi}\right) - 0.5\sigma_{ln}^{\ 2}$$

$$\sigma_{ln} = \left[LN\left(COV_R^2 + 1\right)\right]^{0.5}$$

The above equations follow those from the Transportation Research Circular E-C079. ϕ is a trial resistance factor as used in Equation (7) and therefore does not have to reappear in Eq.(8). Note that the only unknown variable is the nominal live load LL. In the *Monte Carlo* simulation, the magnitude of the nominal load would not affect the result, so that LL maybe simply set to 1 or assume the average magnitude of the predicted drilled shaft capacity of 136 tons. The actually interpreted measured drilled shaft capacity may be assumed as the maximum mobilized resistance. From each group of random loads and resistance, the safety margin was calculated using Eq. (8).

$$g = R_{rnd} - \gamma_{LL} LL_{rnd} - \gamma_{DL} DL_{rnd} \tag{8}$$

The probability of failure is the number of the failed cases (g < 0) over the total number of the cases generated:

$$P_f = \frac{N_{g<0}}{10{,}000} \tag{9}$$

Finally, the reliability index β estimated by an MATLAB function was obtained

$$\beta = -\text{NORMINV}(P_f) \tag{10}$$

The mathematical expression of the above function is complicated and omitted here. Details of this function can be found in the Circular E-C079 by Allen et al. (2005). The *Monte Carlo* simulation is schematically shown in Fig. 4.

If the calculated β value is different from the target reliability index β_T, the trial resistance factor must be changed and iterations are necessary until $\beta = \beta_T$. The corresponding resistance factor is the one calibrated from this procedure. The *Monte Carlo* simulation for skin resistance factors calibration by assuming different magnitude of loads and β converging to β_T results are explained and graphically shown in Fig. 4.

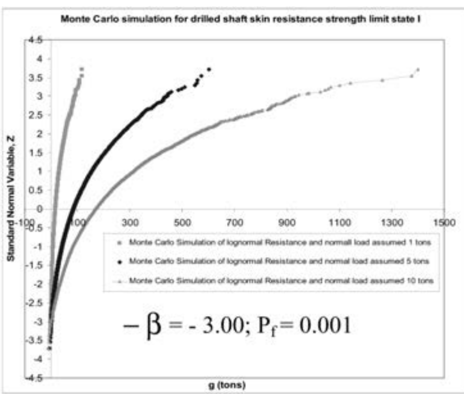

Fig.4. *Monte Carlo* simulation of 10,000 values of g generated for drilled shaft skin resistance strength I limit state (DL/LL=2.0, normal LL with magnitudes of 1 ton, 5 tons, 10 tons, $\gamma_{DL} = 1.25$; $\gamma_{LL} = 1.75$, and lognormal skin resistance distribution assumed) with ϕ_R =0.71 for total and unit skin resistance calibrated.

6. SKIN RESISTANCE FACTORS FOR DRILLED SHAFTS IN SAND AND WEAK ROCK

The resistance factors calibrated from the O-cell test data were summarized in Table 6. Compared with the current skin resistance factor of $\phi =$ 0.55 in sand and 0.60 in IGM weak rock at $\beta_T = 3$ in AASHTO LRFD Bridge Design Specifications (AASHTO, 2006 and 2007), the skin resistance factors obtained in this study are close to the previous calibration based on top-down load tests by Paikowsky (2004) and O-Cell load tests by Yang et al. (2008) as shown in Table 6.

Table 6. Comparison of calibrated skin resistance factors for O-Cell tested drilled shafts

	Total skin resistance factor	Unit skin resistance factor
Target Reliability Index	$\beta_T = 3$	$\beta_T = 3$
Current study	$\phi = 0.71$in sand & weak rock	$\phi = 0.71$ in sand & weak rock
Yang et al. (2008)	$\phi = 0.55$ in sand	$\phi = 0.55$ in sand
AASHTO (2006)	$\phi = 0.55$ in sand $\phi = 0.60$ in IGM or weak rock	$\phi = 0.55$ in sand $\phi = 0.60$ in IGM or weak rock

7. CONCLUSIONS

In this study, the total and unit skin resistance factors of 0.71 have been calibrated and rounded to 0.7 for recommendation of drilled shafts in sand and weak rock. The skin resistance factors were calibrated based on the statistical data collected from seven O-cell tested drilled shafts in sand and weak rock and the FHWA method via SHAFT program by assuming smooth sockets in rock with closed joints. The calibrated and recommended skin resistance factor of 0.70 agrees with the current AASHTO Bridge Specifications, but may seem 117% more confident. The FHWA method seems to conservatively underestimate the total and unit skin resistance of drilled shafts in sand and weak rock from this calibrated skin resistance factors point of view. This study further confirms that with more O-Cell tests and higher resistance factors calibrated at a project site, the cost of uncertainty/risk may be significantly reduced (Hayes, 2008). However, due to the limited size of the quality O-Cell tests database, cautions and engineering judgment need to be taken for the use of these resistance factors calibrated with SHAFT program assumed to be consistent with FHWA (1999) method. It should be noted that low site variability and good drilled shaft construction quality were assumed for the recommended resistance factors. Engineering judgment is necessary for choosing resistance factors if these assumptions are not warranted.

8. ACKNOWLEDGEMENTS

Mr. Tony Allen is acknowledged for making the database available for this study.

9. REFERENCES

AASHTO, 2007. *LRFD Bridge Design Specifications*. American Association of State Highway and Transportation Officials, Third Edition, Washington, D. C.

Allen, T.M., Nowak, A.S., and Bathurst, R.J., 2005. *Calibration to Determine Load and Resistance Factors for Geotechnical and Structural Design*. Transportation Research Circular Number E-C079, Transportation Research Board, Washington, DC, 83p.

Ang, A. H-S., and Tang, W.H., 1975. *Probability Concepts in Engineering Planning and Design, Vol. 1, Basic Principles*. John Wiley & Sons, New York.

Baecher G. B., Christian J. T., 2003. *Reliability and statistics in geotechnical engineering*. Wiley, West Sussex, UK

Barker, R.M., Duncan, J.M., Rojiani, K.B., Ooi, P.S., an, C.K., and Kim, S.G., 1991. *Manuals for the Design of Bridge Foundations*. NCHRP Report 343, TRB, National Research Council, Washington, DC.

Ellingwood, B., Galambos, T.V., MacGregor, J.G., and Cornell, C.A., 1980. *Development of a Probability Based Load Criterion for American National Standard A58*. NBS Special Publication 577, National Bureau of Standards, Washington, DC, 228p.

FHWA, 1999. *Drilled Shafts: Construction Procedures and DesignMethods*. Report No. FHWA-IF-99-025 by O'Neill M. W and Reese L. C., Federal Highway Administration, Washington, DC, 758p.

Fellenus, B. H., 2001a. *What capacity value to choose from the results a static loading test.* Deep Foundations Institute, Fulcrum, May 2001, 4p.

Fellenus, B. H., 2001b. *We have determined the capacity, then what?* Deep Foundation Institute, Fulcrum, Summer 2001, 4p.

Gunnink, B. and Kiehne C., 2002. "Capacity of Drilled Shafts in Burlington limestone", *Journal of Geotechnical and Geoenvironmental Engineering*, ASCE, Vol.128, No. 7, pp. 539-545.

Harr, M. E., 1996. *Reliability-Based Design in Civil Engineering.* Dover Publications, Inc., Mineola, New York.

Hasofer, A.M. and Lind, N.C., 1974. Exact and invariant second moment code format. *Journal of Engineering Mechanics Division*, ASCE, Vol. 100, No. EM1, pp. 111-121.

Hayes, JACK. 2008. *O-Cell Testing for Deep Foundation Design and Construction,* ADSC Foundation Engineering Faculty Workshop Presentations, Chattanooga, Tennessee.

Kulhawy, F.H. and Phoon, K.K., 1993. *Drilled shaft resistance in clay soil to rock, Design & Performance of Deep Foundations: Piles & Piers in Soil & Soft Rock (GSP 38),* Ed. PP Nelson, TD Smith & EC Clukey, ASCE, New York, pp.172-183.

Liang, R. and Li, J. (2009) "Resistance Factors Calibrated from FHWA Drilled Shafts Static Top-Down Tests Data Base", Contemporary Topics in In Situ Testing, Analysis, and Reliability of Foundation (GSP 186). Proceedings of Selected Sessions of *2009 International Foundation Congress & Equipment Expo*, Orlando, FL.

Nowak, A., 1995. *NCHRP Report 368: Calibration of LRFD Bridge Design Code*. Transportation Research Board, Washington, DC.

O'Neill, M.W. and Reese, L.C., 1999. *Drilled Shafts: Construction Procedures and DesignMethods*. Report No. FHWA-IF-99-025, Federal Highway Administration, Washington, DC, 758p.

O'Neill, M.W., Townsend, F.C., Hassan, K.M. and Chan, P.S., 1996. *Load Transfer for Drilled Shafts in Intermediate Geomaterials*. Report No. FHWA-RD-95-172. Federal Highway Administration, McLean, VA, 194p.

Osterberg, J. O., 1984. *A new simplified method for load testing drilled shafts. Foundation Drilling*, 23(6), pp. 9-11.

In situ behaviour of a diaphragm wall

J.R.M.S. Oliveira, M.E.S. Marques
Military Institute of Engineering

D.A. Cabral
Independent Consultant

ABSTRACT: This paper discusses the behaviour of a 10 m deep diaphragm wall constructed in the city of Porto Alegre, south of Brazil. The structure was constructed between existing buildings where four panels enclosed the terrain in a rectangular box-like shape. In order to monitor the horizontal displacements, 3 inclinometers were installed inside the walls, before the concrete casting, and 1 in the soil. In addition to that, 16 steel bars were instrumented with strain gages and installed along 4 levels of the reinforcement steel grid of the wall in order to provide information about traction and compression stresses due to the lateral earth pressure. Two-dimensional numerical analysis was carried out in order to compare with monitoring data.

1. INTRODUCTION

A 10 m, 50 cm thick, deep diaphragm wall was constructed in the city of Porto Alegre, south of Brazil, as part of an educational facility, comprising three underground floors, where two levels worked as intermediate levels of bracing. The structure was constructed between existing buildings where four panels enclosed the terrain in a rectangular box-like shape 75 x 45m wide. The excavation inside the area was carried out in three phases, during four months, with each bracing level being constructed before the next phase.

The first level of excavation was carried out without bracing until 4.5m depth. The first floor level slab, acting as bracing, was constructed at 3m depth. From 7 to 9m depth a berm was cut in order to increase stability (Figure 1). Figure 2 presents a general view and Figure 3 a internal view of the excavation works, where the first intermediate floor is yet uncompleted, with two central holes, in order to provide accessibility to the equipments for the next phases.

Due to the relatively high water table, it was necessary to lower the water table during construction.

The contractor and designers main concern was that considerable settlements, induced by horizontal displacements, could damage the foundations of nearby buildings. Therefore, a monitoring program was conceived in order to evaluate the excavation movements, by means of inclinometer verticals and instrumented steel bars inside the wall.

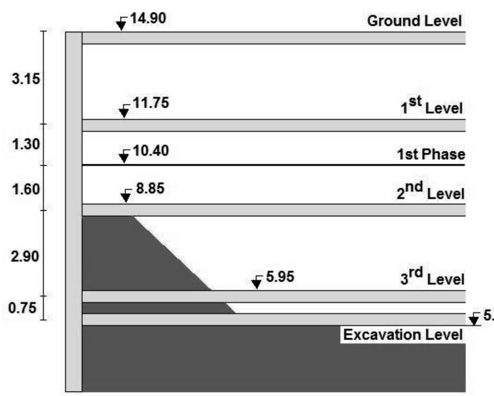

Figure 1. Typical excavation profile (units in meters).

Numerical studies, conducted during the design conception phase, indicate that deformation range around the buildings would be acceptable. The displacements and stresses measured in situ were compared with the predicted values to better understand the soil-structure interaction behaviour.

2. SOIL PROPERTIES

The geotechnical profile of the site is composed by a 1.5m embankment fill, a 1.5m thick layer of silty clay, 2m to 4.5m thick layer of clayey-silty sand, above a layer of gravel and the weathered rock (Figure 4). The top of the sound granite rock varies from 8 to 14m depth. The water table was at 3.5m depth.

Figure 2. General view of the excavation site.

Figure 3. Internal view of the excavation site.

The local soil is lateritic residual yellow well graded clayey-silty sand. Unsaturated shear tests were carried out on a sample collected at 5m depth, which results are shown in Figure 5.

The sand presented a high friction angle (36^{o}) probably due to the angularity and grading effect and an apparent cohesion of 26 kPa.

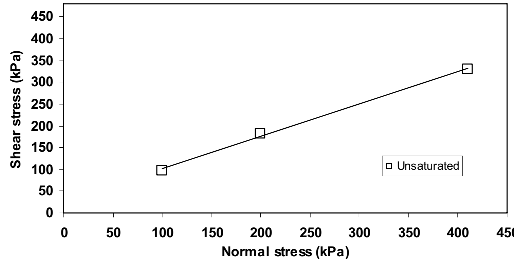

Figure 5. Shear tests results of the clayey-silty sand soil.

3. MONITORING SETUP

The monitoring setup, conceived for this structure, consists of 4 inclinometer verticals and 16 instrumented steel bars. Settlements of an existing building were also measured and controlled during the excavation process (Figure 2).

Dunnicliff (1993) presents some case histories of monitored braced excavations with similar instrumentation. The inclinometer verticals were employed to measure the horizontal displacements along the diaphragm wall profile. Three of them (VT-1, VT-2 e VT-4) were installed inside the walls, before the concrete casting, assuring the best location for movement measurement with the advantage of no drilling operations. The fourth (VT-3) was installed inside the soil, just by the side of one of the instrumented walls, to allow overall behaviour analysis.

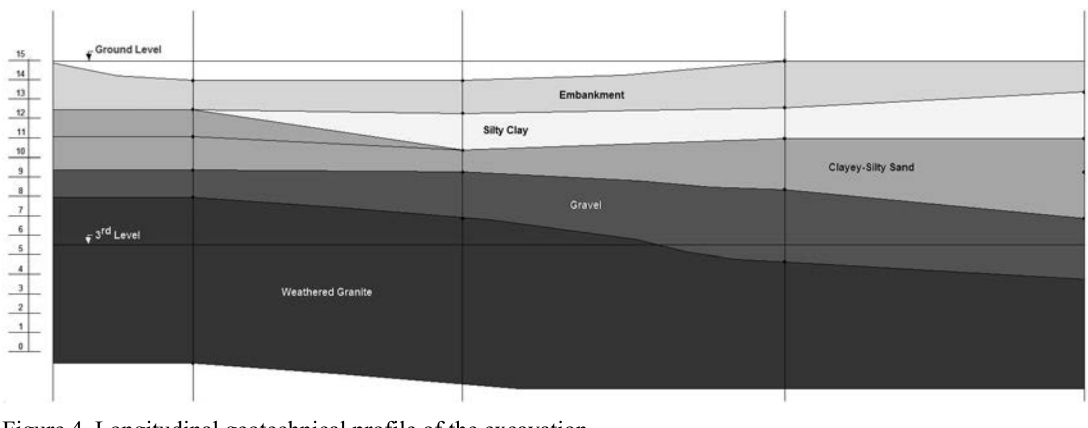

Figure 4. Longitudinal geotechnical profile of the excavation.

Ou et al. (1998; 2000) proposed that since the movement of the soil near the retaining wall is quite close to that of the wall itself the inclinometer casing can also be placed in the soil within 2 m of the outer side of the wall. Figure 6 shows the schematic location of the verticals and the relative position of the instrumented walls (S08, S18 and S60), as well as the location of the existing building settlement measure point (ST-1). Figure 7 shows the inclinometer casing placed inside the wall reinforcement grid.

In order to measure the stress distribution throughout the diaphragm wall reinforcement, 8 steel bars, with 1 m of length and 16 mm of diameter, were equally placed along the front and the back of the steel grid, aligned with the longitudinal reinforcement bars. Walls S08 and S60 were monitored, totalizing 16 reading points.

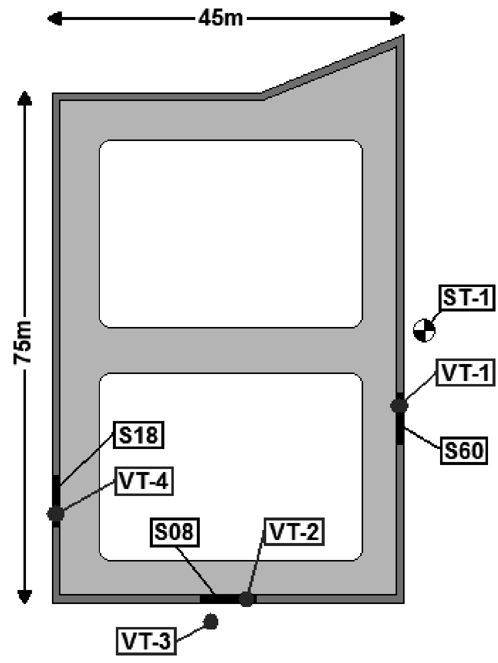

Figure 6. Schematic location of inclinometer verticals.

The instrumented bars consist of two resistance strain gages, placed in diametrical opposite sides of a 16 mm diameter steel bar (Figure 8), and were calibrated for traction and compression (no buckling allowed). The strain gages were protected with a thick plastic waterproof membrane in order to prevent damage. Ou (2006) recommends the use of many layers of water repellent membranes over the steel bar, since it was noted that when the bar is stressed some of the membranes layers may break.

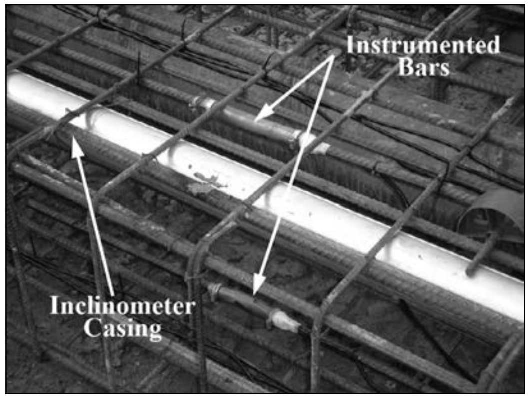

Figure 7. Inclinometer casing inside the wall reinforcement grid.

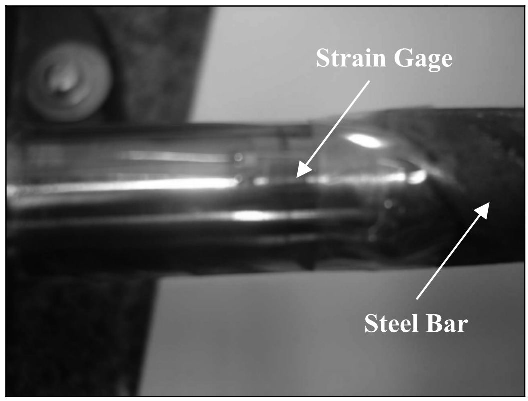

Figure 8. Strain gages being glued on instrumented bars.

4. HORIZONTAL DISPLACEMENTS

The horizontal displacements presented in this paper include the first excavation phase, which is associated to the first floor bracing level (around 3 m depth), and the second one, which is associated to the soil berm represented in Figure 9 (roughly around 6 and 8 m depth). As the bedrock depth varies from 8 to 14m, injected piles were executed, complementarily to the diaphragm wall, in order to anchor the whole structure.

The inclinometer readings associated with the first phase took place 1 month after the beginning of the excavation, while the second set of readings was carried out 3 months later.

As Figure 9 and Figure 10 show that the maximum displacements for the second phase are around 20 and 15 mm for inclinometer verticals VT-01 and VT-03, respectively. Greater values were expected for the VT-01 vertical, relatively to VT-03, since it is located in the larger side of the structure (Figure 6). It can also be noted that the magnitude of displacements between phases is very similar, once the excavation steps are also very close.

Comparisons between verticals VT-02 and VT-03 installed inside the wall and inside the soil, respectively, which are located very close from each other, show very good agreement with for both phases.

Finally, the displacement profiles for verticals located inside the concrete wall show a clear linearity, associated to the rigidity of the structure, whilst for the vertical located inside the soil an inflection can be observed, probably related to the mobilization of soil passive forces.

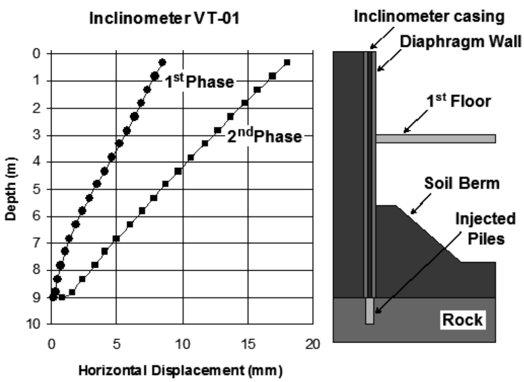

Figure 9. Horizontal displacements in inclinometer vertical VT-01.

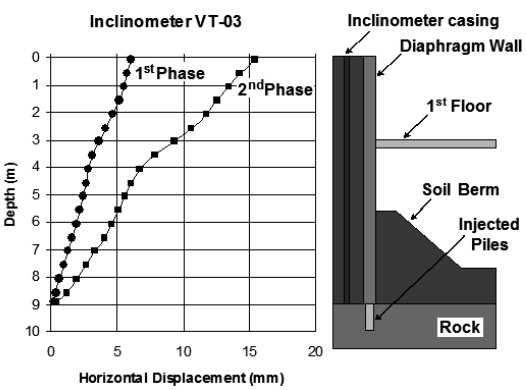

Figure 10. Horizontal displacements in inclinometer vertical VT-03.

5. FORCES AND STRESSES

Two sets of 8 instrumented bars each were equally spaced along the reinforcement grids of walls S08 and S60, half facing the soil (inside position) and half facing the excavation side (outside position).

Tables 1 and 2 show the force measurements for bars located in walls S08 and S60, respectively. The first and second phases are the same considered for the horizontal displacements. Initially, a great number of inoperative instrumented bars can be observed. This problem was probably caused by mechanical breakage of the plastic membrane, responsible for the water sealing, leaving in operation less than one third of the installed transducers. It is important to clarify that for the initial readings, after the concrete casting and before any excavation work, all bar transducers were operational.

Table 1. Force measurements for wall S08.

Number	Position	Depth (m)	1st Phase (kN)	2nd Phase (kN)
1	Inside	1.00	1.59	-
2	Outside	1.00	1.44	2.16
3	Inside	3.05	-	-
4	Outside	3.05	-	-
5	Inside	5.10	2.48	-
6	Outside	5.10	-	-
7	Inside	7.15	0.17	-
8	Outside	7.15	0.45	6.81

Table 2. Force measurements for wall S60.

Number	Position	Depth (m)	1st Phase (kN)	2nd Phase (kN)
1	Inside	1.00	0.57	7.63
2	Outside	1.00	-	-
3	Inside	3.05	-	-
4	Outside	3.05	-	-
5	Inside	5.10	-	-
6	Outside	5.10	-	-
7	Inside	7.15	-	-
8	Outside	7.15	2.69	-

As the operational instrumented bars were located in points of low bending moments, measured force values were kept in Table 1 and Table 2 mainly as a lower bound reference.

6. SETTLEMENTS OF EXISTING BUILDING.

Figure 11 presents the settlement measurement of the tallest existing building around the excavation site (Figure 2). The reference point is just few meters from the excavation area and is represented in Figure 6.

The settlement curve can be divided in two parts: a steeper one which is associated with excavation works with no bracing level (depth shallow than 5 m), and a gentler one after the first level of bracing (depth deeper than 5 m).

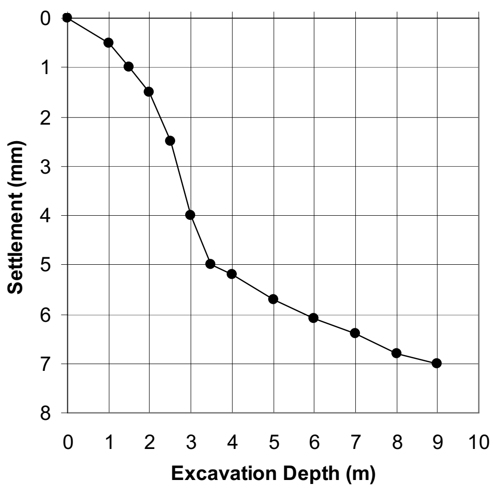

Figure 11 – Settlement evolution of existing building.

7. COMPARISION WITH PREDICTED VALUES

Ng et al. (1999), Liu et al. (2005) and Leung and Ng (2007) measured the in situ performance of diaphragm walls. Hsieh et al. (2003) presented monitoring results of a diaphragm walls in Taiwan where lateral displacement of the walls resulting from basement excavation alone may reach up to 0.3–0.5% of the basement excavation depth under normal construction conditions in silty sand soils. These percentages lead to horizontal displacements from 1.8 to 3.0 cm, associated to a 6 m deep excavation, which are close to the ones measured (around 2.0 cm).

A soil-structure interaction numerical investigation was implemented using the structural matrix analysis program FTOOL, Two-Dimensional Frame Analysis Tool, in an attempt to assess more reliable stress and displacement values.

In that way, elastic simulations of phases 1 and 2 were carried out considering the water table 2 m below ground surface and a set of soil passive reaction springs (K) beginning at 3 m depth, as presented in Table 3. Values of friction angle and cohesion were reduced to consider saturation effects and a minimum factor of safety. Also, water table levels were considered higher than those observed by field investigation.

Table 3. Assumed soil parameters for soil-structure interaction analysis.

Depth (m)	SPT (N)	φ (°)	c (kPa)	K (kN/m)
1	5	28	0	-
2	12	30	5	-
3	2	28	0	-
4	7	28	5	10.000
5	10	10	5	1.500
6	18	10	10	1.500
7	12	10	15	15.000
8	11	10	15	15.000
9	9	10	20	2.000
10	12	15	25	2.500

In phase 1, results considering *in situ* horizontal geostatic forces and a surface surcharge of 50 kPa led to the bending moments and horizontal displacements diagrams presented in Figure 12. The maximum displacement found for the top of the wall was 1.6 cm, which is twice the value measured in the inclinometer verticals. This behaviour is probably associated to the lower values of resistance parameters assumed for this analysis. The maximum traction force found per single longitudinal steel bar was 29.1 kN, which is much lower than the values measured with the instrumented bars.

In phase 2, a one degree of freedom restraint was considered at the top of the wall and at its base, with soil passive reaction springs only from 9 m depth on. This scenario was implemented as the most critical in terms of stress distribution along the wall. Figure 13 presents the results for this simulation, where the maximum displacement was 2.6 cm. This value is not too far from the 1.9 cm measured *in situ*, particularly when considering that for the simulation the soil was 2 m below the real position and that lower resistance parameters values considered and water table differences.

8. CONCLUSIONS

The monitoring setup conceived for this structure consisted of inclinometer verticals, force transducer steel bars and settlement measurements. The inclinometer casings installed inside and outside the wall worked adequately, leading to reliable and correct horizontal displacement measurements.

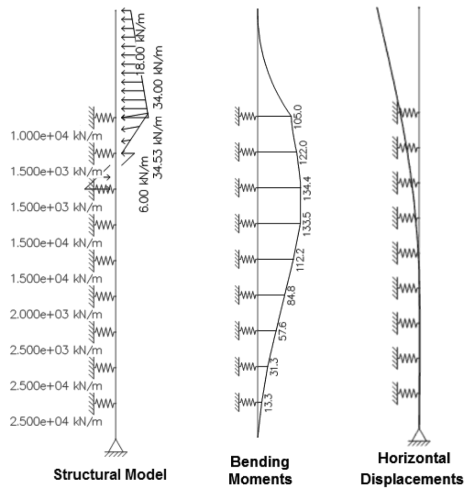

Figure 12. Structural Model, Bending moments (kNm) and horizontal displacements for Phase 1.

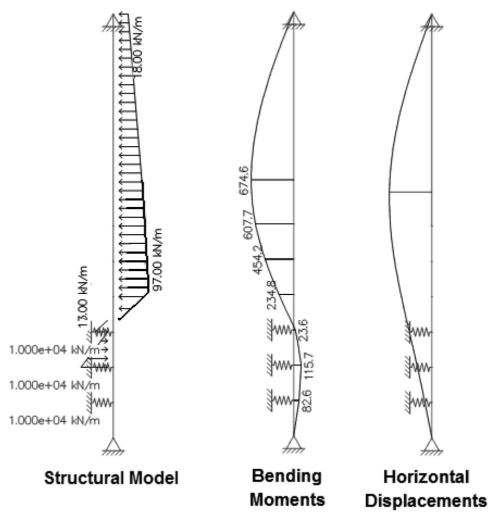

Figure 13. Structural Model, Bending moments (kNm) and horizontal displacements for Phase 2.

On the other hand, the force transducers mounted on steel bars and distributed along the wall reinforcement grid were damaged, even though they have been protected with a thick plastic cover layer before the concrete casting.

The settlement measurement of existing buildings around the excavation site showed the importance that intermediate bracing levels play in displacement control.

Soil-structure interaction simulations are complex problems which usually need powerful computational tools, but approximate results can be achieved via simple algorithms as the elastic structural matrix analysis program. The numerical results compared well with the measured data although the resistance parameters and border conditions were not exactly the same.

9. ACKNOWLEDGEMENT

The authors would like to acknowledge engineers Ricardo Gil Domingues and Alvaro Augusto Dellê Vianna for their help and expertise with the instrumentation setup, as well as graduate student Marcus do Nascimento Rachid for his help with the laboratory tests.

10. REFERENCES

Dunnicliff, J. 1993. Geotechnical instrumentation for monitoring field performance. John Wiley & Sons.

Hsieh, H.S., Wang, C.C. and Ou C.Y. 2003. Use of Jet Grouting to Limit Diaphragm Wall Displacement of a Deep Excavation, Journal of Geotechnical and Geoenvironmental Engineering. ASCE, Vol. 129, No. 2, pp. 146-157.

Leung, E.H.Y. and Ng, C.W.W. 2007. Wall and Ground Movements Associated with Deep Excavations Supported by Cast In Situ Wall in Mixed Ground Conditions. Journal of Geotechnical and Geoenvironmental Engineering Vol. 133, No. 2, pp. 129-143.

Liu, G.B., Ng, C.W.W. and Wang, Z.W. 2005. Observed Performance of a Deep Multistrutted Excavation in Shanghai Soft Clays. Journal of Geotechnical and Geoenvironmental Engineering Vol. 131, No. 8, pp. 1004-1013.

Ng, C.W.W., Rigby D.B., Lei, G.H., and Ng, S.W.G. 1999. Observed performance of a short diaphragm wall panel, Géotechnique 49, No. 5, 681±694.

Ou, C.Y., Liao, J.T. and Lin, H.D. 1998. Performance of a diafragm wall constructed using Top.Down Method, Journal of Geotechnical and Geoenvironmental Engineering, ASCE, Vol. 124, No. 9, pp. 798-808.

Ou, C.Y., Liao, J.T. and Cheng, W. L. 2000. Building response and ground movements induced by a deep excavation, Geotechnique, Vol. 50, No. 3, pp. 209-220.

Ou, C.Y. 2006. Deep Excavation Theory and Practice. Taylor & Francis Group.

Effect of limiting soil pressure on pile group adjacent to a failed excavation

D.E.L. Ong
Swinburne University of Technology, Sarawak Campus

C.F. Leung, Y.K. Chow
National University of Singapore

ABSTRACT: Deep excavation may result in lateral soil movement that may threaten the structural integrity of nearby existing pile foundations. In this paper, a pile group consisting of 4 nos. of 900-mm diameter bored piles was instrumented to provide an in-sight into the study of pile-soil interaction. By chance, the instrumented pile group failed by displacing laterally due to excessive soil movement resulted from a nearby slope excavation. Benchmarking between field data and back-analysis using Finite Element Method (FEM) as well as an established numerical method were carried out to understand the pile group behaviour when subjected to large-strain lateral soil movement or soil flow. The disadvantage of modelling a 3-D pile group in 2-D environment is also addressed.

1. INTRODUCTION

Excavation in soft soil often results in large lateral soil movements, which would induce additional bending moments, shear forces and deflections on piles supporting adjacent structures. Poulos (1997) reported the results of a field study that a building has been severely damaged and eventually demolished due to excessive soil movements caused by soil excavation nearby. Thus, the knowledge of these additional loads/deflections is of great importance to ensure that the structural integrity of the pile foundations can be maintained.

It is the interest of this study to compare the effect of large-strain soil movement or soil flow on pile group responses between these analysis methods:

a) Field measurement vs. 2-D finite element analysis using pile 'smearing' method (continuation of study by Ong et al. (2007) on single pile)
b) Field measurement vs. an established numerical method using important input data of free soil movement and limiting soil pressure

2. PROJECT DETAIL

In this case study, a proposed 7-storey industrial building with one-level basement carpark was to be constructed at a congested site in the city. In order to construct an underground storage facility, a temporary open-cut excavation of a 1V:2.5H slope was proposed. Owing to some unforeseen situations, excessive soil movement had taken place during the slope excavation and caused failure of the instrumented pile group. The post-failure pile behaviour has provided valuable field data for back-analysis.

3. SOIL INVESTIGATION WORK

The soil investigation work consists of:
a) 4 boreholes made using rotary wash boring. Borehole 1 (BH1) was located within the excavation area as shown in Figure 1.
b) Standard Penetration Tests (SPT) with split spoon samplers were carried out to obtain disturbed samples for index property tests.
c) Undisturbed sampling of soil specimens at 1.5m to 3.0m intervals using thin wall samplers for trixial compression tests.
d) Ground water level and pore water pressure measurement using water standpipe and piezometer, respectively.
e) Vane shear tests carried out in borehole to determine the in-situ strength of the soft marine clay.

4. SUB-SURFACE SOIL PROFILE & SOIL PROPERTIES

At BH1, top fill layer was found between depths 0.5 m and 1.5 m. Beneath the fill was the very soft, greenish grey marine clay with thickness ranging between 7.5m and 9.0m. The SPT N values for this layer are less than 4. Layer 3 is about 5 m thick and consists of loose, clayey sand as well as medium stiff sandy clay with SPT N values between 4 and 10. Subsequently, medium dense clayey sand with SPT N values between 10 and 50 were found. Table 1 shows some of the soil input parameters used in the subsequent analyses carried out.

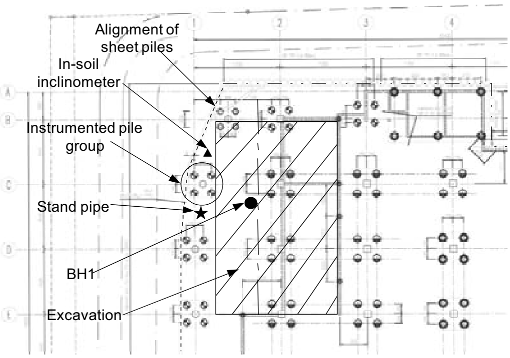

Figure 1. Location of borehole and zone of excavation near the instrumented pile group

Table 1. Input soil parameters

Soil type	c_u (kPa)	c' (kPa)	ϕ' (deg)	E (kPa)
Fill	20	-	-	10,000
Very soft marine clay	10	-	-	4,000
Loose clayey sand (N=4-10)	-	5	28	12,000
Medium clayey sand (N=10-30)	-	10	28	34,000
Dense clayey sand (N=30-50)	-	15	30	68,000

5. FIELD INSTRUMENTATION

Coincidentally, a capped 4-pile group of 900-mm diameter cast-in-situ concrete bored piles located in front of the slope excavation was instrumented. One of the rear piles was installed with an in-pile inclinometer and strain gauges while one of the front piles was only installed with strain gauges. An in-soil inclinometer was also installed adjacent to the pile group to measure the lateral sub-surface soil movement profiles caused by the excavation.

6. PILE CAPACITY

As no massive soil movement has been anticipated in the design, the piles were nominally reinforced with 0.5% steel reinforcement. The cracking moment capacity (M_{cr}) of the piles is about 264 kNm and the ultimate bending moment capacity (M_{ult}) is 520 kNm. These values are obtained by performing a structural moment interaction diagram considering pile properties and combined vertical load and moment acting on it.

7. EXCAVATION SLOPE FAILURE

To facilitate the building basement construction, an unsupported 5-m high slope excavation was carried out in front of the capped 4-pile group of 900-mm diameter cast-in-situ concrete bored piles. Unfortunately, during the course of excavation, the slope failed as a result of heavy rainfall as shown in Figure 2.

Figure 2. Slope failure next to the instrumented pile group

8. METHODS OF ANALYSIS

The two analysis methods used in this study are described in detail hereinafter.

8.1. Method 1: 2-D FE analysis & method of smearing of 3-D pile properties

PLAXIS version 8.2 is a commercial 2-D finite element code and is attempted hereinafter to back-analyse the data obtained. 6-noded triangular elements with each element containing 3 integration points are used for the finite element meshing. Mohr-Coulomb soil model using PLAXIS "Method B" type of analysis was performed. "Method B" type of analysis is one out of three types of analyses coined after the rigorous studies carried out by various institutions worldwide in the back-analysis of the tragic event of Nicoll Highway in Singapore on 20th April 2004. The authors acknowledged that other superior soil models could be used to replicate soil deformation more realistically, but in this particular paper, the more commonly used soil model i.e. Mohr-Coulomb is adopted for the present back-analysis study for simplicity.

"Method B" involves the use of effective stress analysis with a cap on the cohesion values of the soft marine clay as measured by in-situ vane shear. This is to ensure that the cohesion values governed by the linearly elastic-perfectly plastic Mohr-Coulomb soil model are not over-predicted when compared to the actual non-linear soil behaviour. The undrained Young's modulus of the soft marine clay can be best represented by $E_u \approx$ 150-300 c_u or 2000N (N=SPT N value) and relationship between soil E' (effective) and E_u (total) is approximated as $E' \approx E_u/1.15$. Poisson's ratio of 0.3 was used for typical effective stress analysis.

Ong et al. (2007) has successfully used 2-D plane-strain FE analysis to model the smeared 3-D nature of a pile in a 2-D environment for soils stressed within working limits. As such, the actual properties of a 3-D pile are 'smeared' in the plane-strain direction to obtain the 'equivalent' pile properties per m width. Effectively, the 3-D nature of a pile is now represented by an 'equivalent wall'. This can be done by considering the contact areas of a cylinder and a rectangular wall as shown schematically in Figure 3.

However, the limiting soil pressure analysis carried out to assess the response of piles when subject to lateral soil movement in Ong et al. (2007) was for a single pile embedded in stable and sliding soil behind a retaining wall based on centrifuge study. Therefore, the current analysis serves as a continuation of previous work where the analysis is now extended to a real-life situation to demonstrate its applicability in practice.

In this case involving a group of piles, the 3-D single pile properties are multiplied by the number of similar piles in the plane-strain direction and smeared (divided) by the pile group centre-to-centre spacing, s, in the plane-strain direction as shown in Figure 3.

For PLAXIS, the plate element presenting the equivalent wall is represented as a thin plate with a virtual thickness; hence mesh thickness is not important. Nevertheless, the weight of the wall in relation to the surrounding soils can be input when the equivalent wall is defined.

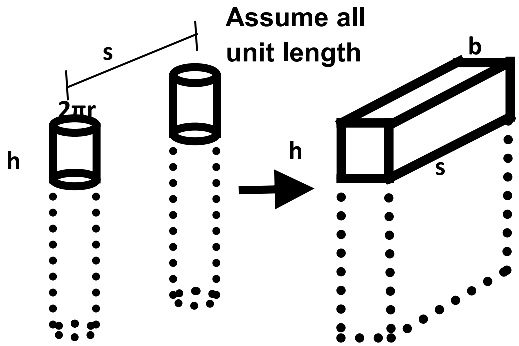

Figure 3. Method of smearing 3-D pile to an equivalent 2-D wall for use in 2-D FE analysis for the case of a group of piles (after Ong et al., 2007)

The input properties of the corresponding equivalent wall, depending on the number of similar piles in the plane-strain direction are tabulated in Table 2.

Table 2. Method of smearing 3-D pile to an equivalent 2-D wall for the case of a group of piles (after Ong et al., 2007)

No. of piles in plane-strain direction (pile spacing, s is 2.7m)	Pile property	2-D equivalent wall
2	Axial rigidity	$2*(E_p*A_p)/2.7$
2	Bending rigidity	$2*(E_p*I_p)/(2.7)$

In general, the formulations used to obtain a 2-D equivalent wall for a group of piles in the plane-strain direction can be written as:

Axial rigidity:

$$n(E_pA_p)/[(n-1)(s)] \quad (1)$$

Bending rigidity:

$$n(E_pI_p)/[(n-1)(s)] \quad (2)$$

where E_p, A_p and I_p are the Young's modulus, cross-sectional area and second moment of area of the pile, respectively, n is the number of piles in the plane-strain direction and s is the centre-to-centre pile spacing between 2 piles in the plane-strain direction.

By converting 3-D piles to equivalent 2-D wall, the magnitudes of bending moment and forces (axial or shear) will be output as kNm/m and kN/m, respectively. In order to obtain the "actual" pile bending moment and forces, multiplication of smeared dimensions is necessary. Table 3 shows the methods of converting response of equivalent wall to that of a pile for a group of piles. Nevertheless, the resulted deflections and rotations remain similar.

Table 3. Method of converting response of equivalent wall to that of a pile for the case of a group of piles (after Ong et al., 2007)

Pile response	Quantity per linear m of wall as output by PLAXIS	Conversion to quantity per pile
Bending moment (BM)	BM in kNm/m	BM*[(n-1)*s]/n to obtain kNm
Axial or shear forces (F)	F in kN/m	F*[(n-1)*s]/n to obtain kN

8.2. Method 2: Established numerical method

A simplified numerical model (Chow and Yong, 1996) is used to back-analyse the responses of the piles subjected to lateral soil movement. The numerical model is described in detail in Ong et al. (2006) and summarised henceforth.

In this numerical method, the pile is modelled as a series of linear elastic beam elements and the soil is idealized using the modulus of subgrade reaction. This numerical method has been adopted successfully to back-analyse the centrifuge model test data on pile subject to excavation-induced soil movement (Leung et al. 2000, 2006) and Ong et al. (2009).

The numerical analysis requires the knowledge of the pile flexural rigidity, E_pI_p, the distribution of lateral soil stiffness, K_h, with depth, the limiting soil pressures, p_y, that acts on the pile and the free-field lateral soil movement profile at the pile location. With the application of p_y values, the non-linear soil model can be simulated to a certain extent. The distribution of lateral soil stiffness with depth, K_h, is assumed to be related to the Young's modulus of the soil, E_s, as follows (Chow and Yong 1996):

$$K_h \approx E_s \quad (3)$$

For lateral loading, Es of clay ranges from 150 c_u to 400 c_u (Poulos and Davis 1980). For the soft marine clay, it is taken that (Ong et al., 2006):

$$K_h \approx E_s = 150\text{-}300\ c_u \quad (4)$$

The following equation proposed by Poulos and Davis (1980) based on a modification of the work of Broms (1964a) for the limiting soil pressure for clay is used in the numerical model:

$$p_y = 2(1+z/d)c_u \le 9c_u \quad (5)$$

where z = depth and d = pile diameter.

Broms (1964b) proposed that the ultimate of limiting soil pressure for cohesionless soils:

$$p_y = 3\sigma_v' K_p \quad (6)$$

is used in this study where σ_v' = effective vertical overburden pressure, $K_p = (1 + \sin\phi') / (1 - \sin\phi')$ and ϕ' = angle of internal friction. The use of limiting soil pressure enables the effect of soil flow around the pile to be considered in the analysis.

Chow (1996) extended the above method to analyse pile groups subject to lateral soil movement. The pile-soil interaction forces acting on the piles and the soil are first considered separately and then combined by considering equilibrium and compatibility. In a nutshell, the following stiffness relationship of the pile group system is obtained considering equilibrium of the interaction forces acting at the pile-soil interface and load-deflection (p-y) relationship of the piles in a group:

$$([K_p] + [K_s])\{y_p\} = [K_s]\{y_o\} \quad (7)$$

The vector $[K_s]\{y_o\}$ represents the induced lateral forces acting on the piles resulting from the lateral soil movement. The pile deformation, $\{y_p\}$, is obtained by solving Eq. (7). Subsequently, by differentiating the pile deformation profile, $\{y_p\}$, the shear force and bending moment profiles can be obtained. Similar to the case for the method of analysis for single pile, the non-linear behaviour of soil can be incorporated by limiting the soil pressure that can act on the pile. The pile cap is simulated by introducing beam elements into the method of analysis to "tie" the pile heads in a group together. Therefore, the bending rigidity of the pile cap, $(EI)_{cap}$, has to be included as part of the input data.

9. ANALYSES PERFORMED

Table 4 shows the attributes of both types of analyses, Methods 1 and 2. The advantage of performing Method 2 analysis over Method 1 is that the former takes into account the flow of the soil past the pile when soil failure occurs. This effect cannot be simulated using a 2-D plane strain FE model as the 'smeared' pile or the 'equivalent wall' does not permit the soil from flowing past it. To properly analyse this problem would, otherwise, require modelling the problem in 3-D finite element modelling, which would require a considerable amount of computer resources and time, besides not being the theme of this paper.

Table 4. Attributes of various analytical methods

Methods of analysis	Source of soil movement as input	Limiting soil pressure
Method 1: 2-D FE analysis & method of smearing of 3-D pile properties	FE analysis	Cannot be considered
Method 2: Established numerical method	Field in-soil inclinometer	Can be considered

10. DISCUSSION AND COMPARISON OF RESULTS

The effect of large-strain soil movement or soil flow on pile group responses are presented hereinafter. Due to the limitation in writing space, only one set of measured of soil movement profiles and pile responses are presented. Nevertheless, this set of data is considered to be representative of the theme of this paper. The development of pile moment of inertia, I from an uncracked (gross) section to a cracked section (pile deflected 135mm, M_{cr} = 264 kNm and M_{ult} = 520 kNm both exceeded) constitutes an important understanding in this back-analysis process and shall be dealt with in detail in future publication as it is not within the scope of this paper. Nonetheless, it should suffice for now to use the uncracked (gross), I_g and cracked, I_{cr} sections of pile, calculated to be 0.03221m^4 and 0.00607m^4, respectively, in subsequent back-analyses. The computation of I can be found in basic reinforced concrete text such as Kongs and Evans (1987).

Table 4. Various analysis cases performed

Analysis cases	I_g of I_{cr}	p_y
1 (Method 1): simulates ignorance of soil flow phenomenon	I_g	Not considered
2 (Method 2): simulates available knowledge on I and p_y	I_{cr}	p_y=6c_u
3 (Method 2): simulates available knowledge on p_y but not on I	I_g	p_y=6c_u
4 (Method 2): simulates absence of knowledge on I and p_y	I_g	p_y=K_h

p_y: limiting soil pressure
K_h: soil spring stiffness not considering p_y

Table 4 shows the various analysis cases performed so as to simulate the understanding level of a designer when confronted with such a case study.

10.1. Field measurement vs. 2-D FE analysis

The finite element mesh set up is shown in Figure 4. The predicted soil movement distribution shown in Figure 5 seems to be limited by the presence of the 'equivalent wall' effect, which negates the natural behaviour of soil movement or widely known as free-field soil movement.

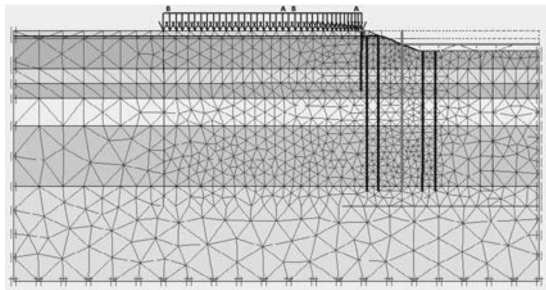

Figure 4. Finite element mesh used in analysis to 'smear' 3-D pile properties in 2-D environment.

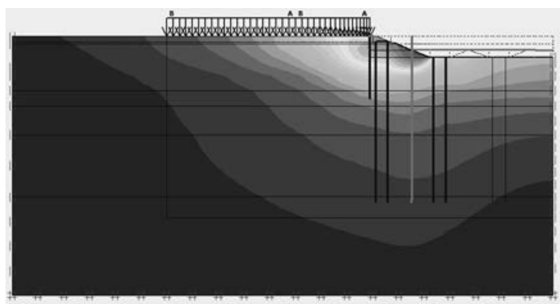

Figure 5. Soil movement distribution around 'smeared' pile group is limited by 'equivalent wall' effect

The predicted and measured lateral soil movement profiles obtained from the 2-D FE modelling above and from field in-soil inclinometer next to the instrumented pile group, are shown in Figure 6, respectively.

The comparison shows that the observed lateral soil movement magnitudes and profiles are quite different. This is due to the fact that in 2-D FE analysis where the piles are 'smeared' in the plane-strain direction, they are effectively represented by an equivalent wall, thus preventing the large-strain deformed soil to squeeze past the piles, which is typically a 3-D phenomenon and observed to occur on site.

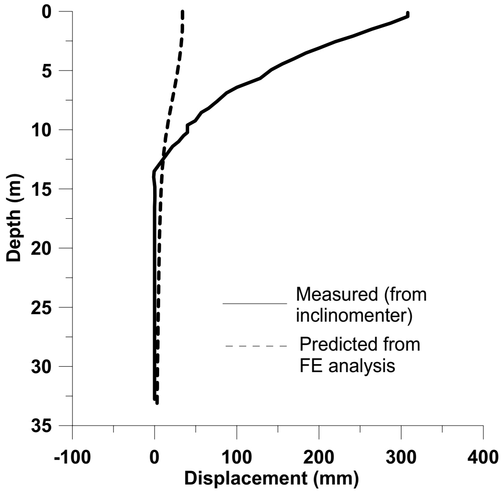

Figure 6. Profiles and sources of lateral soil movement.

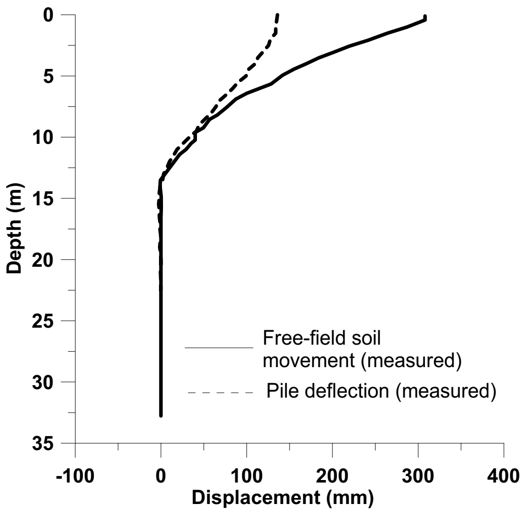

Figure 7. Profiles of free-field soil movement and pile deflection

This is proven by the measured inclinometer readings where the magnitudes of lateral soil movement are much larger than the measured pile deflection (in-pile inclinometer), as shown in Figure 7, thus suggesting that soil flow around the pile has taken place and also highlights the limitation in modelling large-strain soil deformation behaviour in a 2-D environment. However, this method has proven to be viable and effective in situations where large-strain soil deformation is not anticipated or when soil movement is within allowable working limits as described in detailed by Ong et al., 2007.

Figure 8(a) shows the outcome of the pile responses for Case 1 based on Method 1. Front pile is located nearer to the slope than rear pile. In this case, as described above, the natural behaviour of soil deformation is negated by the presence of the 'equivalent wall', resulting in relatively smaller magnitudes than measurements taken on site, as shown in Figure 6. Consequently, the predicted pile responses (bending moment and deflection) are both very much under-predicted, leading to inappropriate design of pile to resist lateral soil movement.

10.2. Field measurement vs. established numerical method

This method of analysis is considered as Method 2, whereby the established numerical method is used in conjunction with the measured lateral soil movement. The advantage of Method 2 is that it is capable of considering the effect of limiting soil pressure, which is an important parameter when dealing with anticipated large-strain soil deformation.

In Case 2, if both I_{cr} and p_y are correctly adopted, Figure 8(b) shows that the prediction of pile responses is very reasonable. This simulates the available and appropriate level of understanding of the back-analysis carried out considering the development on site.

Case 3 simulates the situation where knowledge on limiting soil pressure is available but not on the pile moment of inertia, I. In such a case, the pile bending moment tends to be over-predicted, but the deflection is under-predicted as shown in Figure 8(c). This is due to the pile being assumed to be uncracked (much stiffer) thus attracting high bending moment and low deflection, which does not simulate the behaviour on site as the pile cracking capacity has already been exceeded. This highlights the importance of estimating the pile condition on site when performing back-analysis.

In Case 4, if the back-analysis is carried out without having prior knowledge of estimating limiting soil pressure and pile moment of inertia, I on site, the predicted pile bending moment will be grossly over-predicted as shown in Figure 8(d). However, the 'reasonable' estimation of pile deflection is merely a coincidence.

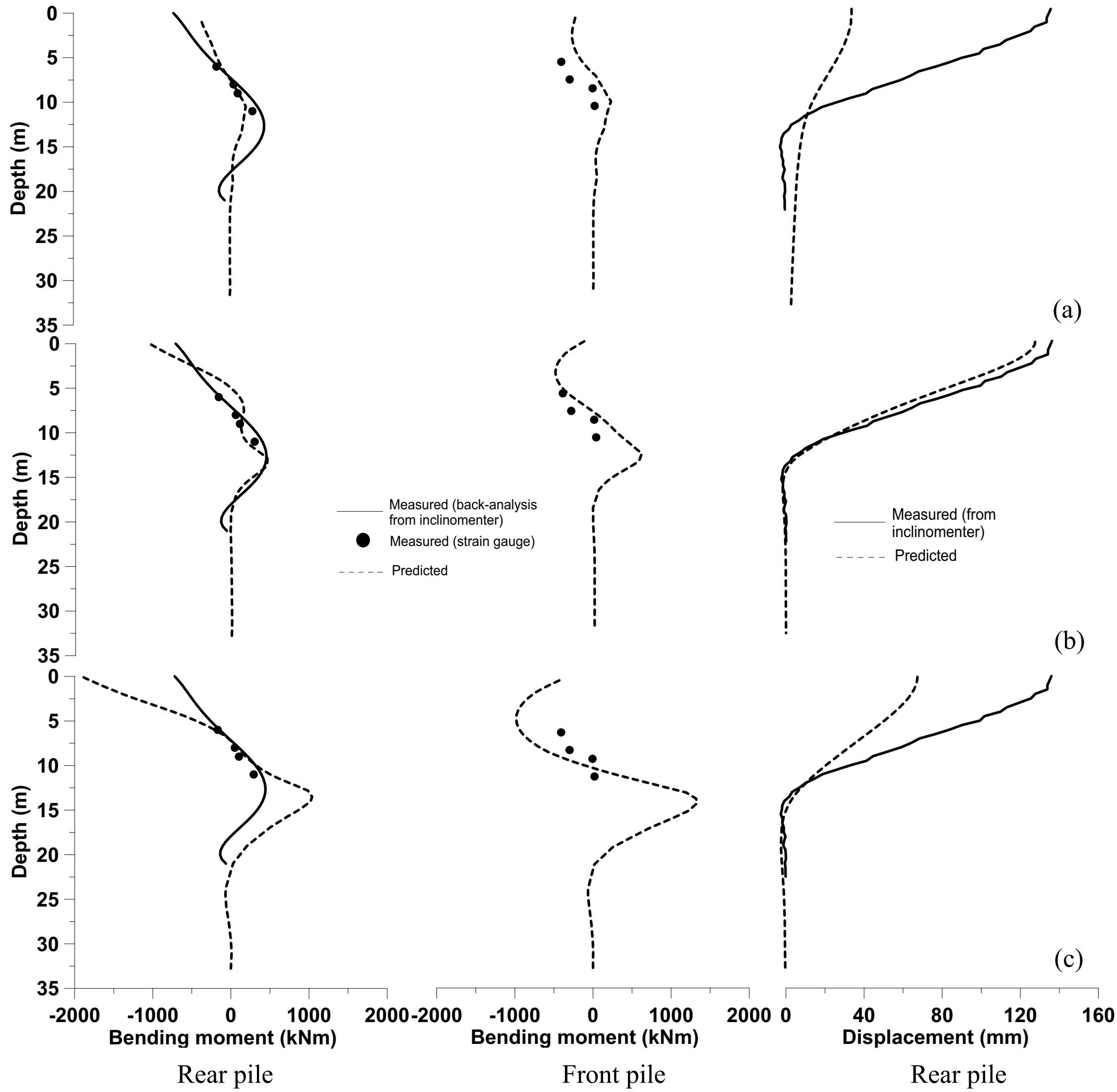

Figure 8. Profiles of measured and predicted rear and front pile bending moment and rear pile deflection

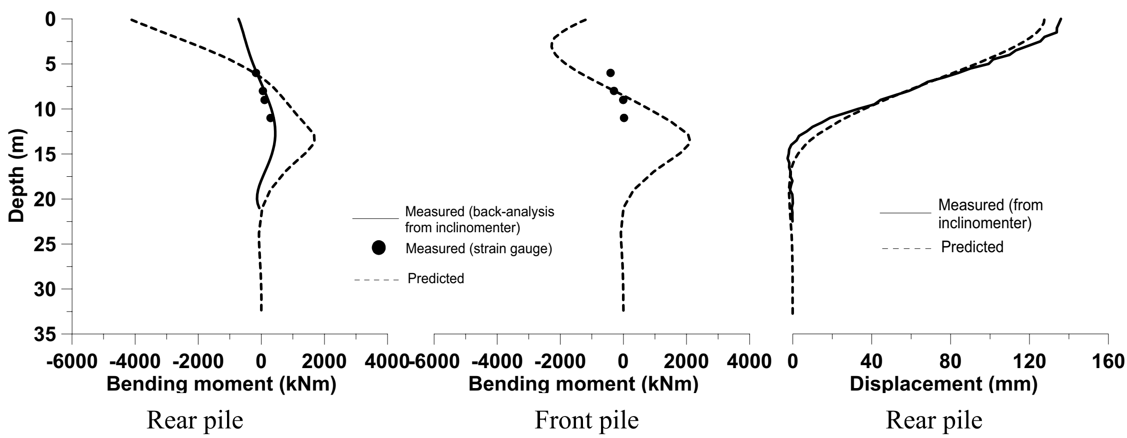

Figure 8(d). Profiles of measured and predicted rear and front pile bending moment and rear pile deflection

Nonetheless, the results are considered 'consistent' as the pile response is a reflection of an unrealistically large imposed soil movement (or pressure) without any specified limiting value. This case of back-analysis is not intuitively correct as soft soil tends to be governed by a set of limiting soil pressures that can act on a pile (Leung et al. (2006), Ong et al. (2009)).

If this case is used in design, construction costs will definitely sky-rocket for the wrong reason. Notwithstanding that, in a routine geotechnical design, it is also not desirable for a pile to be cracked by externally imposed lateral soil movement. As such, a sensible call of informed judgment is required to estimate the input soil and pile parameters to assess pile behaviour subject to imposed soil movement.

11. CONCLUSIONS

This event has successfully highlighted the importance of understanding pile behaviour at limiting condition and its implication on design procedure. It is observed that the magnitudes of pile deflection are considerably smaller than the corresponding soil movement at the same depth suggesting that the phenomenon of soil flow has occurred. At the end of the slope excavation, the measured bending moment has far exceeded its M_{ult} value. This rendered the pile group to be unfit to carry column loads. Thus, the pile group had to be demolished and replaced by another new pile group.

Various back-analysis cases have been carried out to understand pile behaviour when subject to large-strain soil deformation. It has been found that 2-D finite element analysis has under-predicted the true pile responses in the field as the natural behaviour of soil deformation is negated by the presence of the 'equivalent wall' in the analysis, resulting in relatively smaller magnitudes of lateral soil movement being imposed on the pile. It is also observed that two important parameters to consider for successful back-analyses or design situation are the limiting soil pressure, p_y and the condition of the pile (cracked or uncracked) controlled by the second moment of area, I. Reliable free-field soil movement data is also important and is considered a relatively easier parameter to obtain on site as it could be measured by in-soil inclinometer installed nearby a pile foundation.

Back-analyses performed using p_y/c_u ratio of 6 show very reasonable estimation of pile response in this study.

12. REFERENCES

Broms, B. B. 1964a. Lateral resistance of piles in cohesive soils. *Journal of Soil Mechanics and Foundation Engineering Division*, ASCE, Vol. 90, No. SM2, pp. 27-63.

Broms, B. B. 1964b. Lateral resistance of piles in cohesionless soils. *Journal of Soil Mechanics and Foundation Engineering Division*, ASCE, Vol. 90, No. SM2, pp. 123-156.

Chow, Y. K. 1996. Analysis of piles used for slope stabilization. *Int. Journal for Numerical and Analytical Methods in Geomechanics.* Vol. 20, pp. 635-646.

Chow Y.K. and Yong, K. Y. 1996. Analysis of piles subject to lateral soil movements. *Journal of The Institution of Engineers Singapore*, Vol. 36, No. 2, pp. 43-49.

Kong, F. K. and Evans, R. H. 1987. *Reinforced and prestressed concrete*. 3rd Edition. Van Nostrand Reinhold (U.K.) Co. Ltd.

Leung, C. F., Chow, Y. K. and Shen, R. F. 2000. Behaviour of pile subject to excavation-induced soil movement. *Journal of Geotechnical and Geoenvironmental Engineering*, Vol. 126, No. 11, pp. 947-954.

Leung, C.F., Ong, D.E.L. and Chow, Y.K. 2006. Pile behaviour due to excavation-induced soil movement in clay: II: Collapsed wall. *Journal of Geoenvironmental and Geotechnical Engineering*, American Society of Civil Engineers (ASCE), Vol. 132, No. 1, pp. 45-53.

Ong, D.E.L., Leung, C.F. and Chow, Y.K. 2004. Pile behav-iour behind a collapsed wall. *Proc. International Conference on Structural and Foundation Failures*, Singapore, pp. 410-421.

Ong, D.E.L., Leung, C.F. and Chow, Y.K. 2006. Pile behaviour due to excavation-induced soil movement in clay: I: Stable wall. *Journal of Geoenvironmental and Geotechnical Engineering*, American Society of Civil Engineers (ASCE), Vol. 132, No. 1, pp. 36-44.

Ong, D.E.L., Leung, C.F., and Chow, Y.K. 2007. Effect of horizontal limiting soil pressures on pile behaviour". *16th South-East Asian Geotechnical Conference (SEAGC),* 8-11 May 2007, Kuala Lumpur, Malaysia. pp. 427-437.

Ong, D.E.L., Leung, C.F. and Chow, Y.K. 2009. Pile group behaviour due to excavation-induced soil movement in clay. *Journal of Geoenvi-ronmental and Geotechnical Engineering*, American Society of Civil Engineers (ASCE), Vol. 135, No. 10, pp. 1462-1474.

Poulos, H.G. 1997. Failure of a building supported on piles. *Proc. Int. Conf. on Foundation Failures, Singapore*, pp. 53-66.

Poulos, H. G. and Davis, E. H. 1980. *Pile foundation analysis and design*. John Wiley & Sons, New York.

Deep excavations in urban areas – influence on the neighbouring structures; measurements and calculation

H. Popa
Technical University of Civil Engineering, Geotechnical and Foundation Department
Bucharest, Romania

ABSTRACT: The development of the built patrimony in urban environment supposes to affect the existing buildings. The rush for higher and higher buildings, with deeper basements, leads to deeper and deeper excavations in the vicinity of existing buildings. Retaining structures for protecting the existing built patrimony are, therefore, mandatory. The technical solutions are various and they are taking into account a lot of factors: the site, the vicinities, the soil, the groundwater, excavation depth, state of the neighbouring buildings etc.
The paper emphasizes the influence of the deep excavations on the neighbouring buildings, by giving examples on such works from Bucharest. Are included values issued from in situ measurements performed during the excavation works and comparisons between these ones and the calculated values are also shown.

1. INTRODUCTION

Building deep excavations in dense urban areas supposes a previously built retaining structure to secure the neighbouring buildings present in the influence area of the excavation.

The extension of the influence zone depends on the solution adopted for the retaining structure, which is selected taking into account several factors as: site specific, vicinities, soil characteristics, groundwater, excavation depth, state of the neighbouring buildings etc. The complexity and the number of these factors lead to the use of complex models and methods, able to consider all these parameters.

The use of complex models for the calculation of retaining walls for deep excavations in urban areas supposes also a detailed geotechnical investigation able to provide all required parameters. All these aspects can lead eventually to an error accumulation and to quite different results compared to the reality, while the influence on the neighbouring buildings is difficult to estimate accurately.

For this reason, a careful monitoring during the excavation works and during the execution of the structure is required. This monitoring has to extend on the retaining structure (displacements, stresses, structural integrity etc.), but also on the neighbouring buildings (displacements, integrity, fissures, settlements, dewatering works control etc.).

Defining the influence area of a construction should be done considering all phenomena possible to appear in the subsoil and all influences on the neighbouring structures. In case of deep excavations, the factors influencing the existing neighbouring structures depend of the required works for the deep excavation (retaining wall, excavation, dewatering etc.), as well as of the pressures generated into the subsoil by the new building (during the execution and during the operational phase), (Marcu et al., 2008).

All these factors taken together will generate finally displacements into the neighbouring subsoil, e.g. settlements of the subsoil right of the neighbouring buildings. These settlements are in addition of those already generated by the buildings due to their self weight.

The magnitude of the allowable settlements induced by a deep excavation and by a new building is, however, difficult to estimate. Theoretically, the allowable settlement for a structure is a constant. Taking into account the already consumed settlement due to self weight, the allowable settlement due to the deep excavation cannot be too large. The two values should be comprised between the limits provided by specific technical norms or standards for various structure types (e.g. EN 1997-1:2004).

However, many specialists consider that the building structure has adapted itself to the self weight settlements and that the additional settlements produced by a neighbour excavation are not much less than the maximum allowable settlements for the structure itself. On the other way, if lateral displacements occur (tilting) for the building, the allowable settlement is reduced.

Table 1 presents the allowable settlements of a construction due to a deep excavation as proposed by Chang-Yu Ou, 2006.

Table 1. Allowable settlements induced by an excavation, Chang-Yu Ou, 2006.

Foundation	Settlement, mm	Tilt angle	Angular distortion
Raft foundation	45	1/500	1/500
Individual footings	40	1/500	1/500
Brick individual footings	25	1/500	1/2500
Temporary buildings	40	1/500	1/500

2. EVALUATION OF THE INFLUENCE AREA AND OF INDUCED SETTLEMENTS

Settlements induced to an existing building by a new construction requiring a deep excavation can be divided into three categories (Marcu et al., 2008):

A. settlements due to excavation works and deformation of the retaining wall;

B. settlements due to changes in the groundwater regime (dewatering works, cut-off wall etc.);

C. settlements induced by the new building due to its own weight.

A. In general, the first category of settlements represents the greatest part of the total settlement induced to an existing structure. The magnitude of these settlements is directly linked to the horizontal deformations of the diaphragm wall, while the latest are influenced by the following factors: effects of stress changes within the soil, excavation size, soil properties, groundwater conditions, wall stiffness and bracing system, effects of preload in bracing and anchoring system, construction methods and construction workmanship.

Are well known the relationships proposed by Peck (1969) between the retaining wall displacements and the ground settlements behind the wall (figure 1).

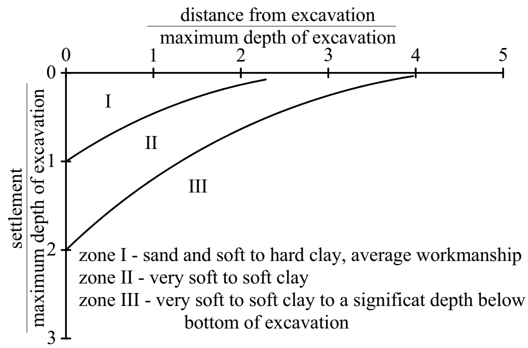

Figure 1. Observed settlements behind excavations (Peck, 1969)

Figure 2 indicates the empirical relationship between the maximum settlement of the ground and the maximum lateral displacement of the retaining wall as resulted from the analysis of various retaining works in clays (Mana and Clough, 1981).

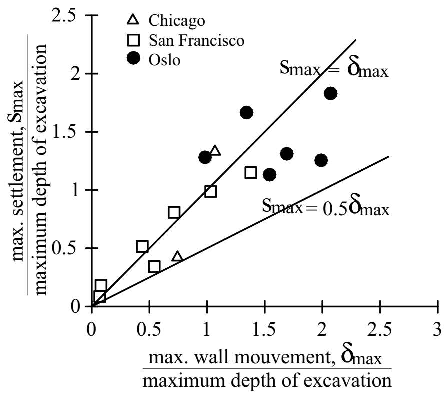

Figure 2. Empirical relationship between maximum settlement and maximum lateral wall movement (Mana and Clough, 1981)

A conclusion that can be drawn from this figure is concerning the equivalency between the maximum settlement of the ground and the maximum displacement of the wall.

Observations made on a large number of retaining structures show that it can be considered, generally on the safe side, that between the maximum settlement of the ground, s_{max} and the maximum horizontal displacement of the wall, δ_{max} there is the following relationship (Marcu et al., 2008):

$$s_{max} \approx 0.5\delta_{max}$$

B. The component of the settlement due to dewatering works is generated by the ground-water table lowering and by the fact that the soil is passing from a submerged to a saturated state, which lead to an almost double of the unit weight (figure 3). Obviously, the settlement value depends on the drawdown of the water table.

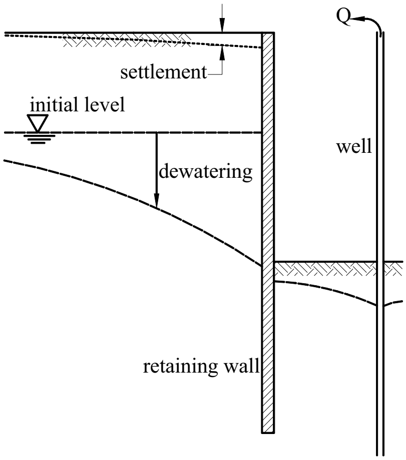

Figure 3. Influence of the dewatering works on the ground settlement

In these conditions is preferred to have a diaphragm wall embedded into an impervious layer. In such way is created an impervious enclosure on both wall and base levels and the dewatering inside the enclosure will no more affect the water level outside the excavation. Obviously, application of this solution depends on the site litho logy. For example, an impervious basis obtained using injections can be too expensive.

C. Pressures generated by the new building will induce deformation into the ground which extends outside the built area (figure 4).

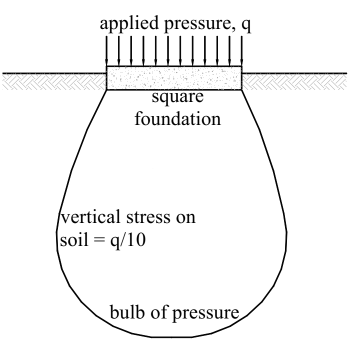

Figure 4. Pressure distribution below a shallow foundation

The extension depends on the foundation system, pressure level and soil characteristics. The influence area can be established only using complex models using methods as finite elements method (FEM) or finite differences method.

3. CASE STUDIES

Here below are presented four case studies from Bucharest, Romania.

The ground in Bucharest area is characterized generally by alluvial strata, composed of medium-soft silty clays or fine – coarse, medium dense sands.

3.1. Case 1

Case 1 presents a deep excavation for 5 underground levels using the top – down technology.

A cross section of this work is presented figure 5 (Marcu and Popa, 2004). The excavation depth is 16.20 m and the diaphragm wall is 26 m long and 0.80 m wide.

The construction procedure was top-down, which supposes to execute the excavation as the underground slabs are being built from top to down, ensuring in the same time the wall propping.

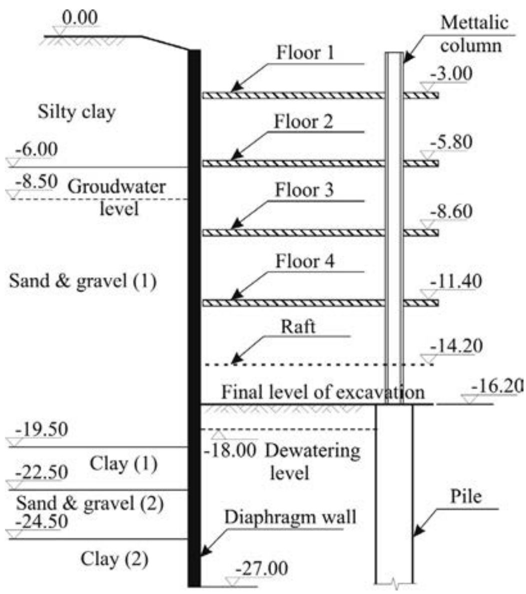

Figure 5. Cross section – case 1

The lithology and soil characteristics are shown table 2.

Table 2. Lithology and soil characteristics – case 1

Layer	Thick-ness, m	γ kN/ m^3	E MPa	ϕ`	c` kPa
Silty clay	6.0	19	25	25	30
Sand & gravel (1)	13.5	19	40	40	0
Clay (1)	3.0	20	25	22	40
Sand & gravel (2)	2.0	19	75	38	0
Clay (2)	16.0	20	75	22	50

In figure 6 is shown a comparison between the calculation results and the in situ measurements.

The calculations have been made using FEM and a Mohr – Coulomb criteria for the soil. The measured horizontal displacements of the wall were generally below the calculated ones, with a maximum of 11 mm. It can also be observed that the ground settlement behind the wall represent about ¼ of the maximum wall displacement.

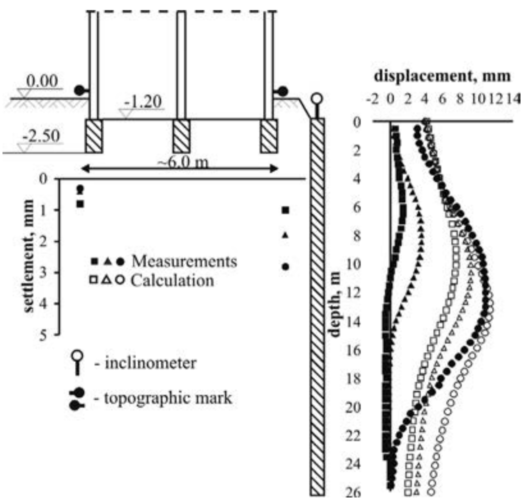

Figure 6. Measured and calculated displacements – case 1

3.2. Case 2

Case 2 presents a deep excavation for 4 underground levels. Figure 7 shows a cross section through the buildings' infrastructure, presenting also the ground lithology. The diaphragm wall is made of panels 80 cm thick and 21 m deep (Popa et al., 2008).

As for the previous case, the top – down technology has been used also. Figure 7 shows the situation corresponding to the last excavation phase, which is also the phase with maximum stresses in the wall.

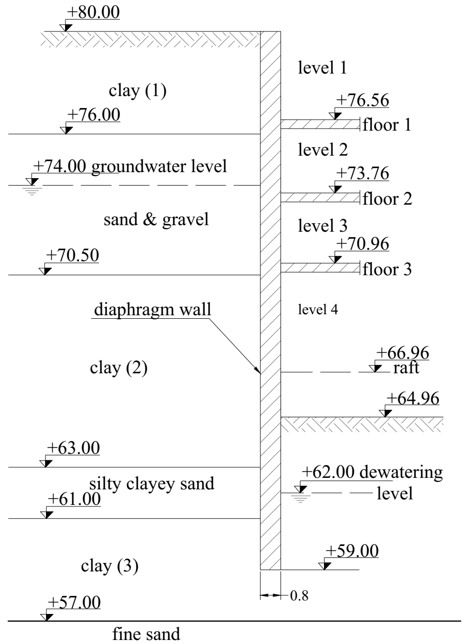

Figure 7. Cross section – case 2

The ground lithology and the design values of the geotechnical parameters are shown in table 3.

Table 3. Design values for the geotechnical parameters

layer	thick-ness, m	γ kN/ m^3	E, MPa	ϕ`	c` kPa
clay (1)	4.0	19	25	25	30
sand & gravel	5.5	20	40	38	0
clay (2)	7.5	20	50	22	50
silty clayey sand	2.0	20	75	28	20
clay (3)	4.0	20	75	22	50
fine sand	7.0	20	75	36	0

The wall calculation has been made using FEM and the same constitutive law as for the previous case.

Figure 8 shows the measured and the calculated lateral displacements of the wall during the last excavation stage (15.04 m depth). It can be seen that, in order to reduce furthermore the risks of a negative influence of the retaining wall on the neighbouring building (at about 6 m distance), a stabilization wall was previously built using cement-based injections.

Concerning the ground settlement behind the retaining wall (at about 1 m distance), the installed extensometers showed a maximum value at ground level of about 7 mm. The settlement evolution versus the depth can also be seen in figure 8 and one can note that it becomes negligible at about 2 – 3 m below walls' toe.

Marks fixed on the neighbouring building at 6 m distance indicated a maximum settlement of 0.7 mm, its integrity not being endangered.

From this point of view it can also be noted the beneficial role of the injection screen, the difference of settlements on one side and the other of the screen being substantial.

Concerning other neighbouring buildings located at about 10 m distance (without stabilization wall), a maximum settlement of about 3 mm was recorded, which is insignificant for their stability.

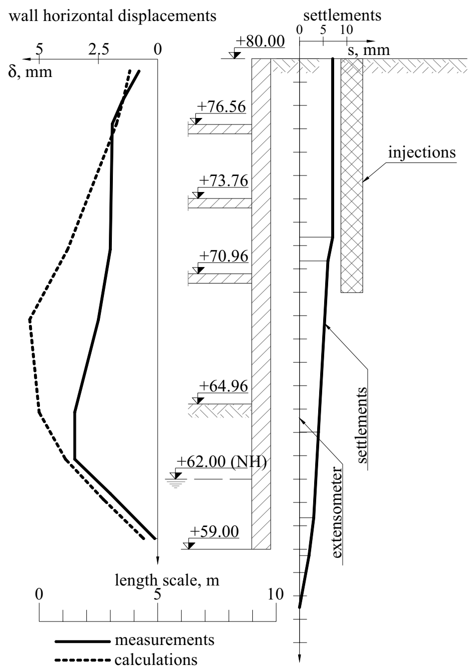

Figure 8. Measured and calculated displacements - case 2

3.3. *Case 3*

Case 3 presents also a deep excavation for 4 underground levels. Figure 9 shows a cross section through the buildings' infrastructure, presenting also the ground lithology. The diaphragm wall is made of panels 80 cm thick and 24 m deep (Popa et al., 2009).

The same construction method (top – down) has been used, but this time the excavation phases comprised 2 underground levels. Thus, in the final excavation stage the wall is propped only through the slabs no. 1 and 3 (figure 9).

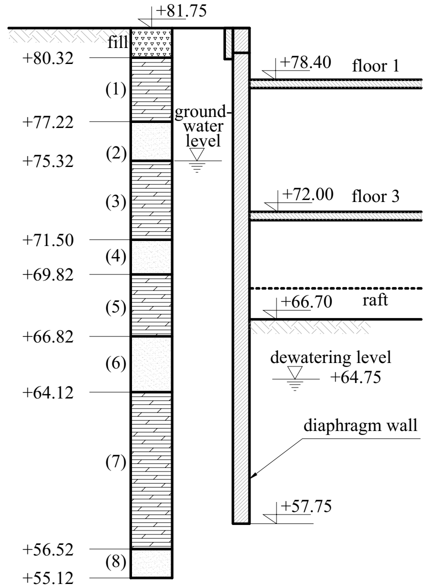

Figure 9. Cross section at final excavation stage – case 3

The geotechnical investigations led to the conclusion that the ground is composed, below a first layer of man-made fill with variable thickness from 0.50 m to 1.50 m, of a succession of cohesive or slightly cohesive soils and granular materials.

Table 4. Geotechnical parameters

layer	thickness, m	E MPa	ϕ`	c` kPa
1	2.6-3.1	11	20	45
2	1.9-2.7	25	32	15
3	4.2-6.3	11	13	45
4	1.3-2.7	30	30	15
5	3.0-3.2	14	18	36
6	0.6-2.7	32	32	5
7	7.3-7.6	23	14	33
8	1.4-1.5	40	34	5
9	0.9-2.6	25	10	45
10	1.5-2.6	40	34	5

The cohesive soils are mainly clays and silty clays with high consistency (stiff to solid), while the granular materials are fine to medium sands, sometimes silty or clayey, in medium dense state. Table 4 shows the mean geotechnical parameters for each layer, layer no. 1 being the first below the man-made fill.

The groundwater table has been found at about 7.4 ÷ 7.9 m below the ground level.

Figure 10 presents the comparison between measured and calculated values for wall displacements and ground settlements. The retaining wall has been modelled using the reaction coefficient method.

A good correlation between measured and calculated values can be seen on the graph for wall displacements. The maximum displacement zone is, however, obtained at a higher depth from calculation than from measurements.

The settlement of the neighbouring buildings has reached values comprised between 5.4 mm and 3.4 mm. The buildings are located at about 3 m distance from the diaphragm wall, and they have one underground level.

The maximum settlement of the diaphragm wall was 7.4 mm (on the side with the buildings), while on the other sides the maximum values were comprised between 5.0 and 6.4 mm. The precision of the measurements is 0.5 mm.

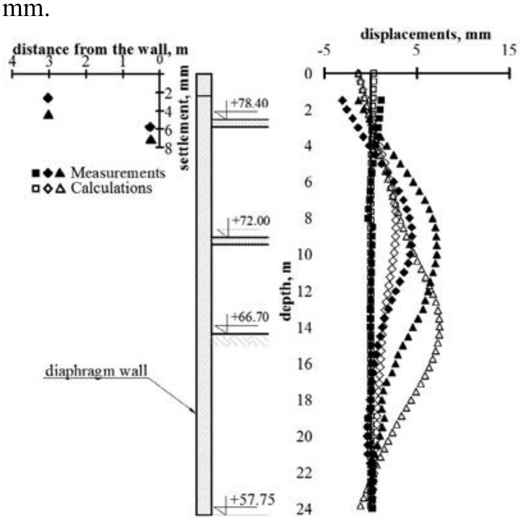

Figure 10. Measured and calculated displacements – case 3

The dewatering system was designed to pump the water only inside the enclosure, so that the outside level not to be influenced. Inside the enclosure the groundwater level has been kept around 17 m depth with ±1.0 m variation. Outside the enclosure was recorded a very slight decrease of the groundwater level. The water pumping has been monitored, no transport of solid particles being recorded.

3.4. *Case 4*

In the case 4 is presented a deep excavation for 2 underground levels. The retaining wall is single propped on top.

Figure 11 presents the cross section through the retaining structure corresponding to the final excavation phase. The diaphragm is made of secant piles made of reinforced and non-reinforced concrete (alternatively), 60 cm in diameter and 11.50 m long, disposed at 45 cm inter-axe (Popa and Batali, 2008).

The excavation is surrounded on three sides by existing buildings having various heights (between 2 and 5 stories) and on the 4th side by a highly trafficked road.

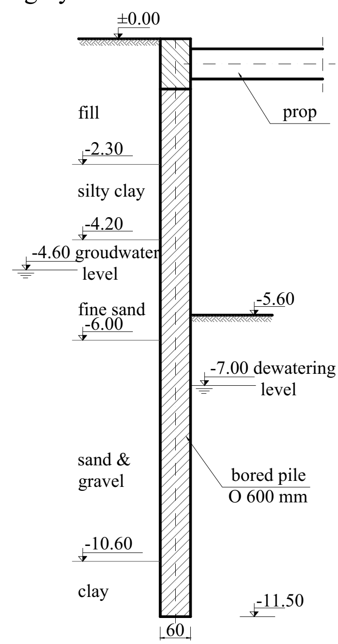

Figure 11. Cross section – case 4

The geotechnical parameters of the soils are given table 5.

Table 5. Geotechnical parameters

layer	thick. m	γ kN/m^3	E MPa	ϕ`	c` kPa
fill	2.3	16	-	-	-
silty clay	1.9	20	25	20	40
fine sand	1.8	20.5	40	25	0
sand&gravel	4.6	20.5	50	32	0
clay	2.0	20	50	17	25

The retaining wall has been modelled using the reaction coefficient method.

The comparison between calculated and measured wall displacements is shown figure 12.

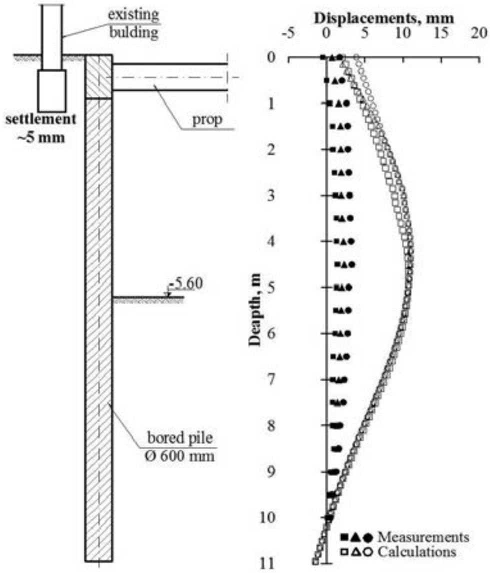

Figure 12. Measured and calculated displacements

Important differences between calculations and measurements can be noted, the measures being 35 – 40 % less than the calculated ones. This can be explained as follows:

- possible errors on the geotechnical characteristics. The geotechnical investigation has been conducted only inside the excavation, where down to 2 – 3 m depth were found ruins of previous buildings;
- difficulties in modelling the neighbouring buildings as no plans were available;
- limitation of the reaction coefficient method.

The settlements of the neighbouring buildings measured using topographic marks were of maximum 5 mm when the final excavation stage has been reached.

4. CONCLUSIONS

A precise evaluation of the influence area and of the ground displacements induced by a deep excavation is difficult event if complex analysis methods are used. From this reason, a careful monitoring of the works and of the neighbouring buildings during the execution is required. More complex the monitoring, more useful data for future analyses on similar works.

Based on the above presented case studies it can be noted that it is difficult to establish a relationship between settlement of the ground behind the wall and the horizontal displacements, even for similar structures and sites.

Thus, if the first three cases are considered (top – down technology in similar site conditions), one can note that the maximum measured settlement is comprised between 1/4 and 1 times the maximum horizontal displacement of the wall.

For the case 4 too it can be observed the equivalence between recorded settlements and maximum wall displacements.

Based on this, one can conclude that settlements have the same order of magnitude as the lateral displacement of the wall.

However, this relationship is influenced by several factors: presence or not of some neighbouring buildings, possible injections previously done for improving the soil (as for case no. 2) etc.

Another observation that can be made through the result analysis is the one concerning the differences, most of the time significant, between the calculation and measurements.

In all cases differences exist even if finite element method or reaction coefficient method has been used. There are, obviously, explanations for this:

- incertitude regarding the geotechnical parameters used for the calculations, especially when complex constitutive laws are used for the soil;
- difficulty in estimation of the initial stress state in the ground, taking into account its lithology, the presence of neighbouring structures, the execution of the retaining wall itself;
- complexity of the numerical model itself, considering all implied parameters;
- difficulty in modelling the neighbouring buildings whose architectural plans were not known (structural type, foundation type, foundation depth etc.) in most of the cases;
- limitation of the used models or methods (Mohr – Coulomb criteria or reaction coefficient method);
- three-dimensional behaviour of the retaining structure.

A second conclusion could be that no matter how complex the structure model is, there is always possibility to have differences between the real and estimated behaviour. More incertitude on the main interaction factors, more significant differences.

This offers another reason for requiring a careful monitoring of the retaining structures and their vicinities, which allows to compare rapidly the real displacements with the estimated ones and to intervene when required. The risk associated to such works is considerably reduced and the observations and measurements can considerably improve further models.

The monitoring costs, although in plus of those related to the building itself, are far less than costs of interventions, repairing, rehabilitation due to possible accidents.

5. REFERENCES

Chang Y.O. 2006. *Deep Excavation. Theory and Practice.* Taylor&Francis, 532 p.

EN 1997-1: 2004. *Eurocode 7: Geotechnical design– Part 1: General rules.*

Mana A.I., Clough G.W. 1981. Prediction of movements for braced cuts in clay. *ASCE J. Geotech. Eng.,* 107, june, 759-777.

Marcu A., Popa H. 2004. La surveillance du comportement d'une structure de soutènement et des bâtiments avoisinants dans la ville de Bucarest, *International Conference on Geotechnical Engineering*, Geo-Beirut 2004.

Marcu A., Popa H., Marcu D., Coman M., Vasilescu A., Manole D. 2008. Impact of deep excavations on the existing buildings - Impactul realizării construcţiilor în excavaţii adânci asupra clădirilor existente în vecinătate. *Revista Construcţiilor, nr. 33/2007 şi 34/2008*, ISSN 1841-1290, pp. 92-96 / 90-94.

Peck R.B. 1969. Deep excavations and tunneling in soft ground. *Proc. 7th Int. Conf. S.M.F.E.,* Mexico City, State of the art volume, 225-290. Sociedad de Mexicana de Mecanica de Suelos.

Popa H., Batali L. 2008. Paroi de soutènement en pieux sécants – calculs et mesures, *Journées Nationales de Géotechnique et de Géologie de l'Ingénieur JNGG'08* - Nantes, France, 18-20 juin 2008.

Popa H., Manea S., Batali L. 2009. Geotechnical design and monitoring of a deep excavation in Bucharest, Romania, *17th International Conference on Soil Mechanics & Geotechnical Engineering*, 5-9 October 2009, Alexandria, Egipt, pp 1985-1988, ISBN 978-1-60750-031-5.

Popa H., Marcu A., Batali L. 2008. Numerical modelling and experimental measurements for a retaining wall of a deep excavation in Bucharest, Romania, *6th International Symposium Geotechnical Aspects of Underground Construction in Soft Ground*, 10-12 April, Shanghai, China.

Surface subsidence control using grouted body method in EPB tunnelling (Case study: seventh line of Tehran subway)

K. Shahriar
Mining, Metallurgical & Petroleum Engineering Department, Amirkabir University of technology, Tehran, Iran

Gh. Sattari
Mining Engineering Department, Faculty of Graduate Studies, Islamic Azad University of South Tehran Branch, Member of young researcher club, Tehran, Iran

H. Zamani
Mining Engineering Department, Tehran University, Tehran, Iran

ABSTRACT: In recent decade, tunneling projects have increased rapidly in populated urban areas. Tunneling in shallow areas may cause hazards that should not be ignored. The most important of these hazards is ground subsidence which has the potential to damage overlying buildings and other installations/infrastructures including utilities. For preventing these problems, it should be controlled with relative standards. In this paper, for prediction of the value of subsidence in the route of seventh line of Tehran subway system, finite difference numerical method is used. Result of using numerical method for this section regarding to tunnel depth (16.1 m) is 8.52 cm subsidence that is more than the critical value (i.e. 2 cm). To reduce ground subsidence, it is proposed to improve ground quality using the grouted body method in this section. Reanalyzing after grouting showed reduction of subsidence value to its critical amount.

1. Introduction

Tunnel excavation lead to remove mass of soil and rock and incidence of significant changes in stress conditions around it. An important result of these changes is occurrence of surface subsidence. This condition is especially important in shallow tunneling in urban areas. In shallow ground this changes can develop to surface and caused surface subsidence. Therefore, many researchers investigated the surface subsidence and its various results due to tunneling. They have adopted appropriate methods to estimate its value before starting excavation and if it is more than the critical value, remedial efforts to control subsidence value considering excavation method should be made.

In general estimation methods of surface subsidence classified into three groups: empirical (such as Peck, 1969; Attewell & Woodman, 1982), analytical (such as Sagaseta, 1987; Verruijt & Booker, 1996; Loganathan & Poulos, 1998; Bobet, 2001; Park, 2005) and simulation using the numerical methods (such as FEM and FDM). Empirical methods, however, have significant shortcomings: (1) they have been developed or have been validated from a limited number of cases, (2) they should be applied only to tunnels that fall within the scope of the cases from which the method was developed, (3) only few soil and geometry parameters are taken into account, (4) they do not consider construction methods and (5) they cannot give the complete solution of a tunnel with support (Bobet & Chou, 2002). Analytical methods are based on simplifying assumptions in terms of geometry, ground structure (single homogeneous layer), selection of constitutive models and definition of boundary and initial conditions. In most cases, the researchers focused on defining the new stress field generated by the excavation; fewer works have been devoted to the evaluation of the distribution of ground movements around the opening and time effects, due to the complexity of such analyses. On the other hand, numerical techniques such as the FEM or FDM take account of heterogeneous ground structures with more sophisticated constitutive models, as well as initial and boundary conditions similar to the actual field conditions, and time dependent effects. They are particularly effective for the study of tunnels excavation in grounds that can be modeled as continuous media, with due account of non-linear behaviors, as well as complex staging and geometrical conditions (ITA-AITES, 2007). Some other efforts has been made to predict and estimate surface subsidence using laboratory model (Atkinson, 1974; Orr & Schofield, 1979) and the technique of artificial neural networks (such as Kim et all, 2001; Neaupane & Adhikari, 2006; Suwansawat & Einstein, 2006) The principle of techniques developed for control and limiting subsidence or its cause during the tunneling project contain:

- Improvement of the overall project conditions
- Improvement of ground characteristics
- Structural improvement of buildings
- Improvement while tunneling with the sequential method
- Improvement with shield tunneling; In this case, all attempts must be made to act upon the subsidence sources and prevent ground decompression:
  - at and ahead of the face
  - above the shield
  - at the tail skin

  Constructional measures to reduce the risk of ground subsidence in shield tunneling include:
  - Prevention of unbalanced pressure at the face.
  - Backfilling of the tail void
  - Ground improvement: Consists of grout injections; jet grouting; grouted body and freezing. Grouting operations aim at increasing the strength and stiffness and/or reducing the permeability of the ground.
  - Prepared stations for TBM: These are predetermined stopping locations for EPB or slurry TBM for maintenance purposes in densely urbanized areas on a long stretch and under difficult geotechnical conditions.
  - Grouting for block (boulder) stabilization: To treat loosened blocks between the cutter head and the face, which may damage the tools on the head and cause over excavation leading to local instabilities.
  - Real underground structures: Such as fore poling, jet grouting arch, pipes umbrella (pipe jacking of a series of tubes filled up by concrete), or even heavier/more complicated structures to allow an adequate reduction of risk.

in this paper the value of subsidence in the location of W_7 borehole of seventh line of Tehran subway system is predicted using finite difference numerical method (convergence-confidence method), to Considering the value of subsidence in this section which is more than the critical value (i.e. 2 cm), it is proposed a grouted body scheme regarding the tunneling excavation method (EPB Shield tunneling) to improve ground quality. Finally the results of these appropriate remedial solutions to diminish the value of subsidence examined with the same numerical method.

2. Seventh line of Tehran subway

According to studies, the final program of Tehran subway is including 9 lines (Figure 1). At this time the line five reached the full exploitation and construction operation of lines 1 and 2 is in its final stages. Executive program of lines 3, 4, 6 and 7 is also in progress. Seventh line of Tehran subway system is including 28 stations which all of them are underground. Length of tunnel counting Length of stations is 26.9 kilometers while length of tunnel without stations is 22.4 km, length of each station is 160 m. Final diameter of tunnel after lining is 8.15 m. Two earth pressure balance shield (EPB) machine with 9.14 m diameter are used for excavation of tunnel in North - South and East - West direction in this line (P.C.E[1], 2007).

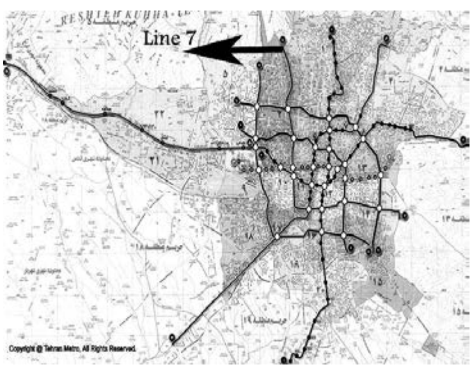

Figure 1. Lines of Tehran subway system (P.C.E, 2007).

The site explorations and surveying were performed by boring 29 boreholes and 11 test pits at proper locations along the proposed

[1] . Pajoohesh consulting engineers

route, in accordance with the specifications and requirements received from the client (P.C.E, 2007).

3. Surface subsidence due to tunneling

The relationship between surface subsidence and tunnel depth is neither simple nor linear. In reality, ground movements depend on a number of factors including (1) geological, hydro-geological and geotechnical conditions, (2) tunnel geometry and depth, (3) excavation methods and (4) the quality of workmanship and management. It is however clear that a shallow tunnel will tend to have a greater effect on surface structures than a deep one.

The construction of a tunnel inevitably affects existing ground stresses and hydro-geological conditions. This redistribution of the natural stress conditions is typically accompanied by a rapid inward displacement of the face and convergence of the tunnel walls (Figure 2) (ITA-AITES, 2007).

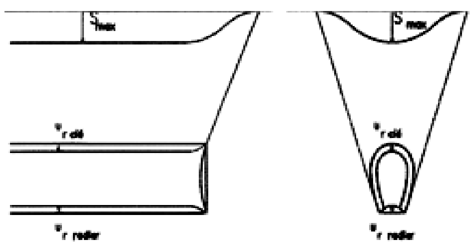

Figure 2. Displacements of the excavation profiles: basic cross-sections (ITA-AITES, 2007).

These ground response mechanisms typically lead to vertical and horizontal displacements that tend to develop at the ground surface as excavation proceeds; these results is referred to as the subsidence trough (Figure 3).

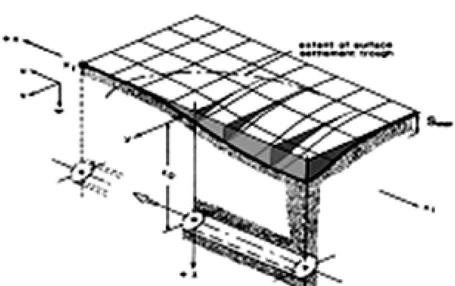

Figure 3. Three-dimensional subsidence trough (Toan, 2006).

For practical purposes, the observed three-dimensional trough is conventionally characterized by means of a transverse trough and a longitudinal trough along the tunnel center-plane (ITA-AITES, 2007).

3.1. Deformation due to closed shield tunneling

Subsidence induced by shield tunneling can be broken down into five components (Figures 4, 5):
- subsidence ahead and above the face (1)
- subsidence along the shield (2)
- subsidence at the shield tail skin (3)
- subsidence due to liner deformations (4)
- subsidence due to consolidation (long term subsidence) (5)

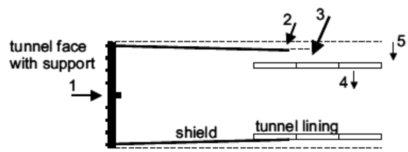

Figure 4. Principal components of ground deformation in closed shield tunneling (Moller, 2006)

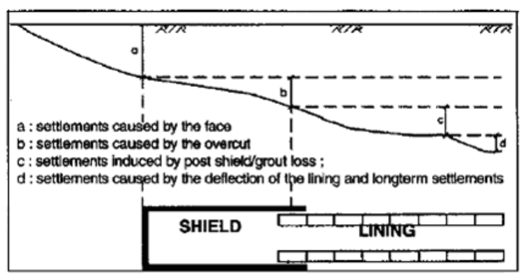

Figure 5. Evolution of subsidence along a shield (Toan, 2006).

For shield tunneling with adequate face support (such as EPB shield), the first component of ground deformation will be relatively small, but the second one may be appreciable; in particular for a somewhat conical shield or in case of over-cutting, as well if there are steering problems in maintaining the alignment of the shield. The third component of ground deformation can be minimized by grouting, but this component is strongly influenced by the experience of the crew and the ground pressure control being implemented. This third component is usually the major cause of subsidence. Component four tends to be of minor importance in relation to conventional tunneling. Component five can be of importance for tunneling in soft soils with low permeability (Moller, 2006).

4. Prediction of surface subsidence in W_7 section

This section is located in 22,650 km of the North – South direction of seventh line of Tehran subway near the W_7 station (Sanat sq) as shown in figure 6.

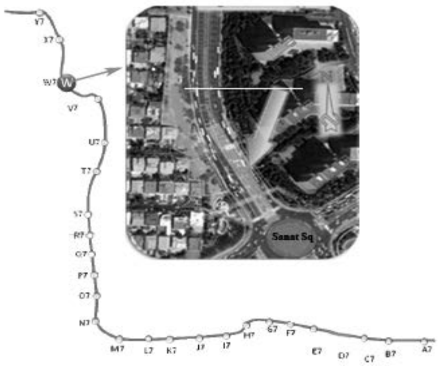

Figure 6. Location of W_7 section in seventh line of Tehran subway (P.C.E, 2007).

The important factors considered for choosing this section in this line to more study and predict surface subsidence are:
- Depth of the tunnel (16.1 m)
- tunnel placed under the groundwater table (depth of groundwater table is 6.6 m)
- Special buildings considerations near this section (existence of buildings with average degree of importance near the section)
- Variety of subsurface stratigraphy of the ground (alternation of fine and coarse grain materials)

According to the information obtained from W_7 borehole, geotechnical characteristics of observed soil are presented in the table 1. It should be mentioned that amount of dry, total and saturated unit weight of soil is 1630, 900 and 2000 kg/m^3, respectively.

As mentioned before maximum subsidence due to shield tunneling with adequate face support (such as EPB shield) occurs at the tail skin area behind the shield (Part 3 in Figure 4 or Part C in Figure 5) so consideration and analysis in this study has focused at the end of shield in tail skin area.

Table 1. Geotechnical characteristics of soil in W_7 section (P.C.E, 2007).

H*	S	ν	E	C	Φ
0 - 1.7	CLG/GCL	0.28	63.74	29.42	32.5
1.7 - 4	CLG	0.3	49.03	29.42	30
4 - 10	GCL	0.27	78.45	29.42	35
10 - 18	CLG/GCL	0.28	63.74	29.42	32.5
>18	CL	0.35	29.42	39.23	27

*In this table; H: depth (m), S: Soil classification (According to BSCS[1]), ν: Poisson Ratio, E: Modulus of Elasticity (MPa), C: Cohesion (KPa), φ: Angle of internal friction (deg)

Through draw of ground reaction curve (GRC) using finite deference numerical method, determination of deconfinement ratio and applying relaxation factor (stress reduction) equal value of wall displacement (i.e., the ratio of the current tunnel traction to the initial tunnel traction) before of support installation in numerical method we can change a three-dimensional problem to a two dimensional solution. For this purpose and to obtain values of wall displacement before support installation and drawing ground reaction curve, convergence-confidence method in FLAC^{2D} software was used. In modeling of tunnel in this section regarding available parameters the Mohr-Coulomb model was used.

Regarding to excavation diameter (9.14 m) and outer diameter of lining (8.85 m) in this line and manner of lining position, the gap in roof of tunnel in tail skin area is 29cm (figure 7).

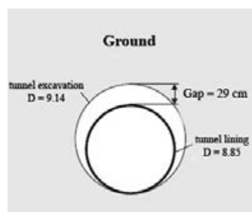

Figure 7. Physical gap between excavation diameter and outer diameter of lining.

Figure 8 shows the GRC in this section. With consideration of max displacement in roof of tunnel due to perfect stress reduction and amount of deconfinement ratio (equal 0.77), value of wall displacement before support installation is 18 cm. therefore stress reduction ratio (equal to this displacement, i.e. 18 cm) obtained 99 percent.

1 . British Soil Classification System

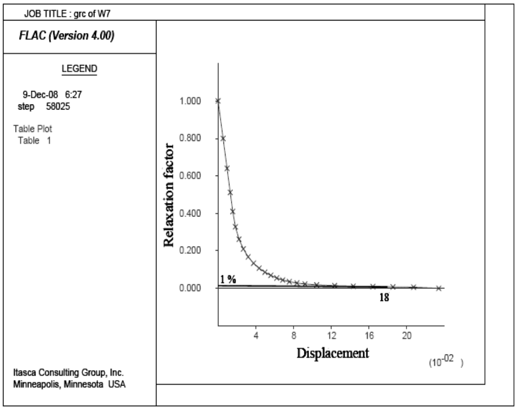

Figure 8. Ground reaction curve in W_7 section.

The next stage after applied reduction stress equivalent to the tunnel convergence is installing support system. For support system of this tunnel, segmental lining with 35cm thickness and outer diameter of 8.85 m will be used. Properties of these segments are given in table 2.

Table 2. Properties of prefabricated segments (P. C. E, 2007).

Elastic Modulus, GPa	UCS, MPa	Passion ratio	Unit Weight, ton/m^3
22.5	34.32	0.15	2.4

In this study analyzes were done in 1 meter of length of support system. After modeling in according framework, max surface subsidence in this section attentive to occurred displacement in roof of tunnel is 8.59 cm. Figure 9 shows the surface subsidence profile in this section.

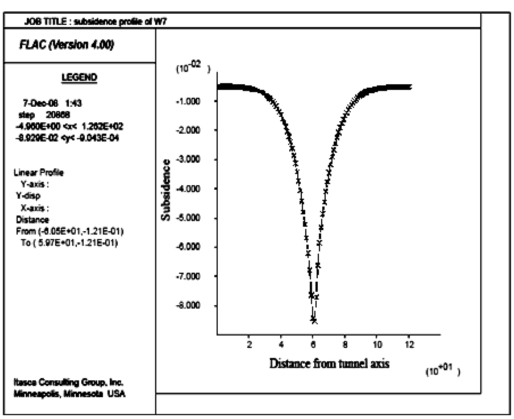

Figure 9. Surface transverse subsidence profile.

As shown above max surface subsidence value calculated (i.e. 8.59 cm) is more than critical value[1] (i.e. 2 cm) where the tunnel axis is under the street and it has suitable distance from surface buildings. Therefore, in this section during the tunnel construction suitable measures such as ground improvement to control and mitigate of surface subsidence damages should be performed.

5- Proposed grouted body scheme to reduce the surface subsidence

Regarding value of subsidence in this section that is more than the critical value and to reduce its magnitude, we proposed two grouted body scheme to improve ground quality according tunneling excavation method (EPB Shield tunneling). In the following section effect of these appropriate measures (remedial solutions) in decreasing the value of subsidence investigated with the same numerical method.

As mentioned in the introduction, there are various and different measures for prevent and control of ground surface subsidence. One of the suitable structural measures for ground improvement is grouting operations. Grouting caused improvement the ground quality (i.e. increase strength and stiffness and decrease permeability). It makes possible advancement of excavation in a safe condition and without delay. Among grouting operations method in EPB and Slurry shield tunneling is grouted body performing around the tunnel.

Generally, TBM drives should avoid the involvement of extra work (ground improvement) as much as possible. But in specific cases, grouted body may form an integral part of EPB and slurry shield drives.

Figure 10 shows six possible cases of executing grouted bodies. Case 1 has only a modest grouting in the roof area, since the ground has a sufficient average cohesion but locally mixed with materials possessing no cohesion. This unsystematic consolidated body needs no statically calculation. Cases 2 to 5 indicate the grouted bodies with a well defined

[1] . In according to survey done, the critical value of surface subsidence under surface building is 1cm and under street is 2 cm in Tehran city.

shape and size and clearly defined shear strength parameters. The most important and most frequently applied body is presented by case 2 and 3. Case 2 is considered preferable by Kovári, however, Kochen (1992) deemed that geometry in Case 3 is better. Grouted bodies according to the cases 4 and 5 are extremely worked intensive and costly. The case 6 shows the prepared stations for the preplanned maintenance work in the TBM's working chamber (Toan, 2006).

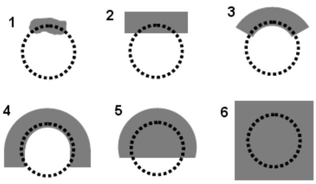

Figure 10. General layout of grouted bodies (Kovári, 2004).

In summary on the discussion about the grouted bodies, following major benefits can be pointed out:
- reduction of support pressure
- high safety against collapse
- reduced ground subsidence
- safety during work in the chamber
- control of time schedule

It should be recalled that, grouting operations for ground improvement in TBM tunneling are uncommon and always expensive; therefore this kind of work should be specified in the technical specifications.

Systematic grouting operations can be executed from inside or outside the TBM as shown in Figure 11.

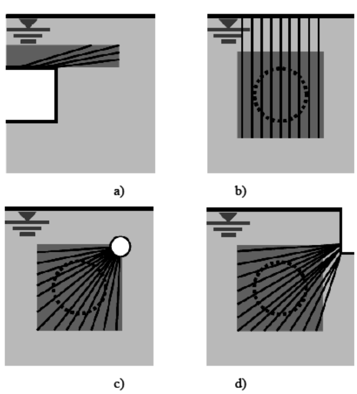

Figure 11. Injection schemes: a) From inside TBM; b) from the surface; c) from an auxiliary adit; d) from a vertical shaft (Kovári, 2004).

According the subjects was presented and considering the type of soil (coarse grain sediments) in this area that gives possibility of grout injection, two grouting schemes as shown in figure 12 are investigated.

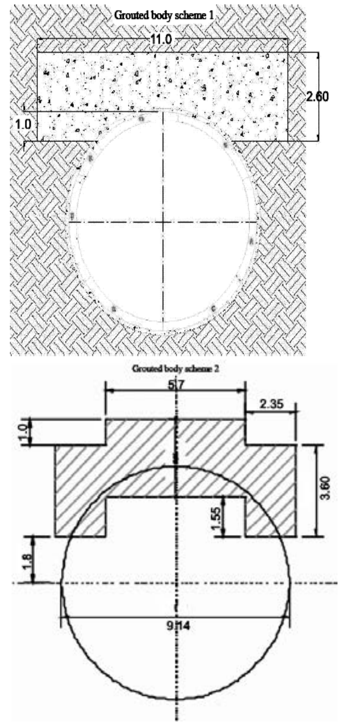

Figure 12. Suggested grouted body schemes.

As shown in figure 12 the pattern of these schemes derived of case 2 and 3 of figure 10 that most important and frequently applied body schemes. To determine the dimensions of the pattern presented, the experiences in Turin Metro are used (Concilia, 2005).

As mentioned before, grouting caused improvement the quality of ground (increase strength and stiffness and decrease permeability), in Tehran Coarse grain sediments studies show that grouting operations caused to increase stiffness value between 10–14 times as much and 6–10 times as much of strength value (A'li, 1999).

5.1. Prediction of surface subsidence for case 1 of grouted body schemes

Figure 13 shows the GRC for case 1 of grouted body schemes. As observation amount of stress reduction (equal of 4.62 cm displacement), 95.5 percent was calculated.

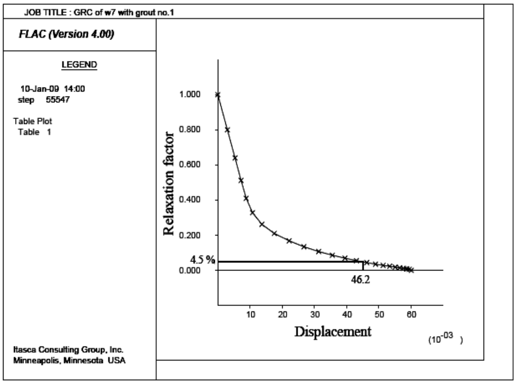

Figure 13. Ground reaction curve for case 1.

Figure 14 shows the surface subsidence profile for case 1. Max surface subsidence according to observed displacement in roof of the tunnel (i.e. 4.62 cm) is 3.45 cm.

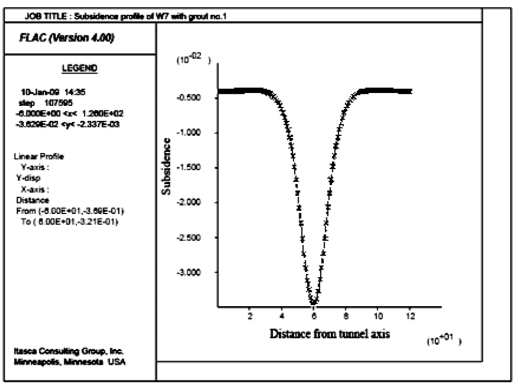

Figure 14. Surface transverse subsidence profile in case 1.

As figures 13 and 14 showed, max surface subsidence for case 1 is more than critical value (i.e. 2 cm) so case 2 of grouted body schemes designed.

5.2. Prediction of surface subsidence for case 2 of grouted body schemes

Figure 15 shows the GRC for case 2 of grouted body schemes. As observed stress reduction 95.5 percent was obtained (equal of 2.68 mm displacement). Figure 16 shows the surface subsidence profile for case 2. Max surface subsidence regarding to observed displacement in roof of tunnel (i.e. 2.68 cm) is 2 cm.

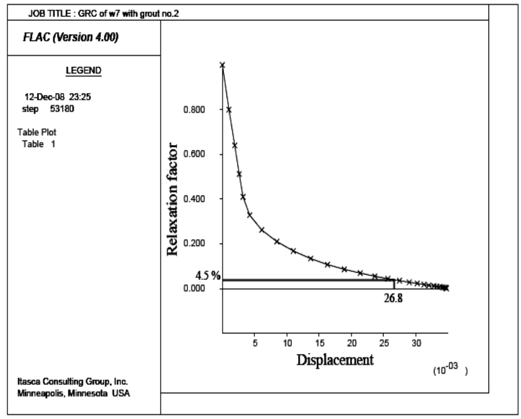

Figure 15. Ground reaction curve for case 2.

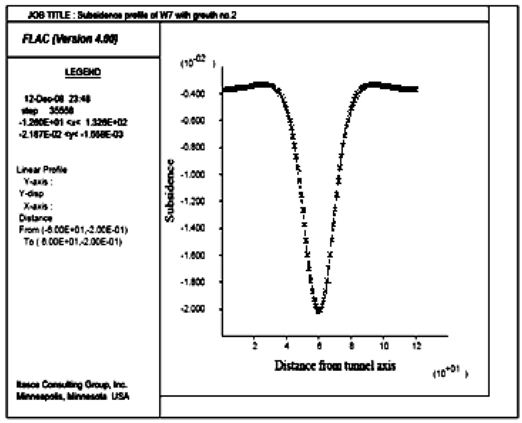

Figure 16. Surface transverse subsidence profile in case 2.

Value of max surface subsidence for case 2 of grouted body schemes, for the situation where the tunnel axis under the street is equal to critical value, so this pattern can be applied for control of subsidence in this section.

6. Technical consideration

The calculated max surface subsidence before and after grouting in this section is given in table 3.

Table 3. Max surface subsidence calculated before and after grouting

Time of analyze		Max surface subsidence, cm
Before grouting		8.59
After grouting	grouting body scheme 1	3.45
	grouting body scheme 2	2

Value of max surface subsidence for case 2 of grouted body schemes is equal to critical value so this pattern can be applied for control of subsidence in this section successfully.

It should be recalled that, grouting operations for ground improvement in TBM tunneling are unusual and always expensive; therefore this kind of work should be used only in special technical conditions.

Regarding tunnel excavation using EPB shield and capability of these shields in control of pressure in tunnel face that causes significant decreasing of ground deformation in this area so can be rely on results of 2D analyze in this study thoroughly.

The proposed grouted body schemes designed according pre-construction information as a strategy of control of surface subsidence. It is quiet obvious that this results can be re-evaluated carefully with increasing more information during tunnel construction.

7. Conclusion

- Max surface subsidence in this section according to occurred displacement in roof of tunnel before install support system is 8.59 cm.
- Value of max surface subsidence calculated (i.e. 8.59 cm) is more than critical value (i.e. 2 cm). Therefore, during the tunnel construction suitable measures should be performed such as ground improvement to control and mitigate of surface subsidence in this section.
- There are various and different measures for prevention and control of ground surface subsidence. One of the suitable structural measures for ground improvement in shield tunneling is grouting operations. Among of grouting operations methods in shield tunneling with adequate face support (EPB and Slurry shield), performing the grouted body scheme around the tunnel is usual.
- Performing of grouting operations cause improvement the quality of ground and decrease surface subsidence. According to grouting plan (normal or strong) and thickness of grouting, value of subsidence decrease between 35 – 75 percent.
- With proposed grouted body scheme, max value of surface subsidence decrease from 8.59 cm to 2 cm (equal of critical value).

8. References

A'li, A.R. 1999. Investigation of consolidation grouting in sediments as an auxiliary support system around the tunnel. MSc Thesis, faculity of mining engineering, Tehran University.

Chou, W.I. & Bobet, A. 2002. Predictions of Ground Deformations in Shallow Tunnels in Clay. *Tunneling Underground Space Technol*, Vol. 17, pp. 3–19.

Concilia, M. 2005. Construction of Lot 5 of the Turin Metro Line 2 Tunnel. Injection of Fines into the Cutterhead Chamber Extends the Ground Range of Application of EPB TBMs. *FELSBAU*.

ITA/AITES Report 2006 on Settlements induced by tunneling in Soft Ground. *Tunneling and Underground Space Technology*, Presented by the WG ‘‘Research; Eric, Leca. & Animateur: Barry, New. 2007. Vol. 22, pp. 119–149.

Kovari, K. & Ramoni, M. 2004. Urban Tunneling in Soft Ground using TBM's. Key note lecture at International Congress on Mechanized Tunneling: Challenging Case Histories. Politecnico di Torino, Italy 16-19 November.

Loganathan, N. & Poulos, H.G. 1998. Analytical Prediction for Tunneling-Induced Ground Movements in Clays. *Journal of Geotechnical and Geoenvironmental Engineering*, Vol. 124, No. 9, pp. 846–856.

Moller, S. 2006. Tunnel Induced Settlements and Structural Forces in Linings. Phd thesis, institute fur geotechnik der universitat, Stuttgart.

Neaupane, K.M. & Adhikari, N.R. 2006. Prediction of Tunneling-Induced Ground Movement with the Multi-Layer Perceptron. *Tunnelling and Underground Space Technology*, Vol. 21, pp. 151–159.

Pajoohesh consulting engineers. 2007. Report of Performance Method of Seventh Line of Tehran Subway. Tehran, Iran.

Pajoohesh consulting engineers. 2007. Report of Geotechnical Study of Seventh Line of Tehran Subway. VOL 1 & 2, Tehran, Iran

Park, H.H. 2005. Analytical Solution for Tunneling-Induced Ground Movement in Clays. *Tunnelling and Underground Space Technology*, Vol. 20, pp. 249–261.

Suwansawat, S. & Einstein, H.H. 2006. Artificial Neural Networks for Prediction the Maximum Surface Settlement caused by EPB Shield Tunneling. *Tunnelling and Underground Space Technology*, Vol. 21, pp. 133–150.

Toan, N.D. 2006. TBM and Lining-Essential Interfaces. Postgraduate master course in Tunneling and Tunnel Boring Machines, V Edition 2005-06, Politecnico di Torino, Italia.

Back Analysis of Tehran Metro Tunnel Construction using the FLAC-3D

N.Shariatmadari
Department of Civil Engineering, Iran University of Science and Technology, Tehran, Iran

M.Mahdi
Department of Civil Engineering, Iran University of Science and Technology, Tehran, Iran

ABSTRACT: An important aspect of planning for shallow tunneling under urban areas is the determination of likely surface movements and interaction with existing structures. Back analysis of built tunnels that their settlements magnitude is available, could aid the designers to have a more accuracy in future projects.

In this paper, one single Tehran Metro Tunnel (at west of Hor square, Jang University Street) was selected. At first, surface settlements of this tunnel were measured in situ. Then this tunnel was modeled using the commercial finite deference software FLAC-3D. Finally, Results of modeling and in situ measurements compared for verification.

1-INTRODUCTION

The need for tunnel design and construction in urban areas, mainly for transportation purposes, has increased markedly in recent years, especially in Tehran city. New tunnels are often required in close proximity to the existing ones and construction must be carried out without damage either to the buildings above the excavation field or to the subsurface infrastructures. During the design stages it is therefore necessary to predict possible interaction effects.

Due to the high interaction between tunneling and existing structures in urban areas, tunneling operations in urban areas draws much attention. This paper describes a thorough analysis of the tunneling influence in soft soils on surface settlements. A combination of in situ observations and numerical modeling was previously adopted to analyze such problem.

The surface settlements, S above a single tunnel constructed in soft ground are usually assumed to follow an inverted Gaussian curve, i.e.

$$S = S_{\max} \exp(-y^2 / 2i^2) \qquad (1)$$

Where S_{max} is the maximum settlement (over the tunnel axis), y is the vertical distance from the tunnel axis and i is the width of the settlement trough (Attewell & Farmer, 1975).

The source of these settlements is the "volume loss" which occurs at the tunnel. It is defined as the additional volume of soil which is excavated over the volume required to house the final lining. As excavation proceeds, the soil ahead of the face is unloaded so it tends to move inwards. Losses also occur behind the face due to the nature of the shield in which the excavation is being carried out. Many field studies have confirmed Equation 1 to be acceptable for green field sites (Mair et al., 1993; Atkinson & Mair, 1981) while, for structures in urban situations, Equation 1 is no longer valid.

The development of transportation systems in Great Tehran city requires the construction of metro tunnels.

In this paper, one single Tehran Metro Tunnel (at west of Hor square, Jang University Street) was selected. At first, surface settlements of this tunnel were measured in situ.

Then this tunnel and that's circumstance was modeled using the commercial finite deference software FLAC-3D. Finally, Results of modeling and in situ measurements compared for verification.

In situ Geotechnical parameters are as below:

$C = 0.3$ kg/cm² $\quad \varphi = 40°$ $\quad \gamma = 20$ gr/cm

2. FIELD SURFACE SETTELMENTS MEASURING

For field surface settlements measuring, surveying technique was selected. In order to achieve the best results in analysis and tracing the surface settlements profiles, 70 points were selected on the field ground surface and dug for rods installation. Recoding the height differences before and after the tunnel construction showed the surface displacement. In this case settlements measured after 2 years from the tunnel construction.

Finally, model verification has been done by comparison between settlements from 3D model and In situ measurements at S1, S2 and C points (Fig 4 to 6).

Figure 1 shows the Locations of points that selected for field measurement on the street surface. The magnitude of this settlement will come in figures 4 to 6 (compared with modeling results).

Using in situ construction procedures, at first the head of the main tunnel with the step of 1 meter is excavated. Having shotcreted the head, the bench excavated (with step of 1 meter), shotcreted and finally lined with reinforced concrete. (Figure 2).

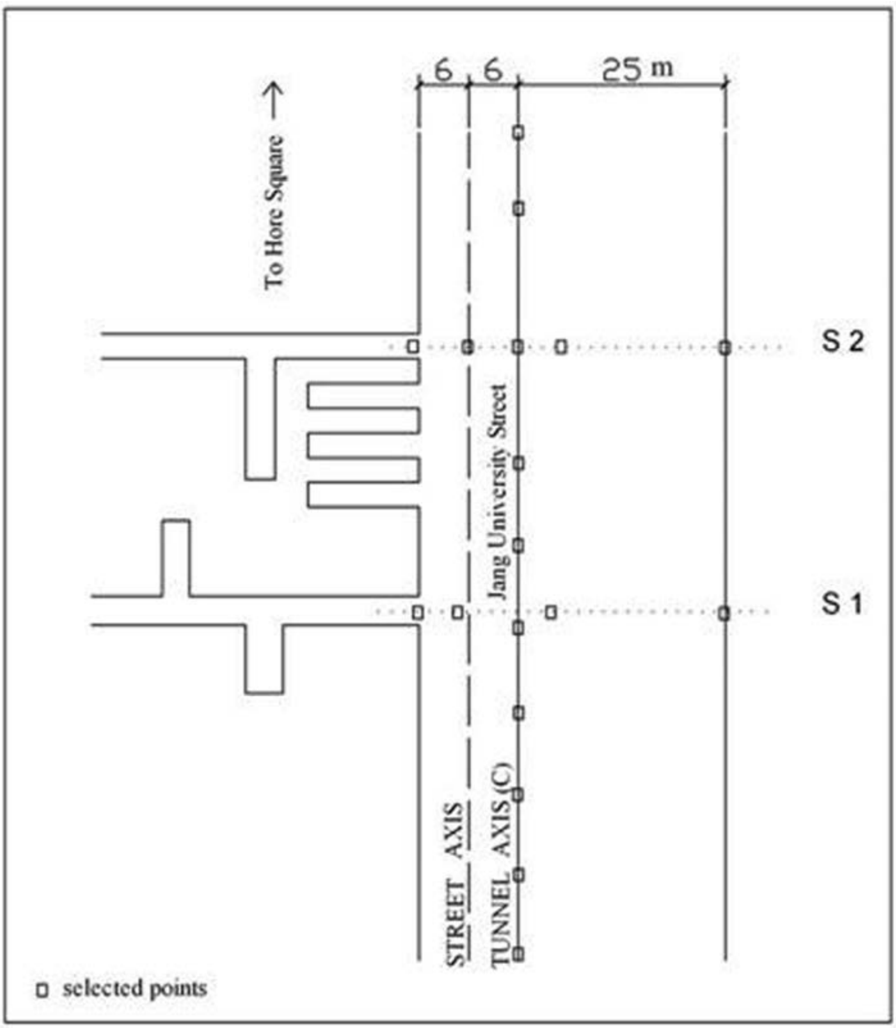

Figure 1. Locations of points for field measurement

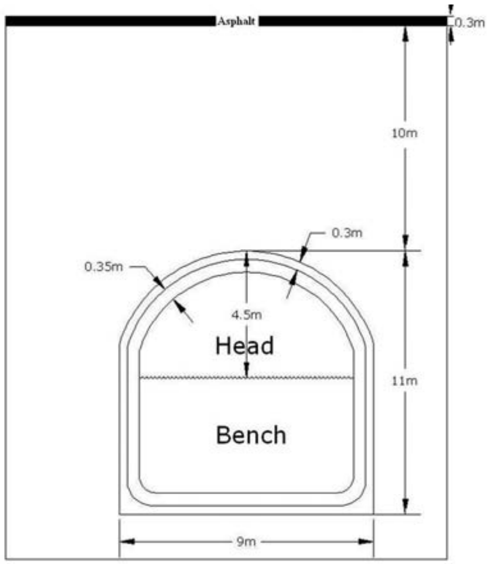

Figure 2. tunnel geometry

3. MODELING WITH FLAC-3D

Fig. 3 shows the mesh used for the tunnels analysis. concerning the boundary conditions, the displacements are constrained in three directions at the bottom, while zero horizontal displacement is imposed at the lateral boundaries (figure 3).

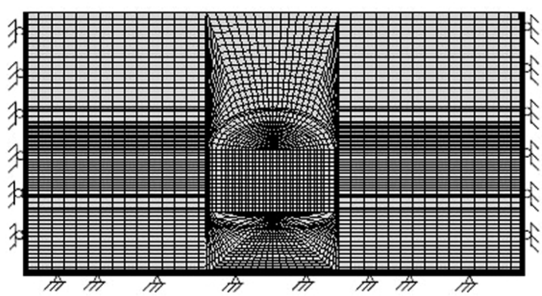

Figure 3. Mesh used in the analysis of tunnels

Table 1 summarizes the properties of the soil and the lining used in this study. The soil corresponds to GW-GM. The coefficient of the lateral stress (K0), thickness of the shotcrete, thickness of the lining and thickness of the asphalt are equal to 0.5, 0.35 m, 0.30 m and 0.40 m, respectively. In all calculations, drainage analysis was performed, meaning that no excess pore water pressures were generated. Consequently, strength parameters based on effective stress were used as indicated in table 1. The results therefore represent the settlements likely to occur over a long period of time. In all calculations, the analysis procedure began with the definition of initial effective stresses prior to tunnel construction, using ratio value of effective horizontal to vertical stress K_0 equal to 0.5.

Table 1. Properties of the soil ratio, shotcrete, lining and asphalt materials

Material	E0 (MPa)	ν	C(kPa)	φ, deg	Dilatancy Angle,deg	Unit Weight (kN/m3)	Type of Behavior
Soil	125	0.3	30	40	5	20	Mohr Coulomb
Shotcrete	20000	0.25	-	-	-	24	Linear Elastic
Lining	26000	0.25	-	-	-	25	Linear Elastic
Asphalt	20000	0.25	-	-	-	24	Linear Elastic

So, seven load stages are accounted as below.

1. Construction of the first tunnel head, simulated by activating the tunnel shotcrete and deactivating the soil elements inside the first tunnel head.
2. Exertion of volume loss and activating the tunnel shotcrete for the first tunnel head.

3. Construction of the first tunnel bench, simulated by the tunnel shotcrete activation, and deactivating the soil elements inside the first tunnel bench.

4. Exertion of volume loss and activating the tunnel shotcrete for the first tunnel bench.

5. Activating the first tunnel lining.

Each load stage was carried out using standard nonlinear solution techniques available in FLAC.

4. RESULTS

Figures 4 to 6 show the comparison of two way ground surface movements' measurements.

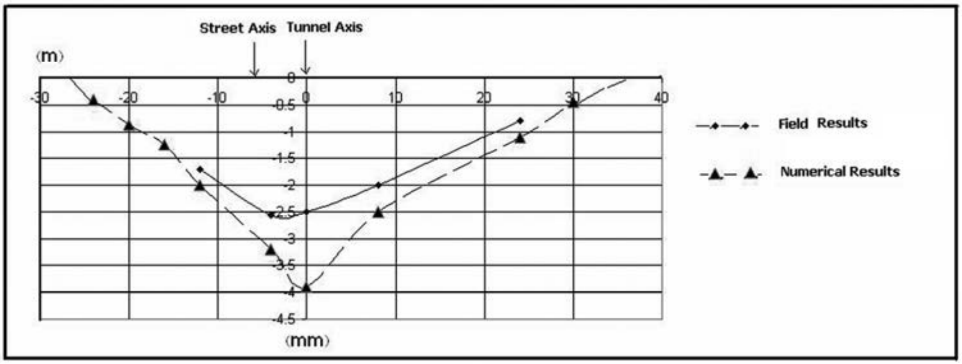

Figure 4. Comparing measured and estimated surface ground settlements in section S1

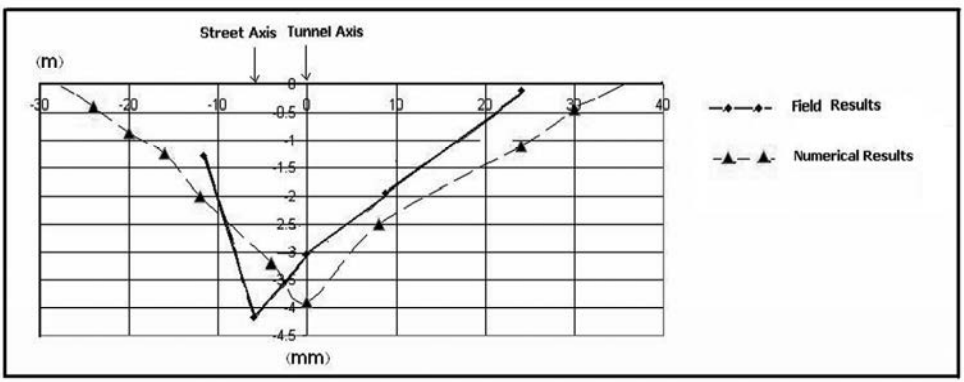

Figure 5. Comparing measured and estimated surface ground settlements in section S2

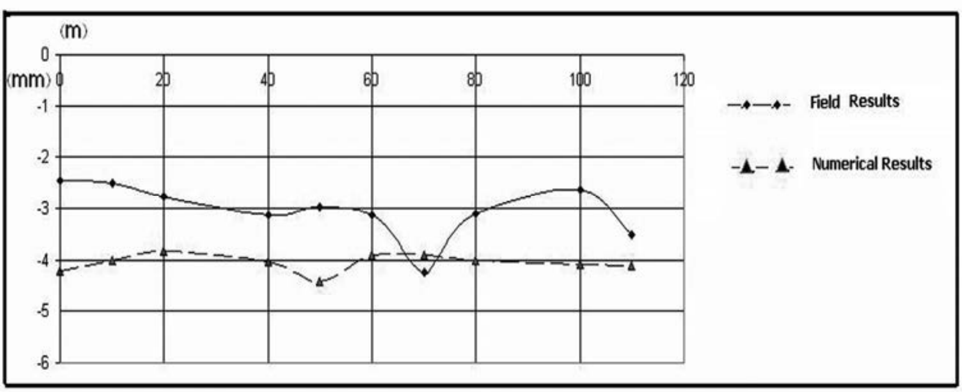

Figure 6. Comparing measured and estimated surface ground settlements section in tunnel axis

Figures 4 to 6 show that the deviation of the results is usually 1-2 mm. This deviation is so little, indicating that the accuracy of the built model is so appropriate.

The deviation may be caused by factors such as: the constant traffic load applied in the model, probably soil parameters variety in layers and existence of zones, likely local groundwater presence, size of model meshes, model dimensions, shotcrete and lining parameters variety in operation, and other variables in field that cannot be considered explicitly in the modeling.

5. CONCLUSIONS

The assessment of the influence of tunneling on adjacent structures is an important issue in urban areas. Therefore, it is necessary to monitor the ground deformation during tunneling not only to ensure the safety of construction but also to provide important information for feedback analyses.

The results of present analyses and field measurements showed that both methods could be used for the preliminary design of NATM tunneling for the conditions used in this research. And the numerical modeling confirmed that the soil laboratory tests and field measurements that performed for soil parameters extract has a good accuracy.

Consequently, we can be sure about the built model, since the resulted deviation is so little to be neglected. These neglect differences also could be due to reasons such like, the constant assumed traffic loading, presence of zones with different mechanical properties, errors due to numerical modeling and etc.

6.REFERENCES

Prinzl & A.R.A Gomes "The requirement of Protective measure for building affected by ground movements due to shield Tunneling in soft ground" Proc.Tunnels and Metro Polises Edited by A.Negro Jr & A.A.Ferreira , vol.2 A.A.Balkema 1998

D.K. Koungelis & C.E. Augarde "Interaction between multiple tunnels in soft ground" .School of Engineering, University of Durham, UK 2004

D.N. Chapman, S.K. Ahn, and D.V.L. Hunt" Investigating ground movements caused by the construction of multiple tunnels in soft ground using laboratory model tests " , Canadian Geotechnical Journal, volume 44, Number 6 jun 2007, ISSN 1208-6010 , Pages 513-523

M.Marata , T.Okazawa " shallow twin tunnel for six lanes beneath densely residential area " Proc.North American Tunneling ,Edited by Levent Ozdemir,A.A.Balkema ,1996.pp 371-380

Xu Guogang, Ma Guoyan, Li Qingbo and Cui Zhifang , " Predicting the settlements above twin tunnels constructed in soft ground " , *Tunnelling and Underground Space Technology*, *Volume 19, Issues 4-5*, *July-September 2004*, *Page 378*

M. Karakus and R. J. Fowell , " Effects of different tunnel face advance excavation on the settlement by FEM " , *Tunnelling and Underground Space Technology*, *Volume 18, Issue 5*, *November 2003*, *Pages 513-523*

Pande G.N,William J.R " Numerical Methods in Rocks Mechanics " John Willy and Sons Ltd 1990.

New B.M ama O'Riely M.P "Tunneling induced ground movements-Predicting their magnitude and effects " .Ground movements and structures vol.4 ,Edited by James D.1991

Tunnelling effect on underground pipelines – a closed-form solution

Y. Wang, Q. Wang
Department of Building and Construction, City University of Hong Kong, Hong Kong, China

K.Y. Zhang
Institute of Geotechnical Engineering, Hohai University, Nanjing, China

ABSTRACT: This paper develops a Winkler-based model for pipe-soil-tunnelling interaction in response to an arbitrary ground settlement profile that is represented by a polynomial function. Governing differential equations are derived, and their closed-form solutions are provided. The commonly used Gaussian type of the settlement profile is shown to be a special case of arbitrary settlement profile, as it can be expressed as an expansion of a polynomial series. The closed-form solutions are validated against finite element models. The model and closed-form solutions are used to explore the effect of different settlement profiles that can be interpreted from the same set of field settlement observations. It is shown that the pipe responses differ significantly when different settlement profiles are used.

1. INTRODUCTION

The underground space in urban areas is frequently congested with utilities, including pipelines and conduits that are affected by underground construction, e.g., tunnelling. Tunnelling-induced ground movements cause pipeline deformation that may disrupt the conveyance of important services and resources (e.g., water, electric power, and telecommunications) and threaten the safety and security of urban inhabitants (e.g., flooding and leakage of combustible gas from ruptured or leaking mains). To evaluate the effects of tunnelling-induced movements on underground utilities, it is necessary to 1) characterize the distributed settlement at shallow depths typical of most utilities, and 2) account rationally for the interaction between pipeline and soil associated with tunnelling-induced patterns of soil movement.

There has been substantial work performed on the characterization of ground movement patterns caused by tunnelling (e.g., Peck, 1969; O'Reilly & New, 1982; New & O'Reilly, 1991; Mair et al., 1993). As shown in Figure 1, distribution of ground settlement, S(x), transverse to the longitudinal axis of the tunnel is commonly described by a Gaussian curve:

$$S(x) = S_{\max} \exp[-\frac{1}{2}(\frac{x}{i})^2] \qquad (1)$$

where S_{max} is the maximum settlement, x is the horizontal distance from the tunnel centerline, and i is distance between the tunnel centerline and inflection point of the Green field settlement trough profile. More recently, investigators have pointed out that approximating the settlement profile by means of a Gaussian curve may lead to errors in estimating settlement (e.g., Celstino et al., 2000; Jacobsz, 2002), and modifications of the Gaussian curve have been proposed to provide a better fit with field measurements and centrifuge test data (Vorster, 2005). However, existing analytical pipe-soil-tunnelling interaction models, such as the Winkler-based model by Attewell et al. (1986) and the elastic continuum model by Vorster et al. (2005) and Klar et al. (2005), were developed only for a Gaussian settlement profile.

This paper develops a Winkler-based model for pipe-soil-tunnelling interaction in response to an arbitrary ground settlement profile. After this introduction, the Winkler-based pipe-soil-tunnelling interaction model is briefly reviewed, followed by development of closed-form analytical solutions for an arbitrary ground settlement profile. Then, the closed-form solutions are validated against finite element simulation results. Finally, the effects of different ground settlement profiles are explored.

2. WINKLER-BASED PIPE-SOIL-TUNNELLING INTERACTION MODEL

Figure 2a shows a schematic view of pipe-soil-

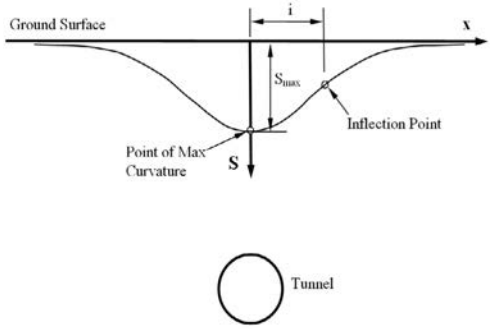

Figure 1. A Gaussian ground settlement profile induced by tunnelling

tunnelling interaction model, in which a tunnel is excavated below an existing pipeline. The tunneling process deforms the soil surrounding the existing pipeline, and through the soil, imposes an equivalent distributed load in the pipeline. As shown in Figure 2b, Winkler-based model (e.g., Attewell et al., 1986) considers the pipeline as an infinite Winkler beam that is supported by an elastic medium with a supporting force proportional to the deflection, v(x), of the pipe at the supporting point with a coordinate x. The equivalent distributed load induced by tunnelling is proportional to the Green field soil settlement S(x). The governing differential equation can be expressed as (Attewell et al., 1986):

$$\frac{\partial^4 v(x)}{\partial x^4} + 4\lambda^4 v(x) = 4\lambda^4 S(x) \tag{2}$$

where $\lambda = \sqrt[4]{\frac{K}{4E_p I_p}}$, E_p is Young's modulus of the pipe, I_p is the moment of inertia of the pipe, and K is the subgrade modulus that represents the pipe-soil interaction. In other words, the pipe-soil-tunnelling interaction is modeled as a Winkler beam subjected to a distributed load equal to KS(x).

Attewell et al. (1986) obtained a numerical solution for Equation (2), and Klar et al. (2005) proposed a closed-form solution using Fresnel integrals. However, it should be pointed out that they focused on the Gaussian type of S(x), and their approaches (e.g., Fresnel integrals) can not be easily extended to an arbitrary type of S(x), a closed-form solution for which is developed in the next section.

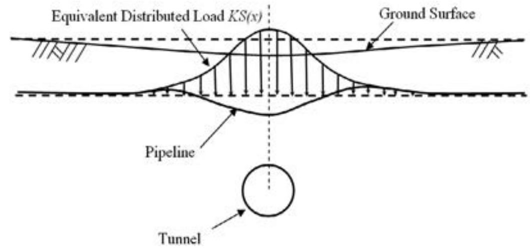

(a) Schematic view

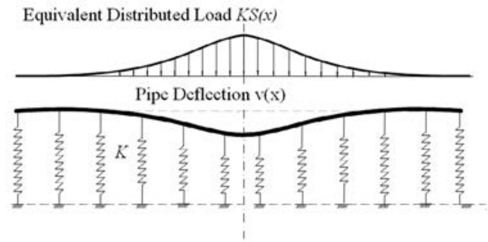

(b) Winkler-based model

Figure 2. Pipe-soil-tunnelling Interaction

3. CLOSED-FORM SOLUTION FOR AN ARBITRARY SETTLEMENT PROFILE

Mathematically, an arbitrary settlement profile, S(x), can be represented by an n-order polynomial series,

$$S(x) = \sum_{i=0}^{n} a_i x^i \tag{3}$$

where a_i are constants in the polynomial series.

When an arbitrary settlement profile S(x) is imposed on pipeline, the Winkler model can be divided into three regions, as shown in Figure 3. The corresponding governing equations for these three regions are given as:

$$\frac{\partial^4 v}{\partial x^4} + 4\lambda^4 v = 0 \qquad -\infty < x \le a \text{ or } b \le x < +\infty$$

(Regions I or III)

$$\frac{\partial^4 v}{\partial x^4} + 4\lambda^4 v = 4\lambda^4 S(x) \qquad a \le x \le b \text{ (Region II)} \tag{4}$$

General solutions for Equation (4) are given as following (Hetenyi 1946):

$$\begin{aligned}
v &= e^{\lambda x}(C_{11}\cos\lambda x + C_{12}\sin\lambda x) + e^{-\lambda x}(C_{13}\cos\lambda x + C_{14}\sin\lambda x) && \text{for } -\infty < x \le a \\
v &= e^{\lambda x}(C_{21}\cos\lambda x + C_{22}\sin\lambda x) + e^{-\lambda x}(C_{23}\cos\lambda x + C_{24}\sin\lambda x) + v_n^* && \text{for } a \le x \le b \\
v &= e^{\lambda x}(C_{31}\cos\lambda x + C_{32}\sin\lambda x) + e^{-\lambda x}(C_{33}\cos\lambda x + C_{34}\sin\lambda x) && \text{for } b \le x < +\infty
\end{aligned} \tag{5}$$

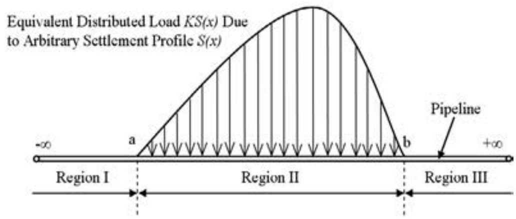

Figure 3. Winkler model for an arbitrary settlement profile

where C_{11}, C_{12}, C_{13}, C_{14}, C_{21}, C_{22}, C_{23}, C_{24}, C_{31}, C_{32}, C_{33}, C_{34} are integration constants, and v_n^* is a particular solution for S(x). v_n^* can be obtained using the method of undetermined coefficients (Miller, 1982), which represents v_n^* as a n-order polynomial series,

$$v_n^* = \sum_{j=0}^{n} b_j x^j \tag{6}$$

where b_j are constants in the polynomial series, and they can be obtained using following equations:

$$\begin{cases} b_n = a_n \\ b_{n-1} = a_{n-1} \quad \text{for } n-4 < i \le n \\ b_{n-2} = a_{n-2} \\ b_{n-3} = a_{n-3} \end{cases}$$

$$b_i = a_i + \sum_{j=1}^{k} (-1)^j \frac{\frac{(i+4j)!}{(i)!} a_{i+4j}}{(4\lambda^4)^j}$$
$$\text{for } i \le n-4 \text{ and } (i+4j \le n) \tag{7}$$

There are twelve integration constants in Equation (5), C_{11}, C_{12}, C_{13}, C_{14}, C_{21}, C_{22}, C_{23}, C_{24}, C_{31}, C_{32}, C_{33}, C_{34}, which are determined from corresponding boundary conditions. It is obvious that for $x \to \pm\infty$, $v = 0$ because soil settlement at $x \to \pm\infty$ is zero. This leads to $C_{13} = C_{14} = 0$ (Region I) and $C_{31} = C_{32} = 0$ (Region III). In addition, continuity condition must be satisfied at x=a or x=b. Therefore, at x=a, the pipe deflections, slopes (i.e., $\theta = v'$), section moments (i.e., $M = -E_p I_p v''$), and shearing forces (i.e., $Q = -E_p I_p v'''$) calculated from the solutions for Region I must equal to those calculated from the solutions for Region II (i.e., $v_{aI} = v_{aII}$, $v'_{aI} = v'_{aII}$, $v''_{aI} = v''_{aII}$, and $v'''_{aI} = v'''_{aII}$). Similarly, four equations at x=b (i.e., $v_{bIII} = v_{bII}$, $v'_{bIII} = v'_{bII}$, $v''_{bIII} = v''_{bII}$, and $v'''_{bIII} = v'''_{bII}$) can be established, resulting in totally eight independent equations for eight unknowns (i.e., C_{11}, C_{12}, C_{21}, C_{22}, C_{23}, C_{24}, C_{33}, C_{34}). Then, these eight integration constants are obtained by solving these eight equations. Accordingly, the pipe deflections are determined by Equation (5), and the pipe section moments are calculated as $M = -E_p I_p v''$. The equations described herein are implemented in Matlab (Mathworks Inc 2007) for facilitating estimate of pipeline responses to tunnelling-induce ground movements.

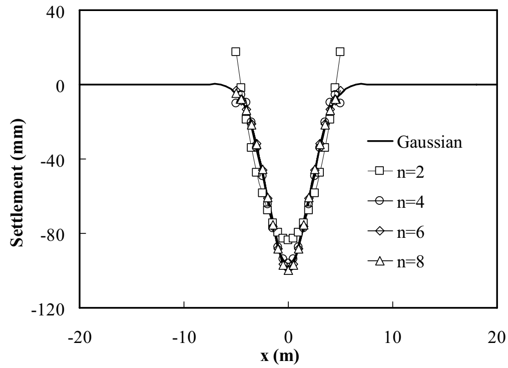

Figure 4. Polynomial series expansion for a Gaussian settlement profile

3.1. Gaussian ground settlement profile

The Gaussian type of settlement profile can be considered as a special case of arbitrary settlement profile. Mathematically, the Gaussian profile given in Equation (1) can be expressed as an expansion of a polynomial series,

$$S(x) = S_{\max} \exp[-\frac{1}{2}(\frac{x}{i})^2] = S_{\max} \sum_{m=0}^{+\infty} \frac{(-1)^{m+2} x^{2m}}{2^m \cdot i^{2m} \cdot m!} \tag{8}$$

Consider, for example, a Gaussian settlement profile with a S_{max} = 100mm and i = 2.0m. Figure 4 shows that the polynomial series approximates the Gaussian profile reasonably well when n ≥ 6.

3.2. Calculation example

Consider, for example, the ground settlement profile shown in Figure 4 which interacts with a steel pipe with an outer diameter and wall thickness of 610mm and 9.5mm, respectively. The pipe is buried in dense sand with a buried depth of 0.9m, unit weight of 20kN/m^3 and friction angle of 40°. The Young's modulus of the pipe is 200GPa, and the soil subgrade

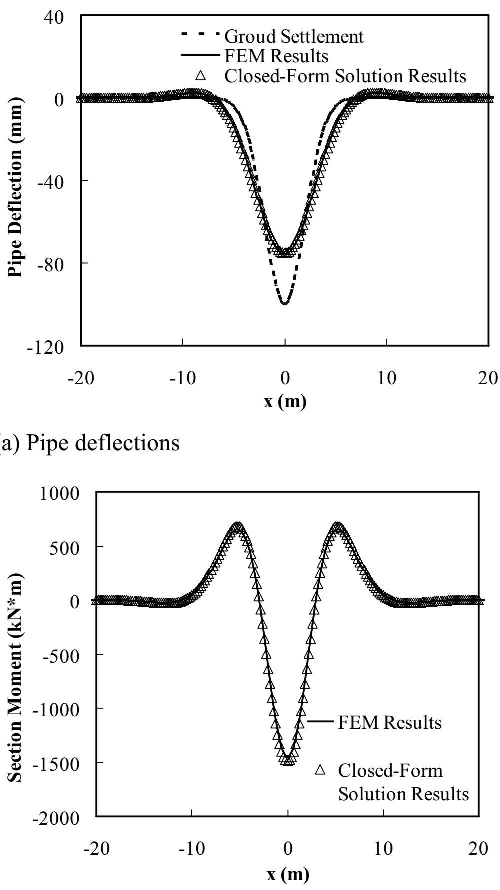

(a) Pipe deflections

(b) Section moments

Figure 5. Comparison of results from closed-form solutions and finite element models

modulus is estimated as 21293 kN/m^2, using the method formulated in the ASCE "Guidelines for the Seismic Design of Oil and Gas Pipeline Systems" (Committee on Gas and Liquid Fuel Lifelines, 1984).

Figure 5a shows the pipe deflections obtained from the closed-form solutions together with the ground settlement profile. As the ground settlement profile is symmetric, the pipe deflections are also symmetric. At the center of settlement trough, the maximum pipe deflection is about 77 mm, which is smaller than the maximum ground settlement (i.e., 100mm). This results in a relative uplift pipe movement at the center of settlement trough, as opposed to the relative downward pipe movement at x= ±5m, where the pipe deflection is larger than the ground settlement. Figure 5b shows the pipe section moments obtained from the closed-form solutions. The pipe section moments are also symmetric, and the maximum section moment of about 1500 kN*m occurs at the center of settlement trough.

3.3. Validation with finite element models

The proposed closed-form solutions for pipe-soil-tunnelling interaction are validated against finite element models (FEM) using the software package ABAQUS (ABAQUS 2006). Continuous pipe segments and pipe-soil interaction are simulated explicitly in the ABAQUS finite element models. Beam elements with pipe cross section are used to simulate pipe segments, and the pipe-soil interaction is modeled by pipe-soil interaction (PSI) elements in ABAQUS. The PSI element in ABAQUS is formulated in accordance with the ASCE "Guidelines for the Seismic Design of Oil and Gas Pipeline Systems" (Committee on Gas and Liquid Fuel Lifelines, 1984) and is consistent with estimate of subgrade modulus for the closed-form solutions. The tunnelling-induced ground displacements are imposed on the PSI elements as distributed displacement boundary conditions. Figure 5 also includes the FEM results, and it is evident that the FEM results (i.e., both pipe deflections and section moments) are virtually identical to those from closed-form solutions.

4. EFFECT OF DIFFERENT SETTLEMENT PROFILES ON PIPE RESPONSES

As pointed out by recent researches (e.g., Celstino et al. 2000, Jacobsz 2002), approximating the tunnelling-induced settlement profile by means of a Gaussian curve may lead to errors in estimating settlement. In addition, the settlement profile is frequently estimated from limited in-situ measurements that are sparsely distributed in the field. Figure 6a illustrates such an example, which contains settlement measurements at eleven points. The settlements can be approximated by either a Gaussian profile (with S_{max} = 100mm and i = 2.0m) or a six-order polynomial profile as shown in Figure 6a. If these two settlement profiles interact, respectively, with the steel pipe that is described in the previous section, the resulting pipe responses may differ significantly. Figure 6b shows the resulting pipe deflections for both Gaussian and polynomial profiles. The pipe deflections under the Gaussian profile are symmetric, while the pipe deflections under the polynomial profiles

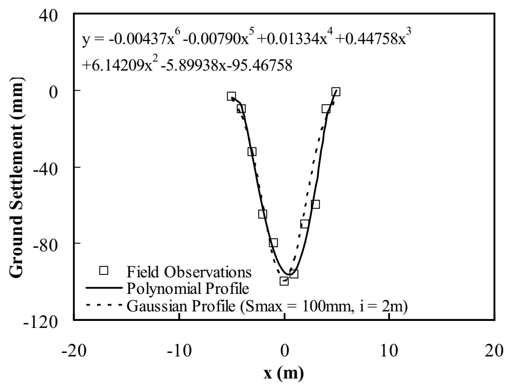

(a) Field observations and two settlement profiles fitted

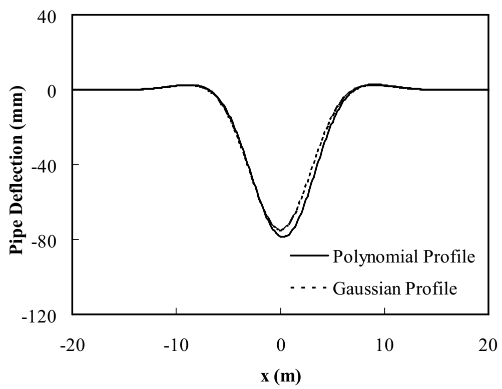

(b) Pipe deflections

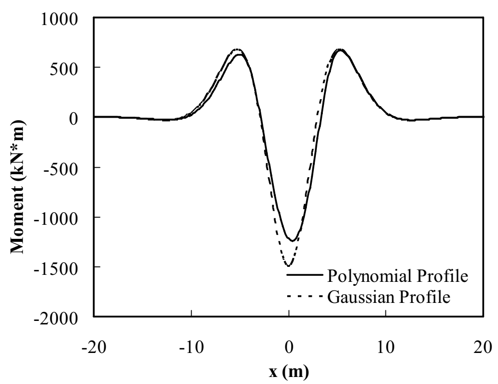

(c) Section moments

Figure 6. Comparison of pipe responses to different settlement profiles

are not. When compared with the deflections under the Gaussian profile, the deflections under the polynomial profiles have relatively large pipe settlements when x > 0m because of the relatively large ground settlements inferred from the polynomial profile at x > 0m (see Figure 6a). Figure 6c shows the resulting pipe section moments for both Gaussian and polynomial profiles. The difference between them is more significant than the difference between pipe deflections. The maximum section moment decreases from about 1500 kN*m for Gaussian profile to about 1200 kN*m for polynomial profile. The different is more than 20%, and the effect of different ground settlement profiles for fitting field observations should be properly accounted for in the analysis.

The closed-form solutions developed in this paper deal with arbitrary types of settlement profile, and hence, they offer flexibility in using different types of settlement profiles and provide a vehicle for assessing the effect of different types of settlement profiles on the resulting pipe responses to tunneling-induced ground movement.

5. CONCLUDING REMARKS

This paper developed pipe-soil-tunnelling interaction models for estimating pipe responses to tunneling-induced ground movement. A Winkler-based model was developed for an arbitrary type of ground settlement profile that is represented by a polynomial function. The pipe-soil-tunnelling interaction is modeled as a Winkler beam subjected to a distributed load proportional to the ground settlement. Governing differential equations were derived, and their closed-form solutions were provided. The commonly used Gaussian type of settlement profile was shown to be a special case of arbitrary settlement profile, as the Gaussian profile can be expressed as an expansion of a polynomial series. The closed-form solutions were validated against finite element models using the software package ABAQUS. It was shown that the finite element simulation results are virtually identical to those from the closed-form solutions.

The closed-form solutions were used to explore the effect of different settlement profiles on pipe responses. Recent researches showed that approximating the tunnelling-induced settlement profile by means of a Gaussian curve may lead to errors in estimating settlement. In addition, the same set of settlement measurements in field can be fitted to different types of curves. When pipes are subject to different settlement profiles, their responses differ significantly. The closed-form solutions developed in this paper deal with arbitrary types of settlement profiles, and hence, they offer flexibility in using different types of settlement profiles and provide a vehicle for assessing the effect of different types of settlement profiles on the resulting pipe responses to tunnelling-induced ground movement.

6. ACKNOWLEDGMENTS

The work described in this paper was supported by a grant from the Research Grants Council of the Hong Kong Special Administrative Region, China [Project No. 9041260 (CityU 121307)]. The authors would also like to thank Mr Aijun Zhang for his assistance in the research described in this paper.

7. REFERENCES

ABAQUS 2006. *User's manual*, ABAQUS, Inc., Providence, RI, USA.

Attewell, P. B., Yeates, J., and Selby, A. R. 1986. *Soil Movements Induced by Tunneling and Their Effects on Pipelines and Structures*, Blackie and Son Ltd., London, UK.

Celestino, T. B., Gomes, R. A. M., and Bortolucci, A. A. 2000. Errors in ground distortions due to settlement trough adjustment. *Tunneling and Underground Space Technology*, 15(1), 97-100.

Committee on Gas and Liquid Fuel Lifeline 1984. *Guidelines for the Seismic Design of Oil and Gas Pipeline Systems*, American Society of Civil Engineers, New York, USA.

Hetenyi, M. 1946. *Beams on Elastic Foundation*, University of Michigan Press, Ann Arbor, Mich.

Jacobsz, S. W. 2002. The effects of tunneling on piled foundations. *PhD thesis*, Engineering Department, University of Cambridge, Cambridge, UK.

Klar, A., Vorster, T. E. B., Soga, K., and Mair, R. J. 2005. Soil-pipe-tunnel interaction: Comparison between Winkler and elastic continuum solutions. *Geotechnique*, 55(6), 461-466.

Mair, R. J., Taylor, R. N., and Bracegirdle, A. 1993. Subsurface settlement profiles above tunnels in clays. *Geotechnique*, 43(2), 315-320.

Mathworks Inc. 2007. *MATLAB – the language of technical computing*, <http://www.mathworks.com/products/matlab/> (March 9, 2007).

Miller, R. K. 1982. *Ordinary Differential Equations*, NY: Academic Press, New York, USA.

New, B. M. and O'Reilly, M. P. 1991. Tunneling induced ground movements: predicting their magnitudes and effects. *Proceedings of the 4th International Conference on Ground Movements and Structures*, Cardiff. Invited review paper, Pentech Press, 671-697.

O'Reilly, M.P. and New, B. M. 1982. Settlement above tunnels in the United Kingdom – their magnitude and prediction. *Tunneling'82*, London IMM, 173-181.

Peck, R. B. 1969. Deep excavation and tunneling in soft ground. *Proceedings of the 7th International Conference on Soil Mechanics and Foundation Engineering*, Mexico City, State of the Art volume, 266-290.

Vorster, T. E. B. 2005. The effect of tunneling on buried pipes. *Ph.D. thesis*, Engineering Department, University of Cambridge, Cambridge, UK.

Vorster, T. E. B., Klar, A., Soga, K., and Mair, R.J. 2005. Estimating the effects of tunneling on existing pipelines. *Journal of Geotechnical and Geoenvironmental Engineering*, 131(11), 1399-1410.

Session 2b

Preservation of historical buildings

Strengthening and reconstruction of foundations

Interaction of foundations

Preservation of historical buildings

Preservation of Saint George's church at Cairo, Egypt

A.A. Antoniou
Geotechnical Division, School of Civil Engineering, National Technical University of Athens, Greece

E.Lekkas
Department of Dynamic Tectonic Applied Geology, Faculty of Geology and Geoenvironment, National and Kapodistrian University of Athens, Greece

N.Chiotinis
Department of Interior Architecture, Decoration and Design, Technological Educational Institute of Athens, Greece

ABSTRACT: Saint George's church represents one of the most important monuments of Greek Orthodoxy heritage at Egypt. The church is a unique and massive building complex combining the elements of a number of different structural systems constructed at different periods of time. This paper presents the ability of the building to resist the potential impacts caused by dewatering operation taking into account the prevailing geological and geotechnical conditions, since cracks and local failures were observed during the abovementioned process. Moreover, the estimated settlements from previous reports were reconsidered and protection measures as well as monitoring methods recommended.

1. INTRODUCTION

The Saint George Church at Mar Girgis, Cairo, Egypt, is a unique and massive masonry building complex combining the elements of a number of different structural systems constructed at different periods of time (Fig. 1). Portions of the existing structures, particularly those lying within the cylindrical portion of the church, are believed to have been erected during Roman times, but foundation elements were encountered that suggest even earlier Pharonic workmanship at the lower levels.

The scope of this paper is to present the ability of the building to resist the potential impacts caused by dewatering operation taking into account the prevailing geological and geotechnical conditions, since cracks and local failures were observed during the abovementioned process as well as to reconsider the estimated settlements and to propose monitoring methods.

1.1. History of the monument

The first written references to Mar Girgis monastery occur in the 14th and 15th centuries; however, the Greek Orthodox community had presence in Old Cairo from 5th century. The three major periods of construction that influence present behaviour are as follows:

- Roman period.
- 1909 construction.
- 1941 reconstruction (extensive demolition, construction of new exterior wall and restoration of many interior surfaces)

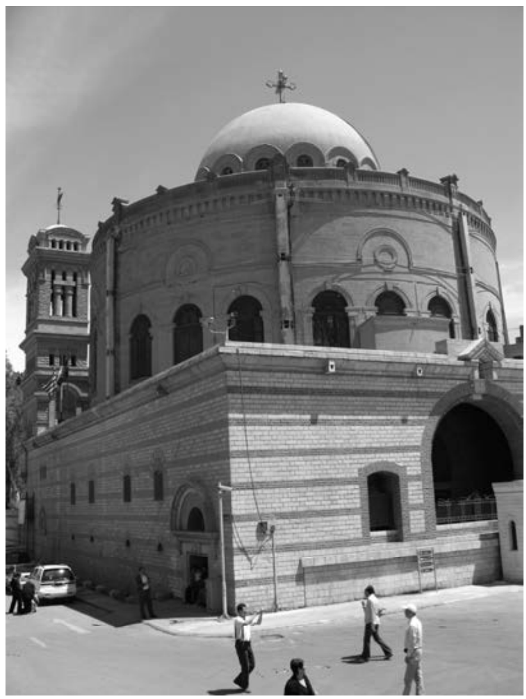

Figure 1. Saint George's church

The substantiation of distress depend largely on how the various components, which were built at different times and with different structural properties, interact with each other under the application of load or deformation (Fig. 2).

The circular Roman tower is certainly one of the most fundamental elements of the church. It was constructed in masonry and measures 28.6m in diameter. It extended to the height of the current upper terrace denoted as level D on Figure 1 and built immediately adjacent to the Nile River. The foundation is believed to have been constructed on native dense alluvial sands, silts and clayey soils, during the low water periods of river flow. Two factors permit the original tower system to carry loads: the massive thickness of the walls and the addition of cross walls.

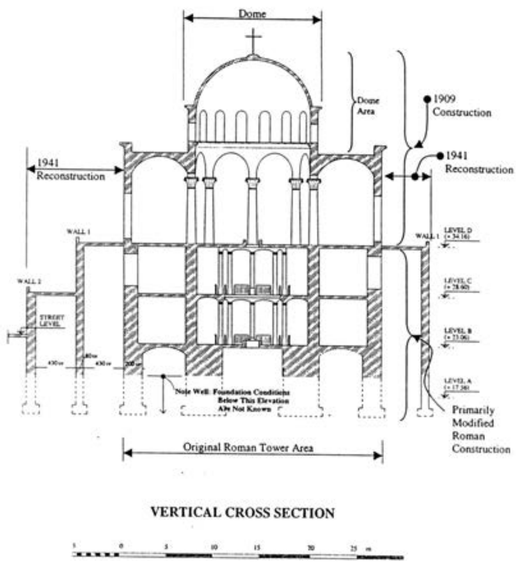

Figure 2. Vertical cross section (after CDM, 2002).

As illustrated on Figure 2 the central elevated dome and its associated walls, built above the present level of the upper terrace, are supported by series of arches that span to a circular colonnade. The flat portion of the roof is carried on a vaulted arch system, while the vault loads are transferred to the inner colonnade and the main exterior rotunda walls. The entire building rests upon a concrete slab located at terrace level D which in turn transfers all loads to the Roman structure below.

During the third period of construction, structural modifications have been performed; particularly between levels B and C where most of the wall surfaces of the Roman tower rebuilt using a hard cement mortar.

1.2. Pathology of the monument

According to CDM report (2002) the masonry church structure is judged to be at moderate risk to continued damage from any external movements caused by excessive construction vibrations, excessive differential settlements from ground water lowering or seismic events. From their point of view some major areas of concern are:

Roof level

- The cupola window arches which are cracked through the entire thickness of the masonry arches.
- Clogged roof drains which allow water to stagnate on the roof, leading to excessive moisture in masonry walls.

Main sanctuary "D" level

- Vertical and horizontal cracks at the base of the perimeter windows at the sill masonry.
- The ceiling of the hollow clay block vaulted roof is cracked around the peak of the vaults.
- The wood framed glass windows of the sanctuary are weathered due to moisture and pollution.
- The bases of six central columns have unsupported areas underneath them.

Third floor "C" level

- The interior central core colonnade of masonry arches supporting the main sanctuary floor are slightly cracked due to stress concentrations.
- There has been some slight movement at the cracks after the 1944 gypsum crack indicator strips were installed.

Second floor "B" level

- The inner radial walls at the door jambs exhibit cracks through the entire thickness of the newer hard masonry shell facing masonry.
- The interior central core colonnade brick arches have two slight cracks at mid span between two sets of columns.

First floor "A" level

- Three of the inner radial walls at the door jambs exhibit cracks through the entire thickness of the newer hard masonry shell facing masonry.
- The eight cracked marble columns in the central well area that are supporting the intermediate period masonry above give the appearance of instability.
- The internal ancient Roman stairway is suffering from deterioration and degradation.

2. GEOLOGICAL AND GEOTECHNICAL CONDITIONS

2.1. Geological conditions at Old Cairo

The Cairo city area is bound to the west by the Nile River and to the east by the Mokattam Plateau. Old Cairo is located at the southwest part of Cairo along the Nile River. The Old Cairo area is generally flat, while ground surface elevations ranging from 22 to m above mean sea level. At the western part, the ground surface slopes to the banks of the Nile River, where the water level is controlled by the Aswan Dam. Prior the construction of the dam the lower part of Old Cairo flood periodically during the wet season.

The meandering and fluctuation of Nile River as well as human activities for more than 5000 years had great effects in the soil deposits beneath Cairo. In general three geological units are present in the Old Cairo city; a man-made (fill) layer, the Nile alluvium layer and a limestone layer. The transition between the fill layer and the Nile alluvium layer is not always clearly differentiated, due to deposition of additional layers of sediments above layers of human activities, during very recent periods of flood.

Man-made layer

This layer consists of varying amounts of gravel, sand, silt and clay. Pottery, asphalt, timber and construction debris were also observed.

Nile alluvium layer

This layer divided in two portions: the upper portion generally consists of layers of clay and silt deposited by the Nile during geologically recent periods of flooding. The lower portion of the Nile alluvium generally consists of coarse to fine graded sand and gravel, while the coarse grained member increases with depth. Occasional pockets or lenses of silt and clay can occur throughout this lower portion.

Limestone layer

Underlying the Nile alluvium layer is limestone bedrock. The bedrock outcrops at cliffs of Mokattam plateau and dips close to Nile River.

2.2. Geotechnical conditions at Saint George's church

Three separate subsurface investigations have been performed in the area of Saint George's church. One by Bondok Consultants and Engineers (1998) and two were performed by Hamza Associates (2000) (in CDM's 2002 report). Based on the results of in situ and laboratory tests on samples from boreholes related to aforementioned investigations the following stratums encountered, according to CDM's report:

Fill layer

This layer ranges in depth from 4,0 to 14,5 meters below ground surface, while the average depth of fill is about 11,5 meters below ground surface. The depth of fill is deeper north of Saint George's church and slopes gradually up towards the south. The fill is comprised of red bricks, pottery, asphalt, timbers, gravel, sand, silt and clay.

Stratum 2

This layer was encountered in all boreholes in Saint George's church. All boreholes were ended in Stratum 2, while its thick was over 13 meters in places, and its depth was significantly deeper than other areas in Old Cairo. This layer was comprised of very loose to dense, yellowish to brown and grey, silty sand and clayey sand with traces of gravel, limestone fragments, clay and red brick fragments in some places. According to Unified Soil Classification System (USCS) this layer characterized as silty sand with no cohesion. In CDM's report stratum 2 divided in two sub-stratums: 2a which is cohesive and 2b which is non-cohesive.

Limestone layer

This layer was not encountered in any of boreholes in Saint George's church area and estimated to be significant deeper in this area than other parts of Old Cairo.

Laboratory tests results of the aforementioned geotechnical units are presented to table 1.

2.3. Groundwater at Saint George's church

Groundwater levels encountered at all boreholes during drilling. The depth to groundwater ranged from 6 to 7.50 meters below ground surface.

Table 1. Mean values of physical parameters of geotechnical units

Soil Type	LL, %	PI, %	w, %	Fine contents, %	Dry unit weight, kN/m^3
Fill	44	15	40	36	17.56
Stratum 2a	41	17	34	75	18.20
Stratum 2b	-	-	23	23	19.72

Water levels measured in the explorations should not necessarily be considered to represent stabilized groundwater levels. In addition, water levels are expected to fluctuate with season, river levels, temperature, climate, construction in the area and other factors.

3. GROUNDWATER LOWERING

3.1. General Description of Groundwater control system

The existing high groundwater level in the Old Cairo area has flooded lower floor levels of some ancient structures. The Contract 102 groundwater control system has been constructed to lower the water table below that floor levels. The groundwater control system consists of groundwater lowering elements and discharge elements. The elements are as follows:

- Perforated shafts (Fig. 3)
- Filter walls adjacent and connected to the perforated shafts
- Horizontal perforated drainage systems below building floor, which will discharge to collection shafts or to the closest perforated shafts
- Discharge pipes installed by using microtunneling technique, and
- Shafts collecting the water from the horizontal drains.

The entire Contract 102 groundwater control system operates by gravity flow. Pumping or electricity is not required to discharge the water into the main sewer. The Contract 102 groundwater control system has been under construction since February 2000.

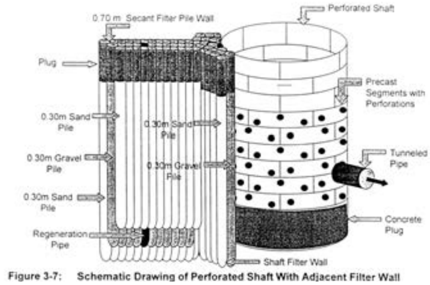

Figure 3. Schematic drawing of perforated shaft with adjacent filter wall (in CDM's report, descriptive sketch by CCJM of Contract 102, Old Cairo dewatering project designer)

3.2. Groundwater control system at Saint George church

According to CDM's report at mid April 2002 the construction has proceeded to the following stage at Saint George's church:

- The perforated shaft southwest of the church and an adjacent filter wall with a length of 33 meters south of the church were installed (Fig. 4). The top of the concrete plug in the perforated shaft was at a depth of approximately 15.3 meters below ground surface. The bottom of the filter wall was at a depth of 15.5 meters below ground surface.
- The horizontal perforated drain system and the non perforated collecting shafts were under construction.

CDM refer that the groundwater will typically be lowered within fill layer, which is a non-homogenous material with a wide range of grain sizes. The CCJM design calculations of the groundwater control system (2000) were based on using a range of permeabilities. The highest permeability assumed was 1.5×10^{-4} m/s and the lowest permeability used was 4×10^{-5} m/s. CDM design calculations were based using permeability equal to 4×10^{-5} m/s.

The drawdown of the water table at a point produces a cone of depression (Fig. 5). The steepness of the water drawdown curve starting from the groundwater control element and the influence area of the groundwater lowering are dependent on the permeability of the soil. In highly permeable material, such as gravel and sand, reaches of long distances away from the drains. The reach is significantly less in low permeability soils, such as silt and clay, and the drawdown curve is steeper.

In order to calculate the radius of influence for various drawdowns and coefficient of permeability the authors used the following equation (Eq. 1):

$$R_0 \sim C*h*k^{0.5} \qquad (1)$$

where R_0 is the radius of influence, C is a factor equal to 3000 for radial flow to pumped wells (simulation of perforated shafts) and between 1500 and 2000 for line inflow to trenches or to a line of wellpoints (simulation of filter walls), h is the drawdown in meters and k is the permeability (m/s). Table 2 presents the radius of influence for given drawdown and coefficients of permeability.

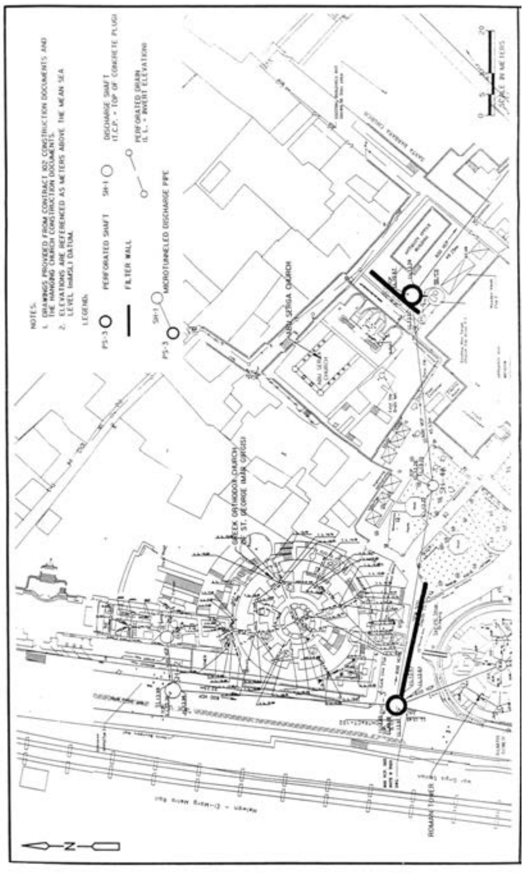

Figure 4. Groundwater control system elements in the Saint George church area (CDM, 2002t).

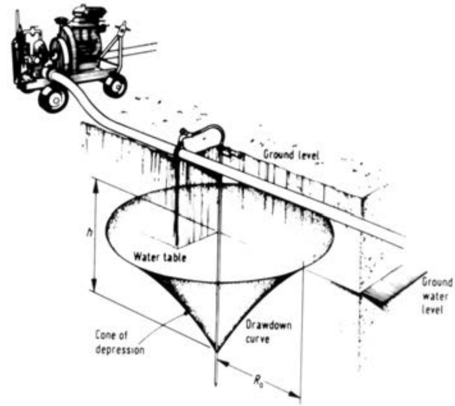

Figure 5. Cone of depression resulting from drawdown (Ciria, 1986).

Table 2. Radius of influence for given drawdown and coefficients of permeability

Drawdown, m	k, m/s	Type of drawdown	R_0, m
2	$4x10^{-5}$	perforated shafts	38
2	$4x10^{-5}$	filter walls	19
2	$1.5x10^{-4}$	perforated shafts	73.5
2	$1.5x10^{-4}$	filter walls	36.7
3	$4x10^{-5}$	perforated shafts	57
3	$4x10^{-5}$	filter walls	28.5
3	$1.5x10^{-4}$	perforated shafts	110
3	$1.5x10^{-4}$	filter walls	55
5	$4x10^{-5}$	perforated shafts	95
5	$4x10^{-5}$	filter walls	47.5
5	$1.5x10^{-4}$	perforated shafts	184
5	$1.5x10^{-4}$	filter walls	92

The percentage drawdown of the water table at any distance from the centre of the cone can be obtained from the following figure (Fig. 6).

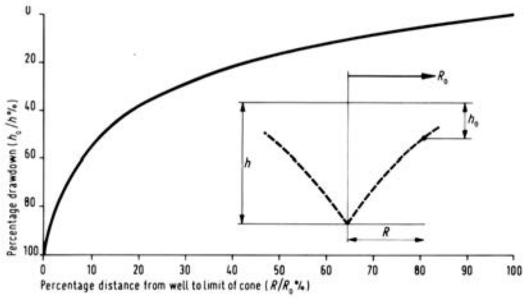

Figure 6. Relation of drawdown to distance from centre of cone of depression (Ciria, 1986).

3.3. Estimation of settlements at Saint George church

Within the cone of depression drawdown will result in an increase in the effective pressure of the ground at the lowered groundwater level and cause consolidation of cohesive and granular materials. In granular soils the pore pressure dissipates almost instantaneously because the water flows easily from the soil so that consolidation also takes place quickly. In cohesive soils the pore pressure are much slower to dissipate because the water flows much slower through the soil so that the consolidation of the soil occurs over a longer period.

The analyses for the estimation of settlements presented hereinafter did not assess the past loads applied to the soils and the historical groundwater levels in the area. These levels have been approximately 5 to 8 meters below the present average levels (2002). For Saint George church the aim was a maximum drawdown of 2.5 meters below the present average level. According to CDM's report (2002) the Old Cairo area has historically flooded periodically before the construction of the Aswan High dam on the Nile River. These floods caused loading and unloading of the soils for at least decades up to hundreds of years as the vertical effective stresses in the soil changed with the rising and falling waters. Having this in mind no settlements or at least only small settlements of a few millimeters are likely to occur due to the groundwater lowering measures, for the following reasons:

- The soil has already experienced numerous loading and unloading cycles, and
- The soil has already been preconsolidated with higher loads than the loads or stresses, which can be caused by the planned lowering measures.

Finally CDM concluded that the maximum settlements varied from 0.7cm to 0.9cm for the most realistic cases.

The authors of this paper estimated the settlements based on the theory of the elastic isotropic half space and taking into account the depth influence factor which considers that the depth of influence below the elevation where the additional load is applied is finite. Usually it is limited by a non compressible soil layer or it is limited in the compressible soil layer by the increase of the additional effective stresses caused by the loads applied compared to the total existing effective stresses of the soil weight. Generally settlements at a level below the depth where the additional stresses are less than 10% of the total effective stresses of the soil weight can be neglected. Thus the estimated settlements concluded inside fill material where the Young's modulus was considered 9MPa, while the range presented in previous geotechnical reports was from 9 to 11MPa. Moreover, in a conservative approach was not taken into account the preconsolidation of fill material. Finally having in mind the fact that the perforated shaft and the filter wall can drawdown the water table to a maximum of approximately 5 meters below the average level but only at the filter wall and the perforated shaft, the settlements estimated to 9mm. In specific distance from shaft or wall figure 6 will be used.

It has to be considered that parts of the church are founded on shallow depth, although the inner part of the church is built on remnants of a Roman tower. This tower has a deep foundation in significantly deeper soils than the foundations of the outer structures. The foundation of the tower is expected to experience almost no settlements, while for the very conservative case, differential settlements of less than 10mm may occur, between the deeply founded interior and the shallower founded exterior structures of the church.

3.4. Monitoring

After the completion of groundwater lowering works and before the inception of dewatering CDM refer that two separate monitoring programs were being performed at the Greek Orthodox church of Saint George, one by the Contract 102 contractor and the other by Cairo University. They refer that the number of monitoring locations is sufficient to monitoring movements, but they also proposed the installation of additional Elevation Reference Points (ERP) mainly in the lower levels of church.

Finally, after the termination of the ground-water lowering, differential settlements were observed between parts of the Roman Tower and the structures around the perimeter terrace. Those settlements were less than one centimetre and substantiate not only CDM's calculations but also author's calculations.

4. RECOMMEDATIONS FOR FURTHER MONITORING OF THE MONUMENT

The authors believe that no more settlements will appear, since water table level persists at the present altitude.

Before the beginning of the renovation of the church, authors suggest another monitoring program with additional ERPs at the inner columns and walls of the outer circle of the Roman Tower and the 1941's additional structures. Readings should be taken for a period of six months to one year (every week) and especially after heavy rainfall events. In case of no additional movements the works of renovation will commence.

5. REFERENCES

Camp Dresser & McKee International (CDM), 2002. *Old Cairo Ground Water Lowering, Greek Orthodox church of Saint George evaluation. Final report*. United States Agency for International Development.

Construction Industry Research and Information Association (CIRIA), (ed.) 1986. *Control of groundwater for temporary works.* Report 113, London.

Johnson C.C. & Malhotra (CCJM), 2000. In CDM's final report, *Contract 102, Old Cairo Area Project. Works at Mar Girgis church.*

Hamza Associates, 2000. In CDM's final report, *Geotechnical investigation, Volume II of IV, Mar Girgis church area.*

Preservation of historical buildings in Albania

Luljeta Bozo
Polytechnic University, Tirana, Albania

Bekim Lila

ABSTRACT: In Albania exist a lot of old churches constructed in the XV-XVI century. They are very interesting by their construction and marvelous paintings. In many of them have appeared damages which sometimes have created serious situations. In many cases the damages have geotechnical origins which are connected with deformable and resistant characteristics of soils. In this paper we would like to present the damage analysis of the Ardenica's monastery near Lushnja city and Saint Maria church near Permet city. Also we wont to present the geotechnical investigation that we made in these areas, to discover the main cause of the damage and the engineering measures taken for the rehabilitation of this objects.

1. INTRODUCTION

Albania is a small country with 28000 km^2 area and about 4million habitants. Albania is situated in south-west part of Balkan and in the littoral of the Jonian and Adriatic seas. Albania has a lot of cultural wealth and it is one of the most ancient population in Balkan and in Europe. A part of this cultural wealth is expressed in the cult objects. We have about 500 churches which are generally small but astonishing from their art which are stone-cutting, wood engraving and chiseling. Also the used construction techniques were particular and the mural paintings are miraculous. The longevity of many churches is tied with the place where they are constructed as in the dense forests, hills, mountains which were protected from different occupations. Also it is tied with the quality of used materials and the best building techniques. In the following part we would like to present the work realized for the reconstruction of two cultural monuments in Albania. This work would be impossible without the research activity to discover the causes of the damages and considering soil-structure interaction.

2. MONASTERY OF ARDENICA

Ardenica's Monastery is one of the most beautiful and known in Albania. It has picturesque view and nice, relaxing landscapes. It has a dominant position in Myzeqe.

2.1. Location of Ardenica monastery

It is located at the top of the hills zone in Myzeqe (central part of Albania) and in the middle of the pine forest. The monastery is confined in the west side by Libofsha field and in the east side by Kolonja field. (Fig1)

Figure 1. View of Ardenica's monastery from above.

2.2. Construction time

Ardenica's monastery was constructed in 3 phases: the first phase was around year 1450 the second phase was from year 1740 to 1750, when was constructed the church of Saint Maria with the famous paintings of Zografi brothers. (Fig2) the third phase was the construction of the bell tower in 1925. (Fig3)

Figure 2. Zografi brothers' paintings

Figure 3. Bell tower.

2.3. Construction type

The church, monastery, library and other annexes are the combination of stone construction (the foundations, walls, columns) with wood construction (inner part, some columns, ceiling, iconostas, ect). The monastery is a two floor building and it is surrounded by high retaining walls.

2.4. The plan and the damages that have appeared

The monastery is deployed in a triangular form at the hill top. It went through many restorations but during 1990-1997 many serious damages appeared as split walls in the first floor, serious deformation of the stone walls as result of their bending and the destruction of some transversal support elements of the retaining walls. (Fig4)

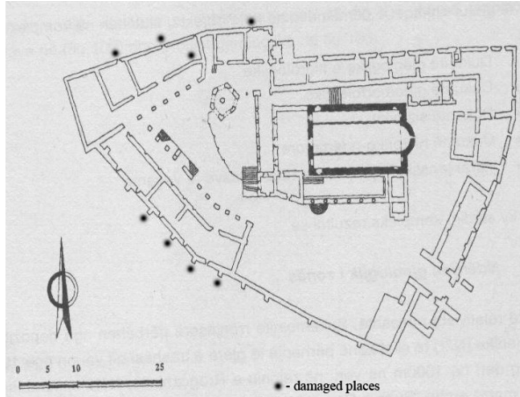

Figure 4. The plan and places of the damages.

We think that all damages are tied with geotechnical phenomena's as partial slide of soils, equilibrium dissolution in some zones by earthquakes, different settlements ect.

2.5. The completed study

To find the damage causes we made a complex study: geological, geomorphologic, seismic, and historical and geotechnical.

The geological situation is that, we have Neogene rocks N_2r thick from 100-1000m composed by alevrolite, conglomerates and sandstones. Over them are situated eluvions and deluvions. The monastery with 2500m^2 area is leaned on the layers with different deformable and resistant characteristics. (Fig 5)

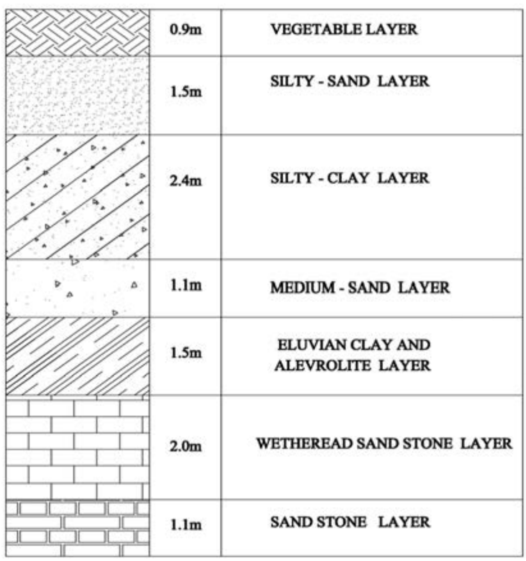

Figure 5. Section from bore-holes 9

From the geomorphologic point of view the object was build in hill's zone and the geological formation which is much altered can show volume changes of soils, change of the mechanical characteristics φ, C, E. We can find this phenomena's until 9m depth.

From the seismically point of view this zone has a high seismic activity (M= 6-6.4). During the last 50 years in (1959, 1962, 1982) happened three strong earthquakes with time length 20-40 seconds. The cyclic loading-unloading has influenced in the diminution of the resistant characteristic of the soils φ, C and in the development of the new active forces in the slide planes, which have the same orientation as the slope.

From the geotechnical point of view the behavior of the soils is different because there are two layers with different characteristics determined by bore-holes and laboratory tests. In the central part we find weathered rock with e=0.39, $E=2.9*10^4$Kpa, R=400Kpa, while in the peripheral part we find the eluvial and deluvial deposits with e=0.85, E= $(0.7 \text{ to } 0.8)*10^4$Kpa, R=200Kpa. In some zones where appeared fissures and deformations in the stone walls, we find weak soils with $E \leq 0.4*10^4$Kpa, $R \leq 200$Kpa. In the zone where the destruction of the transversal support elements of the retaining walls happened the soils have low resistant value $\varphi=18^0$, C=3 to 7Kpa, while in the central part this values are changed to $\varphi=28^0$, C=100Kpa.

From historical point of view we notice that during the 550 years of longevity of this object, except all factors mentioned above and climatic, biologic factors there is even the material ageing that influences in the fissures that appeared in the construction. Finally from the study results that from the geotechnical phenomena's as non uniform settlements, slides, swelling, softening, the new horizontal and vertical displacements by earthquakes had been the causes for further damages in the construction of this object.

2.6. Recommendation of the engineering measures for stabilizing the situation

Noticing that all the damages appeared in the peripheral zone, near the slope or at the top of the hill we recommend.

To stop the superficial sliding must be done a forest planting of the zone.

In the deluvial zone which is in a limit equilibrium state must be prohibited every building construction. The construction of the new transversal support elements of the retaining walls which will rest in the second layer with the following characteristics $\varphi=20^0$, C=23Kpa, $E=1.12*10^4$Kpa, R=250Kpa, e=0.8.

The damaged walls must be reinforced with the combination of concrete and metallic elements.

In the deformable zone must be reinforced the basement by jet ground cement.

3. CHURCH OF SAINT MARIA IN LEUS PERMET

The St. Maria church rises in the middle of a dense but beautiful forest. It has a dominant position over Vjosa valley. It's a place where poets were inspired by the marvelous nature that surrounds it.

3.1. Location of Saint Maria church

The church is located in the south-east part of Permet city (south-west part of Albania). It is constructed in a small hill rounded by dense forest and with a rich water source. (Fig 6) It is famous not only for the construction but also for the mural paintings and iconostasis which is the most beautiful in the Balkan region.

Figure 6 a. View of St. Maria church.

Figure 6 b. View of the churches mural paintings.

3.2. Construction time and type

The St. Maria church was build in1810-1812 and its construction is a basilica with cupola, structure type T_3V_1. (Fig7)

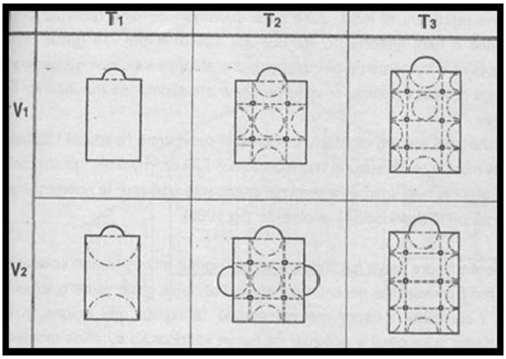

Figure 7. Church typology.

The inner part is composed by two lines of stone columns. They are 10.9m high in the center and 8.8m in the lateral parts. Over the columns rest the arches in two directions creating perfect space structure. In the central part we can see the cylindrical arches which end with cupola. (Fig8)

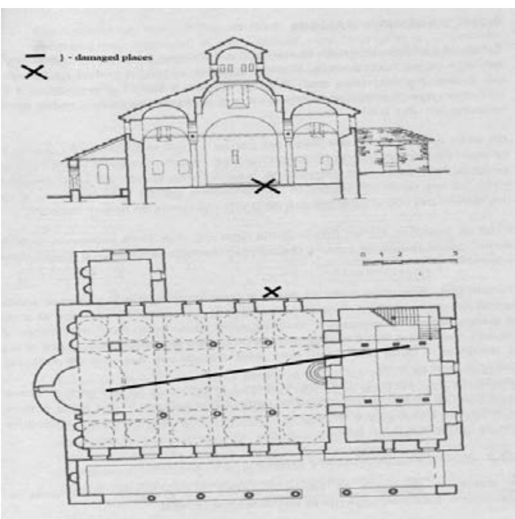

Figure 8. Section and plan of St. Maria church.

3.3. The plan and the damages that have appeared

The church is constructed in a trapezium form platform, with 0.2Ha surface. The church and the graveyard are surrounded by stone walls 3-6m high. The ground under the wall is very inclined. A small and rush torrent flows in the north part of the platform. The water sources are situated 30m far from Leus church. During 1981-1990 some serious damages occurred in the church as: one of the central columns row suffered 10cm settlements; the splitting of the floor in longitudinal direction; the splitting of the arches in different points; the bending and splitting of the longitudinal wall in the south part of the church; the splitting of the stone stair in the churches entry; displacement of the retaining wall near the longitudinal stone wall of the church in its south part. (Look at figure number 8)

3.4. The analysis of the causes of the damages

To do this analysis we undertake a geological and geotechnical research. From this research results: in the geological aspect we have rocks of the Eocene (Pg_2) and Oligocene (Pg_3') composed by calcareous (massive and slab) and mergel package. Also we find quaternary's deposits $Q_{1\text{-}3}$ and $Q_{4dl\text{-}el}$ composed by breccie and flysh. The geomorphology shows that the place of the church is situated in hills zone near a small torrent which has big erosive activity. The inclination of the slope layers is the same with the hill inclination. In the north part the slope inclination is nearly 90^0. (Fig 9) From the climatic condition show that we have a zone with plentiful rains (1000-2000mm rain/year), medium temperature 18.5^0C and many water sources. The zone is relatively quiet from seismic point of view (M 5-5.4) and the last earthquake with M=5.4 happened in 1845. From the hydrological condition we can see that many water sources appear 30-40m above church. The natural drainage (the small torrent) and the geological composition of the land (flysh 40-45% silt) makes possible to have massive water flows in the underground environment and big hydrological gradients. The geotechnical conditions show that we have two layers with the following characteristics: elivium from colluviums with $\varphi=33^0$, C=14Kpa, R>200Kpa, e=0.72 and 63-65% gravel particles; eluvium from flysh with $\varphi=26^0$, C≈0Kpa, R<150Kpa, e=0.8-0.82 and 40-44% silt particles.

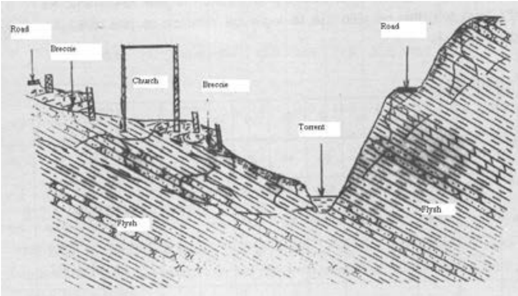

Figure 9. The schematic geologic section

The damage of the church construction is the result of the geotechnical phenomena's happened in the last 30-40 years (1950-1990). These phenomena's are: 1) The presence of the superficial waters, their undisciplined movement and the terrain inclination which have caused very fast water flows, dredge of the silts and sands particles of the flysh, the creation of cavities under foundations, augmentation of the bulk density, the rise of an unpredicted hydrostatical pressure in the retaining walls of the south part. 2) Big supplement settlements of one part of the church foundation (over 10 cm) caused by suffusion phenomena's. 3) The displacement of the north retaining walls caused by hydrostatical pressure and augmentation of bulk density. 4) Small slides in the west part where the inclination of the layers is the same with the slope. 5) The different settlements of the church foundation because they rest in two layers with different deformable characteristics. Beside the geotechnical phenomena's in the object damages have influenced the human activity. 6) The build of the transversally wall which connects the retaining wall with the longitudinal wall of the church. (Fig 10) When the retaining wall moved to stop it, a protective measure was taken to build a transversally wall which was leaned in the longitudinal wall of the church. The new horizontal load caused bending and fissure of the stone wall. In the other hand the build of a pit near the foundation for the collecting of superficial waters caused the development of the suffusion phenomena's in the soils located under the foundation. This was accompanied with supplement settlements.

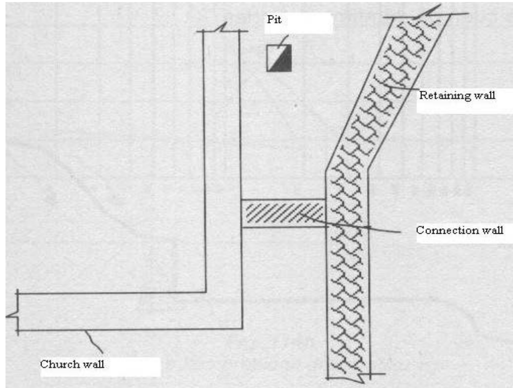

Figure 10. The connecting wall and the pit.

3.5. The engineering measures for the church repair

After the situation analysis and our geological and geotechnical study, we proposed two groups of engineering measures. The first group is: 1) The reconstruction of the foundation realizing the cross concrete beams which will strengthen the church construction and assures the uniform settlement. 2) The reinforcement of all constructive elements as columns, arches, stairs, walls and cupola. 3) The removal of the connecting wall. The second group is for the improvement of the basements conditions, the channeling of the surface waters, and the reinforcement of the retaining structures. We made the design of: 1) The all canal system to collect the superficial waters. 2) The reconstruction of retaining walls by adding new transversal support elements. 3) The construction of the new retaining walls near the torrent to protect the slope behind the church from erosion.

4. CONCLUSIONS

The main damage causes of the old historical, cultural objects in Albania are these three: 1) Factors tied with geo environment as geology, seismic, geotechnical, weathering, erosion, water activity, suffusion, climatic conditions, ect. 2) Factors tied with ageing of construction material and the lost of their quality from the climatic conditions. 3) Factors tied with uncontrolled human activity. To evidence the damage main causes of the different objects should be done: 1) A complex geological, seismic and geotechnical studies. 2) A study to see how the material behavior changed. 3) A study for the soil-structure behavior. The problem solution to repair and reconstruct the cult objects, can be resolved only if we know well the basement and structure behavior and soil structure interaction.

5. REFERENCES

Adhami S. 1989. Voskopoja in her flourishing century. *Tirane: Science Academy (in Albanian)*.

Bozo L. 2000. Rock Mechanics. *Tirane: Polytechnic University (in Albanian)*.

Bozo L. 2001. Geotechnical phenomena's and objects damage. *Tirane: Geotechnical magazine.* No. 1, pp. 10-15 (in Albanian).

Kociaj S. 1985. Earthquake and high seismic resistance projects. *Tirane: Newsletter. No. 6, Science Academy* (in Albanian).

Sulstarova E. 1985. The seismic map of Albania and its use in design. *Tirane: Newsletter. No. 6, Science Academy* (in Albanian).

Thomo P. 1998. After Byzantine churches in south Albania. *Tirane: KOASH press*.

Electrical imaging survey as a tool for the stability analysis of St. Peter's Church, Jaffa (Israel)

V. Frid, G. Liskevich, N. Korostishevsky, D. Doudkinski, A. Averbakh
Isotop, soil and rock mechanics laboratory, Gedera, Israel

ABSTRACT: This paper presents results of electrical imaging survey (EIS) in the vicinity of St. Peter’s Church, Jaffa (Israel). An intensive fracturing of the Church’s walls and uneven suffusion collapse of the lane adjacent to its western wall necessitated this investigation. The aim of the study was to understand the cause for soil failure. High sensitivity of the historical object to any kind of invasion, very dense building of ancient city with extremely narrow lanes of complicated geometry and topography presented a considerable challenge to the investigation methodology. Complex investigations of electrical resistivity, soil moisture, lithology and deformation were carried out. Unsteady soil condition was confirmed by inclinometer measurements.

1. INTRODUCTION

St. Peter's Church (Fig. 1), one of the pearls of Jaffa (Fig. 2), was built in the 19th century on the remains of Crusaders' fortress in the place, where Napoleon camped during his campaign in Middle East in 1799. Intensive fracturing of both bearing walls and decorative elements of the Church building almost at all levels (Fig. 3), drastic swelling, deformation and partial sinking of the floor behind the Church altar, formation of a suffusion crater and soil loosening beneath the lane along the western wall of the Church were responsible for our investigation. The application of destructive investigation methods is in no way desirable and, in places, impossible.

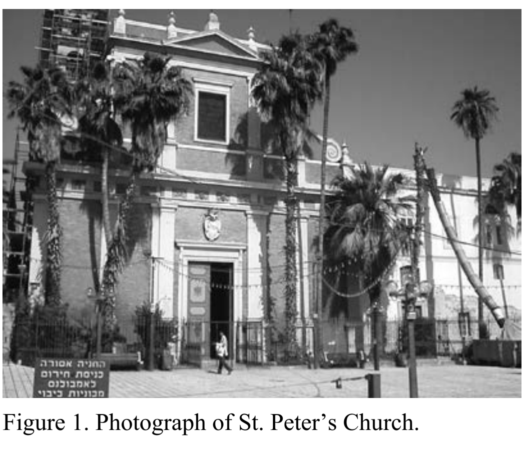

Figure 1. Photograph of St. Peter’s Church.

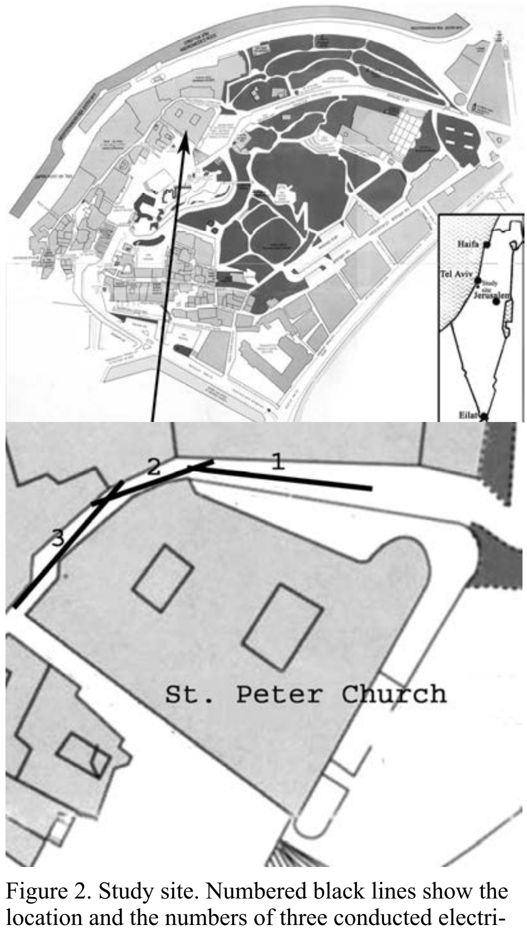

Figure 2. Study site. Numbered black lines show the location and the numbers of three conducted electrical imaging survey lines.

Figure 3. An example of a wall fracture.

Electrical imaging survey (EIS) has been successfully applied to the subsurface characterization for different geo-engineering purposes since the end of the last century (Loke, 2000, Dahlin & Loke, 1998, Dahlin, 2001, Dahlin & Zhou, 2004). Nassir *et al.* (2000) studied the usefulness of EIS for groundwater investigations in coastal areas. It was shown that the fresh-water/saline-water boundary being two-dimensional was a good target for 2D EIS. Panissod et al. (2001) applied the EIS to identify clear resistive features associated with the water losses in Beauce (France). Bowling et al. (2005) constructed a hydrogeological model of investigated site from interpretations of resistivity data obtained. EIS carried out in Hummelstown (PA) for cavern mapping in the region (Recelli-Snyder et al., 1997).

Several examples of EIS employment was provided by Loke (2000) in his comprehensive guide to 2-D and 3-D surveys. Of special interest to us is his case of EIS application to landslide stability control (Cangcat Jering, Malaysia) where water accumulation zone in a hill slope, known to be the source of slope sliding hazard, was delineated by the use of EIS. Hack (2000) discussed applicability of several geophysical methods for slope stability analysis and claimed that application of EIS is promising and may become a standard tool in geotechnical practice. Van Schoor (2002) claimed that EIS is an ideal tool to aid in detecting and monitoring sinkholes and subsurface cavities. Israil and Pachauri (2003) used EIS together with seismic refraction method and spectral analysis of surface waves for determination of the thickness of the landslide body, its possible slip surface and evaluation of hydrological conditions related the occurrence of landslide. Donnely et al. (2005) undertook combined engineering geological investigations and EIS of slopes in the territory of Edinburgh castle. It turned out that slope instability was associated with zones of low resistivity, high water saturation (weak material). Drahor et al. (2006) conducted EIS in a landslide area (Aydin, Turkey) that yielded useful information on the landslide structure, indicated the presence of a fault on the site and revealed the rupture surface. Godio et al. (2006) employed EIS together with seismic refraction tomography and spectral analysis of surface waves to determine the overburden thickness and the geometry of the sliding surfaces. This short review shows successful employment of EIS for groundwater and slope stability investigation. That is why EIS was used for our investigation.

Dahlin and Zhou (2004) numerically investigated ten electrode arrays to compare their resolution and efficiency and found that pole-dipole, dipole-dipole and Shlumberger electrode configurations were the best candidates for the EIS application in a variety of geo-engineering aims. They also showed that a) Pole-Dipole array has a low signal-to-noise ratio while Dipole-dipole is a more at risk of noise contamination than other investigated arrays; b) the main strength of Schlumberger and Wenner arrays is good depth determination while spatial resolution of Wenner array is poorer than that of the Schlumberger. Our own experience of geophysical investigations in situ completely confirms these conclusions. That is why we employed Schlumberger array (see below) that enables to ensure compromise between minimum noise contamination and good spatial resolution.

2. STUDY AREA

St. Peter's Church was built on a peculiar kind of calcareous sandstones belonging to the so-called Kurkar group (Gvirtzman, 1969). The Kurkar group is part of a continuous paleocliff ridge of pre-recent (Neogene) to recent age running parallel to the coastline. Kurkar is a very porous, crossbedded, mostly friable, wind-laid sandstone whose weathering rate is high and hence it is easily quarried.

Several interrelated varieties of the Kurkar are known, e.g. calcareous sandstone (the sandstone with calcitic cement and clastic quartz), calcarenite (sandstone whose clastic component is wholly calcareous), coquina that is made up of cemented shell beds and sands (Gvirtzman, 1969). In the area under investigation the Kurkar constitutes three terraces. St. Peter's Church is located on the uppermost terrace while the middle one is presently under construction and reconstruction. The lowest terrace is the sea front that was already broadened and reconstructed.

Note that the Kurkar is a main coastal aquifer of Israel. In the westmost part (several kilometers away from the coastline) intervening clay layers divide the main aquifer into several subaquifers. These subaquifers have a distinct chemical composition and hydraulic properties because seawater has penetrated to various parts of coastal aquifer, mainly in the uppermost subaquifer. Although water table is known to be at the sea level depth (approximately 19 m lower than the existing ground level), influence of the seawater in the studied area is important.

Changes in slope configuration are frequently known to cause soil instability whose analysis is at times made employing different geophysical methods.

3. METHODS

We combined EIS with careful geological investigation of the soil close to the Church foundation using three shallow boreholes and downhole inclinometer profiles.

The survey was conducted using the Sting R1- Swift system (Fig. 4) manufactured by the Advanced Geoscience, Inc. (USA). It consists of a Sting R1 resistivity meter, automatic multielectrode switching box, cables and special electrode assemblages with stainless steel switches attached to grounded stainless steel rods. Thirty electrodes arranged in a Schlumberger configuration were utilized in each EIS line, enabling us to measure 196 points at 14 levels under each EIS line. Figure 4 shows Sting-R1 Earth resistivity meter, an assemblage of a single electrode and a multielectrode array. Three EIS lines (Fig. 2) were conducted in series along the western wall of St. Peter's Church so that the middle EIS line intersected the area of the lane collapse.

Figure 4. An example of the EIS assemblage in situ.

The interelectrode spacing was 1 m for this line while for two others – 1.5 m. AGI Earth Imager software (version 2.1.6) was employed for apparent resistivity inversion to produce 2D pseudosections using the following main settings: inversion method - smooth model inversion, forward model method - finite element, forward equation solver - Cholesky decomposition, boundary conditions – mixed, number of mesh divisions – 2, optimization method – Gauss-Newton. Such initial settings were employed to produce proper inversion of EIS data by the AGI's recommendations and our own experience.

Three shallow investigation boreholes were drilled on the site - 2, 2.5 and 18 m depth, respectively. The deepest borehole was equipped with an inclinometer (the Slope Indicator Company, USA) to compare EIS data with the direct measurements of soil displacement. The locations of all three boreholes are shown in Figure 5 by black vertical lines.

4. RESULTS

4.1. Site Geology

Drilling results show that the uppermost part of the soil stratigraphy (down to 5 m depth) adjacent to the western wall of St. Peter’s Church is highly uniform consisting of a mixture of moderately wet (see below) clayey sand and lean sandy clay with approximately 5-10% fine to coarse building stone fragments, 5-8% of ancient ceramics and scattered limestone cobbles of about 15 cm in size. The deeper part of the section is composed of yellowish Kurkar.

Two lithological types were found here: the upper part (5 -17 m depth) is made up of yellowish, very friable, disintegrated calcareous sandstone plates, recovered as fine to medium sand to slightly silty sand with approximately 20-30% calcareous sandstone fragments, while the lower part (17-18 m depth) consists of hard fine-grained calcareous sandstone (up to 15-20 cm thick), alternating with thick moist to moderately wet sand and/or slightly silty sand layers.

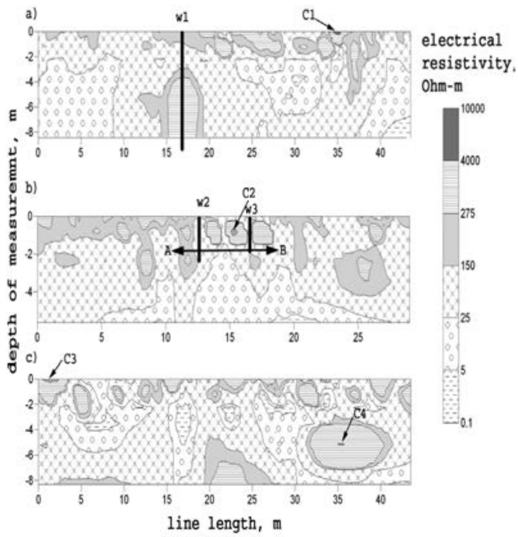

Figure 5. Inverted resistivity sections of three EIS lines. Black-white scale on the right-hand side of Line 1 shows changes of soil resistivity from 0.5 Ohm-m (black) to 10,000 Ohm-m (white). Black vertical lines show the location of three prospecting wells. Double side arrow A-B shows the location of lane collapse. Black arrows C1-C4 indicate zones, where electrical resistivity obtained was over 4000 Ohm-m.

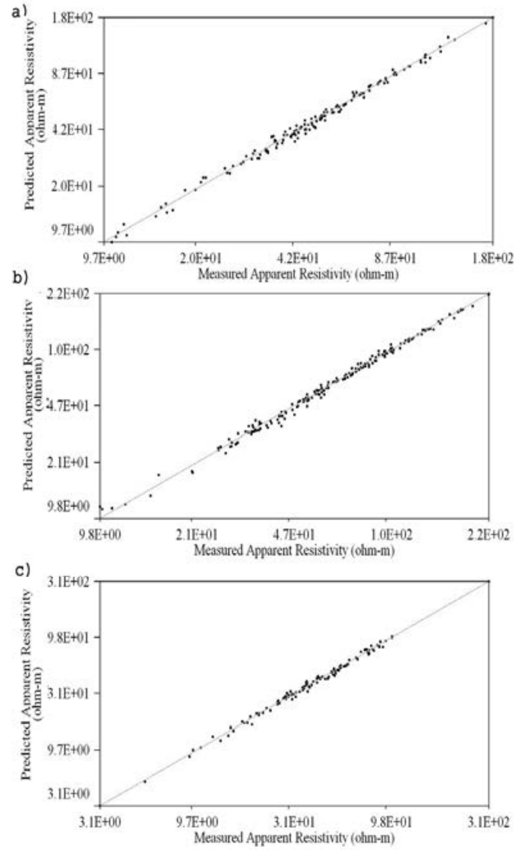

Figure 6. Crossplots of measured vs. predicted apparent resistivity data for three EIS lines. a. Line I: iteration number 5, root mean squared error (RMS) =4.67%, L2=0.87(*), electrode spacing 1.5 m; b. Line II: iteration number 5, RMS= 4.66%, L2=0.87, electrode spacing 1 m; c. Line III: iteration number 7, RMS 4.82%, L2=0.93, electrode spacing 1.5 m.* L2 is measure of data misfit. It is defined as the sum of the squared weighted data errors. When L2≤1 the inversion is converged.

4.2. Results of EIS

Figure 5 shows inverted resistivity sections of three EIS lines conducted in series along the western wall of the Church. Inversion of the EIS data from the first two lines was completed after 5 model iterations and from the third line - after 7. Figure 6 shows three cross plots of measured vs. predicted apparent resistivity whose RMS error varies between 4.66 and 4.82%, indicating a consistency between modelled and measured apparent resistivity.

Analysis of Figs. 5 and 7 shows that the shallow part of inverted resistivity section (0- 3 m depth) offers electrical resistivity range between 25 and 250 Ohm-m.

As mentioned above, results from three prospecting boreholes drilled in the area show the existence of clayey sand-sandy clay mix with some gravel and cobbles fragments. Analysis of soil samples recovered from the wells shows that shallow part of geological section (2-3 m depth) exhibits the moisture between 13-20% (Fig. 7). Note that commonly known values of electrical resistivity for clay, wet sand and sandstone fall in the range of 5-300 Ohm-m (Guerin et al., 2004) that confirms the authenticity of the measured data. Small local maxima of electrical resistivity at the depth of 2.5-3 m from wells w2 and w3 probably correspond to the existence of thin clayey sand layer enriched with Kurkar gravel (approximately 20-25%).

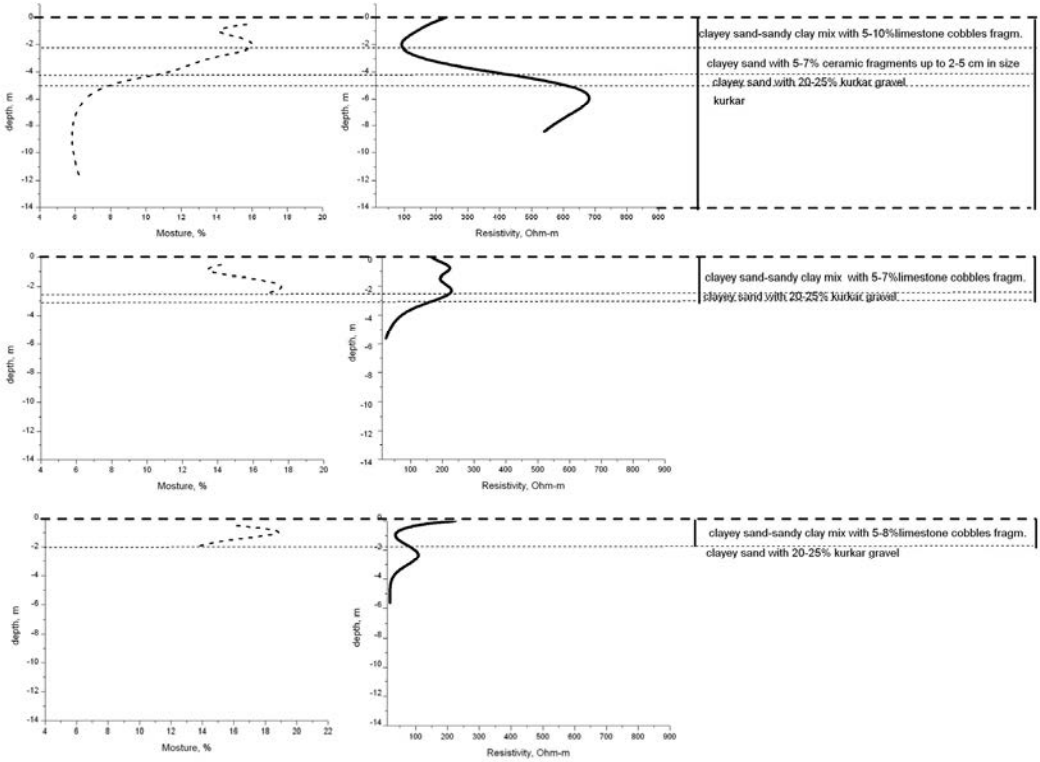

Figure 7. Moisture, electrical resistivity and lithological logs. a - well number 1 (w1), b - well number 2 (w2), c - well number 3 (w3).

Note that values of electrical resistivity in both graphs gradually decrease below 2.5-3 m depth. Electrical resistivity values at the deep part of well w1 gradually increase below the depth of 4 m up to the maximum at the depth of 6 m. Such a maximum seems to us relevant since it corresponds to the boundary between the overlying thin layer including 20-25% of Kurkar gravel and Kurkar itself. Comparison of electrical resistivity with values of moisture at the deep part of section from w1 shows their inverse correlation: a decrease in moisture is followed by an increase in electrical resistivity and vice versa.

The decrease in soil moisture between 5-12 m depth from the well w3 shows that the increased moisture values in the shallow part of all three wells are more likely due to water losses through underground communication and not accountable to the aquifer that was noted above to be at the depth of about 19 m.

Good quality of inverted resistivity sections, good fit between them and the geological prospecting results together with moisture measurements enable us to use our geophysical data to scrutinize geo-engineering situation beneath the lane.

4.3. Analysis of soil stability on the basis of EIS data.

Analysis of all three EIS sections shows their high heterogeneity: electrical resistivity changes from 0.1 to 10,000 Ohm-m, mean and standard deviation vary from 136 to 255 Ohm-m and from 399 to 721 Ohm-m, respectively. Noteworthy is such heterogeneity in the zone of lane collapse shown in Figure 5 (Line 2) by double side arrow A-B, where soil electrical resistivity varied from 5 to over 4000 Ohm-m. The implication of this observation is that there is a close contact between sandy clay (mostly wet) or highly water saturated clayey sand, wet sand, sandstone and loosened dry sand or/and ground water flaw along permeability pathways. Both scenarios could indicate instability source in the zone. This instability could be caused by water penetration from wet to dry sand with resulting decreased cohesion and/or internal friction, diminished bearing capacity of soil. Difference in bearing capacity of nearby parts of soil caused by the differential settling of more humid and less humid parts inevitably ends in soil collapse. The soil suffusion collapse that occurred beneath the lane and motivated our study confirms this scenario. Moreover, arrow C2 indicates the zone where electrical resistivity is even higher than 4000 Ohm-m which could be interpreted as the existence of an underground cavity there, meaning that the process of soil failure is not over yet.

Although percentages of soils featuring electrical resitivity less than 5 Ohm-m and over 4,000 Ohm-m are 8 and 0.4, respectively (that is they are present in insignificant amount) they are worth scrutinizing.

As we noted above, zones with electrical resistivity less than 5 Ohm-m, are interpreted as an accumulation of salt (to available degree) water in the soil. As we noted above, the existence of water in sand soil diminishes its bearing capacity and can dramatically contribute to triggering soil collapse. Note the existence of such zones below the first EIS line and especially below the third EIS line. An additional image obtained from our measurements shows distinct zones of loosened dry sands or/and cavities below the earth surface along all three lines. Formation of subsurface cavities (electrical resistivity higher than 4000 Ohm-m) underground and near the earth surface could be the 'finger prints' of instability/ destruction in the soil. Several such zones are shown by arrows C1-C4 (Figure 5). Note that formation of near surface cavities (C1 and C3) was confirmed by visual observations.

4.4. Measurements of soil deformation

Inclinometer measurements of soil deformation were carried out two, three and five weeks after the installation of inclinometer system. Figure 8 shows that the lowest part of the Kurkar unit (in the interval of 17.2-19 m depth- see sect. 3.1) is autochthonous, i.e. stationary, while the upper part of the Kurkar unit (4.8-17.2 m depth) is allochthonous (non-stationary) and moved together with overlying clay-sandy filling unit (0-4.8 m depth) sliding down the slope. The first two measurements showed progressive sliding of this part northwest (with constant rate of about 0.75 mm/week). However, the last measurement showed a sharp change in displacement direction from NW to SW.

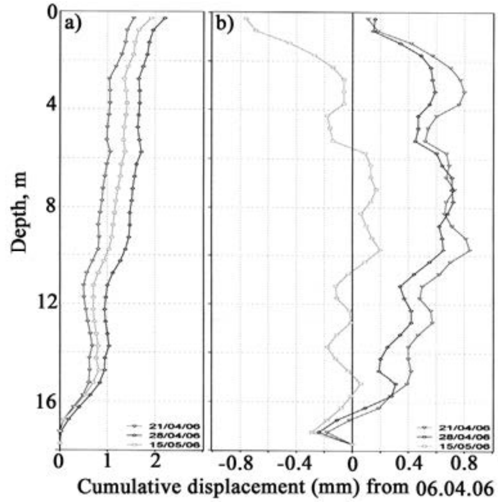

Figure 8. The results of inclinometer measurements: two, three and five weeks after installation of inclinometer assemblage. (a) and (b) are two normal components of soil displacement: a - EW. (positive West), b- NS (positive North).

5. CONCLUSIONS

The site under investigation is characterized by high sensitivity to any kind of invasion and complicated conditions for stability investigation. Analysis of advantages and disadvantages of different methods of stability investigations enabled us to employ combined geotechnical–geophysical methodology ensuring minimal site invasion and comprehensive delicate soil study. The research involved the application of electrical resistivity imaging for assessment of the stability of sandstone bedrocks in the foundation of St. Peter's Church. Comparison between inverted resistivity and geological survey data showed their consistency.

Analysis of inverted resistivity sections shows their significant heterogeneity, where zones of low and high electrical resistivity were found to be in the close vicinity of each otherThis observation was interpreted as a close contact between water saturated and dry sands and formation of groundwater flow pathways. Careful scrutiny of inverted resistivity section in the zone of suffusion collapse showed that process of soil failure there is not over yet. Moreover, it was shown that such potentially dangerous zones exist along all three EIS lines. Penetration of water from wet to dry sands, decreased cohesion and internal friction could trigger local landslides via differential settling of wet/dry parts of soil, resulting in the weakened slope, its sliding, suffusion collapses. Hence, the entire region under investigation is potentially unstable. The last conclusion was supported by our inclinometer investigations showing that Kurkar slope underlying the St. Peter's Church foundation was indeed unsteady.

6. REFERENCES

Bowling, J.C., Rodriguez, A.B., Harry, D.L., Zheng C. 2005. Delineating Alluvial Aquifer Heterogeneity Using Resistivity and GPR Data *Ground Water,* Vol. 43, No.6, pp. 890–903.

Cardarelli, E. & Fischanger, F. 2006. 2D data modelling by electrical resistivity tomography for complex subsurface geology. *Geophysical Prospecting*, No 54, pp. 121–133.

Dahlin, T. 2001. The development of DC resistivity imaging techniques *Computers & Geosciences*, No. 27, pp. 1019–1029.

Dahlin, T. & Zhou, B. 2004. A numerical comparison of 2D resistivity imaging with 10 electrode arrays. *Geophysical Prospecting,* No. 52, pp. 379–398

Dahlin, T. & Loke, M.H. 1998. Resolution of 2D Wenner resistivity imaging as assessed by numerical modeling. *Journal of Applied Geophysics*, No. 38, pp. 237-249.

Donnelly, L. J., Culshaw, M.G., Hobbs, P.R.N, Flint, R.C., Jackson, P.D. 2005. Engineering geological and geophysical investigations of a slope failure at Edinburgh Castle, Scotland. *Bull Eng Geol Environ,* No. 64, pp. 119–137.

Drahor, M.G., Gokturkler, G., Berge, M.A., Kurtulmus, T.O. 2006. Application of electrical resistivity tomography technique for investigation of landslides: a case from Turkey. *Environmental Geology*, No. 50, pp. 147-155.

Godio, A., Strobbi, C., De Bacco, G. 2006. Geophysical characterisation of a rockslide in an alpine region. *Engineering Geology*, No. 83, pp. 273– 286.

Guerin, R., Munoz, M.L., Christophe, A., Laperrelle, C., Hidra, M., Drouart, E., Grellier, S. 2004. Leachate recirculation: moisture content assessment by means of a geophysical technique. *Waste Management,* No. 24, pp. 785–794.

Gvirtzman, G. 1969. The Saqiye Group (late Eocene to early Plistocene) the Coastal plain and Hashephela regions (Israel, v.2 – maps, Geological Survey of Israel Bull.) pp. 51

Gvirtzman, G., Shachnai, E., Bakler, N., Ilani, S. 1983. Stratigraphy of the Kurkar Group (Quaternary) of the coastal plain of Israel. *Geological Survey of Israel Current Research*.

Hack, R. 2000. Geophysics for slope stability, *Surveys in Geophysics.* No. 21, pp. 423–448.

Israil, M. & Pachauri, A.K. 2003. Geophysical characterization of a landslide site in the Himalayan foothill region. *Journal of Asian Earth Sciences,* No. 22, pp. 253–263.

Loke, M.H. 2000. Electrical imaging surveys for environmental and engineering studies (*A practical guide to 2-D and 3-D surveys. 61p.* www.heritagegeophysics.com/images/lokenote.pdf*)*

Nassir, S.S., Loke, M.H., Lee, C.Y., Nawawi, M.N.M. 2000. Salt-water intrusion mapping by geoelectrical imaging surveys. *Geophysical Prospecting*. No. 48, pp. 647-661.

Panissod, C., Michot, D., Benderitter, Y., Tabbagh, A. 2001. On the effectiveness of 2D electrical inversion results: an agricultural case study. *Geophysical Prospecting,* No. 49, pp. 570-576.

Reccelli-Snyder, H.L., Stahl, B.A., Warren, P.G., Warren, J.J. 1997. Electrical imaging: A Method for Identifying Potential Collapse and other Karst Features Near Roadways. (*Science Applications International Corporation, Middletown, Pennsylvania.* www.quality-geophysics.com/50th1.pdf)

van Schoor, M. 2002. Detection of sinkholes using 2D electrical resistivity imaging. *Journal of Applied geophysics*, No. 50, pp. 393-399.

Deep Excavations and Preservation of Historical Buildings and Façades

A. Pinto, X. Pita
JetSJ Geotecnia, Lda., Portugal

ABSTRACT: The aim of this paper is to present a case study of an excavation in Lisbon, where the preservation of historical masonry façades was mandatory. For that purpose integrated special earth retaining solutions (Berlin walls), underpinning solutions (micropiles and jet grouting) and façade retention structures were adopted.

In the paper the following points are pointed out: preservation of existing historical façades, taking into account the main architectural and urban restraints, soil - structure interaction design and calculation models, integrated geotechnical and construction technologies and monitoring and survey.

1. INTRODUCTION

The execution of deep excavations at the down town of the majority of the European cities has demanded, by historical and architectural reasons, the preservation of buildings façades.

The age and integrity of the original façades, together with the site neighbourhood as well as the geological conditions, has leading to some demanding geotechnical and structural solutions. As presented in this paper, this kind of situation has occurred in Lisbon, for a building located at the República Avenue, with a plan area of about 32x36m^2. For the excavation, with 12m depth, it was necessary the underpinning of the existent old and historical façades, for the construction of 4 basement floors, with car parking purpose.

Figure 1. View of the external preserved façades

2. MAIN CONDITIONS

2.1. Geological and geotechnical conditions

The ground at the site is composed by fills, underlying the Miocene layer (Miocene 1, with N_{SPT} lesser than 60 blows and Miocene 2, with N_{SPT} bigger than 60 blows), both formed by clays and claystones, with stiffness and resistance, in general, increasing with depth. The adopted values of the main geotechnical parameters are presented at Table 1.

Table 1. Main geotechnical parameters

Soil Type	E [MPa]	ν [-]	C' [kPa]	∅' [º]
Fill	5.000	0.3	1	28
Miocene 1	30.000	0.3	40	30
Miocene 2	100.000	0.3	70	35

The water table was located below the final excavation level.

2.2. Façades to be preserved

The preserved façades, with about 100 years old, belonged to the original and internally previously demolished building, with 4 upper floors,. The 4 façades were 2 external: located at the República and at the João Crisóstomo Av. (figure 1) and 2 internal, as the excavation overall pit area was bigger than the one of the existent and demolished building.

The façades location, as well as the relative position of the retaining walls, bellow the external façades, demanded the need for the underpinning of all the 4 preserved façades (figure 2).

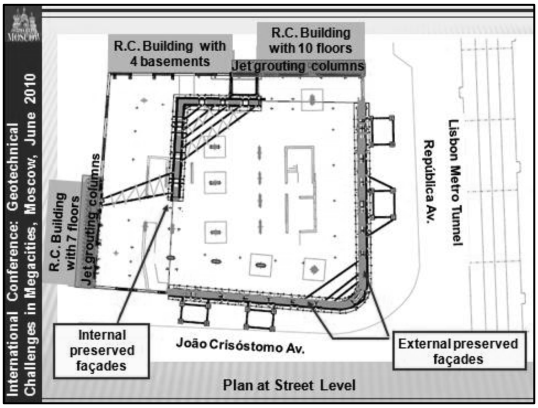

Figure 2. Plan at street level

2.3. Neighbourhood conditions

The main neighbourhood conditions were the 3 contiguous buildings, with reinforced concrete structures, each one with 4 basement floors, 10 and 7 upper floors, the several infrastructures located under the avenues walkways, as well as the Lisbon Metro Tunnel, located under the República Av, just about 8 meters from the excavation pit and having a plain concrete cross section (figures 2 and 3).

The adopted solutions were designed in order to minimize any damage on the neighbourhood structures and infrastructures.

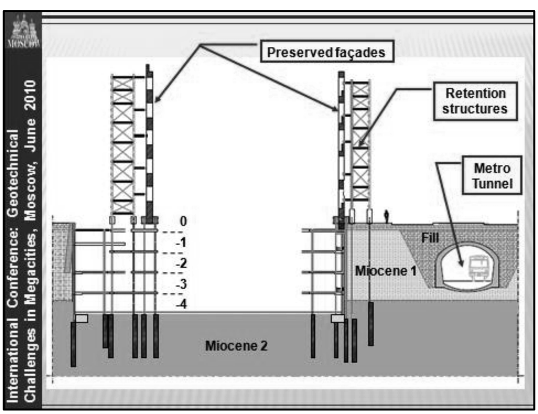

Figure 3. Cross section of the excavation pit and preserved façades

3. MAIN SOLUTIONS

3.1. Retaining walls

The adopted solution for the retaining walls was a King Pile wall (Berlin) with 0,30m thickness reinforced concrete panels, temporally supported on hollow steel tubular micropiles N80 ∅139,7 × 9 mm (API 5A), internally reinforced with one ∅32mm bar. By constructive reasons, the micropiles were located inside and outside the panels, depending on its distance to the façades and neighbourhood buildings.

Due to the site neighbourhood conditions, mainly the proximity of the Lisbon Metro Tunnel, the use of ground anchors was not recommended. For this reason, during the excavation works, the retaining walls were braced, at two levels (0 and -2), by strips of the basement reinforced concrete slabs, acting as horizontal beams, integrated on a stiff frame bracing system. In order to facilitate its disassembly, at the inclined parking access ramps the slabs were replaced by temporary steel trusses (figures 3, 4 and 5).

Where the geological conditions were not favourable and bellow the existing and without basements buildings, the fills and Miocene 1 materials were previously treated using jet grouting technology. Columns with 600mm diameter spaced 500mm were adopted at the fill and Miocene 1 layers. This ground improvement procedure allowed the adoption of the Berlin solution, with only two levels of bracing system, spaced vertically 6m and located at the basement levels 0 and -2, on soft and heterogeneous soils.

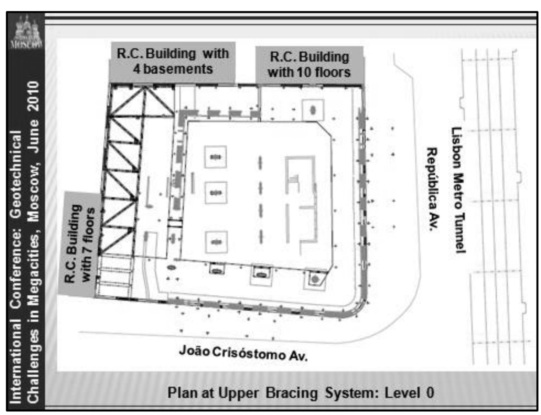

Figure 4. Plan of the upper bracing system (level 0)

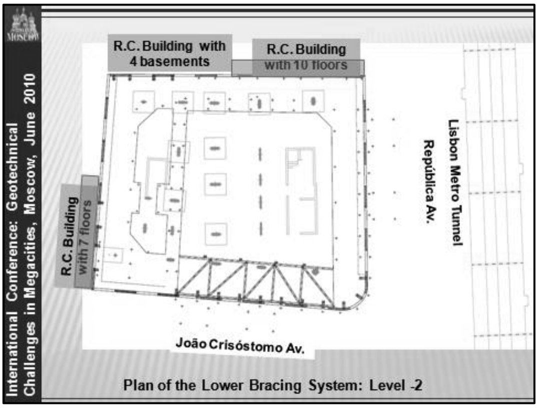

Figure 5. Plan of the lower bracing system (level -2)

3.2. Underpinning of the old façades

The adopted solution for the underpinning of the old masonry internal and external façades included the extensive use of hollow steel tubular micropiles N80 ∅139,7 × 9 mm (API 5A), internally reinforced with one ∅32mm "Gewi" bar, with external couplers at the tubes joints, and capped, in each side, by a reinforced concrete beam.

The cap beams were connected to the façades foundations through pairs of prestressed ∅32mm "Gewi" bars, allowing the load transference to the micropiles (figure 6). In order to prevent buckling, the micropiles were design for buckling coefficient not bigger than 120 and, in consequence, braced, at least, at two levels (0 and -2). As for the retaining walls, the bracing system included strips of the final basement reinforced concrete horizontal slabs, cast against the ground, or temporary steel trusses, at the car parking ramps.

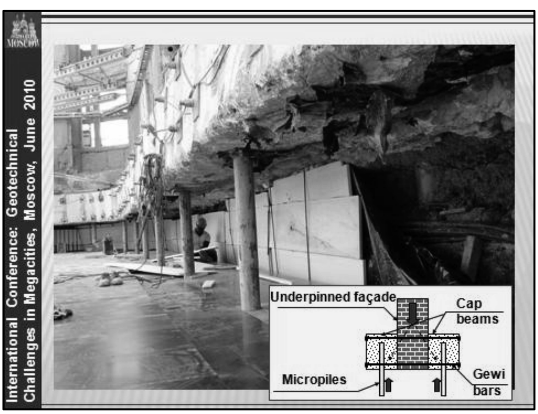

Figure 6. Underpinning of the external old façades

The façades underpinning solutions were complemented with the adoption of upper retention structures to resist to horizontal loads, mainly wind load. For this purpose RMD Kwikform prefabricated solutions were adopted (figures 6 and 7).

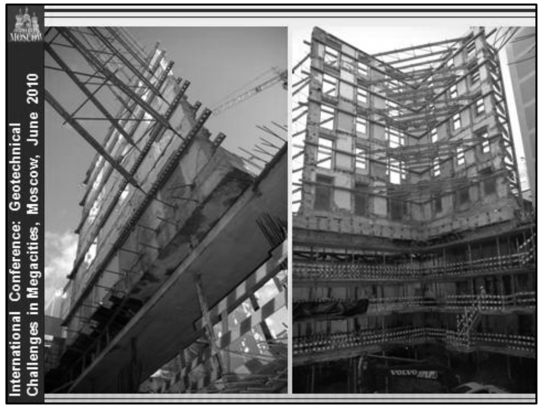

Figure 7. Underpinning of the internal old façades

4. DESIGN

The design of both the underpinning and the retaining walls solutions, including the bracing systems, was performed using a 2D and 3D FEM geotechnical and structural models: Plaxis Professional V9.02 and SAP2000 V.14.

Internal forces and displacements at the retaining walls and microplies, as well as at the supported soil and Metro Tunnel, were analyzed and predicted for all the main construction stages (figures 8 and 9). All the main geotechnical parameters were established taking into account the results of previous laboratorial and in situ tests (table 1).

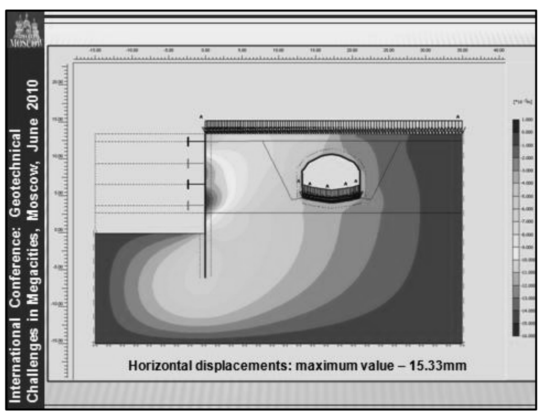

Figure 8. Results of static calculation using Plaxis software

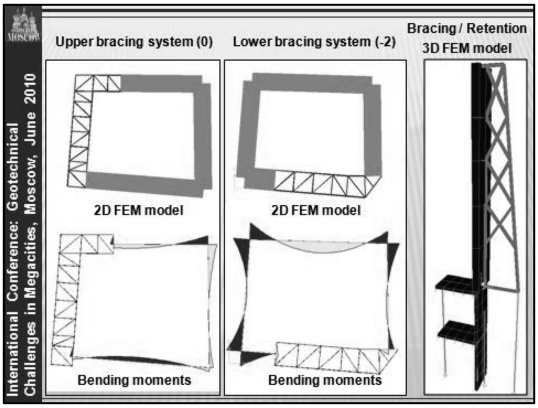

Figure 9. Results of numerical calculation using SAP2000 software

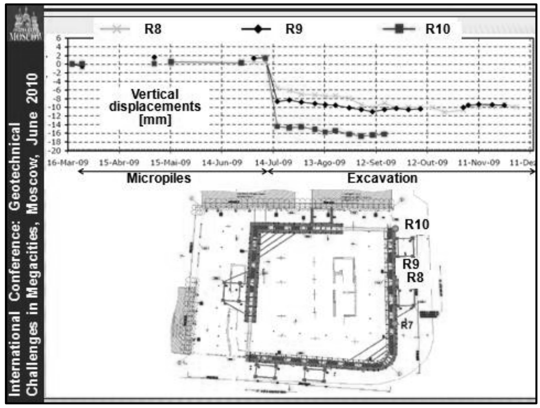

Figure 11. Main results of topographic rules (R)

5. MONITORING AND SURVEY PLAN

Considering the scenario and the complexity of the described solutions, a wide monitoring and survey plan was applied, taking into account the need to perform the underground construction in safe and economical conditions for both the site and the neighborhood conditions. The following main devices were installed:

- 36 topographic targets (TT), at the preserved façades and neighborhood buildings and 15 topographic targets (TT), at the Metro tunnel;
- 10 topographic marks (TM), at the Metro tunnel;
- 11 topographic rules (R), at the preserved façades and neighborhood buildings;
- 4 inclinometers (I).

The location of the main monitoring devices is indicated in Figure 10. Measurements were performed, at least, once a week.

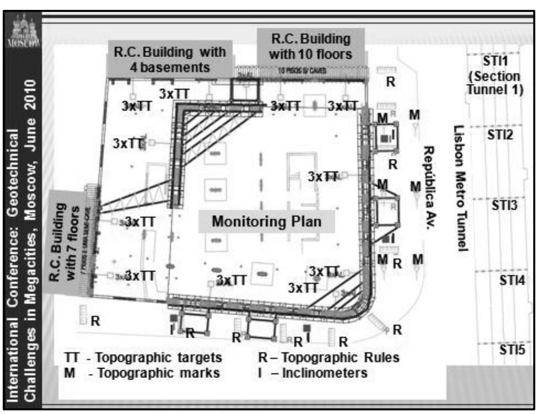

Figure 10. Plan of the monitoring devices

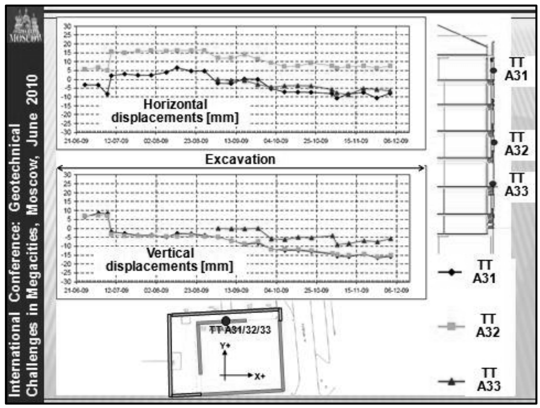

Figure 12. Main results of topographic targets (TT)

Based on the calculation results, alert and alarm criteria were established for the measurements regarding the displacements of the retaining walls, preserved façades and the Metro Tunnel (MT). Reinforcement construction measures were established, in case the alert or alarm criteria could have been reached.

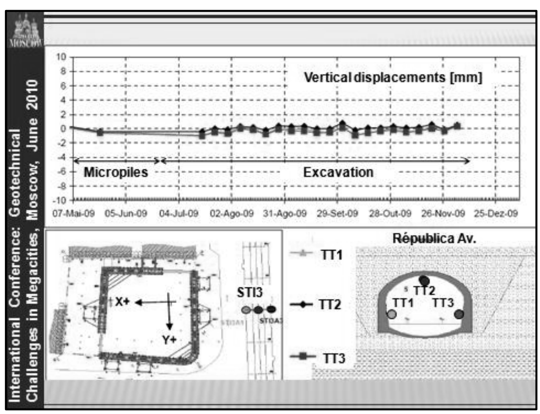

Figure 13. Main results of topographic targets at MT

Figure 14. View of the jet grouting works

The main results of the monitoring and survey plan confirmed the site and neighborhood buildings and Metro Tunnel good behavior. The maximum horizontal and vertical displacements at the site, measured at the preserved façades, were not bigger than 20mm (figures 11 and 12). These maximum values occurred when the façades loads were transferred from the original arch foundations to the micropiles. The displacements at the Metro Tunnel were negligible (figure 13).

6. MAIN QUANTITIES

It is possible to point out the following main quantities, regarding the geotechnical works:

- 2.600m of vertical micropiles N80 ∅139,7 × 9 mm (API 5A), internally reinforced with 1 ∅32mm "Gewi" bar;
- 200m of horizontal ∅32mm "Gewi" bars;
- 500m of ∅600mm jet grouting columns;
- 15.000 m^3 of soil excavation.

Figure 15. View of the initial excavation works

Figure 16. View of internal façades bracing system

7. MAIN CONCLUSIONS

The demand for underpinning has increased steadily in the last years as renewals and refurbishment works have gained popularity. As example, the presented case proved how the versatility of some underpinning techniques can fit the uniqueness and restraints of complex scenarios, involving old and historic sensitive structures. In this context, it is also important to point out that underpinning works requires design and execution expertise, especially when the underpinned buildings or façades have an old structure and a special architectural/historical interest and therefore are protected from demolition or alteration. In these situations, considerable care is required on previous tasks, as for example: monitoring and survey, geological and geotechnical site investigation, as well as structural stiffen, grout and strut, in order to carefully prepare these old structures and their original foundations for the complex underpinning works.

Figure 17. External micropile - wall connection

Figure 18. View of the steel truss at the lower bracing system (level -2)

Taking into account the described scenario, in this paper the main design and performance issues of unusual urban excavation in central Lisbon, including the underpinning works of old and historical façades were presented. The main adopted conditions and solutions were described (figures 14, 15, 16, 17, 18, 19 and 20) and the main monitoring and survey results were presented. Those results show that the obtained displacements were small and, in general, lesser than the estimated ones, confirming, as well as with the accomplishment of both the initial predicted schedule and main quantities, the overall suitability of the adopted solutions

8. ACKNOWLEDGEMENTS

The authors are grateful to the Building owner, *CERQUIA S.A.*, for his permission to the presentation of this paper.

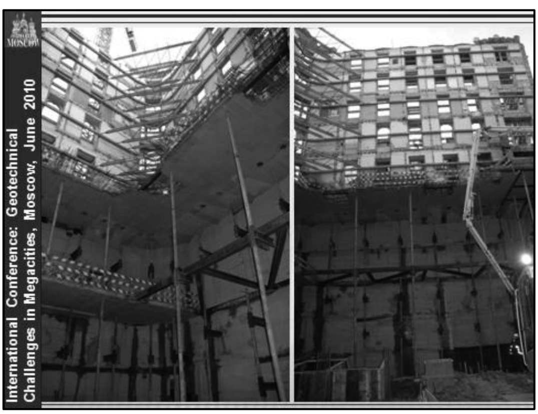

Figure 19. View of the underpinned external old façades

Figure 20. View of the final excavation works

9. REFERENCES

Bullivant, R. A. & Bradbury, H. W. 1996. *Underpinning – A practical guide*. Oxford, Blackwell Science.

Bustamante, M. and Doix, B. 1985. Une méthode pour le calcul des tirants et des micropieux injectés (in french). *Bull. Liasion Labo. P. et Ch., nº140*, p.75-92.

Bustamante, M. et al. 1997. Underpinning of the Bordeaux Pont-de-Pierre: A First Empire masonry. *Geotechnical Engineering for the Preservation of Monuments and Historic Sites*, p. 551-559. Rotterdam, Balkema.

Kutzner, C. 1996. *Grouting of Rock and Soil*. Rotterdam, Balkema.

Pinto, A.; Ferreira, S.; Barros, V.; Costa, R.; Lopes, P.; Dias, J. 2004. *Sotto Mayor Palace – Design and Performance of Retaining and Underpinning Structures*, Journal Reconstruction of Cities and Geotechnical Engineering, Vol. Nº 8, pp. 30-36. ASV Publishers – Moscow & Georeconstruction Engineering Co. – Saint Petersburg (in Russian).

Pinto, A. & Gouveia, M. 2004. *Teatro Circo: Underpinning works for the underground enlargement of a Centenary Theatre*. Journal Reconstruction of Cities and Geotechnical Engineering, Vol. Nº 7, , pp. 169-174. ASV Publishers – Moscow & Georeconstruction Engineering Co. – Saint Petersburg (in Russian).

Analysis of historical monuments condition using soil-structure interaction approach

V.M. Ulitsky
Saint Petersburg State Transport University, Russia

A.G. Shashkin, K.G. Shashkin, M.B. Lisyuk
NPO “Georeconstruction-Fundamentproject”, Saint Petersburg, Russia

ABSTRACT: Many important historical monuments in Saint Petersburg have been analysed by the authors using soil-structure interaction (SSI) approach. Among them are the Admiralty building in central Saint Petersburg and St. Nicholas Naval Cathedral in the town of Kronshtadt near Saint Petersburg. They are presented in this paper. It is shown that SSI is a very powerful tool in analysing historical monuments. The potential of this method lies in the complete description of the stress-state of the monuments and in possibility to develop measures of the monuments’ remediation. To fulfil this method successfully a comprehensive survey of the monuments is needed. Essential parts of this survey are: survey of structural elements and foundations, geophysical research, soil sampling and testing, in-situ testing of soils. All these findings can be used in SSI analysis.

1. INTRODUCTION

Analysis of historical buildings condition is very important for projects dealing with preservation or reconstruction of historical monuments and their foundations (Burghignoli, Jamiolkowski, and Viggiani, 2007, Powderham, 2003, Ulitsky et al, 2003).

Such analysis should include the following steps:

- Analysis of the actual stress - strain conditions of subsoil of preserved buildings, and, if necessary, of adjacent buildings;
- Estimation of the influence of present vibration background on settlement development;
- Estimation of ongoing settlements of buildings (under own weight and outside factors), that is defined through calculations or observations the location of geodetic marks and gauges;
- Estimation of the allowable additional settlement of the existing buildings during reconstruction works or new development.

For important projects it is also necessary to make historical analysis of foundation behaviour of preserved/reconstructed buildings and buildings adjacent to reconstructing object or to new development together with substructure behaviour of the existing buildings;

In this paper analyses of stress-strain state of 2 historical monuments are presented.

2. ANALYSIS OF THE ADMIRALTY BUILDING IN CENTRAL SAINT PETERSBURG

First example deals with the Admiralty building in central St. Petersburg (Fig. 1). The building has well pronounced cracks. The purpose of the historical analysis in this case was to find out the reason of these cracks development to make decision about further strengthening or preservation of the monument.

The Admiralty tower was constructed in 1734 by I. Korobov. In 1811-1823 the Admiralty was reconstructed by A. Zakharov, who enlarged the tower and made some structural rearrangements.

The tower has a rigid structure. It rests on stone foundations supported by wooden piles (Fig 1b). The subsoil under the tower is loaded more than under the adjacent lower wings of the building. Therefore the tower suffered bigger settlement than the adjacent wings. The cracks appeared in the wings near the location of windows.

The subsoil of the Admiralty is comprised of fine-grained saturated sand of medium density and soft clayey sands. A thorough survey of the foundation has been made. The stone foundations were inspected by a mini TV camera lowered down the survey holes predrilled through the stone foundations.

(a)

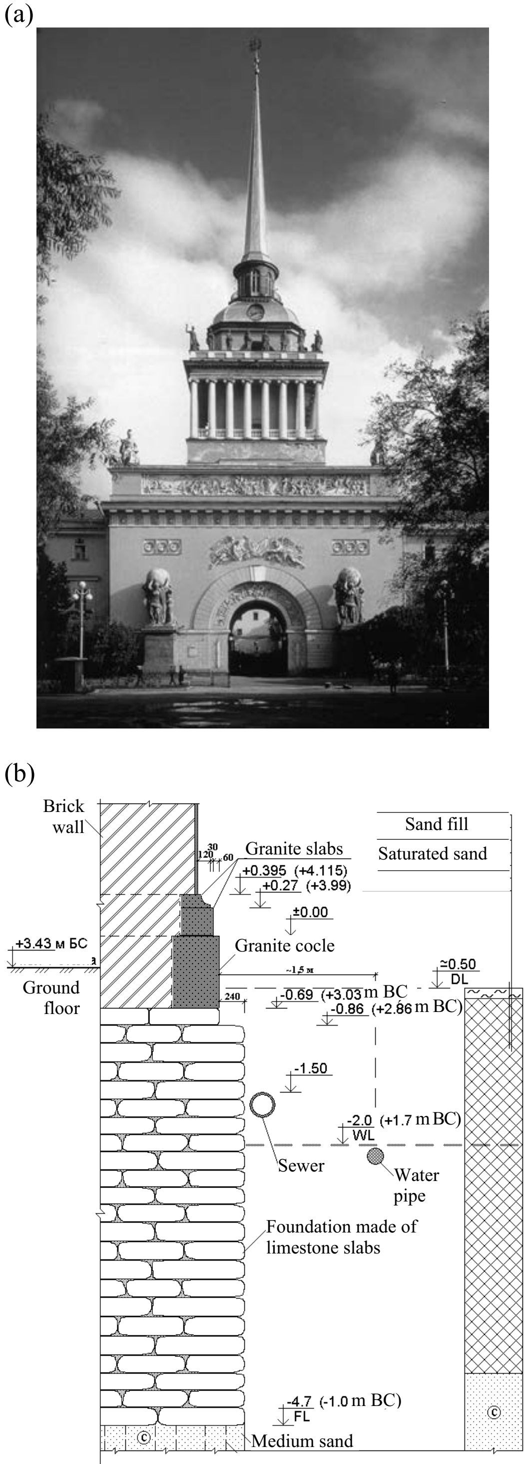

Fig. 1. (a) The building of the Admiralty, (b) historical foundation under the Admiralty tower

It was found out that the average percentage of voids in the foundation body was in the range of 1 to 10%. General condition of the foundations was found to be satisfactory, except for one part of the foundation under a transverse walls of the tower.

The structural survey of the building made it possible to identify all cracks in the walls. It was discovered that many cracks appeared in the bearing walls of the tower.

To find out the reasons of the cracks development in the tower a 3D soil-structure interaction analysis has been performed. All findings made during the geotechnical and structural survey of the building have been taken incorporated into the design scheme.

Initial construction and consequent reconstruction of the building was modelled. First the deformations of old Korobov's Admiralty tower (1732) were assessed, and then the modifications of the design scheme were made with account of the added walls (1816) and additional loads (Fig. 2). Thus, the real construction history had been simulated.

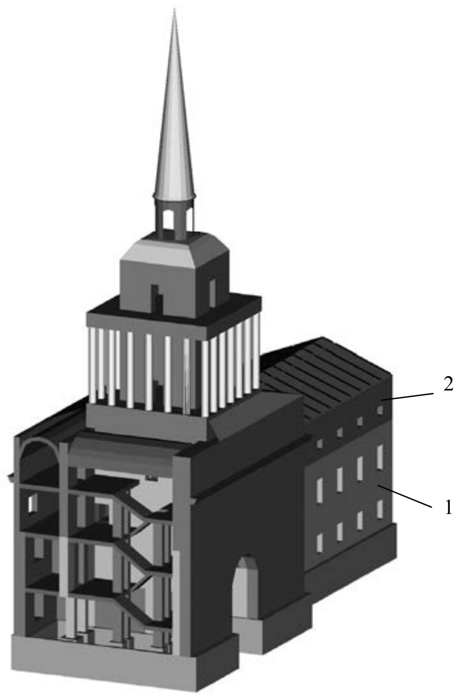

Fig. 2. Part of the calculation profile for the Admiralty building: 1 – masonry of 1732, 2 – masonry of 1816. Subsoil not shown but it is incorporated into the calculation profile

The contours of settlements accumulated after reconstruction of the building are shown in

Fig. 3. The total estimated settlements have a value of about 20 cm. It should be noted that the soil model used in the analysis can take into account a long-term creep of the Admiralty's subsoil.

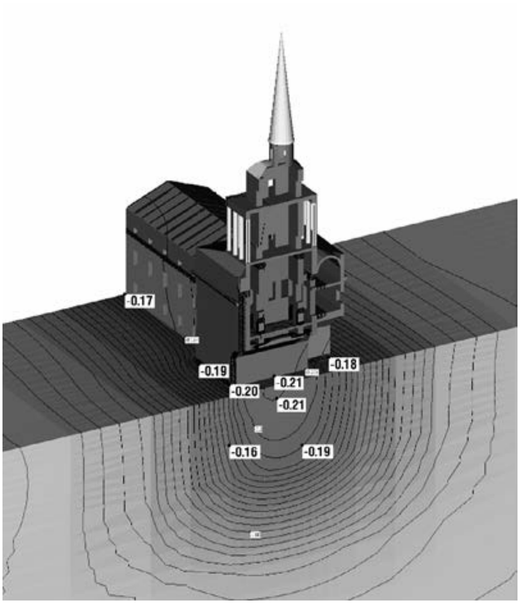

Fig. 3. Contours of computed of settlements of the Admiralty (cross section along the symmetry axis), cm

The performed analysis has made it possible to identify the reasons of the cracks development in the structural elements of the building. The main crack appeared in the tower wall adjacent to the lower wing. The reason of this crack development is the non-uniform settlement of the building. The development of settlements may still go on, which can be explained by a long-term creep of the subsoil. The non-uniform settlement leads to the generation of shear stresses in the walls with their maximum values up to 235 kPa (Fig. 4a).

The shear stresses cause the development of the cracks in the tower walls (fig 4b). There is a good correspondence between the soil-structure interaction calculation results and the observed behaviour of the building (fig. 5).

Thus, the conducted historical analysis of this geotechnical problem taking into account joint behaviour of the Admiralty' structure and subsoil as well as the construction history helped to identify the reasons of the deformation of this famous monument in the central Saint Petersburg.

(a)

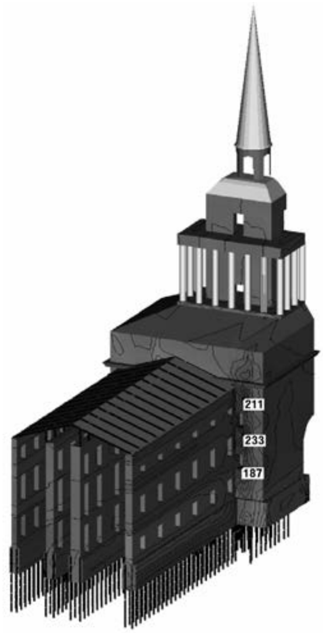

(b)

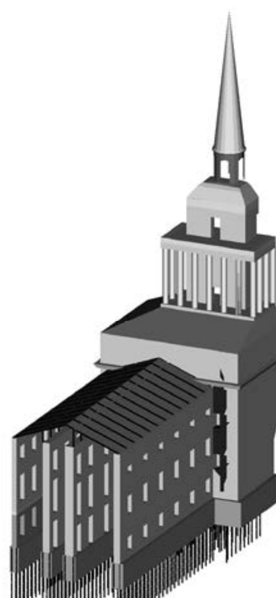

Fig. 4. Analysis of the structure of the building: (a) contours of the shear stresses in the masonry (kPa), caused by the differential settlement of the tower and the lower wing; (b) zones of the possible development of the cracks caused by shear deformations of the transverse wall

Fig. 5. Development of cracks in the Admiralty tower

3. ANALYSIS OF ST. NICHOLAS NAVAL CATHEDRAL IN KRONSHTADT NEAR SAINT PETERSBURG

St. Nicholas Naval Cathedral is located in the town of Kronshtadt (Fig. 6). It was built in 1902-1913 according to the project of V.A.Kossiakoff. In this cathedral an idea of a classical cruciform church with a domed roof was fulfilled. This idea was realized first in the famous St. Sophia Cathedral in Constantinople.

In fulfilling ancient architectural traditions new structural materials, introduced in the beginning of the 20 century, have been used. The main dome is supported by the system of steel beams. The dome is made of the reinforced concrete. Four big pillars are the main supporting elements of the cathedral.

Geological investigations were made in 1897 and 1902. Eighteen boreholes were bored to the depth of 27.7 m. The bearing layer of subsoil is a coarse sand with pebbles (thickness of the layer is 1.1-4.3. m.). This layer is underlain by moraine loams with boulders (thickness 6.4 m) and hard clays.

Due to the presence of the boulders the author of the project decided to construct foundations made of cast-in-place reinforced concrete avoiding construction of piles.

Fig. 6. St. Nicholas Naval Cathedral in Kronshtadt

Immediately after the construction completion the differential settlement was recorded with the value of about 4 cm.

During the Cathedral's life a lot of cracks have been developed. In May 2009 a sharp local increase of a crack in one of the abutments was observed. This endangered the stability of the whole structure. A special programme of cathedral structural survey, research and development of salvation measures was put forward. The key issue of this investigation was to find out the reasons of cracks development.

Some dangerous cracks in the cathedral's structures are shown in Fig. 7 and 8.

Fig. 7. Cracks in the vaults of the cathedral

Fig. 8.Cracks in the wall of stairwell passage

The scope of the survey works was the following:

- Full structural survey of the cathedral was completed

- 11 holes have been drilled through the foundations body to the subsoil. Scheme of test boreholes is shown in Fig. 9. The condition of the foundations and subsoil was estimated.

- Dynamic sounding of the subsoil was made

- A detailed geophysical investigation was made. This investigation showed that there are several zones of subsoil local softening due to leakage of water. These zones are located in the vicinity of the engineering networks. Around the cathedral a partially decayed timber sheet pile wall was found out.

- Soil samples from the holes were taken; main properties of soil were determined.

It was found out that the condition of subsoil and foundations was satisfactory.

A series of soil-structure interaction computations has been performed with the help of *FEM models 2.0* software (Ulitsky V.M. et al, 2003). The computation profile is shown in Fig. 10. All main structural elements, foundations, and subsoil layers have been incorporated in the computation profile. All main findings during the condition survey of structural elements, foundations, and subsoil have been taken into account in computations.

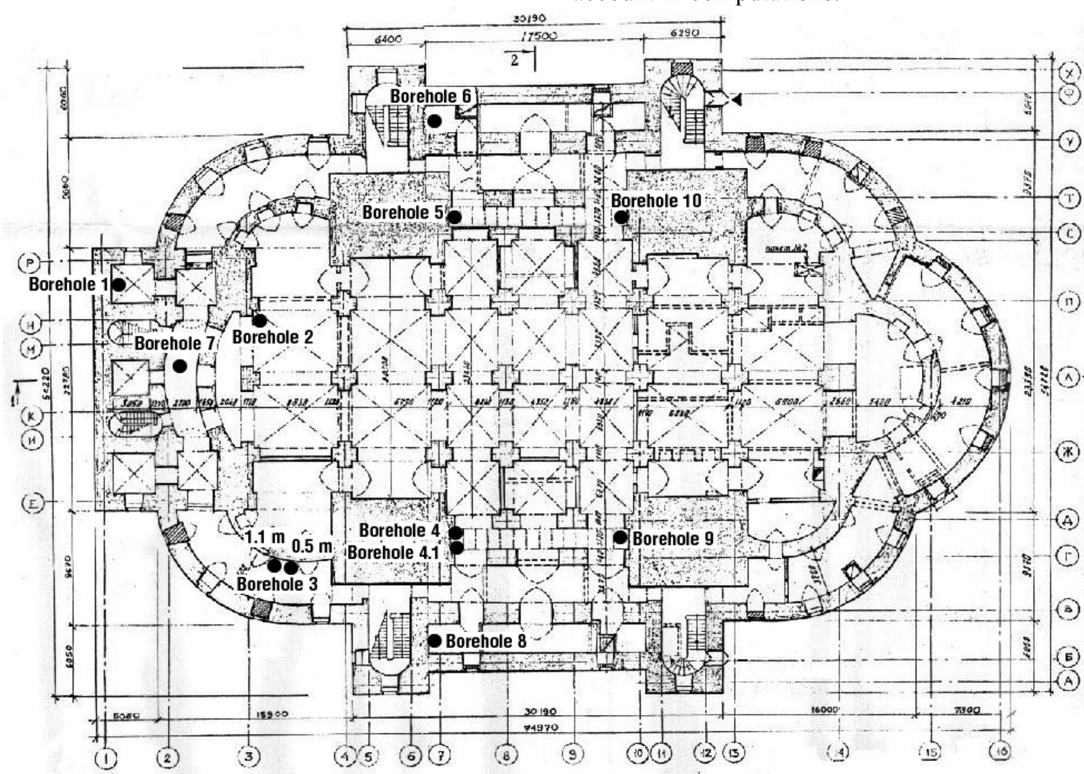

Fig. 9. Location of test boreholes drilled through foundation body to the subsoil

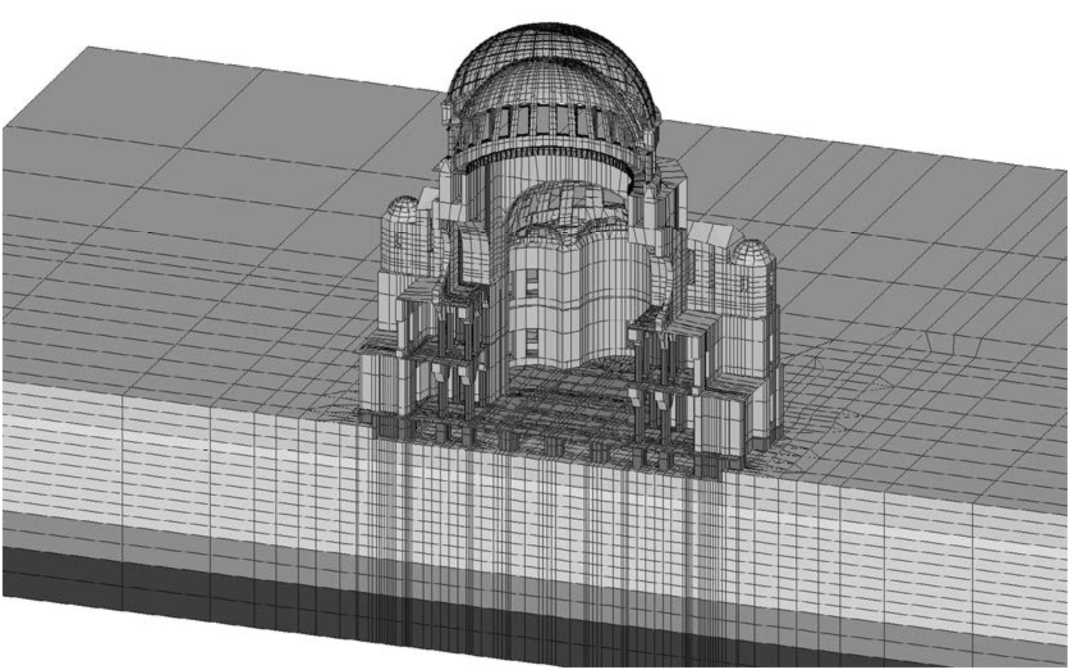

Fig. 10. Computation profile of the cathedral

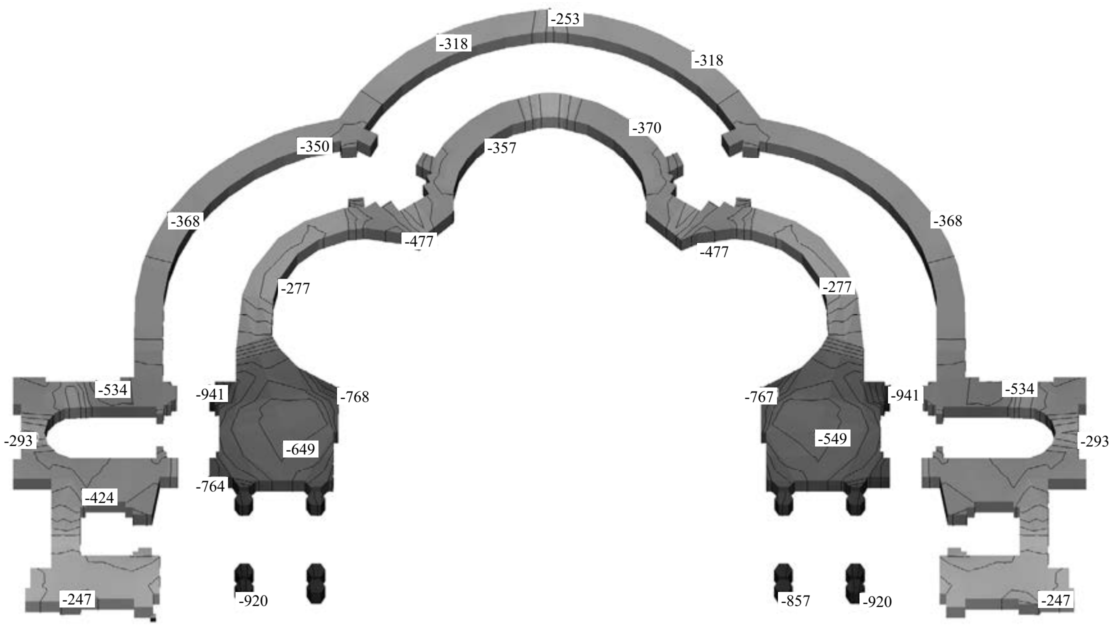

Fig. 11. Distribution of vertical stresses (kPa) in the main bearing structures of the Cathedral on the level of the 1st floor. The most heavily loaded are the main pillars, the least loaded are the walls of the outer galleries

Soil-structure interaction calculations showed that the cathedral is subject to non-uniform settlements. The reason of these settlements is the different loads acting to the main bearing structures of the Cathedral (Fig. 11, 12). Such non-uniformity of loads is quite typical for the temples characterized by cross-cupola structural scheme. The most heavily loaded are central pillars by which the central cupola is supported. Hence, the pillars are subject to bigger settlements. The calculated non-uniform settlements (Fig. 12) correspond well to the results of the geodetic measurements. The observed settlement differential is about 13-22 mm.

Computations show that the zones of development of tensile stresses in brickwork well agree with the locations of actual cracks. In particular, taking into account non-uniform settlements we have a characteristic system of cracks in the semi-domes in altar and Western parts of the Cathedral (Fig. 13 and 14).

The main conclusion of the conducted investigations and SSI computations is that currently there is no danger of an immediate collapse of the Cathedral.

Local mostly endangered structural elements are: the main dome, its supporting elements and semi-domes in Eastern and Western parts of the cathedral. Local reinforcement must be provided as soon as possible. This reinforcement must be based on the detailed analysis.

The computations of the system "subsoil-foundations-superstructure" show that all main cracks in the structural elements of the cathedral are caused by differential settlements of the monument (Fig. 12), conditioned by the non-uniform loading of the subsoil. The most dangerous cracks caused by differential settlements are the cracks in semi-domes in Eastern and Western parts of the cathedral.

General strengthening of the monument must be realized on the basis of SSI computations as required both by local codes (TSN 50-302-2004) and International codes, for example Eurocode 7 (Frank, 2006).

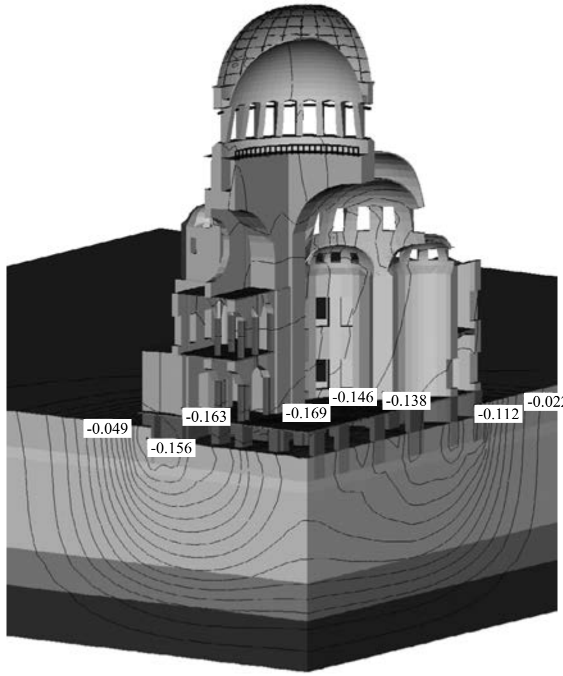

Fig. 12. Contours of computed of settlements of the Cathedral, cm

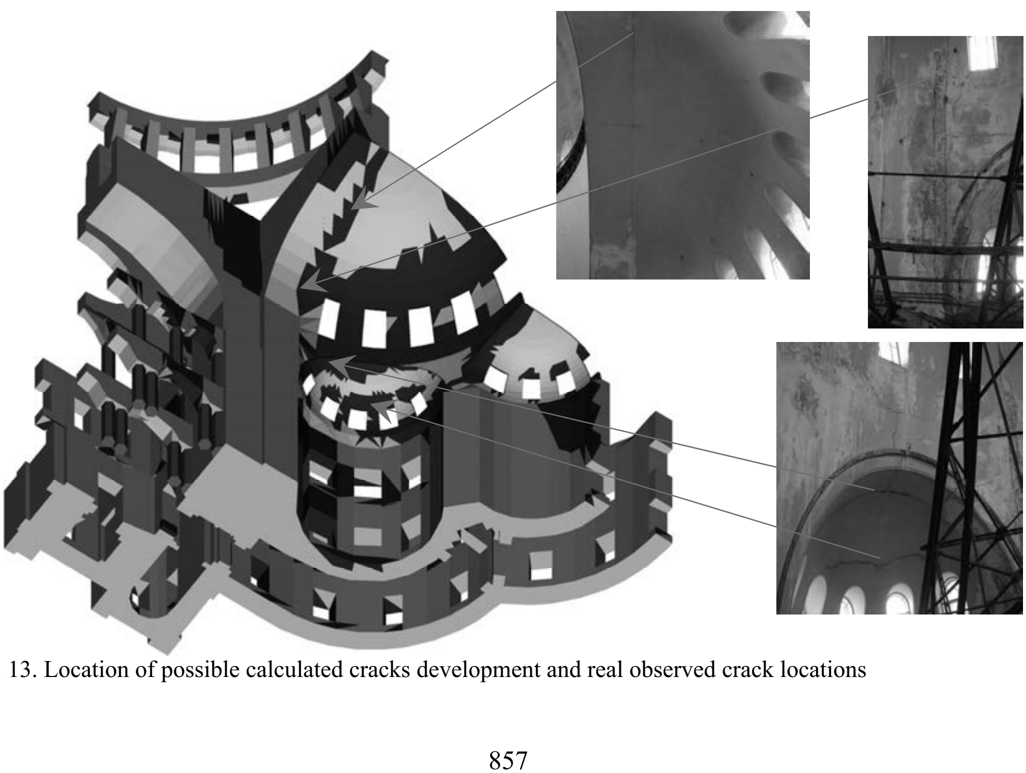

Fig. 13. Location of possible calculated cracks development and real observed crack locations

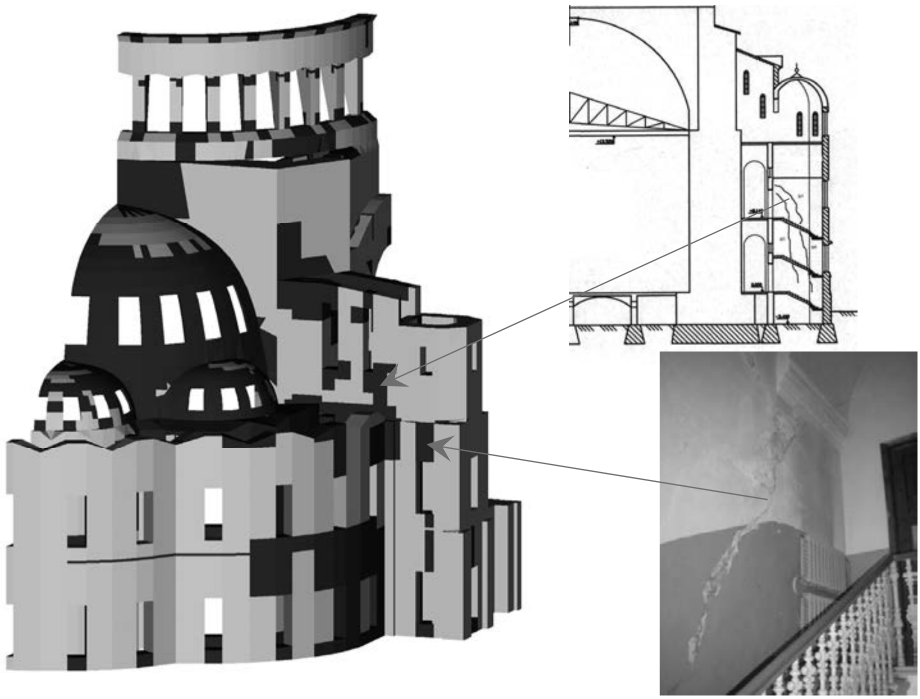

Fig. 14. Location of possible cracks development by calculations as compared with the real observed cracks

4. CONCLUSIVE REMARKS

Two examples of historical monuments are presented in this paper - the Admiralty building in central Saint Petersburg and St. Nicholas Naval Cathedral in the town of Kronshtadt near Saint Petersburg.

As these examples show, it is very important to use soil-structure interaction approach in design monuments preservation in urban areas. SSI approach is very efficient at all stages of analysis of monuments. It is a very powerful tool in prediction of behavior of preserved buildings and structures.

Successful application of SSI approach requires a very comprehensive survey of the monuments. Essential parts of this survey are: survey of structural elements and foundations, geophysical research, soil sampling and testing, in-situ testing of soils. Results of these investigations must be used in SSI analysis.

5. REFERENCES

Burghignoli, A. Jamiolkowski, M., and Viggiani, C. 2007. Geotechnics for the preservation of historic cities and monuments: components of a multidisciplinary approach. General report. *Proc. of XIV European conference on Soil Mechanics and geotechnical Engineering "Geotechnical Engineering in Urban Environments"*, Madrid, Volume 1.

Frank R. 2006. Some aspects of soil-structure interaction according to Eurocode 7 'Geotechnical design', *Engenharia Civil/Civil Engineering*, Universidade do Minho, Portugal , No. 25, pp.5-16.

Powderham, A. 2003. Protecting historical infrastructure using the Observational Method. *Proceedings of the geotechnical conference "Reconstruction of historical cities and geotechnical engineering"*. St. Petersburg, 16-18 September 2003. Vol. 1, pp. 243-250.

TSN 50-302-2004. *Design of foundations for buildings and structures in St. Petersburg*. Local constructional codes for St. Petersburg. Government of Saint Petersburg, 2004.

Ulitsky, V.M., Shashkin, A.G., Shashkin, K.G., and Lisyuk, M.B. 2003. Soil-structure interaction: methodology of analysis and application in design. ASV Publishers. St. Petersburg – Moscow. 40 p. (in English)

Ulitsky, V. 2003. Geotechnical challenges in reconstruction of historical cities (as may be illustrated by St. Petersburg). *Proceedings of the geotechnical conference "Reconstruction of historical cities and geotechnical engineering"*. St. Petersburg, 16-18 September 2003. Vol. 1, pp. 13-28.

Strengthening and reconstruction of foundations

Performance of CSM stabilised soils in geotechnically complex formations.

M.Grisolia, I.P. Marzano, D. De Lentinis, E. Leder
Sapienza Università di Roma

ABSTRACT: The paper represents an initial part of an more extensive study aimed at developing simple operative criteria to optimise the cutter soil mixing process in the presence of geotechnically complex formations (e.g. layered subsoil with high variability of mechanical and hydraulic properties). To achieve homogeneity along the depth of a column it is necessary to adapt the treatment to the different soil strata. For this purpose, an extensive laboratory testing programme was carried out to examine the effect of cement contents on the mechanical and physical properties of different treated soils. The study shows that relatively homogenous results in terms of compressive strength and permeability may be reached by modifying the treatment parameters. The results constitute a preliminary useful guide to adapt the construction techniques in actual field applications.

1. INTRODUCTION

Deep mixing is a relatively new in-situ treatment technology aimed to improve the mechanical and hydraulic properties of soils. Wall panels are constructed using sets of multiple mixing tools combined into a single unit using a rotary drilling technology.

In contrast, the new Cutter Soil Mixing or CSM technique is derived from the cutter technology. The soil is loosened and broken down by cutter wheels, and in-situ mixed by the rotating cutter wheels to form a soil-slurry mortar.

CSM offers versatile construction solutions suitable to various types of ground improvement and retaining structures as circular shafts, temporary walls for urban excavations, Berlin walls, etc.

Grout composition and construction parameters allow to achieve specific permeability and strength, providing an efficient and effective retaining solution.

CSM walls are generally made of successive primary and secondary panels, as usually done on traditional diaphragm walls. The secondary panels may be done either in fresh primaries or in hardened ones (a couple of days after primary panel installation).

If needed, a CSM panel can be reinforced by insertion of steel beams into the fresh mixed material to resist bending moments. This reinforcement requires generally a simple crane with no additional vibration means.

Compared to traditional diaphragm wall techniques, the CSM is more environmental friendly due to the low production of wasted material. The treatment of contaminated soils can save the cost of expensive waste disposal.

Compared to other deep mixing techniques, CSM can also penetrate layers of stiff to hard layers into geotechnically complex formations characterised by unpredictable and strong variation of the geotechnical properties.

The result of treatment, in terms of homogeneity and continuity, is a function of the construction techniques that must be adapted to the different crossed soil layers.

In general it could be assumed that in the first working phase, the preliminary crashing of the hard material layer will produce a mix with the fine graded material. This loose and broke down soil, which composition is a function of the frequency and stiffness of the crossed layers, will be subsequently encompassed in the self hardening slurry.

In reference to the typical sequence of Italian turbiditic complex formations between arenaceous (A) and pelitic (P) layers (A.G.I. 1979 Figure 1), the average composition of the loose and broke down material was simulated in laboratory by assigning different initial granulometric compositions to the soils to be tested. With reference to the Figure 1, three kind of soils were preventively selected.

This work has been carried out as part of a large international collaborative study with the objective of comparing the effect of treatment parameters on the geotechnical properties of cement-stabilised soils.

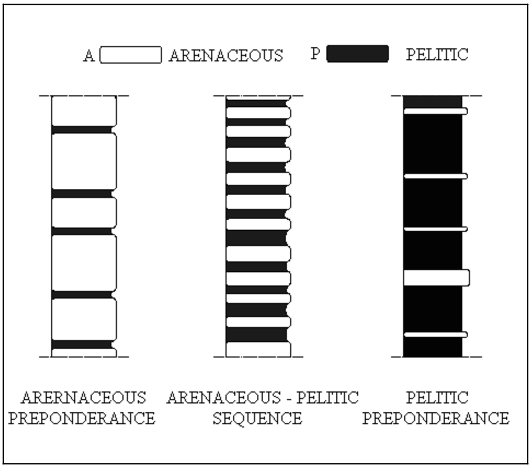

Figure 1. Typical sequences in turbiditic geotechnically complex formations.

2. EXPERIMENTAL WORK

The effect of the binder content on the mechanical and hydraulic properties of treated soils, namely unconfined compressive strength, secant modulus and permeability, was analysed on about 200 laboratory tests.

Duplicate samples were used for permeability testing and triplicate samples for the UCS test.

Three different natural soils, namely sand and gravel (I), silty sand (II) and clayey silt (III), were tested with the aim to simulate different initial stratigraphic sequences of a geotechnical complex formation (Figure 1). The top size of the gravel was artificially limited to 10 mm due to the adopted specimens dimension.

Table 1. Soil type tested.

Soil type	Clay [%]	Silt [%]	Sand [%]	Gravel [%]	Water content [%]
I	13	14	40	33	8
II	18	20	40	22	36
III	24	34	24	18	30

The clayey silt had a Plastic Limit (w_P) of 19.0% and a Liquid Limit (w_L) of 37.0%, classified as CL according to the Casagrande Plasticity Chart.

Portland cement (32,5 R obtained from CementirItalia S.pA, IT) was used as the wet binder at a 5, 10 and 15% addition by weight and was applied at a water:cement ratio of 1.

The mixer used for the soil and soil-binder mixing is shown with the plastic moulds used (of about 50 mm inner diameter and 100 mm height) in Figure 2.

Figure 2. Mixer and plastic moulds.

2.1. Testing procedures

The initial water content of the natural soil was adjusted to the prefixed value by mixing operations (Table 1). The mixing process was stopped several times to remove and add back manually the soil portion sticking to the mixing wings and the bowl and continued until a homogeneous soil mix was formed.

Afterwards a Portland cement and water slurry (at a weight ratio of 1:1) was added to the soil and it was then mixed for the standard time of 10 minutes. During the mixing process, every 3 minutes or so, the mixer was turned off to obtain a homogeneous mix. The same mixing blade (‘K’ shape), time of mixing and spin velocity were always used in order to ensure the same mixing conditions for each sample.

After mixing, the treated soil was moulded in specific plastic cases (Figura 2) by dynamic compaction or rodding. The procedure consists of filling the mould in three stages. The compaction was performed by rodding each layer for 30 times with a 8 mm diameter “rod” (Figure 3).

The samples so obtained were stored in special curing tanks at 95% relative humidity. In each case the temperature was controlled and fixed at 20°C.

After about a week of curing the samples were demoulded and stored in the same tanks and under the same conditions of humidity and temperature.

After a preset curing time each sample was tested with an automatic uniaxial compression apparatus with digital data logging. Before the tests the specimens were measured and weighed and if necessary trimmed (to ensure horizontal surfaces). The compression rate was 1.0 mm/min and the tests were stopped when the post failure compressive stress was sufficiently reduced.

After the tests representative parts of the specimen were taken for water content measurements.

Figure 3. Rod and last step of the dynamic compaction.

Similar procedure was adopted for permeability tests that were carried out in triaxial cells with the constant head bottom-up flux at 4 bar cell pressure and 2 bar back pressure.

3. RESULTS AND ANALYSIS

The results of the experimental work are presented in three different sections to show the effects of the soil type and binder content on unconfined compressive strength (UCS), stiffness (E_{50}) and permeability (k).

3.1. Unconfined compressive strength (UCS)

Figure 4 shows the relationship between the average UCS values after a standard curing time of 28 days for each soil type treated at three different cement content.

The figure clearly shows, for all the analysed cement contents, a decay of strength passing from the soil type I to III. Such differences of strength increase with higher cement content.

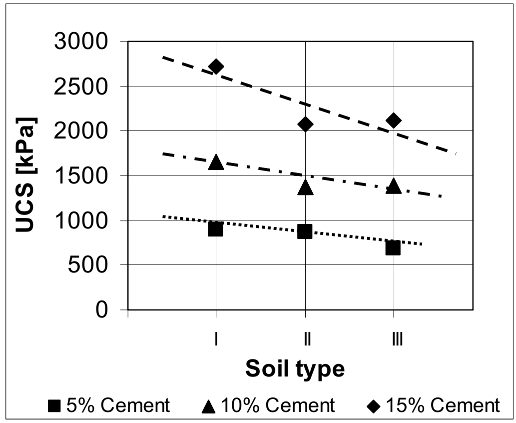

Figure 4. UCS vs. soil type for different cement contents at 28 days.

The average values of the UCS for each soil type at 15% cement content and at varying curing time are shown in Figure 5.

The results show that the soil type has a great influence not only on the strength but also on its variation with time. Figure 5 shows that after 56 curing days similar average UCS values are obtained for the three type of soil at 15% cement content.

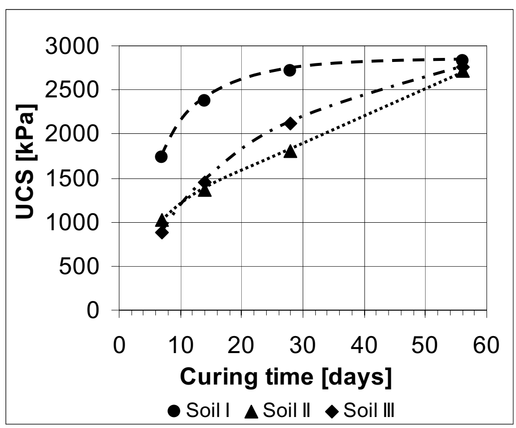

Figure 5. UCS vs. curing times for different soil types and 15% cement content.

3.2. Secant modulus (E_{50})

Figure 6 shows the average secant modulus (E_{50}) values for each Type of soil tested at three different cement contents and at the same standard curing time of 28 days.

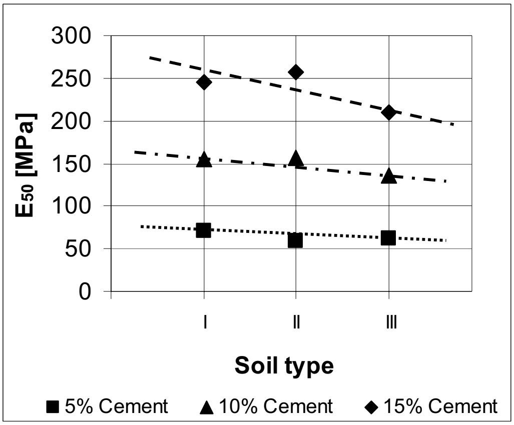

Figure 6. E_{50} vs. soil type for different cement contents at 28 days.

Similarly with the UCS tests, results show a reduction of the treated soil stiffness moving from soil type I to III. Even in this case the trend appears more evident when the cement content increases.

Figure 7 shows, for the 15% cement content, the E_{50} measured average values with the corresponding curing days for each treated soils.

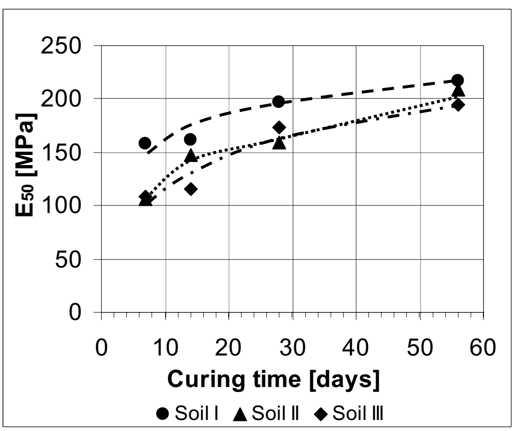

Figure 7. E_{50} vs. curing times for different soil types and 15% cement content.

The stiffness of the treated soils increases with the curing time in function of the soil type.

Similar to the UCS results, the E_{50} is significantly affected by the soil type and cement contents.

Figure 8 shows the relationship between E_{50} and the UCS obtained for the investigated soils.

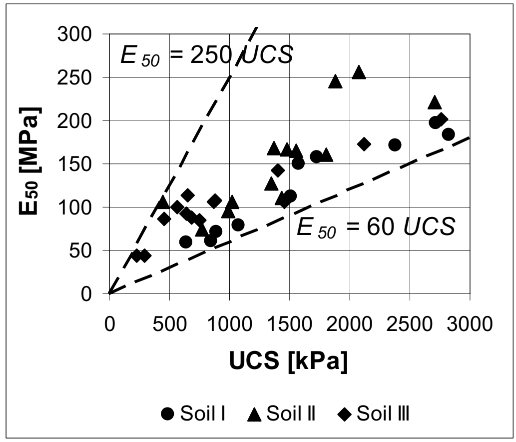

Figure 8. Obtained relationship between the UCS and E_{50}.

3.3. Permeability (k)

Figure 9 shows the average permeability values for each of the treated soils at 15% cement content and at two different curing times (7 and 28 days).

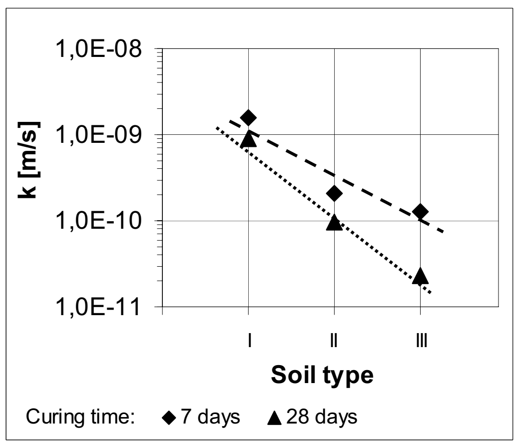

Figure 9. Permeability vs. soil type for different curing time at 15% cement content.

The initial soil composition has a great influence on the permeability of stabilised soils. After 28 curing days there is a difference of an order of magnitude in the permeability of soil I and III. Such difference increases with the curing time.

Figure 10 shows the permeability average values for each tested soil at three different cement contents and at the standard curing time of 28 days.

An increase of the cement content produces positive effects on the coefficient k.

A permeability value of 1.0E-9 m/s or less is usually required for permanent seepage control (i.e. waste and contaminant barriers to prevent groundwater pollution).

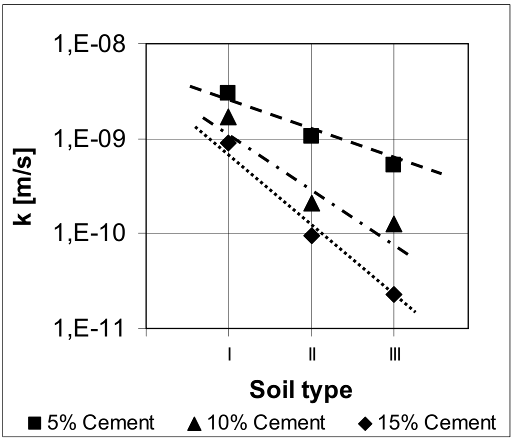

Figure 10. Permeability vs. soil type for different cement contents after 28 days.

Figure 10 shows that for the soil II and III in order to obtain such value it is sufficient a cement amount of about 10%, while for the soil I not even 15% is suitable. Also considering that the lab-measured values of the permeability may differ from the ones in situ even of one order of magnitude, in actual applications it may be necessary to increase the cement content or change the grout composition by adding bentonite.

This can be achieved by modifying the grout flux and/or penetration (or retrieval) speed or by using a computer controlled grout mixers that allow changes in the slurry composition.

3.4. Relationship between UCS and k

Figure 11 shows the relationship between the UCS and permeability coefficient k for the investigated soils at 28 days curing time.

It is clear how the permeability values decrease while the UCS increases for all investigated soils.

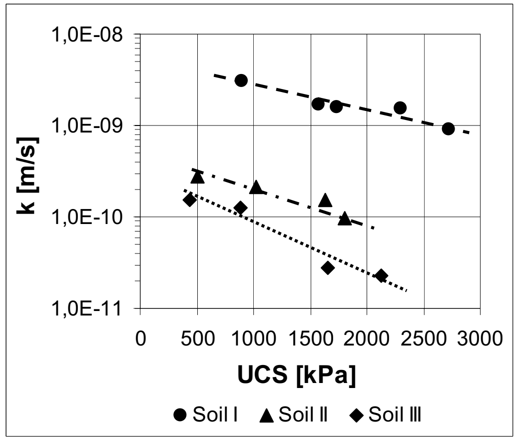

Figure 11. Obtained relationships between the UCS and k.

In a semi-log scale, for each treated soil, the points are well fitted from a two parameters exponential equation:

$$k = \alpha\, USC^{-\beta x}$$

where empirical α e β for the different soil types are represented in Table 2.

Table 2. Empirical α e β values.

Soil type	α	β
I	4,83E-09	-5,29E-04
II	4,30E-10	-7,42E-04
III	2,97E-10	-1,26E-03

4. CONCLUSIONS

The laboratory tests allowed to simulate the influence on the CSM treatment of the different strata sequence in a turbiditic structurally complex formation .

To obtain homogeneous geotechnical characteristics, in terms of unconfined compressive strength and permeability, it may be necessary to modify the main treatment parameters through the available CSM machinery such as the breaking down energy of the cutter wheels, time of retrieval, amount of slurry injected and even, with the newest equipments, the grout composition with the depth.

In any case, a preliminary significant characterization of the material to be treated is needed.

5. REFERENCES

A.G.I. 1979. Some Italian experiences on the mechanical characterization of structurally complex formations. *Proc. IV Int. Congr. ISRM (Montreux) 1, 827–846*.

Al-Tabbaa A. 2003. Soil Mixing in the UK 1991-2001: State of Practice Report. *Journal of Ground Improvement, Thomas Telford, Vol. 7, No. 3, pp. 117-126.*

ASTM 2002. Standard method for compressive strength of moulded soil-cement cylinders. *Test Method D1633-00, American Society for Testing of Materials. 04.08(I): 161 – 164.*

Bergado D. T., Lorenzo G. A. 2005. Economical Mixing Method for Cement Deep Mixing. *Proc. of ASCE GeoFrontiers Conference, GSP-136 Austin, Texas, U.S.A.*

Bringiotti M., Dossi M., Nicastro D. 2009, Miscelazione profonda dei terreni: metodi classici e tecnologie innovative – *CSM by BAUER. Geofluid 2009 (in Italian)*

Bringiotti M., Fiorotto R., Bringiotti G. 2004. Dal Cutter Soil Mix al Triple Auger I p. *Quarry & Construction, 9-2004, Edizioni Pei, Parma (in Italian)*

Bringiotti M., Fiorotto R., Bringiotti G. 2004. Dal Cutter Soil Mix al Triple Auger II p. *Quarry & Construction, 11-2004, Edizioni Pei, Parma (in Italian)*

Bringiotti M., Fiorotto R, 2005. CSM Cutter Soil Mixing - Una nuova tecnologia nel Soil Mixing per la costruzione di gallerie artificiali ed opere varie in sottosuolo mediante paratie di ritenuta. *Gallerie e Grandi Opere Sotterranee n. 74, SIG, 5-2005 (in Italian)*

Bruce D., Bruce M. 2003. The Practitioner's Guide to Deep Mixing. *Third international conference on Grouting and Ground treatment, New Orleans, USA, Geotechnical Special Publication ASCE, vol. 1, pp. 474-488.*

Hansbo S., Massarsch, K. 2005. Standardisation of Deep Mixing Methods. *Proceedings of the International Conference on Deep Mixing – Best Practice and Recent Advances, Deep Mixing'05, Stockholm, Sweden, May 23 – 25, pp. 3-10.*

Marzano I.P., Al-Tabbaa A., Grisolia M. 2009. Influence of moulding procedure, curing temperature and mixing time on the strength of cement stabilised artificial clays. *Proc. International Symposium on Deep Mixing & Admixture Stabilization, Okinawa.*

Marzano I.P., Osman A.A-M., Grisolia M., Al-Tabbaa A. 2009. Mechanical performance of different stabilised soils for application in stratified ground. *Proc. 17th ICSMGE Alexandria, Egypt.*

Mathieu F., Borel S, Lefebvre L. 2006. CSM: an innovative solution for mixed-in-situ retaining walls, cut-off walls and soil improvement. *Proceedings - DFI/EFFC 10th International Conference on Piling and Deep Foundations, Amsterdam, The Netherlands.*

Porbaha A., Shibuya S., Kishida T. 2000. State of the art in deepmixing technology. Part III: Geomaterial characterization. *Ground Improvement 4, No.3, 2000, 91-110.*

Stoetzer E., Brunner W.G., Fiorotto R., Gerressen F.W., Schoepf M. 2006. CSM cutter soil mixing – a new technique for the construction of subterranean walls initial experiences gained on completed projects. *Proceedings - DFI/EFFC 10th International Conference on Piling and Deep Foundations, Amsterdam, The Netherlands.*

O'Rourke T. D., McGinn A. J., Dewsnap J., Stewart H. E. 1998. Case History of an Excavation Stabi zed by Deep Mixing Methods. *Proceedings of Sessions of Geo-Congress 98, Geotechnical Special Publication No. 83. ASCE, Eds., 41-62 p.*

On the effect of pre-stressing using micro-pile injection

Božo Soldo
University of Zagreb; Faculty of Geotechnical Engineering

Matija Orešković
Polytechnic in Varaždin; Study Civil Engineering

Aleksej Aniskin
Polytechnic in Varaždin; Study Civil Engineering

ABSTRACT: When damages occur on structures due to their base giving in, strengthening of that base, i.e. of the foundation soil is performed. One possible method of strengthening is through the use of pipe micro-piles and pressure injection, which is the subject this paper deals with. The effect of pipe micro-pile injection, the process and successful repair are described below.

1. INTRODUCTION

Small diameter piles (micro-piles) have low rigidity and bearing capacity, but carry a very specific and important role, and can be repaired using supplementary injection. Injection of the injection mixture leads to pre-stressed surrounding soil, and after the mixture hardens, to compression pre-stressing of the hardened mixture next to the micro-pile pipe. This type of pre-stressing results in favourable features in low-permeation high-deformity soil.

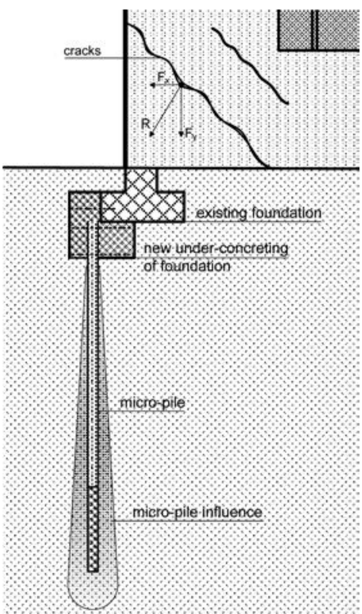

Fig. 1 Some of possible micro-pile applications: - prevention of the soil creeping under load, - decrease of settling, - prevention of differential settling

There are also more modern methods of strengthening the soil below structures, such as expansion resin (also used for soil pre-stressing). Injecting this resin into the area below the foundation has numerous advantages: no digging/excavation is necessary, there is safe laser-based movement control, the operation is quick, efficient, simple, it does not pollute the environment, there is direct contact between the soil and the construct, there are no dynamic effects, etc.

2. ABOUT MICRO-PILOTS AND INJECTING

2.1. About the micro-pilot and injection process

The steel pipe is outfitted with a sharp point at the top and lateral perforations approximately 1.0 m (depending on the length of the micro-pilot) from the top of the pipe, in order to allow seepage of the injection mixture (Figs. 1 and 3). Spiking the sharpened micro-pile pipe or its placement into a drilled bore-hole 4-5″ in diameter when faced with a low-permeation high-deformity soil is quite simple. When the steel pipe reaches the planned depth, spiking is ceased and now begins the operation of sealing the ring-shaped area between the pipe and the surrounding soil on a segment approximately 1 m below the surface of the soil. The most important operation before injection is setting the appropriate packer (Fig. 2) in the upper portion of the pipe so that the seepage of the injection mixture to the surface during injection is prevented. Next, injection is used to facilitate injection pre-stressing of the contact zone between the pile and the surrounding soil. Under pressure, the injection mixture exits the pipe through the perforations, but due to high density (and thereby high viscosity), the injection mixture, being a pressed-in fluid, cannot propagate through filtration into the surrounding soil (because the soil is not permeable enough); instead, there is an effect of compaction grouting, i.e. injected surface being created in the soil.

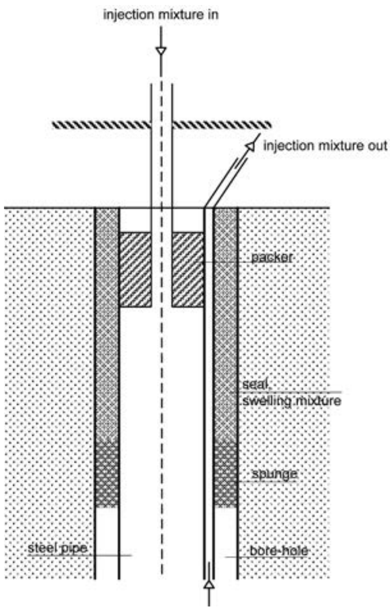

Fig. 2. Detail at the outlet of the bore-hole injection

2.2. Pipe micro-pile injection characteristics

This type of soil pre-stressing appears due to the inability of filtration seepage of the injection mass into the surrounding soil (due to low soil permeability and high density, i.e. very high viscosity of the injection mixture). Soil pre-stressing in this case also appears due to high level of deformity of the surrounding soil and due to forces speared by high working pressures ($\mathbf{p_{rad}}$) during the injection into the pipe and the underground space surrounding the pipe, especially around the top of the pipe, where perforations were made in order to facilitate injection mixture seepage.
Estimate of successful creation of pre-stressed soil around the pipe micro-pile is determined by measuring return pressures ($\mathbf{p_{pov}}$), and the volume can be ascertained according to the quantity of injection mixture used.
The total volume of the mixture used (V_u) for the pile in question contains two components: V_o = volume of the mixture contained within the steel pipe and V_g = volume of the mixture outside the pipe, with the ratio being:

$$V_u = V_o + V_g \quad (1)$$

Coefficient of realized injection volume κ may be formulated as follows:

$$\kappa = \frac{V_g}{V_o} = \frac{V_u - V_o}{V_o} = \frac{V_u}{V_o} - 1 \quad (2)$$

In theory, the coefficient may have values between: $0 \le \kappa \le \infty$ (most often 2 to 10).
If the return pressure is very low and the coefficient **κ** is close to zero, that means the soil features low deformability (semi-hard or hard clay).
If the return pressure is low and κ is high, the soil is very deformable, which may mean:
- The soil contains cracks or other paths (for example, holes along dead roots, ground hog holes, etc.)
- The soil contains intercalations (or thicker layers) of high permeability
- The injection mixture entered the holes (in some underground areas, etc.)
- Due to overly high pressure, the ground fractured *(fracturing - hydrofracture grouting)*, and the injection mixture filled the cracks
- In very soft, non-consolidated and water-saturated dusty/muddy layers there exists a high probability for the injection mixture heterogeneously mixing with the muddy materials (creating round, bubbly accumulations). The effect of stress in the soil is partially transformed and weakened, although the coefficient κ may carry a high value. The quality of the above process is shown through increased density and total stiffness of the injected zone, decreasing the total soil deformability along the micro-pile pipe.

The average strain effect surrounding the pipe micro-pile is estimated using two parameters:
p_{povr} >1 bar (better: p_{pov} >5 bar)
κ >1 (better: **κ**>3)

2.3. Effect of soil strain due to injection

When the injection mixture is allowed to solidify, i.e. become properly dense (minimum

of 30 minutes, usually around 60 minutes), packers are taken down from the micro-pile pipe. In order to prevent the rising seepage of the mixture due to return pressure, it is necessary to hold initial pressures in the soil (especially those in contact with the surrounding soil) to levels as high as possible.
After a few days the injection mixture hardens, and fluid pressure fills the stress area; however, the area of the contact with the surrounding soil will keep the pre-stress effect, manifesting in the surrounding soil increasingly pressuring the hardened contents within the pre-strained area.
Said phenomenon has a positive effect on the pile bearing capacity from two aspects:
- The hardened injection mixture is exposed to increased spatial pressure stress (pre-stressing), increasing its resistance to rifts in the pipe
- Soil around the stress contour is in high-compression state, resulting in decreased porosity and deformability, and to increased bearing capacity.

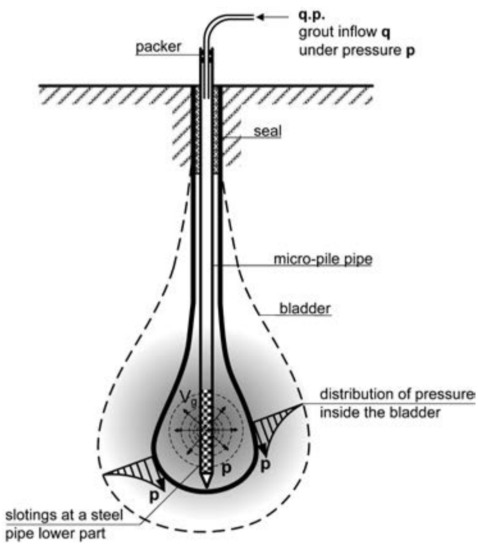

Fig. 3. Effect of pressure pre-straining of hardened contents (ideal case diagram)

3. EXAMPLE OF SALT SILO FOUNDATION REPAIR

A large number of silos have been constructed lately only by installing them on standard foundations and only with a visual examination of the foundation soil, without any pre-construction geotechnical examinations (Fig. 4). After filling the silos up with 100 tons, or 80% of their capacity, settling and leaning of the silos was noticed, both phenomena increasing significantly in a short time period. Counter-measures were introduced right away: surveying of settling and geotechnical investigations. The silo foundations at the depth of 1.3 m were set on hard clay, but from the depth of 2 m (where the water level is), there was soft clay. After geotechnical investigations, a means of repair/improvement (i.e. preventing further settling) was suggested – driving a micro-pile into the foundation soil to below the present foundations, then injecting and thereby improving the soil, as will be shown below.

Fig. 4. Salt silo:
a) Silo photograph b) Silo foundations at the depth of 1.3 m, diagram of the foundations and driven-in micro-piles

The chosen repair method using micro-piles is the simplest, fastest and the most economical means of improvement for the presented situation. The following was performed on 4 foundation footings (4 micro-piles per foundation): pre-drilling and driving in the pre-perforated steel pipes 6.00 m long, 101 mm in diameter, wall thickness of 3.60 mm, installation of rubber packers and injection of a certain quantity of cement suspension under pressure, thereby forming return pressure (Fig. 5).
The entry pressure (pre-injection) was 12 bar. Through the measurement of return pressure, it was ascertained that injection was successful and yielded the pressure of 3 bar, while the volume of used mixture was approximately 2.5 times larger than the volume of the drill-hole. The contents and the characteristics of the

injection mixture per 100 kg of dry cement: water (42 kg), bubbling additive -"Interplast – A" (0.5 kg or 0.17 l). The average mixture density $\rho_{smjese,}$ based on the formed injection mixture, was 1.9 t/m^3.
The operation also called for filling in the area between the pipe and the footing wall using an appropriate adhesive with a bubbling additive in order to ensure a long-lasting bond.

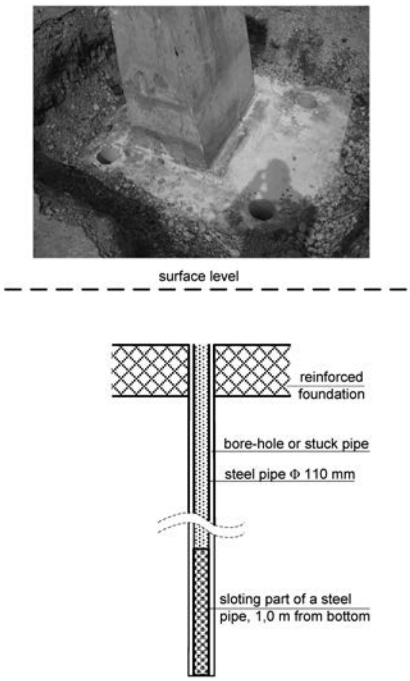

Fig. 5. Foundation, bore-hole, steel pipe

Settling is coupled with surveying equipment monitoring. The diagram of the time-based settling of the silo (i.e. the 4 foundations) was drawn according to collected data.
The diagram shows that the repair of the soil was successful, i.e. further settling was stopped (Fig. 6).

Fig. 6. Time-based diagram of silo settling

An estimated calculation (not taking in consideration the pre-stress) of the pile at the depth of 6 m and estimated diameter of 0.2 m using the alpha (α) method with non-drained stiffness $c_u = 70\,kN/m^2$ gave us the total bearing capacity of one pile of Q_t>230 kN, which is a significant increase per foundation.

4. CONCLUSION

Introducing pipe micro-piles with injection may in many cases present a quick, cost-efficient and effective solution. It is important to add that for this kind of a intervention and similar interventions, an important role belongs to the collection and processing of data used to make estimates on location; we should also point out the importance of cooperation between the designer and the works contractor. The example of micro-pile-based repair we chose was performed in a very short time period. However, each location needs to be looked at separately. Based on the use of the injection mixture and measured return pressure, it is assumed that settling could be stopped. This type of repair/recovery was proven to be very successful on a number of cases.

LITERATURE

Soldo, B. 2005. Geotehnički elaborat za temeljenje silosa soli u Ivancu, Geotehnički fakultet Sveučilišta u Zagrebu, (2005) Istražni radovi i proračuni, Varaždin

Muhovec, I. 2000. Osvrt na učinak injekcijskog prednaprezanja kod izvođenja cijevnih mikropilota u slabopropusnom deformabilnom tlu, Croatian Geotehnical Journal, vol 8 No: 15 – 16, Varaždin

Al-Alusi, H. R. 1997. Compaction Grouting: From Practice to Theo, Grouting: Compaction, Remediation and Testing, American Society of Civil Engineers.

Web. 2010. http://www.builderbill-diy-help.com/underpinning.html, repair and strengthening of faulty foundations.

Web. 2010. http://www.joostdevree.nl/shtmls /compenserend_grouten.shtml, compenserend grouten

Interaction of foundations

An analytic method to measure the earth pressure resulting from the surcharge on retaining walls

Mojtaba Ahmadabadi
Assistant Professor, Civil Engineering, College of Technics and Engineering, Islamic Azad University, Sepidan

Dr. Ali Ghanbari
Assistant Professor, Civil Engineering, College of Technics and Engineering, Tarbiat Moallem University, Tehran

ABSTRACT: In order to calculate the extra pressure made by the surcharge on retaining walls, boussinesq method is usually being used in case of elastic behavior. Supposing elasto-plastic behavior, in this research we are presenting a new method for calculating the active pressure on retaining walls, despite the line load surcharge. In this method the effect of rake, friction between soil and wall, side slope and internal friction angle of soil have all been concerned in the final formulization. So, first the analytic relations based on equilibrium assumption and gaining the desired balance in critical failure wedge have been obtained. Based on this proposed method, soil failure wedge angle has been reached through active condition and active pressure distribution on the wall in regard with line load surcharge and strip load surcharge. Then it is compared with the ordinary method. And the case that the surcharge is effective in pressure distribution on the wall has also been discussed.

1. INTRODOUCTION

To calculate the soil active pressure on retaining walls is one of the basic problems in foundation engineering. This problem is usually being considered according to Coulomb theory (1773) or Rankine theory (1857). On the other hand, the active pressure under external loads, effective on the soil, is located behind the same wall. In order to calculate the extra pressure resulting from surcharge on retaining walls, boussinesq method has usually been used in case that soil elastic and congenial behavior is presented. However, the researchers' surveys show that the above pressure distribution for calculating the effect of surcharge has a significant difference with the actual results. Georgiadis and Anagnostopoulos (1998) have compared the results of measuring the pressure on shields under line load with the results of different methods including elastic pressure, the approximate 45-degree slope and also the result of Coulomb method. According to the results of this research, elastic method has a big difference with actual amounts.

Kim and Barker (2002) have studied the effect of the live surcharge, resulting from traffic load, on retaining walls. These researchers have presented an analytical way to measure the horizontal active pressure on retaining walls by the use of bent slope.

Greco (1999, 2003, 2005 and 2006) has considered the effect of strip load surcharge on active pressure on retaining walls based on Coulomb theory, and then has proposed an analytical method to measure the amount of pressure and its point effect resultant.

Das (1992), on the other hand, while considering the differences between the results of elastic boussinesq way for measuring the surcharge with actual amounts, has also proposed the following terms to show the calculations of pressure resulted from line load surcharge on retaining walls.

$$Pa = \frac{4q(a^2b)}{\pi H(a^2 + b^2)^2} \qquad a>0.4 \qquad (1)$$

$$Pa = \frac{q(0.203\ b)}{H(0.16 + b^2)^2} \qquad a<0.4 \qquad (2)$$

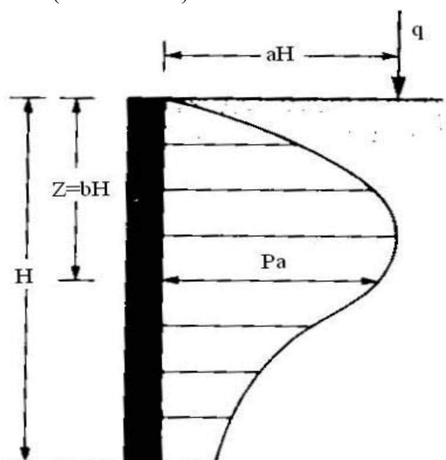

Figure 1. Das (1992) proposed method for measuring the horizontal pressure resulted from surcharge

In these terms, Pa is the horizontal pressure resulting from line load surcharge on the wall, *q* is the amount of surcharge, H is the height of the wall and the other parameters have been shown in figure (1).

In all of these terms, elastic behavior for environment and Poisson's ratio (ν = 0.5) are taken into consideration.

According to Coulomb failure theory in this paper, for a retaining wall with declination from virtual line and the sleep soil behind it, the change in failure wedge angle and also soil pressure distribution resulted from line surcharge activities are being discussed.

2. ACTIVE PRESSURE FORMULATION WITH THE EFFECT OF LINE SURCHARGE ON THE WALL

If the surcharge is only located in the area of failure wedge, then it will be able to affect on the soil behind the wall. In this figure, the wall and the soil both are supposed to be sleep and friction between soil and the wall is taken into account. Considering the base of balance for the pressures on the wedge, we will have the followings:

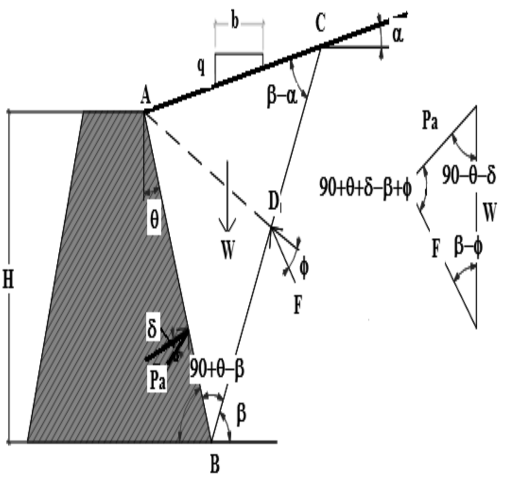

Figure 2. Pressure balance in failure wedge without the surcharge effect

$$P_a = \frac{\sin(\beta-\phi)}{\sin(90+\theta+\delta-\beta+\phi)}(W+bq) \qquad (3)$$

In equation (3), all of the parameters are the same as figure (2). In figure (2) *b* is surcharge width, *q* is the amount of failure wedge and *w* is the weight of failure wedge. According to the rules of trigonometry we can show that:

$$W = \frac{1}{2}\gamma H^2 \frac{\cos(\theta-\beta)\cos(\theta-\alpha)}{\cos^2(\theta)\sin(\beta-\alpha)} \qquad (4)$$

After inserting terms (3) & (4) in the general term for measuring the pressure on the wall with surcharge, the followings are emerged:

$$P_a(\beta) = \left[f(\beta)\right]\left[\frac{1}{2}\gamma H^2 g(\beta) + qb\right] \qquad (5)$$

$$f(\beta) = \frac{\sin(\beta-\phi)}{\sin(90+\theta+\delta-\beta+\phi)} \qquad (6)$$

$$g(\beta) = \frac{\cos(\theta-\beta)\cos(\theta-\alpha)}{\cos^2(\theta)\sin(\beta-\alpha)} \qquad (7)$$

In the above equations, Pa Is the active pressure on the wall with surcharge, f (ß) and g (ß) are functions that according to soil and wall qualities are reached based on the above mentioned figures. Figure (5) shows the amount of active pressure along with the failure wedge with angle (ß). If the angle showing extreme amount of Pa is equal with the failure wedge, in order to calculate ß, P's derivate has to be considered zero based on ß.

$$\partial P_a / \partial\beta = 0 \qquad (8)$$

So we will have:

$$\frac{1}{2}\frac{FAE}{B^2D} + \frac{1}{2}\frac{\gamma h^2 AIK}{B^2G} - \frac{1}{2}\frac{\gamma h^2 IAEG}{B^2D^2} + \frac{1}{2}\frac{\gamma h^2 IAEH}{B^2DC} + bq\left(K + \frac{EH}{C}\right) = 0 \qquad (9)$$

To determine ß, we can solve equation (9) via try and error, with the factors given in table (1).

Table 1. Defining the factors of equation 9.

$\cos(\theta-\alpha) = A$	$\sin(\theta-\beta) = F$
$\cos(\theta) = B$	$\cos(\beta-\alpha) = G$
$\sin(\frac{\pi}{2}+\theta+\delta-\beta+\phi) = C$	$\cos(\theta-\beta) = I$
$\sin(\beta-\alpha) = D$	$\cos(\frac{\pi}{2}+\theta+\delta-\beta+\phi) = H$
$\sin(\beta-\phi) = E$	$\cos(\beta-\phi) = K$

3. VALIDATION

In figure (3), pressure distribution on the wall resulting from surcharge is drawn and compared with Das (1992) stress distribution. In figure (4) side pressure distribution on the wall is shown in two forms "with and without surcharge".

According to the results, the surcharge increases earth pressure on the top of the wall and creates no line pressure distribution.

In figure (5), you can see the comparison between failure wedge on the walls with internal friction angle in two different situations: "with and without surcharge", and it has also been compared with Coulomb (ß = 45+Ø/2).

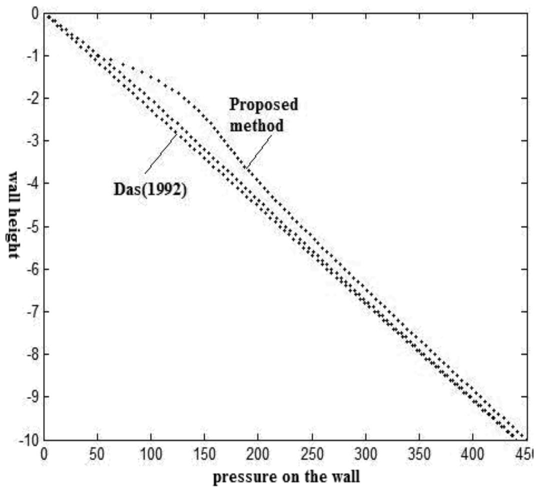

Figure 3. Pressure distribution on the wall with surcharge, according to proposed method and Das (1992) method

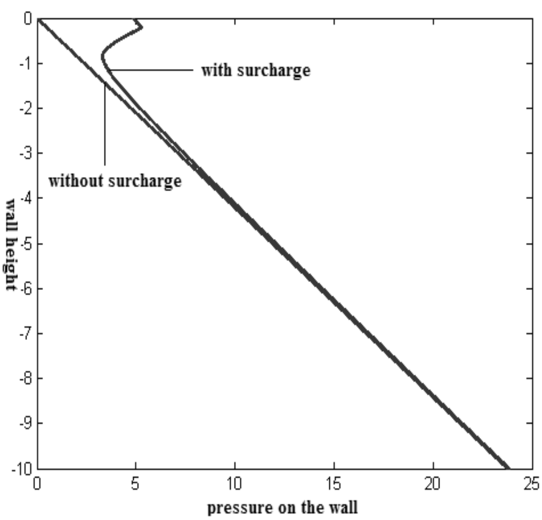

Figure 4. Earth pressure distribution on the wall "with and without surcharge"

To survey the validation of the formulas offered in the current paper, the results have been compared with both Rankine method and Ahmadabadi & Ghanbari new procedure (2009); and its conclusion has been brought in table 2 and table 3.

Table 2.Comparison of results for Ahmadabadi & Ghanbari (2009) and proposed methods

A: Ahmadabadi & ghanbari(2009) B: Proposed methods					
		δ=10		δ=20	
		A	B	A	B
φ=20	β	50.9	51.0	48.1	48.0
	ρ_a	446.7	446.7	426.9	426.9
φ=25	β	54.5	55.0	52.2	52.0
	ρ_a	372.6	372.6	357.4	357.4
φ=30	β	57.7	58	55.9	56
	ρ_a	309.08	308.45	297.9	297.31

		Rankine method	Proposed methods
$\phi = 20$	β	55.0	55.0
	ρ_a	490	490.3
$\phi = 25$	β	57.5	57.5
	ρ_a	406.0	405.9
$\phi = 30$	β	60	60
	ρ_a	333	333.66

Table 3.Comparison of results for Rankine and proposed methods

4. CONSIDERING THE EFFECTS OF SOIL SURCHARGE QUALITIES ON THE EARTH PRESSURE ON THE WALL

In order to evaluate the different soil qualities and surcharge, on earth pressure on the wall, according to the above figures, the effect of the change in internal soil friction angle, surcharge amount, friction angle between soil and wall and wall steep on the mentioned pressure, are being considered. In table (4) you can see the features of the wall, used in the analysis. You can also see the results in figures (6-9). These results prove that any decrease in internal soil friction and the increase in wall steep angle result in more pressure on the wall and the deeper the wall is, the more pressure we will have. On the other hand, surcharge leads to no line earth pressure distribution on the wall and therefore, the center of soil active pressure which is supposed to be in the lower 1/3, rises toward the higher positions. We should bear in mind that the deeper the wall is, the more decrease you see in surcharge role to change tension distribution. However, friction angle between wall and soil has a stable role in changing the earth pressure distribution.

As the mentioned angle increases, first earth pressure decreases and then it starts rising again. So with some friction angles, that should be between 5 to 15 Degrees, and the least pressure will be on the wall.

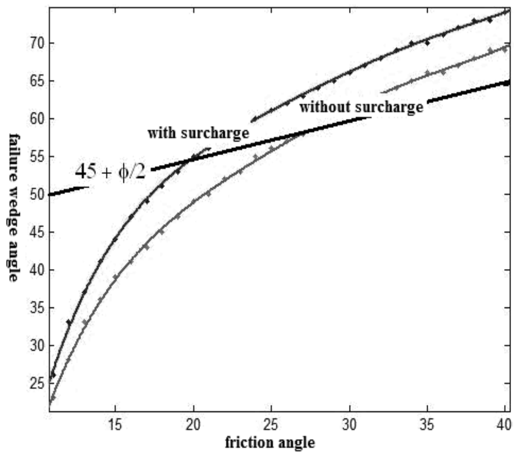

Figure 5. Failure wedge angle in two proposed forms "with and without surcharge"

5. CONSIDERING THE EFFECTS OF STRIP LOAD SURCHARGE DISTANCE IN EARTH PRESSURE DISTRIBUTION

The farther the surcharge is from the outset of the wall, the less effect it has on the same wall. Therefore, according to the assumption of creating equilibrium for failure wedge based on hit balance, after sometime the wedge gets out and you will notice line pressure distribution on the wall. From now, the surcharge has no effect on the pressure distribution. The results of this observation are shown in figure (10).

Table 4. Features of the wall being analyzed

Series Analysis	Internal Friction Angle (degree)	Adherence (Newton Kilo on Square Meter)	Wall Height (Meter)	Wall Steep Angle (Degree)
A	40−10	0	10	20
B	30	0	10	20
C	30	0	10	20
D	30	0	10	20−0
Series Analysis	Friction Angle between Soil & Wall (degree)	Soil Specific Gravity (Newton Kilo on Square Meter)	Earth Steep Angle (Degree)	Surcharge Amount (Newton Kilo on Square Meter)
A	10	20	10	50
B	10	20	10	150−0
C	20−0	20	10	50
D	10	20	10	50

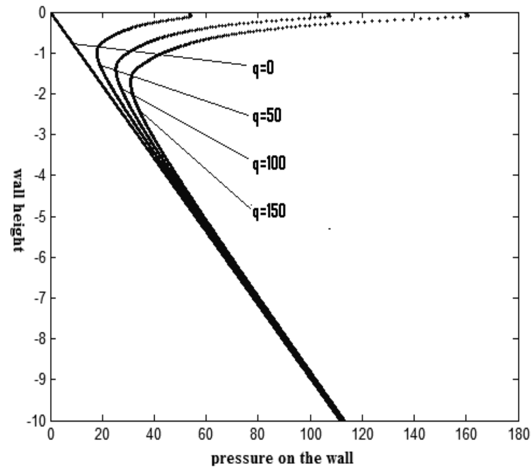

Figure 6. Earth pressure distribution on the wall with the change of Soil Internal Friction Angle

6. C0NCLUSION

In this essay, we talked about the effect of surcharge on pressure distribution on the wall and also the change in failure wedge angle and a new formulation was gained based on hit balance for failure wedge. The following shows a summary of these results:

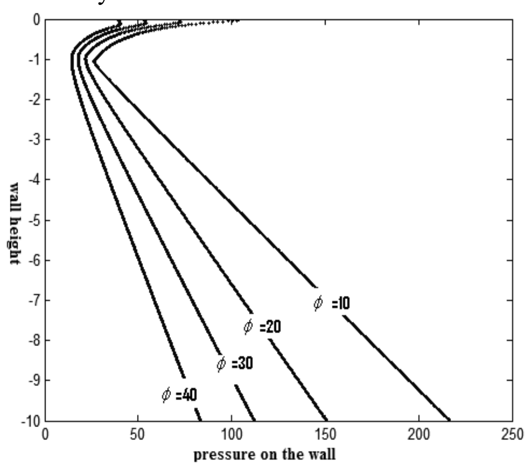

Figure 7. Earth pressure distribution on the wall with the change of Surcharge Amount

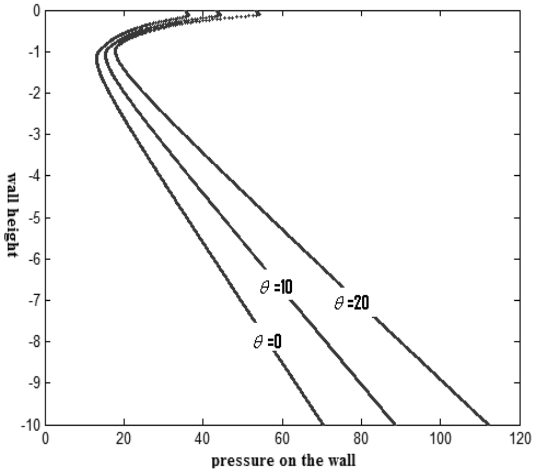

Figure 8. Earth pressure distribution on the wall with the change of friction angle between soil and wall

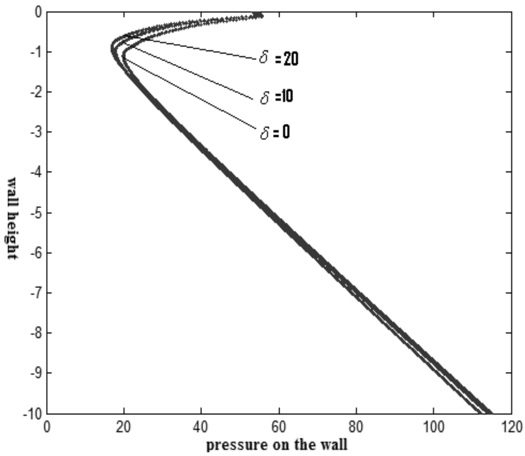

Figure 9. Earth pressure distribution on the wall with the change of wall steep

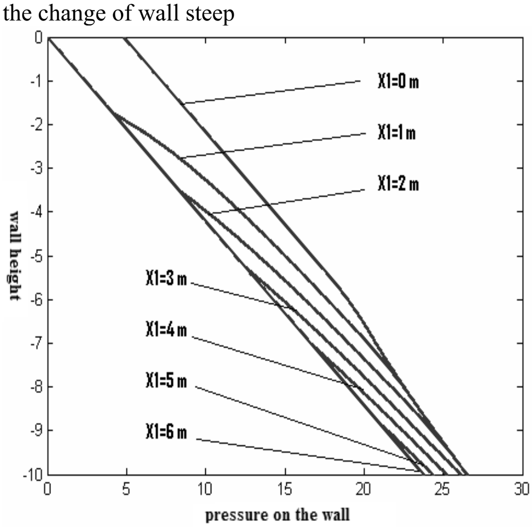

Figure 10. Change process in earth pressure distribution on the wall with a change in surcharge effect

1) A new relation was found to calculate pressure distribution with line and strip load surcharge in retaining walls. Wall steep, earth steep, friction angles between wall and soil are taken into consideration in drawing this relation out. This distribution is reached based on the elasto-plastic behavior and is somehow different with Das (1992) pressure distribution (Elastic behavior).

2) There is a new relation for calculating the angle of failure wedge along with surcharge and it is being compared with a no surcharge situation. If you consider the results, you will notice that the presence of surcharge results in.

3) After studying the soil and wall qualities in changing stress distribution, we came into the conclusion that reducing soil internal friction angle and increasing wall steep angle results in increasing the pressure on the wall. And if the depth of the wall increases, the above mentioned pressure increases afterwards.

4) Based on some friction angles between soil and wall, supposed to be approximately 5 to 15 degrees, the least earth pressure would be on the wall.

7. REFERENCES

Ahmadabadi, M. and Ghanbari, A., 2009. New procedure for active earth pressure calculation in retaining walls with reinforced cohesive-frictional backfill. Geotextiles and Geomembranes 27 (2009) 456– 463.

Arango, I. (1969) Personal communication to Seed and Whitman, reported in Seed, H. B. and Withman, R. V., (1970) Design of earth retaining structures for dynamic loads. Proceedings of ASCE Specialty Conference on Lateral Stresses in Ground and Design of earth retaining Structures. Cornell University , Ithaca, NY, pp. 103-147.

Choudhury D, Ahmad S.M. Stability of waterfront retaining wall subjected to pseudo-static earthquake forces, Ocean Engineering 2007; 34: 1947-1954.

Choudhury D, Nimbalkar S.S. Seismic passive resistance by pseudo-dynamic method, Geotechnique, London, 2005; 55 (9): 699-702.

Choudhury D, Nimbalkar S.S., 2006. Pseudo-dynamic approach of seismic active earth pressure behindretaining wall, Geotechnical and Geological Engineering, Springer, The Netherlands; 24(5): 1103-1113.

Choudhury, D., Nimbalkar, S.S., 2008. Seismic rotational displacement of gravity walls by pseudo-dynamic method, International Journal of Geomechanics 8(3), 169-175.

Coulomb, C. A. (1773), Essai sur une application des règles de maximis et minimis a quelques Problèmes de statique relatifs a l'architeture, Mémoires de savants étrangers de l'Académie des Sciences de Paris, V, 7.

Coulomb, C.A. 1776. Essai sur une application des regles de maximis et minimis a quelqes de stratique relatifs a l' architecture. In Memoires de mathematique et de physique. Presentes a l' academie royale des sciences, Paris, 7: 343-82.

Das, B.M., Puri, V.K., 1996. Static and dynamic active earth pressure. Geotechnical and Geological Eng. 14, 353-366.

Georgiadis, M. and Anagnostopoulos, C. (1998) "Lateral Pressure on sheet pile walls due to Strip load", J. Geotech. Geoenviron. Eng. , ASCE , 124(1), 95-98.

Gnanapragasam, G., 2000. Active earth pressure in cohesive soils with an inclined ground surface. Canadian Geotechnical J. 37, 171-177.

Greco, V. R. (1999) "Active earth thrust on cantilever walls in general conditions", Soils Found., 39(6), 65-78.

Greco, V. R. (2003) Pseudo-static analysis for earth thrust computations, soils Found., 43(2), 132-140.

Greco, V. R. (2005) "Active earth thrust by backfills subject to a line surcharge" Can. Geotech. J. 42(5): 1255–1263.

Greco, V. R. (2006) "Lateral Earth Pressure due to Backfill Subject to a Strip Surcharge" Geotechnical and Geological Engineering, Springer, (24), 615-636.

Jahanandish, M., Keshavarz, A., 2005. Seismic bearing capacity of foundations on reinforced soil slopes. Geotextiles and Geomembranes 23 (1), 1–25.

Kim, J. S. and Barker, R. M. (2002) Effect of live load surcharge on retaining walls and Abutments, J. Geotechn. Geoenvirom. Eng., ASCE, 128(10), 808-813.

Lee, K.Z.Z., Wu, J.T.H., 2004. A synthesis of case histories on GRS bridge-supporting structures with flexible facing. Geotextiles and Geomembranes 22 (4), 181–204.

Rankine, W. J. M. (1857) on the mathematical theory of the stability of earthwork and Masonry, Proceedings of Royal Society, vol. 8.

Visualization of soil mobility surrounding a model pile using thermography

M.J. Arai
System Measure Co.,Ltd., Japan

M. Fujii
Tokai University, Japan

K. Watanabe
Tokai University, Japan

ABSTRACT: The advantage of use the screw piles for installations of pile foundations in metropolitan areas is an environmentally friendly method that generates minimal noise, vibration and waste soil. However, results in disturbance in the surrounding of the pile. The real area of soil disturbance cannot be easily evaluated due to the difficulty in accessing the area beneath the surface. It has been found that the bearing capacity of the pile was affected by the shear stress of soil under the tip of the pile. The area influenced is decided only on the basis of estimation from the results of load tests. This paper proposes a method of visualization using thermography suitable for the evaluation of possible construction methods of pile and ground improvement.

1. INTRODUCTION

In geotechnical and foundation engineering, there have been many studies on the use of thermography. Since it is a non-destructive method, for determining the properties or interior conditions of a test sample based on temperature changes measured on its surface, thermography has been used in numerous applications, such as for detecting cracks in walls(Barreira et al., 2007), for evaluating the energy-dissipating ability of soil (Luong,2007), for identifying the existence of eroded caves behind shotcrete-protected slopes (Wu et al., 2005), and for determining the water content of soil (Gotoh et al, 1995).

A common feature of these studies is that the amount of water in soil particles is the decisive factor for visualizing differences in the temperature of the ground surface by thermography. With this approach, it is possible to evaluate the behavior of surface soil that has been disturbed by the penetration of a screw pile.

The screw pile, a steel pipe pile with a helicoidal wing at the bottom for screwing into the ground, is widely used in Japan. A screw pile was used in this study because of its high load capacity compared to a straight pile. However, the nature of the disturbance of the soil surrounding a screw pile in use has mostly been estimated solely from the results of load tests.

Infrared imaging is considered to be the most suitable method for examining this problem.

This paper summarizes a method for producing such artificial soil and introduces an imaging method for evaluating the soil that uses thermography during penetration of the pile.

2. THERMOGRAPHY EQUIPMENT

Infrared thermography is a non-destructive method for detecting and visualizing infrared energy emitted from an object at a temperature above absolute zero (0K) and for displaying images of temperature distribution.

The equipment used in this investigation is based on the principle shown in Fig.1. The infrared camera detects infrared energy emitted from a test object (surface of the model soil), converts it to temperature, and displays an image of temperature distribution, as shown in Fig.2.

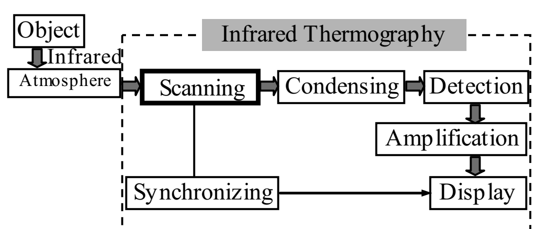

Figure 1. Schematic drawing of the thermography equipment (Nec-Avio)

The details of the equipment used (NEC/AVIO TH7800) are listed in Table1.

Figure 2. Measurement conditions

Table1. Details of the thermography equipment

	Description
Range	-20 to 100℃
Resolution	0.05℃(Range 1 at30℃,Σ16) 0.01℃(Range 1 at30℃,60Hz)
Accuracy	±2℃ or 2% of reading
Detector	Uncooled focal plane array
Spectral range	8 to 14μm
Thermal image pixels	320(H)×240(V)
Focusing Range	50cm to ∞
I.F.O.V.	1.5mrad
Field of View	27°(H)×20°(V)
S/N improvement	OFF, Σ2, Σ8, Σ16, and spatial filter ON/OFF
Operating temperature	-15 to 45℃, 90%RH or less

3. EXPERIMENTS AND EQUIPMENT

3.1. Model Soil

To determine the most suitable mixture for making this model soil, siliceous sand No.7, Kasaoka clay and water mixed at different ratios. The grain-size distribution curves of siliceous sand No.7 and Kasaoka clay are shown in Fig.3.

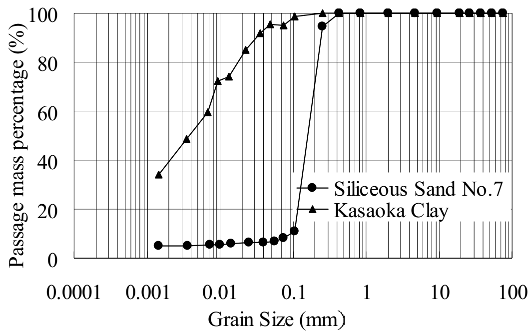

Figure 3. Grain-size distribution curves of Siliceous sand No.7 and Kasaoka Clay

To identify the most appropriate mixing ratio and water content for visualizing the variation in temperature by thermography, 9 samples were prepared with different mixing ratios of sand and clay (9:1, 8:2, 7:3, 6:4, 5:5, 4:6, 3:7, 2:8, and 1:9), each with eight water contents (0, 1, 3, 5, 6, 7, 8 and 10%), to give a total of 72 samples. Figure 4 shows representative pictures of the experiment and the area of each nine samples analyzed by thermography.

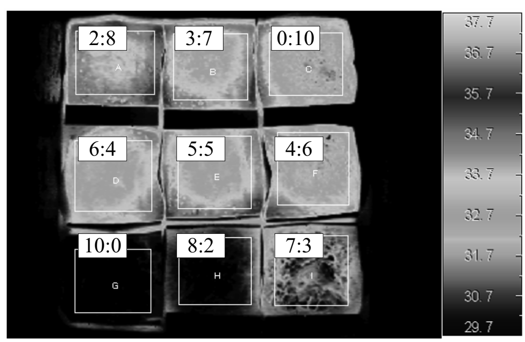

Figure 4. Thermal image of samples at 7% water content (sand: clay mixture ratio)

Each sample (200g) was placed on a paper plate (100mm x 100mm) and heated for 30min by a 500W lamp (the distance from the test samples to the lamp was 80cm). The surfaces of the samples were measured by thermography three times (before heating (t_0), after 30min of heating (t_{30}), and after cooling for 30min (t_{60})).

The mixture ratio selected for further studies was that with a stable temperature difference at each water content.

The temperature difference (ΔT℃) for all samples in the natural state, increased with the water content, as shown in Fig. 5(a). On the other hand, the temperature difference became unstable after heating (t_{30}) and cooling (t_{60}), except for the samples with a water content of 7%. Figure 5(b) shows the change in temperature (ΔT%) with a given sand: clay mixture ratio for each water content before heating (t_0). As the proportion of sand increases, the variation in temperature decreases, and this trend is enhanced when the water content increases.

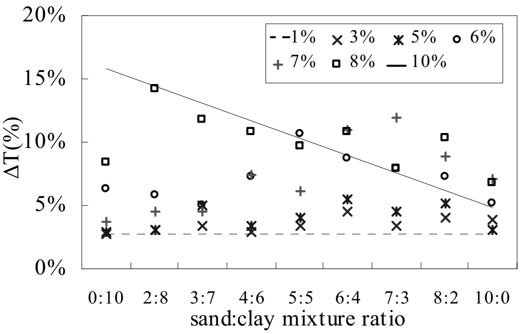

Figure 5(a). Relationship between the difference in temperature with water content before, after 30min of heating and after 30min of cooling

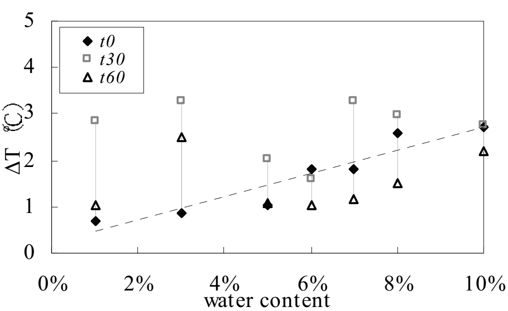

Figure 5(b). Variation in temperature with the mixture ratio and water content

However, there was a large variation in temperature with a sand: clay mixture ratio between 6:4 to 8:2, specifically at a water content of 7%.

Moreover, the relationship between the difference in temperature with water content at the maximum, mean and minimum temperature (Fig. 5(c)), remained fairly constant (within the approximated curve of the minimum and maximum values) at a water content of 7% compared to the other proportions.

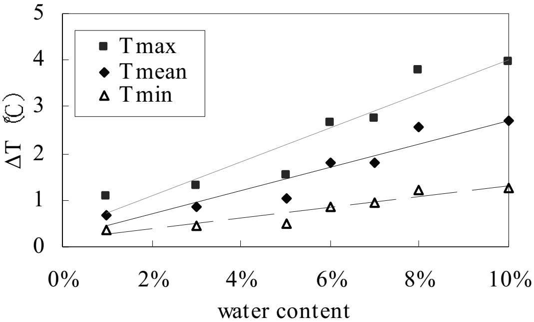

Figure 5(c). Difference in temperature with the water content for T_{max}, T_{ave} and T_{min}

According to Luong (2007), thermography offers the possibility of evaluating the energy-dissipating ability of soil subjected to stress.

To verify the nature of these internal forces acting on soil by thermography, and based on the results of the preliminary experiment, a 7:3 mixture of siliceous sand No.7 and Kasaoka clay with a water content adjusted to 7% was prepared for testing. A load pressure of 1.5N/mm^2 was applied to the upper part. One side of the mold was then removed and half of the sample was scraped off and heated for 30sec at a distance of 20cm. The temperature distribution was measured by thermography.For comparison to the results obtained by thermography, a linear computational analysis (FEM) was used (Table 2).

Based on the model of initial concrete failure under triaxial stress conditions described by Chen (1985), the correlation between thermography and the compression of soft rocks by Ohta et al. (1992) and a simulation of mortar failure by 2D RBSM (Nagai et al., 2004), the results of FEM analysis and the distribution temperature obtained by thermography were similar, as shown in Fig. 6.

There was a significant correlation between the stress value obtained by of FEM analysis and the temperature distribution, as shown in Fig. 7.

Based on these results, for further analysis we used a mixture of siliceous sand No.7 and Kasaoka clay at a ratio of 7:3 with a water content of 7%.

Table 2. FEM input criteria *(AIJ, 2001)

FEM Input Conditions		Value	Model
Height		100	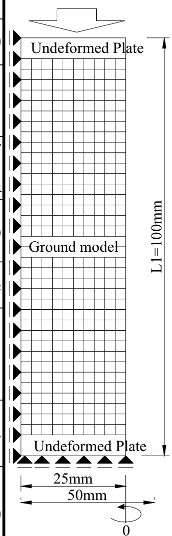
Width		50	
Deformation displacement		26.5	
Load		Top / bottom	
Deformation orientation		Top	
L_1 restrition		None	
Experimental Soil*	Young modulus *(N/mm^2)	0.065	
	Poison ratio* (N/mm^2)	0.4	
Undeformed material	Young modulus (N/mm^2)	5000	
	Poison Ratio (N/mm^2)	0.3	

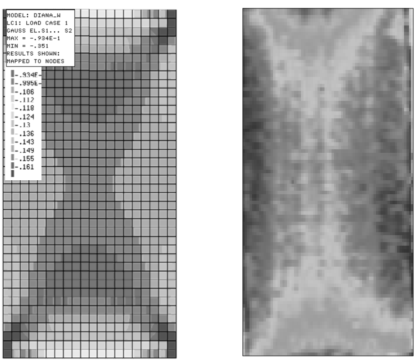

Figure 6.Comparative analysis of FEM stress results (left) and a thermography image (right)

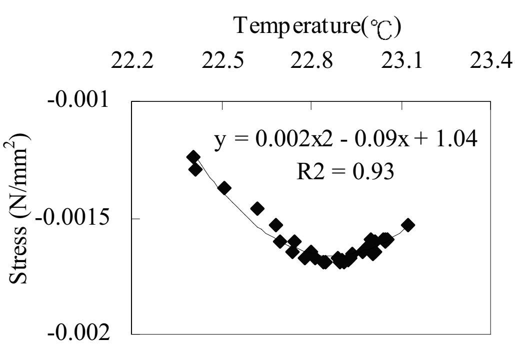

Fig. 7. FEM stress results and temperature

The distribution curve of grain size for the artificial soil mixture is shown in Fig. 8.

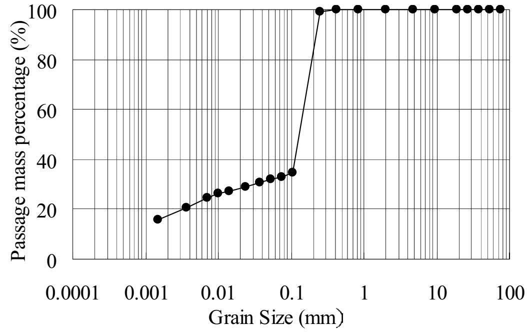

Figure 8. Grain- size distribution for a sand: clay ratio of 7:3

3.2. Pile Penetration and Bearing Device

The penetration equipment (Fig. 9) has a motor attached to the axis of the screw pile both for rotation and for moving the pile up and down.

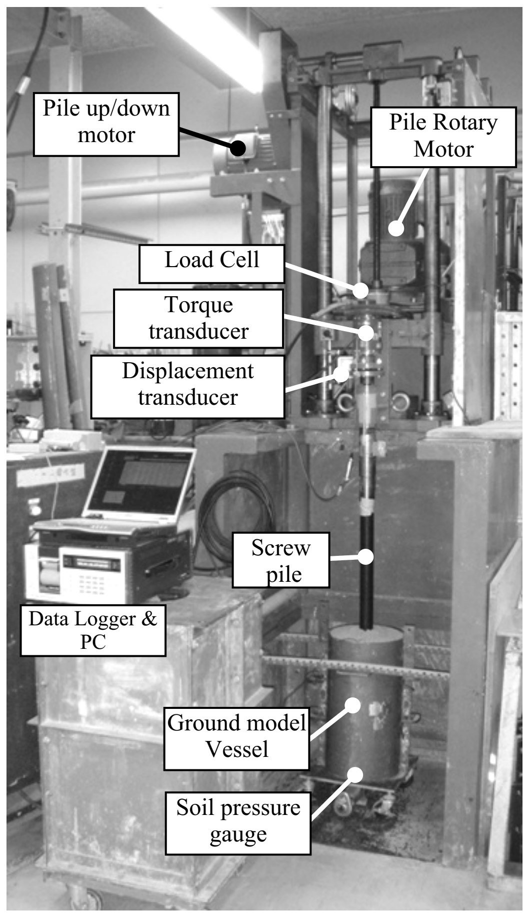

Figure 9. Penetration equipment

Thrust is applied to a vessel containing artificial soil in the direction of drilling. Moreover, this equipment can measure both the thrust of the driving force, torque and the depth of penetration into the soil.

The vessel is made of steel, and is 260mm in diameter and 500mm high. It consists of two parts, and thus the soil can be cut perpendicularly after installation of the pile. A soil-pressure gauge was buried at the bottom of the vessel to measure soil pressure with penetration of the screw pile.

The artificial soil was divided into five layers at a density of $1.3 g/cm^3$. Each layer measured 9cm, of which 2cm was colorized to visually verify the behavior of the soil and the pile at each penetration speed.

The pile was driven into the artificial soil (depth of 300mm) at 4 different penetration speeds (45, 90, 180 and 270mm/min). After each penetration test, the screw pile was pushed 50mm into the vessel containing artificial soil. One side of the vessel was removed horizontally, and half of the soil was removed. An infrared camera was used to measure the temperature distribution at the cutting plane by thermography. A hardness tester was also used to compare the hardness of the soil with the temperature distribution at each intersection in a 20mm mesh.

3.3. Model pile

The screw pile shown in Fig. 10, and has a shaft diameter of 48.7mm and a wing diameter of 72.8mm. The pitch of the wing is 13.7mm and the height of the digging edge of the wing is 18.2mm.

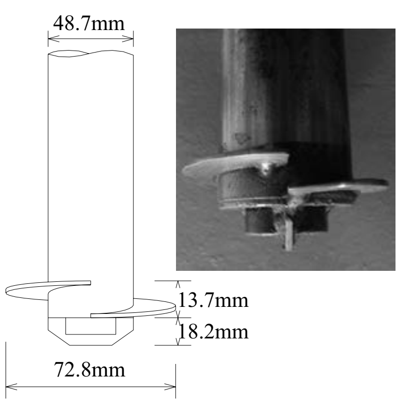

Figure 10. Dimensions of the screw pile

3.4. Experimental results and considerations

Figures 11 (a) and (b) show the results of the driving force, torque, soil pressure and penetration velocity during penetration.

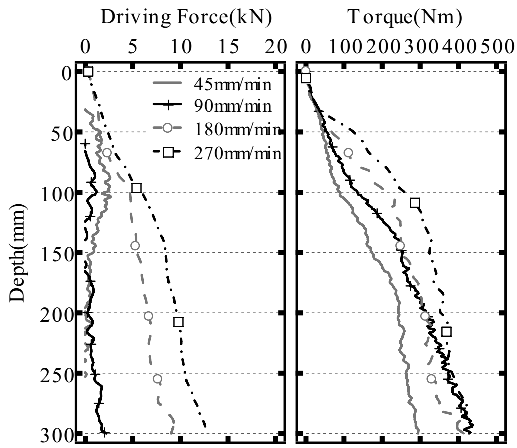

Figure 11(a). Driving force and torque during penetration

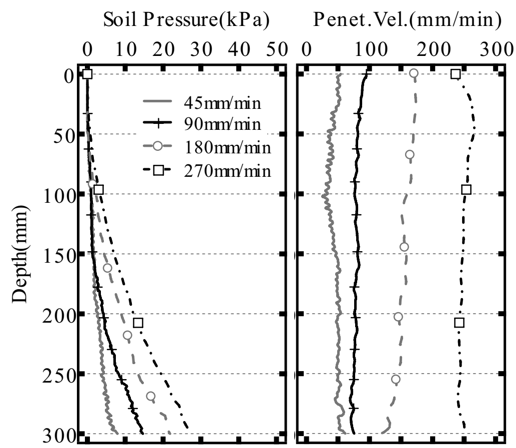

Figure 11(b). Soil pressure at the bottom of the vessel and penetration velocity during penetration

While the driving forces with penetration velocities of 45 and 90mm/min are equivalent at 180 and 270mm/min the driving force increases 3-fold and 5-fold, respectively. Regarding the torque force at penetration velocities of 90 and 180mm/min, a similar torque must be applied for the pile to penetrate into the soil. The soil-pressure gauge installed at the bottom of the vessel showed that the pressure increased in proportion to the penetration velocity.

Figure 11(c) shows the results of the load test and the reaction of the soil during the experiment as detected by the soil-pressure gauge at the bottom of the vessel, after penetration of the screw pile. As shown, the ultimate load on the soil decreases as the penetration velocity decreases.

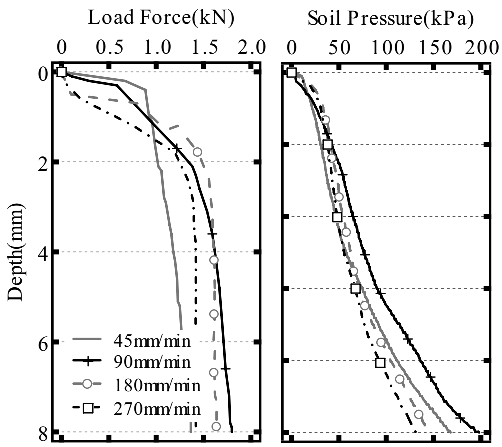

Figure 11(c). Load test and soil pressure after pile penetration

Figure 12 (a) to (d) show the results regarding the strength distribution as determined by a hardness tester and the distribution of temperature by thermography after the pile penetrated 300mm into the ground for each penetration velocity. The initial strength of the soil before the tests was 1.7N/mm^2.

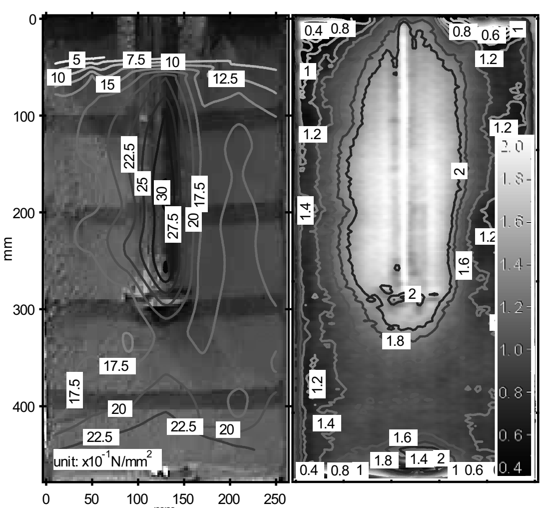

Figure 12(a). Strength and temperature distributions for a penetration velocity of45mm/min

At a penetration speed of 45mm/min (Fig.12(a)), the difference in temperature increased up to 2, due to friction with the soil, and only the area around the pile was affected.

In Fig.12(b), at a penetration speed of 90mm/min, it is easy to see the relationship between the temperature distribution and the strength distribution. For each 0.2℃ increase in temperature, strength increases by 0.25N/mm^2. At this penetration velocity, the soil was not disturbed compared with greater velocities.

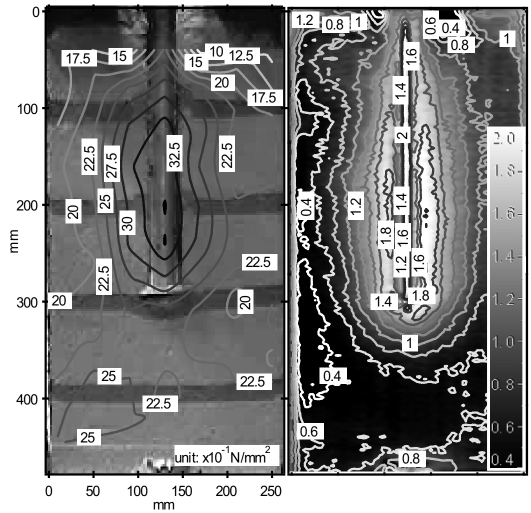

Figure 12(b). Strength and temperature distributions for a penetration velocity of 90mm/min

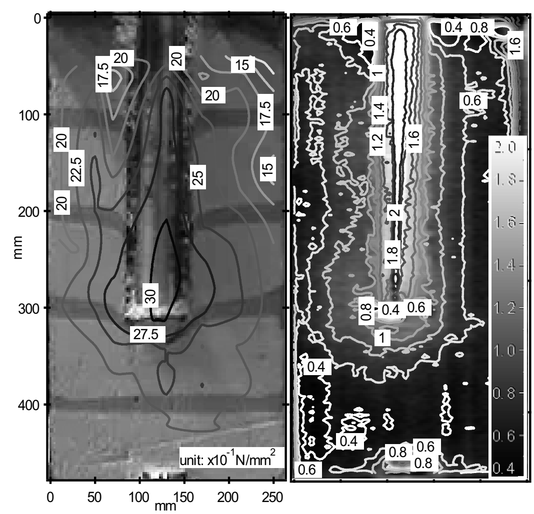

Figure 12(c). Strength and temperature distributions for a penetration velocity of 180mm/min

In Fig. 12(c) and (d), the screw pile was pushed straight into the soil instead of being rotated. The soil around the pile was disturbed. The temperature distribution is different around the tip of the pile, due the incorporation of air into the soil and the change in temperature.

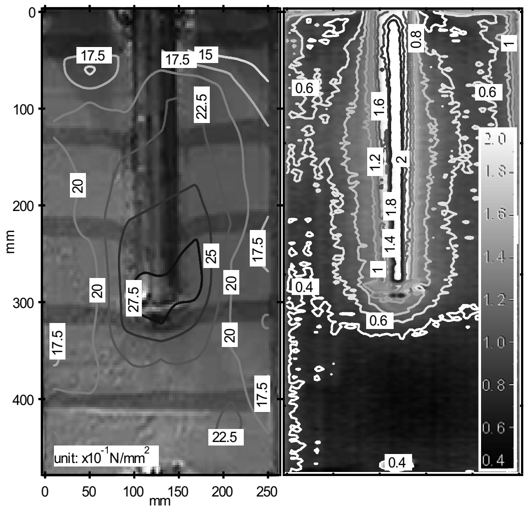

Figure 12(d). Strength and temperature distributions for a penetration velocity of 270mm/min

Figures 13 (a) to (d) show the strength distribution as determined by a hardness tester and the temperature distribution as determined by thermography after the pile penetrated 30mm into the soil and was then pushed 50mm for each penetration velocity.

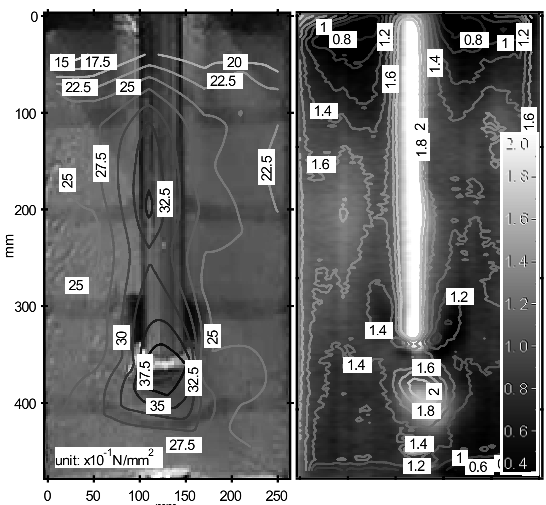

Figure 13(a). Strength and temperature distributions after the pushing test for a penetration velocity of 45mm/min

When the pile was pushed an additional 50mm, the temperature appears to be especially high in the region directly under a wing (best visualized in Figs.13(a) to (c)). As shown in Fig.13(d), penetration at this velocity completely disturbed the soil. The length of the vertical directions is equivalent to a part for the diameter of a wing. It is aimed at N value of the ground of the domain, which is experimentally equivalent to the diameter of a wing when calculating the tip bearing capacity of screw pile. Thermography corroborated this finding.

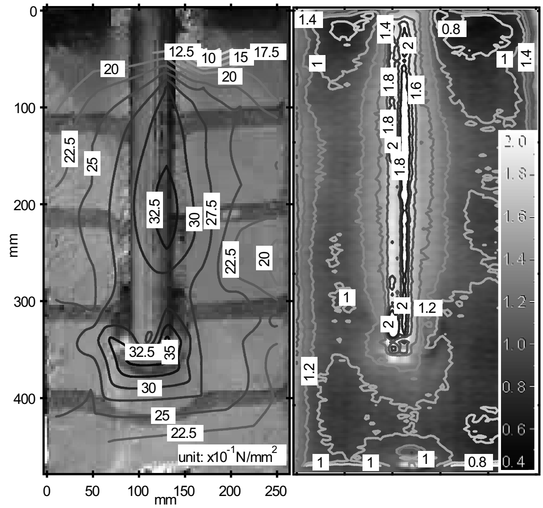

Figure 13(b). Strength and temperature distributions after the pushing test for a penetration velocity of 90mm/min

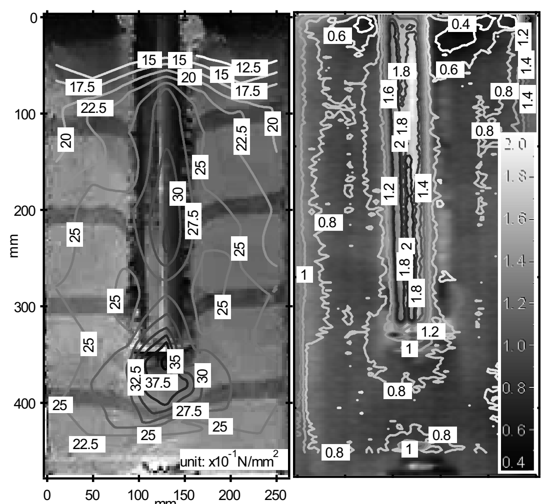

Figure 13(c). Strength and temperature distributions after the pushing test for a penetration velocity of 180mm/min

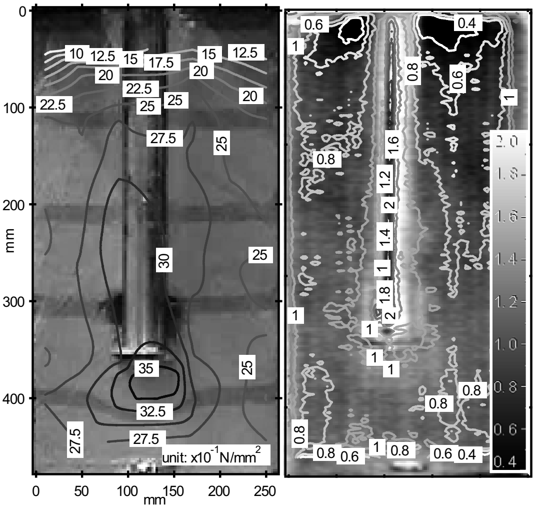

Figure 13(d). Strength and temperature distributions after the pushing test for a penetration velocity of 270mm/min

If we consider all of the results, the soil is disturbed by this screw pile up to a depht of 100mm independent of the penetration speed.

The soil turbulence in the area surrounding the pile during penetration can be revealed by thermography. If a colored layer and a hardness tester are used, this condition can be demonstrated more accurately.

4. CONCLUSIONS

The present results suggest the following:

-The correlation between the temperature distribution and stress appears most clearly by thermography with a sand:clay mixing ratio of 7:3 and with a water content of 7%.

-The hardness distribution by the hardness tester for each penetration speed, the changes in the colored layer, and the temperature distribution by thermography.

-The penetration velocity of a screw pile has an important effect on the soil disturbance around the pile, as demonstrated by thermography and other methods.

As these results show, it is possible to evaluate the performance of a screw pile and the mobility of soil using thermography images.

5. ACKNOWLEDGMENTS

This study was supported by a Grant-in-Aid for Scientific Research Project from the Japan Society for the Promotion of Science.

6. REFERENCES

Architectural Institute of Japan, 2001. Recommendations for Design of Building Foundations. *AIJ*, pp142-150. (in Japanese)

Chen, W.F., Plasticity in reinforced concrete, 1985.*Maruzen*.pp.40-43. (in Japanese)

Gotoh, K., Chen, Y.,1995. A Fundamental study on the utilization of infrared thermography as a tool for the management of materials in soil construction. *http//Itpwww.gsfc.nas.gov/ISSSR-95/ afundame.htm*.

http://www.nec-avio.co.jp/en/products/ir-thermo /what-thermo .html

Luong, M.P.,2007. Introducing infrared thermography in soil dynamics. *Infrared Phys & Technol*, No.49, pp. 306-311.

Nagai, K., Sato, Y., Ueda, T. 2004. Mesoscopic simulation of failure of mortar and concrete by 2D RBSM. *Journal of Advanced Concrete Technology*, Vol. 2, No. 3, pp. 359-374.

Ohta, H., Hideshima, Y., Onodera, Y., 1992. Thermographic Observations of compression processes on soft rock. *Monthly Report of the Civil Engineering Research Institute*, No.472, pp.9-16. (in Japanese)

Wu, J., Lin, H., Lee, D., Fang, S.,2005. Integrity assessment of rock mass behind the shotcreted slope using thermography. *Engineering Geology*, No. 80, pp.164-173.

3-D Nonlinear Ground-Foundation Computational Analysis

Ahmed Elgamal
University of California, San Diego, Department of Structural Engineering, La Jolla, CA, USA

Jinchi Lu
University of California, San Diego, Department of Structural Engineering, La Jolla, CA, USA

Zhaohui Yang
Caltrans, Oakland, CA

Thomas Shantz
Caltrans Division of Research and Innovation, Sacramento, CA

ABSTRACT: This paper presents a robust and versatile framework that helps streamline the use of finite elements for seismic response of soil-structure systems. In this regard, a Windows-based graphical-user-interface OpenSeesPL is developed for pile-ground interaction analyses. Particularly suited to static as well as seismic applications, the open-source computational platform OpenSees (http://opensees.berkeley.edu) is employed throughout. To illustrate the capabilities of OpenSeesPL, two studies are presented. Lateral spreading effects on pile foundations are modelled, followed by an investigation of ground remediation effects in a mildly sloping soil stratum. Along with the insights gained from these studies, the reported effort aims to highlight the analysis framework capabilities, and the range of potential soil-structure interaction applications.

1. INTRODUCTION

With the recent developments in numerical modeling techniques and high-speed efficient computers, three-dimensional (3D) nonlinear finite-element (FE) methods are becoming increasingly feasible for geotechnical studies. Particularly suited to seismic applications, the open-source computational platform OpenSees (Mazzoni et al. 2006) provides such 3D simulation capabilities.

However, in conducting numerical simulations, preparation of the FE input files is a step that requires careful attention. A minor oversight might go undetected, leading to erroneous results. Numerous opportunities for such small errors abound, and a user-friendly interface can significantly alleviate this problem, and allow for high efficiency and much increased confidence.

On this basis, a graphical user interface "OpenSeesPL" is under development (Figures 1 and 2), to allow for the execution of push-over and seismic footing/pile-ground simulations (Lu et al. 2006, http://cyclic.ucsd.edu/openseespl). Various ground modification scenarios may be also studied by appropriate specification of the material within the pile zone.

In the following sections, an overview of OpenSeesPL capabilities is presented, followed by a range of potential simulation scenarios. As such, the aim is to highlight the analysis framework capabilities and range of potential applications.

2. COMPUTIONAL FRAMEWORK

The open-source platform OpenSees (http://opensees.berkeley.edu, Mazzoni et al. 2006) is employed throughout. OpenSees is a software framework for developing applications to simulate the performance of structural and geotechnical systems subjected to earthquakes. OpenSees can be used to study the performance of infrastructure facilities (bridges, buildings, etc.) under static loads, and during earthquake events.

In the OpenSees platform, a wide range of linear and nonlinear soil and structural elements is available (details are included in the Appendix). The reported pre- and post-processing scenarios are generated by the user interface OpenSeesPL which allows for: i) convenient creation of the mesh and associated boundary conditions and loading parameters (FE input file), ii) execution of the computations using the OpenSees platform, and iii) graphical display of the results for the footing/pile and the ground system.

3. MODELING CONFIGURATION

The OpenSeesPL graphical user interface (pre- and post-processor) is focused on facilitating a wide class of 3D studies (with additional capabilities yet under development). The basic default configuration is in the form of a 3-dimensional soil island with the possibility of including a footing/pile/pile-group model. Full-mesh, half-mesh, or quarter mesh configurations may be analyzed, as dictated by symmetry considerations.

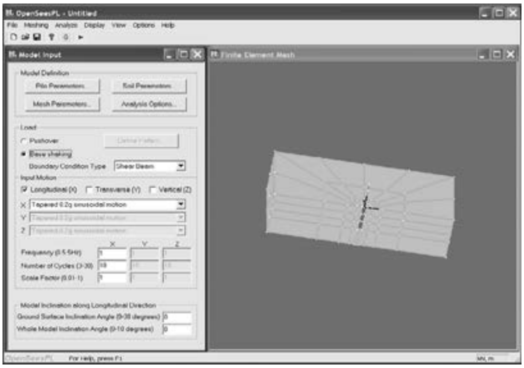

Figure 1. OpenSeesPL user interface showing (1/2 mesh due to uniaxial lateral loading symmetry) a circular pile in level ground (Lu et al. 2006).

In OpenSeesPL, the mesh configuration may be easily modified to: i) change the pile diameter, depth of embedment, height above ground surface and number of pile beam-column elements, and ii) refine the ground mesh domain in the lateral and vertical directions (Figure 3).

Square or circular pile cross-sections may be specified. As such, the pile model may be employed to study the response of a tall building that can be modeled as a bending beam (Figure 4). Shallow foundations (rigid) in square or circular configurations may be also conveniently analyzed (Figure 5).

Independent control over the pile zone material may be exercised, allowing for a wide range of ground modifications studies (Figure 6). Of particular importance and significance in these scenarios is the ability to simulate the presence of a mild infinite-slope configuration, allowing estimates of accumulated ground deformation, efficacy of a deployed liquefaction countermeasure, pile-pinning effects, and liquefaction-induced lateral pile loads and resulting moments/stresses.

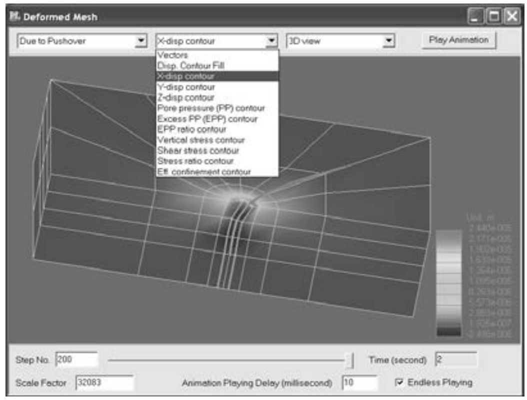

Figure 2. Push-over analysis and deformed mesh window in OpenSeesPL (Lu et al. 2006).

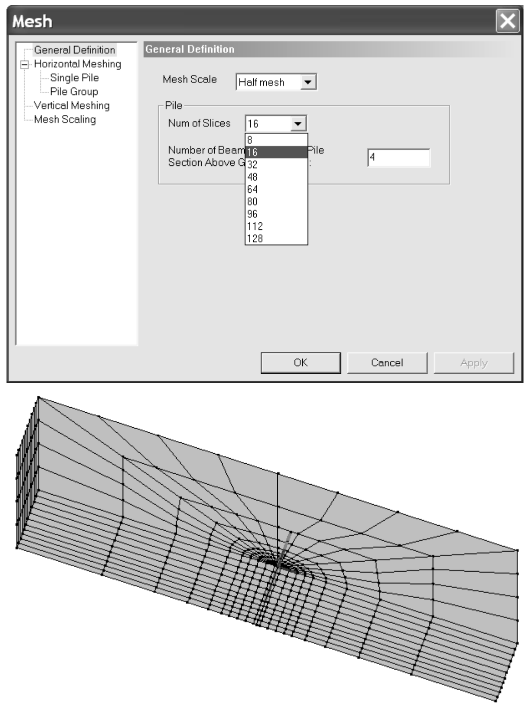

Figure 3. Mesh refinement in OpenSeesPL.

Material for the pile-soil interfacing zone may be also specified by the user, permitting scenarios such control over pile-soil friction and potential no-tension interaction during lateral deformation (Figure 7). In addition to the footing and single pile configurations, pile groups may be also represented in the free head or fixed head configurations (Figure 8).

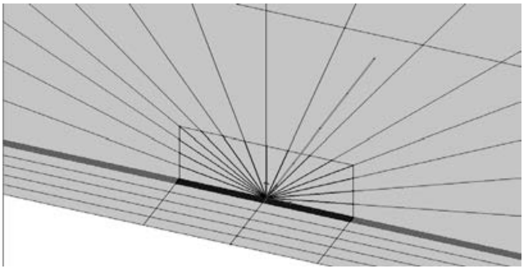

Figure 4. Building modeled as a bending beam on a shallow foundation embedded in the ground.

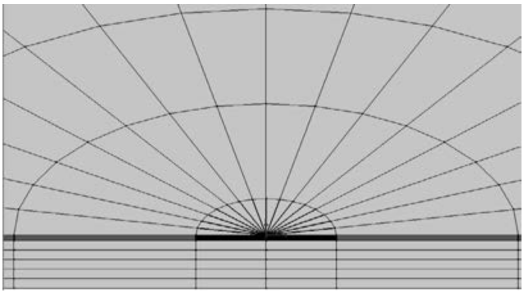

Figure 5. Circular shallow foundation model.

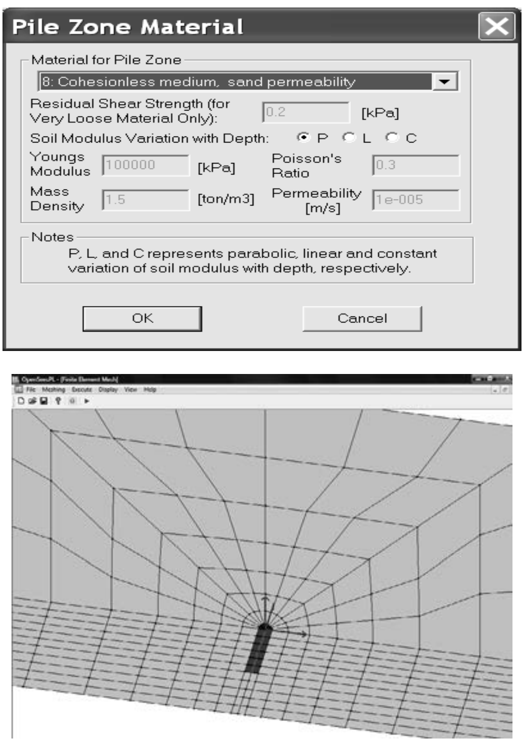

Figure 6. Control over specification of soil inside the pile zone.

4. LOAD APPLICATION

Static and dynamic loads may be applied. For static loading, push-over type analyses may be conducted where the loads/moments are directly applied to the pile top or footing surface, in force or in displacement modes (Figure 9). Capabilities are provided for monotonic loading, cyclic loading, and for user-defined load patterns to be uploaded as text file. Push-over along the finite element mesh boundary may be also specified, for instance to explore loads on pile foundations due to lateral ground displacement (Figure 10).

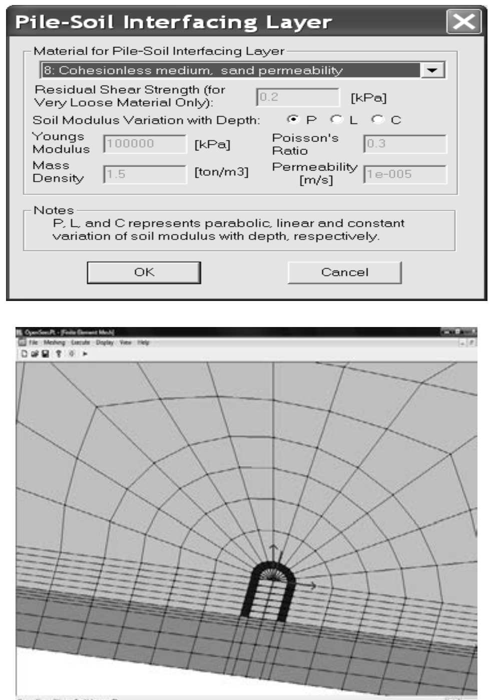

Figure 7. Control over specification of pile-soil interfacing zone.

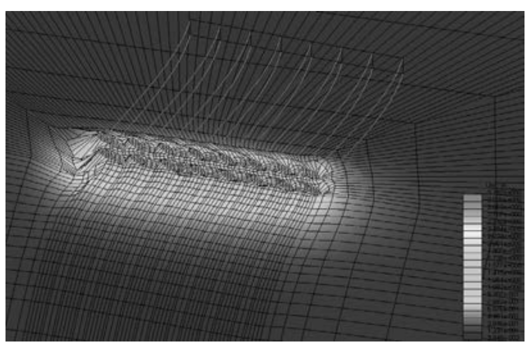

Figure 8. Large pile group model (1/2 mesh configuration).

Dynamic and earthquake shaking may be also imparted along the soil lower boundary (base). Shaking is allowed in 3D with a small set of available motions, and a capability to upload user specified base shaking excitation (Figure 11).

5. SOIL MESH BOUNDARY CONDITIONS

For static loading on the pile or footing system, a fixed boundary condition may be specified along the base and lateral boundaries of the soil mesh. For dynamic/earthquake excitation, ground motion is specified uniformly along the soil model base as mentioned earlier. Along the lateral boundaries, users can choose between fixed, shear beam, or periodic boundary conditions.

6. SOIL PROPERTIES

Linear and nonlinear elasto-plastic cyclic soil modeling capabilities are available. For nonlinear soil response, pressure independent (Mises or J_2) plasticity and pressure dependent (Drucker-Prager cone yield surface) models are available (Elgamal et al. 2003, Yang et al. 2003). The available solid-fluid coupled formulation allows for conducting

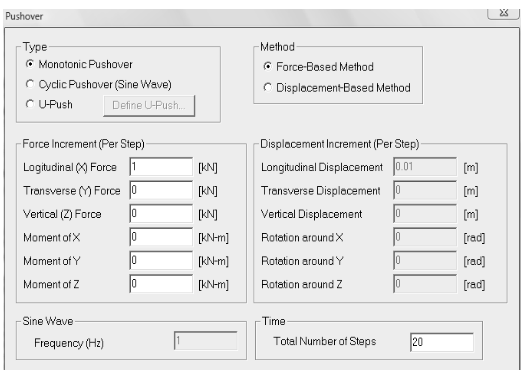

Figure 9. Push-over load application in force or displacement modes.

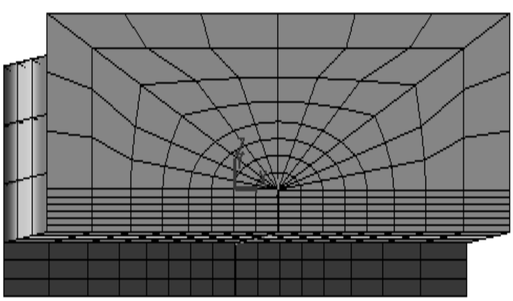

Figure 10. Push-over for lateral ground displacement studies.

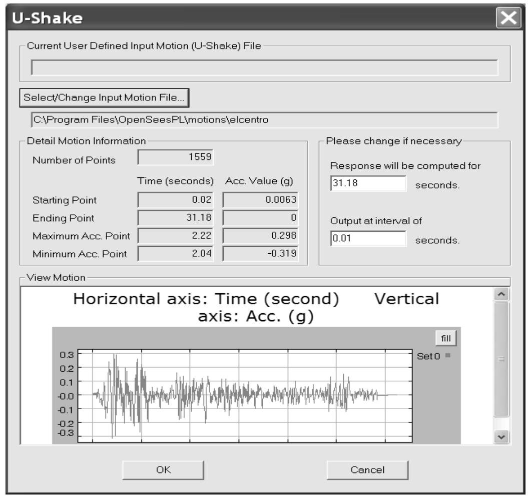

Figure 11. User-uploaded earthquake base excitation.

liquefaction-type analyses (Yang et al. 2003). Selection may be made from a set of available soil model properties, or by user-defined input modeling parameters (Figure 12).

7. BEAM-COLUMN ELEMENTS

OpenSeesPL employs state-of-the-are beam-column element formulations through the FE analysis engine OpenSees (Mazzoni et. al 2006). In addition to static analysis, these elements allow for dynamic/cyclic earthquake-type simulations. Linear, bilinear hysteretic, and nonlinear fiber element formulations are available (Mazzoni et al. 2006), based on steel and concrete cyclic constitutive models. Using OpenSeesPL, the beam column modeling properties may be specified, and the resulting moment-curvature relationship can be generated as shown in Figure 13.

8. VISCOUS DAMPING

For dynamic computations, viscous damping at the level of the entire model may be specified conveniently. A dedicated interface allows users to define damping ratios at two different frequencies, according to the Rayleigh mass-stiffness damping logic. Conversely, the mass and stiffness matrix viscous damping multipliers may be specified directly (Figure 14).

9. POST-PROCESSING

Upon specification of the model parameters, the interface accesses the FE OpenSees platform to conduct the computations. If needed, own weight is applied first (soil domain followed by superstructure), nonlinear material properties are activated, and the specified loading scenario is finally executed (static or dynamic/earthquake loading).

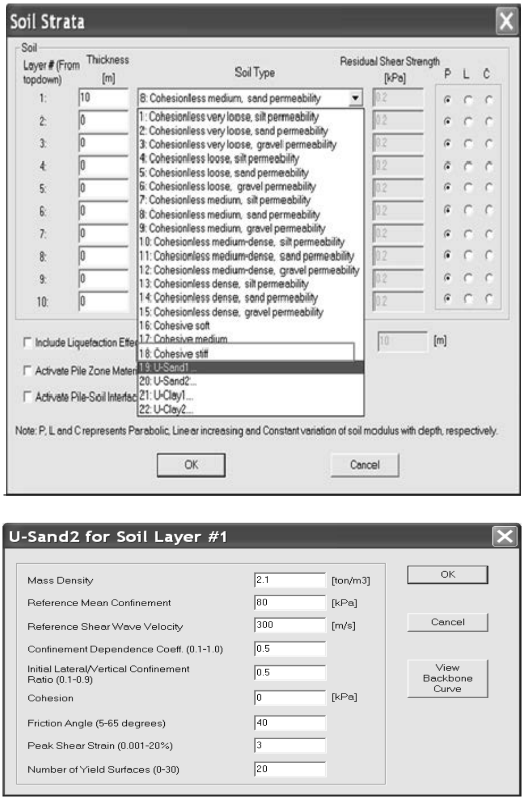

Figure 12. Menu of soil properties, and user-defined parameters.

Upon completion of the computational phase, display of the results is initiated by OpenSeesPL. The structure response may be viewed as time histories and/or as response at various levels of the applied static load (Figures 15 and 16). The deformed mesh may be also viewed (Figures 2 and 8), with capabilities for animation and display of conditions after application of own weight only, and after execution of the static/dynamic load computations. Contour quantities such as displacement, strain, stress, pore pressure, and stress-ratio (stress-state relative to failure condition) may be viewed (Figure 10).

10. EXAMPLE SIMULATION SCENARIOS

I. Elgamal and Lu (2009a) conducted a pilot study of lateral loading on a 3x3 pile group. A single-pile FE model was first calibrated in the linear range based on the 3D analytical solution of Abedzadeh and Pak (2004). Response of this linear pile in an idealized nonlinear undrained-clay material was then computed and compared to the linear solution. The corresponding 3x3 pile group response was also addressed, as a function of pile-spacing for the above linear and nonlinear soil cases (Figures 17 and 18).

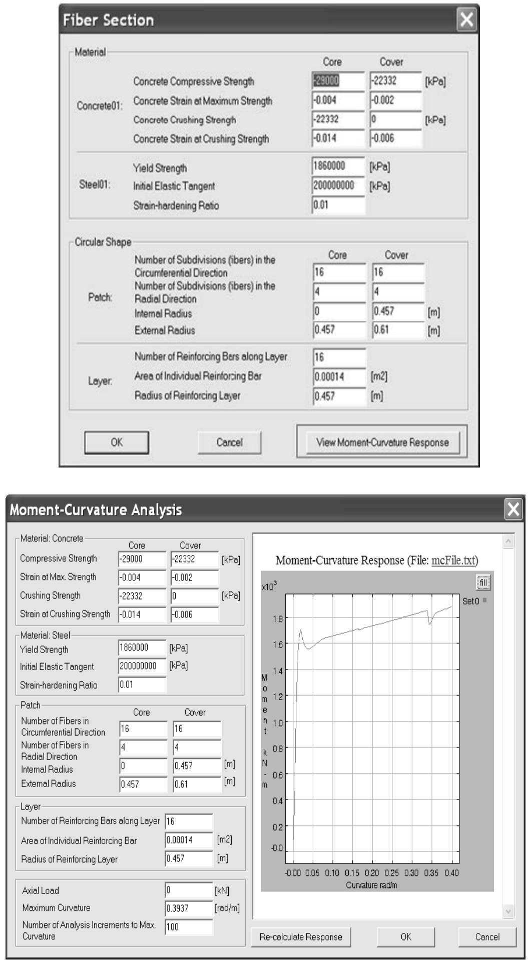

Figure 13. Fiber section and moment-curvature relationship.

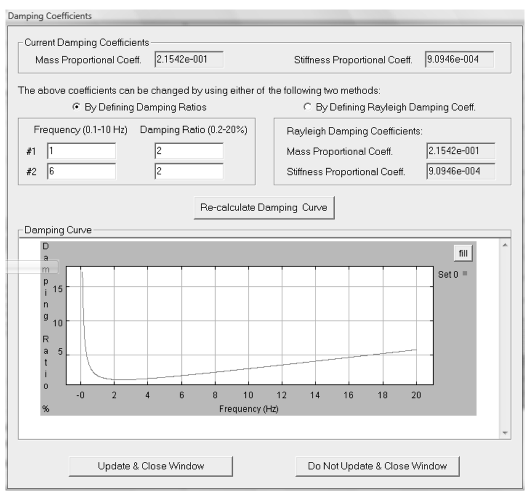

Figure 14. Control over Rayleigh mass, stiffness viscous damping.

II. In a remediated area of large spatial extent (Figure 19), the periodic boundary technique offers an effective approach for conducting 3D analyses (i.e., symmetry allows the investigation of a representative remediated "cell"). On this basis, Elgamal et al. (2009b) conducted a 3D FE ground modification parametric study (Figure 19), to evaluate mitigation of liquefaction-induced lateral soil deformation by the stone column and the pile pinning approaches. An effective-stress plasticity-based formulation was employed.

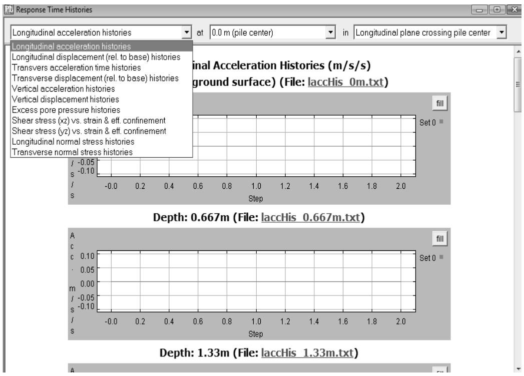

Figure 15. Display of response time histories.

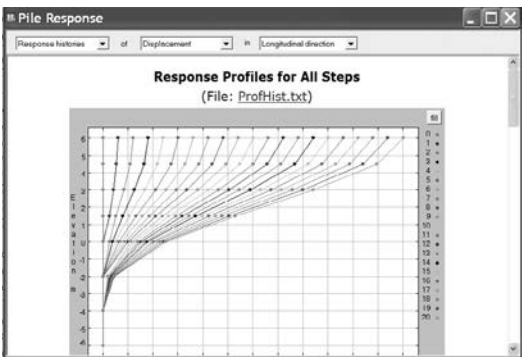

Figure 16. Pile displacement load-step display (monotonic load).

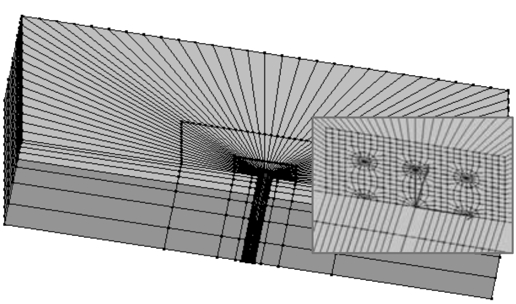

Figure 17. FE mesh of 3x3 pile group (1/2 mesh due to symmetry).

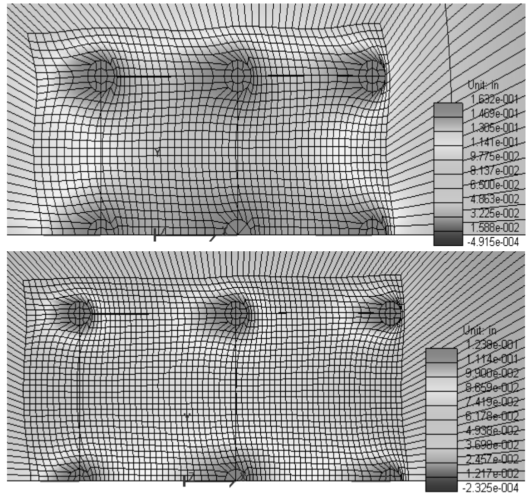

Figure 18. Plan view of displacement around piles for 5 (above) and 7 (below) pile-diameter spacing (1/2 mesh configuration, with red color denoting the large displacement zones).

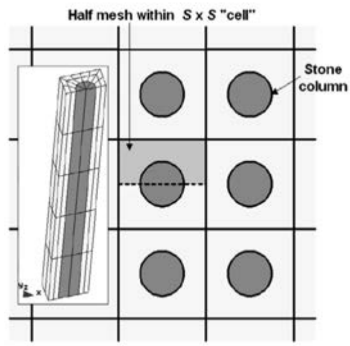

a)

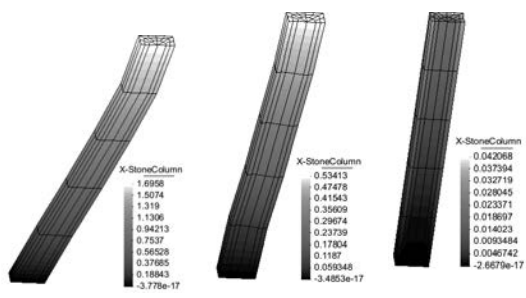

b) c) d)

Figure 19. Ground modification study for mitigation of liquefaction-induced lateral deformation: a) cellular ground modification and FE mesh (1/2 mesh due to symmetry); b) - d) final deformed mesh for cases of medium silt, 20% stone-column replacement ratio, and pile-pinning effect, respectively (factor of 5; contour fill shows longitudinal displacement in meters).

Using OpenSeesPL, a half-mesh was studied due to symmetry (Figure 19). A 10 m depth mildly-inclined (4 degrees) saturated layer was analyzed, with the remediated zone diameter maintained at 0.6 m throughout. Liquefaction-induced lateral deformation and remediation procedures for mildly sloping sand and silt strata were investigated under the action of an applied earthquake excitation. The extent of deployed remediation (area replacement ratio) and effect of the installed stone column permeability were analyzed. Effect of lateral spreading on the pile response was also investigated.

11. SUMMARY AND CONCLUSIONS

A robust and versatile framework for computational analysis of pile-ground systems was presented. The open-source platform OpenSees is employed throughout. For illustration, scenarios of lateral response of pile groups, as well as ground remediation against liquefaction-induced lateral spreading were discussed. The conducted investigations aim to highlight the analysis framework capabilities and range of potential applications.

ACKNOWLEDGMENT

The authors are grateful for the funding provided by the Pacific Earthquake Engineering Research (PEER) Center, the US National Science foundation Grant No. 0529995, and the PEER Lifelines program.

APPENDIX

The employed FE analysis platform OpenSees http://opensees.berkeley.edu) includes a large library of element and material models that are particularly suited to earthquake engineering simulation (Mazzoni et al. 2006). Among the main capabilities accessible via the user interface OpenSeesPL are:

1) Solid elements and soil models

For the soil domain, 3D brick elements are included in OpenSees with coupled solid-fluid capabilities (Yang and Elgamal 2002), following the original *u-p* formulation (Chan 1988), in which *u* is displacement of the soil skeleton, and *p* is pore pressure. This implementation is based on the following assumptions: small deformation and rotation, solid and fluid density remain constant in both time and space, porosity is locally homogeneous and constant with time, soil grains are incompressible, and solid and fluid phases are accelerated equally.

In addition, multi-yield surface soil models (Yang et al. 2003) are available for the pressure-independent (J_2 plasticity) and pressure-dependent Drucker-Prager scenarios (Figure 20). The pressure-dependent (Yang and Elgamal 2002; Elgamal et al. 2003) was developed based on the multi-surface-plasticity theory for frictional cohesionless soils proposed by Prevost (1985). This model was developed with emphasis on simulating the liquefaction-induced shear strain accumulation mechanism in clean cohesionless soils (Yang and Elgamal 2002; Elgamal et al. 2003). The above soil elements and models allow for simulation of dry/fully saturated soil conditions.

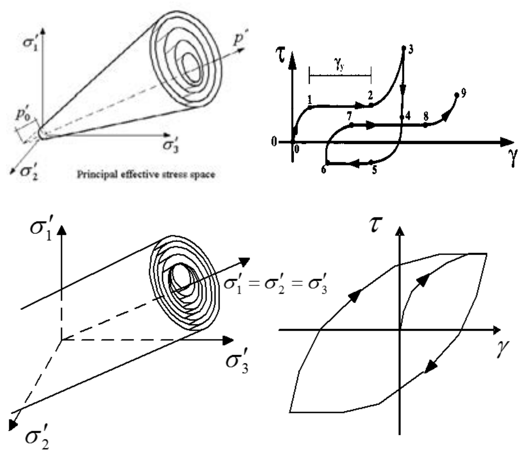

Figure 20. . Multi-yield surface soil models available in OpenSees (J_2 and Drucker-Prager).

2) Beam-column elements

In OpenSeesPL, the OpenSees beam-column linear, bilinear and fiber force-based elements may be directly accessed (Spacone et al. 1996; De Sousa 2000; McKenna and Fenves 2001). For the fiber element, the uni-axial Kent-Scott-Park model (Kent and Park 1971; Scott et al. 1982; Mander et al. 1988) with degraded linear unloading/reloading stiffness is used to model the concrete (Figure 21). The reinforcing steel is represented by a uni-axial bilinear inelastic model with kinematic hardening (equivalent to a 1-D J_2 plasticity model with linear kinematic hardening) as shown in Figure 22.

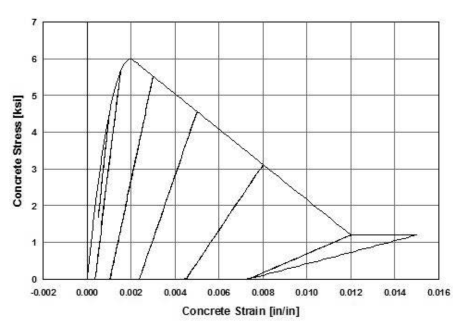

Figure 21. Concrete Kent-Scott-Park model with degraded linear unloading/reloading stiffness (Mazzoni et al 2006).

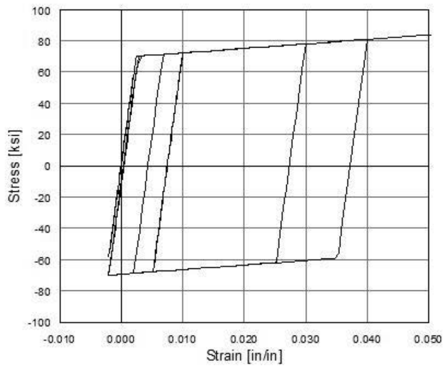

Figure 22. Steel bilinear inelastic model with linear kinematic hardening (Mazzoni et al 2006).

REFERENCES

Abedzadeh, F., and Pak, Y.S. 2004. Continuum mechanics of lateral soil–pile interaction. *Journal of Engineering Mechanics*, 130(11): 1309-1318.

Chan, A.H.C., 1988. A unified finite element solution to static and dynamic problems in geomechanics, PhD Thesis, University College of Swansea, U. K.

De Sousa, R. M. 2000. Force-based finite element for large displacement inelastic analysis of frames, *Ph.D. Dissertation*, University of California, Berkeley.

Elgamal, A., Yang, Z., Parra, E., and Ragheb, A. 2003. Modeling of cyclic mobility in saturated cohesionless soils. *International Journal of Plasticity*, 19(6), 883-905.

Elgamal, A., and Lu, J. 2009a. A framework for 3D finite element analysis of lateral pile system response, *Proceedings of the 2009 International Foundation Congress and Equipment Expo, Contemporary Topics in In Situ Testing, Analysis, and Reliability of Foundations, ASCE GSP 186*, M. Iskander, D. F. Laefer, and M. H. Hussein, Editors, Orlando, Florida, March 15–19, pp. 616-623.

Elgamal, A. Lu, J., and Forcellini, D. 2009b. Mitigation of liquefaction-induced lateral deformation in a sloping stratum: 3D numerical simulation, *Journal of geotechnical and geoenvironmental engineering*, 135(11), 1672-1682.

Kent, D. C., and R. Park, 1971. Flexural members with confined concrete, *J. Structural Engineering Division., ASCE*, 97(7), 1969–1990.

Lu, J., Yang, Z., and Elgamal, A. 2006. OpenSeesPL three-dimensional lateral pile-ground interaction version 1.00 user's manual, *Report No. SSRP-06/03*, Department of Structural Engineering, University of California, San Diego, La Jolla, CA.

Mander, J. B., M. J. N.Priestley and R. Park, 1988. Theoretical stress-strain model for confined concrete, *Journal of the Structural Engineering*, 114(ST8), 1804-1826.

Mazzoni, S., McKenna, F., and Fenves, G. L. 2006. Open system for earthquake engineering simulation user manual, Pacific Earthquake Engineering Research Center, University of California, Berkeley (http://opensees.berkeley.edu/).

McKenna, F. T., and G. L. Fenves, 2001. *The OpenSees Command Language Manual, Version 1.2*, Pacific Earthquake Engineering Research Center, University of California, Berkeley.

Prevost, J.H. 1985. A simple plasticity theory for frictional cohesionless soils. *Soil Dynamics and Earthquake Engineering*, 4(1), 9-17.

Scott, B. D., R. Park, and M. J. N. Priestley, 1982. Stress-strain behavior of concrete confined by overlapping hoops at low and high strain rates, *ACI Journal*, 79(1), 13-27.

Spacone, E., F. C. Filippou, and F. F. Taucer, 1996. Fiber beam-column model for non-linear analysis of r/c frames: part I. formulation, *Earthquake Eng and Structural Dynamics*, 25(7), 711-725.

Yang, Z. and A. Elgamal, 2002. Influence of permeability on liquefaction-induced shear deformation, *Journal of Engineering Mechanics*, ASCE, 128(7), 720-729.

Yang, Z., Elgamal, A., and Parra, E. 2003. A computational model for cyclic mobility and associated shear deformation, *Journal of Geotechnical and Geoenvironmental Engineering*, 129(12), 1119-1127.

Kinematic interaction for piles embedded in soils with a shear modulus increasing with depth

M. Maugeri, E. Motta, E. Raciti
University of Catania, Department of Civil and Environmental Engineering

ABSTRACT: Pile kinematic deformation has triggered structural damage in many strong earthquakes, but they can be distinguished from inertial deformations only when mechanical discontinuities are found at a certain depth. In this work kinematic interaction is analysed for single piles embedded in normally consolidated soil deposits, with a linearly increasing Young modulus with depth. Kinematic bending moments, in this case, reach a peak near the ground surface, were there is the maximum mechanical difference between soil and pile; moreover here the inertial effect has its maximum value. When the phase difference between kinematic and inertial effects is null, they sum each other, so destructive effects could arise.

1. INTRODUCTION

Deep foundation analysis and design is a main problem in engineering practise, especially in megacities and in the most urbanised areas, where skyscrapers, viaducts and other man made works are often founded on piles.

Pile foundation dynamic behaviour is quite complex and not deeply known. It is affected by non linear phenomena taking place in the soil rounding piles and by kinematic effects connected to ground shaking. Mylonakis et al, (2006) explain soil-foundation-overstructure dynamic interaction phenomena as a series of effects of strains and the following induced stresses linked together. In reality, inertial forces arising from the over-structure and soil deformations arising from seismic waves act contemporarily, but in technical literature, many times, inertial interaction, due to over-structure and kinematic interaction, due to soil deformations caused by seismic waves, are analysed separately and then, hypothesizing small strains, the superimposition effect is applied.

During the last thirty years a deep improvement in knowledge has been established about dynamic soil-structure interaction. Theoretical studies and experimental observations (Mizuno, 1987; Tazoh et al., 1987; Matsui e Oda, 1996; Boulanger et al., 1999) are now available. In particular, Mizuno (1987) observed seismic pile failures in Japan and concluded that most of them arose from inertial effects transmitted by the superstructure or from liquefaction-induced soil deformations. However, in several cases the location of pile failure was too deep to be caused by loading from the top (that is inertial interaction), while liquefaction could not possibly have occurred. The observed damage was instead associated with the presence of discontinuities in strength and stiffness of the soil profile. So Kavvadas & Gazetas (1993) deduced that the most likely cause was the relatively large pile curvatures imposed by the surrounding soil deformed by seismic waves, that is “kinematic interaction”.

A comprehensive survey of the dynamic and seismic response of piles has been presented by Novak (1991). Eurocode EC8 (2003), and various recent national seismic regulations (among which AASHTO, 1983; JSCE, 1988; AFGP, 1990 and the Italian DM 14/01/2008) have recognized the importance of this type of loading and require to take into account the dynamic soil-structure interaction in seismic foundation design, in terms of both kinematic and inertial effects. Despite this, kinematic deformation and potential failure has not received proper attention in professional practise. In the past engineers used to design the piled foundation merely against head loading, ignoring kinematic effects because easy application analysis methods were missing and the application of simplified methods to evaluate the maximum kinematic bending moments (Margason e Holloway, 1977; Dobry e O'Rourke, 1983; Nikolau e Gazetas, 1997; NEHRP, 1997) is not widespread.

On the other hand, great geotechnical experience can be found about the equivalent static analysis for the inertial loading, but no specific methods are proposed in EC8 or in the abovementioned national codes to predict kinematic deformations and bending moments. So, in the last period, many researches arose about this theme with the aim of both a better comprehension of those phenomena through experimental observations and analytical and numerical modelling and that of finding useful methods for professional applications.

In technical literature, dynamic simulations on physical models and numerical analysis in various load conditions have been developed. The results of those studies show that kinematic interaction effects could be very onerous. However, kinematic interaction is usually analysed for two-layered deposits with high stiffness contrasts (Dente, 1999; Nikolau et al., 1995; Nikolau et al., 2001; Cairo et al., 2006; Cairo et al., 2007 a and b; Maiorano et al., 2007; Ardita et al., 2008, Maugeri et al, 2009a; Maugeri et al, 2009b, etc.), and the maximum values of kinematic bending moments are reached near an alternation between a soft and a rigid soil layer interface, while inertial interaction effects are prevalent near the ground surface.

In this work kinematic interaction is analysed for single piles embedded in soils, laying on a bedrock, with linearly increasing Young modulus, that represent normally consolidated soil deposits. The bedrock is considered as a rigid material. The system is subjected to upward propagating harmonic shear waves. For the aim of this work, a computer program is developed and a parametric study is brought about. The results are shown through a comparison between the kinematic behaviour of a pile embedded in a Gibson soil with that of the same pile embedded in a soil with a constant Young modulus. It will be shown that kinematic bending moments, in this case, reach their peak near the ground surface, were there is the maximum difference between soil and pile Young modulus, and were inertial bending moments are greater. These two effects have usually a phase difference but if, in the worst conditions, the phase difference is null, they sum each other and destructive effects could arise.

2. THE CALCULATION MODEL

To analyse soil-foundation dynamic behaviour, the application of rigorous analytical tools would be desirable, but in design practise this is too onerous, especially when a frequency domain seismic analysis is brought about, as pile response should be evaluated with so a high frequencies number (thousands) that it would be enough to cover the seismic signal frequency content.

In this work a simplified analytical model presented by Ardita et al. (2008), Maugeri et al (2009a) and Maugeri et al (2009b) will be developed for a multi-layered soil profile and then applied to analyse pile seismic behaviour in the case of a soil deposit, with a linearly increasing with depth Young modulus, such as a normally consolidated clay deposit.

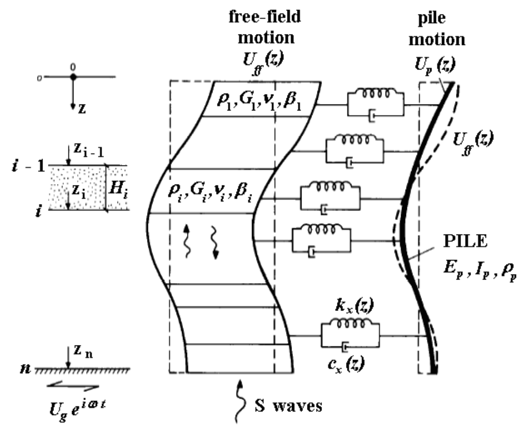

Figure 1. BDFW model for a multy-layered soil and a free-head pile (modified from Kavvadas and Gazetas, 1993).

The proposed calculation model is a BDWF (Beam on Dynamic Winkler Foundation) type, applied for the first time by Kavvadas and Gazetas (1993) to the case of a two-layered soil deposit. It retrieves a scheme already analysed for applications to cases of layered soils with two or three homogeneous layers (Ardita et al., 2008; Maugeri et al., 2009a; Maugeri et al., 2009b), but it relies on a more detailed discretizzation, so that it allows also an application, though approximate, to the case of soils with properties linearly increasing with depth, based on effective stress. Soil around piles is hypothesised in free-field conditions, so seismic S-waves propagate vertically, not influenced by pile presence.

To determine the soil free-field displacement, a one-dimensional S-wave propagation can be used, assuming a linear hysteretic soil behaviour. The loading corresponding to free field motion related to undisturbed soil, $u_{ff}(z,t)$, is transmitted to the pile through an interface of springs and dumpers distributed continuously along the pile shaft (Figure 1) whose features are described by a impedance function. The determination of the springs and dashpot mechanical parameters (stiffness and viscosity), that are functions of the input frequency, is one of the most critical aspects in modelling the soil-pile system.

It is necessary to take into account both the pile with the involved soil layers parameters, and the interface parameters, that are, however, functions of both soil and pile geometrical and physical features.

Each layer is characterized by a complex shear wave velocity. To determine the soil fundamental natural frequency, Rayleigh method is used. Boundary conditions will be chosen taking into account the particular geometrical conditions of the analysed problem.

Pile deformations, shear and bending moments can be obtained, as functions of both the depth z and the time t, solving the following differential equation:

$$E_p \cdot I_p \cdot \frac{\partial^4 u_p}{\partial z^4} + m_p \cdot \frac{\partial^2 u_p}{\partial t^2} = S_x \cdot \left(u_{ff} - u_p\right) \qquad (1)$$

where $E_p \cdot I_p$ is the pile bending stiffness, m_p is the unit length mass, u_p is the pile displacement.

S_x, called "complex stiffness", represents the interface features through which free-field motion transmits the seismic solicitations to the pile, and it is a function of the oscillation frequency ω, according to the following expression:

$$S_x = k_x + i \cdot \omega \cdot c_x \qquad (2)$$

Soil-pile interface is represented through springs, with a stiffness k_x, and dumpers, with a viscosity coefficient c_x, independent each other. The parameters k_x and c_x are functions of physical and geometrical features of both the soil and the pile. As a first approximation, the spring stiffness, k_x, can be considered frequency-independent and it can be expressed as a multiple of the local soil Young modulus, E_s:

$$k_x \approx \delta \cdot E_s \qquad (3)$$

where δ is a frequency-indipendent coefficient, assumed constant (i.e. the same for all layers and independent of depth), whose values have been determined by Kavvadas and Gazetas (1993) by FEM analyses.

The stiffness parameter, c_x, represents both radiation damping, arising from waves originating at the pile perimeter and spreading laterally outward, and material damping, deriving from hysteretically-dissipated energy in the soil. Kavvadas and Gazetas (1993), for example, use an algebraic expression based on the work of Roesset and Angelides (1980), Krishnan et al. (1983) and Gazetas and Dobry (1984a, 1984b):

$$c_x \approx (c_x)_{radiation} + (c_x)_{hysteresis} \qquad (4)$$

or the following other expression:

$$c_x \approx 2 \cdot d \cdot \rho_s \cdot V_s \cdot \left[1 + \left(\frac{V_c}{V_s}\right)^{5/4}\right] \cdot a_0^{-1/4} + 2 \cdot k_x \cdot \frac{\beta}{\omega} \qquad (5)$$

Where $a_0 = \omega \cdot d / V_s$ is the dimensionless frequency and V_c is the apparent velocity of the extension-compression waves, taken as the Lysmer's analogue velocity, introduced by Gazetas and Dobry (1984a, 1984b).

$$V_c \approx \frac{3{,}4 \cdot V_s}{\pi \cdot (1 - \nu)} \qquad (6)$$

At all depths except near the ground surface $(z \le 2{,}5 \cdot d)$ where three dimensional effects arising from the stress-free boundary are better reproduced by use of $V_c \approx V_s$.

In case of a multy-layered soil profile with N layers ($j = 1, 2, \ldots, \mathrm{N}$), equation (1) will be applied to each layer interface, so, for each soil deposit mechanical discontinuity, 4 arbitrary constants will be determined through congruence and equilibrium equations at the interface between one layer and the adjacent other one. Adding boundary conditions at the pile cap and at the pile tip, a system of $4N$ equations with con $4N$ arbitrary unknown constants will be obtained.

3. NUMERICAL APPLICATIONS

In the numerical applications, the behaviour of a single pile embedded in a homogeneous soil has been compared with those of the same pile embedded in a Gibson soil, that is a soil with a linearly increasing with depth Young modulus, with the following equation:

$$E_s = \vartheta \cdot z \tag{7}$$

This condition is typical of normally consolidated soil deposits.

A system made of a single floating pile restrained at the head is analysed. The pile has a length $L = 20m$ and diameter $d = 0{,}60m$ embedded in a soil deposit with a total height $H = 30m$. The soil is divided in fifteen layers, all with the same thickness, $h = 2m$. A bedrock is located at the base. S-waves propagates from the bedrock toward the ground surface, and they cause a horizontal harmonic motion that can be described by the following equation:

$$u_g(t) = U_g \cdot \exp(i \cdot \omega \cdot t) \tag{8}$$

For as regards the soil deposit, a damping ratio $\xi_i = 5\%$, a soil unit weight $\gamma_i = 19kN/m^3$ and a Poisson ratio, $\nu_i = 0.40$ have been hypothesized for all the layers.

For as regards the mechanical features, the soil has been hypothesized as a linearly hysteretic material and the two following cases have been compared:

(a) Soil Young modulus linearly increasing with depth, following equation (4) (Figure 2 *a*);

(b) Soil Young modulus constant and equal to its average value along the pile shaft in case '*a*' (Figure 2*b*).

To simulate E_s linear increment, for the generic layer i it is assumed:

$$E_{si} = \vartheta \cdot h \cdot \left(i - \frac{1}{2} \right) \qquad i = 1,\ 2,\ \ldots,\ 15 \tag{9}$$

Instead, for as regards the case of the pile embedded in a homogeneous soil, the following assumption has been made:

$$E_{si} = E_{s\_av} = \frac{L}{2} \cdot \vartheta \quad i = 1,\ 2,\ \ldots,\ 15 \tag{10}$$

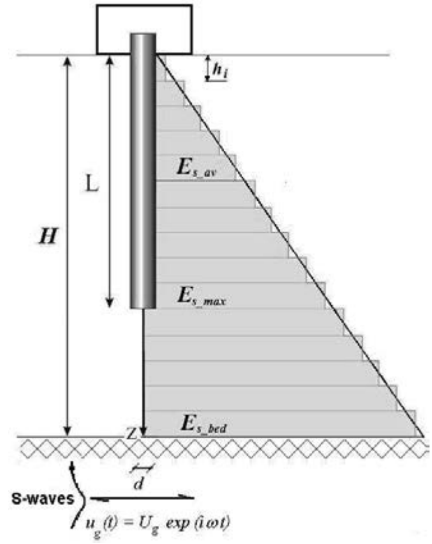

(a)

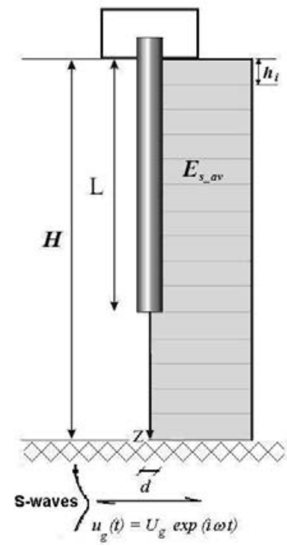

(b)

Figure 2. Examined cases. (*a*) Soil Young modulus linearly increasing with depth; (*b*) Soil Young modulus constant and equal to its average value in case *a*.

The pile has been schematised as an elastic beam with unit weight $\gamma_p = 24kN/m^3$.

Analyses have been brought about assigning as bedrock motion frequency both that of the system of case '*a*' (ω_a) and that of the system of case '*b*' (ω_b).

4. RESULTS

In Figure 3 the soil displacements in free field conditions are plotted for the two cases analysed in this work. Figure 3a refers to a harmonic solicitation with a excitation frequency $\omega = \omega_a$, while Figure 3b the case $\omega = \omega_b$.

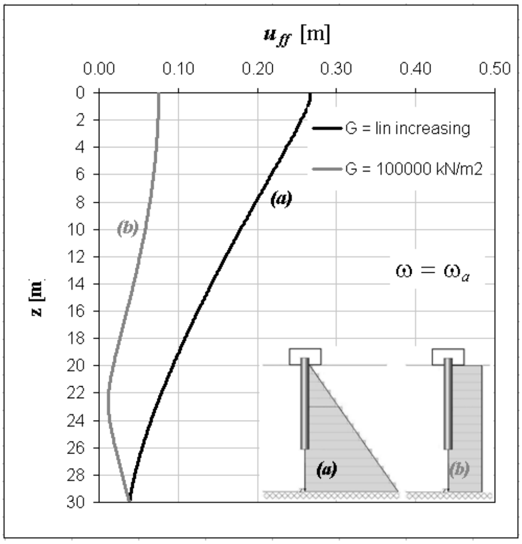

(*a*)

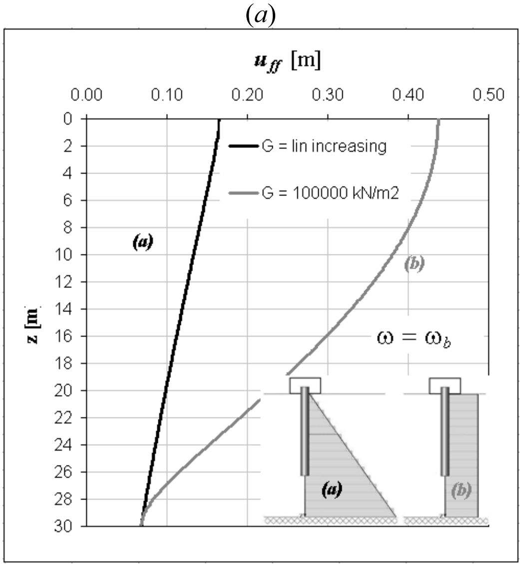

(*b*)

Figure 3. The displacement fields in free field conditions for the following two solicitation conditions: (a) harmonic with $\omega=\omega_a$ as excitation frequency (b) harmonic with $\omega=\omega_b$ as excitation frequency.

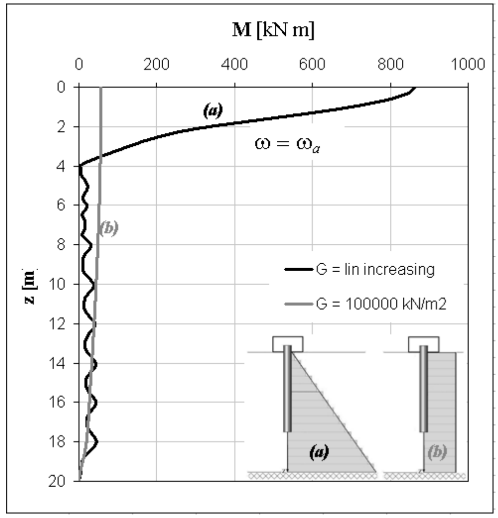

(*a*)

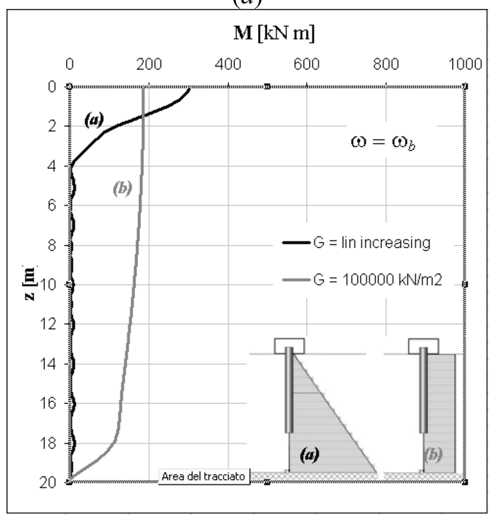

(*b*)

Figure 4. The bending moments moduli for the two analysed soil conditions, for the following two solicitation conditions: (a) harmonic with $\omega=\omega_a$ as excitation frequency (b) harmonic with $\omega=\omega_b$ as excitation frequency.

As expected, the displacements fields are exalted in agreement with the soil fundamental natural frequency: this impact on the response in terms of shear and bending moments; in particular the bending moment is exalted by the harmonic frequency.

In Figure 4 the bending moments moduli are plotted versus depth. Figure 4a refers to a harmonic wave with $\omega = \omega_a$ as excitation frequency, while Figure 4b refers to the case $\omega = \omega_b$. The analysis shows that the bending moments due to kinematic interaction for a pile embedded in a "Gibson soil" are in both cases greater near the ground surface than in the case of a homogeneous soil, with a shear modulus constant with depth. In particular, analysing figure 4a, with $\omega = \omega_a$ (the harmonic frequency is the "Gibson soil" fundamental natural frequency), it can be observed that the maximum bending moment at the ground surface deduced for the "Gibson soil" is about 15 times greater than that determined for a homogeneous soil.

Similarly, analysing figure 4b, with $\omega = \omega_b$, (the harmonic frequency is the homogeneous soil fundamental natural frequency), it can be observed that the maximum bending moment at the ground level deduced for the "Gibson soil" is in both cases greater than that determined for a homogeneous soil. However, in this case the former is only 1,5 times greater than the latter. It can be also observed that the bending moments induced at the pile head could be severe. However, this response is often "covered" by inertial interaction effects at the pile head induced by the overstructure. Moreover, it is known in literature that the results obtained using a single harmonic input method may overestimate the maximum bending moment along the pile. To solve this question, we can refer to the dimensionless bending moment defined by Kavvadas and Gazetas (1993):

$$\frac{M_{\max}}{\rho_p \cdot d^4 \cdot A} \tag{11}$$

To obtain the real value of the maximum bending moment due to a measured accelerogram, the right value of the operative harmonic amplitude "A" should be chosen. For example, Maugeri et al. [2009], compare the results obtained by Cairo and Dente [2007] by a FEM model applied to the geometrical scheme represented in Fig. 5 using eighteen different real Italian recorded accelerograms as input (see Table 1) with those obtained in their work by a closed form analytical solution for the same geometrical scheme in Figure 5, using a harmonic input with a frequency equal to the fundamental natural frequency of the studied system. "A" operative values are obtained as the ratio between the maximum bending moment obtained by the two different methods. The assumed V_{si} values for each layer are listed in Table 2.

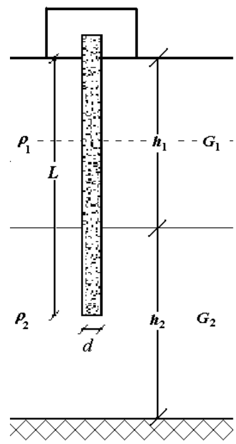

Figure 5: The calculation model used by Maugeri et al. (2009b).

Table 1. The Italian seismic records used to calibrate the model (Maugeri et al., 2009b).

File name	Date	Seismic station	Earthquake	Main Dir.
A-TMZ270	06/05/1976	Tolmezzo-Diga Ambiesta	Friuli	WE
A-TMZ000	06/05/1976	Tolmezzo-Diga Ambiesta	Friuli	NS
A-STU270	23/11/1980	Sturno	Campano-Lucano	WE
A-STU000	23/11/1980	Sturno	Campano-Lucano	NS
A-AAL018	26/09/1997	Assisi-Stallone	Umbria-Marche	NS
E-NCB090	06/10/1997	Nocera Umbra-Biscontini	Umbria-Marche (aftershock)	WE
E-NCB000	06/10/1997	Nocera Umbra-Biscontini	Umbria-Marche (aftershock)	NS
R-NCB090	03/04/1998	Nocera Umbra-Biscontini	Umbria-Marche (aftershock)	WE
J-BCT000	14/10/1997	Borgo-Cerreto Torre	Umbria-Marche (aftershock)	NS
J-BCT090	14/10/1997	Borgo-Cerreto Torre	Umbria-Marche (aftershock)	WE
E-AAL018	06/10/1997	Assisi-Stallone	Umbria-Marche (aftershock)	WE
B-BCT000	26/09/1997	Borgo-Cerreto Torre	Umbria-Marche	NS
B-BCT090	26/09/1997	Borgo-Cerreto Torre	Umbria-Marche	WE
TRT000	11/09/1976	Tarcento	Friuli (aftershock)	NS
C-NCB000	03/10/1997	Nocera Umbra-Biscontini	Umbria-Marche (aftershock)	NS
C-NCB090	03/10/1997	Nocera Umbra-Biscontini	Umbria-Marche (aftershock)	WE
R-NC2090	03/04/1998	Nocera Umbra 2	Umbria-Marche (aftershock)	WE
R-NC2000	03/04/1998	Nocera Umbra 2	Umbria-Marche (aftershock)	NS

The studied soil deposits have been distinguished in soil types C and D (EC8 - EN [1998-1, 2003]) based on the V_{s30} values obtained with the following equation:

$$V_{s30} = \frac{30}{\sum_{i=1}^{N} \frac{h_i}{v_i}} \quad (12)$$

The operative "A" values obtained by the authors are listed in Table 3.

Table 2.. The soil types analysed by Maugeri et al. (2009b).

	Soil type C			
V_{S1} [m/s]	300	150	150	150
V_{S2} [m/s]	300	300	400	600
V_{s2}/V_{s1}	1	2	2.67	4
V_{S30} [m/s]	300	200.00	218.18	240.00
w_S [1/s]	17.99	11.413	12.686	14.173

	Soil type D			
V_{S1} [m/s]	150	100	100	100
V_{S2} [m/s]	150	200	300	400
V_{s2}/V_{s1}	1	2	3	4
V_{S30} [m/s]	150	133.33	150	160
w_S [1/s]	8.994	7.608	8.783	9.448

Table 3.. The values of the operative harmonic amplitude " A " (in units of g) corresponding to the Italian seismic records used to calibrate the model (Maugeri et al., 2009b).

File name	V_{s2}/V_{s1}							
	Values of A for soil type C				Values of A for soil type D			
	1	2	2.67	4	1	2	3	4
A-TMZ270	0.14	0.14	0.12	0.16	0.12	0.09	0.14	0.14
A-TMZ000	0.07	0.05	0.06	0.08	0.05	0.04	0.05	0.05
A-STU270	0.08	0.07	0.07	0.10	0.07	0.08	0.07	0.06
A-STU000	0.09	0.13	0.10	0.03	0.11	0.09	0.11	0.12
A-AAL018	0.08	0.06	0.07	0.10	0.04	0.03	0.03	0.05
E-NCB090	0.02	0.02	0.02	0.03	0.02	0.02	0.03	0.02
E-NCB000	0.03	0.03	0.03	0.03	0.02	0.01	0.02	0.03
R-NCB090	0.02	0.02	0.02	0.03	0.01	0.01	0.02	0.02
J-BCT000	0.03	0.03	0.03	0.04	0.02	0.02	0.02	0.02
J-BCT090	0.05	0.04	0.05	0.06	0.04	0.04	0.05	0.05
E-AAL018	0.03	0.03	0.03	0.03	0.02	0.01	0.02	0.02
B-BCT000	0.03	0.02	0.03	0.03	0.02	0.02	0.03	0.02
B-BCT090	0.03	0.02	0.03	0.05	0.02	0.01	0.02	0.02
TRT000	0.04	0.04	0.04	0.05	0.02	0.03	0.02	0.02
C-NCB000	0.02	0.02	0.02	0.03	0.01	0.01	0.01	0.01
C-NCB090	0.02	0.02	0.02	0.03	0.01	0.01	0.01	0.01
R-NC2090	0.03	0.03	0.03	0.03	0.02	0.01	0.02	0.02
R-NC2000	0.02	0.02	0.02	0.02	0.01	0.01	0.02	0.02

5. CONCLUSIONS

This work puts in evidence that kinematic interaction, that, as known, is conditioned both by the harmonic frequency and intensity, is of course insidious in case of a mechanical discontinuity inside the soil deposit (Gazetas and Mylonakis, [1998]), but it could be significant also in normally consolidated soils. In such deposits in fact, it is reasonable to hypothesize a Gibson soil behaviour, with a shear modulus linearly increasing with depth. That should be taken into account for as regards kinematic interaction induced solicitations, during deep foundation design and verification phases.

6. REFERENCES

AASHTO (American Association of State Highway and Transportation Officials). 1983. Guide specifications for the seismic design of highway bridges, Washington D.C.

AFGP (Association Francaise du Genie Parasismique]. 1990. Recommandations pour la redaction de regles relatives aux outrages et installations a realizer darts les regions sujettes aux seismes, 183 pp. Paris.

Ardita, D., Armenia, F., Motta, E. & Raciti, E. 2008. 'Kinematic interaction of a single pile in a heterogeneous soil: preliminary results'. IARG 2008, Geotechnical Engineering in Italy. Catania, 15-17 September 2008. Editor M. Maugeri. Patron Editore – Bologna (in Italian).

Boulanger, R.W., Curras, C.J., Kutter, B.L., Wilson, D.W. & Abghari, A. 1999. Seismic soil-pile-structure interaction: experiments and analyses, *J. Geotech. Eng., ASCE*, 125, 9, pp. 750-759.

Cairo, R. & Conte, E. 2006. Settlement analysis of pile groups in layered soils. Canadian Geotechnical Journal, 43, 8, 788-801.

Cairo, R. & Dente, G. 2007a. Un metodo per l'analisi dell'interazione cinematica palo-terreno nei depositi orizzontalmente stratificati. XII Convegno ANIDIS, L'Ingegneria Sismica in Italia, Pisa, memoria n. 378.

Cairo, R. & Dente, G. 2007b. Kinematic interaction analysis of piles in layered soils. XIV European Conference on Soil Mechanics and Geotechnical Engineering, ISSMGE-ERTC 12 Workshop "Geotechnical Aspects of EC8", Madrid, Pàtron Editore, Bologna, cd-rom, paper n. 13

D.M. 14/01/2008 – "Nuove norme tecniche per le costruzioni", supplemento ordinario n. 30, Gazzetta ufficiale n. 29 - 4 febbraio 2008.

Dente G. 2005. Pile foundations – Guidelines on geotechnical aspects of seismic design Publisher: Patron, Bologna – (Provisional edition, in Italian) -pp. 147-160, March 2005.

Dente, G. 1999. Seismic response of pile foundations (in Italian) Publisher: Hevelius, Benevento.

Dobry R. & O'Rourke M.J. 1983. Discussion on

"Seismic response of end-bearing piles" by Flores-Berrones R. and Whitman R.V. *Journal of Geotechnical Engineering. Diision, ASCE*, 109.

EC8-Part 5, 2003. Design of structures for earthquake resistance. Part 5: Foundations, retaining structures and geotechnical aspects. Technical Committee CEN/TC250, Ref.No.prEN 1998-5: Final draft.

Gazetas, G. & Dobry, R. 1984a. Horizontal response of piles in layered soils. J. Geotech. Engng Dia. Am. Sot. Cio. Engrs 110, No. 1, 20-40.

Gazetas, G. & Dobry, R. 1984b. Simple radiation damping model for piles and footings. J. Engng Mech. Div. Am. Sot. Civ. Engrs 110, No. 6, 937-956.

Gazetas, G. & Mylonakis, G. 1998. Seismic soil-structure interaction: new evidence and emerging issues. *Geotechnical Special Publication No. 75, 2, ASCE*, 1119-1174.

JSCE (Japanese Society of Civil Engineers) 1988. Earthquake engineering design for civil engineering structures in Japan. Tokyo.

Kavvadas, M. & Gazetas, G. 1993. Kinematic seismic response and bending of free-head piles in layered soil. *Géotechnique*, Vol. 43, No 2, pp. 207-222.

Krishnan, R., Gazetas, G. & Velez, A. 1983. Static and dynamic lateral deflexion of piles in non-homogeneous soil stratum. *Geotechnique* Vol. 33, No. 3, 307-325.

Maiorano, R.M.S., Aversa, S. & Wu, G. 2007. Effects of soil non-linearity on bending moments in piles due to seismic kinematic interaction. *Proceedings of 4th International Conference on Earthquake Geotechnical Engineering*, Greece, 2007, paper No. 1574.

Margason E. & Holloway D.M. 1977. Pile design during earthquakes. *Proceedings of 6th World Conference on Earthquake Engineering,* New Delhi, 237-243.

Matsui, T. & Oda, K. 1996. Foundation damage of structures. *Soil and Foundations*, special issue on Geotechnical aspects of the January 17, 1995 Hyogoken-Nambu Earthquake, JGS.

Maugeri M., Motta, E., Raciti, E. & Ardita D. 2009a. 'Kinematic interaction of a single pile in heterogeneous soil'. *Proceedings of 7th International Conference on Earthquake Resistant Engineering Structures (ERES 2009)*, Cyprus, 11-13 May 2009.

Maugeri M., Motta, E. & Raciti, E. 2009b. 'Seismic response of single piles due to kinematic interaction'. *Proceeding of TC4 Satellite Conference. Earthquake Geotechnical Engineering.* Alexandria, Egypt, 2-3 October 2009.

Mizuno, H. 1987. Pile damage during earthquake in Japan (1923-1983). Dynamic response of pile foundations: experiment, analysis and observation, *Geotechnical Special Publication No. 11*, ASCE, 53-78.

Mylonakis G., Nikolaou S. & Gazetas G. 2006. Footings under seismic loading: Analysis and design issues with emphasis on bridge foundations. *Soil Dynamics and Earthquake Engineering* Vol. 26, No 9, pp. 824-853.

NEHRP 1997. Recommended provisions for seismic regulations for new buildings and other structures. Building Seismic Safety Council, Washington D.C.

Nikolaou A.S. & Gazetas G 1997. Seismic design procedure for kinematically loaded piles. Proc. 14th Int. Conf. Soil Mech. Found. Engng, Hamburg, Special volume, ISSMFE TC4 Earthquake geotechnical engineering, pp. 253-260.

Nikolaou, S., Mylonakis, G. & Gazetas, G. 1995. Kinematic bending moments in seismically stressed piles. Rep. NCEER-95-0022, National Center for Earthquake Engineering Research, Buffalo, N.Y.

Nikolaou, S., Mylonakis, G., Gazetas, G., & Tazoh, T. 2001. Kinematic pile bending during earthquakes: analysis and field measurements. Géotechnique, 51 (5), 425-440.

Novak M., 1991. Piles under Dynamic Loads: State of Art. *Proc. 2nd Int. Conf. on Recent Advances in Geotechnical earthquake Engineering and Soil Dynamics*, St. Louis, Vol.3, pp. 2433-2456.

Roesset, J. M. & Angelides, D. 1980. Dynamic stiffness of piles. Numerical methods in offshore piling, pp. 75-81. London: Institution of Civil Engineers.

Tazoh, T., Shimizu, K. & Wakahara, T. 1987. Seismic observations and analysis of grouped piles. Dynamic response of pile foundations: experiment, analysis and observation, Geotech. Spec. Publ. No. 11, ASCE, 1-20.

Session 3a

Geofailures & risk assessment
Improved soils
Geological risks in urban planning

Geofailures & risk assessment

Geotechnical Aspects on Earth Excavation Collapse – A Case of Kampala City

D. Kalumba
Department of Civil Engineering, University of Cape Town, Cape Town, South Africa

U. Bagampadde, B.M Kiggundu
Department of Civil Engineering, Makerere University, Kampala, Uganda

ABSTRACT: The economic growth in Uganda since 1986 after years of political instability has greatly increased the number and size of construction projects especially in and around Kampala - the capital city. Consequently, besides the lateral expansion of the city, several old structures have been pulled down so as to put up taller and better ones on the same foot print. Several of the mega projects have presented enormous challenges some of which have resulted into excavation collapses. These collapses have claimed tens of lives and leading to loss of property worth millions of dollars. The authors, who were part of investigation teams of some of these failures, present three of the most publicized excavation failures.

1. INTRODUCTION

Competition for limited space, amongst other urban problems, is becoming increasingly serious due to unprecedented economic growth of megacities in developing countries. Effects of the aforementioned problem are typified by frequent demolition of short buildings and replacing them with taller ones with attendant deep excavations (> 10m). This is aimed at allowing for maximum space utilization in form of underground floors and off-street parking.

Kampala city in Uganda (East Africa) is a typical city in the developing world characterized by an urban sprout of tall buildings with geotechnical challenges accompanying deep excavations. Having a day-population of about 4 million and land area of 176 km^2, this city has an infrastructural development pattern whereby the highly expensive hill tops and low lying wetlands are avoided in erecting tall buildings. Between these two extreme altitudes where most high rise construction is concentrated, the top 10 m of earth generally constitute deposition material which is rather un-indurated. Consequently, deep vertical excavations have lately exhibited earth collapses leading to deaths.

This paper reviews three recent cases of earth excavation collapses in the Ugandan capital city which were fatal. The paper points out the possible main causes of these excavation failures so that lessons learnt can be utilised in many deep excavations else where.

2. LUMUMBA AVENUE

On 14th October 2008 at around 11:00 am, a portion of a 17 m deep foundation excavation, on the eastern side of a proposed multi-storey structure at Plots 15A, 15B & 17 Lumumba Avenue in Kampala, collapsed (Figure 1). The accident killed 7 workers and injuring a couple of others. In addition, a servants' quarter on the neighbouring Plot 18 Nakasero Road was completely destroyed during the incident. At the time of the tragedy, excavation had advanced to about 12 m below Lumumba Avenue level and 17.1 m below the existing ground level on the eastern side.

Figure 1. Failure of 14th Oct. 2008

The project area was bordered by a residential property and a public meeting hall at the east, Kyagwe Road on the south, Lumumba Avenue on the west and an office one storey block on the north. The project was to exploit the full development potential of the site giving it 100% plot coverage. The proposed building had 525 parking spaces, and was to be an ultramodern building with 4 levels of basement parking, 2 floors in the podium, a middle tower of 23 floors and two smaller towers of 7 floors each. The structure was designed to significantly contribute to the improvement of the skyline of Kampala City.

2.1. Excavation process

Excavations of the big foundation pit were executed in three stages by excavating to the depths of: 6, 8 and 12 m with respect to Lumumba Avenue. The first level was done by excavating the entire area and reducing to level, with the cut inclined at approximately 75° and the entire earth between the cuts removed. In order to protect the sloped surfaces from erosion, the cut surfaces were plastered with 50-75 mm cement-sand lean class 30 concrete reinforced with chicken wire mesh fastened to the cut with iron bars. The first cut was separated from the second by a platform (chair) approximately 1 m wide. The second level was a vertical cut, protected with 2 no. 50 mm thick timber shoring slotted between flanges of 160x80x6 mm steel I-sections driven into the ground (Figure 2). The steel sections were propped by 220 mm round pipes, leaning on the I-sections as diagonal braces. At the time of the accident, the contractor was in the third and final stage of excavation.

The method of excavation for the second and third stages was by driving the 3-metre long piles of steel I-sections using a hydraulic press to a depth of approximately 2.4 m, welding another 3-metre long I-section and driving the pile to a depth of 6 m. The piles were positioned at approximately 4 m apart. The earth would then be excavated in the two stages. In the second stage, excavations would be done from the 6-m level to 8 m below Lumumba Avenue. The web would be exposed and the pile supported along the exposed flange. The shoring timber battens would then be stacked. This constituted the first shoring. The third stage of excavations would be done after the first shoring. The works were being done in a sequence as in the second excavation.

In all stages of excavation, the excavated material was disposed off site.

Figure 2 Temporary earth retaining system at the accident spot with rows of inserted steel bars at top and shoring at bottom of cut.

2.2. Temporary earth retaining system

Clause 18.2 of the General Conditions of Contract stated that the contractor was to be responsible for the design of all temporary works and was to submit specifications and drawings showing the proposed temporary works to the consultant. The consultant was to approve such specifications and drawings if they complied with the specifications and drawings in the statements of requirements. Consequently, the temporary earth retaining system in this project fell under temporary works. Accordingly, it had to be designed by the contractor and approved by the consultant. A combination of inserting steel bars in the upper 10 m and shoring in the lower 7 m were selected as the most locally and economically feasible methods (Figure 2).

Supporting the sloped section of the cut involved driving continuously 32 mm diameter high tensile steel bars pneumatically into the soil at an inclination of 45°. The bars were inserted at 2.0 m centre-to-centre (vertically and horizontally) and were driven into the soil as far as they could go with the embedment length ranging between 3 – 6 m.

The pushing of the bars into the soil was done using the back of an excavator bucket. This push, according to information gathered from the local consultant, applied a 1.6-2 tonne force on the rod and thus it would have required the same amount of force to pull it out of the soil. Unfortunately, this procedure was techniquely inadequate as it had no scientifically proven basis. A proper conventional procedure would have involved careful drilling past the slip surface, inserting the bar, grouting around it, and providing a rigid anchorage plate for the bar on the cut surface.

It was established during the interviews with the local contractor and consultant that no geotechnical and structural analysis for this method of soil support was undertaken for the selection of steel bars, their embedment length, spacing or inclination angles, or the shoring system at the bottom. Additionally, no rigorous slope stability analysis was ever conducted or any other scientific computation undertaken to predict possible shear planes in the slopes. A safe support system needed to be designed for after careful analysis of all parameters.

2.3. Mode of failure and possible causes

It was apparent, from the site visit, that the slope failed by a top-down rotational slide forcing a huge soil mass from the cutting to slip down to the bottom of the excavation, burying some of the workers who were around that spot at the time. The soil mass, which measured about 4 m into the neighbouring plot, 30 m along the plot boundary and 10 m high (Figures 1, 2 and 3), collapsed after a period of heavy rain the night prior to the accident. Incidentally, heavy rains were experienced that whole week.

The slip failure was as a result of one or a combination of the following:

i) The shearing forces due to the weight of the soil mass and the house located at the edge of the cutting, became greater than the resultant shearing resistance of the soil,
ii) Water ingress from the surface run off at the top of the slope (following heavy rains that week) causing the pore water pressure at the slip surface to increase, reducing the effective normal stress and thus diminishing the restraining friction along the slip line.
iii) The inadequate temporary soil-retaining system. This was exemplified by a failure which occurred next to the first, exactly one month after the first later (Figure 4).

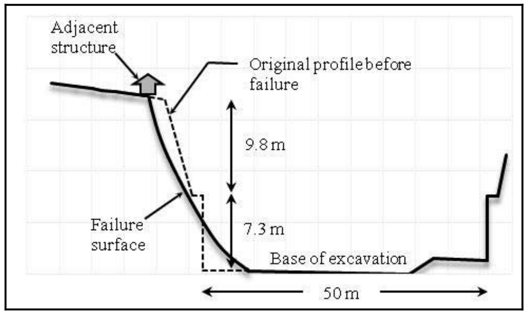

Figure 3. Diagrammatic representation of the section through the circular rotational slide.

Figure 4. Another larger failure 1 month later which occurred near the first failure.

2.4. Situation Analysis

It was observed that the excavation slope was made at 70°-90° at the top and bottom respectively hence much greater than the natural angle of repose (Ministry of Works and Transport, 2001). Consequently, there was need to reinforce the slopes and analyse their stability so as avoid the horrific incident.

To do that, the project required enough

technical skills in geotechnical engineering. However, none of the staff employed on the local contractor or consultant's team had the expertise or experience in that area.

The influence of the excavation extended well beyond the excavation itself both vertically and horizontally into the adjacent plots. A site investigation of these neighbouring sites before and during works was necessary. This had not been done. In fact, the geotechnical investigation of the project site had been conducted in 2001 (Ministry of Works and Transport, 2001), 7 years before the project started. If investigations in the bordering sites been conducted, they would have established among others:

- the surface run off and drainage characteristics in the neighborhood plots and beyond,
- the overall stability of the proposed excavation work,
- the most appropriate support system,
- the magnitude of expected ground movement, and
- the effect of excavation on the adjacent plots,

all of which would have been essential for a proper geotechnical analysis.

3. SNAY BIN AMIR STREET

On 26th February 2009 at around 12:00 noon, 1 worker was killed and 5 injured on Plot 5 Snay Bin Amir Street at a foundation excavation site for the proposed 14 storey Shopping Arcade and Hotel complex (Figure 5). The building was to have three floors in the basement. The incident occurred when a huge mound of soil on the western excavation end slipped from the top of the cutting, plunging down onto the workers at the bottom of the pit 9.5 m below Market Street (7.5-metre on the Bin Amir Street). The site initially sloped North to South towards Bin Amir Street.

The 35 m by 33 m project site is located between Market Street in the north, Duster Street in the west, Snay Bin Amir Street in the south and two one-storied structures in the east. The design was such that the development occupied the entire plot.

Figure 5. Accident spot shown by the arrow.

3.1. Excavation

Foundation excavations involved digging the entire plot and reducing the levels to approximately 9.5 m below Market Street. At the time of tragedy, most of the excavated material had been disposed off site. Generally, the cut surfaces at the upper levels were approximately vertical. The local contractor excavated further into the ground at the toe (under scouring). This occurrence was within 1 to 2.5 m of reaching the foundation base line level (Figures 6 and 7). This was done without any precautionary measures to safety. Interviews with the contractor revealed that it was done in order to create room for installing formwork for the foundations. However, this action of excavating further into the earth at the toe further undermines the stability of the slope due to the loss of toe support.

Figure 6. Soil excavated with a lot of under scouring at the bottom. Profiling boards nailed into the earth for setting out the foundation.

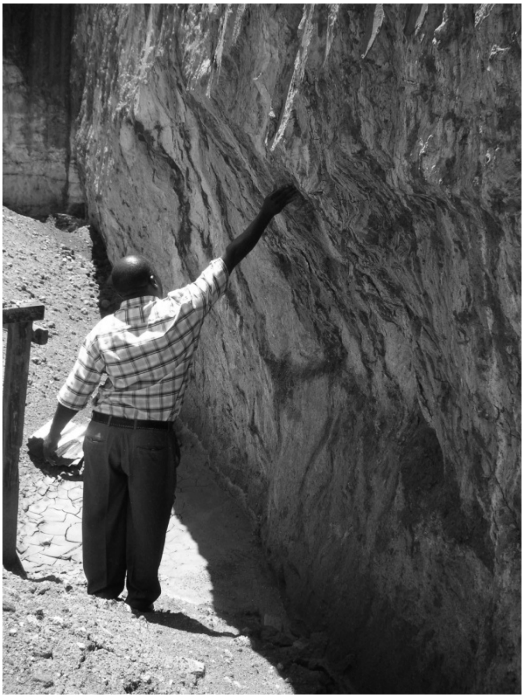

Figure 7. Another excavated section with under scouring at the bottom.

The cut surfaces were neither protected from erosion nor was the soil supported against slope instability, leaving the workers on site and the general public at large vulnerable to the impending tragedy.

3.2. Probable cause of failure

With no shoring system put in place, it was impossible for the soil to stand unsupported for long. Therefore, the primary cause of collapse was likely to be due to no shoring provided as well as heavy vehicles plying with in 3 m of the edge of the excavation along Duster Street and those parked near on the road side.

3.3. Situation Analysis

From the information gathered from the private developer, the works were being conducted without the expertise of a geotechnical engineer and that no geotechnical investigations were ever carried out prior to construction. Apparently the developer and contractor opted for the cheapest option of rapid excavation, with no support, and then raising the basement immediately. However, with no geotechnical assistance, they could not recognise that this was unattainable.

The action of excavating further into the earth at the toe of the cut further undermined the stability of the slope due to the loss of toe support.

Through guided site visits critical observations were made. There was evidence that storm water from the neighbouring properties (on the northern side) was getting into the site. On the eastern side of the site (opposite site from where the accident occurred), a one storied structure was only 1 m from the edge of the unsupported vertical cut (Figure 8). Significant signs of distress involving continuous structural cracks were noticed both in the interior and outside of the walls close to the excavated slope. In addition, there were floor cracks in the interior, and examination of the ground floor revealed that the gable wall moved slightly laterally. A section of the old strip foundation was partly hanging and supported by props of dry eucalyptus (Figure 9). This structure was soon condemned after the accident.

Of course, while some buildings have been constructed in the city following the building set of laws, unfortunately the regulations were not enforced on this particular project due to a number of reasons. The possible ones include graft, inspector malfeasance, or a lack of enforcement resources. It is probably that the developer and contractor ignored the regulations requiring them to secure the cuts safely in order to save money. In this case though, collapse and fatality was a prime example of what occurs when some contractors ignore or subvert the shoring requirements contained in the building regulations.

Due to the size, depth and scale of excavation, the restricted working area, the steep cut slopes and the consequences to life and property in case of failure of the excavated faces, it was essential to protect the cut surfaces from erosion as well so as to keep the sides of the deep excavation stable. The protection would also ensure that movements in the surrounding soil did not cause damage to any neighbouring structures.

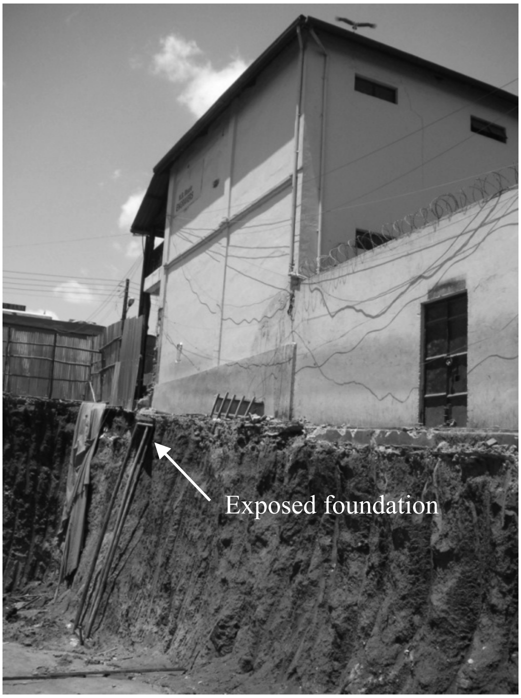

Figure 8. One storied structure on the edge of the cutting.

Figure 9. Closer shot of exposed foundation due to excavation in adjacent plot.

4. NASSER ROAD

At around 3:00 pm March 13th, 2009 two people were killed and twenty one injured when an accident occurred close to another foundation excavation site for a proposed Commercial Building on Plot 5B Nasser Road, Kampala. The tragedy arising from the collapse of a cut slope severely damaged Mirembe Shopping Arcade, a 2 storey building on Plot 5A Nasser Road, which plunged down into the excavation bottom. The excavation was being undertaken for a proposed Commercial Building, to be built on the 12.5 m by 30.5 m site. Once completed, it was to have 5 floors above ground and 1 basement floor for parking. At the time of the accident, the excavation had reached 8 m below the ground level with no provision for shoring.

Figure 10. Severely damaged Mirembe Arcade minutes after collapse.

Figure 11. Volunteers in action at the accident site trying to rescue the victims.

4.1. Cause of failure

With the local developer after the development of the entire plot, the contract embarked on excavating up to the boundaries of properties in the bordering plots. This left the shallow foundations of these properties compromised as noticed in Figures 12 and 13. All cut faces were nearly vertical, very close to existing structures and not maintained by any shoring system.

The weight of Mirembe arcade super structure, then sitting on the edge of the unsupported vertical slope, contributed to active earth pressures in the underlying soil which were far beyond the resisting shear stresses in the slope. This should have triggered the material under the foundations to slip further undermining the whole structural integrity of the building. It is also possible that before total collapse, that the soil underneath the foundations of Mirembe Arcade had started being displaced as noted in Figure 13 of the boundary property on the opposite side of the one which collapsed.

Figure 12. Excavation extended to the boundaries of the nearby properties leaving their foundations exposed and in some cases hanging out.

Figure 13. Close shot of the foundations of the adjacent property foundation. Note the undermined sections of the foundations indicated by the arrows.

Figure 14. Neighbouring property whose foundation was undermined was also still under construction.

4.2. Situational analysis

Since the entire site was 100% excavated, there was no room left for the much needed site office. It was evident then that progress of works was not adequately monitored.

The way the project had been run, compounded by a catalogue of geotechnical engineering blunders, showed a lack of a whole range of supervising professionals and a competent contractor. This deprived the project of the much-needed expertise in the day-to-day supervision. In fact according to the information gathered on site the Contractor did not employ registered engineers on site for such complex earth works in contravention of sections 21 and 29 of the Uganda Engineers Registration Act (1969), a requirement that the project Consultants should have addressed.

As is the case of majority of Ugandan projects, the Contractor had the responsibility of designing and implementing temporary works, including excavations. With no shoring system in place, it is implied that the designs were none existent. This omission was definitely to cut project costs.

5. CONCLUSIONS

It is evident from the information of the Kampala past fatal accidents that the stability of deep earth excavations and their adjacent slopes can be affected if the excavations are not properly carried out. In this case, the main factors contributing to the excavation failures were: absence of an adequate drainage system leading to ingress of surface runoff water, inadequate earth supporting system (includes situations where no shoring was used) and loss of toe support. These failures could have been due to inadequate contract specifications of the earth works (which fell under temporary works), or non-compliance with specifications or both.

Digging deep is fraught with challenges: ground stability, water tightness, impact on existing structures near the excavation and safety of workers on site and general public. It is therefore crucial that excavations comply with the latest regulations

Tighter controls with close supervision by local authorities during construction in almost all deep excavations must be enforced

6. REFERENCES

Uganda Engineers Registration Act 1969, *unpublished.*

Ministry of Works and Transport, 2001. Geotechnical Investigation Report for the Proposed NSSF Headquarters Building at Plots 15A, 15B & 17, Lumumba Avenue, Central Materials Laboratory.

NSSF General Conditions of Contract of the Proposed NSSF Headquarters Building at Plots 15A, 15B & 17, Lumumba Avenue.

Relationships of Modified Mercalli Intensity with Return period and Pick Ground Acceleration for Hormozgan Province in Southern part of Iran

Mohammad Kavei
Department of Physics, Hormozgan University, Bandarabbas, Iran

M.K. Ghassem Alaskari
Petroleum University of Technology, Ahwaz, Iran

S.D. Gore
Department of Statistics, Pune University, Pune, India

N.J. Pawar
Department of Geology, Pune University, Pune, India

Mahboobeh Kavei
Department of Physics, Center of Education, Bandarabbas, Iran

Mohsen kavei
Department of Civil Engineer, Center of Education, Bandarabbas, Iran

ABSTRACT: Hormozgan Province (52º 30' - 59º E, 25º –29º N) is located in the Southern part of Iran. Historical earthquakes show this region has had more than 880 events with magnitude 3 to 7 in the period of 1930 – 2007. In this paper a method is developed to produce civil engineer codes for the desired relationships between such ground motion parameters as Modified Mercalli Intensity (MMI) and their average return periods for Bandarabbas Zone, Hajiabad Zone and Minab Zone of Hormozgan province. In addition we have calculated a relationship between return period and MMI and also seven relationships were suggested between MMI and Peak Ground Acceleration (PGA) for Hormozgan province. There is a fairly remarkable agreement between the PGA vs. MMI found in this study and the correlation calculated by others for a few regions.

1. INTRODUCTION

Seismic intensity and ground motion acceleration are two important parameters that describe the degree of ground shaking for earthquakes.

Seismic intensity is based on human response to ground motion, damage observations, and earthquake effects. There are commonly measured using the Modified Mercalli Intensity (MMI) scale, which is expressed as Roman numerals between I and XII (Wood and Newman, 1931;Richter, 1958). A more objective representation of the degree of shaking is given by the ground motion acceleration that is measured using accelerometers and is expressed in cm/s2, gals, or as a percentage of the gravity acceleration. The Peak Ground Acceleration (PGA) is used here as the maximum absolute value of acceleration found for particular strong motion recorded.

Onur et al., (2008) can present the distribution of earthquake shaking probabilities across Canada within a 50-year period. They use a relationship that is suggested by Wald et al., 1999. Their equation is a relationship between Modified Mercalli Intensity (MMI) and Peak Ground Acceleration (PGA). Linkimer (2008) develops relationship between Modified Mercalli Intensity (MMI) scale and the horizontal component of Peak Ground Acceleration (PGA) for Costa Rica region. He uses regression analysis of 108 earthquakes that occurred in that zone between 1983 and 2004. Hormozgan Province is located south of Iran (52º 30' - 59º E, 25º –29º N). This area is taken as a case for the present study, alike to others Iran has many faults and each region has unique seismicity, seismotectonics and geological formations (Nowroozi, 1976, Berberian, et al., 1978). The main goal of this study is to develop a relationship that can be used to estimate seismic intensity rapidly given by instrumental ground motion recordings for the Hormozgan region. Pervious studies have suggested that empirical relationships between ground motion parameters and MMI are specific and therefore they should be carefully calculated for a particular region (Murphy and O'Brien, 1977; Kaka and Atkinson, 2004, Fielding et al, 2005, Faenza et al. 2007). Other contributions to this subject have been presented by Newman (1954), Gupta (1980), Schenk et al. (1990), Atkinson and Boore (1995), Atkinson and Sonley (2000), Atkinson (2001), Boatwright et al. (2001), Wu et al. (2003) and Kavei et al., (2007). One evident application of the MMI vs. PGA correlation is to obtain MMI information from available PGA data. This study can be the first step in Hormozgan Province for the development of shaking intensity maps like those created in California, a few minutes after the occurrence of felt earthquakes. These maps are created using empirical relationships between ground motion parameters in MMI and give a rapid representation of potentially damaged regions that can be used for emergency response and public information through the media (Wald et al., 1999b).

2. DESCRIPTION OF THE DATA

Since 1973, Building and Housing Research Center (BHRC, 2005) has installed accelerometers in different cities and villages throughout Iran. Figure 1 shows accelerometer stations in Hormozgan province. The data of Peak ground acceleration are available in Building and Housing Research Center, Tehran, Iran (BHRC, 2005). These events occurred for period of 1973 to 2007. Each record has: Name of station; Longitude and Latitude of station; Date of earthquake; Longitude and Latitude of epicenter; Distance between epicenter and nearest station; Body wave magnitude; longitudinal component of PGA; and Soil type (IIEES, 2003 and IRSC, 2007). Figure 2 shows distribution of body wave magnitude and distribution of earthquake in order to find distance between epicenter and nearest station. Figure 3 shows distribution of PGA values for soil types. Figure 4 shows distribution of soil types (hard rock, soft rock, soil and soft soil).

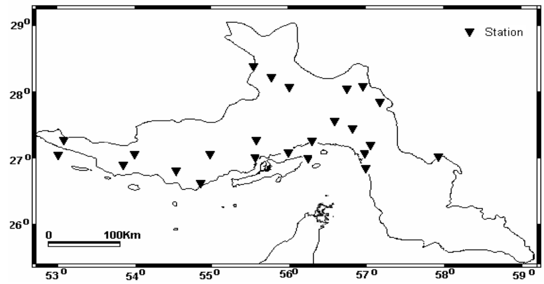

Figure 1: Location of stations (accelerometers).

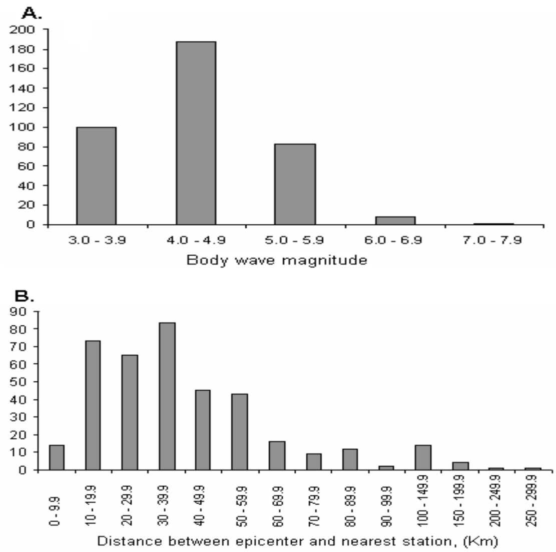

Figure 2: A) Distribution of body wave magnitude.
B) Distribution of earthquake in order to distance between epicenter and nearest station.

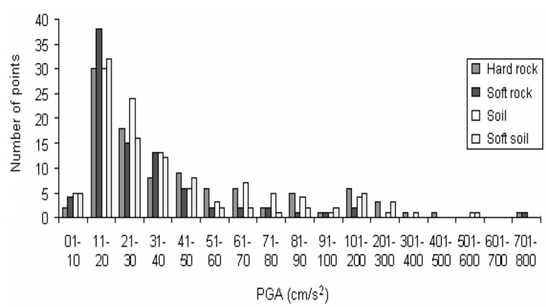

Figure 3: Distribution of PGA values for soil types.

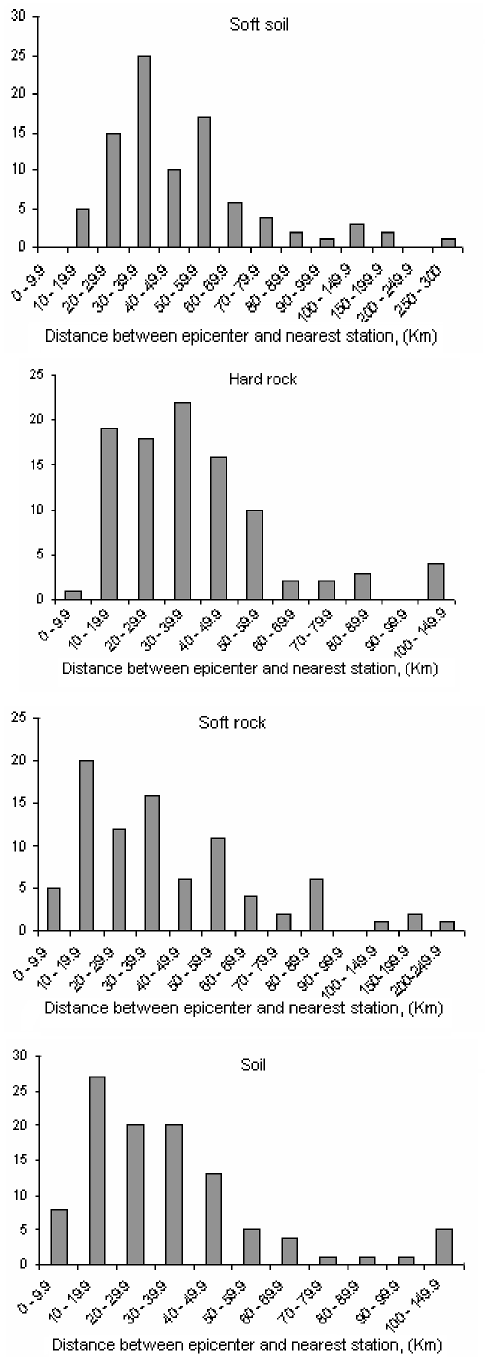

Figure 4: Distribution of soil types (hard rock, soft rock, soil and soft soil).

3. METHODOLOGY AND RESULTS

There are various faults in the province of Hormozgan. All the major faults in this province are shown in Figure 5. This province has had more than 880 earthquakes from 1930 to 2007. Figure 6 shows all earthquakes in this province and also the frequency of events in some regions as well as three seismic zones with high frequency. These regions are: Bandarabbas Zone (BZ), Hajiabad Zone (HZ) and Minab Zone (MZ), (Kavei et al, 2008). In this article we have established a relationship between Modified Mercalli Intensity and return period of earthquake for three zones of Hormozgan Province (Kavei, 2009) using historical earthquakes of Hormozgan province, depth and the distance between hypocenter and station for each earthquake, length of each fault, average number of earthquakes in excess of magnitude 3 per year per unit length of fault and b-Value for each zone. The above-mentioned method has been applied to calculate the following typical values of the parameters and site constants which are applicable to three particular zones in Hormozgan province:

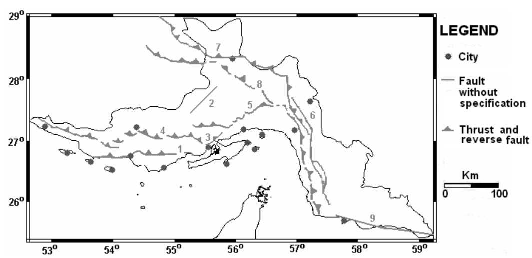

Figure 5: Major faults of Hormozgan province (1: Charak, 2: Moran basement, 3: Khamir basement, 4: Zagros mountain front, 5: Khurgu basement, 6: Zendan-Minab, 7: Main Zagros Reveres, 8: High Zagros Reverse, 9: Makran (after Kavei et al, 2008).

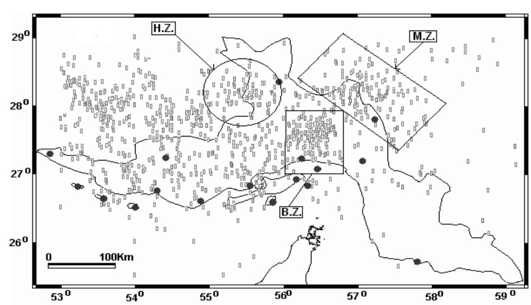

Figure 6: Earthquake epicenters with magnitude 3 -7, Bandarabbas zone (B.Z.), Hajiabad zone (H.Z.) and Minab zone (M.Z.), Rectangles denotes the location of earthquake epicenters and circles denote the location of cities.

3.1. Bandarabbas zone

Bandarabbas Zone is located in the center of Hormozgan province (Figure 7), southern part of Iran (27º - 28º N, 56º - 57º E). In this region, over n = 186 earthquakes have been recorded between 1949 and 2007. The locations of these events related to some active faults and seismically active tectonic zones in this region. The major fault system in this area is Khurgu fault (fault number 5 in Figure 7). The b-value for Bandarabbas Zone is 1.22 (kavei et al. 2008).

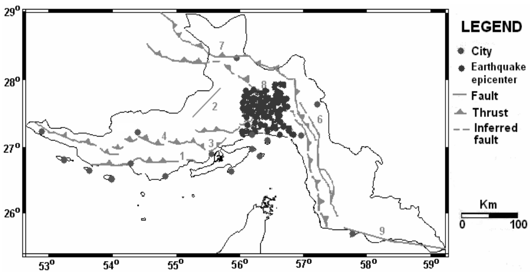

Figure 7: Earthquake epicenters (1949–2007) in Bandarabbas Zone, Southern part of Iran.

The intensity at this site with return period T (kavei, 2009) is Equation 1:

$$MMI = 0.42Ln(549.4T) \quad (1)$$

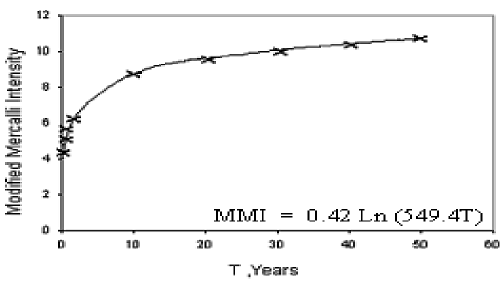

Figure 8: Intensity versus return period for Bandarabbas city, Center of Hormozgan province, Southern part of Iran.

3.2. Hajiabad zone

Hajiabad zone is located in the north of Hormozgan province (Figure 9), southern part of Iran (27.85º - 28.70º N, 54.6º - 56º E).

In this region, over n = 86 earthquakes have been recorded between 1936 and 2007. The locations of these events related to some active faults and seismically active tectonic zones in this region. The famous faults in this area are High Zagros Reverse fault (HZF) in the north, Main Zagros Reveres (MZRF) in the center (fault number 7) and Moran basement fault (fault number 8) in the southeast (Figure 9). This region of Iran is very active and was the seat of many destructive and major earthquakes in the past. The major fault system in this area is Main Zagros Reverse fault (fault number 7 in Figure 9). The b-value for Hajiabad Zone is 0.92 (kavei et al. 2008).

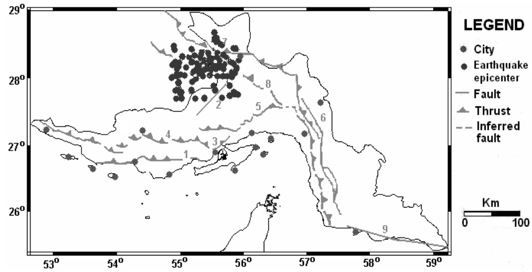

Figure 9: Earthquake epicenters (1936–2007) in Hajiabad Zone, Southern part of Iran.

The intensity at this site with return period T (kavei, 2009) is Equation 2:

$$MMI = 0.56Ln(484T) \quad (2)$$

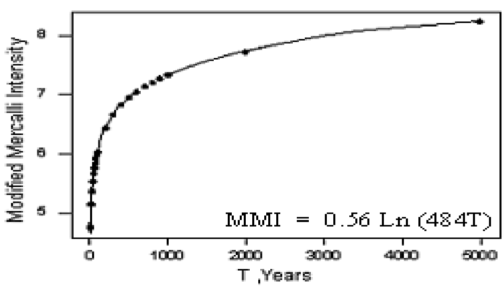

Figure 10: Intensity versus return period for Hajiab city, Southern part of Iran.

3.3. Minab zone

Minab zone is located in the northeast of Hormozgan province (Figure 11), southern part of Iran (27.35º - 29º N, 56.25º - 58.1º E). In this region, over n=190 earthquakes have been recorded between 1933 and 2007. The locations of these events related to some active faults and seismically active tectonic zones in this region. This region of Iran is very active and was the seat of many destructive and major earthquakes in the past. The famous faults of this region are Zendan (Minab) fault (fault number 6) and Main Zagros Reverse fault (fault number 7) in Figure 11. The b-value for Minab Zone is 0.93 (kavei et al. 2008).

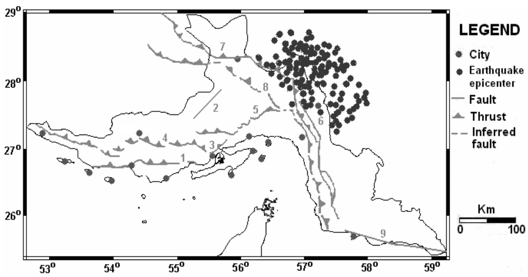

Figure 11. Earthquake epicenters (1933–2007) in Minab Zone, Southern part of Iran.

The intensity at this site with return period T (kavei, 2009) is Equation 3:

$$MMI = 0.55Ln(121.78T) \tag{3}$$

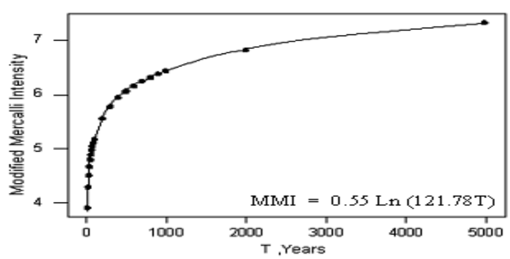

Figure 12: Intensity versus return period for Minab city, Southern part of Iran.

4. RELATIONSHIPS BETWEEN MMI AND PGA

Seismic intensity and ground motion acceleration describe the degree of seismotectonic activities for each zone.

Seismic intensity is based on earthquake effects. Peak Ground Acceleration (PGA) is used here as the maximum value of acceleration found for particular strong motion record. Data is used in this section are 382 PGA.

For each longitudinal component of PGA (PGAL), a single MMI value is assigned based on Kavei (2009) and the geographic proximity of the station. First linear regression between MMI and log (PGAL) for each soil type is estimated. Equations 4 to 10 show relationships between MMI and PGAL (longitudinal component) for four soil types in Hormozgan Province.

$$\begin{aligned}&MMI = 3.141\log(PGA_L),\\&R^2 = 0.696 \text{, for Hard rock,}\\&\text{II} \le \text{MMI} \le \text{V, No} = 67\end{aligned} \tag{4}$$

$$\begin{aligned}&MMI = 3.1\log(PGA_L) - 0.054,\\&R^2 = 0.779 \text{, for all data,}\\&\text{II} \le \text{MMI} \le \text{VII, No} = 382\end{aligned} \tag{5}$$

$$\begin{aligned}&MMI = 3.06\log(PGA_L),\\&R^2 = 0.835 \text{, for Soft rock,}\\&\text{II} \le \text{MMI} \le \text{VII, No} = 87\end{aligned} \tag{6}$$

$$\begin{aligned}&MMI = 2.81\log(PGA_L) + 0.375\\&R^2 = 0.792 \text{, for Hard rock,}\\&\text{II} \le \text{MMI} \le \text{VII, No} = 99\end{aligned} \tag{7}$$

$$\begin{aligned}&MMI = 3.06\log(PGA_L),\\&R^2 = 0.738 \text{, for Soil,}\\&\text{II} \le \text{MMI} \le \text{VII, No} = 105\end{aligned} \tag{8}$$

$$\begin{aligned}&MMI = 3.87\log(PGA_L) - 0.987\\&R^2 = 0.826 \text{, for Soft Soil,}\\&\text{II} \le \text{MMI} \le \text{VII, No} = 91\end{aligned} \tag{9}$$

$$\begin{aligned}&MMI = 4.22\log(PGA_L) - 1.55\\&R^2 = 0.814 \text{, for Soft soil,}\\&\text{II} \le \text{MMI} \le \text{V, No} = 64\end{aligned} \tag{10}$$

Here are showed various correlations that have been published by others for particular regions:

Gutenberg, Richter (1942;1956) and Richter(1958) show :

MMI =3.0 log (PGAave) +1.5 for Western USA.

Hershberger (1956) show: MMI =2.33 log (PGAave) +2.11 for Western USA.

Trifunac & Brady (1975) show:

MMI =3.33 log (PGAave) – 0.47 (IV<MMI<X for Western USA.

Murphy & O'Brien (1977) show:

MMI =2.86log (PGAave) – 1.24 (IV<MMI<X for
Western USA, Japan, and Southern Europe.

Murphy & O'Brien (1977) show:

MMI = 4.0 log (PGAmax) – 1 (IV<MMI <VIII) for Western USA, Japn, and Sothern Europe.

Sauter & Shah (1978) show:

MMI = 3.62 log (PGAave) – 0.9 for Unspecified region. Wald et al., (1999a) show:

MMI + 2.2 log (PGAmax) + 1 (MMI<1) and

MMI = 3.66 log (PGAmax) – 1.66 (V<MMI<VIII) for California.

Linkimer (2008) shows:

MMI=2.33log (PGAmax) + 0.92 (II<MMI<V),

MMI=3.82log (PGAmax) - 1.78 (V<MMI<VII),

MMI=2.33log (PGAmax) + 0.76 (II<MMI<V), and

MMI=4.60log (PGAmax) - 3.38 (V<MMI<VII)

for Costa Rica. Figure 13 shows distribution of Modified Mercalli Intensity and Figure 14 shows distribution PGA and MMI.

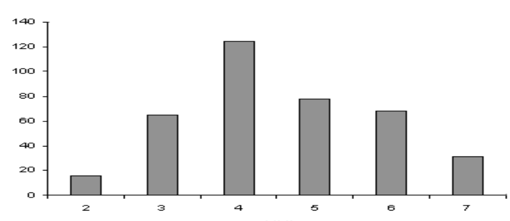

Figure 13: Distribution of Modified Mercalli Intensity.

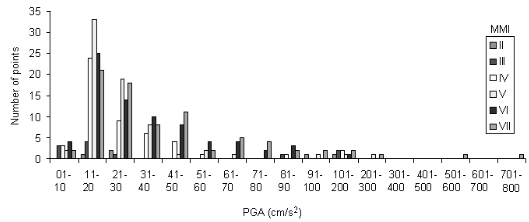

Figure 14: Distribution PGA and MMI.

5. CONCLUSIONS

First of all, this study introduces a method for the evaluation of the seismic risk at Hormozgan Province where this region is one of the most seismicity region in the world.

Return period of earthquakes shows activities of seismicity in this region. These activities are modifier of seismotectonics of the region. Frequency of earthquakes demonstrate the regional seismotectonic activity in about from 52.5° to 59° for East longitudes and 25° to 29° for North latitudes. The results are in terms of Modified Mercalli Intensity and return period. This study proposed two relationships between Modified Mercalli Intensity and return period for Bandarabbas city, Hajiabad city and Minab city. Using these relationships one can estimate return period for definite earthquakes. Besides, the first relationship between MMI and the longitudinal component of PGA (PGAL) is developed for four soil types using regression analysis of 370 earthquakes that took place between years 1973 and 2007. It is clear that the tendency of PGA increase as MMI increases. Best fit lines showing this tendency are calculated between MMI and PGA for four soil types. As we showed in this analysis, the conclusions appear in an easily applied, easily interpreted form, suitable for review for reliability and sensitivity to assumptions. So these methods can be used for other Province in Iran.

6. REFERENCES

Atkinson, G.M. & Boore, D.M. 1995. Ground motion relations for Eastern North America, Bulletin of the Seismological Society of America, 85(1), 17-30.

Atkinson, G.M. 2001. Linking historical intensity oboobservations with groud-motion relations for eastern North America. Seismol. Res. Let. 72 (5): 560-574.

Atkinson, G.M. & Sonley E, 2004. Empirical

relationships between Modified Mercalli Intensity and response spectra, Bulletin of the Seismological Society of America, 90: 537-544.
Berberian, M. , & Papastamatiou, D. & Qoraishi, M. 1978. Khurgu (North Bandarabbas, Iran) earthquake of March 21, 1977: A preliminary field report and a seismotectonic discussion, Bulletin of the Seismological Society of America, 68(2), 411-428.
BHRS (Building and Housing Research Center, .http://www.bhrc.ac.ir), 2005. Iranian Code of Practice for Seismic Resistance Design of Buildings, Standard No. 2800, Third Edition.
Boatwright, J. & Thywissen, K. & Seekins, L. 2001. Correlation of ground motion and intensity for the 17 January 1994 Northridge, California earthquake. Bulletin of the Seismological Society of America, 91: 739-752.
Faenza, L. & Hainzl, F. Scherbaum & Beauval C. 2007. Statistical analysis of time-dependent earthquake occurrence and its impact on hazard in the low seismicity region Lower Rhine Embayment. Geophys. J. Int. 171, 797-806.
Fielding, E. J. & Talebian, M. & Rosen, Nazari, P.A. H. Jackson, J.A. & Ghorashi, M. & Walker, R. 2005. Surface ruptures and building damage of the 2003 Bam, Iran, earthquake mapped by satellite synthetic aperture radar interferometric correlation. Journal Geophysics Research, 110, B03302, doi: 10.1029/2004JB003299.
Gupta, I., 1980. A note on the correlation of Modified Mercalli Intensity with peaks of far-field ground motion, Bull. Seismol. Soc. Amer. 70: 925-932.
Gutenberg, B. & Richter, C.F., 1956. Frequency of Earthquakes in California. Bull. Seism. Soc. Am., 34: 185-188.
Hershberger, J., 1956. A comparison of earthquake accelerations with intensity ratings,Bull. Seismol. Soc. Amer. 46: 317-320.
IIEES, 2003. International Institute of Engineering and Seismology, Tehran, Iran, http://www.iiees.ac.ir
IRSC, 2007, Iranian Seismological Center, Institute of Geophysics, University of Tehran, Iran, http://www.irsc.ut.ac.ir
Kavei, M., & Gore, S.D. & Pawar, N.J. 2007. Seismotectonic and calculation the return period in Hormozgan province, Southern Iran, Ecol. Env. & Cons., 13(1): 35-38.
Kavei, M., S.D. Gore, & Pawar N.J. & Sukhtankar, R.K. 2008. Establishing a relationship between the frequency and magnitude of earthquakes for some parts of Hormozgan province, Southern Iran, Acta Ciencia Indica, Vol. XXXIV P, No. 1, 35-50.
Kavei, M., 2009. Ph.D. thesis, entitled: “Investigations on seismotectonics in some parts of Hormozgan province, Southern Iran”.
Linkimer, L. 2008. Relationship between peak ground acceleration and Modified Mercalli Intensity in Costa Rica, Revista Geológica de América Central, 38: 81-94.
Murphy J.R. & O’Brien, L.J. 1977. The correlation of peak ground acceleration amplitude with seismic intensity and other physical parameters, Bull. Seismol. Soc. Amer. 67: 877-915.
Newmark, N.M. 1967. Design Criteria for Nuclear Reactors Subjected to Earthquake Hazards, Urbana, III.
Onur, T. & Seemann, M., & Halchuk, S. and J. Adams 2008, Probabilities of significant earthquake shaking in communities across Canada, The 14th World Conference on Earthquake Engineering October 12-17, 2008. Beijing, China.
Nowroozi, A. A. 1976. Seismotectonic provinces of Iran, Bulletin of the Seismological Society of America, Vol. 66, No. 4, 1249-1276.
Richter, C. F. (1958). Seismic regionalization, Bull. Seism. Soc. Am. 49, 123-162.
Sauter, F. & Shah, H.C., 1978. Estudio de seguro contra terremoto, 250 pags, Franz Sautery Asociados Ltda, San Jose, Costa Rica.
Schenk, V., & Mantlík, F., & Zhizhin, M.N. & Tumarkin, A.G. 1990. Relationship between macroseismic intensity and instrumental parameters of strong motion- a statistical approach. – Natural Hazards, 3: 111-124.
Trifunac, M.D. & Brady, A.G., 1975. on the correlation of seismic intensity scale with the peaks of recorded strong ground motion, Bull. Seismol. Soc. Amer. 65: 139-162.
Wald D. J., & Quitoriano, V. T. & Heaton, H., & Kanamori, H., 1999a. Relationships between peak ground acceleration, peak ground velocity and modified Mercalli intensity in California, Earthquake Spectra, Vol. 15, No. 3, 557-564.
Wald, D.J., & Quintoriano, V. & Heaton, T.H. & H. Kanamori., & Scrivner, C.W. & Worden, C.B. 1999b. TriNet “ShakeMaps”: Rapid generation of peak ground motion and intensity maps for earthquake in Southern California. Earthquake Spectra, 15: 537-555.
Wood, H.O. & Newman, F. 1931. Modified Mercalli intensity of 1931, Bull. Seismol. Soc. Amer. 21:277-283.
Wu, Y., T. Teng, T. Shin, and N. Hsiao 2003. Relationship between peak ground acceleration, peak ground velocity, and intensity in Taiwan. Bulletin of the Seismological Society of America, 93:386-396

Two dimensional surface topography considering in earthquake hazard zonation

H. Khodadadi Tirkolaei, MSc of Geotechnical Engineering
Arak Branch, Islamic Azad University, IRAN

M. Jiryaei Sharahi, Assistance Professor
Arak Branch, Islamic Azad University, IRAN

ABSTRACT: In order to mitigate the risk from earthquakes and to ensure the safety of structures under earthquake loading, dynamic effects should be taken into consideration in design codes. This problem are often considered using zoning maps based on geological assessments of seismic hazards and little attention has been paid to the geotechnical assessments such as amplification. Nonlinearity and non-homogeneity are two effective factors on amplification effects. In this study we focused on the surface topography effects, as a type of the non-homogeneity. Hence, a topographic site under earthquake and by using FE computer code has parametrically been analyzes. The surface topographic site analysis under real ground motion has not been performed yet.

1. INTRODUCTION

One aspect of safety against earthquake hazards is softly of a site itself related with geotechnical phenomena such as amplification. In order to mitigate the risk from earthquakes and to ensure the safety of structures under earthquake loading, dynamic effects have been taken in to consideration in design codes with different accuracy, often using zoning maps based on geological assessments of seismic hazard which are embodied in building codes or regulations.

However, little attention has been paid to the assessment of geotechnical phenomena such as amplification in the form of regulations on land use. Generally, there are three grades of seismic zonation that describe quality level of geological and geotechnical investigations.

Grade-1 or general zonation is the first level of zonation based on compilation and interpretation of existing information available from historic documents, published reports and other available data bases. This is the crudest approach and doesn't give a good estimation of hazards distributions.

Grade-2 or detailed zonation is the improved quality of the grade-1 zonation map by making use of additional sources of data, for example aerial photographs, older photographs, additional field studies, geotechnical engineering reports from governmental or local or prefectural agencies and private companies, additional field and laboratory test data. Micro tremor measurements can also be utilized to obtain more detailed information. This approach permits a substantial upgrading of the zonation maps.

Grade-3 or rigorous zonation is applied where a very high and very detailed level of zonation is required our purpose in this level is most accurate result obtaining;

Hence, it is necessary to use computer modeling of ground response to achieve zoning to grade-3.

The first and most widely used analytical method for site response in grade-3 zonation is to make use of the multiple reflection models for the propagation of s-waves in a one- dimensional column (e.g.Haskell, 1953). In this method the soil column is modeled as series motions that are considered representative of those likely to occur in the region of interest. Finally, in the zonation mapping of an area, amplification factors are determined for each element in the mesh, typically around 1*1 Km in size. The other one of the major issues in evaluating site effects for rigorous zonation is nonlinearity of site response. Evidence of nonlinear behavior has been detected in observed earthquake ground motion records (e.g.Tokimatsu & Miderikawa, 1982), (Change et al., 1991), SHAKE (Schnabel et at., 1972), a computer code based on equivalent linear analysis, is widely utilized for computing nonlinear site response. The equivalent linear method doesn’t give a satisfactory approximation for short period high amplitude motion on thick soil deposits.

The next less attended method to Grade-3 seismic zoning is to take into account the non-homogeneous nature of natural ground, such as surface topography effect on seismic response of site, by two- or three- dimension analysis. The different numerical methods, such as the finite element method, the finite difference method, the boundary element method, the finite difference method, the boundary element method and the hybrid method, have been developed to analysis. Because the complex nature of the seismic wave scattering by non-homogeneous structures can only be solved by numerical method, accurately and economically.

In this study we focus on the surface topography effects, as a type of the non-homogeneity. Despite of the documented observation of destruction distribution. After seismic events that suggest to topography effects on site response (Boore, 1972; Brambati et al., 1980; Siro, 1982; Levert et al., 1986; Celebi, 1987; Kawase &Aki, 1990 & Restrepo &cowan, 2000) there is very few consideration of this effect to seismic zoning and attempts have seldom been made to formalize a standard approach in terms of regulations or code requirements. (At present, the Eurocode8 and AFPS 90 are only two codes that considered this issue). This problem is for lake of the enough powerful special computer instruments. The existing usual tools are only able to model topographic asperities in form of the isolated ridges or depressions on the surface of homogeneous and linearly elastic half spaces. Furthermore, seismic input is usually modeled as monochromatic or narrow-band waves that cannot describe the broad-band of true earthquake motion. Indeed, there exist very few – if any – well documented case studies where topography effects are illustrated for strong ground motion.

In this study, we investigated the topographic site response under real ground motion by using a FE computer code (Plaxis 2D v.8.2). This computer code has not been applied for these problems yet, and we used it for first time (Davoodi & Akbari, 2007; Sigaran-Loria & Hack, 2007; & Visone et al, 2008; use Plaxis for site effect analysis but not under earthquake). Although, the finite element method has a restriction in finite dynamic modeling for infinite media, but this problem has been solve land spurious reflections from the artificial boundaries can be partly eliminated by viscose boundary technique used in this program. The finite element method is a powerful numerical technique for detailed description of site topography and layering and with this method. it is possible to calculate the response of two-dimensional configuration for nonlinear stress-strain material behavior.

However, the boundary element methods have been more extensive used for unbounded medium but this is not powerful to solve problems with in homogeneities and nonlinearity. The hybrid type techniques, which combine the effective characteristic of two or more methods, have been proven but they also have difficulties in implementation and programming.

In this paper, 2D parametric study on trapezoidal shaped valley under Manjil earthquake (Iran, 1990). Is performed and the topography effects on site response are diagramed.

2. NUMERICAL MODELING

2.1. Verification of Program

There are very few documents which used Plaxis for site effects analyses (Davoodi and akbari, 2007; Sigaran-Loria and Hack, 2007; Visone et al, 2008). In three following sections, the verification of the program is shown. These schemes were chosen because the solutions of the problems are available in literature and some comparisons can be easily done.

2.1.1. Free Field Motion of Half-Plane Subjected to Incident SV Wave of Ricker Type

We analyzed the site response of a linear elastic, homogeneous half-plane, which is considered as a layered system, subjected to vertical propagating incident SV wave of the Ricker type:

$$F(t) = A_{max}\,[1-2(\pi\, f_p\,(t-t_0))^2]\; e^{-(\pi\, fp(t-t0))^{\wedge}2} \qquad (1)$$

f_p, t_0 and A_{max} denote the predominant frequency, the time shift parameter of time history and maximum amplitude of the time history which are chosen to be 2.5 HZ, 0.4 sec and 0.001m, respectively.

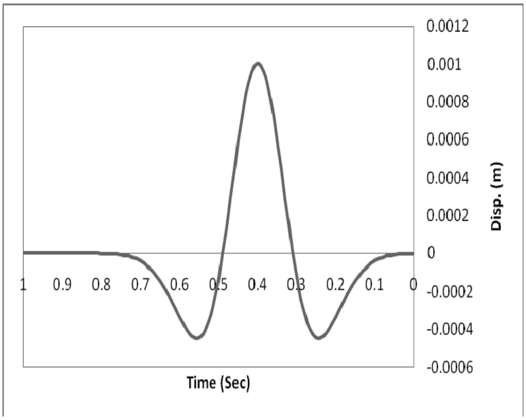

Fig.1. Displacement time history of the incident wave of Ricker type used in analysis.

The finite element model and material properties of the layer are plotted in Fig. 2 and Table 1, respectively.

The geometry model is constituted by a rectangular domain 1000m wide and 70 m height. In order to detract the influence of excess scattered waves from boundaries to medium the lateral boundaries placed far enough (even though no clear indications exist in literature on this aspect), as well as, the absorbent boundaries are employed.

The initial stress generation is obtained by the k_0-procedure in which the value of the earth pressure at rest, k_0 is chosen by means of the well-known formula for the elastic medium:

$$K_0 = \nu / (1-\nu) = 0.389 \qquad (2)$$

For accurate representation of wave transmitted in the model, the element sizes should be selected small enough to satisfy the following criteria expressed by Kuhlemeyer and Lysmer (1973):

$$L_e \leq \lambda/8 \qquad (3)$$

Where λ is the wave length associated with the highest frequency component that contains appreciable energy and L_e is the length of element.

In this case, the average element size (AES) has been selected about 10m, though it could be selected greater value.

The 15-node triangular elements are employed.

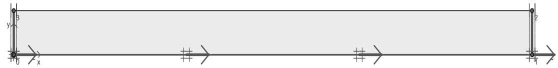

Fig. 2. The model utilized in FE dynamic analysis.

Table 1. Material Properties of the Layer

Material Model	Linear Elastic
γ (KN/m^3)	15.5
E (KN/m^2)	5.31×10^5
ν	0.28
V_s (m/s)	362.1

Figure 3 shows the horizontal and vertical displacement time histories calculated at the ground surface. As expected, there exists good agreement between obtained results and analytical solution. The Total horizontal displacement is equal to twice the incident motion and the total vertical displacements are equal to zero.

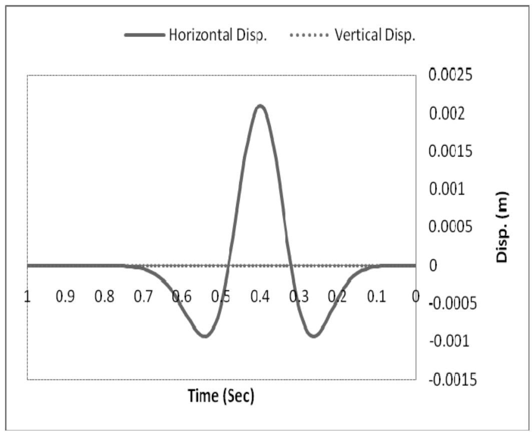

Fig. 3. Horizontal and vertical displacement time histories at surface of the half-plane

2.1.2. Free field motion of half-plane subjected to earthquake.

Here, the model with the similar material and geometry to illustrated model in previous section (as plotted in Fig. 2 and Table 1) is subjected to real ground motion. Also, the AES has been selected about 5m.

The imposed earthquake was registered at AB-Bar station (Manjil earthquake, IRAN, 1990). The sampling frequency, duration and peak acceleration are 200HZ, 53 sec and 5.82m/s^2, respectively. The baseline corrected and filtered signals are used for input motion.

The result explained in frequency domain (see Fig.4). The predominant frequency is very close to the expected theoretical value (Rosset, 1970):

$$A.F = 1/\sqrt{(\cos^2((2\pi.\ H/V_s).\ f_n) + ((2\pi.\ H.\ D/V_s).f_n))} \quad (4)$$

Where,
A.F: the amplification function;
H: layer thickness;
V_s: shear wave velocity;
D: material damping (Here, D=5%) and
f_n: nth natural frequency of the layer = V_s /4H (2n-1).

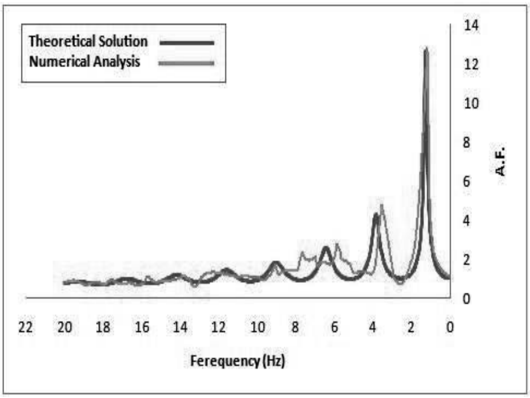

Fig. 4. Earthquake seismic response of free space in frequency domain.

2.1.3. semi-circular non-alluvial valley subjected to incident SV wave of Ricker type.

Figure 5 shows a semi-circular non-alluvial valley subjected to vertically propagating SV wave of the Ricker type. This problem was studied by Dravinski and Mossessian (1987).

The material properties and inputted motion are similar to what that explained in former section (as plotted in Fig. 1 and Table 1).

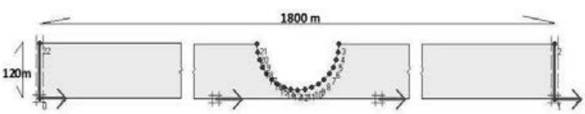

Fig. 5. The FE model of semi-circular valley (Width=1800m, Height=120m, Radius of Valley=100m)

Figure 6 compares the numerical result with those obtained by Dravinski and Mossessian (1987). The acceptable agreement exists, too.

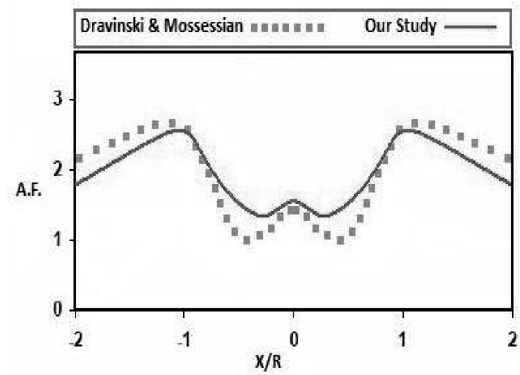

Fig. 6. Comparison between amplification of surface Horizontal displacement, obtained by FE analysis and Dravinski and Mossessian (1987)

2.2. Topographic site under earthquake

Very few numerical studies exist that investigated site effects, especially topography effects, under the real strong ground motion (Sigaran-Loria and Hack, 2007; Visone et al, 2008).

With reference to mentioned in foregoing, it can be concluded that Plaxis v.8.2 is acceptable computer program for dynamic analyses of irregular site under the earthquake.

In this section, in order to evaluation of topography effects and its shapes on seismic response of site, numerical parametric analyses on trapezoidal shaped valley (non-alluvial) under Manjil earthquake (Iran, 1990) have been done (by using Plaxis v.8.2). Geometrical parameters, 2D FE model, material properties and geometrical ratios have been shown in Fig. 7, Fig. 8, Table 2 and Table 3, respectively.

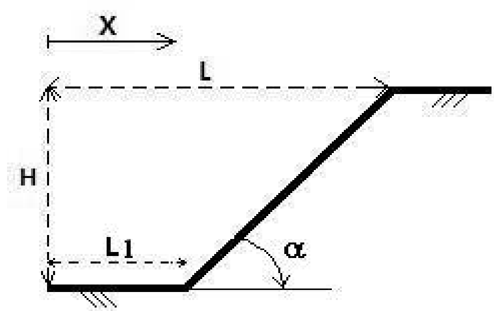

Fig. 7. Geometrical parameters of studied model

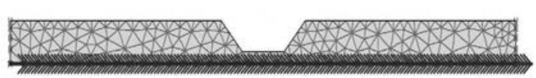

Fig. 8. 2D FE model used in dynamic analysis

As observed in Fig. 8, the model dimension no indicated, since the model dimensions vary by valley size and there is not any specific ratio between them. The model dimensions are obtained after some sensitivity analysis for each valley size.

Table 2. Material Properties of Trapezoidal Valley

Material Model	Linear Elastic
γ (KN/m^3)	27.1
E (KN/m^2)	7×10^6
ν	0.25
V_s (m/s)	1006

The material used here only consist of a dry rock mass and are not took alluvial layers situation into account to investigate geometrical shape effect of valleys, clearly.

Two series of model with different height of valley (H=50m, 100 m) analyzed. Other parameters obtained from following ratios:

Table3. Ratios between Parameters

L1/L	H/L		
	0.2	0.6	1
0	α=11.31°	30.96°	45°
0.25	14.93°	38.66°	53.13°
0.5	21.8°	50.19°	63.43°
0.75	38.66°	67.38°	75.96°

Finally, the results are diagrammed in terms of shape ratio (H/L), dimensionless distance (X/L), ratio of bottom length to crest length (L1/L) and amplification factor (see Fig. 9):

$$A.F. = PGA_x(\text{valley}) / PGA_x(\text{free field}) \qquad (5)$$

Where,
(A.F.): Amplification factor;
PGA_x(valley): Peak ground horizontal acceleration across valley;
PGA_x(free field): Peak ground horizontal acceleration on free field.

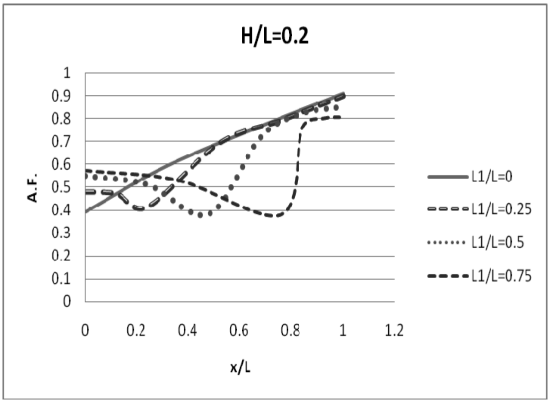

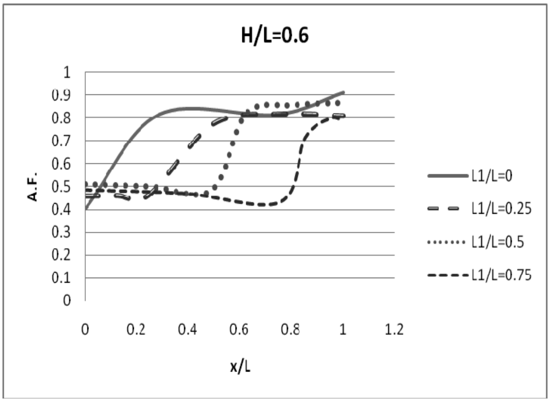

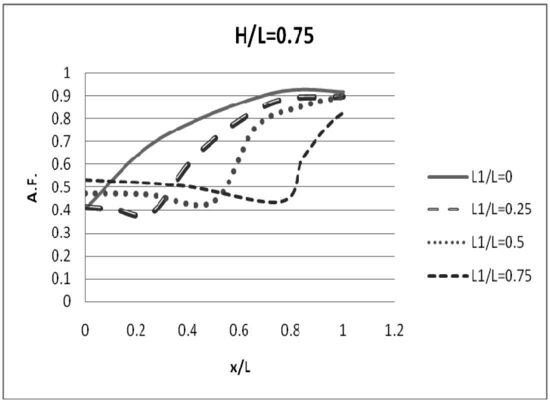

Fig. 9. Results of numerical analysis of trapezoidal valley

3. CONCLUSION

In this paper, a powerful FE program applied to carry out site response analysis of two-dimensional topographic structures subjected to earthquake.

Here, the applicability and efficiency of PLAXIS v.8.2 have been demonstrated through some examples of site response analysis, including half-plan subjected to incident SV wave and earthquake and semi-circular valley subjected to incident SV wave. Then, this program used in performing site response parametric analysis of trapezoidal valley structures. Numerical results show this computer code is very powerful, user friendly and time-saving than other different presented hybrid algorithms, which have particularly been programmed for this problem and unable to consider the real ground motion and nonlinear behavior of material for practical engineering projects.

Numerical analyses of trapezoidal non-alluvium valleys show that slopes of valleys are critical regions during earthquake. The response intensity increasingly varies of minimum amplification value at the toe to maximum amplification value at the crest of slope. Also, shape of valley further influence in seismic response of slopes.

4. REFERENCES

Ambraseys N.N., 1960. *On the Shear Response of a Two Dimensional Wedge Subjected to an Arbitrary Disturbance*, Bul. Seismol., Vol. 50, 45-56

Assimaki D., E. Kausel, G. Gazetas, 2004. *Topography effects in the 1999 Athens earthquake: engineering issues in seismology*, Proc. 11th ICSDEE and 3rd ICEGE, UC Berkeley, January, 7-9, 2, 31-38

Athanasopoulus G.A., P.C. Pelekis, E.A. Leonidou, 1999. *Effects of surface topography on seismic ground response in the Egion (Greece) 15 June 1995 earthquake*", Soil Dynamics and Earthquake Engineering, 18: 135-149

Bouchon M., J.S. Barker, 1996. *Seismic response of a hill: The example of Tarzana, California*, Bul. Seismol., 86(1A): 66-72

Bouckovalas G.D., A.G. Papadimitriou, 2005. *Numerical evaluation of slope topography effects on seismic ground motion*, Soil Dynamics and Earthquake Engineering, 25: 547-558

Brinkgreve R.B.J., 2002, *Plaxis 2D version8,* A.A. Balkema Publisher, Lisse

Celebi M., 1987. *Topographical and geological amplifications determined from strong-motion and aftershocks records of the 3 march 1985 Chile earthquake*, Bul Seismol, 77, 1147-1167

Dravinski M., T.K. Mossessian, 1987. *Scattering of plane harmonic P, SV, and Reyleigh waves by dipping layers of arbitrary shape*, Bull. Seismol. Soc. Am., 77, 212–235

Geli L., P.Y. Bard, B. Jullien, 1988. *The effect of topography on earthquake ground motion: A review and new results*, Bul. Seismol, 78: 42-63

Havenith H.B., D. Jongmans, E. Faccioli, K. Abdrakhmatov, P.Y. Bard, 2002. *Site effect analysis around the seismically induced Ananevo rockslide, Kyrgyzstan*, Bul. Seismol, 92(8): 3190-3209

Idriss I.M., H.B. Seed, 1967. *Response of earthbanks during earthquakes*, J. Soil Mech. Found. Div. ASCE, 93(SM3), 61-82

Idriss I.M., 1968. *Finite element analysis for the seismic response of earth banks*. J. Soil Mech. Found. Div. ASCE, 94(SM3)

Kovacs W.D., et al., 1971. *Studies of seismic response of clay banks*, J. Soil Mech. Found. Div. ASCE, 97(SM2)

Kuhlmeyer R.L, J. Lysmer, 1973. *Finite Element Method Accuracy for Wave Propagation Problems*, J. Soil Mech. & Found. Div., vol.99 n.5, 421-427

Kamalian M., M.K. Jafari, A. Sohrabi-bidar, A. Razmkhah, B. Gatmiri, 2006. *Time-domain two-dimensional site response analysis of non-homogeneous topographic structures by a hybrid BE/FE method*, J. soil dynamic & earthquake Eng., Elsevier, 753-765

Lokmer I., M. Herak, G.F. Panza, F. Vaccari, 2002. *Amplification of strong ground motion in the city of Zagreb, Croatia, estimated by computation of synthetic seismograms*, Soil Dynamics & Earthquake Eng., 22:105-113

Lysmer J., R.L. Kuhlmeyer, 1969. *Finite Dynamic Model for Infinite Media*, ASCE, J. Eng. Mech. Div., 859-877

Paolucci R., 2002. *Amplification of earthquake ground motion by steep topographic irregularitie*s, Earthquake Engineering & Structural Dynamics, 31:1831-1853

Papalou A., J. Bielak, 2004. *Nonlinear seismic response of earth dams with canyon interaction*, J. Geotechnical & Geoenvironmental Eng., ASCE, January: 103-110

Psarropoulos P.N., Y. Tsompanakis, Y. Karabatsos, 2007. *Effects of local site conditions on the seismic response of municipal solid waste landfills*, Soil Dynamics & Earthquake Eng., 27: 553-563

Roesset J.M., 1977. *Soil Amplification of Earthquakes, Numerical Methods in Geotechnical Engineering*, Chapter 19, [Ed. Desai C.S., J.T. Christian], McGraw-Hill, 639-682

Semblat J.F., M. Kham, E. Parara, P.Y. Bard, K. Pitilakis, K. Makra, D. Raptakis, 2005. *Seismic wave amplification: Basin geometry vs soil layering*, Soil Dynamics & Earthquake Eng., 25: 529-538

Sigaran-Loria C., H.R.G.K. Hack, 2007. *Verification of two-dimensional numerical earthquake site effects on a dam site, Costa Rica*, Proc. 11th Congress of the International Society for Rock Mechanics: The Second Half Century of Rock Mechanics. Taylor & Francis/ Balkema, Leiden, 1203-1207

Sincraian M.V., C.S. Oliveira, 2001. *A 2-D sensitivity study of the dynamic behavior of a volcanic hill in the Azores Islands: Comparison with 1-D and 3-D models*, Pure and Applied Geophysics, 158:

2431-2450

Thimus, J.F., P. Delvosal, S. Waltener, C. Schroeder, N. Boukpeti, 2006. *Analysis of seismic wave propagation in soils*, In P. Verona & R. Hart (eds.), FLAC and Numerical Modeling in Geomechanics, Proc. 4th International FLAC Symposium, 29-31: 181-186

Trifunac M.D., 1973. *Scattering of plane SH-waves by a semi-cyliderical canyon*, Earth. Eng. and-struct. Dyn. , 1, 267-281

Visone C., E. Billota, F. Santucci de Magistris, 2008. *Remarks on site response analysis by using Plaxis dynamic module, Plaxis Bulletin*, issue 23, 14-18

White W., S. Valliappan, I.K. Lee, 1977. *Unified boundary for finite dynamic models,* J. Eng. Mech. ASCE, 964-969

Wolf J.P., 1985. *Dynamic soil-structure interaction*, Prentice Hall, Englewood Cliffs, NJ

Zhang L., A. K. Chopra, 1991. *Three-Dimensional Analysis of spatially varying ground motions around a uniform canyon in a homogeneous half-space*, Earth. Eng. and Struc. Dyn., 20

An empirical prediction of maximum horizontal displacements caused by the construction of diaphragm wall panels

D. L'Amante, A. Flora, G. Russo, C. Viggiani
Department of Hydraulic, Geotechnical and Environmental Engineering – University of Napoli Federico II, Napoli, Italy

ABSTRACT: Displacements caused by large urban excavations are often estimated at a preliminary stage by using simple charts and empirical relationships. These charts refer to the effect of the main excavation. In the last years these displacements are getting smaller and smaller because of the improvement in construction practice and technology. As a consequence, the displacements caused by the construction of the retaining structure may become significant, and therefore need to be evaluated. In the paper, available field data were first collected and analysed. Then, a simple formula able to catch the effect of geometrical and mechanical properties on the maximum horizontal displacement in the soil caused by panel construction was proposed and validated by numerical 3D calculations.

1. INTRODUCTION

Deep excavations connected with transportation infrastructures are generally placed in densely urbanized areas; they raise important geotechnical challenges, especially if located in the vicinity of historical or valuable buildings. One of the main design requirements is the prediction of displacements caused in the surrounding soil by the excavation process and of the consequent damages to nearby structures. Several empirical methods to estimate the maximum horizontal displacement δ_{max} of the retaining structure have been proposed (Mana and Clough, 1981; Clough *et al.,* 1989; Fernie and Sucking, 1996; Boone and Westland, 2006). A classical chart for the evaluation of δ_{max} in excavations in soft clays is reported in Fig. 1; values of δ_{max} as large as 1% of the vertical spacing h between props are indicated for stable systems. In the case of stiffer soils, Clough and O'Rourke (1990) have collected a large number of case histories, showing typical values of δ_{max} smaller than 0,5% h (Fig. 2).

Recent observations (L'Amante, 2009) on a number of deep excavations in urban areas seem to indicate that these charts significantly overestimate the expected horizontal displacements; similar conclusions can be drawn for vertical displacements. Such a finding may be justified by a number of factors, as the use of increasingly stiff retaining structures and props, ground anchors, as well as the adoption of ground improvement techniques and more refined excavation procedures (e.g. top down).

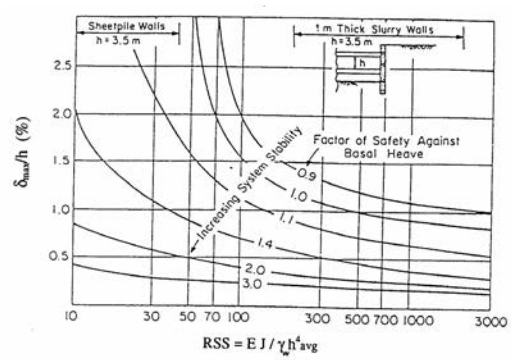

Fig. 1. Normalised maximum horizontal displacement δ_{max} of the wall versus retaining system stiffness (RSS) as a function of the factor of safety against basal heave (Clough *et al.,* 1989).

This progress in construction practice demands for an improvement in the ability to predict displacements caused by excavation, making use of both empirical methods and advanced numerical analyses. To this aim, new experimental data from well documented case histories are needed to upgrade the empirical charts; on the other hand, the numerical analyses have to take into account apparently minor aspects of the construction process, usually neglected, that may significantly concur to the smaller overall displacements.

Recent studies (e.g. Poh and Wong, 2000; Koutsoftas *et al*., 2000) show that the horizontal displacements *s* caused by the construction of the retaining structure (typically, excavation under bentonite slurry followed by placement of the reinforcement cage and concreting) may be of the same order of magnitude of those caused by the main excavation. As a consequence, the computation of displacements at the design stage should include such additional contribution. Furthermore, the construction process of the retaining structure modifies the stress state in the surrounding soil mass and therefore has an influence on the overall construction behaviour.

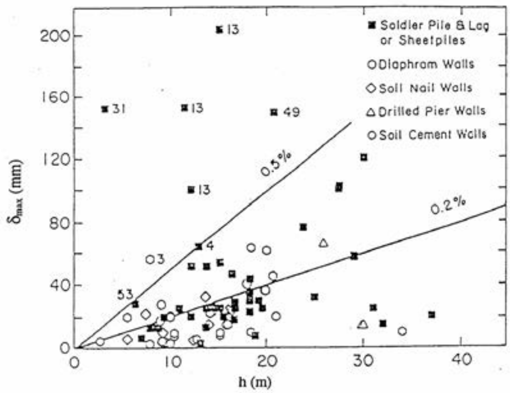

Fig. 2. Maximum horizontal displacement of the wall δ_{max} versus excavation depth h for stiff clays and sands (after Clough & O'Rourke, 1990).

The evaluation of the maximum horizontal displacement s_{max} is therefore an important issue, and there are experimental indications of its dependence on some of the main geometrical properties of the panel (e.g. Poh and Wong 1998, 2001; de Wit et al. 2002; Lachler et al. 2006).

In this paper, some available in situ measurements of soil horizontal movements caused by panels constructions will be considered. A simple way to predict s_{max} will then be proposed, taking into account the more relevant geometrical and mechanical factors.

2. CONSTRUCTION SEQUENCE

The initial in situ horizontal stress in the soil is defined by the coefficient of earth pressure at rest K_0. Significant changes may occur around a panel depending on the construction procedure. The construction is typically carried out in subsequent stages as follows: primary panels are first excavated, supporting the hole with bentonite slurry; the hole is then filled from the bottom by a tremie tube, with wet concrete that pushes up the lighter slurry and hardens in time. The adjacent panels, called secondary panels, are then installed following the same procedure. The stress state around each panel is modified during the process of construction by all these actions. The prediction of the stress changes around the panel is a complex task for the following main reasons: (i) the problem is three-dimensional; (ii) in fine grained soils, the process is mostly undrained. However, these changes may be relevant in determining the true initial conditions to be considered in the analysis of the diaphragm wall during the main excavation stage.

The net final effect of the construction process is generally a displacement towards the panel in overconsolidated soils, and towards the soil in soft normally consolidated deposits.

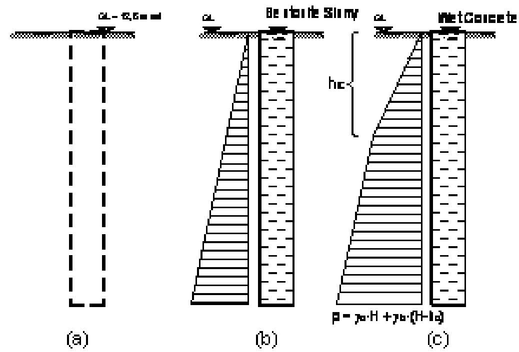

Fig. 3. Schematic horizontal pressure of bentonite slurry (b) and wet concrete (c).

The horizontal stress exerted by the bentonite slurry on the excavation wall is hydrostatic; its intensity is ruled by the unit weight γ_b of the slurry (Fig. 3). The horizontal stress exerted by the fresh concrete is not so straightforward to define. There is a general agreement in considering for it a bilinear distribution. In the top part, down to a critical depth h_c, the gradient is the concrete unit weight γ_c. At depths larger than h_c, the gradient is the bentonite unit weight γ_b. Being γ_c (22÷25 kN/m^3) much larger than γ_b (11÷13 kN/m^3, Filz *et al.*, 2004), the depth h_c controls the overall boundary conditions applied to the surrounding soil and hence plays a relevant role on the horizontal displacement caused by panel construction.

L'Amante (2009) has collected a number of case histories in which the critical depth h_c was either measured or estimated on site (Tab. 1). For a large range of excavation depths H, h_c ranges from 5 to 10 m and is not directly related to H. The ratio h_c/H decreases as the height of the excavation H increases (Fig. 4). In the following, when direct measurements are not available, the horizontal stress at the panel-soil interface will be evaluated assuming h_c=7.5 m, corresponding to the dotted line reported in Fig. 4.

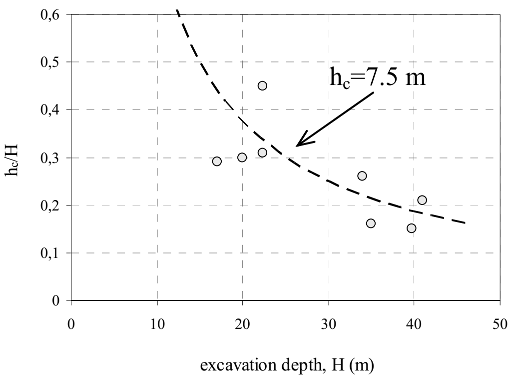

Fig. 4. Values of critical depth hc inferred from observations.

3. A SIMPLE FORMULA

The available experimental evidence is summarized in Tab. 1, and refers to case histories in fine grained soils. The maximum horizontal displacement s_{max} is directed towards the panel in stiff clays, and towards the soil in soft clays. Usually, s_{max} does not take place at ground level. As expected, the value of s_{max} decreases as the distance from the excavated panel increases.

Based on a careful screening of the available experimental data, and considering the relevant geometrical and mechanical variables, a simple formula for a first evaluation of s_{max} may be formulated as follows:

$$\frac{s_{max}}{H} = \alpha \cdot C_g \cdot C_m \qquad (1)$$

where H is the full panel depth, α is a dimensionless parameter, C_g a factor depending on geometrical variables and C_m a factor depending on mechanical variables.

C_g is expressed as:

$$C_g = \chi^{\beta} \cdot \sqrt{\xi} \qquad (2)$$

where χ and ξ are the two angles (in radians) shown in Fig. 5 - along with all the geometrical variables of interest -, expressing respectively the influence of the depth and the width of the panel. By adopting the angles χ and ξ instead of the size of the panel, the effect of the distance at which s_{max} is computed is explicitly taken into account and finite values of s_{max} are obtained even for a distance from the panel d = 0. The depth H shown in Fig. 5 is the panel length if the surrounding soil is homogenous; it is the depth of the softer layer in a layered soil profile.

Table 1. Summary of the collected case histories.

Author	H (m)	h_c (m)	Hole size (m, m^2)	s_{max} (cm) (referred to the whole wall)	Depth of s_{max} (m)	Distance from panel (m)
Gatti and Garassino 1989	22,4	7 ÷ 10	d = 1,0 (pile)	-	-	-
Uriel and Oteo 1977	34	9	Not known	-	-	-
Di Biaggio 1972	20	6	1 x 5	-	-	-
Ling et al. 1994	17	5	0,6 x 8,5	-	-	-
Ng et al. 1999	39,7	6	0,8 x 2,8	-	-	-
Lachler et al. 2006	41	8,5	1,2 x 7,5	-1,3 ÷ -2,6	8	1.9 ÷ 3,8
de Wit et al. 2002	37	6	0,8 x 6,2	-3 ÷ -14,3	9	1,2 ÷ 7,2
Poh and Wong 2001	12 ÷ 32	Not known	Variable	-1.5 ÷ 2,2	2 ÷ 30	1 ÷ 6,5
Koutsoftas et al. 2000	20	Not known	0,9 x 3,7	-0,4 ÷ - 4,2	10	1 ÷ 21

The values of the two angles can be simply calculated (Fig. 5) as:

$$\chi = \tan^{-1}\left(\frac{h}{d}\right) \tag{3}$$

$$\xi = \tan^{-1}\left(\frac{\frac{b}{2}-a}{d}\right) + \tan^{-1}\left(\frac{\frac{b}{2}-a}{d}\right) \tag{4}$$

The mechanical factor C_m should take into account the stiffness of the soil and the coefficient of earth pressure at rest K_0 on one hand, and the construction sequence on the other.

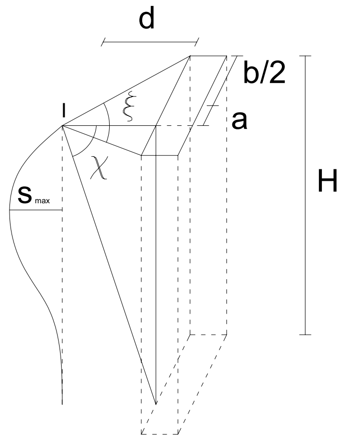

Fig. 5. Sketch of the panel and of the geometrical parameters (eqs. 3 and 4).

It has been found (L'Amante, 2009) that the intermediate step of excavation sustained by slurry pressure is extremely important for stability, but has a minor influence on final displacements. Therefore, the proposed expression for C_m is:

$$C_m = \left(\frac{\gamma_c \cdot h_c}{E_s}\right) \cdot \left[1 - \sqrt{\left(\frac{R_c}{R_s}\right)}\right] \tag{5}$$

in which γ_c is the unit weight of the concrete, E_s is the Young modulus of the soil (in clayey soils, it is the undrained modulus), R_c is the resultant force of the horizontal pressures applied on the panel wall by the fresh concrete, and R_s is the resultant force of the initial (undisturbed) total horizontal soil stress on the panel lateral surface. Assuming the distribution reported in Fig. 3, R_c can be calculated as:

$$R_c = \gamma_c \left(H \cdot h_c - \frac{{h_c}^2}{2}\right) + \frac{\gamma_b}{2}\left(H - h_c\right)^2 \tag{6}$$

The first factor in eq. (5) grossly represents a strain level caused by fresh concrete; the second factor controls the sign of the coefficient, which is related to the versus of the displacement, being it negative for displacements towards the soil and positive for displacements towards the panel.

At the end, the value of s_{max} (eq. 1) depends on the two parameters α and β, which in this work were calibrated on the available experimental data (Tab. 1), adopting an original best fitting procedure suggested by L'Amante (2009):

α=0.19
β=1.36

Figs. 6 and 7 show the relationship between measured and calculated values of s_{max}. The circular marks indicate the data set on which eq. (1) was calibrated, while the square marks are the data (Lachler *et al.,* 2006) used to check the accuracy of the proposed formula. The adopted calibration procedure is conceived to weigh the larger displacements more than the smaller ones. This choice was taken both because the smaller displacements are affected by larger measuring uncertainties and because they are less important from an engineering point of view. Fig. 6 confirms the better agreement of the formula with the larger measured displacements, while Fig. 7 allows to appreciate the capability of the formula to predict the correct sign of the maximum displacement.

Eq. (1) is certainly easy to use, but has some limitations: first of all, it does not take into account the effect of construction duration, which certainly has an influence. However, most times such a duration is not known *ex ante*, and so this is an unavoidable limitation. Furthermore, as previously mentioned, eq (1) does not consider the intermediate stress condition applied by bentonite.

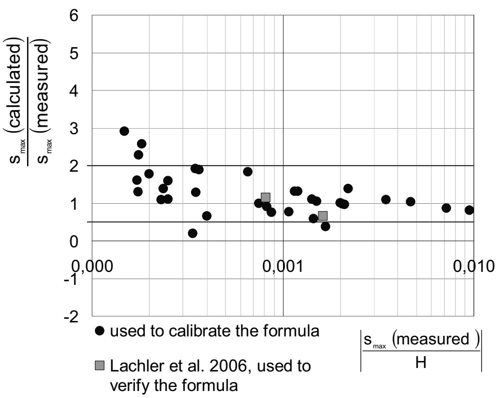

Figura 6. Relationship between measured and calculated (eq. 1) s_{max}.

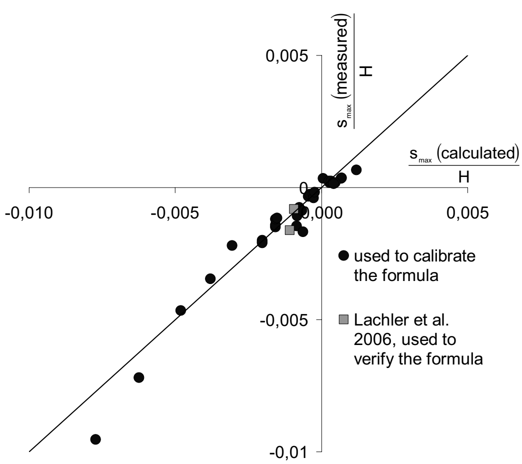

Figura 7. Relationship between measured and calculated (eq. 1) s_{max}.

4. NUMERICAL SIMULATIONS

Numerical analysis have been carried out as a tool to gain a better understanding of the mechanisms and to validate the simple empirical formula proposed in the previous paragraph. The analyses are based on a 3D FE model built and solved by the code Plaxis 3D foundation.

A total of 9 cases has been analysed. In Tab. 2 the main features of each case are summarized, along with the calculated value of s_{max}.

The soil has been modeled in the simplest possible way as a linear elastic-perfectly plastic material with a Mohr-Coulomb yield surface. Being the analyses dedicated to the simulation of the relatively quick construction process in clayey soils, undrained conditions were assumed.

The 3D mesh shown in Fig. 8 was used in all cases, taking profit of two planes of simmetry. The mesh is composed by 34000 wedge elements and its global size is 70 m x 50 m x 50 m.

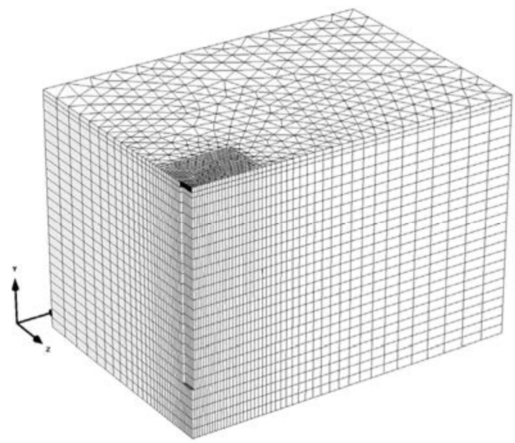

Figure 8. Three-dimensional finite element mesh.

The excavation of the panel has been simulated removing the soil elements by 4 m deep steps, and applying horizontal forces given by the pressure of the bentonite slurry. At the bottom of the excavation, a vertical load equal to the maximum horizontal pressure was applied. The adopted unit weight for the bentonite slurry was 12 kN/m^3, in agreement with Filz et al. (2004).

The concreting stage with the progressive upwards slurry removal has been simulated by progressively adding loads on 4 m long pieces of the exposed face, to represent the increased pressure exerted by the wet concrete, consistently with the scheme shown in Fig. 3. The critical depth was considered constant (h_c=7.5 m), γ_{soil}=20 kN/m^3 and $\gamma_{concrete}$ = 25 kN/m^3.

The results summarized in Tab. 2 show that the sign of s_{max} is ruled by K_0, consistently with eqs. (5) and (6). Furthermore, taking soil properties constant, s_{max} increases with panel width b for a given value of H and, for a given width, it decreases as H increases. In both cases, there is a beneficial 3D effect that reduces s_{max} as b/H decreases. However, increasing H has a more pronounced effect, and this can be simply explained by the larger increase of soil loads with depth compared to fresh concrete loads. This feature is well kept by the proposed simplified formulation: in eq. (5), in fact, the ratio R_c/R_s decreases with depth, the overall effect being ruled by both K_0 and h_c eq. 6).

Table 2.Parameters used in the analysis and calculated values of s_{max}.

test	H (m)	b (m)	K_0	E_u (kPa)	s_{max} (mm)
clay 1	20	6	0,577	11540	-73,1
clay 2	20	6		23080	-36,5
clay 3	20	3		23080	-28,2
clay 4	20	3		11540	-56,5
clay 5	16	3		23080	-27,5
clay 6	16	3		11540	-54,9
clay 7	40	6		11540	-37,5
clay 8	40	6		23080	-18,7
clay 9	20	6	1,5	23080	30

In Fig 9 typical calculated horizontal displacements are plotted. In the selected case (clay 1) horizontal displacements directed towards the soil were obtained, with the largest value located in the upper part of the panel. On the contrary, when the calculated horizontal displacements are directed towards the panel, s_{max} is usually located in the lower part of the panel.

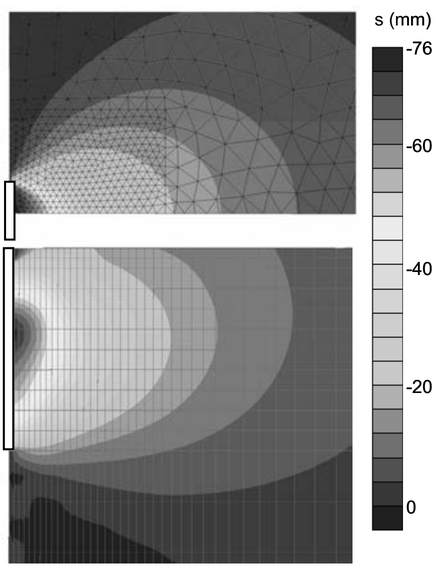

Figure 9. Horizontal displacements in a vertical and an horizontal section (case clay1).

Fig 10 shows the very large influence of K_0 on the calculated profile of displacements. With the largest value of K_0 (clay 9), displacements are towards the panel, while the opposite happens for the smaller value of K_0. As previously stated, Fig. 11 show that for the 40 m deep panel, the maximum displacement s_{max} is still towards the soil and at a small depth because of the small value of K_0; however, the displacements profile has a more complex shape, with displacements towards the panel in the bottom part of the panel where, because of the large depth, soil loads are larger than fresh concrete ones.

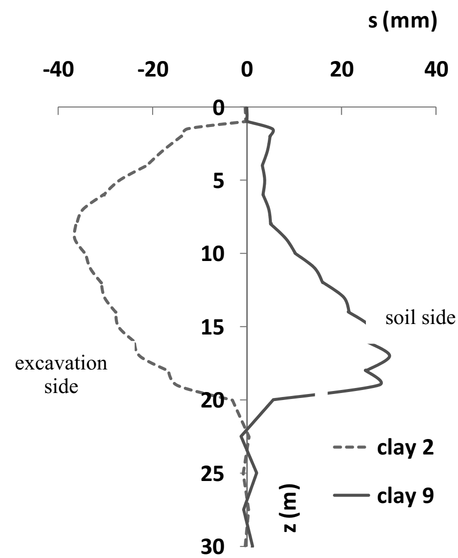

Figure 10. Horizontal displacements in the mid section and close to the panel.

The analyses refer to the construction of just one panel, while the formula refers to the displacement caused by the construction of the whole diaphragm wall. However, the construction of adjacent panels should produce negligible effects on the value of s_{max} calculated close to the mid section of the panel. Therefore, such values of smax were selected to validate eq. (1). Fig. 12 shows that there is a quite good agreement between eq. (1) and FEM results, with a general tendency of the proposed formula to overestimate the maximum displacement.

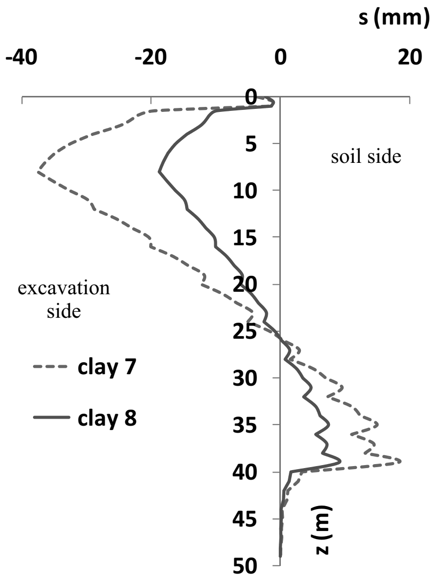

Figure 11. Horizontal displacements in the mid section and close to the panel.

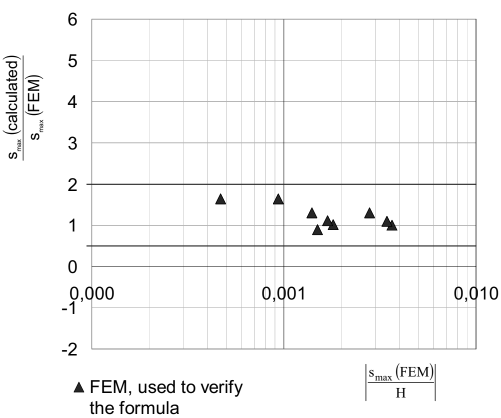

Figure 12. Relationship between FEM and calculated (eq. 1) values of s_{max}.

In Fig. 13 the FEM values of s_{max} along a cross section are compared with the ones obtained by eq. (1), with a general overall agreement. Such an agreement may be the outcome of two opposite effects: on one hand the simple constitutive model tends to overestimate the displacements at large distances from the panel. On the other, the FEM simulations were carried out on a single panel, thus without taking into account the obvious increments of s_{max} caused by the adjacent panels, whose relevance increases with distance.

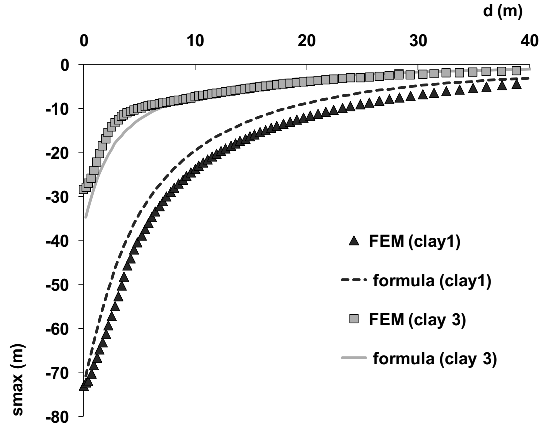

Figure 13. Calculated (by eq. 1) and computed (by FEM) s_{max} versus distance

5. CONCLUSIONS

The evaluation of the horizontal displacements caused by panels construction is becoming more and more important. Obviously, such an evaluation refers to stable panels for which, at the design stage, the overall stability has been checked.

The proposed formula could be a simple yet useful tool to get a preliminary estimate of the maximum displacement at any location in the soil around the panel. Such displacement must be added up to the displacement related to the main excavation, which can be also evaluated at a preliminary stage by using simple charts, as the ones reported in Figs. (1) and (2). Of course, the relevance of the effect of panel construction does not only refer to the displacements field in the soil, having also a relevant effect on the stress state within the soil mass and therefore on soil loads on the retaining structure.

Further validation of eq. (1) has to be carried out in the future, based on the availability of new well documented and reliable field data.

6. REFERENCES

Boone S.J., Westland J. 2006. Building Estimating displacements associated with deep excavation , *Proc. Of the Int. Symp. On Geotechnical aspect of underground construction in soft ground*. London.

Clough G.W., O'Rourke T.D. (1990). Construction Induced Movements of In-Situ Walls, *ASCE, Geotechnical Special Publication* No. 25 – Design and Performance of Earth Retaining Structures, 439-470.

Clough G.W., Smith E.M, Sweeney B.P. (1989).

Movement Control of Excavation Support Systems by Iterative Design, *Proceeding, ASCE, Foundation Engineering Congress: Current Principles and Practices*, Vol. 2, 869-884.

de Wit, J.C.W.M., Lengkeek, H.J. 2002. Full scale test on environmental impact of diaphragm wall trench installation in Amsterdam. *Proc. Int. Sym. On Geotechnical Aspect of Underground Construction in Soft Ground*, Toulose, France

Di Biaggio, E., ROTI, J. A. 1972. Earth pressure measurements on a braced slurry-trench wall in soft clay. *Proceedings of 5-th European Conference on Soil Mechanics and Foundations Engineering*, Madrid, vol. I, pp. 473-483

Fernie R., Sucking T. 1996. Simplified approach for estimating lateral wall movement of embedded walls in UK ground. *Proc. Of the Int. Symo. on* Geotechnical *aspect of underground construction in soft ground*. London.

Filz, G.M. 2004. Stability of Long Trenches in Sand Supported by Bentonite-Water Slurry. *J. of Geotechnical and Geoenvironmental Engineering*, ASCE pp.915-921.

Gatti, G., Garassino, A. L. 1989. Determi-nazione sperimentale della portata laterale di pali trivellati in terreno granulare. *Atti del XVII Convegno Nazionale di Geotecnica* Taormina 231-239 (in italian)

Koutsoftas D.C., Frobenius P., Wu C.L., Meyershon D., Kulesza R. (2000): Deformation during Cut-and-Cover Construction of MUNI Metro Turnback Project. *J. of Geotechnical and Geoenvironmental Engineering*, ASCE 344-359.

Lachler, A., Neher H.P., Gebeyehu, G. 2006: A comparison between monitoring data and numerical calculation of a diaphragm wall construction in Rotterdam. *Numerical Modelling of Construction Process in Geotechnical Engineering for Urban Environment* 83-95

L'Amante, D., 2009. Comportamento di grandi opera di sostegno in ambiente urbano. *PhD Thesis* (in Italian)

Lings, M.L., Ng, C.W.W., Nash, D.F.T. 1994. The pressure of wet concrete in diaphragm wall panels cast under bentonite. *Proc. of the Institution of Civil Engineers*, Geotechnical Engineering

Mana, A.I., Clough G.W. 1981. Prediction of movement for braced cuts in clay, *Journal of the Geotechnical Division*, ASCE, pp.759,777.

Ng, C.W.W., Yan, R.W.M. 1999. Three-dimensional modelling of a diaphragm wall construction sequence. *Geotechnique*, 825 - 834

Poh, T.Y., Wong, I.H. 1998. Effect of Construction of Diaphragm Wall Panels on Adjacent Ground: Field Trial. *J. of Geotechnical and Geoenvironmental Engineering*, ASCE 749-756.

Poh, T.Y., Wong, I.H. 2001. Ground Movements Associated with Wall Construction: Case Histories. *J. of Geotechnical and Geoenvironmental Engineering*, ASCE 1061-1069.

Uriel, S., Oteo, C., S. 1977. Stress and strain beside a circular trench wall. *Proc. 9th Int. Conf. soil mechanics and foundation engineering*, Tokyo, vol. 1,pp. 781-788 ;

Risk assessment of highway embankments based on embankment failures caused by 2007 Noto Peninsula earthquake

T. Matsumoto, S. Kobayashi, Y. Nishiki
Graduate School of Kanazawa University, Kanazawa, Japan

H. Kawai
Government Corporation of Highways, Ishikawa Prefecture, Japan

P. Kitiyodom
Geotechnical & Foundation Engineering Co., Ltd., Bangkok, Thailand

ABSTRACT: Noto Peninsula of magnitude 6.9 on the Richter scale occurred on 25 March 2007 at 9:42 local time (0:42 GMT) in the Hokuriku region of Japan, near the Noto Peninsula. During the earthquake, failures of high embankments having heights of 30 to 35 meters occurred at a total of 11 locations on the Noto highway connecting the Noto Peninsula and Kanazawa city. In this paper, static and dynamic analyses of one of the embankment failures are carried out. Practically feasible approaches for risk assessment of existing highway embankments are discussed based on the observations and the analyses of the highway embankment failures of the Noto highway.

1. INTRODUCTION

Highways connecting cities and industrial areas are very important infrastructures. If a highway is damaged by a disaster and blockaded, huge influence on social activities is induced. Huge earthquakes repeatedly occurred in Japan, such as Hanshin-Awaji earthquake in 1993, Miyagiken hokubu earthquake in 2003, Niigataken Chuetsu earthquake in 2004, Noto Peninsula earthquake in 2007, Niigataken Chuetsuoki earthquake in 2007 and so on. In reality, a number of failures of highway embankments and natural slopes were caused by these earthquakes. In several cases of damages of highways, it took several months to restore the damaged highways. Such damages of the highways caused isolation of residential areas, backset of transportation of aid supplies and delay of restoration works. Hence, risk assessment of existing and planned highways against future earthquakes takes an important role to ensure safe and secure life in rural cities as well as in megacities.

An earthquake of magnitude 6.9 on the Richter scale occurred on 25 March 2007 at on 9:42 local time (0:42 GMT) in the Hokuriku region of Japan, near the Noto Peninsula (see Fig. 1). The earthquake left huge damages especially in Ishikawa Prefecture. In Ishikawa Prefecture, it is reported that about 650 houses were collapses and about 25,000 houses were partially damaged (Exploratory Committee, 2008). Besides high casualties and damage to various engineering structures and buildings, slope and embankment failures of a highway and country roads occurred. Failures of high embankments occurred at a total of 11 locations on the Noto highway connecting the Noto Peninsula and Kanazawa city during the earthquake (Exploratory Committee, 2008). Figure 1 shows the locations of the epicentre and the embankment failures. The distance from the epicentre to each location of embankment failure ranges from 17 to 20 km.

In this paper, practically feasible approaches for risk assessment of existing highway embankments are discussed, based on post-earthquake observation highway and analyses of one of embankment failures, T06-embankment, caused by 2007 Noto Peninsula earthquake.

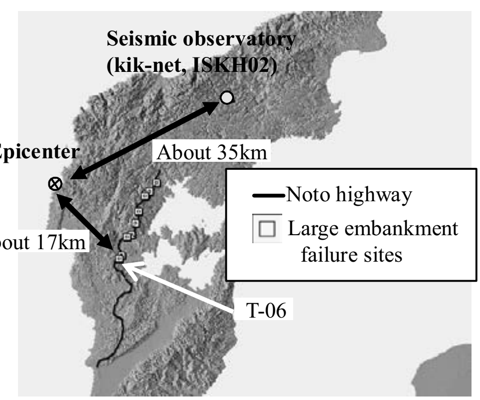

Figure 1. Location of epicentre of Noto Peninsula Earthquake in 2007.

2. OUTLINE OF T-06 EMBANKMENT FAILURE

Figures 2 and 3 show the plan view and an aerial view of the post-failure embankment. The length of the embankment failure was 65 m, and the disrupt soils reached the paddy field developing form the toe of the embankment as shown in Fig. 3.

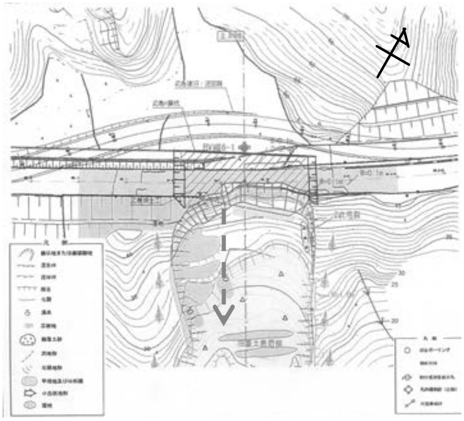

Figure 2. Plan view of T-06 embankment (Exploratory Committee 2007).

Figure 3. Aerial view of T-06 embankment failure (Exploratory Committee 2007).

Borehole investigations and surveying were carried out 10 days after the occurrence of the earthquake. Figure 4 shows cross sections of both pre- and post-failure geometries and the observed failure surface. The configuration of the embankment near the shoulder after the failure was about 5:3 (v/h; about 58 degrees). The observed slip line took an almost circular shape, but the slip occurred along the interface between the fill and the original ground (natural ground) for x greater than 65 m. Two borehole investigations were carried out at locations No. 1 and No. 2.

Figure 5 shows profiles of soil layers and SPT N-values at the embankment. The SPT N-values in the fill typically ranged from 2 to 10, while the SPT-N values of the bed rock were typically larger than 30. The groundwater table estimated from the borehole investigations is indicated in the Fig. 4.

Soil samples were taken from the site after the earthquake to obtain the physical and mechanical properties of the fill material. Sieving tests, maximum and minimum density tests, soil particle density tests and direct shear tests were carried out using the disturbed soil samples. Table 1 summarises the physical properties of the fill material. The relative density, D_r, was 60 %. The fill material contains relatively high fraction of fine-grains of 40.5 %.

Direct shear tests of the disturbed dry soil samples were carried out, setting the relative density D_r, = 60 %.

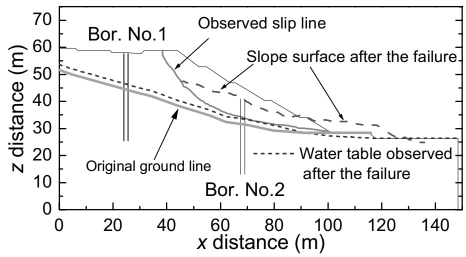

Figure 4. Cross section showing pre- and post-failure geometries, and failure surface (Exploratory Committee 2007).

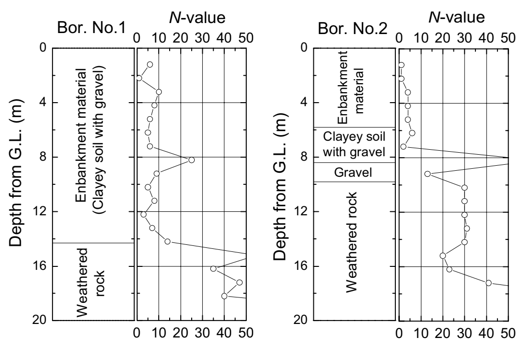

(a) No.1 borehole (b) No.2 borehole

Figure 5. Profiles of soil layers and SPT N-value. (Exploratory Committee 2007).

Table 1. Physical properties of the fill material.

Wet density at site, ρ_t (t/m^3)	1.536
Water content at site, w (%)	41.4
Dry density at site, ρ_d (t/m^3)	1.086
Maximum dry density, ρ_{dmax} (t/m^3)	1.251
Minimum dry density, ρ_{dmin} (t/m^3)	0.903
Relative density at site, D_r (%)	60.3
Density of soil particle, ρ_s (t/m^3)	2.747

3. STRESS-DEFORMATION ANALYSES OF T-06 EMBANKMENT FAILURE

3.1. Static analyses

The borehole investigations were carried out 10 days after the earthquake as mentioned. Hence, it will be reasonable to think that the groundwater table measured during the borehole investigations does not necessarily correspond to the groundwater table at the occurrence of the earthquake, because the slope configuration and the hydraulic conditions were totally changed after the earthquake. Hence, it is required to estimate a probable groundwater table at the occurrence of the earthquake. For this purpose, stability analyses of the embankment in usual condition (only gravity acceleration is applied) were carried out using a finite difference method FLAC3D (Itasca, 2002) prior to dynamic analyses.

Figure 6 shows the finite difference mesh used for the embankment in plane strain (two-dimensional) condition. In the static analysis, vertical displacements at the bottom of the bedrock and horizontal displacements at both sides were fixed.

The fill material was modelled by non-associated elastic-perfectly plastic constitutive model with Mohr-Coulomb yield criterion, while the bedrock material was modelled as liner elastic material. The analysis parameters are summarised in Table 2. Cohesion, c', and internal friction angle, ϕ', of the fill material were determined from the direct shear tests of the soil specimens sampled from the embankment.

Shear moduli, G, of the fill and the bedrock were estimated from the following empirical equation (1) proposed by Imai (1977) using SPT N-value and Eq. (2) of the elastic stress-wave theory.

$$V_s = 91N^{0.337} \text{ (m/s)} \quad (1)$$

$$G_0 = \rho_t V_s^2 \quad (2)$$

where V_s: velocity of shear wave (m/s), N: N-value, G_0: initial shear modulus at small strain, ρ_t: wet density of soil

Poisson's ratio, ν, was assumed to be 0.3 because fully-drained condition was assumed in the static analyses.

The factor of safety, F_s, and the corresponding deformation of the embankment were calculated using "shear strength reduction (SSR) method" (Zienkiewicz et al 1975) implemented in FLAC3D.

Figure 7 shows the groundwater tables (W.T.) assumed in the analyses. W.T. 1 corresponds to the groundwater table measured after the earthquake.

Figure 8 shows the calculated shear strain increments where the measured groundwater level (W.T. 1) was assumed. The calculated F_s was 1.80 indicating that the embankment had a sufficient safety margin in usual condition.

Table 2. Analysis parameters.

	Fill	Bed rock
N-value (Average) *1	7	60
Wet density ρ_t (t/m^3) *2	1.54	1.9
Saturated density ρ_{sat} (t/m^3) *2	1.69	2.0
Cohesion c' (kPa) *2	0.4	-
Internal friction angle ϕ' (deg.) *2	38.0	-
Initial shear modulus G_0 (MPa) (Saturated soil) *3	46.2	3000
Poisson's ratio ν (Static analyses and partially saturated soil in dynamic analyses) *4	0.3	0.3
Poisson's ratio ν (Saturated soil in dynamic analyses) *4	0.49	0.49

*1 Field investigation, *2 Direct shear test, *3 Equation (1), *4 Assumed

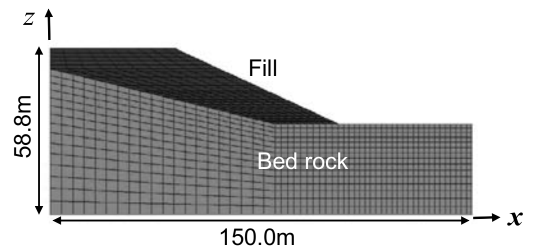

Figure 6. Finite difference grid used for the analyses of T-06 embankment.

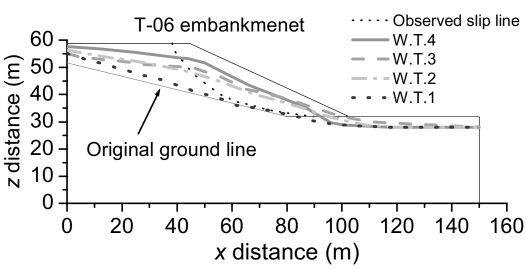

Figure 7. Groundwater tables assumed in the analyses of T-06 embankment.

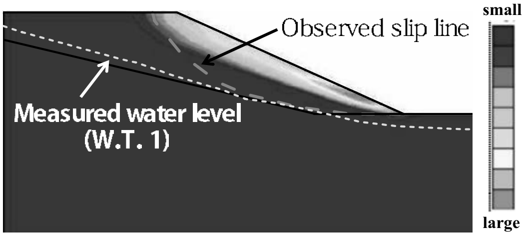

Figure 8. Calculated shear strain increment in static stability analysis of T-06 embankment (W.T.1, F_s = 1.80).

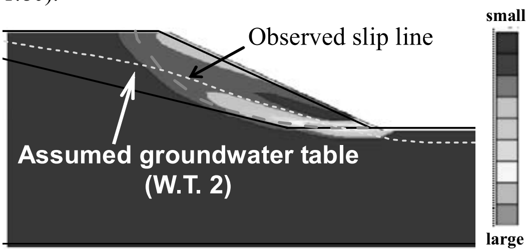

Figure 9. Calculated shear strain increment in static stability analysis of T-06 embankment (W.T.2, F_s = 1.71).

It is seen from the figure that shear strain increments concentrate at shallow depths in the slope, especially near the slope toe. That is, the potential slip line is located is far from the observed slip line. Therefore, static analyses were iterated with raising the groundwater level gradually.

Figure 9 shows the calculation results when W.T. 2 was assumed. Although F_s reduced a little bit to 1.71 from 1.80 in this calculation, the shear strain increments developed to deeper depths in the embankment and the potential slip line conformed to the observed result well. It should be noted that the expected slip lines were shallower than the observed slip line when groundwater levels lower than W.T. 2 were assumed in the analyses. Therefore, it may be reasonable to judge that the groundwater level at the occurrence of the earthquake was not below W.T. 2 indicated in Figure 7 or 9. Thus estimated groundwater level (W.T. 2) is used in the dynamic analyses described later.

3.2. Dynamic analyses

Dynamic analyses of the embankment during the earthquake were carried out using FLAC. The finite difference mesh (Fig. 6) is used also in the dynamic analyses. In the dynamic analyses, excitation accelerations are applied at the bottom of the bed rock with infinite boundaries at both sides.

As acceleration records are not available at the location of the embankment, excitation accelerations at the embankment were approximated from the acceleration records of the engineering bedrock measured at Yanagida station of KiK-net with an attenuation (scaling-up) factor derived from an empirical equation (3) proposed by Fukushima and Tanaka (1990).

$$\log A_{\max} = 0.41M_s - \log(R + 0.032\times 100.41M_s) \\ -0.0034R + 1.30 \tag{3}$$

where $A_{\max}$: maximum acceleration (cm/s^2), R: shortest distance to fault (km), M_s: Surface wave magnitude.

The distance between the epicentre and Yanagida station is 35 km and that between the epicentre and T-06 embankment is 17 km. Hence, the acceleration records (accelerations in NS, EW and UD directions at Yanagida station) were scaled-up using the relation of Eq. (3) to obtain the dynamic excitations at T-06 embankment. As the dynamic analyses were carried out in plane strain condition, horizontal accelerations in x-direction were constructed from NS- and EW-accelerations at T-06 embankment. The horizontal and vertical input accelerations thus obtained are shown in Fig. 10.

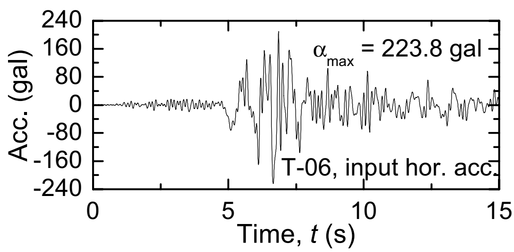

(a) x direction

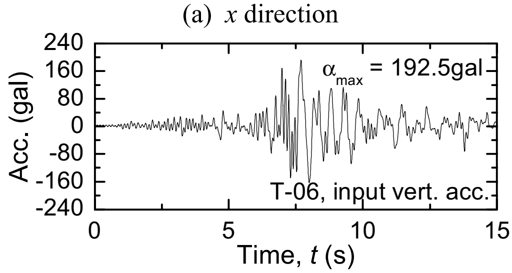

(b) z direction

Figure 10. Input dynamic excitation components at T-06 embankment.

Two dynamic analyses were carried out with the estimated groundwater table (W.T. 1). obtained in the static analyses. In an analysis

(Case 1) horizontal excitation alone was considered, while both horizontal and vertical excitations were accounted for in the other analysis (Case 2). Uncoupled analyses under fully-undrained condition during the earthquake were carried out. Hence, Poisson's ratios, ν, of saturated soils were set as 0.49 (see Table 1) to approximately simulate fully-undrained condition. Note, however, that pore pressures and effective stresses of the ground were calculated through self-weight analysis prior to the dynamic analyses for the initial state of the dynamic analysis.

Figure 11 shows the calculated shear strain increments in Case 1 at time t = 15 s. Larger shear strains occur at very shallow depths in the embankment.

Displacements were checked in the calculation along the sections shown in Fig. 12. Figure 13 shows the calculated changes in distributions of horizontal displacements relative to that of the bottom of the bedrock with time along section No. 5. It is seen that the horizontal relative displacements are very small especially in the bedrock, and that definite slip line (failure zone) is not generated although relatively large gradients of relative horizontal displacement occur in the fill just above the interface between the fill and the bedrock.

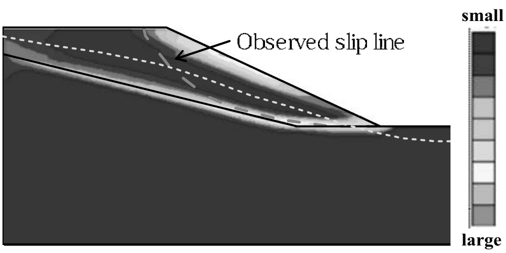

Figure 11. Calculated shear strain increment in dynamic response analysis of T-06 embankment (horizontal acceleration alone, at t = 15 s).

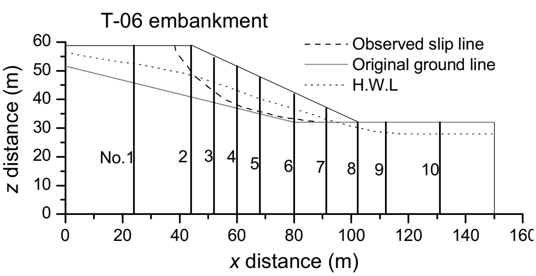

Figure 12. Section numbers to check horizontal displacement.

Figure 14 shows the calculated shear strain increments at time t = 15 s in Case 2 where vertical excitation as well as horizontal excitation was input at the bottom of the bedrock. In this case, large shear strain increments are generated deep depths in the fill especially along the zone just above the interface between the fill and the bedrock. The zone of the calculated shear strain concentration coincides well with the observed slip line.

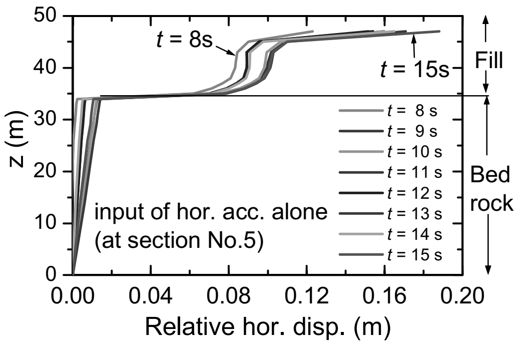

Figure 13. Changes in distributions of horizontal displacements with time along section No. 5 relative to that of the bottom of the bedrock in Case 1.

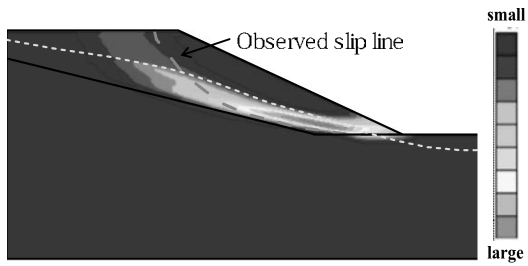

Figure 14. Calculated shear strain increment in dynamic response analysis of T-06 embankment (horizontal and vertical accelerations, t = 15 s).

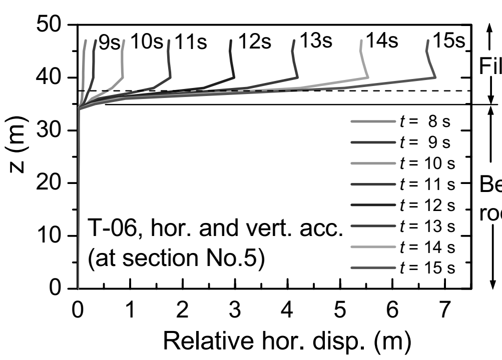

Figure 15. Changes in distributions of horizontal displacements with time along section No. 5 relative to the that of the bottom of the bedrock in Case 2.

Figure 15 shows the calculated changes in distributions of relative horizontal displacements with time along section No. 5. It is seen that very large relative horizontal displacements occur in the fill section. It is also seen that large horizontal displacement gradients are generated within a zone of 1.5 m thick above the interface between the fill and the bedrock, which can be regarded as slip (failure) zone.

The calculation results shown in Figs. 14 and 15 in Case 2 simulate well the observed behaviour of the embankment failed by the earthquake, compared to the calculation results in Case 1. This fact clearly indicates that consideration of the vertical input accelerations in the dynamic analysis is inevitable to accurately assess the stability of the embankment during the earthquake. Furthermore, this fact suggests that consideration of seismic coefficient, k_v, as well as horizontal seismic coefficient, k_h, is necessary even when quasi-static analysis is employed to assess slope stability of an embankment during an earthquake.

4. PRACTICAL RISK ASSESSMENT OF EMBANKMENT

It was demonstrated in the previous section that dynamic stress-deformation analysis approach is a useful tool to estimate the stability of an embankment during a big earthquake. However, such approach is often difficult in practice to assess stability (risk of failure) of many existing embankments and embankments to be constructed in future. Hence, quasi-static stress-deformation analysis and quasi-static limit equilibrium analyses of T-06 embankment are carried out in this section to explore the applicability of the quasi-static analyses approaches for risk assessment of the embankment. And, an intuitive method of use of the results of quasi-static analyses for risk assessment is discussed

4.1. Quasi-static stress-deformation analysis

A series of quasi-static stress-deformation analyses (SSR analyses) were carried out using the finite difference mesh of Fig. 6. In the analyses, combinations of horizontal and vertical seismic coefficients, k_h and k_v, that gives F_s = 1 were sought. Figure 16 shows the calculation results (shear strain increments) from one of the quasi-static analyses in which W.T. 2 was assumed. Factor of safety F_s = 1 was obtained when k_h = 0.19 and k_v = 0 were assumed. It is seen from the figure that the slip line derived from the quasi-static analysis is very similar to that obtained the static analysis shown in Fig. 9 and the observed slip line.

Combinations of k_h and k_v giving F_s = 1 for various groundwater tables calculated using FLAC are shown in Fig. 17. It is clearly seen that linear relationship between k_h and k_v is found for each groundwater table. This fact means that only two analysis results are sufficient obtain combinations of k_h and k_v for each groundwater table.

It may be worth to describe that the slip lines derived from the quasi-static analyses were almost equal to those derived from the static stability analyses, although factors of safety from the static and the quasi-static analyses were, of course, different.

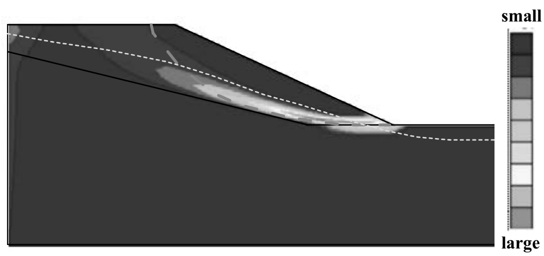

Figure 16. Calculated shear strain increment in pseudo-static stability analysis of T-06 embankment (W.T.2, F_s = 1.00 for k_h = 0.19 and k_v = 0).

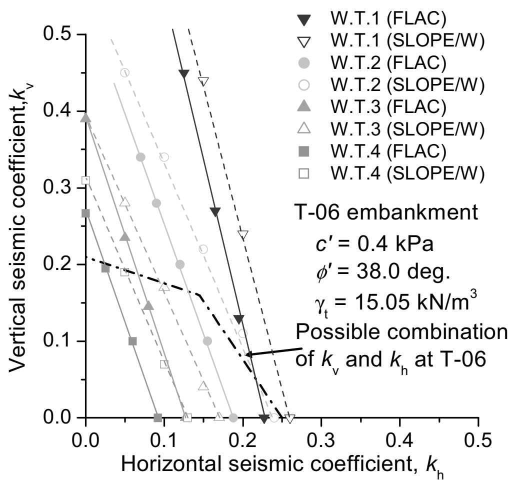

Figure 17. Combination of k_h and k_v which provide safety factor F_s = 1 obtained from stress-deformation analysis (FLAC) and limit equilibrium analysis (SLOPE/W).

4.2. Quasi-static limit equilibrium analysis

Limit equilibrium analysis has been most widely used for stability analyses of embankments in Japan. In this research, quasi-static limit equilibrium analyses of T-06 embankment were also carried out using Morgenstern-Price method (Morgenstern and Price, 1965) implemented in SLOPE/W program (Geo-Slope Int., 2007).

Figure 18 shows the results of stability analyses of the embankment in usual condition ($k_h = k_v = 0$). Factors of safety and corresponding slip lines are indicated in the figure for various groundwater tables. The results from the limit equilibrium analyses are comparable to the stress-deformation analysis results in Figs. 8 and 9. The deduced potential slip lines are not so far from the observed slip line.

Figure 19 shows the results of one of quasi-static limit equilibrium analyses, in which W.T. 2 was assumed in the analysis.

Combinations of k_h and k_v giving $F_s = 1$ for various groundwater tables calculated using the limit equilibrium analyses (SLOPE/W) have been indicated in Fig. 17. Linear relationship between k_h and k_v is found for each groundwater table, as was seen in the FLAC analysis. It should be noted that the limit equilibrium analysis (SLOPE/W) gives higher values of k_h and k_v for each groundwater table, compared with the stress-deformation analysis (FLAC).

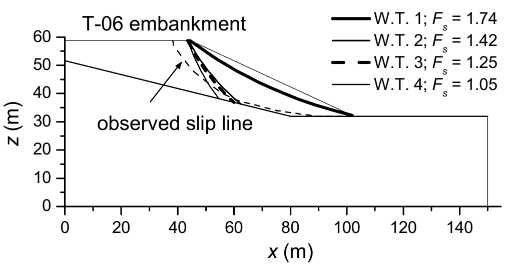

Figure 18. Slip lines of T-06 embankment estimated from limit equilibrium analyses in usual (static) condition.

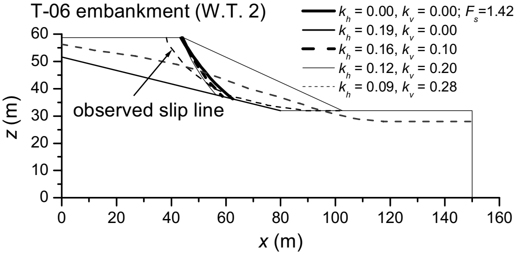

Figure 19. Slip lines of T-06 embankment estimated from limit equilibrium analyses in pseudo-static condition with W.T. 2.

This result indicates that the limit equilibrium analysis always overestimates the factor of safety.

4.3. Use of quasi-static analysis results for risk assessment

A problem, e.g. how to utilise the design chart for risk assessment of the embankment, may arise, even if a design chart as shown in Fig. 17 is constructed. In other words, what values of k_h and k_v should be selected for a given embankment. Practically applicable intuitive approaches are attempted below.

Figure 20 shows the evolution of horizontal and vertical excitation accelerations, α_x and α_z, at T-06 embankment which was constructed from the input dynamic excitation components in Fig. 10. It is seen that trace of acceleration fluctuates within a closed envelope surface (the dotted line).

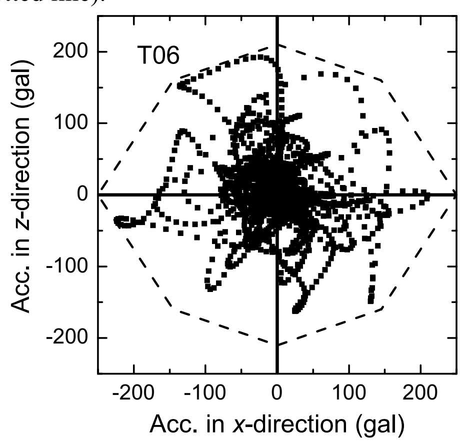

Figure 20. Evolution of horizontal and vertical excitation accelerations at T-06 embankment.

From the calculation results in the dynamic analysis, the horizontal displacements of the embankment relative to the bedrock continue to increase regardless of directions of excitation accelerations (see Fig. 15). Hence, the evolution of absolute values of α_x and α_z are shown in Fig. 21. The dotted line in Fig. 21 is approximated limits of α_x and α_z at this particular site. This line has been indicated in Fig. 17 and Fig. 20.

Although it seems conservative that the evolution of absolute values of α_x and α_z hown in Fig. 21 are utilised for an assessment of seismic resistance (the chain-dot line in Fig. 21 shows a safe approximation for combination of α_x and α_z), it is difficult at present to make further discussion on selection of combination of α_x and α_z.

It is worth mentioning that embankments of Noto Highway were designed by a quasi-static limit equilibrium method considering a horizontal coefficient, k_h, equal to 0.2 and $k_v = 0$.

The approach presented in this paper will be applied to the other embankments failed by 2007 Noto Peninsula earthquake and the other big earthquakes.

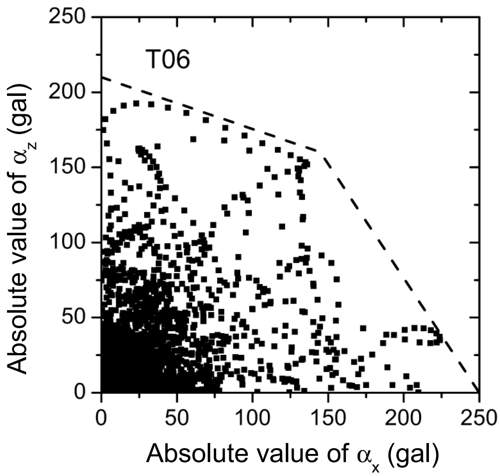

Figure 21. Evolution of absolute values of horizontal and vertical excitation accelerations at T-06 embankment.

5. CONCLUDING REMARKS

In this article, stress-deformation analyses of the T-06 embankment in Noto Highway failed by 2007 Noto Peninsula Earthquake have been carried out to explore major influential factors on the stability during the earthquake.

Main findings from this research are summarised as follows:

(1) Factor of safety of the embankment in usual condition is controlled by groundwater table as widely recognised.

(2) Failure pattern (configuration of slip line) is sensitive to groundwater table.

(3) The slip line calculated from the static stability analysis in usual condition is similar to that calculated in the dynamic analysis.

(4) Consideration of vertical input accelerations as well as horizontal accelerations is necessary to accurately estimate the dynamic behaviour of the embankment during the earthquake.

Based on the above findings, quasi-static analyses of the embankment were carried out using stress-deformation analysis method and limit equilibrium analysis method to discuss the applicability of the quasi-static approaches for risk assessment of embankments. Main findings from the quasi-static analyses are as follows:

(5) Limit equilibrium analysis is used as an alternative to stress-deformation analysis, although the former analysis method gives dangerous side design compared to the latter analysis method.

(6) Selection of vertical seismic coefficient, k_v, was discussed using the input accelerations neglecting amplification of accelerations in the embankment. It was inferred that k_v/k_h is higher for lower k_h and k_v/k_h is lower for higher k_h. However, no definite conclusion was derived from limited analyses in this paper. Further consideration based on analyses of the other embankment failures is needed for this aspect.

6. ACKNOWLEDGEMENTS

The authors acknowledge National Research Institute for Earth Science and Disaster Prevention (NIED) for use of KiK-net seismic records in this research.

7. REFERENCES

Exploratory Committee of Restoration Method for Noto Highway, Ishikawa Prefectural Government and Government Corporation of Highways of Ishikawa Prefecture 2008. Report of Sub-Committee of Earth Work in Exploratory Committee of Restoration Method for Noto Highway damaged during 2007 Noto Peninsula Earthquake.

Fukushima, Y. & Tanaka, T. 1990. A new attenuation relation for peak horizontal acceleration of strong earthquake ground motion in Japan. *Bull. Seism. Soc. Am.* Vol 84, pp. 757-783.

Geo-Slope Int. 2007. Stability Modeling with SLOPE/W.

Imai, T. 1977. P- and S-wave velocities of the ground in Japan. *Proc. 7th ICSMFE*, Tokyo, Vol 2, pp. 257-260.

Itasca Consulting Group, Inc. 2002. FLAC^{3D} manual, Itasca Consulting Group, USA.

Morgenstern, N.R. & Price, V.E. 1965. The analysis of the stability of general slip surface. *Géotechnique*, Vol. 15, No. 1, pp. 79-93.

Zienkiewicz, O.C., Humpheson, C. & Lewis. R.W. 1975. Associated and non-associated visco-plasticity and plasticity in soil mechanics. *Géotechnique*, Vol. 25, No. 4, pp. 671-689.

A Study on the Effects of Soil-Structure Interaction in Seismic Evaluation of Short Structures

M.A. Shayanfar
Civil Eng Dept. Iran University of Science and Technology,
Narmak, Tehran-16, Iran

M. Ghanooni Bagha
Civil Eng Dept. Iran University of Science and Technology,
Narmak, Tehran-16, Iran

ABSTRACT: In this paper first, three buildings have been modelled and then analyzed using nonlinear static analysis method (Nonlinear SAP 2000 software) under two different conditions. In the first condition the interaction of soil adjacent to the walls of basement is ignored while in the second case this interaction has been modelled using Gap elements of the software. Finally, by comparing the results of the two models, the effects of soil-structure on period, target point displacement, internal forces, shape deformations and base shears have been studied. According to the results, this interaction has always increased the base shear of buildings, decreased the period of structure and target point displacement, and often decreased the internal forces and displacements.

1. INTRODUCTION

As the people living in regions prone to having earthquakes are exposed to many detriments such as injuries, building damages, and economic losses, these damages should be considered in vulnerability and risk analysis of the area. Besides, one can mention the type of soil and the faults of the area as the earth properties of region, and enumerate the PGA, amplitude of vibrations, duration, and released energy as the properties of earthquake.

Thus by furthering our knowledge about earthquakes and the growth in concepts of retrofitting, consideration of structure's behavior in its realty have become of great importance. Consideration of factors such as effects of soil beside the structure in either viewpoint concerned to prediction and evaluation of possible damages or appreciation of soil's behavior adjacent to the structure have become of our great interest. Moreover, as there are many structures having basements, below stories adjacent to surrounding soil of structure, study of their behavior in presence of soil's stiffness in one hand and the behavior of soil on the other hand, seem to be necessary.

Generally, to consider the linear and nonlinear effects of soils on structures in Softwares such as nonlinear SAP2000 or Etabs, one can utilize the Link elements [1]. In the current work, the results of nonlinear static analysis of three structures without consideration of soil-structure interaction effects are compared to those of their models considering this effect using GAP elements. In addition, the maximum stress in the soil surrounding the structure is controlled by [2].

2. DESCRIPTION OF BUILDINGS AND THEIR LOADINGS

The structures considered here are comprised of a three story steel skeletal structure named as S1, a three and a four story concrete structures having skeletal system named as C1 and C2, respectively. All three structures have solid deck roofs. The plan views of these structures are shown in Fig.1.

Dead load considered for all the stories of three structures equals 550 Kg/m^2. According to [3], as the structures are belonged to schools, the live load equals 500 Kg/m^2 for corridors, 350 Kg/m^2 for classes and the minimum of 750 Kg/m^2 for the libraries. In addition, according to [4], the effective coefficient of live load in stories of schools equals 0.4, while for the roofs of structures this coefficient equals 0.2 and the loads belonged to the walls are assigned at their exact places.

The information for type of soil have been derived from analysis results of soil mechanics laboratory, and the seismic characteristics of the site of construction are defined using the regulations of [4].

Table 1. Specifications of structure's

Building ID	C1	C2	S1
Cross section of columns cm	40×40	40×40	2IPE16 2 IPE18
Cross section of beams cm	35×35	40×40	IPE20 IPE14
Height of basement m	3.6	3.4	3.6
Height of stories m	3.2	3.2	3.2
Height of ground above the foundation m	2.6	2.2	2.6
Soil allowed strength Kg/m^2	16900	12400	14600

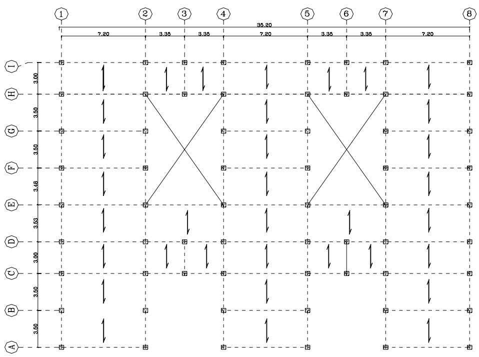

Fig1 (a): C1 Structure

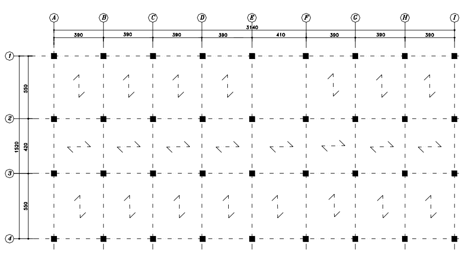

Fig1 (b): C2 Structure

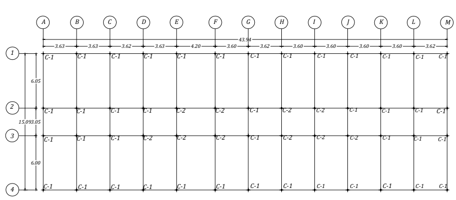

Fig1 (c): S1 Structure

More details about these structures as well as allowable stress for their surrounding soils are presented in table 1. For S1 structure, the bracing member cross section in ground floor is UNP10, while in1st and 2nd floors are UNP8.

3. NONLINEAR STATIC ANALYSIS

The structures have been analyzed toward satisfaction of life satisfy performance. In all three structures, the load combinations are derived from [2] so that the lateral loads are assigned to the structures after the vertical loads. Besides, in the nonlinear static load case, a unified load and a load according to first mode of vibration are assigned as well. In addition, according to [2], the method of coefficients of displacement has been chosen for calculation of displacement of target point and has been adjusted according to the primary analysis based upon efficient period of structure and the control point have been observed on the roof of structure.

In extreme points of concrete beams of C1 and C2 structures, according to the ratio of longitudinal bars of cross section to balanced bars and regarding the maximum allowable interval between stirrups next to the point of conjunctions to the columns, as well as consideration of shear made in them in their first analysis, hinges have been assigned to them and modifications in further analyses regarding the variations of the shear have been made. In order to define the hinges in the columns, the tool for assignment of axial loads in SAP.Ver.12 was efficiently utilized. Besides, as in a number of columns for C1 and C2 structures, the regulations for anchorage of bars are not satisfied, especial considerations are assigned to hinges [2].

In the S1 structure, the connections of columns to the foundations are hinged support. In addition, regarding the little values of moments made in the lower regions of columns, no hinges were assigned to them. Thus the columns are controlled by forces rather than moments. Moreover, as the connections of beams to the columns are of simple type, they do not participate in seismic behavior of structure, and they are only designed for gravity loads of the structure. In this structure, the force hinges are merely applied to the midpoint of bracings.

4. SOIL-STRUCTURE INTERACTION

The Nonlinear Gap elements are utilized in the current work to measure the allowable stress in the soil surrounding the basement and the modeling and analysis processes will be defined later [5]. In order to clarify the place of usage for Gap elements, it is worthy of notion that the basement has an opening with height of 80 *cm* from the bottom of ground story's floor. As it can be viewed in Fig.2 the Gap elements are located in connection to circumferential columns with the maximum distance of 50 *cm* to each other.

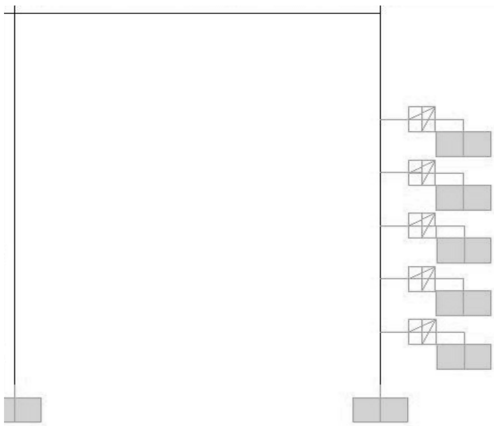

Figure 2. Gap elements connected to circumferential columns of basement

In order to calculate the stiffness of Gap elements connected to basement columns, the loading area of each column as well as the stiffness of adjacent soil are utilized. In other word we have:

$$K_{GAP} = Area \times k_s \qquad (1)$$

Where, k_s is the stiffness of soil in kg/m^3, calculated by laboratory of soil mechanics. The analysis results in compact forces in Gap elements and the stresses in soil have been calculated, consequently. On the other hand, the loading capacity of soil considered equal to six times of allowable stress of it. In other words:

$$Q_{CE} = 3 \times 2 \times q_{all} \qquad (2)$$

Where, q_{all}represents the allowable stress of soil in kg/m^2.

In order to be more realistic to the results of soil mechanic laboratory, the multiplier 2 has been entered to Eq.2.

The Gap elements are divided into two general groups: first group comprises of the elements connected to inner columns located at the circumference of the plan of basement and the second group contains those elements connected to columns located at the corners of the plan. The elements considered in the aforementioned groups are also divided into the elements completely buried in the soil and those located on the surface. The soil stiffness, K_s, stiffness of Gap elements and other details for a few elements have been presented in table.2.

Table 2. Parameters calculated for Gap elements located on the perimeter of the basement

Building ID	C1	C2	S1
Number of Gap Elements	5	4	5
Soil Stiffness kg/m^3	2020000	1665000	1780000
Loading area for buried elements m^2	1.75×0.5	1.95×0.5	1.80×0.5
Stiffness of buried elements kg/m	1767500	1623375	1602000
Loading area for surface elements m^2	1.75×0.25	1.95×0.25	1.80×0.25
Stiffness of surface elements kg/m	883750	811687.5	801000

Besides, for the Gaps located at the corners of the basement, the associated values presented in the table.2 should be halved.

5. STRESS CONTROL IN SOIL

Generally modelling the soil around the structure enables us to control the behaviour of structure and soil simultaneously, and the latter satisfies the need for experimental calculations toward control of stresses in soil. In order to calculate the stresses in soil, one can utilize the forces made in the Gap elements of the model and divide them by the loading area of the elements. This stress should be compared to the expected capacity of soil equal to six times of allowable capacity of soil [2]. The four left columns of table.3 represents the loading areas and forces, calculated for sample elements in addition to concerned stresses and loading capacities of the soil, and the fifth column controls the ratio of present stress to loading capacity of soil.

Table 3. Sample control of stresses in soil adjacent to basement's walls of three structures

C1 Structure					
Gap ID	Force (Kg)	Area (m^2)	Present Stress (Kg/m^2)	Capacity (Kg/m^2)	Ratio
1	42402	0.87	48459	101400	0.48
2	36745	0.87	41994	101400	0.41
3	15809	0.44	36136	101400	0.36
4	16782	0.44	38402	101400	0.37
C2 Structure					
Gap ID	Force (Kg)	Area (m^2)	Present Stress (Kg/m^2)	Capacity (Kg/m^2)	Ratio
1	37480	0.98	38441	74400	0.52
2	35864	0.98	36783	74400	0.49
3	14454	0.49	29650	74400	0.40
4	17718	0.49	36382	74400	0.49
S1 Structure					
Gap ID	Force (Kg)	Area (m^2)	Present Stress (Kg/m^2)	Capacity (Kg/m^2)	Ratio
1	34627	0.9	38474	87600	0.44
2	27641	0.9	30712	87600	0.35
3	12993	0.45	28873	87600	0.33
4	14352	0.45	31893	87600	0.36

As it can be obviously observed in table.3 in any of the structures, the ratio of Present Stress to the Loading Capacity of Soil does not reach the unit value, and the latter demonstrates that the soils' capacity satisfies our demand.

6. INTERPRETATION OF THE RESULTS

In this section, first the analytical characteristics of the three structures have been calculated under two conditions. The first condition comprises of a nonlinear static analysis regardless of presence of soil surrounding the walls of basement, and the second condition consists of a push over analysis regarding the soil-structure interaction effects on the structure's behavior. In table.4, the period, displacement of target point and the base shear of structures are calculated under uniform loading pattern in the two aforementioned conditions and the results are compared, consequently.

Table 4. Analytical characteristics of the structures

Building ID	Condition 1			Condition 2		
	T_x (Sec)	δ_x (m)	V_x (Kg)	T_x (Sec)	δ_x (m)	V_x (Kg)
C1	0.667	0.076	685300	0.591	0.065	758600
C2	0.617	0.064	394000	0.510	0.056	617300
S1	0.691	0.078	988200	0.614	0.068	1129000
Building ID	Condition 1			Condition 2		
	T_y (Sec)	δ_y (m)	V_y (Kg)	T_y (Sec)	δ_y (m)	V_y (Kg)
C1	0.643	0.085	625800	0.557	0.077	659400
C2	0.555	0.072	362500	0.460	0.061	400650
S1	0.572	0.102	725000	0.496	0.89	895000

As it can be obviously seen, the confining effects of soil on the displacements of the structures, also affect the periods of them and this can be a cause to diminish the displacements of target points in structures. According to the Eq. (3), the displacement of target point is derived by coefficients of displacements method.

$$\delta_t = C_0 C_1 C_2 C_3 S_a \frac{T_{eff}^{\ 2}}{4\pi^2} g \qquad (3)$$

In which, C_0 to C_3 are modifier coefficients, S_a is the acceleration read from the spectrum of maximum accelerations, T_{eff} is the effective period of structure and ***g*** represents the ground acceleration.

The comparison made between the final results of analysis of structures in two different conditions demonstrates that, the consideration of effects of surrounding soil on behavior of structures increases the *C* coefficients and reduces the periods of structures. Consequently, these variations cause an increase in base shear and a decrease in displacement of target point. Besides, it can be concluded that although the base shear of structures have been increased, because of the occurred decrease in displacement value of the target point, the number of members in which the nonlinear hinges have passed the acceptance criteria are lessened. The results for control of members in passing the acceptance criteria are presented in table.5.

Table 5. Nonlinear SAP 2000 outputs for acceptance criteria of using the loading patterns

C1 structure- in X-direction					
Conditions	A-B	B-IO	IO-LS	LS-CP	CP-E<
1	571	214	62	48	1
2	565	225	63	41	2
C2 structure- in X-direction					
Conditions	A-B	B-IO	IO-LS	LS-CP	CP-E<
1	568	64	60	68	0
2	568	64	124	4	0
S1 structure- in X-direction					
Conditions	A-B	B-IO	IO-LS	LS-CP	CP-E<
1	248	40	2	0	0
2	254	35	1	0	0
C1 structure- in Y-direction					
Conditions	A-B	B-IO	IO-LS	LS-CP	CP-E<
1	629	208	12	30	17
2	648	185	22	30	11
C2 structure- in Y-direction					
Conditions	A-B	B-IO	IO-LS	LS-CP	CP-E<
1	598	54	52	56	0
2	598	54	88	20	0
S1 structure- in Y-direction					
Conditions	A-B	B-IO	IO-LS	LS-CP	CP-E<
1	249	38	3	0	0
2	256	33	1	0	0

In order to compare the types of nonlinear hinges created in the structures in the two different conditions, the hinges created on an internal frame of *C*2 structure are represented in Figs.3 (a) and 3(b).

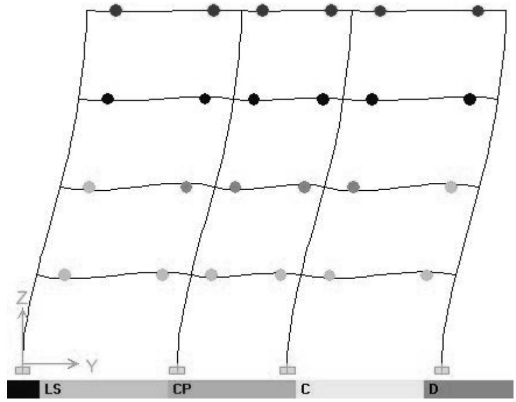

Figure 3(a). Types of nonlinear hinges without consideration of soil- structure interaction

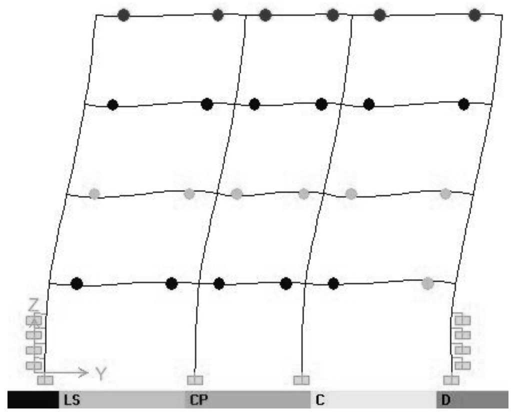

Figure 3(b). Types of nonlinear hinges with consideration of soil- structure interaction.

It is worthy of notion that although the axial forces in columns of structures, especially in S1 structure, have been increased, the final forces did not pass the acceptance criteria, therefore this increase can be treated as a more realistic behavior of structure adjacent to soil.

Finally, a comparison between the capacity curves, that is the diagram of base reaction against displacement of target point, is made for two conditions. The results demonstrate that considering the soil-structure interaction decreases the displacement of target point and increases the base shear of structure. The schematic representations of capacity curves of three structures for two different conditions are shown in Fig4.

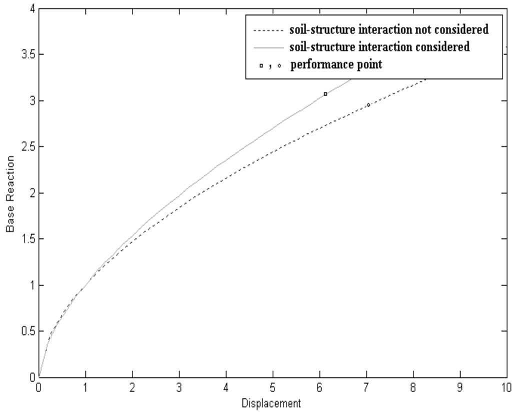

Figure 4. Comparison of capacity curves in two conditions

As it can be observed in Fig.4 although considering the soil-structure interaction increases the base shear, the efforts of structure and nonlinear hinges controlled by shape deformations will be controlled in smaller displacements and this leads to better performance in life safety performance.

7. CONCLUDING REMARKS

According to necessity of seismic retrofitting of structures especially for schools and emergency centers in seismic regions in one hand, and enormous expenses of it on the other hand, consideration of factors which impact on the structural behavior of buildings and lead to more realistic models of them seems to be crucial. The effect of soil-structure interaction is one of the aforementioned definitive factors which was modeled in the current work using the Gap elements that has no stiffness in tension. Modelling the soil around the structure enables us to control the behaviour of structure and soil simultaneously; so there will be no need for experimental calculations toward control of stress in soil, consequently.

In addition, modeling the soil surrounding the basement's walls increases the whole stiffness of structure and decreases its effective period. It also increases the coefficients of *C* which is utilized in calculation of displacement for target point and base shear of structure.

It can be inferred that in comparison to effects of *C* coefficients, the period of structure has more impact on the displacement of target point. In other words when the soil-structure interactions are considered, although the *C* coefficients have been increased and this causes an increase in forces made in some of members, because of the decrease occurred in the effective period of structure the displacement of target point have decreased. The aforementioned variations caused an improvement in structures' performance and aided the structure not to pass the acceptance criteria in life safety performance.

8. REFERENCES

[1] CSI, (2000). SAP-2000, three dimensional static and dynamic finite element analyses of the structures. Computers and Structures, Inc., Berkeley, CA

[2] FEMA,(2000). NEHRP recommended provisions for seismic regulations for new buildings. Report no. 356, Federal Emergency Management Agency, Washington D.C.

[3] Iran National Building Code, 519, 2000; Housing and Municipal Engineering Ministry.

[4] ICBO, 1997, Uniform Building Code, International Council of Building Officials, Whittier, CA

[5] T. Takeda, M.A. Sozen, N.N. Nielsen, "Reinforced Concrete Response to Simulated Earthquakes," J. Struct. Engrg. Div., ASCE, V. 96, No. 12, 1970, pp. 2257-2573

Retaining wall movements due to deep excavation in Zagreb

I. Sokolić,
Faculty of Civil Engineering Zagreb, Zagreb, Croatia

G. Plepelić
Geotehnički studio d.o.o., Zagreb, Croatia

ABSTRACT: In this paper several case studies of deep excavations in Zagreb are presented, containing the basic information of retaining structure geometry, geotechnical profile and inclinometer measurements. Horizontal displacements of the retaining structure are analyzed taking into account dimensions of the excavation pit and retaining structure, geotechnical soil profile, safety factor of base heave, stiffness of the retaining wall and stiffness of the complete retaining structure together with geotechnical anchors. The analysis has been performed according to the well established method proposed by Bjerrum & Eide 1956, Clough et al. 1989 and Clough & O'Rourke 1990. The results are compared to database of around 300 retaining walls from all over the world, summarized by Long 2001.

1. INTRODUCTION

Ground movements are of little consequence where there is nothing to be affected by them. However, in most urban locations where embedded retaining walls are likely to be installed, they can be of great importance. The decision to set particular wall deflection and ground movement limits can be of significant economic importance. The setting of appropriate limits should be considered carefully. Measurements of wall deflection and ground movement and the use of numerical analysis over recent years have improved understanding of ground behavior. The assessment of ground movements is not straightforward and much experience is required to make appropriate use of numerical analysis. It is there essential that best use is made of precedent in comparable conditions trough the use of case history data (Gaba et al. 2003).

Zagreb city, the capital of Croatia is developing very quickly in recent years and there is a constant need for more living space. One way to solve the problem leads to underground excavations. New retaining structures are installed every day to ensure stability of deep excavations and to prevent damage of nearby structures. Unfavorable cracks or even structural damage of nearby structures can occur depending on stiffness and strength of the structure and ground displacement developed during the excavation. The only way to control the displacement of retaining structure during construction is by field measurements. In recent years many retaining structures of different types in Zagreb were monitored during the excavation, using inclinometer installations inside or behind the structure (Krajnović 2005, Kralj 2004, 2005, Šilhard et al. 2002, Škacan et al. 1994, Sokolić & Vukadinović 2007, Sokolić 2008, Szavits-Nossan et al. 1999, 2009, Tomac & Marić 2006, Vukadinović 2004).

In this paper several case studies of deep excavations in Zagreb are presented, containing the basic information of retaining structure, geotechnical profile and inclinometer measurements. Horizontal displacements of the retaining structure are analyzed taking into account dimensions of the excavation pit and retaining structure, geotechnical soil profile, safety factor of basal heave, stiffness of the retaining wall and stiffness of the complete retaining structure together with geotechnical anchors.

The analysis of horizontal displacement is performed according to the well established method proposed by Bjerrum & Eide 1956, Clough et al. 1989 and Clough & O'Rourke 1990. The results are compared to database of around 300 retaining walls from all over the world, summarized by Long 2001. The database contains different types of retaining structure and soil profiles so it was necessary to isolate the data comparable with typical geotechnical soil profile in the area of Zagreb city.

2. HORIZONTAL DISPLACEMENTS OF RETAINING STRUCTURES

Widely used Semi-empirical design method for predicting horizontal displacements of retaining structures leads to the use of dimensionless base stability number defined by Bjerrum & Eide 1956 (Milligan et al. 2008). Safety factor for base heave (*FOS*) includes the critical information on excavation geometry, surcharge loading and average undrained soil strength. The equation for calculating FOS is based on 'reverse bearing capacity' analysis for base heave failure of the deep excavations of limited width:

$$FOS = \frac{N_c c_u}{\gamma D + q} \tag{1}$$

where *FOS* is safety factor for base heave, N_c bearing capacity factor c_u average undrained soil strength, γ unit weight of soil, *D* excavation depth and *q* surcharge load (Figure 1. and 2).

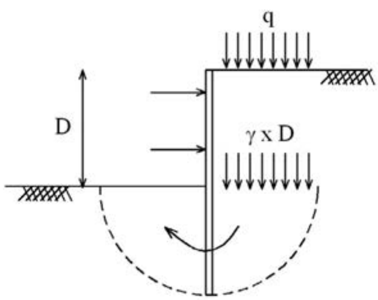

Figure 1. Failure mechanism for estimating safety factor for base heave *FOS* (Bjerrum & Eied 1956).

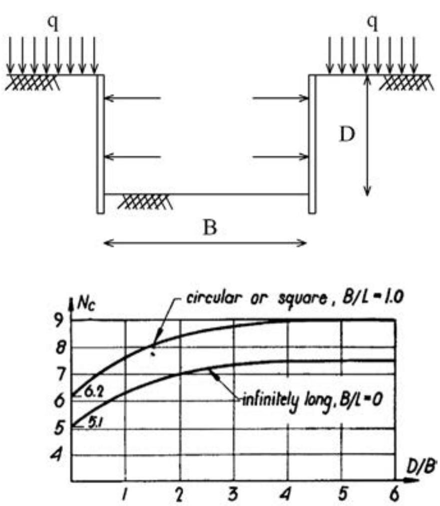

Figure 2. 'Bearing capacity' value N_c for estimating safety factor *FOS* (Bjerrum & Eied 1956).

Horizontal displacement of retaining structure depends both on soil and retaining structure stiffness. Clough et al. 1989 proposed the semi-empirical estimation of horizontal displacement, normalized to the depth of the excavation, that is taking into account both influences on the same chart (Figure 3). The stiffness of the soil is defined using base heave safety factor *FOS*. For very soft clays *FOS* takes value of approximately 1.0 and rises over 3.0 for stiff soils. The stiffness of the retaining structure include the retaining wall stiffness and horizontal support geometry. Normalized value of stiffness can be calculated using next equation:

$$\frac{EI}{\gamma_w s^4} \tag{2}$$

where *E* is Young modulus of wall material (2.5×10^7 kN/m^2 for concrete and 3×10^8 kN/m^2 for steel), *I* moment of inertia of the wall cross section, γ_w unit weight of water and *s* vertical displacement of anchor rows.

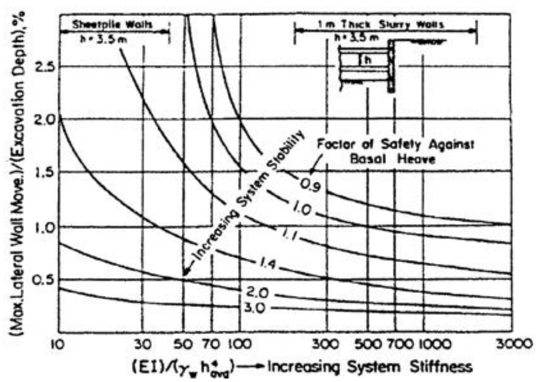

Figure 3. Semi-empirical design method for estimating horizontal wall displacement taking into account both soil and retaining structure stiffness (Clough et al. 1989).

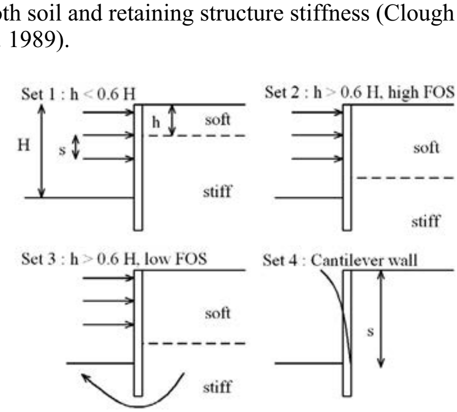

Figure 4. Soil profile classification (Long 2001).

Using the described method for estimating horizontal displacement very big database containing around 300 case histories of deep excavations all over the World was collected by Long 2001. The data was analyzed separately in four different sets of characteristic soil profiles (Figure 4.) depending on the soil stiffness and the geometry of the soil. Set 1: Case histories where the ground conditions comprise dominantly stiff/medium dense soils and the thickness of soft soil $h < 0.6H$ (Figure 6); Set 2: Situations similar to Set 1 but with $h > 0.6H$ and with a high *FOS* against excavation base heave, due to toe being embedded in a stiff stratum; Set 3. As set 2 but with a low FOS against excavation base heave; Set 4: Cantilever walls with *s* defined as retaining height plus fixity depth. The database contains the following details:

- location of the excavation pit
- type of soil
- undrained strength for cohesive material and *SPT* value for non cohesive
- total depth of the excavation *H*
- average vertical distance of support *s*
- wall type (diaphragm, secant pile, sheet pile or contiguous wall)
- wall stiffness *EI*
- support configuration (multiprop, single prop, props + berms, topdown)
- support spacing
- maximum horizontal and vertical displacement of the retaining structure
- case study reference

3. DEEP EXCAVATION IN ZAGREB

In the early nineties the population of the Zagreb city started to grow rapidly and since then the living space value is increasing continuously, especially in the central urban area. For that reason almost every new building, especially business centers, are reaching for underground space, used mostly for warehouse and parking places, to the maximum depth of nearly 20 meters.

Typical soil profile in the area of city of Zagreb is characteristic for alluvium of Sava River and consists of three dominant layers. Surface layer of low to medium stiffness formed of humus fill, low plasticity clay and sand, extending to depths of ~3.5 m. The second layer formed of alluvial deposits of loose and dense gravel, mostly mixed with clay, extending to depths of ~12.0 m. The bottom layer is stiff Pliocene clay. Underground water level at the depth of ~5.0 m varies with the season and it is mostly governed by the water level of Sava River. Usual geotechnical investigation works consist of in-situ penetration tests to determine gravel compactness and laboratory tests to determine undrained strength of stiff clay and its stiffness. The basic request for the retaining structure is to prevent the water seepage into the excavation pit which is mostly achieved with impervious diaphragm walls and sheet walls embedded in the stiff clay with low water seepage coefficient (Figure 5).

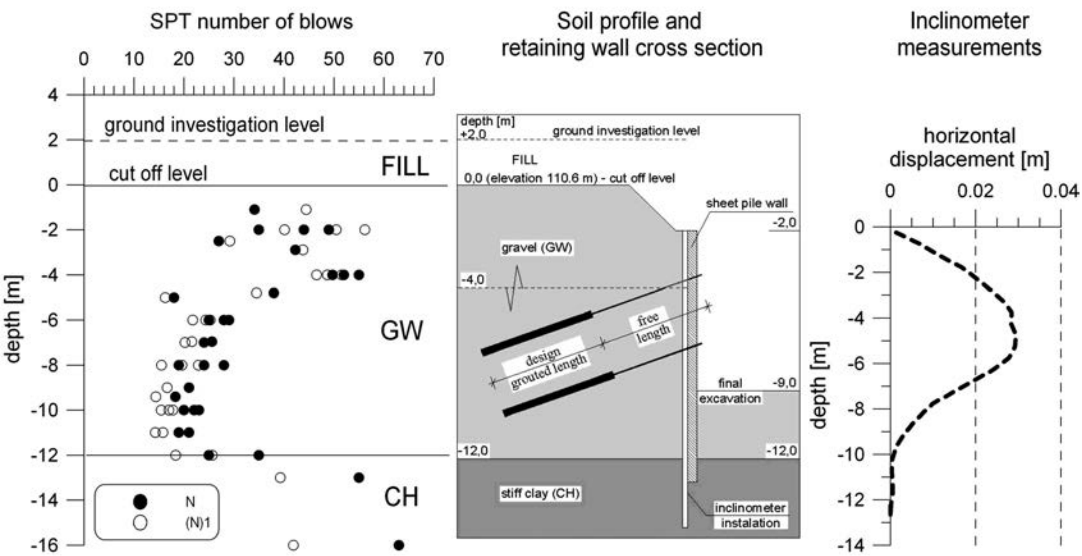

Figure 5. Characteristic of deep excavation in Zagreb

4. HORIZONTAL DISPLACEMENT OF RETAINIG WALLS IN ZAGREB

In recent years it is almost an everyday practice in Zagreb to monitor the horizontal displacement of the retaining structure by inclinometer measurements installed in the retaining wall (possible in the case of diaphragm) or behind the wall (in the case of soldier and sheet pile walls). The inclinometer consists of casing installed in the ground and the portable probe that is reading the inclination of the casing that occurs during the excavation. Adding up the incremental displacement that results from incremental inclination, from the bottom of the casing to the top, it is possible to calculate the relative horizontal displacement. To calculate the absolute horizontal displacement it is necessary to perform geodetic survey of the top of the casing.

In this paper total number of 17 case studies were analyzed based on detailed review of available national and international references containing information of deep excavation in Zagreb. For most of them the normalized horizontal displacement is evaluated for final excavation depth and for some of them also for earlier excavation phases (Table 1). The results are compared to the database summarized by Long 2001. The following assumptions were made to calculate the normalized displacement and the stiffness of the retaining structure:

- failure plane of base heave going completely through the stiff clay
- average value for undrained strength of the stiff clay c_u = 125 kN/m^2
- bearing capacity coefficient N_c = 7
- soil unit weight γ= 20 kN/m^3
- excavation depth H for normalizing the horizontal displacement equal to the distance from the top of the retaining wall to the bottom of the excavation H_w

The comparison between the case histories in Zagreb and other throughout the world is made for soil profile Set 1. which mostly suits the soil profile in Zagreb (Figure 6.)

To be able to make the best comparison of case studies in Zagreb with data summarized by Long 2001, it was necessary to search for the data where soil type is similar to the soil type typical for Zagreb, gravel & clay (Figure 7.)

The comparison was also made to the support configuration of the structure used for different retaining structure stiffness (Figure 8.)

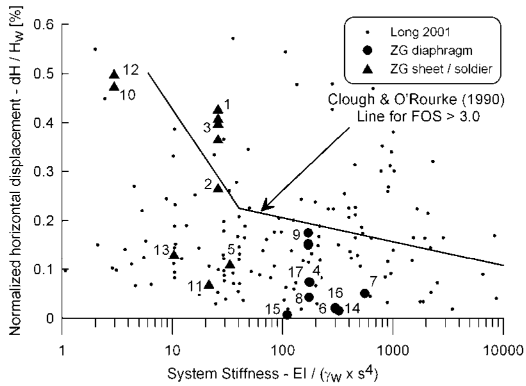

Figure 6. Set 1. data from database of deep excavation case studies all over the world summarized by Long 2001, compared with case studies in Zagreb

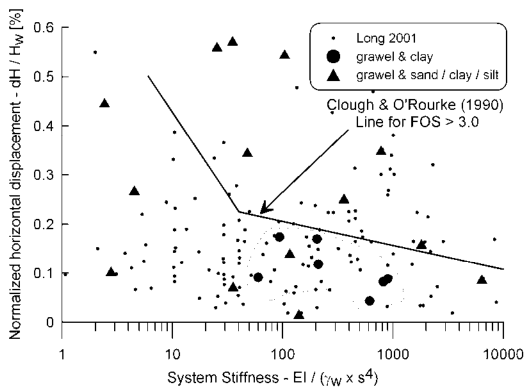

Figure 7. Set 1. data from database of deep excavation case studies all over the world summarized by Long 2001, with emphasis on the data comparable with typical soil profile of Zagreb (gravel & clay)

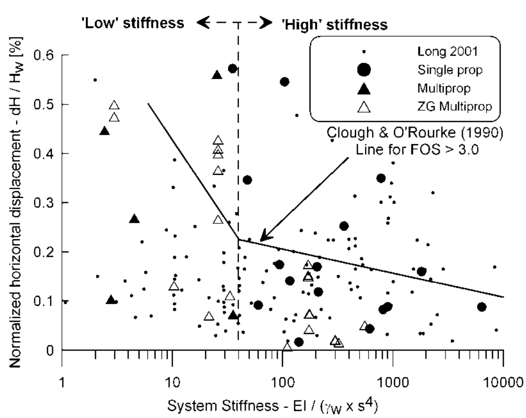

Figure 8. Set 1. data from database of deep excavation case studies all over the world summarized by Long 2001, with emphasis on the support configuration, compared with retaining walls in Zagreb

Table 1. Summary of case studies in Zagreb

wall no.	Location	GPS N-north ; E-east	H_S [m]	H_W [m]	H_E [m]	L [m]	H [m]	h_C [m]	h_W [m]	q [kN/m^2]	wall type	EI [kN/m^2]	a [ ]	s [m]	dH [mm]	dH/H_W [%]	EI/(γ_w x s^4)	FOS	References
1	PC 2000 (Radnička) - wall 1	45°48'10.86''N 16°00'12.23''E	2,0	7,0	4,0	11,0	9,0	1,0	4,5	0	Sh	21.000	2	3,0	30,0	0,43	26	5,5	Krajnović 2005., Sokolić & Vukadinović 2007
			2,0	4,5	4,0	8,5	6,5	1,0	4,5	0	Sh	21.000	2	3,0	18,0	0,40	26	8,0	
2	- wall 2		5,0	6,0	4,0	10,0	11,0	1,0	6,5	0	Sh	21.000	2	3,0	16,0	0,27	26	5,1	
			5,0	4,5	4,0	8,5	9,5	1,0	6,5	0	Sh	21.000	2	3,0	12,0	0,27	26	6,3	
3	- wall 3		1,0	10,0	4,0	14,0	11,0	1,0	6,5	0	Sh	21.000	2	3,0	41,0	0,41	26	4,2	
			1,0	6,0	4,0	10,0	7,0	1,0	6,5	0	Sh	21.000	2	3,0	22,0	0,37	26	6,7	
4	Radnička (Bunićeva) - wall 1	45°48'13.75''N 15°59'53.26''E	0,0	13,5	4,0	17,5	13,5	5,3	6,0	100	D	260.417	3	3,5	10,0	0,07	174	2,4	Szavits-Nossan et al. 2009.
5	- wall 2		2,0	9,0	2,0	11,0	11,0	3,5	3,0	120	Sh	50.000	2	3,5	10,0	0,11	33	2,7	
6	Grand cenar (Radnička)	45°48'15.98''N 15°59'44.70''E	0,0	11,5	5,6	17,1	11,5	2,5	5,7	0	D	260.417	3	3,0	1,8	0,02	322	3,8	Kralj 2005.
7	Branimir centar (Branimirova)	45°48'21.93''N 15°59'04.84''E	3,2	12,8	5,2	18,0	16,0	6,2	5,8	0	D	450.000	4	3,0	6,5	0,05	556	3,0	Šilhard et al. 2002.
8	Avenue mall (Siget)	45°46'35.53''N 15°58'43.87''E	3,0	7,0	9,0	16,0	10,0	2,0	7,0	0	D	260.417	1	3,5	3,0	0,04	174	5,1	Tomac & Marić 2006.
9	Importane Gallery (Ibler)	45°48'48.47''N 15°59'05.33''E	1,0	17,0	5,0	22,0	18,0	8,0	10,0	0	D	10.066.666	3	5,0	26,0	0,15	1611	2,5	Szavits-Nossan et al. 1999.
			1,0	10,0	5,0	15,0	11,0	8,0	10,0	0	D	10.066.666	3	5,0	15,0	0,15	1611	4,2	
			1,0	4,0	5,0	9,0	5,0	8,0	10,0	0	D	10.066.666	3	5,0	7,0	0,18	1611	9,7	
10	Euroherc (Almerija) - wall 1	45°48'08.01''N 16°00'44.48''E	2,3	4,0	2,0	6,0	6,3	0	6,3	0	So	8.367	3	4,1	19,0	0,48	3	8,5	Vukadinović 2004. Kralj 2004.
11	- wall 2		1,0	7,1	1,9	9,0	8,1	0	8,1	0	So	8.367	3	2,5	5,0	0,07	21	5,8	
12	- wall 3		2,3	4,0	2,0	6,0	6,3	0	6,3	0	So	8.367	3	4,1	50,0	1,25	3	8,5	
13	- wall 4		0,9	6,1	2,0	8,1	7,0	0	7,0	0	So	8.367	3	3,0	8,0	0,13	10	6,7	
14	Importane center (Esplanade)	45°48'19.22''N 15°58'37.50''E	0,0	13,7	5,2	18,9	13,7	6,2	7,0	0	D	450.000	3	3,5	3,0	0,02	300	3,2	Škacan et a. 1994.
15	Dubrava market (Dubrava)	45°49'52.34''N 16°03'24.27''E	0,0	14,2	8,8	23,0	14,2	13,5	8,0	0	D	450.000	3	4,5	1,0	0,01	110	3,1	Tomac & Marić 2006.
16	Agram Genera (Holjevćeva)	45°47'38.51''N 15°58'47.59''E	2,7	10,2	6,8	17,0	12,9	5,2	6,6	0	D	450.000	2	3,5	2,0	0,02	300	3,8	Tomac & Marić 2006.
17	Eurotower (Humboltova)	45°47'57.62''N 15°58'10.98''E	0,0	15,0	5,0	20,0	15,0	10,0	7,2	0	D	450.000	3	4,0	11,0	0,07	176	2,9	Tomac & Marić 2006.

H_S [m] - denivelation from the ground surface to the top of the retainig wall (slope hight); **H_W** [m] - denivelation from the top of the retaining wall to the final excavation;
H_E [m] - embedded length of the retainig wall; **L** [m] - total length of the retaining wall L = H_W+ H_S ; **H** [m] - total depth of the excavation pit H = H_S+ H_W; q [kN/m^2] - surcharge load;
h_C [m] - tickness of the clay layer at the back of the wall; **h_W** [m] - underground water level depth; **E** [kN/m2] - Young modulus of the retaining wall; **I** [kN/m4] - moment of inertia of the retainig wall cross section; **EI** [kNm2]- stiffness of the retainig wall; **a** - number of anchor rowes; **s** [m] - average anchor rowe distance; **dH** [mm] - maximum horizontal displacement of the retaining wall; **dH/H** [%] - normalized horizontal displacement of the retaining wall; **γ_w** [kN/m3] - unit weight of water; **EI/(γ_w x s^4)** - normalized retainig structure stiffness;
FOS - safety factor for basal heave (Nc = 7, cu = 125); **D** - diaphragm wall; **Sh** - sheet pile wall; **So** - solider pile wall; **GPS** - Global Positioning System coordinate

5. DISCUSSION

Looking at the range of horizontal displacement proposed by Clough et al. 1989 it can be seen that usual values for stiff soils with FOS above 3.0 are less than 0.5 % ($dH / H < 0.5\%$). Calculated values of FOS for case histories in Zagreb are in the range from 2.4 – 9.7 depending on the type of the wall and geometry of the retaining structure, especially on the embedded length of the wall. 'Low stiffness' structures, such as sheet pile walls and soldier walls, reach the $FOS \approx 6.0$ while 'high stiffness' structures, diaphragm walls, reach $FOS \approx 3.0$. Those values are expected to be even higher in reality because minimum value of the 'bearing capacity' N_c =7.0 is used for calculation of *FOS*, average undrained strength of the stiff clay is used considering that the failure plane of base heave goes completely through the stiff clay but usually it goes manly through the gravel with higher strength.

Comparing the results of horizontal displacement from case histories in Zagreb it can be seen that for calculated *FOS* the data are matching the range proposed by Clough et al. 1989 very well (Figure 6.) Comparing them to the data summarized by Long 2001 we can conclude that the soil profile typical for Zagreb corresponds to the Set 1. soil profile proposed by Long 2001. As the safety factor *FOS* is even higher than 3.0 the values are mostly below the proposed line for $FOS = 3.0$ as expected. There are only two retaining structures above the expected line, case history 1. and 3. which can be due to low global safety factor for temporary sheet pile wall (F_s =1.2), and due to self -boring geotechnical anchors used that require some initial displacement to achieve support force (Krajnović 2005, Sokolić & Vukadinović 2007, Sokolić 2008). It is evident from Figure 6. that the 'low stiffness' retaining structures (sheet pile walls and soldier pile walls) develop higher values of horizontal displacement while the 'high stiffness' structures develop small displacements and the trend is similar as proposed by Clough et al. 1989. Horizontal displacement of diaphragm walls in Zagreb, marked with circle dots on the Figure 6, fall mostly well below the line for $FOS = 3.0$, which is also below the data from other case histories with similar soil profile and soil type typical for river alluvium, gravel & clay (case histories from Salzburg, Paris, Geneva, Dusseldorf, Duisburg etc, are marked with circle dots on Figure 7, falling within the shadowed area). As the safety factor of those structures is around $FOS = 3.0$ the difference can be due to some other influence such as very high stiffness of the anchor used or even due to inclinometer measurement error, because the measured displacement are very small (around 3.0 mm), barely above the accuracy of the inclinometer probe.

Final stiffness of the anchors depends not only on the quality of the steel used but also on the type of the anchor and its geometry. Geometry characteristic can be very dominant in the case of big excavation where the upper anchors are used to locally stabilize the upper part of the structure but do not contribute to the global safety of the complete structure. The influence of anchor stiffness is not included in the normalized retaining structure stiffness proposed by Clough et al. 1989. but it can affect the horizontal displacement as we can see by comparing the case histories no. 1, 2 and 3 with no. 5. They are situated in almost the same ground conditions, only 400 m away, they both consist of sheet pile wall with almost the same normalized stiffness (in the logarithm scale, Figure 6.) but the horizontal displacement of the case histories no. 1, 2 and 3 are around two times higher than in no. 5. In the first case the 'short' pre stressed self boring anchors are used while in the second case 'long' pre stressed geotechnical anchors are used (Szavits et al. 2009, Krajnović 2005).

One of the influences that affect the horizontal displacement of the retaining structure is also number of support rows used. On the Figure 8, an emphasis is made on the support configuration used for different stiffness of the structure. It can be seen from the database summarized by Long 2001. that usually for 'low stiffness' structures (below ~ 40) only single prop is used while for 'high stiffness' structures multi props are used. This is not the case in Zagreb where almost always multi props are used not depending on the stiffness of the structure. It should be noted that the comparison is made for the similar sol types and similar soil profiles.

One of the great advantages of the method used is that we can predict final displacement of the structure if we have information of the displacement in some excavation stage. If we look at the case histories no. 1, 2, 3, and 9., we can see that the data for different excavation phase fall almost at the point in the normalized diagram. For example for case history no. 9 the normalized displacement value $dH/h_w \approx 0.15$ for excavation depth in the range of 4 to 17 meters.

6. CONCLUSION

Typical soil profile for Zagreb can be classified as Set 1 type according to Long (2001) classification.

Generally the results of horizontal displacement of the retaining structures fall within the area proposed by Clough & O'Rourke (1990) which means that proposed diagram can be used for safe design of retaining structures in typical Zagreb soil profile.

Looking at the diaphragm displacements it seems that the structures in Zagreb are little bit more rigid than usually.

Looking at the same retaining structure in different excavation phases, almost the same point appears in the diagram for different excavation depths and for corresponding maximum horizontal displacement. So it is possible to predict the final displacements if displacements in some excavation phases are known.

The efficiency of the pre stressed geotechnical anchor to minimize the wall displacement, over the nail-anchor is evident.

The presented methodology of horizontal displacement analysis seems to be very useful to accumulate the experience for future design.

7. REFERENCES

Bjerrum, L. & Eide, O. 1956. Stability of Strutted Excavation in Clay, *Géotechnique,* Vol. 6, pp. 32-47.

Claugh, G.W., Smith, E.M. & Sweeney, B.P. 1989. Movement control of excavation support system by iterative design. *Proc. ASCE Found. Enging. Current Principles and Practice.* Vol. 2, ASCE, New York, pp. 869-884.

Clough, G.W. & O'Rourke, T.D. 1990. Construction induced movements of insitu walls. *Proc., ASCE Conf. on Design and Performance of Earth Retaining Sructures, Goetechnical Special Publication No. 25, ASCE, New York,* pp. 439-470.

Gaba, A.R., Simpson, B., Powrie, W. & Beadman, D.R. 2003. Embedded retainig walls – guidance for economic design, *CIRIA Report C580, London*

Gill, S.A. & Lukas, R.G. 1990. Ground movement adjacent to braced cuts. *Proc., ASCE Conf. on Design and Performance of Earth Retaining Sructures, Goetechnical Special Publication No. 25, ASCE, New York,* pp. 471-488.

Krajnović, D. 2005. Poslovni centar 2000, Građevina za zaštitu građevinske jame. *Glavni projekt zaštite građevne jame, Geotehnički studio d.o.o., Zagreb, Croatia.*(in Croatian)

Kralj, N. 2004. Almeria, zaštita građevne jame. *Inklinometarska mjerenja, završni izvještaj, Geo-Eko d.o.o., Zagreb, Croatia* (in Croatian)

Kralj, N. 2005. Oskulatacije građevne jame Grand centar. *Završno izvješće o mjerenju. Geotehnički studio d.o.o., Zagreb, Croatia.*

Long, M. 2001. Database for Retaining Wall and Ground Movements due to Deep Excavations. *Journal of Geotechnical and Geoenvironmental Engineering,* Vol. 127, No. 3, pp. 203-224.

Milligan, G.W.E., John, H.D.ST. & O'Rourke, T.D. 2008, Contribution to *Géotechnique* 1948-2008: Retaining structures. *Géotechnique,* Vol. 58, No. 5, pp. 377-383.

Šilhard, V., Verić, F. & Ivšić, T. 2002. Protection of deep excavation for the ''Branimir'' Center. *3rd Cunference of the Croatian Society for Soil Mechanics and Foundation Engineering, Geotechnics trough Eurocode 7, Hvar, Croatia,* pp. 415-422. (in Croatian)

Šilhard, V., Ivšić, T. & Kovačević, M. 2002. Monitoring of displacement of diaphragm wall and adjacent buildings during excavation of deep construction pit in Zagreb. *3rd Cunference of the Croatian Society for Soil Mechanics and Foundation Engineering, Geotechnics trough Eurocode 7, Hvar, Croatia,* pp. 423-430. (in Croatian)

Škacan, B., Verić, F. & Szavits-Nossan, A. 1994. Retaining structure for the open excavation of Esplanade center. *Geotehnika prometnih građevina, Novigrad, Croatia,* Vol. 1, pp. 479-489. (in Croatian)

Sokolić, I. & Vukadinović B. 2007. Soil parameter analysis based on inclinometer measurements of sheet pile displacement. *14th European Conference on Soil Mechanics and Geotechnical Engineering, Madrid,* Vol. 4, pp. 665-670.

Sokolić I. 2008. Sheet pile wall analysis by computer program Plaxis using different constitutive models for soil. *International Geotechnical Conference Development of Urban Areas and Geotechnical Engineering, Saint Petersburg,* Vol. 1, pp. 331-336.

Szavits-Nossan, A., Kovačević, M.S. & Szavits-Nossan, V. 1999. Modeling of an anchored diaphragm wall. *Proc. Interntl. FLAC Symposium on Numerical Modeling in Geomechanics: FLAC and Numerical Modeling in Geomechanics*. Minneapolis, pp. 451-458.

Szavits-Nossan, A., Sokolić, I. & Plepelić, G. 2009. Design of anchored retaining structures by numerical modeling, *17th International Conference on Soil Mechanics & Geotechnical Engineering, Alexandria, Egypt.* Vol. 3.

Tomac, I. & Marić, B. 2006.. Deep excavation case histories in the city of Zagreb. 13th Danube-European conference on getechnical engineering, Lubljana, Slovenia, pp. 515-519.

Vukadinović, B. 2004. Zaštita građevne jame, Poslovno trgovački kompleks *Almeria*, *Glavni projekt zaštite iskopa, Geotehnički studio d.o.o.*

About dimensional ratios of elements in protection of construction pits

B. Soldo
University of Zagreb, Faculty of Geotechnical Engineering

A.A. Aniskin, M. Oreskovic
Polytechnic in Varaždin, Study of Civil Engineering

ABSTRACT: One of the most complex typical geotechnical works in urban areas are construction pits. The complexity of their performance depends on the characteristics of the underground environment and pit sizes. Construction or design and execution of construction pits needs to be adjusted to the conditions at the site. Unwanted situations can sometimes occur due to unforeseen influences. This paper deals with the most sensitive issues in connection with construction pits. More precisely, it deals with dimensional ratio of penetration depth of the cantilever sheet pile in the construction pit and the length of the anchor. The paper also contains the commentary on the constructing of protection for the construction pit where unwanted consequences ensued, i.e., there was damage of the surrounding, neighbouring buildings.

1. INTRODUCTION

Cantilever sheet pile walls stabilized by being placed far below the planned bottom of the pit and by anchoring in the sides of the construction pit, are often used as protection for construction pits. The very problem lies in the fact that behind the sheet pile wall material causes lateral pressure. Often the question is what the depth of penetration of the sheet pile wall is and what the length of anchors in a stable zone is. Due to inadequate size of developed location, there exists the possibility of damages or even destruction of the construction pit protection.

It is known that during mid-18th century the French engineer Charles Coulomb dealt with the amount of lateral load acting on the retaining wall. Nowadays his discoveries are applied in everyday engineering practice, and are also essential for designing sheet pile walls with anchors. The situation is even more complex due to the fact that presently many buildings are built with construction pits, especially those near or next to already existing buildings. Certain methods of embedment of the wall below the bottom of the construction pit will be displayed in the section that follows, as well as the required length of anchors required for the embarkation of the pit in a stable zone.

2. METHODS OF DETERMINATION OF WALL EMBEDMENT DEPTH

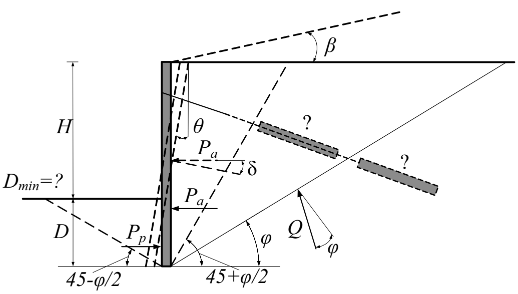

Figure 1. Selection of location and depth of anchoring

There are three most common methods of determining the minimum depth of sheet pile wall penetration (D): FMM - Factored Moment Method, FSM - Factored Strength Method, NPPM - Net Passive Pressure Method. Inflection point, i.e. the minimum depth D_{min} can be obtained from the equalization of moments of force of active pressure and passive pressure:

$$M_a = M_p,$$

$$\frac{\gamma \cdot (H+D)^2}{2} \cdot K_a \cdot \frac{H+D}{3} = \frac{\gamma \cdot D^2}{2} \cdot K_p \cdot \frac{D}{3},$$

$$D = \frac{H}{\sqrt[3]{\frac{K_p}{K_a} - 1}}$$

With the FSM method, the safety factor used for the friction angle is usually 1.25, while the FMM and NPPM methods use $\varphi = \varphi_d$. With the NPPM method, the safety factor used is $(FS)_r$ = 1,5, i.e. $M_a = 1/1{,}5 \cdot M_p$ and the distribution of stress differs. With the FMM method the taken safety factor is $(FS)_p = 2$, i.e. $M_a = 1/2 \cdot M_p$. To calculate the active pressure and passive pressure, we will use Coulomb's expressions for the calculation of the active pressure coefficient (K_a) and passive pressure (K_p), which depend on angles $\delta, \theta, \varphi, \beta$. By inserting the known values in the given expressions we get the minimum penetration depth D of the wall. The result of comparing the ratio floor height H and the minimum penetration depth D of the wall obtained by all three methods in the function of the friction angle is the graph shown in Figure 2.

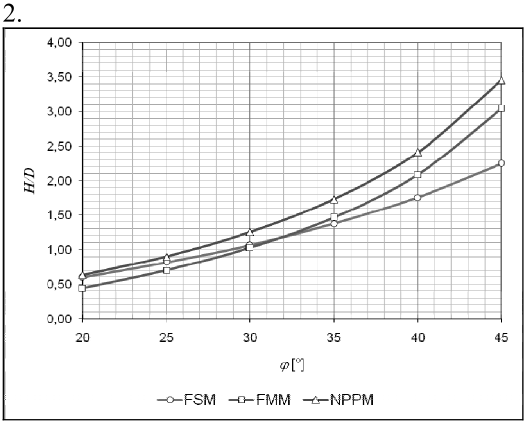

Figure 2. Graph of the variation of H / D using the soil friction angle φ (FSM, FMM, NPPM)

The graph shows that the NPPM method results in the largest ratio of H / D. The FMM method is the safest one for soil with the friction angle φ of 20° to 30°, while the FSM method is the safest for the soil friction angle of 30° to 45°.

3. ABOUT ANCHOR LENGTH IN NON-COHERENT SOIL

Higher loads and heights of sheet pile walls lead to landslides and deformation of cantilever sheet pile walls. In order to avoid this, we use anchors. The question is, what is length of anchors?

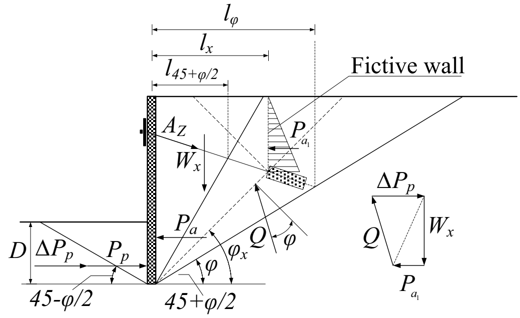

Figure 3. The force polygon

For our case we shall use the situation as shown in Figure 3 above, anchoring on the section between the active surface pressure 45 + φ/2 and deep failure surface at angle φ. We can see that the anchoring section is located in the zone of active pressure. Active pressure P_{a1} is formed behind the fictive wall, which needs to be equated with the passive pressure ΔP_p. In this case the soil can slide over the surface shown in Figure 3 using the dotted line, i.e, creeping is possible on surfaces at angle greater than φ.

Furthermore, looking at the situation without the anchor, we compare the two force polygons as shown in Figure 4. The first force polygon is the force for the active wedge acting as failure surface, and the other is the force polygon of the deep failure surface at angle φ. We see that the weight of the wedge of the deep failure surface is in equilibrium with the friction on the failure surface, while this is not true for the failure surface 45 + φ/2. Therefore, we can conclude that all the surfaces at an angle greater than φ are not in balance with the force of friction on the surface.

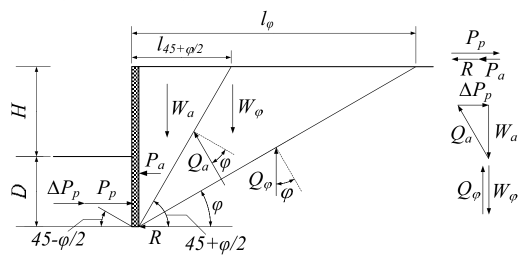

Figure 4. Polygon force for the failure surface 45 + φ/2 and φ

As a result, the additional passive pressure ΔP_p is activated, which returns the system to the state of equilibrium. Wall rotation occurs if the potential of passive pressure P_p is used. That proves that the anchor section needs to be performed behind the section of the deep failure surface at the angle φ. If the anchor section is performed in the active zone, in front of the deep failure surface, the soil behind the wall crawls along with the anchor and results in deformation of the wall. To annul this, we need to perform the anchor in a stable zone of angle φ. This conclusion is confirmed by the DIN standard.

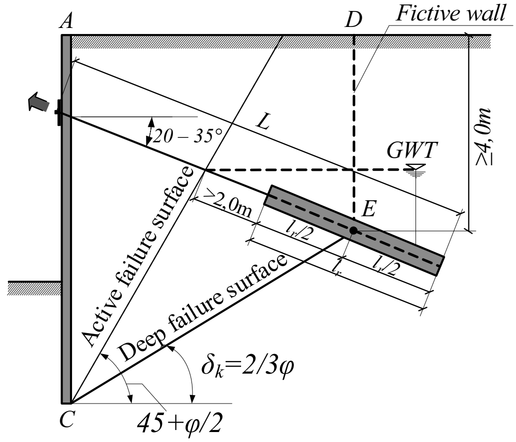

Figure 5. Recommended length of anchors designed according to DIN standard.

The DIN standard advocates safety, assuming deep failure surface at an angle of $\delta = 2/3 \cdot \varphi$.

In coherent soil, in expressions for P_a and P_p cohesion is present. Cohesion contributes to the reduction of active pressure, and increases passive pressure. The contribution of cohesion should also be taken with care, especially when it comes to strain, time and conditions of effectiveness.

Additional load on the protection of the construction pit is the load in the pit surroundings, as well as loads due to groundwater. If load is present at the upper portion of the construction pit, which is most often the case in practice, active pressure demands additional individual calculation.

Flow of water in the soil occurs due to the difference of levelling of the groundwater in the construction pit. According to Darcy's law, we can describe this using the equation $v=k \cdot i$. Prolonged flow of water in the soil leads to flushing of small particles, i.e. granulometry of the soil changes. Coefficient of permeability depends on soil granulometry and may be obtained from the relation $k=1000 \cdot D_{10}^2$ (m/day) (estimation of permeability). Flushing of small particles increases the coefficient k, and consequently the current velocity v of water through the soil. It also increases the potential for ground settlement, which reflects adversely on the buildings around the building pit. There are also problems with the disturbance of pressure in the soil, i.e. the active pressure increases and the passive pressure is reduced. The expressions for specific gravity take the following forms: in case of active pressure $\gamma'' = \gamma' + i \cdot \gamma_w$ and in case of the passive pressure $\gamma'' = \gamma' - i \cdot \gamma_w$, which is a very unfavorable situation. In such a case, determining the penetration depth of sheet pile wall and the length of the anchors is often a very delicate matter.

Example from practice: construction of buildings with underground floors, i.e. where protection of the construction pit with a sheet pile wall was needed. After some time, significant cracks appeared in the surrounding buildings and the foundations far removed from the construction pit as shown in Figure 6.

A lot can be said about the origination of significant damage of buildings surrounding construction pits. The most important ones were discussed in this paper. The basic determination to be made is to distinguish the influence of static equilibrium in relation to deformities. Furthermore, special attention needs to be paid to additional impactful effects such as water, filtering through the soil and active duration of certain specific situations.

4. CONCLUSION

This text is of primarily engineering character. Its intention is to show that some purely technical oversights and mistakes can occur in construction, as evidenced in literature, but also in practice. The paper gives emphasis to the boundary angle between stable and unstable zones. Boundary stability and instability of a zone is where mistakes can occur; sometimes without any consequences, but when it comes to distortion effects, unwanted consequences may occur - especially when it comes to ground water, its depth of embedment and stability boundary zones. Such situations must not be underestimated in designing stages.

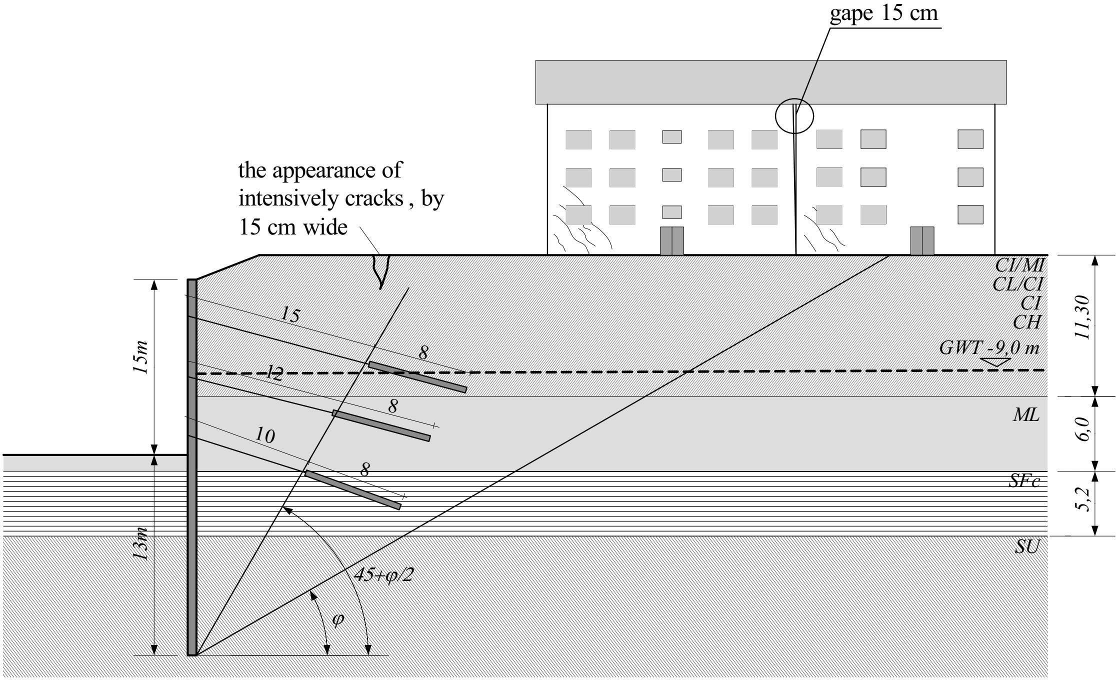

Figure 6. Example from practice, schematic view

LITERATURE

Budhu M. 2000. Soil Mechanics and Foundations, University of Arizona, Department of Civil Engineering & Engineering Mechanics, John Wiley & sons, Inc., New York, N.Y.

Muhovec, I., Soldo, B. 2009. Coulomb´s Unintentional Risk, Faculty of Geotechnical Engineering, University of Zagreb, Varaždin.

Soldo, B., Muhovec, I., 2009. Nadvještačenje, Izvori rizika u geotehničkim zahvatima, Osijek.

Tsytovich, N.A. 1983. Soil mechanics, fourth edition, adapted and supplemented, MOSCOW HIGH SCHOOL, Moscow.

Seelye, E. E. 1956. Foundations – Design and Practice, John Wiley & sons, Inc., New York, N. Y.

Das, B. M. 2008. Fundamentals of Geotechnical Engineering, sixth edition, Thomson Learning, UK.

Spigolon, J. S. 2001. The McGraw-Hill Civil Engineering PE Exam Depth Guide, first edition, McGraw – Hill.

Smoltczyk, U. 2002. Geotechnical Engineering Handbook, Ernst & Sohn - A Wiley Company, Berlin.

Dörken, W., Dehne, E. 2005. Baugruben und Gräben, Spundwände und Verankerungen, Böschungs- und Geländebruch, 2. neu bearbeitete Auflage, Werner Verlag, Duesseldorf.

Perau, E., Haubrichs, K. 2006. Numerische Berechnungen zum Nachweis der Standsicherheit tiefer Baugruben, ELE, Erdbaulaboratorium Essen, Essen.

Improved soils

Settlements of silos founded on compressible soils reinforced by stone columns

R. Bahar, O. Sadaoui
Laboratoire de Géomatériaux, Environnement et Aménagement, Université Mouloud Mammeri de Tizi-Ouzou, Tizi-Ouzou, Algérie

E. Vincens
Université de Lyon, Laboratoire de Tribologie et Dynamique des systèmes, Ecole Centrale de Lyon, France

ABSTRACT: This paper deals with an analysis of observed settlement of a battery of ten steel silos founded on compressible soils reinforced by stone columns. The geotechnical survey shows a succession of sedimentary layers of silts and muddy silty sands up to 30 m of depth, under consolidated, characterized by a low bearing capacity and a high compressibility, which require improvement. The settlements measured over 545 days are analysed and discussed. The settlement evolution indicates that 50 % of the total settlements are reached over the first six months of the structure exploitation. Some problems are observed on the foundation raft starting from a differential settlement of about 7 cm, corresponding to 1/400 of the silo diameter.

1. INTRODUCTION

The deposits of fine grained soft and compressible soils (clays, muds...) or loose sands resulting from the recent alluvial deposits are frequent in the valleys, around the rivers and in littoral coast. In Algeria, with a rapid pace of industrialization, structures have been designed and constructed on these soils. Therefore, reinforcement of these types of soils to increase the bearing capacity and to reduce settlement and potential liquefaction before structures are constructed is frequently required. Various methods are available to stabilize these soils. Stone columns is one technique of soil reinforcement which is frequently used in soft cohesive soils (Dhouib and Blondeau , 2005)

The stone columns technique was used for the improvement of the soils of the harbour zone in Béjaia town, located at about 250 km east of Algiers in Algeria (Bahar and Sadaoui, 2008; Sadaoui, 2007). This paper deals with an analysis of observed settlement, measured over 545 days, of silos founded on compressible soils reinforced by stone columns.

2. SITE CONDITIONS AND DESCRIPTION OF THE PROJECT

2.1. Geological and geotechnical conditions

The city of Bejaia was clinging to the slopes of Gouraya mountain, then spread southward across the plain. The plain covers an area of approximately 750 hectares. This area had not experienced in the past urban development due to various risks highlighted by hydraulic and geotechnical studies conducted in the region. The low bearing capacity of the soil and its high compressibility and the risk of flooding from the river Soummam are among these risks and are a constraint on urbanization and require reasonable accommodation to limit the damage.

The plain consists of sedimentary soil deposits of Quaternary age. The geologic formations found in the region are (Roth, 1950):

- Old alluvia: they are represented by marl gravel, pebble and sand enveloped in silt matrix.
- Swamp alluvia: they consist of fine elements represented by silt and mud with intercalations of fine sand.
- Recent Alluvia: The deposits are slightly muddy and cover the most of the plain.
- Fill: These embankments are not compact, except in the first meter, they are composed of heterogeneous soil represented by gravelly clay with a presence of few blocks.

The geological history indicates that the port area extending the alluvial plain is composed of fine materials (silt, clay) more or less muddy and sand deposited in bedrock encountered at approximately 30 to 50 m depth.

Many geotechnical surveys are carried out in the region to evaluate the resistance of soils and their degree of constructability. It appears that the surface layers of alluvial nature, predominantly sandy clayey and sometimes heterogeneous have not yet reached a sufficient degree of consolidation, therefore their bearing capacity is low and their compressibility is high. These soil conditions require their improvement for heavy construction works. Soil substitution and pile foundations are not always the best solutions, in terms of technical and economical, to solve the stability problems of foundations. Several cases of structures founded on shallow foundations in the harbor area of Bajaia have suffered damages: collapse of oil tanks of Sonatrach Company, settlement of abutment Bridge of Saghir river (Sonatrach, 1991, 2004).

The geotechnical investigation consisted of achieving three borings to 36 m depth and twelve heavy dynamic penetrometer tests to 12 m depth. This investigation shows a succession of sedimentary layers of silts and muddy silty sands up to 30 m of depth, under-consolidated, characterized by a low bearing capacity and a high compressibility, then encounters a layer of plastic marl (Fig. 1). The level of groundwater was observed 2 m depth below the ground level. All soil studies conducted in the immediate vicinity of the project confirm this lithology. Pressuremeter tests conducted in the immediate vicinity of the site were then used (Fig. 2).

The physical and mechanical properties are summarized in Figures 1 and 2. The sedimentary layers of silts and muddy silty sands are characterized by a void ratio varying between 1,0 and 1,30 and a compressibility index C_c varying between 0,37 and 0,54. These results indicate clearly the soft nature of the soils and their high compressibility. The dynamic penetrometer tests showed some horizontal homogeneity of the alluvial formation. The lower values of the dynamic resistance are 0,80 to 1,0 MPa on the first twelve meters. From this depth the dynamic resistances vary between 10 and 15 MPa. The limit pressures measured from pressuremeter tests on the first twelve meters vary between 0,10 and 0,46 MPa.

2.2. Silos of ECI factory

The structure is localised at the harbour zone in Bejaia city. It consists on a battery of ten steel silos of circular cross-section, arranged in two rows (Figs. 3 and 4). It was constructed for the storage of cereals which have a total capacity of 76000 tons. The height of each silo is 27 m and the diameter 23 m. The dimensions of raft foundation are 51x122 m^2 and 0.70 m thick.

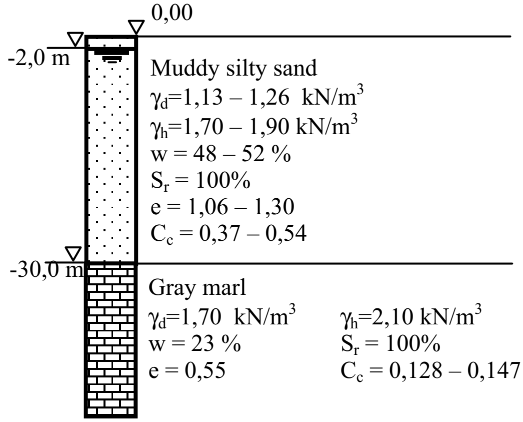

Figure 1. Typical soil profile.

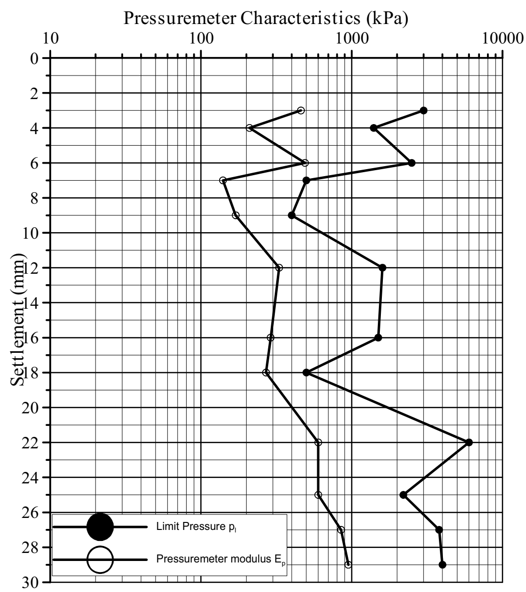

Figure 2. Pressuremeter characteristics.

Figure 3. Silos view.

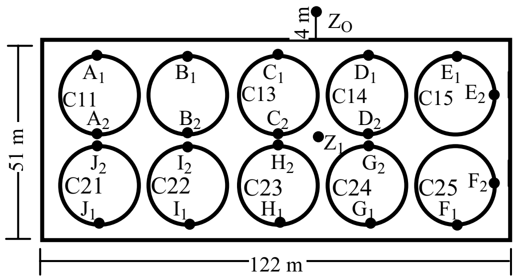

Figure 4. Schematic plan of the silos.

2.3. Bearing capacity and settlements

At the design stage, bearing capacity and settlement analyses were carried out for the silos. For an anchoring of the foundation raft of 1,50 m, the allowable bearing capacity estimated from the different test results is variable, the most unfavorable is estimated to 110 kPa. The oedometer method was used to estimate the settlements. For an allowable bearing capacity of 120 kPa, the consolidation settlements of 40 m thick of alluvial layers are estimated to 160 cm. These results are not tolerable. Therefore, there is need a deep foundations or to carry out the improvement of the soils. The experience already gained in previous projects realized in the harbor area of Bejaia made that the project owner opted to improve the soils by stone columns. This choice is also justified by the cost of execution compared to deep foundations, the local availability of substitute material (ballast) and timeliness of the process.

2.4. Soil improvement

The large raft is anchored on 12 m reinforced soil by stone columns. This depth has been reached on the basis of the dynamic penetrometer tests which have given the dynamic resistance, $R_{p,}$ varying from 10 to 15 MPa from 12 m depth (layer of fine dense sand). The stone columns have an average diameter of 1 m and a length of 12 m. The diameter of 1 m was verified after stripping of the column test conducted near the site. The mesh really made in the field is regular and rectangular, 5.80 m ^{2} (2,39 x 2,43). These dimensions represent respectively the space between the stone columns in the transverse and longitudinal. The total number of columns made on the area of 5871 m ^{2} is 1100 columns and the approximate volume of rolled ballast used is estimated to 10400 m $^{3.}$

The settlement calculation after soil improvement is performed by the Priebe method (Priebe, 1995). After improvement, the total settlement calculated for allowable bearing capacity of 130 kPa is 58,30 cm. However, the settlement calculated for a mesh size (1,80x1,80 m $^{2)}$ and a depth of stone columns of 30 m under allowable bearing capacity of 140 KPa is 27 cm. The same results are obtained using the homogenization method.

For verification of the design and certification of stability and serviceability, a load test on a single stone column was performed according to standards by the company responsible for carrying out the work under the supervision of an authorized body and the owner of the work. The load settlement behaviour of the improved ground as observed for single column tests is presented in Figure 5. The measured settlement is less then 10 mm for a maximum load of 375 kN, corresponding to 1,5 ultimate state limit.

Twenty heavy dynamic penetrometer tests were carried out on stone columns in order to determine their mechanical properties according to the requirements of the DTU 13-2, 1978. The analysis results showed that only 25% of tests gave a dynamic resistance above 15 MPa from 1 m depth. 75% of tests give dynamic resistance varying between 3 and 9 MPa between 2 and 4 m depth. This is probably due to the deviation stems outside of the columns or the crossing of very soft layers which offer no resistance to lateral ballast. Some tests are characterized by refusal surface because of the blocking on coarse elements of the ballast. Under the regulations rules, these results are not conclusive.

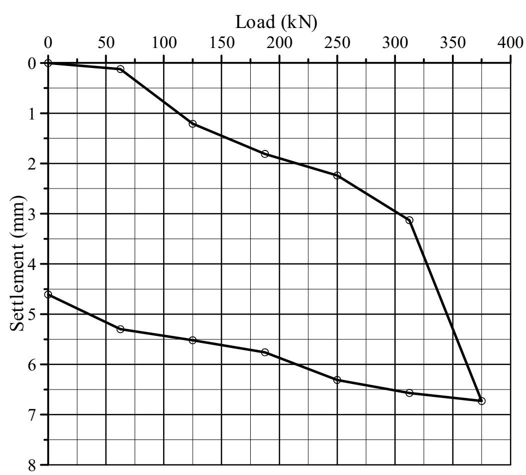

Figure 5. Results of a single stone column load test.

3. MONITORING INSTRUMENTATION

For verification of the design and the stability of the silos during the cereal storage, the structure was monitored to evaluate vertical settlement. The settlements were made by tacheometric aimings on twenty fixed reflective targets (points A1, B1, C1, D1, E2,……. given in Figure 4). Four stations (ST1 to ST4) were located on the site. The stations are installed sufficiently far from the silos to avoid the influence of the loading of the silos and vibration devices. To avoid possible relative movements of the stations, they were fixed on reinforced concrete caissons isolated by polystyrene. The reflectors were fixed on both outer edges and central part of the silos to the same initial side elevation (Z_{ref}=12,138 m). The condition surveys are conducted in accordance with the general loading and unloading of the silos. The observations were made on 545 days from 01/09/2005 to 01/03/2007. Two independent stations, Z_0 and Z_1 are also located respectively outside and on the center of the raft (Fig. 4).

4. MEASUREMENT RESULTS

Figure 6 shows an example of loading of the silos in time recorded on 545 days of assessment. The distribution of foundation settlements in time for some measuring points (B1, B2, E1, E2 G1 and G2) is shown in Figures 7 and 8. Figure 9 shows the settlements against the silo load at points G1 and G2. Figures 10 and 11 show the silo loads and their corresponding settlements respectively at 01/03/2007. Figure 12 shows a distribution profile settlements in the longitudinal direction (A2 - E2).

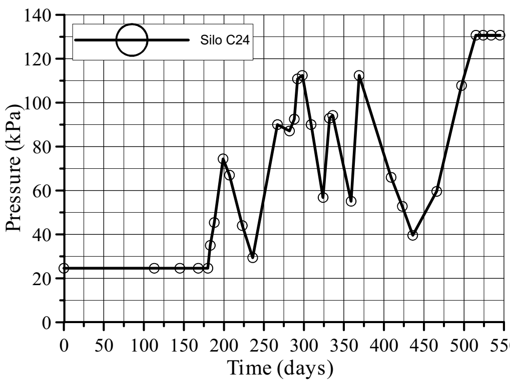

Figure 6. Loading of the Silo C24 from 01/09/2005 to 01/03/2007.

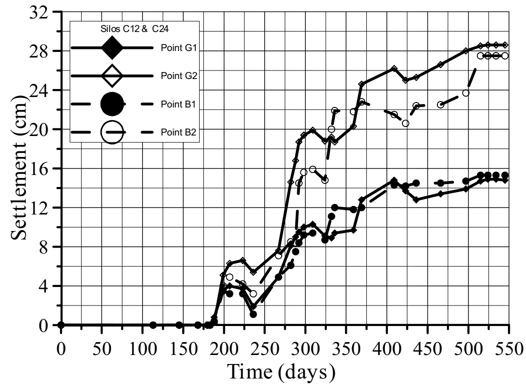

Figure 7. Settlements at points G1, G2, B1, and B2 from 01/09/2005 to 01/03/2007.

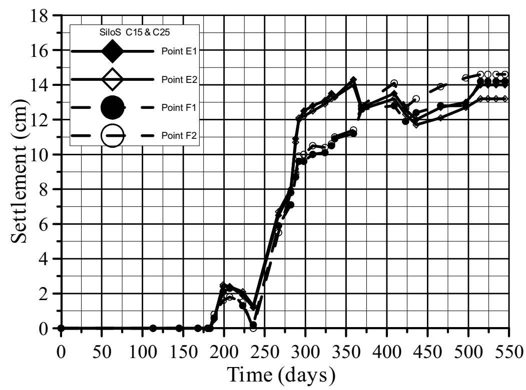

Figure 8. Settlements at points E1, E2, F1, and F2 from 01/09/2005 to 01/03/2007.

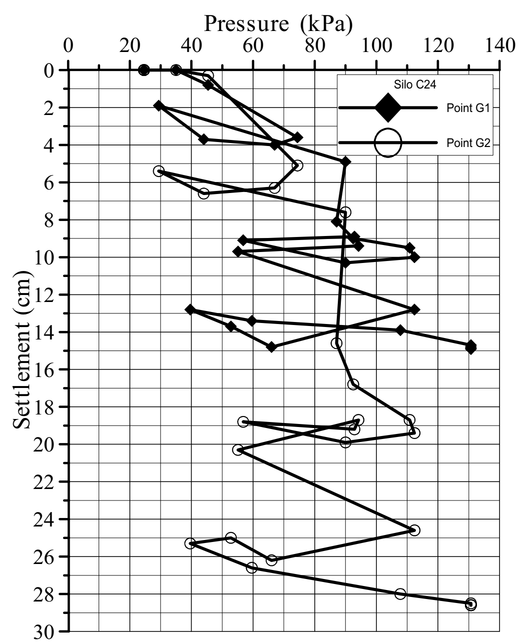

Figure 9. Settlements at points G1 and G2.

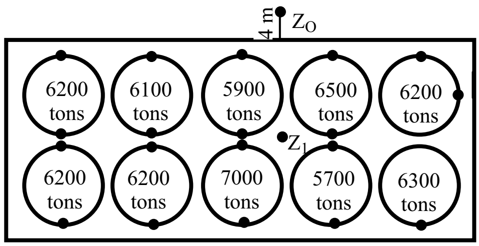

Figure 10. Loading of the silos in tons at 01/03/2007.

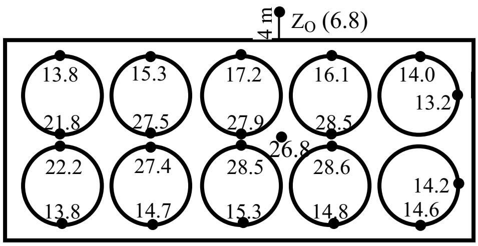

Figure 11. Settlements in (cm) at 01/03/2007.

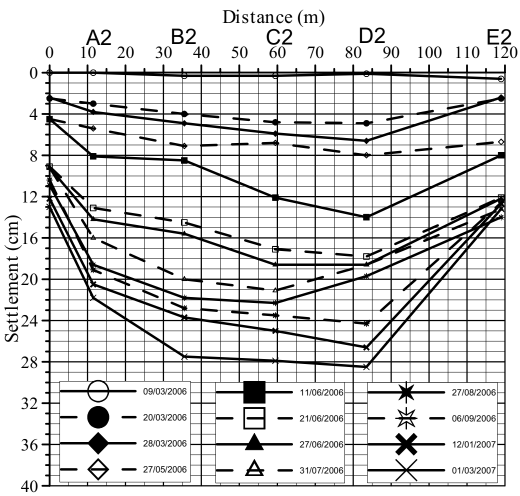

Figure 12. Settlement profiles during loading stages (profile A2-E2).

The analysis of measured settlements permitted the following observations:

- During the first five months of loading and unloading of the silos, the foundation settlements developed rapidly to about 15-20 cm on the center of the raft and to 7-13 cm on the edges of the raft. The maximum differential settlement is 10, 80 cm which is measured in the silo C23 (between H1 and H2). The differential settlement occurred is prejudicial to the stability of the structure that the first signs of tilting and deformations at the base of the silos began to appear at the central area (silos C13, C14, C23 and C24).

- The loading evolution to a value of 130 kPa and maintained constant during one month generated a total settlement of 28 cm in the central area and 17 cm at the edges. The differential settlement is about 11 to 13,80 cm between center and periphery of the raft.

- The examination of the deformation distribution of the raft in the transverse and longitudinal direction clearly shows the bending of the raft in the two directions. The indices of excessive settlements appear on site by observed deflection, the change of the slope of the cover raft toward the central part, important deflection of the road, cracks and tilting of the silos particularly the silos C13, C14, C23 and C24 (Figs 13, 14, 15 and 16).

Figure 13. Observed cracks on the raft.

Figure 14. Observed cracks and deflection of the road.

Figure 15 : Observed settlement at the edge of the raft.

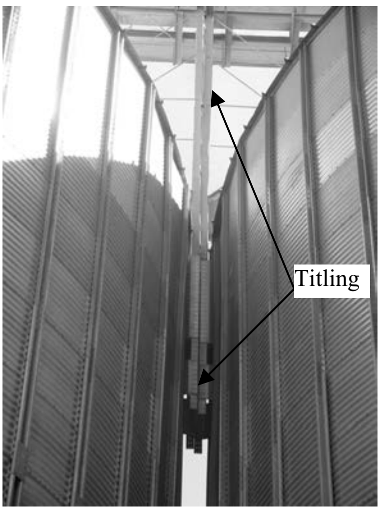

Figure 16. Titling of the silos.

- The soil improvement has done only under the raft; it was arrested at the edge of the raft. The difference in behavior between the two areas, virgin soil (outwards of the raft) and improvement soil (under of the raft) supported the development of the differential settlements. The measured settlement at point Z_0 located at 4 m from the edge of the raft is about 7 cm.

- The maximum total settlement measured at the center of the raft is 28 cm. This result is obtained for loading varying from 24.60 to 130 kPa. The settlement tends to stabilize because it is stationary for a month of observation with a constant loading. However, regarding to floating stone columns, it is necessary to understand the consolidation settlement of compressible layer that lies between the base of the stone columns and the marl bedrock (18 to 23 m thick). The settlement obtained by the method of Priebe for a stress of 130 KPa is 58,30 cm, with 14,60 cm obtained in the treated layer . This result seems reasonable owing to the fact that the in-depth influence of the raft foundation and a settlement of untreated layer will appear in the long term.

5. CONCLUSIONS

The settlements of a battery of ten steel silos measured over 545 days are excessive. Some problems (cracks, tilting, deflection,…) are observed on the foundation raft starting from a differential settlement of about 7 cm, corresponding to about 1/400 of the silo diameter. The settlement evolutions indicate that fifty percent of the total settlements are reached over the first five months of the structure exploitation. These observations show a lack of the geotechnical survey carried out at the design stage leading to under estimate the thickness of the soil reinforcement. Moreover, the realization of only one single stone column load test cannot validate a design method.

REFERENCES

Bahar, R. & Sadaoui O. 2008. Analyse des tassements de silos fondés sur des sols compressibles renforcées par des colonnes ballastées : cas de la zone portuaire de Béjaia. *International Conference on Geotechnical Engineering. Hammamet.* Tunisie, 139-148.

Dhouib, A. & Blondeau, F. 2005. Colonnes ballastées. *Edition Presses des Ponts et Chaussées.* Paris.

Documents Techniques Unifiés (DTU n° 13.2), 1978. Fondations profondes : colonnes ballastées. Paris.

Priebe, H.J. 1995. The design of vibro replacement. Ground Engineering*, Keller Grundbau GmbH:* 31-37.

Roth, J.P. 1950. Les séismes de Kherrata et la sismicité de l'Algérie. *Bulletin de service de la carte géologique de l'Algérie* n° 3.

Sonatrach, 1991. Documents techniques sur les bacs de stockage et étude de sol pour la reprise en sous œuvre des bacs R13, R21 et C9, *Document interne de Sonatrach TRC Béjaia.*

Sonatrach, 2004. Rapport sur les relevés des affaissements des bacs de stockage confortés. *Document interne de Sonatrach TRC Béjaia*

Sadaoui, O. (2007). Tassements de silos sur des sols compressibles renforcés par des colonnes ballastées. *Mémoire de magister, Université de Béjaia.*

Analysis of the consolidation influence in a strutted excavation in soft soil reinforced with a jet-grout base slab

J.L. Borges, R.P. Pinto
Department of Civil Engineering, Faculty of Engineering, University of Porto, Porto, Portugal

ABSTRACT: One possible solution to improve stability against bottom heave failure in strutted excavation in soft soils consists of extending the wall below the excavation base and, before excavation, constructing a jet-grout slab to support the wall below the excavation level. Using a computer code based on the finite element method, the consolidation effect on a strutted excavation in soft soil reinforced with a base jet-grout slab is analysed. The numerical model incorporates the Biot consolidation theory (coupled analysis) with soil constitutive relations simulated by the p-q-θ critical state model. Special emphasis is given to the analysis, during and after the construction period, of the pore pressures, stress levels and displacements in the ground, as well as strut compression loads, wall displacements and bending moments, earth pressures on the wall faces and compression loads and bending moments on the *jet-grout* slab.

1. INTRODUCTION

Several solutions can be used in practice to improve stability against bottom heave failure in strutted excavation in soft soils. One solution consists of extending the wall below the excavation base, usually down into a stronger stratum (hard stratum). In this case, in simple terms, earth pressure on the wall, below the excavation bottom, is transferred to the hard stratum and to the lower strut levels. However, in practical terms, this solution may not be practicable if the hard stratum lies deeply. If this is the case, one possible solution consists of extending the wall a few meters below the excavation base and, before excavation, constructing a jet-grout slab to support the wall below the excavation level. The retaining wall can be founded, for instance, on steel piles extended to the hard stratum.

Another pertinent question is the excess pore pressure generation during excavation and its dissipation after that period (consolidation). After construction, there are pore pressure gradients in the ground that determine a consolidation process. This process is dependent on both the magnitude of excess pore pressure at the end of excavation and the long-term equilibrium conditions regard to pore pressure.

In the paper, the consolidation effect on a strutted excavation in soft soil is analysed using a computer code, developed by Borges (1995), based on the finite element method. A base jet-grout slab is considered in order to improve stability against bottom heave failure and minimize wall displacements.

Basically, for the present applications, the finite element program uses the following features: a) plane strain conditions; b) coupled formulation of the flow and equilibrium equations with soil constitutive relations formulated in effective stresses (Biot consolidation theory) (Borges, 1995; Lewis and Schrefler, 1987; Britto and Gunn, 1987), applied to all phases of the problem, both during excavation and in the post-construction period; c) utilisation of the p-q-θ critical state model (Borges, 1995; Lewis and Schrefler, 1987), an associated plastic flow model, to simulate constitutive behaviour of soil; d) use of the 2D elastic linear model to simulate constitutive behaviour of the wall (reinforced concrete) and of the jet-grout slab; e) utilisation of the 1D elastic linear model to simulate the constitutive behaviour of the struts; f) use of joint elements with elastic perfectly plastic behaviour to simulate the soil-wall and soil-slab interfaces.

2. DESCRIPTION OF THE PROBLEM

The problem concerns a 10 m deep excavation with width of 12 m (Fig. 1). The retaining structure consists of a 0.7 m thick diaphragm wall of reinforced concrete with length of 12.5 m (2.5 m below the excavation base). Three steel strut levels are considered at depths of 1 m, 4 m and 7 m. The excavation is carried out in a total time of 25 days at a uniform rate. In order to increase stability against bottom heave failure and minimize the wall displacements, a 1.3 m thick jet-grout slab is included (constructed by secant columns) to support the wall below the excavation base (Fig. 1). Due to hydraulic reasons, “dissipation holes” in the jet-grout slab (see Fig. 1b) are constructed after excavation in order to avoid long-term over-pressures on the lower face of the slab. Therefore, it is assumed that, after the end of excavation, the water flows through the “dissipation holes”, being pumped within the excavated area. This corresponds to define the boundary condition of pore pressure on the lower face of the slab equal to 13 kPa (considering the unit weight of water equal to 10 kN/m^3 and that the thickness of the slab is 1.3 m).

The ground consists of a 30 m thick soft clay overlying a “hard stratum”. The water table is at the ground surface.

Circular steel tubes, spaced of 2.5 m in the horizontal direction, are used for the struts. Their cross sectional area is indicated in Fig. 1.

Fig. 2 shows the finite element mesh of the problem. Two types of the six-noded triangular element are considered: (i) the coupled element, for the clay elements where consolidation is considered; (ii) the non-coupled element, for the wall and jet-grout slab elements, considered as “impermeable”. All six nodes of the coupled element have displacement degrees of freedom while only the three vertice nodes have excess pore pressure degrees of freedom. The six nodes of a non-coupled element have only displacement degrees of freedom.

The struts are modeled with three-noded bar elements with linear elastic behaviour. Six-noded joint element (three nodes at each face) with elastic perfectly plastic behaviour are used to simulate the soil-wall and soil-slab interfaces. Since the jet-grout slab is constructed after the wall and there is no liaison (continuity) between them, joint elements are also considered for slab-wall interfaces, supposing that a fine portion of soil remains between these two materials.

Regarding the boundary conditions, no horizontal displacement is allowed on the vertical boundaries of the mesh while the bottom boundary is completely fixed in both the vertical and horizontal directions. The left vertical boundary corresponds to the symmetry line of the problem. In hydraulic terms, it is assumed that, in the supported side, the water level remains on the ground surface (which is a conservative and simplified assumption and presupposes that there is a flow that provides water to the ground) and, in the excavated side, the water level coincides, at each stage of excavation, with the excavation base (which means that the water, inside the excavated area, is assumed to be pumped). A fully coupled analysis is performed both during and after the excavation period.

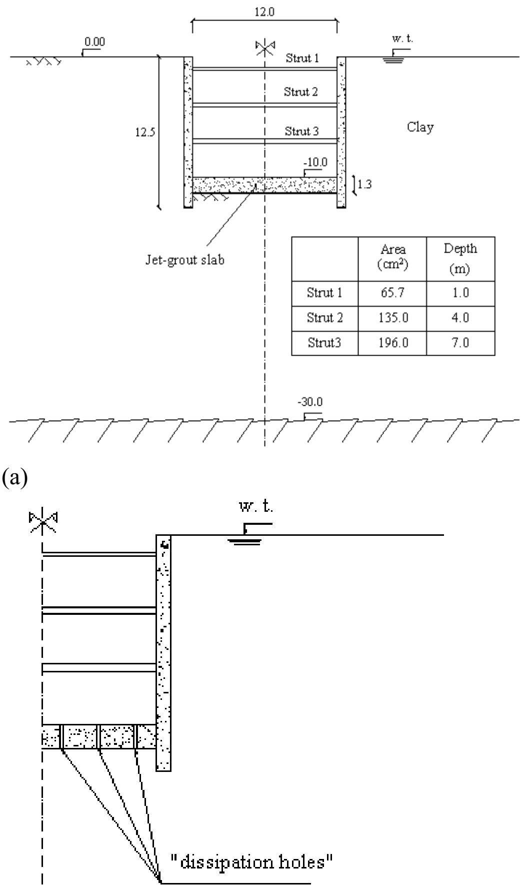

Figure 1. (a) Cross section of the strutted excavation; (b) “dissipation holes” holes” in the jet-grout slab.

The constitutive behaviour of the clay is modeled by the p-q-θ critical state model (Borges, 1995; Lewis and Schrefler, 1987). The values of its parameters are indicated in Table 1 (λ, slope of normal consolidation line and critical state line; k, slope of swelling and recompression line; Γ, specific volume of soil on the critical state line at mean normal stress equal to 1 kPa; N, specific volume of normally consolidated soil at mean normal stress equal to 1 kPa; ϕ', angle of friction defined in effective terms). Table 2 shows other geotechnical properties of the clay: γ, unit weight; ν', Poisson's ratio for drained loading; k_h and k_v, coefficients of permeability in horizontal and vertical directions; K_0, at rest earth pressure coefficient; OCR, over-consolidation ratio. The values adopted for the clay are similar to those used by Finno *et al* (1991) regarding an excavation in soft soils constructed in Chicago, USA.

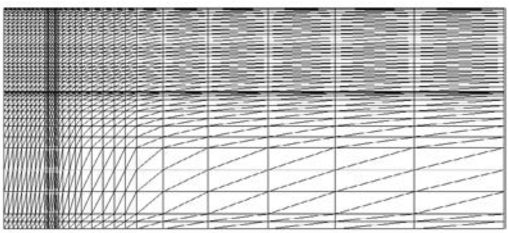

Figure 2 – Finite element mesh.

Table 1. Parameters the p-q-θ critical state model.

	λ	κ	N	Γ	ϕ' (º)
CLAY	0.18	0.025	3.158	3.05	26

Table 2. Geotechnical properties of the soil.

	γ (kN/m³)	K_0	OCR	ν′	k_x=k_y (m/s)
CLAY	16	0.5	1.0	0.25	10^{-9}

The reinforced concrete wall is modeled as an isotropic elastic material with a Young's modulus (E) of 18 GPa and a Poisson's ratio (ν) of 0.2. The isotropic elastic model is also considered for the jet-grout slab, adopting values of 150 MPa and 0.2 for E and ν, respectively.

The one-dimensional isotropic elastic model is used in the strut simulation, with a Young's modulus of 206 GPa for the steel. However, due to the difference usually observed in practice between theoretical and effective stiffnesses, the later was considered equal to half the theoretical stiffness, as suggested by O'Rourke (1992).

The soil-wall interfaces are modeled with joint elements with elastic perfectly plastic behaviour defined in total stresses. Taking into account the results of laboratorial tests performed by Fernandes (1983), the soil-wall interface strength was considered equal to the shear strength of the soft soil. To define the elastic tangential modulus of the interface, it was supposed that a tangential displacement of 1 mm is reached when shear strength is mobilised, also based on what Fernandes (1983) proposed.

3. ANALYSIS OF RESULTS

3.1. Construction period

Figures 3 shows results of excess pore pressure at several stages during excavation. Excess pore pressure is defined as the difference between pore pressure at a particular instant and its initial hydrostatic value.

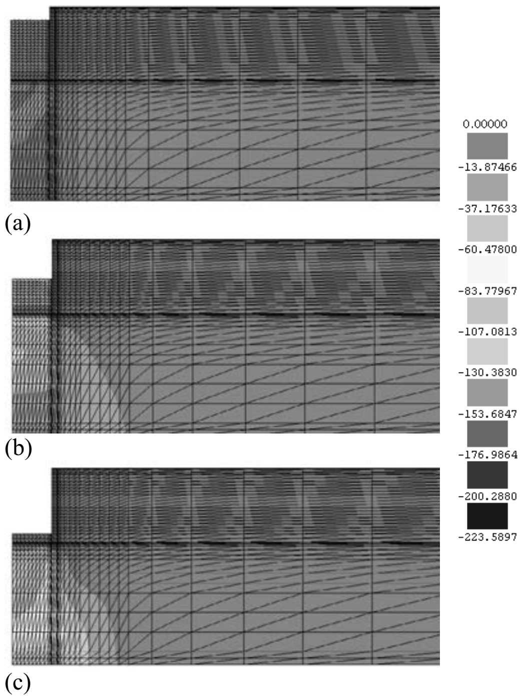

Figure 3. Excess pore pressure during excavation: a) 2 m excavated; b) 6 m excavated; c) 10 m excavated (end of excavation).

These results show that negative values are generated during excavation, increasing as excavation progresses, as expected. Highest absolute value of excess pore pressure occurs below the excavation base near the left boundary (symmetry line). This is explained by the highest decrease of total mean stress associated to the excavation, which occurs in that zone. On the supported side of the ground, a tendency of generating negative excess pore pressure is also observed, although with lower values than on the excavated side. This is explained not only by the lower decrease of total mean stress on that side (because there is no excavation on the supported side) but also by the presence of the wall and, mainly, of the base slab, which decisively contributes to avoid a ground decompression with similar magnitude to that on the excavated side. Below the wall tip, this effect does not take place and consequently higher absolute values of excess pore pressure are observed on the supported side.

Principal effective stresses at the end of excavation are shown in Figure 4. Rotations of the principal stress directions on both sides of the wall, mainly below the wall tip, can be observed in this figure, which means that large shear stresses (deviatoric stresses) occur on those zones.

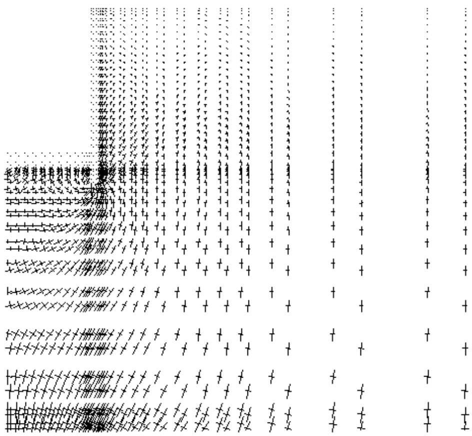

Figure 4. Principal effective stresses at the end of excavation.

Figure 5 shows distributions of stress level, *SL*, in the ground at several stages during excavation. *SL* measures the proximity to the soil critical state. In normally consolidated soils, *SL* varies from zero to 1, the latter being the critical state level. In overconsolidated soils, because of the peak strength behaviour, stress level may be higher than 1.

Figure 5 shows that *SL* significantly increases during excavation, which is basically related with the increase of deviatoric stress. At the end of excavation, stress level takes values close to 1, below the wall tip on both sides of the wall. Lower values of *SL* are observed above the wall tip on both sides of the wall, which corroborates the roll of the jet-grout slab in the stability improvement against bottom heave failure.

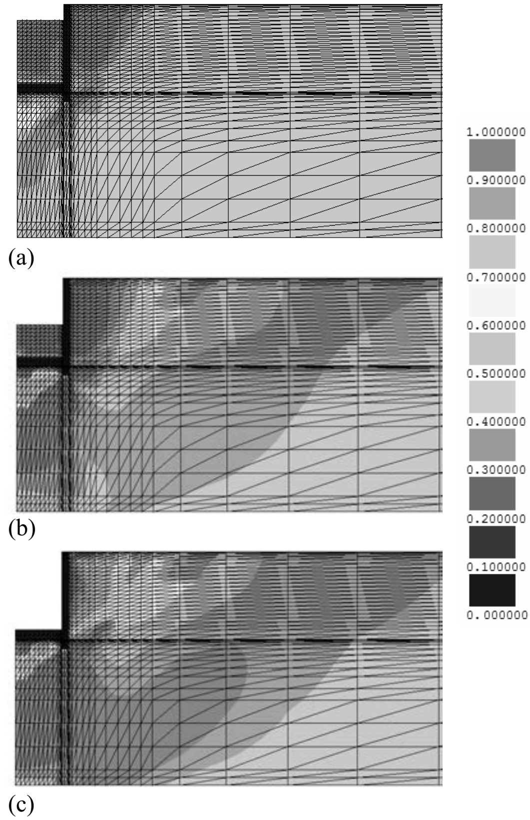

Figure 5. Stress level during excavation: a) 2 m excavated; b) 6 m excavated; c) 10 m excavated (end of excavation).

Wall horizontal displacements at several stages during excavation are shown in Figure 6. Unlike what usually happens in strutted excavations without a base slab, Figure 6 shows that the displacements decrease with depth at all stages of construction; i.e., the maximum horizontal displacement takes place on the top of the wall. This behaviour is obviously due to the base slab support.

Settlements on the ground surface, on the supported side, are shown in Figure 7, for several depths of excavation. These results show that the maximum settlement takes place close to the wall, and another local maximum occurs approximately 20 m away from the wall. It should be noted that, as said above, the wall-soil interface reaches its shear strength for 1 mm of tangential displacement, which explains that high settlements may occur on that interface, as observed in Figure 7.

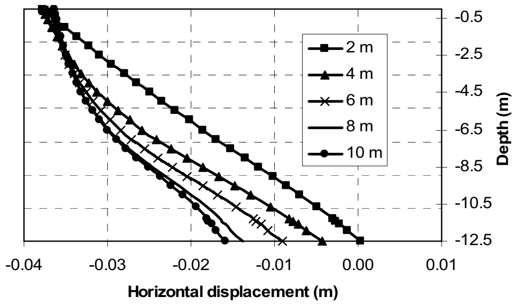

Figure 6. Wall horizontal displacements at several depths of excavation.

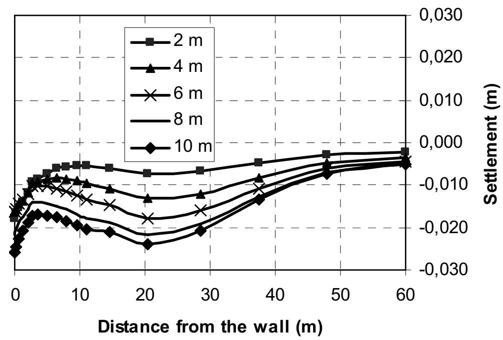

Figure 7. Settlements on ground surface at several depths of excavation.

Figure 8 shows the excavation bottom vertical displacements (on the upper face of the jet-grout slab) for several depths of excavation. These results show that upward displacements are higher on the left boundary (middle of the slab), reaching a value of 11.28 cm at the end of excavation. Near the wall, upward displacements are smaller, which is justified by the tangential stress mobilized on the soil-wall interface. However, this stress does not impede that high values are also reached on that zone (approximately 9 cm), since the strength of the interface is mobilized for a small value of 1 mm of tangential displacement, as said above.

Strut compression loads for several stages of excavation are illustrated in Figure 9. Compression load of 1st strut level increases with excavation until 2nd strut level is installed. After that, its compression load decreases. Similar effect is observed on the 2nd strut level, i.e. its compression load also increases with excavation, decreasing after 3rd strut level is installed. The decreasing effect is more expressive on the 1st level than on the 2nd level.

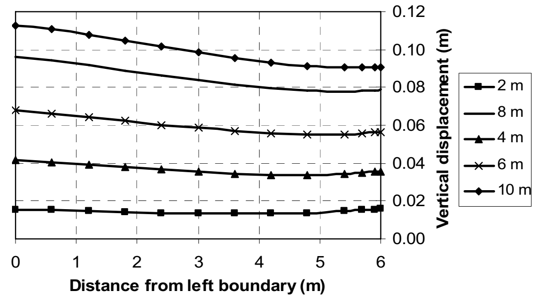

Figure 8. Excavation bottom heave for several depths of excavation.

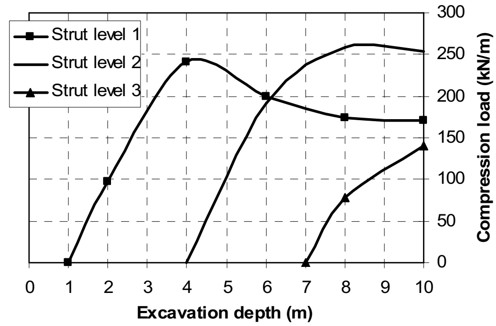

Figure 9. Strut compression loads during excavation.

Bending moment diagrams in the wall at several stages of construction are illustrated in Figure 10. These results show that near the excavation base the sign of the bending moment changes, which is explained by the base slab support that works as a kind of a fixed support. Below excavation base, bending moment increases with excavation whereas above that level the evolution is different, i.e. the maximum value is reached at 6 m of excavation and reduces after that. This reduction is determined by the installation of the 3rd strut level at 7 m of depth.

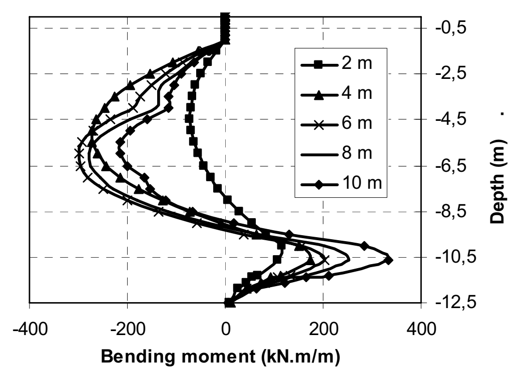

Figure 10. Bending moment in the wall at several stages of excavation.

Compression loads in the jet-grout slab are illustrated in Figure 11. This figure shows that compression load increases as excavation progresses, as expected, and does not significantly vary along the slab at each stage.

Bending moment diagrams in the jet-grout slab are shown in Figure 12. These results illustrate that bending moments also increase with excavation and are higher at the slab extremities.

It should be noted that, at the end of excavation, highest values of compression load and bending moment are applied near the extremities of the slab, which implies that the minimum and maximum values of compression stress on the most unfavorable cross section (extremity of the slab) are 56.06 kPa (lower fiber) and 857.14 kPa (upper fiber) respectively; the latter is significantly smaller than the jet-grout strength values usually reported in bibliography for this kind of soils. If that was not the case, or traction stress was detected on the jet-grout slab, the slab thickness should be enlarged in design.

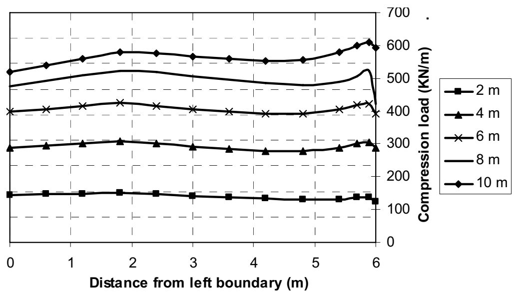

Figure 11. Compression loads in the jet-grout slab at several stages of excavation.

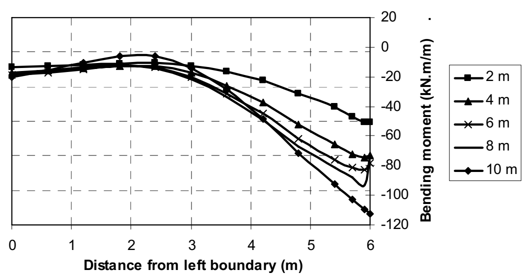

Figure 12. Bending moment in the jet-grout slab at several depths of excavation

3.2. Post-construction period

After construction, the behaviour of the problem is globally determined by the consolidation process associated to the dissipation of the excess pore pressure gradients generated during construction. Therefore a transient water flow takes place in time until hydrodynamic equilibrium is reached. In this case, the long term hydrodynamic equilibrium is determined by the difference of the hydraulic load of 10 m caused by the water table lowering on the excavated side.

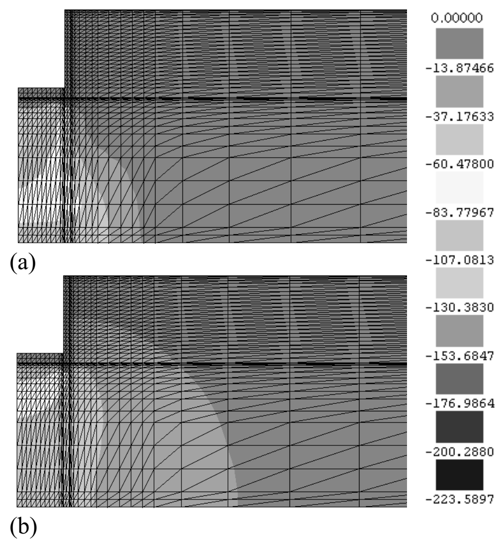

Figure 13. Excess pore pressure at: a) end of construction; b) end of consolidation.

Figure 13 shows results of excess pore pressure at the end of excavation and at the end of consolidation (long term behaviour). It should be noted that, as said above, excess pore pressure is considered herein (as defined in the computer code) the difference between pore pressure at a particular instant and its initial hydrostatic value (before excavation), and not its final value at the end of consolidation. With the consolidation, the most significant variations are observed on the excavated side where water pressure increases (reduction of the absolute value of excess pore pressure). On the supported side, the evolution is contrary, although with low magnitude: there is a small increase of the absolute value of excess pore pressure which correspond to reduction of the water pressure (which is related with downward water flow), especially below the excavation base level. At the end of consolidation, very typical shapes of isovalue curves of excess pore pressure are observed. These curves are normal to the flow lines of the steady flow reached at end of consolidation (determined, as said, by the 10 m lowering of the water table on the excavated side).

After construction, stress level (Figure 14) increases on the excavated side below the excavation bottom which is due to the reduction of mean effective stress on that zone, whereas on the supported side the contrary effect is observed: stress level decreases, since mean effective stress increases.

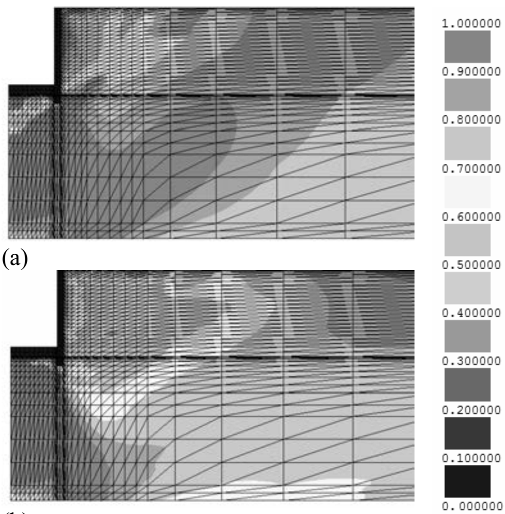

Figure 14. Stress levels at: a) end of construction; b) end of consolidation.

Diagrams of earth pressure (total horizontal stress, i.e. sum of pore pressure and horizontal effective stress) on both faces of the wall at ends of excavation and consolidation are shown in Figure 15 (pressure on the excavated face is illustrated with negative sign). A large increase of earth pressure is observed during consolidation on the excavated face. This is due to the swelling effect of the soil (associated to the decrease of mean effective stress, as seen above) as consolidation takes place in that zone. The soil swelling is partially impeded by the wall in the horizontal direction, which increases the earth pressure on the wall face.

On the supported side, above the excavation level, a small decrease of earth pressure is observed. This fact is justified by an effect contrary to what happens on the excavated side; i.e., as seen above, an increase of effective mean stress occurs with consolidation on the supported side, which provokes reduction of the soil volume and therefore decrease of earth pressure on the wall.

In overall terms, wall horizontal displacements do not change significantly with the consolidation, as shown in Figure 16. The most expressive variation is observed below depth of 9 m, where displacements reduce with consolidation. This effect is explained by the increase of earth pressure on the excavated face, as mentioned above.

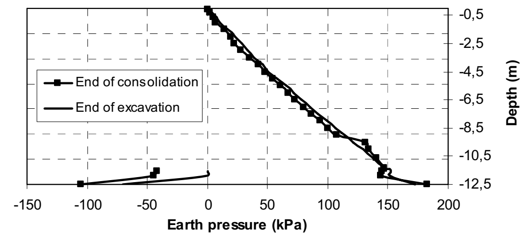

Figure 15. Earth pressure on the wall faces at ends of excavation and consolidation.

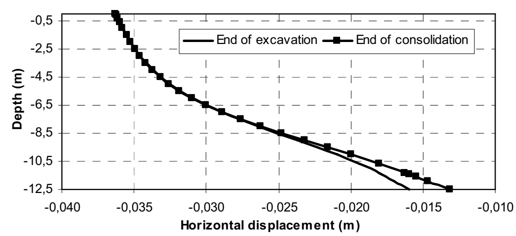

Figure 16. Wall horizontal displacement at ends of excavation and consolidation.

Diagrams of vertical displacement on the supported ground surface are illustrated in Figure 17. These results show that, with the consolidation, there are expressive downward displacements on the supported ground. This effect is justified by the reduction of volume on the supported soil, as discussed above.

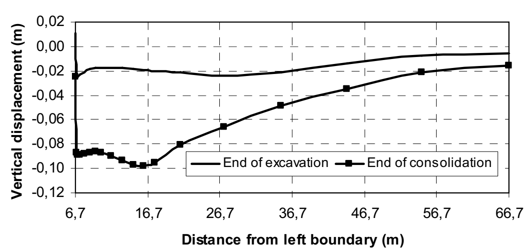

Figure 17. Vertical displacement on supported ground surface at ends of excavation and consolidation.

Diagrams of wall bending moments at ends of construction and consolidation are illustrated in Figure 18. With the consolidation, there is an increase of bending moment in the upper zone of the wall and a decrease in the lower zone. This is due to the above-mentioned increase of earth pressure on the wall on the excavated side.

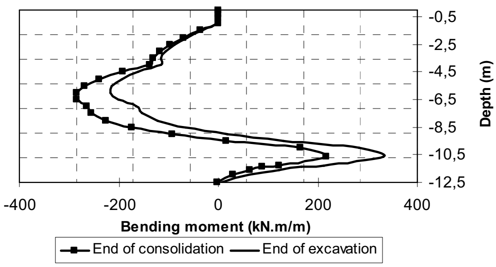

Figure 18. Wall bending moments at ends of construction and consolidation.

Figure 19 shows that during the consolidation the compression load on the jet-grout slab reduces. This is due to the increase with consolidation of the earth pressure (total horizontal stress) on the wall face of excavated side, as discussed above, which decreases the load that the wall transfers to the slab. Figure 20 shows that, during consolidation, the absolute value of bending moment on the jet-grout slab globally increases, the maximum value (at extremities of the slab) increasing 33%.

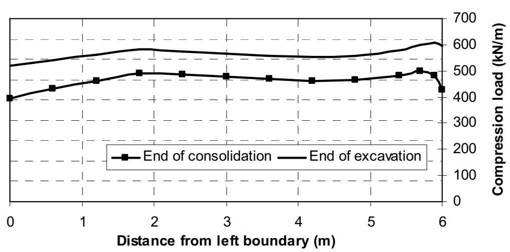

Figure 19. Compression loads on the jet-grout slab at ends of construction and consolidation.

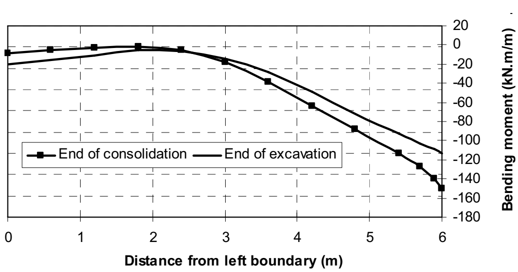

Figure 20. Bending moments on the jet-grout slab at ends of construction and consolidation.

4. CONCLUSIONS

The influence of the consolidation on a strutted excavation in soft soil incorporating a jet-grout base slab was analysed using a finite element program. Some overall conclusions are pointed out below on the results of the numerical analysis.

(1) During excavation, negative excess pore pressures are generated in all zones of the ground. After construction, with the consolidation, water pressure increases on the excavated side and decreases on the supported side.

(2) Stress level significantly increases during excavation, especially below the wall tip. After construction, stress level increases below the excavation bottom, whereas decreases on the supported side of the wall.

(3) Unlike what usually happens in strutted excavations without a base slab, the maximum wall displacement takes place on the top of the wall at all stages of excavation and post-excavation.

(4) During consolidation, there are expressive downward displacements on the supported ground surface.

(5) During construction, below the excavation base, the wall bending moments increase as excavation progresses.

(6) With consolidation, the compression load of the jet-grout slab reduces whereas its bending moments globally increase.

5. REFERENCES

Borges, J.L. 1995. *Geosynthetic-reinforced embankments on soft soils. Analysis and design*. PhD Thesis in Civil Engineering (in Portuguese).

Britto, A.M. & Gunn, M.J. 1987. *Critical soil mechanics via finite elements*. Ellis Horwood Limited, England.

Fernandes, M.M. 1983. *Flexible structures for earth retaining: New design methods*. PhD Thesis in Civil Engineering (in Portuguese).

Finno, R.J.; Atmatzidis, D.K.; Perkins, S.B. 1989. Observed performance of a deep excavation in clay. *Journal Geotech. Eng. Div.*, ASCE, 115: 1045-1064.

Lewis, R.W. & Schrefler, B.A. 1987. *The finite element method in the deformation and consolidation of porous media*. John Wiley and Sons, Inc., New York.

O´ Rourke, T.D. 1992. Base stability and ground movement prediction for excavations in soft soil. *Proceedings of the International Conference on Retaining Structures*, Cambridge, UK, pp. 657-686.

A Study on Application of PBD Method for Double Layered Soft Clay Improvement in Deep Depth

Yo-Seph Byun, Hyoung-Nam Kang
Dept. Civil of & Environmental Engineering, Hanyang University

Kyung-Min Kim
Geotechnical Engineering & Tunneling Research Division, KICT

Byung-Sik Chun
Dept. Civil of & Environmental Engineering, Hanyang University

ABSTRACT: The consolidation characteristics and mechanical behavior characteristics of soft ground are very complicated. They are very different according to a deposit origin and improvement method of soft ground(geological history). Accordingly, it is very important to grasp a mechanical behavior characteristics of soft ground with evaluating a characteristics of soil to geological formation age. The basic research is very necessary about these contents at deep soft ground and sites with different deposit origin in Korea. In this study, it was operated compound drainage capacity test and numerical analysis were done to analyze application of PBD(Plastic Board Drain) method applied in double layered soft clay in deep depth according to different deposit origin. As a result, the settlement was gradually occurred with increase of surface load. The consolidation settlement was processed with dissipation of pore pressure after surface load of 0.5MPa. It was also found that the drainage capacity of vertical drains was considerably reduced with pressure increase and time elapse. In case of the numerical analysis, total settlement was an almost same in case that single core PBD and double core PBD were applied, and it was showed a similar trend as a result of compound drainage capacity test.

1. INTRODUCTION

As environmental protection is becoming a global issue in recent years, collection of natural sand is restricted. Accordingly, many consolidation acceleration methods, using artificial materials as drain materials in place of natural materials like sand have been proposed. Among them, the plastic board drain(PBD) method using a plastic porous drain material is a useful method of soft ground consolidation acceleration method. The vertical drain method using PBD is known to have been first used by Kjellman(1948) who used a plate-shaped cardboard for soft ground improvement, and the utility of PBD began to be noticed after the 1960's and until now more than 50 types of PBD (Plastic Board Drain) have been developed since all over the world(Holtz et al., 1991). The drainage capacity of the PBD drain material has been analyzed by many researchers so far. Oosstveen et al.(1990) proposed an experiment for analyzing the drainage capacity of drain materials under the condition that drain materials are installed in a cell and lateral pressure is applied. According to the American Standard Test Method(ASTM D4716-01), drain materials without any banding or folding were installed horizontally between the upper and lower plate and sealed, and a load was applied to give the desired stress. After adjusting the height of the external water under an arbitrary hydraulic gradient condition, water was made to flow inside the drain materials and the flow rate over time was measured to analyze the drainage capacity of the drain materials. Koener and Lawrence(1988) also made a tester called Drexel, and conducted in a way similar to the American Standard Test Method(Yoo et al., 2008). In this study an indoor model experiment was conducted with regard to the consolidation behavior of the soft clay ground where the PBD was installed for analysis of the applicability of the PBD method to the deep soft ground. At this time, an experiment was conducted with regard to cases where the properties of the PBD filter and core were varied, and the overburden pressure was varied according to the passage of time in each phase. Also, the resulting consolidation subsidence, excessive pore water pressure, and drainage capacity were measured.

2. LABORATORY MODEL TEST

2.1. *Outline of the experimental apparatus*

In this study, as illustrated in Figure 1, a compound drainage capacity tester was made and the drainage capacity under a certain overburden pressure was measured after the drain materials were installed in the ground in the indoor test. The compound drainage capacity tester used in this experiment was made of a cylindrical steel frame which was 50cm across and 105cm tall, and ports for measuring excessive pore water pressure according to the progress of consolidation were installed at intervals of 10cm on the side of the tester. At the bottom three ports were installed for measurement of excessive pore water pressure by distance from drain materials, and the dissipation of the excessive pore water pressure according to the progress of consolidation were measured. The excessive pore water pressure was recorded by the Digital Transducer.

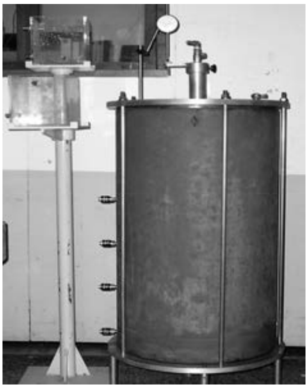

Figure 1. compound drainage capacity tester

2.2. *Simulated ground*

The samples used in the compound drainage capacity experiment are the cohesive soil collected from the deep soft ground. As it is very difficult to get undisturbed samples, in this experiment, samples were collected in the disturbed state, and they were sieved with a No. 10 sieve. In this process big pieces of soil, likely to affect the results of the experiment, or impurities like shells were removed. The soil properties of the samples used in this experiment are shown in Table 1.

Table 1. The soil properties of the soft ground

Contents	Properties
Soil classification	CH
No.200 passing percentage	98%
Specific gravity	2.682
Liquid limit (LL)	47.32%
Plastic limit (PL)	26.66%

2.3. *Target drain materials*

As shown in Figure 2, as for the drain materials used in this experiment, the single core PBD consists of a harmonica-type core, which has a 100mm(±5mm) wide and 5.0mm(±0.5mm) thick cross section, and a pocket-type filter, while the double core PBD is 100mm(± 0.5mm) wide and 7.0mm(± 0.5mm) thick, and the core has the cross section of a double filter made of 2 interlocked cores so that there is a drainage passage at the center. The properties of the single core PBD and the double core PBD used in this experiment are shown in Table 2.

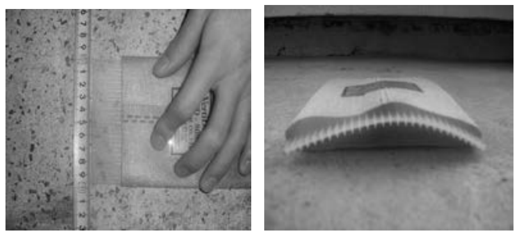

(a) The single core PBD

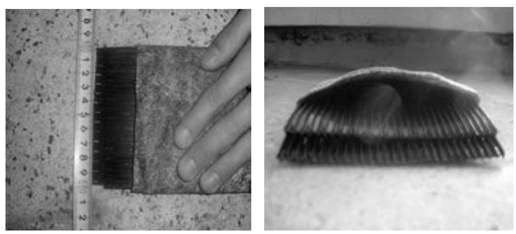

(b) The double core PBD

Figure 2. The drain materials used in this experiment

Table 2. The properties of the single core PBD and the double core PBD

Contents	The single core PBD	The double core PBD
Filter material	Polypropylene	Polypropylene
Core material	Polypropylene	Polypropylene
Total wide	100mm(± 5mm)	100mm(± 5mm)
Thick	5mm(± 0.5mm)	7mm(± 0.5mm)
The maximum tensile strength	Above 20000 (kN/wide)	Above 25000 (kN/wide)
The core type	Harmonica-type	Pocket-type filter

2.4. Experimental methodology and conditions

In the drainage capacity experiment conducted in this study, to simulate the conditions of the site as much as possible, drain materials were installed inside the tester filled with clay, and a certain vertical load was applied to measure the influence of clay on the filter of the drain materials through the compound drainage capacity experiment. Also, the drainage capacity (Q_w) was measured when the drain materials are bent as the clay was consolidated. The final overburden pressure in this experiment was increased to 500kPa in consideration of the depth of the site. If 500kPa pressure is applied at once to the cell filled with clay, a sudden increase of load may rapidly increase the excessive pore water pressure, and the sample is expected to be unstable. So the pressure was increased by 50kPa at a time for this experiment. The compound drainage capacity experimental conditions applied in this experiment are shown in Table 3.

Table 3. Drainage capacity experimental conditions

Experimental item	Experimental conditions
Drain material	The single core PBD, The double core PBD
The primary drain material length	560mm
Load	Maximum 500kPa (From 50kPa by 50kPa at a time)
Hydraulic gradient	0.5
The primary sample hight	560mm
The primary moisture content	73~77%

3. EXPERIMENTAL RESULTS AND ANALYSIS

3.1. Results of the single core PBD experiment

Figure 3 illustrates the changes in subsidence with the passage of time. If the pore water pressure was thought to be dissipated after the application of the overburden pressure starting with 50kPa, the pressure was increased again by 50kPa until it became 500kPa. As a result, subsidence occurred gradually, and after the overburden pressure became 500kPa, the dissipation of the pore water pressure led to consolidation subsidence in this experiment.

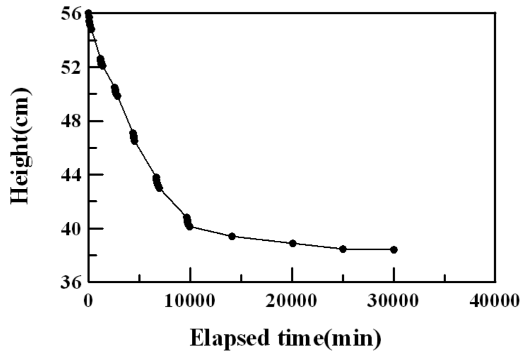

Figure 3. The consolidation subsidence curve with the passage of time (the single core PBD)

Figure 4 illustrates the rise of the pore water pressure due to the load, and the pore water pressure dissipation curve according to the progress of consolidation by load stage. As compared to Figure 3, it was revealed that the changes in subsidence by load state were due to the dissipation of the pore water pressure, and after the overburden pressure reached 500kPa, the pore water pressure tended to be decreased by the consolidation behavior under a certain load.

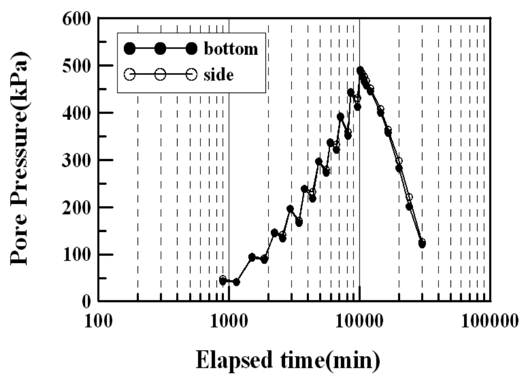

Figure 4. The pore water pressure dissipation curve with passage of time(The single core PBD)

Figure 5 illustrates the changes in the drainage capacity with the passage of time. It was revealed that the drainage capacity drastically decreased as pressure increased and time passed. The drainage capacity was reduced considerably in the pressurization stage, and after the overburden pressure reached 450kPa, the drainage capacity was smaller than 10cm^3/sec, and after the overburden pressure became 500kPa, it gradually decreased and after about 10000 minutes (about 7days) the drainage capacity was 2.8cm^3/sec and was constant with hardly any change. The deformation of the drain materials due to the consolidation subsidence of the clay layer and the clogging of the drain material filter due to the increase of the lateral pressure had a great influence on the reduction of the flow channel.

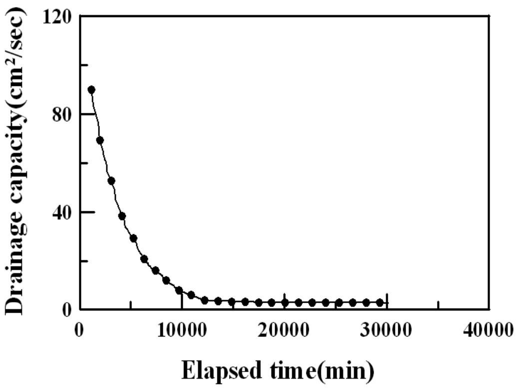

Figure 5. The change curve of the drainage capacity with passage of time(The single core PBD)

The result of the above experiment showed that, due to the load of the initial overburden pressure, the deformation ratio and the drainage capacity rapidly changed. Accordingly, due to the bending of the drain materials with the progress of consolidation and the creep and clogging of the filter caused by the lateral pressure, the drainage capacity became much smaller than the general membrane locking drainage capacity, and at this time if the overburden pressure exceeds 500kPa, the minimum drainage capacity was decreased to 2.8cm^3/sec.

3.2. Results of the double core PBD experiment

To understand the changes in the drainage capacity along with the consolidation subsidence of the ground in case the double core PBD is used to improve soft ground deeper than 40m, the compound drainage capacity experiment was conducted, and the drainage capacity was measured as time passed by load stage the same way as in the single core PBD experiment.

In Figure 6, the overburden pressure was applied starting with 50kPa, and if the pore water pressure was thought to be dissipated, it was increased again by 50kPa until it reached 500kPa. The result showed that subsidence occurred gradually, and after the overburden pressure reached 500kPa, consolidation subsidence took place according to the dissipation of the pore water pressure in this experiment.

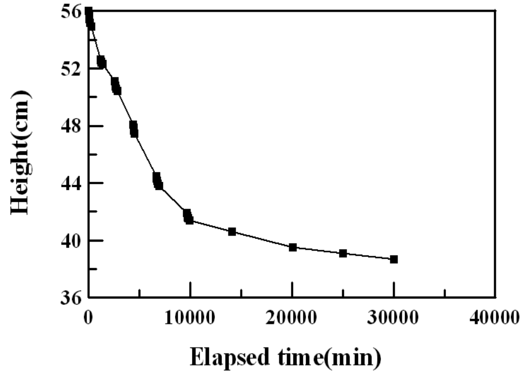

Figure 6. The consolidation subsidence curve with the passage of time (the double core PBD)

Figure 7 illustrates the rise of the pore water pressure due to the load and the pore water pressure dissipation curve according to the progress of consolidation by load stage. As compared to Figure 6, it was revealed that the changes in subsidence by load stage were due to the dissipation of the pore water pressure, and after the overburden pressure reached 500kPa, the pore water pressure tended to decrease due to the consolidation behavior under a certain load.

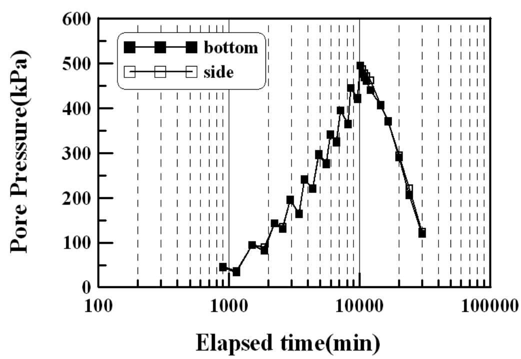

Figure 7. The pore water pressure dissipation curve with passage of time (The double core PBD)

Figure 8 illustrates the changes in the drainage capacity with the passage of time. The drainage capacity was drastically reduced as the pressure increased and time passed. The drainage capacity was considerably decreased when the overburden pressure increased, and after the overburden pressure reached 500kPa, it slowly decreased, and after about 10000 minutes (about 7 days) the drainage capacity was about 9.8cm3/sec and was constant with hardly any change. As the drainage capacity was rapidly decreased in the load stage, the deformation of the drain materials due to the consolidation subsidence of the clay layer and the clogging of the drain material filter due to the increase of the lateral pressure had a great influence on the reduction of the flow channel.

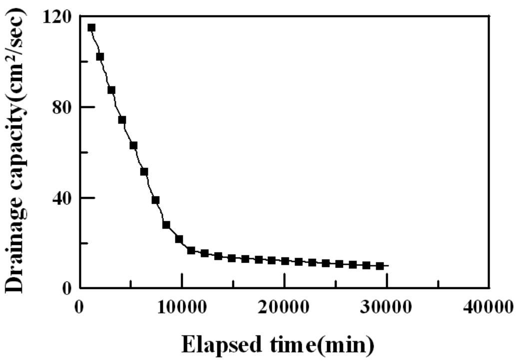

Figure 8. The change curve of the drainage capacity with passage of time (The double core PBD)

The result of the above experiment showed that, due to the load of the initial overburden pressure, the consolidation subsidence of the ground was similar in each load stage even though the drainage capacity rapidly dropped. Accordingly, after the bending of the drain materials with the progress of consolidation and the increase of the lateral pressure, the drainage capacity became much greater than that of the single core PBD as the central flow channel was secured, and at this time if the overburden pressure exceeds 500kPa, the minimum drainage capacity was greater than 9.8cm^3/sec.

3.3. Determination of the drainage capacity of PBD

The drainage capacity of the single core PBD, obtained as a result of the compound drainage capacity experiment, was stabilized at the minimum value as it became about 2.8cm^3/sec when the lateral pressure was 500kPa, and the hydraulic gradient, and had a constant value. Accordingly, existing domestic researches showed that the drainage capacity must be 3~10cm^3/sec, whereas foreign researches required a drainage capacity of 3~5cm^3/sec. The minimum drainage capacity in consideration of variables affecting the drainage capacity was about 5.3cm3/sec. In addition, considering the fact that the result of the experiment using the compound drainage capacity tester was 2.8cm^3/sec, it would be reasonable that the minimum required drainage capacity of 3cm^3/sec should be reflected in the design. However, this site is soft clay ground deeper than 40m, and selection of drain materials satisfying the drainage capacity is important. As the drainage capacity was obtained from the compound drainage capacity experiment based on the drain materials which improved the discharge performance in case the lateral pressure was 500kPa and the hydraulic gradient was 0.5, different drain materials had a different drainage capacity. So if the thickness of the soft layer is less than 40m when the drainage capacity is about 5~10cm^3/sec, the single core PBD is the right choice, and if the thickness of the soft layer exceeds 40m, the double core PBD is the right choice.

4. CONCLUSION

To analyze the applicability of the PBD method to deep soft ground, an indoor model experiment was conducted with regard to the consolidation behavior of the soft clay ground where the PBD was installed. The results can be summarized as follows:

(1) As the overburden pressure increased, subsidence occurred gradually, and after the overburden pressure reached 500kPa, consolidation subsidence took place due to the dissipation of the pore water pressure. Accordingly, it was confirmed that the changes in subsidence by load stage were due to the dissipation of the pore water pressure.

(2) It was predicted that the rate of subsidence of the double core PBD with a relative large drainage capacity would be faster than that of the single core PBD, but the rate of subsidence was almost identical, and as the load increased and time passed, the subsidence was almost identical.

(3) The drainage capacity was reduced considerably in the pressurization stage, and after the overburden pressure reached 500kPa, it

began to decrease slowly. After about 10000 minutes(about 7days) there was hardly any change in the drainage capacity of the single core PBD and the double core PBD, and it was constant. The deformation of the drain materials due to the consolidation subsidence of the clay layer and the clogging of the drain material filter due to the increase of the lateral pressure had a great influence on the reduction of the flow channel.

5. REFERENCES

ASTM D 4716-01. 2001. Test method for determinig the (in plane) flow rate per unit width and hydraulic transmissivity of of geosynthetic using a costant head. *Annual Book of ASTM Standards. ASTM*, Vol. 04.09-(□), pp. 1054-1062.

Holtz, R.D., Jamiolkowisk, M., Lancellotte, R., and Pedroni, S. 1991. Laboratory testing of prefabricated wick drains. *GEO-COAST '91 ICGED,* Yokohama, pp.311-316.

Kjellman, W. 1948. Consolidation of Fine-grained Soils by Drain Wells. Trans, *ASCE*, No.113, pp. 748-751.

Koemer, C.M. and Lawrence, C.A. 1988. Flow behavior of kinked strip drains. *Proc. of ASCE Symposium on Geosynthetics for soil Improvement*, Nashvile, Tenn., Geotechinicak Special Publication, No.18, pp.22-35.

Oosstveen, J.P. and Troost, G.H. 1990. Dicharge index tests on vertical drains. *Geotextiles, Geomembranes and Related Products*, pp.345-350.

Yoo, N. J., Kim, D. G., Park B.S., Jun, S.H. 2008. Geotechnical Engineering:Development and Applicability of Discharge Capacity Testing Apparatus Using Penetration Method. *Journal of The Korean Society of Civil Engineers*, Vol.28, No.5, pp.313-320.

Improvement of a subsoil by microblasts

E. Dembicki
Gdańsk University of Technology, Faculty for Civil & Environmental Eng.
Department of Geotechnics, Geology and Maritime Eng., Gdańsk, Poland

R. Imiołek
Chairman of Polbud-Pomorze Ltd.

ABSTRACT: In the paper a technology of the improvement of a subsoil, both non-cohesive (granular) as well as cohesive ones by microblasting technique together with theoretical considerations is discussed. The description of approximated empirical solutions based on the experiments and verified in geotechnical practice is presented.

1. INTRODUCTION

Developing urbanization and increasing shortage of good construction sites necessitates the engineers and investors to use a subsoil which is considered as weak one and was treated in the past as useless for any infrastructure. Nowadays, the localization of any construction is rarely related with favourable foundation conditions.

The improvement of a subsoil does not only regard subsurface soil layers but goes deeper up to several or even several tens of meters depending of the character and importance of a structure which is to be founded in a given area.

In general, one can distinguish two groups of techniques of subsoil improvement:

- Techniques in which a soil undergoes some modification due to application of various type of grout in order to achieve more compacted or less plastic subsoil. The modification relies on reinforcing the contacts between particular soil grains and increasing its number which simultaneously reduces soil porosity. This group can be named as soil improvement techniques.
- Techniques which take advantage of inserting into the soil some material (elements) in order to increase its total mechanical strength. They can be named as soil reinforcement techniques.

Nowadays, new soil improvement or reinforcement techniques are applied for more and more important constructions of long-term serviceability live and environmental impact.

2. COMPACTION OR IMPROVEMENT OF A SUBSOIL BY MICROBLASTS

This technology aims at the improvement of physical and mechanical parameters of a subsoil by compaction of granular soils or formation of draining sandy piles in weak (high plasticity) cohesive soils. The piles are formed by microblasts of blasting material located in natural soil or fill, which is to be compacted or consolidated.

2.1. Microblast-induced compaction of granular soils

Compaction process of granular soil during the blast can be described as follows:

- the gaseous block created by the microblast propagates in a soil mass causing changes in soil skeleton, which manifests a re-arrangement of soil grains or particles due to large shear strains and next due to soil liquefaction and pore-water pressure dissipation. Explosion of the charge causes rapid increase of pore-water pressure in the soil destroying its existing unstable structure.
- the re-arrangement of grains causes subsequently soil compaction depending on the soil type and its permeability, location of the blasting material and volume of soil to be compacted. Microblast-induced compaction mechanism of granular soil was shown in Fig. 1.

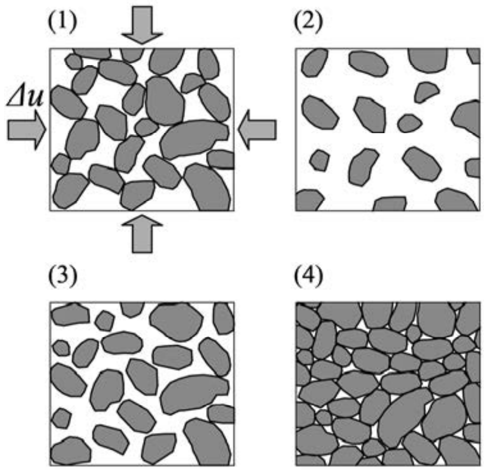

Figure 1. Phases of compaction process of granular soil by microblast.
1 – initial state; 2 and 3 – intermediate states; 4 – final stable state

The microblast acts on granular soil structure causing large degree of its destruction. Repeated process of microblasting leads to the increase of compaction of loose soil zones resulting in creation of uniformly compacted soil structure.

In very permeable soils, such as e.g. rock fill, the microblasts cause large volumetric deformation and outflow of water from pores can occur directly due to shock wave. In this case the compaction process will mainly depend on the microblasting impact on soil skeleton.

3. MICROBLAST-INDUCED COMPACTION SCHEMES OF UNDERWATER GRANULAR SOILS

3.1. Underwater microblasts

Scheme of the impact of underwater microblast together with impact parameters are presented in Fig. 2.

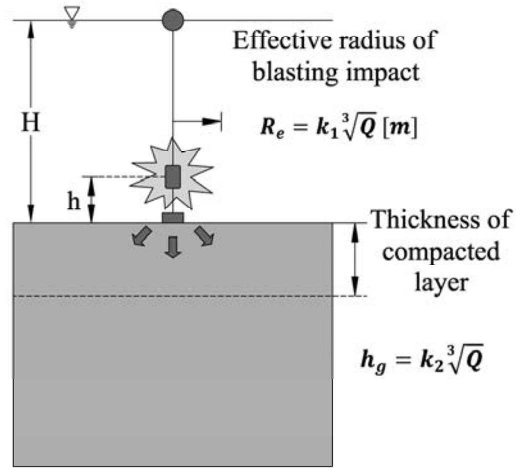

$$k_1 = 1,6 \div 3,0\,;\; k_2 = 4,5 \div 5,0\,;\; Q = 0,1H^{2,46}\,;$$

$$h = k_3\left(\sqrt[3]{Q}\right)^{1,95}\,;\; k_3 = 0,355$$

Figure 2. Scheme of underwater microblast.

3.2. Hidden microblasts with concentrated and elongated charges.

Scheme of such microblast together with its parameters are presented in Fig. 3.

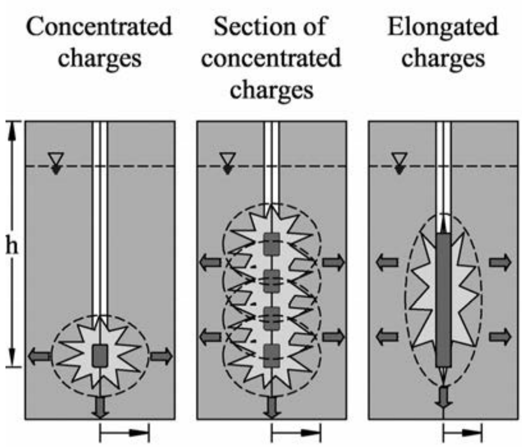

$R_e = k_4\sqrt[3]{Q_1}$, $Q_1 = 0,055h^3$, $k_4 = 2,5 \div 3,0$

$R_e = k_4\sqrt[3]{Q_1}$

$R_e = 0,71k_5\sqrt{Q_2}$, $k_5 = 2,5 \div 3,0$, $[Q_2] = kg/m$

Figure 3. Hidden microblasts with concentrated and elongated charges

3.3. Microblast series

In order to achieve respective degree of the compaction of granular soil the microblasts should be carried out in several series. Based on the experiments performed it was found that the most effective are four series of microblasts, which lead to achievement of optimal granular soil compaction. Sequence and execution of microblasts in series is shown in Fig. 4.

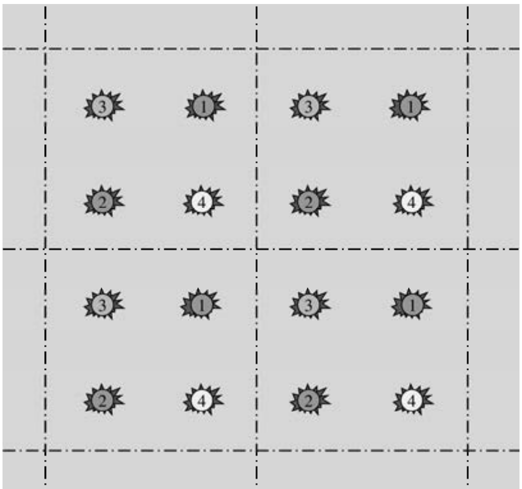

Figure 4. Part of the area subjected to microblast-induced compaction – 4 series of microblasts.

4. HIDDEN MICROBLASTS WITH ELONGATED CHARGES IN WEAK COHESIVE SOILS

In weak cohesive soils the microblasts serve for formation of sandy piles (vertical drains) made of sand lying on the surface of weak soil layer. In the case when such sandy layer does not exist it should be artificially deposited in the form of sandy fill, 1.5 to 2.0 m thick. Scheme of microblast execution in weak cohesive soil was shown in Fig. 5, whereas the formation of sandy pile was presented in Fig. 6.

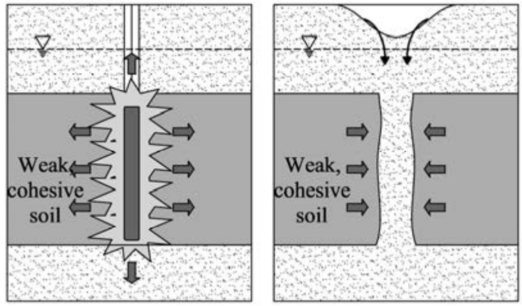

Figure 5. Scheme of formation of sandy piles (drains) in weak cohesive soils

Formation of the pile (drain) develops in the following stages:

- deposition of additional sandy layer,
- installation of elongated charges in the subsoil,
- explosion,
- formation of stable hole (D = 0.1 ÷ 2.0 m), with simultaneous pore water pressure generation around it,
- liquefaction of the granular soil in additional sandy layer and its flow down into the hole upto its complete filling which causes local settlement (depression) of the surface,
- quick dissipation of the excess pore water pressure throughout formed sandy piles which work partially as drains and partially as supporting columns.

The effectiveness of the technique and the consolidation progress are examined by the measurements of a subsidence of the improving area.

Microblasts applied to weak cohesive soils can be also executed in respectively designed series and sequence, which increases the effectiveness of the method and additionally accelerates the seepage to the neighbouring sandy drains.

Interaction mechanism of neighbouring sandy drains with effective interaction radius (R_e) is shown in Fig. 6.

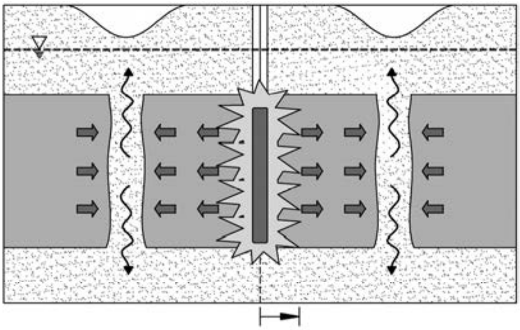

$$R_e = k_6 Q^{1/2}\ , k_6 = 3,5 \div 4,5$$

Figure 6. Mechanism of the interaction between neighbouring sandy drains in designed blasting series

5. PRACTIACL EXAMPLES AND COMPACTION EFFECTIVENESS

In Fig. 7 an example of the compaction of loose granular soils deposited on large depth, for the subsoil improvement under the foundation of nuclear power plant in Żarnowiec, Poland is presented. In turn, the compaction of the body of rubble mound breakwater in Iciči yacht port (near Rijeka, Croatia, 1989) is shown in Fig. 8.

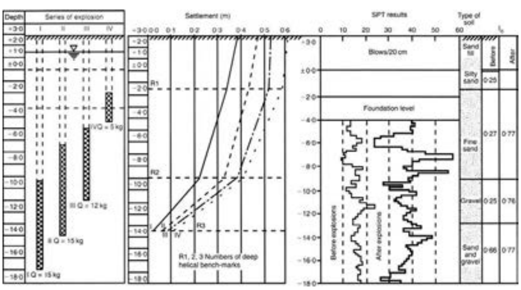

Figure 7. Compaction of loose granular soils by microblasts in the designed nuclear power plant in Żarnowiec, Poland, 1984, 4 blasting series.

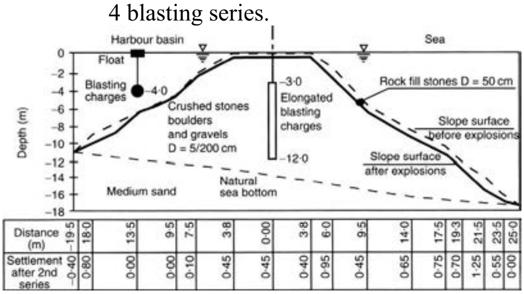

Figure 8. Rubble mound breakwater in Iciči yacht port (near Rijeka, Croatia, 1989).

In Fig. 9 the characteristic after-blast depression network indicating the location of formed sandy piles along the access route to Jan Paweł II bridge in Gdańsk, (2000) is presented.

Figure 9. Access routes to Jan Paweł II bridge in Gdańsk, (2000). Characteristic, after-blast depression network (sandy piles formation).

Exemplary after-blast depression shape observed during the subsoil improvement for the construction of A4 highway in Poland, (2000/2003) is presented in Fig. 10.

Figure 10. A4 highway (2000/2003). After-blast depression shape.

In Table 1 the list of more important construction sites with the subsoil improved in terms of microblasting technique applied by the Authors is given.

Table 1.

Date	Place	Soils, micro-blasting type	Volume $[m^3]$
1979	Gdańsk North Port	Loose sands, underwater blasts	126.000

1980	Gdańsk North Port	Weak mud and loose sands, sandy piles, hidden blasts	2.500.000
1983/ 1985	nuclear power plant in Żarnowiec	Loose sands, hidden blasts with elongated charges	1.600.000
1985	Gdynia Port	Loose sands, underwater blasts	105.000
1986	Szczecin Port	Weak peat, sandy piles, hidden blasts	280.000
1988	sewage-treatment plant in Tczew	Weak peat and mud, sandy piles, hidden blasts	510.000
1989	Breakwater in Iciči, Croatia	Loose stony fill and gravel, underwater and hidden blasts	50.000
2000	Acces routes to Jan Paweł II bridge, Gdańsk	Weak mud, sandy piles, hidden blasts	330.000
2002	Express-way Warszawa-Gdańsk-Elblag	Weak mud and peat under the bridge abut-ment, hidden blasts	300.000
2003	A4 high-way, Katowice	Weak clays, sandy piles, hidden blasts	70.000
2004/ 2005	A2 high-way, Kościelec	Weak peat, sandy piles, hidden blasts	1.403.000
2005	A2 high-way, Wartko-wice	Weak mud, sandy piles, hidden blasts	66.000

6. THEORETICAL SOLUTIONS

Theoretical solutions of the problem of granular soil compaction by microblasts can be found in papers of Dembicki et el. (1989), Raju V.R. (1994) and N. Tomaskovics (2001). In the mathematical description of the compaction process of granular soil by microblasts both heterogeneities of the soil properties as well as geometrical nonlinearity of the process were taken into account. For a determination of basic equations governing the compaction process the methods of continuum mechanics and constitutive equations given originally by Lachow (1959) were incorporated and adapted for three-phase granular medium (soil skeleton + pore water + gas). For the theoretical model the following assumptions were taken:

Reaction of spherical space with after-blast gas. It has been assumed the blasting material at t=0 time is placed in spherical hole with the radius $r_0(t{=}0) = R_0$ and after the blast it transforms to the gaseous bubble with the initial pressure p_0. Thermodynamic state of the blasting gas during explosion is isotropic (no heat exchange). Pressure change of blasting gas can be described by function p(t).

Mechanical model. Shock wave caused by microblast, propagating from the spherical hole outside, can be described by function $r_1(t)$.

Mechanical properties of granular soil can be described by quasi-linear three-phase model of mixture consisting of:

- compressible gas,
- incompressible water,
- incompressible solid particles.

The density of granular soil changes gradually from the initial density ρ_0 at adiabatic process of gas compression. During compression process the mixture remains incompressible.

During initial expansion of gaseous spherical bubble all mixture components move linearly with the same velocity v(R,t). Soil movement between traveling hole of blasting gas r_0 (t) and wave front $r_1(t)$ can be described by displacement field u(R,t).

Stress state in the soil between traveling hole of blasting gas and wave front can be described by pressure field p(R,t).

In the constitutive law assumed the dissipation process is not taken into account.

The details of theoretical solutions based on the above assumptions have been given by Dembicki et al. (1989).

7. CONCLUSIONS

Based on the numerous engineering applications of the technique described, supported by theoretical solutions, the following practical conclusions can be formulated:

Microblasting technique is a simple and efficient method of compaction of granular, saturated and loose soils.

The technique can also serve for the improvement of weak cohesive soils (sandy piles, hidden blasts with elongated charges).

In the case of fine sands or weak cohesive soils microblasts can sufficiently accelerate the consolidation rate.

Directly after the blast vertical strains induced vary from 5 to 10% indicating the efficiency of the technique.

The efficiency of the technique as well as the degree of compaction can be assessed by penetration tests carried out prior to and after the blasting.

A potential threat for neighbouring objects can be minimised by respectively planned and monitored trail blasts.

Microblasting technique is also economically attractive comparing to other soil improvement techniques.

8. REFERENCES

Charlie W.E., Jacobs P.J., Doehring, D.O., 1992. Blast-induced liquefaction of an alluvial sand deposit, Geotechnical Testing Journal 15 (1), 14-23.

Dembicki E., Kisielowa N, 1983, Technology of soil compaction by means of explosions. Proc. VIII. E.C.S.M.F.E., Helsinki, 229-230.

Dembicki E., Kisielowa N., Nowacki W. K., Raniecki B., 1988, Dynamische Bodenverdichtung durch Tiefensprengungen. Bautechnik 65, H. 10, 336-340.

Dembicki E., Kisielowa N., Nowacki W. K., Raniecki B., 1989, Theoretische Analyse der dynamischen Bodenverdichtung durch Sprengung. Bautechnik 66, H.2, 50-54.

Dembicki E., Imiołek R., Kisielowa N., 1992, Soil compaction with the blasting method. In Geomechanics and Water Engineering in Environmental Management, Chapter 20, edited by R.N. Chowdury, Balkema, 599-622.

Dembicki E., Zadroga B., 1997, Polish experience in soil improvement using explosion techniques. Ground lmprovement 1, 19-24.

Dembicki E., Zadroga B., Bona R., Imiołek R., Kisielowa N., Semrau J., 1987, Changes in ground-water levels due to dynamic compaction of subsoil by hidden underground explosions. Proc. of the IXth European Conf. on Soil Mechanics and Found. Eng. Dublin, 599-602.

Gandhi S.R., Dey A.K. Selvam S., 1999, Densification of pond ash by blasting. Journal of Geotechnical and Geoenvironmental Engineering 125, No 10, 889-899.

Green r.A., 2001, Energy based evaluation and remediation of liquefiable soils, PhD thesis, Faculty of the Virginia Polytechnic Institute and State University.

Gohl W.B., Jefferies M.G., Howie J.A., Diggle D., 2000. Explosive compaction: design, implementation and effectiveness, Geotechnique 50, No.6, 657-665.

Hryciw R.D., 1986. A study of the physical and chemical aspects of blastdensification of sand, PhD thesis, Northwestern University, Evanston, 229 pp.

Ivanov P.L., 1983.Uplotnenie malosvlaznih gruntov vzrivami, pp. 230, ref. 50. Izdtielstvo Niedra, Moskva.

Ivanov P.L., 1983. Prediction and control techniques to compact loose soils by explosions. Proc. 8th European Conference of Soil Mechanics and Foundation Engineering, Helsinki, 253-254.

Mitchell J.K., Gallagher P.M., 1998. Guidelines for ground improvement of civil works and military structures and facilities, Publication No. ETL 1110-1-185, US Army Corps of Engineers, Washington, DC, 109.

Raju V.R., Gudehus G., 1994. Compaction of loose sand deposits using blasting, Proc. 13th International Conference of Soil Mechanics and Foudation Engineering, New Delhi, 1145-1150.

Solymar Z.U., 1984. Compaction of alluvial sands by deep blasting. Canadian Geotechnical Journal 21, 305-321.

Tamaskovics N., 2001. Veröffentlichungeen des Instituts für Geotechnik der Technischen Universität Begakademie Freiberg. Heft 3, Freiberg 2001. ISBN 3-86012-155-3.

Van Impe W.E., 1989. Soil improvement techniques and their evaluation, Balkema, Rotterdam, pp. 125.

SOIL MIX walls as retaining structures – critical analysis of the material design parameters

P. Ganne, N. Huybrechts
Belgian Building Research Institute, Division of Geotechnics, Brussels, Belgium

F. De Cock
Geotechnical Expert Office Geo.be, Belgium

B. Lameire
Belgian Association of Foundation Contractors ABEF, Belgium

J. Maertens
KULeuven, Jan Maertens & partners, Belgium

ABSTRACT: The application of soil mix technology in Belgium is sharply increasing. Next to soil improvement applications, soil mix walls are extensively used for excavation support. The compressive strength and elastic modulus of the soil mix material are essential parameters in the design of these retaining structures. This paper describes a procedure for the estimation and measuring of the compressive strength and the elastic modulus of soil mix material. These procedures are based and validated on a large population of laboratory test results on in situ cored soil mix material, realized in Belgian soils. Furthermore, a procedure to define the 5% fractile characteristic value of the compressive strength of soil mix material is proposed and validated.

1. INTRODUCTION

Since several decennia, the (deep) soil mix technique is known as a ground improvement technique (Probaha, 1998). Therefore, the ground is in situ mechanically mixed while a binder, based on cement and lime (Probaha et al., 1998), is injected. The results of national and European research programs have been published in multiple interesting reports (such as Eurosoilstab, 2002), while also the European standard for the execution of deep mixing "Execution of special geotechnical works – Deep Mixing" (EN 14679) was published in 2005. Most of these research projects focussed on the global stabilisation of soft cohesive soils such as peat, clay, gyttja, silt, …

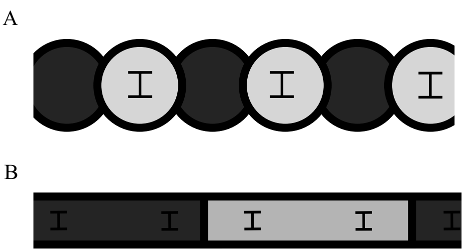

Figure 1. Schematic plan view of the secant execution of (A) cylindrical soil mix columns and (B) rectangular soil mix panels.

More recently, soil mix is increasingly used for the retaining of soil and water in the case of excavations as a more economical alternative for concrete secant pile walls and even for king post walls (i.e. soldier pile walls). The soil mix cylindrical columns or rectangular panels are placed next to each other, in a secant way. By overlapping the different soil mix elements (Rutherford et al., 2007), a continuous soil mix wall is realised (Figure 1 and 2). Steel H or I-beams are inserted into the soil mix before curing to resist the shear forces and bending moments in the retaining wall. The maximum installation depth of the soil mix walls lies – so far – in the order of 20 m. The main structural difference between these soil mix walls and the more traditional secant pile walls is the constitutive wall material which consists of a mixture of soil and cement in stead of traditional concrete.

Figure 2. Photo of a soil mix wall with a ground and water retaining function (CVR).

So far, three main types of soil mix systems are used in Belgium: CVR C-mix®, TSM and CSM. The characterization of the resulting soil mix material is a difficult issue. This paper firstly describes the different types of soil mix systems, whereupon the determination of the compressive strength and of the elastic modulus of the soil mix material is discussed.

2. SOIL MIX SYSTEMS IN BELGIUM

The CVR C-mix®, the TSM and the CSM are the three most used types of soil mix systems in Belgium. All three are wet soil mixing systems.

2.1. CVR C-mix®

The CVR C-mix® is performed with an adapted bored pile rig and a special designed shaft and mixing tool. This tool rotates around a vertical axis at about 100 rpm and hence, cuts the soil mechanically. Simultaneously, the water\binder mixture (water\binder ratio between 0.6 and 0.8), is injected at low pressure (< 5 bar). The injected quantity of binder amounts mostly to 350 and 450 kg binder/m³, depending on the soil conditions. The binder partly (between 0% and 30%) returns to the surface. This is called ‘spoil return’.

The resulting soil mix elements are cylindrical columns. The diameter of the soil mix columns is the diameter of the mixing tool, of which the nominal diameter varies between 0.43 and 1.03 m. When the soil mix is used as a retaining structure, the production rate is about 160 m² of soil mix wall per day.

In order to increase the production rate, a CVR Twinmix® and a CVR Triple C-MIX® is used. A twinmix has two mixing tools, mixing two overlapping cylindrical columns (total wall length of 0.8 to 1.2 m) at the same time. The daily return increases till 210 m². A CVR Triple C-mix® has three mixing tools in line, with an overall wall length of 1.5 to 1.8 m. The production rate increases to 300 m² per day.

2.2. Tubular Soil Mix (TSM)

The TSM technique uses a mechanical and a hydraulical way of mixing. Apart from the rotating (around the vertical axis) mixing tool, the soil is cut by the high pressure injection (till 500 bar) of the water\binder mixture. The water\binder ratio of the mixture can be chosen between 0.6 and 1.2. The injected quantity of water\binder mixture amounts mostly to 200 and 450 kg binder/m³, depending on the soil conditions. Part of the binder (between 0% and 30%) returns to the surface as spoil return.

The resulting soil mix elements are cylindrical columns with a diameter between 0.38 and 0.73 m. The production rate is about 80 m² of soil mix wall per day.

Again, a twin and a triple version exist. The total wall length of the two (three) cylindrical columns of a twin (triple), varies between 0.8 and 1.4 m (1.2 and 2.1 m). In this way, the production rate is increased till about 180 (twin) and 250 m² (triple) of soil mix wall per day.

2.3. Cutter Soil Mix (CSM)

A CSM device is commercially available. It makes use of two cutting wheels that rotate independently about a horizontal axis, cutting the soil. At the same time, the water\binder mixture is injected at low pressure (< 5 bar). The water\binder ratio can be chosen between 0.6 and 1.2. The injected quantity of binder amounts mostly to 200 and 400 kg binder/m³, depending on the soil conditions. Part of the binder (between 0% and 30%) returns to the surface as spoil return.

The resulting soil mix elements are rectangular panels. In Belgium, these panels have a length of 2.4 m and a thickness of 0.55 m, though cutter devices with other dimensions are internationally available. The production rate is about 100 m² to 250 m² per day.

2.4. Advantages of soil mix walls as retaining structures

The use of soil mix as ground and/or water retaining structures has some specific advantages.

No important vibrations are caused by the execution of soil mix. As the stress relaxation of the soil is limited, soil mix can be executed nearby existing constructions.

Contrary to concreted secant pile walls, the execution of the soil mix walls does not suffer from delayed supply (e.g. due to traffic jams) of the fresh concrete.

Another interesting advantage, compared to jet-grouting is the limited amount of spoil return.

3. TEST PROGRAMME

Cores of soil mix have been drilled horizontally on 23 different job sites in Belgium, with different soil conditions and with different types of soil mix systems. All in all, 950 unconfined compressive tests and 100 determinations of the elastic modulus have been performed on these cores. Also wet grab samples and laboratory samples have been analysed.

3.1. Execution of unconfined compressive tests

The laboratory test to determine the unconfined compressive strength (UCS) is performed by a MFL 250 kN loading machine. The loading rate amounts to 2.5 kN/s. The samples have a diameter between 85 mm and 115 mm. The accuracy of the diameter of the cores is 0.3 mm. The height to diameter ratio is 1 (EN 206). All test samples with soil inclusions > 1/6 of the diameter are rejected, on condition that no more than 15% of the test samples from one particular site are rejected. This possibility to reject test samples results from the reflexion that a soil inclusion of 20 mm or less will not influence the behaviour of a soil mix structure, conversely, a soil inclusion of 20 mm in a test sample of 100 mm diameter will influence the result of the test significantly. Of course, this condition is only suitable if one assumes that in the soil mix structure, no soil inclusions larger than 1/6 of its width occur.

3.2. Execution of elastic modulus tests

The laboratory test to determine the elastic modulus is unconfined performed (MFL 250 kN) on in situ cored test samples with a diameter between 85 mm and 115 mm. The accuracy of the diameter of the cores is 0.3 mm. The height to diameter ratio is 2. For the tests of the elastic modulus, cores with a visual better quality are selected, in order to preserve a uniaxial behaviour of the tested samples. The elastic modulus is determined on a secant way by a cyclic loading between 10% and 30% of the estimated UCS of the test samples. The loading rate amounts to 2.5 kN/s. The sample deformations during these loading cycles are measured by three couples of demec points. Once the mean difference of the measured deformation, caused by each cyclic loading, is smaller than 1.10^{-5} Strains (NBN-B15-203), the secant elastic modulus is calculated. Thereafter, the loading is continued to determine the UCS.

3.3. Comparison of cored and wet grab samples

Further on in paragraphs 4 and 5, only laboratory tests using drilled cores are considered. This has been decided after a comparative study of the UCS of cored as well as wet grab samples. Indeed, at two job sites, also wet grab sampling has been performed. In the first half hour after the mixing of the soil with the binder, a specially designed cylindrical wet grab sampling tool is pushed in the fresh soil mix element. This sampler stays closed until it reaches the depth of 2 ± 0.2 m. At this moment, the sampler opens over a height of 0.2 m. After the soil mix material fills the sampler, it is locked and pulled up. The material is preserved in a cylindrical mould (diameter = 113 mm; height = 220 mm) in an acclimatised room (humidity > 98%; temperature = 20 ± 2°C). Two weeks later, the same soil mix elements are cored at the same location (at 2.0 ± 0.2 m depth). The cores and the wet grab samples are tested on the same day (curing time = 14 days). This procedure is applied twice on a job site in Ghent (CSM in tertiary sand) and twice on a job site in Louvain (CSM in tertiary sand). The differences between the mean UCS of drilled cores and of wet grab samples varies between -10% and +35% (Table 1). These differences can not be explained by the variation of the test results only (Larsson, 2005). Probably, also the curing conditions have a significant influence.

Table 1. Comparison between the UCS results at 14 days on cored and wet grab samples (# is the number of test samples, μ is the mean UCS and σ is the standard deviation of the UCS tests).

	Drilled cores	Wet grab
Site - element	UCS [MPa]	UCS [MPa]
Ghent Element I	$\mu = 2.37$ $\sigma = 0.36$ # = 5	$\mu = 2.61$ $\sigma = 0.23$ # = 4
Ghent Element II	$\mu = 1.60$ $\sigma = 0.25$ # = 5	$\mu = 1.85$ $\sigma = 0.10$ # = 4
Louvain Element I	$\mu = 3.98$ $\sigma = 0.78$ # = 4	$\mu = 3.68$ $\sigma = 0.21$ # = 4
Louvain Element II	$\mu = 4.99$ $\sigma = 0.71$ # = 5	$\mu = 3.64$ $\sigma = 0.45$ # = 4

3.4. UCS in top of wall

It has also been observed on different sites that the soil mix UCS over the first meter is strongly influenced by the execution procedure at the start and the stop of an element (e.g. infiltration of rinsing water). As an example, Figure 3 shows that on the site of Bruges (CSM in quaternary sand), the UCS of samples over the first meter is only about 60% of the mean UCS at larger depth. Consequently, the top of the wall is not representative for the dieper part. Therefore, paragraphs 4 and 5 consider only laboratory tests on samples, cored deeper than the first 1 m below surface.

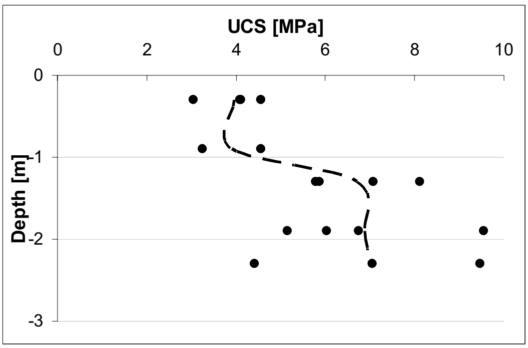

Figure 3. UCS results of samples, cored at different depths (site Bruges: CSM in quaternary sand).

3.5. Influence of the curing time on the UCS of soil mix test samples

The UCS of a soil mix sample depends among others on the curing time. In this article, the curing time of the tested soil mix samples varies between 14 days and 180 days. Therefore, laboratory mixed samples are used to determine the influence of the curing time.

The mixing of the soil and the binder is performed in laboratory using a specific procedure:

- mixing the water and the cement during two and a half minute (in a Zyklos mixing apparatus,
- the dried soil is introduced during one minute,
- continuing the mixing during two and a half minute,
- moulding the soil mix in cylindrical moulds (diameter = 113 mm; height = 220 mm).

For homogeneity reasons, each set of 24 test samples is realized during the same mixing. After 3, 7, 14, 28, 56 and 91 days, the UCS of 4 samples are determined. Using the average of the UCS of 4 samples as a function of time, the following formula is fitted:

$$f_{cm}(t) = \beta_{cc}(t)\ f_{cm} \qquad (1)$$

where $f_{cm}(t)$ is the evolution of the UCS with time [MPa]; f_{cm} the 28 days UCS [MPa] and

$$\beta_{cc}(t) = \exp(s(1-\sqrt{\frac{28}{t}})) \qquad (2)$$

where t is the curing time [days] and s the fitted parameter (EN 1992-1-1).

Depending on the soil conditions, the type of binder, the amount of binder and the amount of water, the influence of the curing time is tested in 11 different conditions. According to the soil conditions in Belgium, the applied water and cement content and the type of binder (see paragraph 2), the fitted parameter s varies between 0.96 to 0.99 (cement used by CSM) and between 1.28 and 1.71 (cement used by CVR C-mix®).

4. RESULTS OF UCS AND ELASTIC MODULUS OF CORE SAMPLES

950 UCS tests and 100 test of elastic modulus are performed on samples, cored at 23 different job sites in Belgium. The soil is mixed with the water\binder mixture by the soil mix systems and the typical execution parameters, used in Belgium (see paragraph 2). It is obviouss that the UCS and the elastic modulus are influenced by these execution parameters, the soil conditions and so forth.

4.1. Influence of the soil conditions on the UCS of soil mix samples

In order to focus on the influence of the soil conditions, the UCS results in this paragraph are corrected to a curing time of 28 days (based on paragraph 3.4).

To determine the influence of its nature, the soils are classified as (A) quaternary or tertiary sand, (B) silt or (C) alluvial clay. Figure 4 to 6 show the histograms of the UCS test results of the soil mix samples, corrected to a curing time of 28 days, according to the nature of the soil. It is clear that the UCS of soil mix from sands is generally higher than the UCS of soil mix from clays. 80% of the soil mix samples has a UCS at 28 days higher than 4.5 MPa (sand), 3.0 MPa (silt) and 1.7 MPa (clay). It is also noticed that a large variability of the UCS is present, with no regards to the nature of the soil.

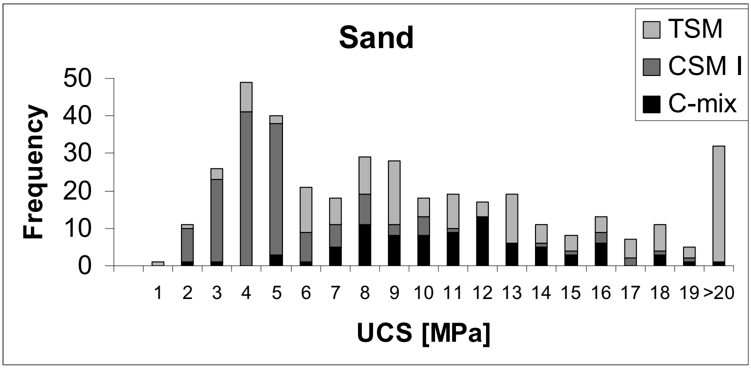

Figure 4. Histogram of UCS [MPa] of cored samples of soil mix material, mixed in quaternary and tertiary sand by a TSM, CSM or CVR C-mix®. The test results are corrected to a curing time of 28 days.

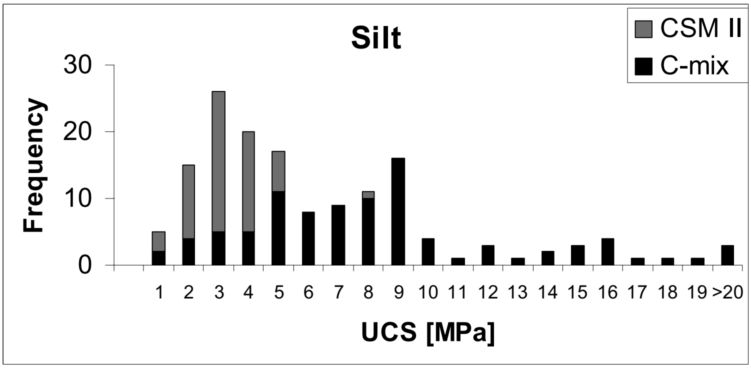

Figure 5. Histogram of UCS [MPa] of cored samples of soil mix material, mixed in silt soils by a CSM or CVR C-mix®. The test results are corrected to a curing time of 28 days.

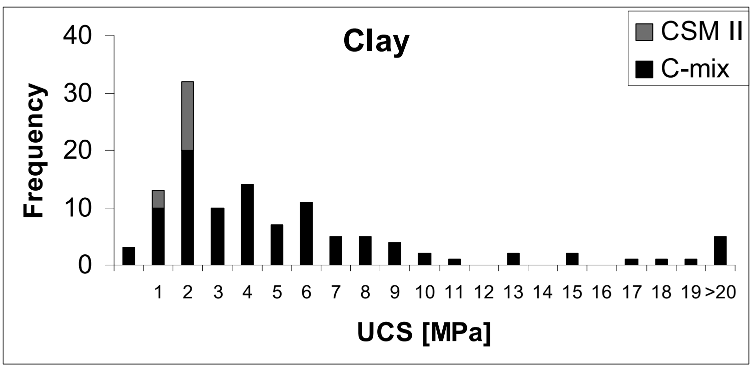

Figure 6. Histogram of UCS [MPa] of cored samples of soil mix material, mixed in alluvial clay soils by a CSM or CVR C-mix®. The test results are corrected to a curing time of 28 days.

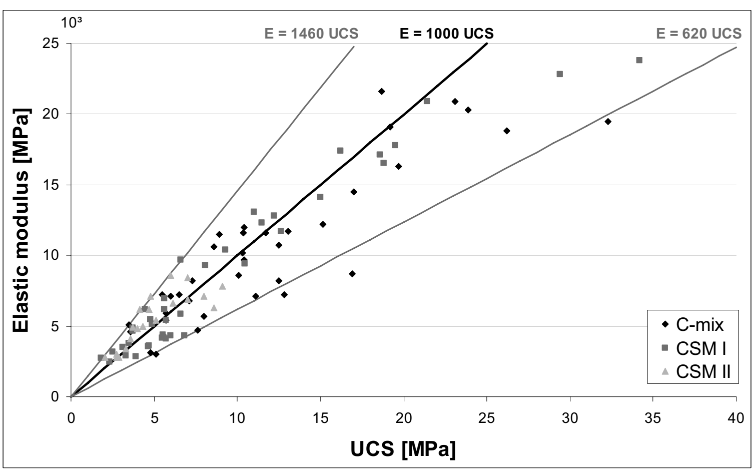

Figure 7. Elastic modulus [MPa] as a function of the UCS [MPa] of soil mix material in different types of soil.

4.2. Elastic modulus of soil mix material

The secant elasticity modulus has been determined on 100 cored soil mix samples. After the cyclic loading for the determination of the elastic modulus, the test is pursued until failure to define the UCS (as described in paragraph 3). These samples are cored in soil mix walls, executed on 17 sites, with various soil conditions and various execution parameters (paragraph 2). The curing time of the tested soil mix samples varies between 14 days and 180 days. Since the aim of this paragraph is to determine the correlation between the elastic modulus and the UCS of the soil mix material in general, the test results in this paragraph are not corrected for the curing time.

Figure 7 shows the elastic modulus as a function of the UCS of the tested soil mix material, without distincting for the soil type. A linear relation between the elastic modulus and the UCS is fitted. Doing so, the best estimated value of the elastic modulus of the soil mix material is roughly:

$$E = 1000\,UCS \tag{3}$$

where E is the secant elastic modulus [MPa] and UCS the unconfined compressive strength [MPa] of the soil mix material. A lower 5% fractile estimation of the elastic modulus of the soil mix material is:

$$E = 620\,UCS \tag{4}$$

A higher 5% fractile estimation of the elastic modulus of the soil mix material is:

$$E = 1460\,UCS \tag{5}$$

These estimations are only valid for the range 2 MPa < UCS < 30 MPa.

5. DETERMINATION OF CHARACTERISTIC VALUE OF THE UCS

The UCS (tested as in paragraph 3) is used as a quality control for the in situ soil mix material. The aim is to estimate a 5% fractile characteristic value of the UCS that may be considered in the design. The conventional method to estimate a characteristic value, is to assume a Gaussian population of the test results. In this case, the 5 % fractile characteristic value is estimated as (neglecting student t - correction):

$$X_{k,0.05} = \overline{X} - 1.64\,\sigma \tag{6}$$

where $X_{k,0.05}$ is the estimated 5% fractile characteristic value, $\overline{X}$ the mean value and σ the standard deviation of the population of the test results.

This method is considered in Belgium to give by far too pessimistic results for populations of UCS of soil mix material. This is demonstrated in Table 2, which compares the 5% fractile lowest test result (as determined on the test population), with $X_{k,0.05}$ (Eq. 6). For example, the UCS results of samples from Ghent KII (TSM in tertiary sand) show a $X_{k,0.05}$ of -0.7 MPa. Remark that a negative characteristic UCS value has no physical sense. Though, the 5% fractile lowest test result of the population amounts to 6.3 MPa. This substantial difference is caused by the non-symmetrical and non-Gaussian distribution of the UCS test results (Figure 8). Furthermore, the UCS results above 25 MPa causes an important increase of the standard deviation and, hence, a decrease of the $X_{k,0.05}$.

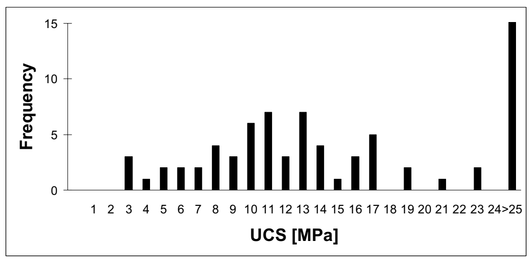

Figure 8. Histogram of the UCS test results of soil mix samples, cored at the site Ghent KII (TSM in tertiary sand).

The estimation of the characteristic value, assuming a log-normal distribution, gives a more realistic estimation. For example in the case of Ghent KII, the estimated characteristic value, assuming a log-normal distribution, amounts to 5.0 MPa. This value is to be compared to the 5% fractile lowest test result (as determined on the test population: 6.3 MPa). The 20% underestimation of the characteristic value of the UCS is due to the non-perfect log-normal distribution of the test results. Figure 9 shows the histogram of the base-10 logarithm of the test results of the UCS on soil mix cores from Ghent KII. This graph suggests that the population of the test results consists of two subpopulations (a population around 1.1 (thus 13 MPa) and one around 1.5 (thus 32 MPa)).

Table 2. Comparison of 5% characteristic value of the test results of the UCS on soil mix material, determined assuming a Gaussian distribution and assuming a log-normal distribution. Per site, the UCS tests are executed on samples, cored on the same depth (± 0.2 m) with about the same curing time. Samples from different sites may be cored at miscellaneous depths or may have different curing time

Site	Soil mix system	Soil	Mean value of UCS test results [MPa]	Standard deviation of UCS test results [MPa]	Coefficient of variation [%]	Number of tested samples [-]	5% fractile characteristic UCS value [MPa] (testpopu-lation)	5% fractile characteristic UCS value [MPa] (Gaussian)	5% fractile characteristic UCS value [MPa] (log-normal)
Bruges	CSM	Quaternary sand	6.3	1.6	25.4	39	4.1	3.8	4.0
Seabruges	CSM	Quaternary sand	6.5	0.8	12.3	38	4.8	5.3	5.3
Ghent KI	TSM	Tertiary sand	9.8	4.6	46.9	60	3.6	2.3	3.6
Ghetnt KII	TSM	Tertiary sand	17.2	10.9	63.4	52	6.3	-0.7	5.0
Antwerp	CVR C-mix®	Quaternary sand	11.9	4.1	34.5	50	6.5	5.2	6.4
Lommel	CVR C-mix®	Quaternary sand	18.6	3.9	21.0	39	11.6	12.2	12.4
Tongeren	CSM	Silt	5.3	1.6	30.2	33	2.8	2.7	2.7
Sint-Lievens Houtem	CVR C-mix®	Silt	10.8	4.9	45.4	31	4.8	2.7	4.5
Limelette	CVR C-mix®	Silt	14.8	5.4	36.5	38	7.4	6.0	7.8
Anderlecht	CVR C-mix®	Silt	8.0	5.8	72.5	64	2.0	-1.6	1.9
Ghent	CVR C-mix®	Alluvial clay	8.6	7.0	81.4	41	1.5	-2.8	1.6
Borgloon	CVR C-mix®	Alluvial clay	5.7	3.1	54.4	26	1.0	0.6	1.4
Knokke	CVR C-mix®	Clay	7.3	7.2	98.6	25	0.5	-4.5	0.9
Erembode-gem	CVR C-mix®	Alluvial clay	8.0	4.6	57.5	25	2.3	0.4	2.4

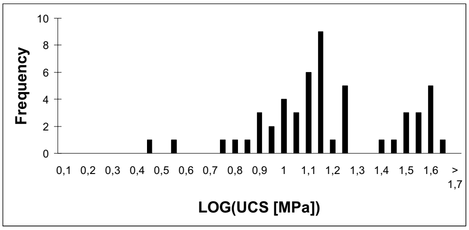

Figure 9. Histogram of the base-10 logarithm of the UCS test results of soil mix samples, cored at the site Ghent KII (TSM in tertiary sand).

In general (Table 2), the estimation of the characteristic value, assuming a log-normal distribution, is more realistic than the estimation, based on the Gaussian approach. Remark that the characteristic value of the UCS of soil mix material, is obtained by testing samples of about 100 mm in length and of about 100 mm in diameter. Further research will be performed to analyse the "size" dependency of this characteristic value that may be considered in the wall design criteria.

6. CONCLUSIONS

The application of the soil mix technology for the realisation of soil and water retaining structures is sharply increasing in Belgium, as in other parts of the world.

Using the soil mix technology for retaining structures, the quality in general, the UCS and the elastic modulus of the soil mix material should be estimated in advance. For this purpose Figures 4 to 7 can be used in Belgian-like soils (if the execution parameters are similar). After the mixing, laboratory tests of in situ cored soil mix material are to be executed to confirm the estimated parameters. Therefore, a procedure to determine the characteristic UCS of soil mix material is proposed and validated. This research is financially supported by the Belgian Normalisation Institute (NBN; BBRI, 2009 – 2010).

The question of an adapted methodology for the mechanical calculation of the soil mix structures taking into account the heterogeneities and soil-inclusion, remains unanswered. End 2009, the BBRI has started a research project about the calculation methodology of soil mix material, focussing on :

1. the compressive strength of soil mix structures considering the influence of soil inclusions,
2. the adherence between the soil mix material and the steel reinforcement elements,
3. the durability of soil mix material,
4. the permeability.

The aim is to obtain a calculation methodology for the soil mix structure, accounting for the presence of the heterogeneities and soil-inclusions, the scale effects and the time-effects such as curing time and creep. This new research project is performed in collaboration with the Catholic University of Leuven and the Belgian Association of Foundation Contractors (ABEF) and is financially supported by the Agency for Innovation by Science and Technology of the Flemish region (IWT; BBRI 2009-2013).

7. REFERENCES

BBRI, 2009. SOIL MIX in constructieve en permanente toepassingen – Karakterisatie van het materiaal en ontwikkeling van nieuwe mechanische wetmatigheden IWT 080736 (in Dutch)

BBRI, 2009. BESCHOEIINGEN – Richtlijnen voor het ontwerp, de uitvoering en de monitoring van klassieke en nieuwe beschoeiingstechnieken. NBN CC CCN/PN/NBN – 613 (in Dutch)

Eurosoilstab. 2002. Development of design and construction methods to stabilise soft organic soils. Design Guide Soft Soil Stabilisation. EC project BE 96-3177.

EN 1992-1-1, 2004. Eurocode 2: Design of concrete structures – Part 1-1: General rules and rules for buildings. CEN

EN 14679, 2005. Execution of special geotechnical works – Deep mixing. CEN TC 288 WI 011.

NBN EN 206-1, 2006. Concrete – Part 1: Specification performance, production and conformity. NBN.

Larsson, S. 2005. State of Practise Report - Execution, monitoring and quality control. In International Conference on Deep Mixing. Best Practise and Recent Advances; Proceedings of the International Conference on Deep Mixing (Deep mixing '05), Stockholm, Sweden, May 23-25, 2005, pp. 732-786. Swedish Deep Stabilization Research Centre.

NBN B15-203, 1990. Proeven op beton – Statische elasticiteitsmodulus bij druk. NBN (in Dutch).

Probaha, A. 1998. State of the art in deep mixing technology: part I. Basic concepts and overview. *Ground Improvement*, Vol. 2, pp. 81-92.

Probaha, A., Tanaka H. & Kobayashi M. 1998. State of the art in deep mixing technology, part II. Applications. *Ground Improvement Journal*, Vol. 3, pp. 125-139.

Rutherford C.J., Biscontin G., Koutsoftas D. & Briaud J.L. 2007. Design process of deep soil mixed walls for excavation support. *International Journal of Geoengineering Case Histories*, Vol. 1, pp. 56-72.

Improvement of silty sand unconfined compression strength by using Epoxy resin

M.Ghorbanalizadeh
Civil Engineering Department Imam Khomeini International University, Qazvin, Iran

S.A. Naeini
Civil Engineering Department Imam Khomeini International University, Qazvin, Iran

ABSTRACT: Materials engineers are continually confronted by the depletion of quality construction materials for road and airfield construction available megacities. This study reports on a laboratory experiment was conducted to evaluate the stabilization of a silty-sand (SM) material with epoxy resin (bisphenol A) stabilizer. All specimens were prepared at dry density of 17 $kn/m^{3.}$ Specimens were prepared by adding different amount of epoxy resin polymer emulsion (3%, 4%, and 5 %) to silty sand with (0%, 10%, 20%, 30%, 35%, 45% and 60%) silt content. Average unconfined compressive strength of specimens determined with uniaxial test. The results of this study indicated that the addition of epoxy resin improves significantly the Compressive strength of samples under dry condition. This improvement depends on the content of polymer and silt.

INTRODUCTION

In developing countries like Iran, the biggest handicap to provide a complete network of road system is the limited finances available to build roads. Use of local materials, including local soils, can considerably lower down the construction cost. If the stability of the local soil is not adequate for supporting wheel loads, the properties are improved by soil stabilization techniques. The stabilization of soil for use in subgrade for pavement is an economic substitute of costly paving materials. There are many techniques for soil stabilization, either mechanical or chemical, but all of them require skilled manpower and equipment to ensure adequate performance.

The alteration of soil property to improve its engineering performance is known as soil stabilization (Lambe and Whitman, 1979). The chief soil properties of concern in soil stabilization are mechanical properties, permeability, volume stability, and durability. The polymeric materials used for soil stabilization may be either natural or synthetic. Natural polymers, for example, liquid asphalts, have been used for stabilization and surfacing of low-volume roads (Mamlouk and Zaniewski, 1999). Palmer et al. (1995) have demonstrated that lignin, a natural polymer, introduces better improvement for ground modification compared to non-organic stabilizers. Lignin is also used in combination with other chemicals to achieve soil improvement (Puppala and Hanchanloet, 1999). acryl ate, epoxy (Ajayi-Majebi et al., 1991), Polysiloxane, and latex acrylic copolymers (Petry and Little, 2002). In a research paper studying many non-traditional stabilizers, Santoni et al. (2002) found that polymers have the best potential to increase strength of silty-sand soils under wet and dry conditions. They reported that the examined polymers maintained good strength potential in both dry and wet conditions. A waterborne polymer emulsion system has been used to introduce structural modification of sandy soil (Al-Khanbashi and El-Gamal, 2003). The system was found to enhance the mechanical properties and reduce the hydraulic conductivity ofsand by incorporating small percentages of polymer. Notwithstanding the good results polymers give in soil stabilization, their use – and non-traditional stabilizers in general – is considered limited due to the lack of adequate studies and publications. In this study the effect of different amounts of polymer emulsion on strength parameters of silty sand was surveyed.

2. METHODS AND MATERIALS

2.1 Materials

A commercial product of Epoxy Resin (bisphenol A) and a polyamide hardener was used in this research. A multicomponent resin grout that usually provides very high, tensile, compression, and bond strengths. The additive mixture was composed of a 1:0.15 ratio of epoxy resin to polyamide hardener, respectively. Some important properties are given in Table 1. Seven silty sand soils with different percents of silt content (0, 10, 20,30,35,45 and 60 wt. % (% by dry density)) were used in this research. The mine silty sand used in this study was obtained from Caspian mine in the Alamot region of the Iran. The sand was characterized by grain sizes ranging from 0.075 to 4.75 mm and with a specific gravity of 2.68. The silt was characterized by grain sizes ranging from 0.075 to 0.002 mm and with a specific gravity of 2.67. The sand and silt was used was classified based on the Unified Soil Classification System (ASTM D2487) as well graded sand (SW) and low plasticity silt (ML) , respectively. The grain size distributions of soils are shown in Fig.1. The optimum moisture content and the maximum dry density as determined by the Modified Test Procedure (ASTM D1557) were 7% and 22.3 (KN/m^3), respectively, as shown in Fig. 2.

Table 1. Physicochemical properties of as- received emulsion

Name	Epoxy Resin
Density (KN/m^3)	22
Solvability in Water	Insoluble in water
Chemical type	$C_3H_5O\ [C_{18}H_{19}O_3]_n\ C_{18}H_{19}O_3$
Elastic modules (GPa)	20
Boiling point (°C)`	>200°C

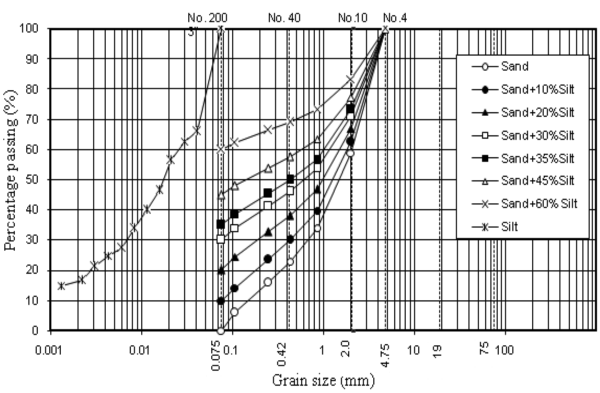

Figure1. Grain size distribution curves

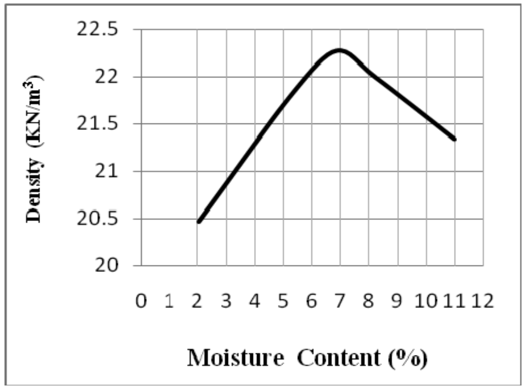

Figure 2.Moisture – Dry Density

2.2. Specimen preparation

Specimens with specified amount of polymer added to the dry silty sand were prepared by mixing the polymer with silty sand in the loose dry density equal to 17 KN/m^3. The soil/polymer mixture was processed into dough using a mechanical kneader. The uniformly mixed dough was subsequently placed into a steel mold measuring 89 mm in height and 38 mm in diameter. Finally, the molded specimens were left to cure, at room's temperature. Specimens containing 3,4,5 wt.% (% by dry weight) polymer and 0,10,20,30,35,45 & 60 wt.% (% by dry density) silt were prepared using this method. We couldn't make specimen containing 3wt. % polymer and 60wt. % silt, because polymer couldn't cover all of sample's area. Samples used in this study were prepared for testing mechanical properties. All specimens used were cylindrical in shape, measuring 89 mm in length and 38 mm in diameter, with a length –to- diameter ratio of 2.34, a value falling within the range specified by ASTM D 4219 for unconfined compression tests. Figure.3, An SEM photograph of the microstructure of impregnated Qazvin soil.

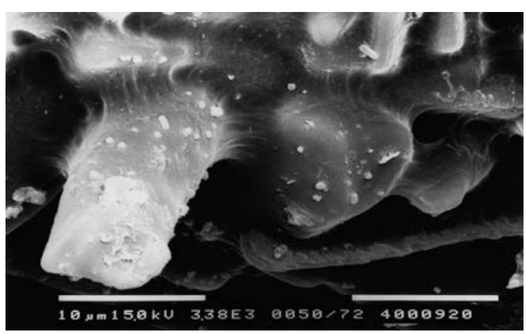

Figure 3. SEM photograph of the microstructure of epoxy-impregnated soil

2.3. Curing time

Curing times of 1, 2, 4, 6 and 8 days were used in this research. Two samples for each curing time were prepared in order to provide an indication of reproducibility as well as to provide sufficient data for accurate interpolation of the results. Additional curing times beyond 8 days may be desired in some cases to investigate longer term changes in strength.

2.4. Unconfined Compressive Strength Testing (ASTM D 2166-00)

Unconfined compressive strength testing was performed on all extracted specimens using a strain rate of approximately one percent per minute. A data acquisition system was used to record the applied load and deformation. Corrections to the cross-sectional area were applied prior to calculating the compressive stress on the specimen. Each specimen was loaded until peak stress was obtained, or until an axial strain of approximately 15% was obtained.

3. RESULTS AND DISCUSSION

The following section presents the results of laboratory tests performed for silty sand soils that have caused problems during construction or resulted in poor performance in service.

The seven soils were obtained from Caspian site of the state: 40 km from North Qazvin, Iran.

3.1. Testing Program

For this research, it was desired to evaluate the effectiveness of the stabilizer mixed with soils at the dry condition. Low to high dosage rates were used for soils at dry condition. The stabilizer dosage rates and soil dry condition used for this study are summarized in the table 2.

Table 2. Dosage Rates for North Qazvin Silty Sand

Silt content(% by dry weight)	Amendment	Amendment Dose Rate (% by dry weight)		
		Low	Medium	High
0%	Epoxy Resin	3%	4%	5%
10%	Epoxy Resin	3%	4%	5%
20%	Epoxy Resin	3%	4%	5%
30%	Epoxy Resin	3%	4%	5%
35%	Epoxy Resin	3%	4%	5%
45%	Epoxy Resin	3%	4%	5%
60%	Epoxy Resin	3%	4%	5%

3.2 Effect of curing time on soils strength

The unconfined compression strength of stabilized samples increases with time. Specimens containing polymer content of 3 wt. % were having curing time equal to 6 days and Specimens containing polymer contents of 4, 5 wt. %, having curing time equal to 4 days. When we increased the time, cross linking between polymer network increased and as the strength soil increased. The results of curing times and polymer contents on unconfined compression strength listed in Tables 3, 4&5 and figures 4, 5 & 6.

Table 3. The UCS results of specimens at different curing periods, with 5% polymer (MPa)

Silt content(% by dry weight)	Curing time(hours)					
	12	24	48	96	144	192
0	3	4.35	4.37	4.4	-	-
10	-	1.43	1.8	2.9	3.1	-
20	-	1.06	1.36	2.2	2.2	-
30	-	0.54	0.75	1.3	1.3	-
35	-	0.37	0.42	0.6	1.1	1.2
45	-	0.26	0.39	0.5	0.6	0.6
60	-	.15	0.16	0.24	0.29	0.3

Table 4. The UCS results of specimens at different curing periods, with 4% polymer (MPa)

	Curing time(hours)					
	12	24	48	96	144	192
0	2.1	3.09	3.12	3.19	-	-
10	-	0.91	1.12	1.69	1.7	-
20	-	0.4	0.59	1.15	1.17	-
30	-	0.17	0.33	0.36	0.40	-
35	-	0.05	0.06	0.15	0.21	0.21
45	-	0.04	0.05	0.12	0.19	0.20
60	-	0.041	0.048	0.11	0.16	0.17

Table 5. The UCS results of specimens at different curing periods, with 3% polymer (MPa)

Silt content(% by dry weight)	Curing time(hours)					
	12	24	48	96	144	192
0	1.08	1.27	1.49	2.21	2.3	-
10	-	0.18	0.26	0.53	0.64	0.65
20	-	0.045	0.062	0.1	0.18	0.19
30	-	0.027	0.031	0.06	0.084	0.087
35	-	0.015	0.019	0.024	0.045	0.051
45	-	0.008	0.012	0.017	0.035	0.041
60	-	-	-	-	-	-

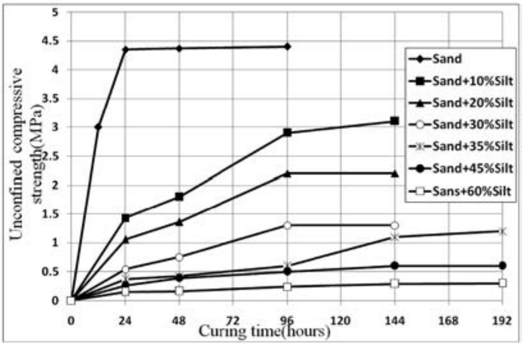

Figure 4. Effects of curing time on compressive strength of specimens, with 5% polymer (MPa)

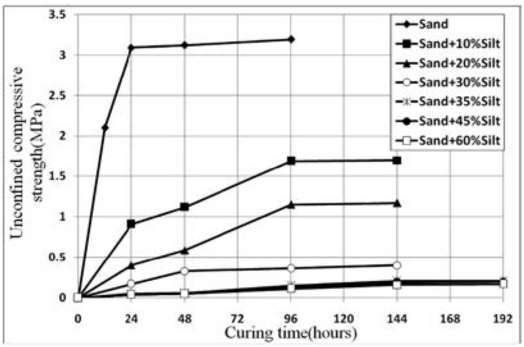

Figure 5. Effects of curing time on compressive strength of specimens, with 4% polymer (MPa)

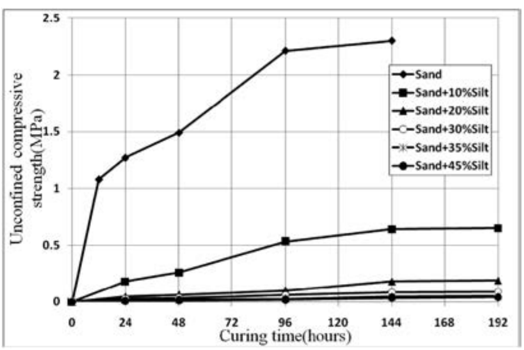

Figure 6. Effects of curing time on compressive strength of specimens, with 3% polymer (MPa)

3.3. Effect of silt content on soils strength

The results of unconfined compression strength on stabilized soils are presented in Figure 7. Stabilized soils with the 3% polymer have lower strength than 4%&5% polymer. For each specimen, the unconfined compression strength decrease with increment silt content. This means that the soil becomes weakened with an increase in the silt content up to 60%. This phenomenon is explained by the fact that the fine grains of silt positioned around and among the sand grains, the polymer cannot cover all of sample's area.

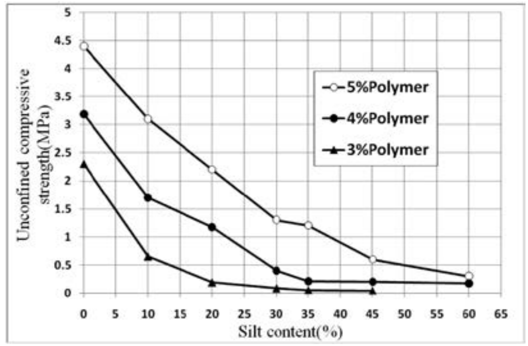

Figure 7. Variation of the unconfined compressive strength, for specimens modified with the different silt contents, as a function of silt content

3.4. Effect of polymer content on soils strength

Effects of polymer content on unconfined compression strength stabilized soils are presented in Figure 8. The unconfined compression strength increases with increment polymer content. This phenomenon is explained by the fact that with increment polymer content, bonding between particles increase.

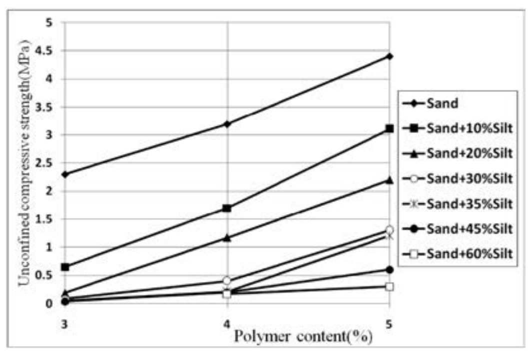

Figure 8. Variation of the unconfined compressive strength, for specimens modified with the different emulsions, as a function of polymer content

3.5. Modulus of elasticity

Several methods are available for determining (actually estimating) the stress-strain modulus, one of several methods is unconfined compression test. Unconfined compression tests tend to give conservative values of E_s; i.e., the computed value (usually the initial tangent modulus) is too small, resulting in computed values of ΔH being large compared with any measured value. In this study, we computed Secant modulus (E_{50}) for strain equivalent 0% & 50% strain maximum unconfined strength, as are shown in table 6.

Secant modulus is the slope of a straight line connecting two separate points of the curve.

Table 6. Variation of the modulus of elasticity (MPa)

Silt content (%)	Polymer content (%)		
	3%	4%	5%
0	114	361	503
10	29	85	210
20	21	51	150
30	16.5	29	80
35	6.3	20	51
45	3.1	6.75	39
60	-	5	25

3.5.1. Effect of silt content on Modulus of elasticity

The variation of the modulus of elasticity of the siltysand/polymer system as a function of silt content for the specimens modified with the different silt contents is shown in Figure 9. When we increased silt contents, the fracture of specimens were soft as modulus of elasticity decreased.

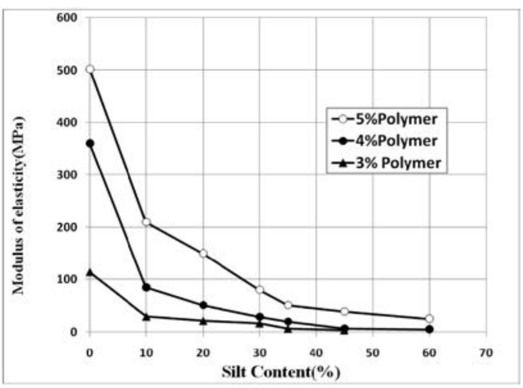

Figure 9. Variation of the modulus of elasticity, as function of silt content (MPa).

3.5.2. Effect of polymer content on Modulus of elasticity

The variation of the modulus of elasticity of the siltysand/polymer system as a function of polymer concentration for the specimens modified with the different contents is shown in Figure 10. Modulus of elasticity increased linearly with a polymer concentration up to 5 wt. % for the entire polymer contents used. A very important characteristic is the rate of increase of strength and modulus (slope of trend line) for each of the specimens. The rate increased at higher polymer percentages. It is obvious that the slopes of the trend lines for specimens including fine grains had espianade. Note that with increase of fine grain diminished cross linked of polymer.

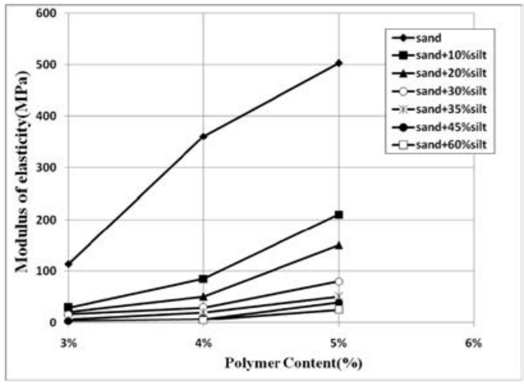

Figure 10. Variation of the modulus of elasticity, as function of polymer content (MPa).

4. RESULTS

This study was undertaken to investigate the influence of polymer percentage and curing time on the unconfined compression strength of stabilized dry silty sandy soils. The results of the study are presented in fallowing conclusions:

1. The overall increase in mechanical properties of the polymer-modified silty sand specimens is attributed to the increased interparticle friction associated with the deposited polymer film and to the interparticle ties. Another very important factor is the adhesion where neighboring silty sand particles are in contact, where the polymer acts as an adhesive that adjoins them. This adhesion, in addition to the friction between silty sand particles enhanced by the polymer coverage of particle surfaces, and the polymer ties between neighboring silty sand particles that are not in contact, are the structural changes that affect the mechanical properties of the silty sand.
2. The unconfined compression strength of silty sand increases with increment of poly-

mer. However, the strength of silty sand is less than the clean sand.

3. The strength of sand will decrease with increment of silt contents up to about 35% and above 35% silt content, the strength of the soil almost becomes constant. This phenomenon is explained by the fact that the fine grains of silt positioned around and among the sand grains, the polymer cannot cover all of sample's area.
4. The strength of specimens will increase with increment of polymer contents, that this phenomenon is explained by the fact that with increment of polymer, the polymer can cover all of sample's area and increase cross links.

5. REFERENCES

Ajayi-Majebi, A., Grissom, W.A., Smith, L.S. and Jones, E.E (1991)"Epoxy – resin – based chemical stabilization of a fine, poorly graded soil system", Transportation Research Record 1295, National Research Council Washington, D.C.

AlKhanbashi, A.and El Gamal, M. (2003) "Modification of sandy soil using waterborne polymer", Journal of Applied Polymer Science, 88, 2484–2491.

Lambe, T.W. and Whitman, R.V. (1979) "Soil mechanics, SI version", Wiley, New York.

Mamlouk, M.S. and Zaniewski, J.P. (1999)"Materials for Civil and Construction Engineers", Addison Wesley.

Palmer, J.T., Edgar, T.V. and Boresi, A.P. (1995) "Strength and Density Modification of Unpaved Road Soils due to Chemical Additives", Mountain-Plains Consortium, Report no. 95–39, Fargo, ND.

Petry, T.M. and Little, D.N. (2002) "Review of stabilization of clays and expansive soils in pavements and lightly loaded structures – history, practice and future", Journal of Materials in Civil Engineering, 14, 447–460.

Puppala, A.J. and Hanchanloet, S. (1999)" Evaluation of a new chemical (SA-44/LS-40) treatment method on strength and resilient properties of a cohesive soil." 78th Transportation Research Board Annual Meeting, Paper no. 99–0389, Washington, D.C.

Santoni, R.L., Tingle, J.S. and Webster, S.L. (2002) "Nontraditional Stabilization of Silty-Sand." 81st Transportation Research Board Annual Meeting, Paper no. 02-3756, Washington, D.C.

Analysis of Strength Development in Blended Cement Admixed Bangkok Clay

S. Horpibulsuk, A. Sudeepong
Construction Technology Research Unit, School of Civil Engineering, Suranaree University of Technology, Nakhon Ratchasima, THAILAND

ABSTRACT: Fly ash has been widely accepted as a replacement material in cement admixed clay. The role of fly ash is to disperse large clay-cement clusters into smaller clusters. This dispersing effect is regarded akin as an addition of cement. Based on this premise, the clay-water/cement ratio hypothesis for blended cement admixed clay is proposed for analyzing the strength development. The role of the clay-water/cement ratio, w_c/C, on the strength development in the blended cement admixed clay is presented. The lower the w_c/C, the greater the strength. The interrelationship among strength, clay-water/cement ratio, curing time, and fly ash content is proposed.

1. INTRODUCTION

Soft clay formations especially when their in-situ water contents are closed to or higher than liquid limit have low inherent shear strength and large potential for settlement. One of the effective ground improvement techniques is in-situ deep mixing (DM). The DM method has been developed during last over two decades primarily to effect columnar inclusions into the soft ground to transform such whole soft ground to composite ground. It has been applied popularly and successfully in Southeast Asia.

For soft Bangkok clay deposit, DM technology has been extensively applied in road embankments, retaining walls, and slope stability, etc. The major cementing agent used in DM method is Portland cement due to cost effectiveness. The soft Bangkok clay is classified as non- to low swelling clay that the swelling potential increases with depth (Horpibulsuk et al., 2007). The analysis of strength development in cement admixed Bangkok clay by the clay-water/cement ratio, w_c/C based on the Abrams' law (Abrams, 1918), has successfully done by Horpibulsuk et al. (2009b). The generalized strength prediction equation of the cement admixed Bangkok clay has been proposed and verified. It is possibly applied to the other non- to low swelling clays.

For cost effectiveness, it is worthwhile to replace pozzolanic material (fly ash) to Portland cement for ground improvement. Recently, Horpibusuk et al. (2009a) have investigated the role of the fly ash on the strength development in the blended cement stabilized clay based on macro- and micro-structural observations. They have demonstrated that for cement stabilized clay that an input of cement is relatively low compared to concrete, pozzolanic reaction is minimal due to low $Ca(OH)_2$ to be consumed. The role of fly ash is mainly to disperse large clay-cement clusters formed due to physico-chemical interaction into smaller clusters. It results in the increase in the reactive surface and hence strength enhancement.

The present paper attempts to investigate and analyze the laboratory strength development in the blended cement admixed Bangkok clay. The clay-water/content ratio hypothesis (Miura et al., 2001) is adapted for this analysis.

2. CLAY-WATER/CEMENT RATIO HYPOTHESIS FOR BLENDED CEMENT ADMIXED CLAY

Cement and clay are interacting materials with water. Fly ash, silt, and sand are non-interacting materials, primarily due to their low specific surface and non-electrical nature of surfaces. Due to physicochemical interactions with water, the soft clay would have a specific micro-fabric formed due to the interacting nature of the clay. The cement can be premised to drift to pore space (the spacing between clusters to clusters) and weld the fabric by gel as subsequent hydration of cement takes place.

Horpibulsuk & Miura (2001); Miura et al. (2001); and Horpibulsuk et al. (2005) have demonstrated that it would be advantageous to have a parameter to reflect the combined effects of clay, cement and water in the analysis of strength and deformation of cement admixed clays. This parameter is designated as clay-water/cement ratio, w_c/C, which is defined as the ratio of clay-water content to cement content. The cement content is the ratio of dry weight of clay to weight of cement. It is a structural parameter, reflecting the effect of the fabric and cementation bond. While the clay water content reflects the microfabric of soft clay, the cement content would influence the level of bonding of that fabric. The application of the w_c/C to predict the strength development in cement admixed clays is successfully done by Horpibulsuk et al. (2003) and Horpibulsuk et al. (2009b).

For the blended cement admixed clay, fly ash as a non-interacting material disperses the large clay-cement clusters into smaller clusters, resulting in the increase in reactive surfaces, and hence cementitious products (Horpibulsuk et al., 2009a). It has been illustrated based on microstructural investigation (Scanning electron microscope, mercury intrusion porosimetry, and Thermal gravity analysis) that the pozzolanic reaction is minimal. This dispersing effect can be regarded akin as an addition of cement. By considering that the input of fly ash can be equivalent to cement content (Papadakis and Tsimas, 2002), the equivalent cement content (C_e) is equal to ka where k is efficiency factor and a is fly ash content. The cement content (C) is thus the summation of input of cement (C_i) and equivalent cement content (C_e). As such, the clay-water/cement ratio hypothesis for the blended cement admixed clay is developed: "For given set of blended cement admixed clay samples, the strength development depends only on clay-water/cement ratio, w_c/C.

3. LABORATORY INVESTIGATION

3.1. Soil Sample

Soil sample is Bangkok clay collected from Ladkrabang district, Bangkok, Thailand at 3 meter depth. The soil is composed of 3% sand, 27% silt and 70% clay. Its specific gravity is 2.63. The liquid and plastic limits are in the order of 89 and 30 percent, respectively. Based on the Unified Soil Classification System (USCS), the clay is classified as high plasticity (CH). Groundwater was about 1.0 m from surface. Natural water content was 85 percent. Grain size distribution curve of the clay is shown in Figure 1.

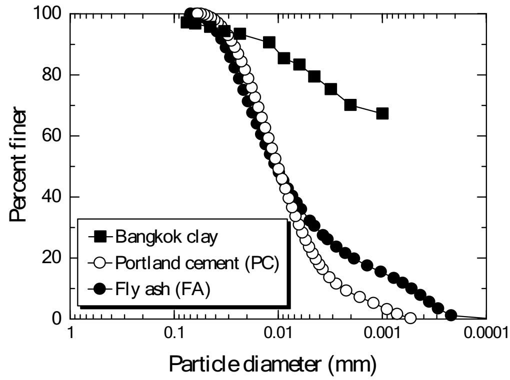

Figure 1. Grain size distribution of Bangkok clay, PC, and FA.

Table 1. Chemical composition of Bangkok clay, PC and FA

Chemical composition (%)	PC	FA
SiO_2	20.90	44.72
Al_2O_3	4.76	23.69
Fe_2O_3	3.41	11.03
CaO	65.41	12.67
MgO	1.25	2.63
SO_3	2.71	1.28
Na_2O	0.24	0.07
K_2O	0.35	2.87
LOI	0.96	1.42

3.2. Cement and fly ash

Type I Portland cement (PC), fly ash (FA) from Mae Moh power plant in the north of Thailand, and tap water were used in this study. Chemical composition of PC and FA is given in Table 1. The FA was passed through sieve No. 325 to remove larger particles. Total amount of the major components SiO_2, Al_2O_3, and Fe_2O_3 in FA is 79.44%. FA is classified as class F fly ash in accordance with ASTM C 618. Grain size distribution curves of PC, and FA are also shown in Figure 1. These curves were obtained from the laser particle size analysis. It is found that the grain size distribution curves of PC and FA are similar. D_{50} of PC is 0.01 mm (10 micron) being almost the same as that of FA.

Specific gravities of PC, and FA are 3.15 and 2.54, respectively. From the grain size distribution curves, it is found that the particles of Bangkok clay are much smaller than those of PC, and FA.

3.3. Methodology

Bangkok clay was passed through a 2-mm sieve to remove coarser particles. The water content was adjusted to the range of liquidity indices (*LI*) i.e., 1.0, 1.5, and 2.0. The liquidity index has been used in this investigation as an indicator to refer the initial water content of the clay in relation to plasticity characteristics of the clay before cement is admixed as has been done by Horpibulsuk et al. (2003 and 2009b). This intentional increase in water content is to simulate water content increase, taking place in wet method of dispensing cement admixture in deep mixing. The clay with its water content, corresponding to the above levels of *LI* is thoroughly mixed with the cement and fly ash. Cement content, C_i, varies from 0 to 30%, FA content, a, varies from 0 to 60% by weight of cement ($a = FC_i$ where $F =$ 0 to 60%). The mixing time was arbitrarily fixed at 10 min as recommended by Miura et al. (2001); and Horpibulsuk et al. (2005). Such a uniform paste was transferred to cylindrical containers of 50 mm diameter and 100 mm height, taking care to prevent any air entrapment. After 24 hours, the cylindrical samples were dismantled. All the cylindrical samples were wrapped in vinyl bags and stored in a humidity room of constant temperature (20±2°C) until lapse of different curing times as planned. Unconfined compression (UC) tests were run on samples after 7, 14, 28, 60, 90, and 120 days of curing. The rate of vertical displacement in UC tests was 1 mm/min.

4. TEST RESULTS

4.1. Strength development with w_c/C

Figure 3 shows the influence of fly ash content on the strength development in the FA blended cement admixed Bangkok clay cured for 28 days. It is noted that initially the strength increases with fly ash content and attains the peak value at F = 25%. For F > 25%, the strength considerably decreases. It is thus concluded the optimal F is 25% where the dispersing effect is the most effective. When F > 25%, fly ash particles surround the cement grains and obstruct the interaction between water and cement grains, resulting in less cementatious products and hence strength.

The dispersing effect for $F \leq 25\%$ can be regarded akin to an increase in cement. Based on the Abrams' law and the clay-water/cement ratio hypothesis for blended cement admixed clay, the following strength equation is proposed.

$$q_u = \frac{A}{\left(\dfrac{w_c}{C_i + C_e}\right)^B} \tag{1}$$

$$q_u = \frac{A}{\left(\dfrac{w_c}{C_i\left(1 + kF\right)}\right)^B} \tag{2}$$

where q_u is the compressive strength of blended cement admixed clay at a specific curing time, w_c is clay water content, A and B are empirical constants. The three parameters A, B, and k for a particular curing time can be determined from a non-linear regression.

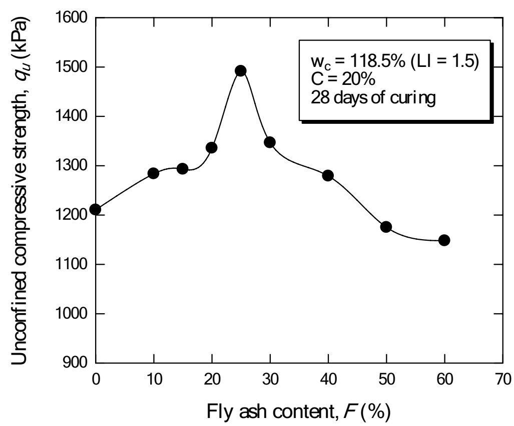

Figure 2. Influence of fly ash on the strength development of blended cement admixed clay.

Figure 3 shows an analysis of strength development in the FA blended cement admixed Bangkok clay. It is shown that the strength development for F = 0 to 25% at a particular curing time can be described by Eq. (2). The variation of parameter A is marked and is dependent on curing time. The variation of parameter B in the liquidity range of 1 to 2 is only between 1.25 and 1.29, and irrespective of curing time, which is a typical feature for cement admixed clays (Horpibulsuk et al., 2003 and 2009b). The parameter *k* insignificantly changes with curing time, varying between 0.72 and 0.79. The practical constant *k*-value for all curing times implies that the pozzolanic reaction is minimal, which is different from concrete that *k*-value increases with curing time (Papadakis and Tsima, 2002).

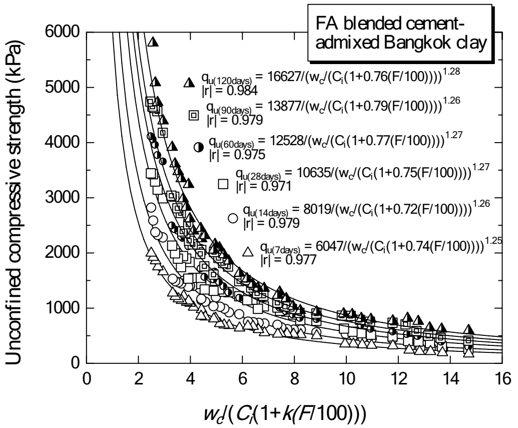

Figure 3. Analysis of strength development in the FA blended cement admixed Bangkok clay using extended clay-water/cement ratio hypothesis.

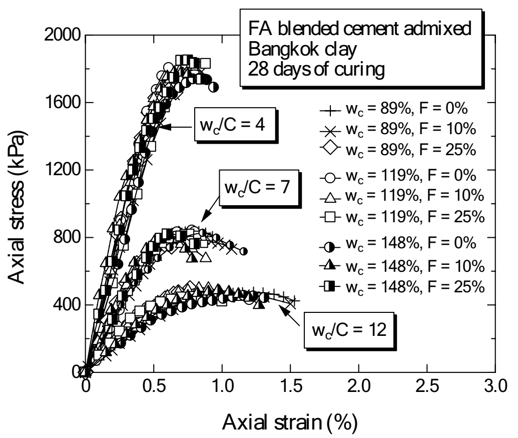

Figure 4. Stress-strain relationship of FA blended cement admixed Bangkok clay samples, having the same w_c/C under unconfined compression test.

The role of w_c/C on the strength development of the blended cement admixed clay is shown in Figure 4. It shows the stress-strain relationship of the blended cement admixed Bangkok clay samples, having the same w_c/C of 4, 7, and 12 but with different combinations of water content, cement content and fly ash content after 28 days of curing. The samples were made up from three conditions of clay water content; i.e., 89%, 119%, and 148% and three conditions of fly ash content; i.e. 0, 10, 25. The *k*-value of 0.75 is taken for determination of the mix proportion. It is noted that the lower the w_c/C, the greater the enhancement of the cementation bond strength, inducing higher strength. The similar stress~strain behavior of all admixed samples, having the same w_c/C, is also figured out.

4.2. Strength ratio at a particular curing time

At a particular curing time, the parameter *A* is eliminated by taking the ratios of strength developed at different clay-water/cement ratios. This is based on the fact that the parameter *A* has a specific value for a blended cement admixed clay at a specified curing time. This results in the following relation:

$$\left\{\frac{q_{(w_c/C)_1}}{q_{(w_c/C)_2}}\right\} = \left[\left(w_c/C\right)_2 - \left(w_c/C\right)_1\right]^{1.27} \quad (3)$$

where $q_{(w_c/C)_1}$ is the strength to be estimated at clay-water/cement ratio of $(w_c/C)_1$ and $q_{(w_c/C)_2}$ is the strength value at clay-water/cement ratio of $(w_c/C)_2$. The value of parameter *B* is taken as 1.27 as recommended for the cement admixed Bangkok clay by Horpibulsuk et al. (2009b). The implication of the above relation is that one laboratory test value of strength developed over a specific curing time at any clay-water/cement ratio is needed. From the above equation, it would be possible to assess the strength at any other clay-water/cement ratio.

4.3. Strength development with time

The strength development with curing time plots is shown in Figure 5 for the FA blended cement admixed Bangkok clay at the liquidity index of 1 to 2. It is noted that strength development with curing time (days) in natural logarithmic scale can be expressed as linear variation. From the above observation, it is evident that at a particular w_c/C, the strength development with time is controlled by the *A*-value only since the *B*- and *k*-values for all practical purposes can be regarded as constant.

Horpibulsuk et al. (2003 and 2009b) have shown that even though the *A*-values of different clays are different due to composition of clay and pore fluid, the rate of strength development with time is identical for various cement admixed clays since the hydration products influence the rate predominantly. Consequently, the strength development with time is a unique relationship for any cement admixed clay. Practically, it is desired, if the strength of cement admixed clay can be assessed in terms of curing time along with the changes in clay-water/cement ratio.

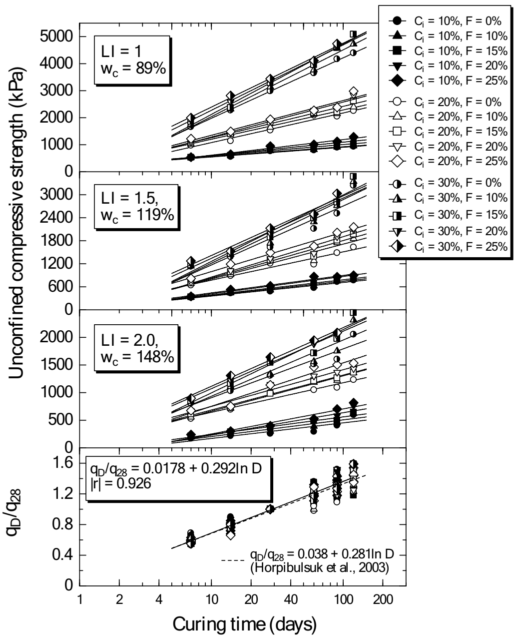

Figure 5. Strength development in the FA blended cement admixed clay and its generalization.

An attempt to generalize the strength development in cement admixed clay has successfully done by the authors (Horpibulsuk et al., 2003; 2009a; and 2009b). They have used the 28-day strength as a reference value. The same generalization of strength development is possibly performed for the blended cement admixed Bangkok clay for different water contents, cement contents, and fly ash contents. This is because the main chemical reaction is also hydration (minimal pozzolanic reaction). The strength ratio plots after normalization for the FA blended cement admixed Bangkok clay is also shown in Figure 5.

It is of very interest to mention that the generalized strength development proposed for cement admixed clays (Horpibulsuk et al., 2003) can represent the strength development in the FA blended cement admixed Bangkok clay. The generalized strength development has been presented in the form:

$$\frac{q_D}{q_{28}} = 0.038 + 0.281 \ln D \tag{4}$$

where q_D is the strength after D days of curing, q_{28} is the 28 day-strength, D is the curing time (days). The generalization accounts for the effects of clay water content, cement content, and fly ash content.

4.4. Interrelationship among clay-water/cement ratio, curing time, and strength

In the development of the interrelationship among clay-water/cement ratio, curing time, and strength, the B value of 1.27 and the k value of 0.75 for LI = 1 to 2 are considered. Consequently, the generalized interrelationship among strength, curing time and w_c/C for predicting strength development of the blended cement admixed clay in which the w_c/C ranges from 2.5 to 15 is expressed by combination either of Equations (2) and (4).

$$\left\{\frac{q_{(w/C)_D}}{q_{(w/C)_{28}}}\right\} = \left[\frac{\left(w_c/\left(C_i+0.75F\right)\right)_{28}}{\left(w_c/\left(C_i+0.75F\right)\right)_D}\right]^{1.27} \left(0.038 + 0.281 \ln D\right) \tag{5}$$

where $q_{(w_c/C)_D}$ is the strength of cement admixed clay to be estimated at clay-water/cement ratio of $\left(w_c/\left(C_i+0.75F\right)\right)_D$ after D days of curing and $q_{(w_c/C)_{28}}$ is the strength of cement admixed clay at clay-water/cement ratio of $\left(w_c/\left(C_i+0.75F\right)\right)$ after 28 days of curing.

5. CONCLUSIONS

This paper analyzes the strength development in the blended cement stabilized clay. The following conclusions can be advanced from this study.

1. Clay-water/cement ratio is a prime parameter governing the strength development in the blended cement admixed clay. Even with the difference in clay water content, cement content and fly ash content, the strength of the blended cement admixed samples are identical as long as the w_c/C is the same.

2. Since the role of the fly ash in the cement stabilization is to disperse the clay-cement clusters into smaller clusters (minimal poz-

zolanic reaction), the *k*-value is practically the same for all curing time.

3. Based on the clay-water/cement ratio hypothesis for blended cement admixed clay, the interrelationship among strength, clay-water/cement ratio, and curing time is proposed. The formulation of the proposed relationship is on sound principles. It is possibly applicable for the other non- to low-swelling clays. For the other medium to high swelling clays and fly ashes, the constants, *B* and *k* can be further refined with the analysis of more data generated for this specific purpose.

6. ACKNOWLEDGEMENT

The financial support provided from Suranaree University of Technology is appreciated.

7. REFERENCES

Abrams, D.A. 1918. Design of Concrete Mixtures. *Structural Materials Research Laboratory*, Lewis Institute, Chicago, Bulletin 1, 20p.

Horpibulsuk, S. & Miura, N. 2001. A new approach for studying behavior of cement stabilized clays. *Proceedings of 15th International Conference on Soil Mechanics and Geotechnical Engineering (ISSMGE)*, Istanbul, Turkey, Vol. 3, pp. 1759-1762.

Horpibulsuk, S., Miura, N., and Nagaraj, T.S. 2003. Assessment of strength development in cement-admixed high water content clays with Abrams' law as a basis. *Geotechnique*, Vol. 53, No. 4, pp. 439-444.

Horpibulsuk, S., Miura, N., and Nagaraj, T.S. 2005. Clay-water/cement ratio identity of cement admixed soft clay. *Journal of Geotechnical and Geoenvironmental Engineering*, ASCE, Vol. 131, No. 2, pp. 187-192.

Horpibulsuk, S., Shibuya, S., Fuenkajorn, K, and Katkan, W. 2007. Assessment of engineering properties of Bangkok clay. *Canadian Geotechnical Journal*, Vol. 44, No. 2, pp. 173-187.

Horpibulsuk, S., Rachan, R., and Raksachon, Y. 2009a.Role of fly ash on strength and microstructure development in blended cement stabilized silty clay. *Soils and Foundations*, Vol. 49, No. 1, pp. 85-98.

Horpibulsuk, S., Rachan, R., and Suddeepong, A. 2009b. Strength development in cement admixed Bangkok clay: laboratory and field investigations. *Soils and Foundations* (under review).

Miura, N., Horpibulsuk, S., and Nagaraj, T.S. 2001. Engineering behavior of cement stabilized clay at high water content. *Soils and Foundations*, Vol. 41, No. 5, pp. 33-45.

Papadakis V.G. & Tsimas. S. 2002. Supplementary cementing materials in concrete Part I: efficiency and design. *Cement and Concrete Research*, Vol. 32, pp. 1525-1532.

Fully coupled numerical modelling of vacuum consolidation

J.P. Hsi
SMEC Australia Pty Ltd, North Sydney, NSW, Australia

C.H. Lee
SMEC Australia Pty Ltd, North Sydney, NSW, Australia

ABSTRACT: This paper presents the simulation of the behaviour of soft soils treated with the vacuum consolidation technique using a fully coupled numerical method. A bridge approach embankment adjacent to a creek is underlain by soft clays up to 25m in thickness. To enable safe construction of the embankment and speedy consolidation of the soft clays, vacuum consolidation was chosen as a means of ground improvement. Detailed instrumentation and monitoring was undertaken to closely monitor the performance of the embankment. A fully coupled numerical modelling method which considers soil-groundwater interaction was used to simulate the behaviour of soft soils subjected to vacuum loading. The measured settlements and pore water pressures at various embankment loading stages were back-analyzed. The geotechnical model representing the site conditions was refined so that the numerical predictions matched the field measurements.

1. INTRODUCTION

Ballina Bypass is a section of the Pacific Highway to be upgraded in the north-east region of New South Wales, Australia. The project involved the construction of approximately 11.4km length of four-lane dual carriageway bypassing the Ballina town centre.

A large portion of the road embankments is located in the areas underlain by deep soft clays. The construction of road embankments in these areas poses significant risks involving embankment instability, and excessive (short and long term) settlements. To reduce these risks, treatment of the soft clays is required prior to the construction of the road embankments.

A bridge approach embankment adjacent to the future bridge over Emigrant Creek North (ECN) is underlain by very soft to firm clays up to 25m thick (see Figure 1). Due to the presence of thick soft clays, embankment stability and settlement become a major concern in the absence of appropriate ground improvement. To enable safe construction of the embankment and speedy consolidation of the soft clays, the vacuum consolidation method was chosen as a means to improve the ground. To increase the ground treatment efficiency, preloading and surcharging have been incorporated with the vacuum consolidation method.

Vacuum consolidation is a technique used to improve the strength of soft clays where the change in pore water pressure produced from the applied vacuum pressure induces discharge of water and thereby increases the shear strength of the soil (e.g. Mohamedelhassan & Shang, 2002).

Various field instruments, such as settlement plates, vibrating-wire piezometers and inclinometers, have been installed to monitor the ground responses associated with the ground treatment.

This paper presents the site geological conditions, the vacuum consolidation method used for ground improvement, the interpreted geotechnical model adopted for the numerical analysis, the fully coupled numerical method (Hsi & Small 1992a, Hsi & Small 1992b, Hsi 2000) and the detailed methodology adopted for the back-analysis of vacuum consolidation.

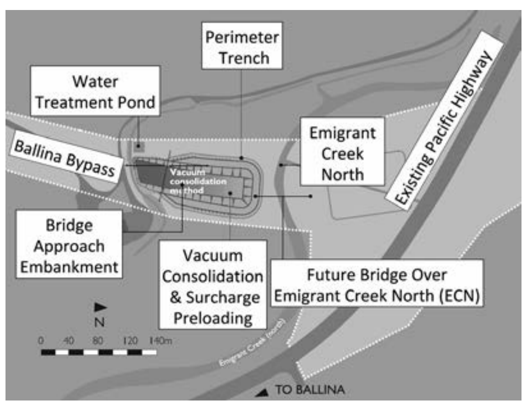

Figure 1. Site layout plan of bridge approach at Emigrant Creek North, ECN (after RTA 2006).

2. PRINCIPLES AND MECHANISM OF VACUUM CONSOLIDATION

The conventional preloading method increases the effective stress in the ground through an incremental change in the total stress. This can be achieved by placing preload fill on top of the existing ground. On the contrary, the vacuum consolidation method preloads the entire soil mass by reducing the pore pressure in the soil mass at a constant total stress (Ihm & Masse 2002).

This method was first introduced by Kjellman (1952) to improve the strength of soft clay. The principles and mechanism of vacuum preloading have been reported in various published literatures (e.g. Kjellman 1952, Chu et al. 2000, Ihm & Masse 2002, Indraratna et al. 2004). The mechanism of vacuum consolidation can be readily elicited by revisiting Terzaghi's (1943) effective stress expression. Note that the atmospheric pressure, P_a is not considered in the effective stress calculation because the effect is self-cancelling. In order to examine the principle of vacuum consolidation, it is necessary to introduce the atmospheric pressure, P_a in the effective stress calculation. The total stress and pore water pressure of the ground is given by

$$\sigma_t = \gamma h + P_a \quad (1)$$

$$u = \gamma_w h + P_a \quad (2)$$

$$\sigma' = \sigma_t - u \quad (3)$$

Substituting equations (1) and (2) into equation (3) leads to

$$\sigma' = \gamma h - \gamma_w h \quad (4)$$

in which σ_t = total stress, σ' = effective stress, u = pore water pressure, γ = unit weight of soil, γ_w = unit weight of water and h = depth below the ground surface.

As shown in equation (4), the effective stress of the ground is not affected by the atmospheric pressure. However, if the atmospheric pressure is removed from the pore water pressure by applying an equivalent vacuum suction i.e. $-P_a$, the final effective stress increases as a result of the unbalanced atmospheric pressure acting above the ground, as shown in equation (5)

$$\sigma' = \gamma h - \gamma_w h + Pa \quad (5)$$

The mechanism of the vacuum consolidation system can also be illustrated using the spring analogy proposed by Chu et al. (2000). In Figure 2, the vacuum pressure is denoted by $-\Delta u$. In the instance when the vacuum pressure, $-\Delta u$, is applied, the pore water pressure in the soil is still P_a. Gradually, the pore pressure decreases and the spring compresses. That is, the soil skeleton starts to gain effective stress. Upon completion of the vacuum consolidation, the gain in the effective stress is equal to Δu, i.e. the applied vacuum pressure.

Note that the incremental change in effective stress equals to the amount of dissipated pore water pressure, Δu, which will not exceed the atmospheric pressure, P_a. In practice, typical gains in effective stress are ranging from 65kPa to 80kPa, depending on the efficiency of the vacuum consolidation system.

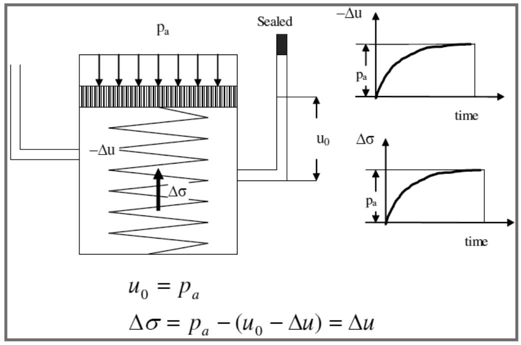

Figure 2. Spring analogy of vacuum consolidation process (after Chu et al. 2000).

3. SITE GEOLOGY

An area of approximately 9400m^2 at the bridge approach embankment of the future bridge over Emigrant Creek North (ECN) had been treated with vacuum consolidation for approximately eight months. The soil profile along the bridge approach embankment prior to the vacuum consolidation treatment is shown in Figure 3. As seen, the embankment is underlain by Holocene alluvial deposits over Pleistocene stiff clay, residual soils and weathered argillite. The Holocene alluvial deposits comprise a thin upper crust underlain by very soft to firm clay up to a depth of 25m with a minimum undrained shear strength, C_u of about 8kPa at the ground surface. Figure 4 shows that the shear strength increases monotonically to approximately 40kPa at a depth of about 25m below the ground surface.

4. CONSTRUCTION HISTORIES AND VACUUM CONSOLIDATION SYSTEM

The key construction history is summarized in Table 1. A total of 8.5m thick embankment was constructed between late November 2006 and mid July 2007. This included a 2.0m thick layer of working platform and sand blanket, which was needed for the installation of the vertical vacuum transmission pipes and also served as a drainage layer.

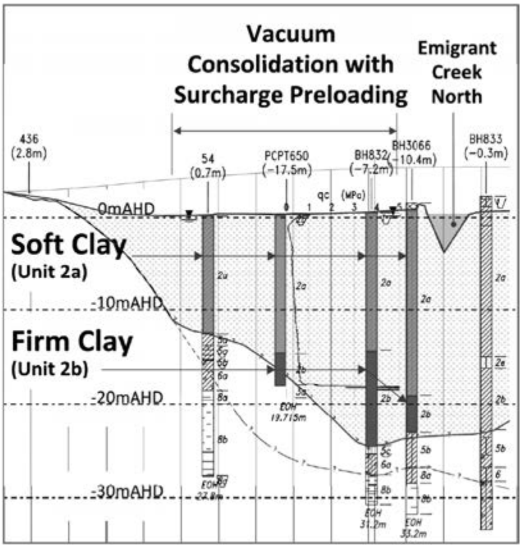

Figure 3. Soil profile along the bridge approach embankment.

The vacuum pressure was transmitted into the ground through 34mm diameter vertical vacuum transmission piles installed in a square grid pattern at 1.0m c/c. These vertical vacuum transmission piles had been extended to approximately 20m depth. Figure 5 shows that the impervious membrane was laid on top of the working platform to ensure an airtight region above the vertical vacuum transmission pipes. Some horizontal drains in the transverse and longitudinal directions had been installed to increase the treatment efficacy. Subsequently, these horizontal drains were connected to vacuum pumps. The edge of the impervious membrane was sealed by a bentonite slurry trench as shown in Figure 5.

Figure 6 shows the schematic diagram of the vacuum consolidation system. The key advantage of this arrangement is that the suction head, generated by the pump, propagates along the soil surface and down the vertical transmission piles within the airtight region, accelerating the dissipation of excess pore water pressures. However, the efficacy of the entire system depends on the ability of the membrane to prevent any air leaks to sustain a sufficient suction head (e.g. Indraratna et al. 2004).

Table 1. Key construction histories of the approach embankment.

Timeline	Total Fill Thickness [m]	Equivalent Fill Thickness[1] [m]	Vacuum Pressure [m]
11/12/06	1.00	1.00	0.00
28/02/07	2.00	1.99	0.00
19/03/07	2.00	1.82	-7.56
22/03/07	2.68	2.46	-8.02
23/05/07	5.40	4.68	-7.77
06/07/07	8.50	7.30	-7.38
06/07/07	8.50	6.73	-6.90

Note 1: Refer to Equation 7.

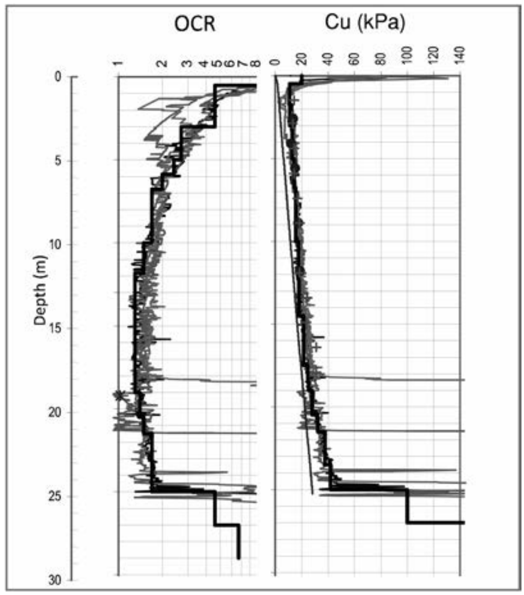

Figure 4. In-situ OCR and C_u profiles prior to vacuum consolidation derived from piezocone results.

A vacuum pressure in the order of 70kPa was applied to the ground between early March 2007 and late November 2007 (i.e. after completion of the 2.0m thick working platform and sand blanket) over a distance of 120m along the bridge approach embankment.

Table 1 also presents the equivalent fill thickness adopted for the numerical analysis. The equivalent fill thickness, as derived in Equation 7, has taken into account the submerged effect of the settled fill.

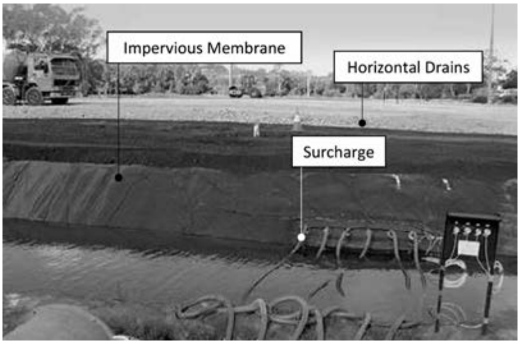

Figure 5. Working platform and impervious membrane that form part of the vacuum consolidation system.

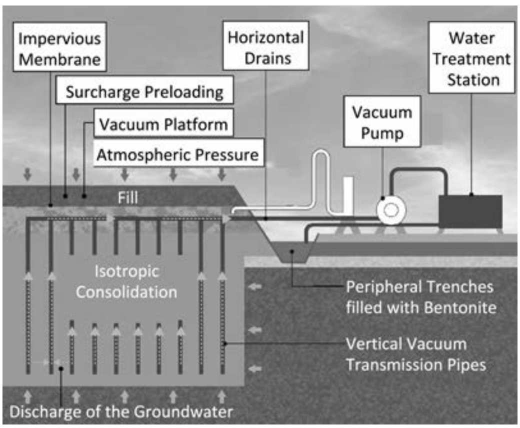

Figure 6. Schematic diagram of the vacuum consolidation system (after RTA 2006).

5. FULLY COUPLED NUMERICAL METHOD

The numerical analysis of vacuum consolidation and preloading involves the prediction of changes in pore water pressure and soil deformation. Such a problem involves interaction between the soil skeleton and the groundwater present in the pores of the soil. To solve this problem, a sophisticated numerical process which is capable of analysing soil deformation and groundwater flow simultaneously is required.

A finite element program COFEA (COupled Finite Element Analysis), developed by Hsi (1992), Hsi & Small (1992a & 1992b) and Hsi (2000), implementing the fully coupled numerical method is considered suitable, where deformation of the soil is calculated simultaneously with the rise/fall of the water table and change in water pressure. Note that one of the key advantages of COFEA is that the pore water pressure boundaries can be prescribed in order to model the applied vacuum pressures.

6. GEOTECHNICAL MODEL

The geotechnical model adopted for the back-analysis is shown in Table 2. The subsoil profile and geotechnical parameters were derived based on the results of the site investigations and the back-analysis of the field monitoring data.

In Table 2, OCR is the over-consolidation ratio, k_v and k_h are vertical and horizontal permeability values, C_c and C_r are compression and recompression indices and γ_{sat} is saturated unit weight of soil. The initial void ratio e_o is assumed to be 2.1 for both Units 2a and 2b.

Table 2. Subsoil profile and geotechnical parameters.

Depth [m][1]	Soil Unit	γ_{sat} [kN/m^3]	k_v [m/day][2]	OCR	C_c	C_r
0.5	2a	18.0	2.0×10^{-04}	20.00	0.93	0.19
2.0	2a	14.5	3.1×10^{-04}	5.00	1.40	0.19
4.0	2a	14.5	3.2×10^{-04}	2.50	1.40	0.19
6.0	2a	14.5	2.6×10^{-04}	2.00	1.40	0.19
8.0	2a	14.5	6.6×10^{-05}	1.50	1.55	0.19
11.0	2a	14.5	5.6×10^{-05}	1.40	1.55	0.19
15.0	2b	14.5	4.6×10^{-05}	1.31	1.55	0.19
17.0	2b	15.0	3.2×10^{-05}	1.25	1.24	0.19
19.0	2b	15.0	2.9×10^{-05}	1.22	1.24	0.19
21.0	2b	15.0	1.3×10^{-05}	1.20	1.24	0.19
23.0	2b	15.0	1.2×10^{-05}	1.18	1.24	0.19
25.0	2b	15.0	1.0×10^{-05}	1.17	1.24	0.19

Note 1: Depth to bottom of the layer.
2: $k_v = k_h/2$.

7. ANALYSIS METHODOLOGY

The actual construction sequence was modelled in the COFEA analysis. The geotechnical model was calibrated to match the prediction with the time settlement curve, excess pore pressure and total settlement inferred based on the Asaoka Method (Asaoka, 1978).

7.1. Modelling of vacuum consolidation

For the vertical vacuum transmission pipes that are installed in a square grid pattern, the effective zone of influence around each pipe takes the form of a cylindrical column. The equivalent diameter of the cylindrical column of soil affected by each vertical vacuum transmission pipe is 1.13×s, in which s is the spacing between the centres of the transmission pipes. During the vacuum consolidation process, the change in pore water pressure produced by the applied vacuum pressure induces discharge of pore water toward the vertical vacuum transmission pipes.

At the centre of the bridge approach embankment, the ground is expected to experience one-dimensional consolidation. Therefore, the vacuum transmission pipe and the surround soil can be simulated as an axisymmetric problem. The applied vacuum pressure can be prescribed along the pipe.

7.2. Finite element mesh and boundary conditions

The finite element mesh, as shown in Figure 7, consists of 240 8-noded isoparametric elements. This mesh is designed to solve axisymmetric problems. Integration with 2×2 Gaussian points was used to solve the consolidation problem. Horizontal fixities ($U_x = 0$) were prescribed to the outer vertical geometry lines and full fixities ($U_x = U_y = 0$) were prescribed to the bottom horizontal geometry line to model the one-dimensional consolidation settlement.

The following drainage boundary conditions were prescribed to the nodal points representing the vertical vacuum transmission pipes:

- Prior to the application of vacuum pressure, zero excess pore pressure was prescribed to model the behaviour of a vertical drain.
- During vacuum consolidation, the vacuum pressure (-65kPa to -80kPa) was prescribed to model the vacuum pressure.
- In the long-term, zero excess pore pressure was prescribed along the vacuum transmission pipe after the vacuum is switched off.
- Throughout the analysis, impermeable boundary conditions were prescribed to the outer cylindrical column of soil to model the effective influence zone of a vertical vacuum transmission pipe.

7.3. Modelling of elasto-plastic behaviour of soft clays

The Modified Cam-Clay (MCC) soil model was adopted to model the multiple stress loading history of the Holocene clays. The MCC parameters adopted for the back-analysis were derived from the geotechnical parameters given in Table 2. The detailed derivations of the MCC parameters are widely available in published literature (e.g. Wood, 1990).

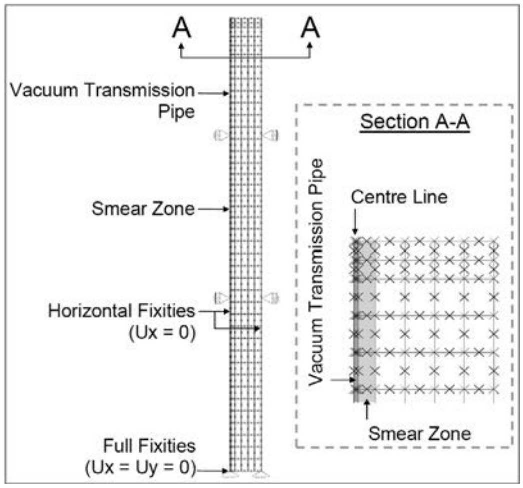

Figure 7. Axisymetric finite element mesh.

7.4. Modelling of initial in-situ stresses

The initial in-situ stresses of the ground are crucial to the numerical modelling as they influence the magnitude of ground displacement. These stresses are affected by the previous stresses experienced by the soil.

In the finite element model, the in-situ stresses are generated using the k_0-procedure. In this approach, the horizontal effective stress is calculated from the vertical effective stress and the coefficient of lateral earth pressure at rest (k_0).

Note that k_0 is dependent on the geological and stress history. In the estimation of k_0, the geological and stress history of the soil can be expressed by its OCR. The k_0 value for an over-consolidated soil is usually higher than that for a normally consolidated soil. Numerous relationships have been proposed for estimating k_0 for over-consolidated soils and most of them are related to the OCR. In this study, Mayne & Kulhawy's (1982) empirical equation for k_0 was used as shown below

$$k_0 = (1 - \sin\varphi')\, OCR^{\sin\varphi'} \quad (6)$$

in which φ' = effective angle of friction (in radians) and OCR = over-consolidated ratio.

7.5. Modelling of smear effects

The soil adjacent to the drain can be disturbed due to the installation process of the vertical vacuum transmission pipe. As a result, the permeability of the disturbed soil decreases causing a reduced consolidation process. This effect is described as 'smear'. The smear effect was modelled in the finite element analysis by defining a small smear zone, adjacent to the circular drain, as shown in Figure 7. The zone of smear is assumed to have a reduced permeability, k_{hs} and a radius, r_s measured from the centre of the drain, as shown in Figure 8. The r_s and k_{hs} are calculated from $r_s/r_p = 4$ and $k_h/k_{hs} = 4$, in which r_p is the radius of the circular drain (i.e. 0.017m) and k_h is the undisturbed soil permeability. The r_s/r_p and k_h/k_{hs} were selected to match the measured excess pore pressures and fall within the range of published data.

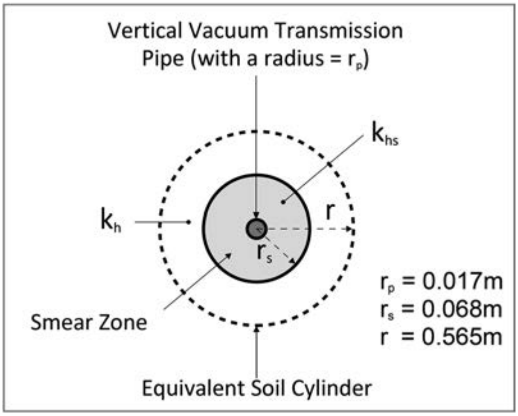

Figure 8. Equivalent soil cylinder around a vacuum transmission pipe.

7.6. Modelling of fill loading

The fill loading, σ_{fill} is calculated as the sum of the full embankment loading above the water table and the submerged fill loading below the water table as shown below:

$$\sigma_{fill} = H_{eq}\,\gamma_{fill} \tag{7}$$

$$= (H - \delta)\,\gamma_{fill} + \delta\,(\gamma_{fill} - \gamma_w) \tag{8}$$

H_{eq} is the equivalent fill thickness, H is the full embankment thickness, γ_{fill} is the unit weight of fill (assumed to be 21kN/m^3) and δ is the fill settlement. The water table is assumed to be at the ground level. Refer to Figure 9 for details.

8. RESULTS OF BACK-ANALYSIS

In this section, the rates of settlements and pore water pressures at various embankment loading stages, obtained from the numerical predictions, are compared with the actual field measurements. The predicted total settlements are compared to that inferred from the Asaoka Method.

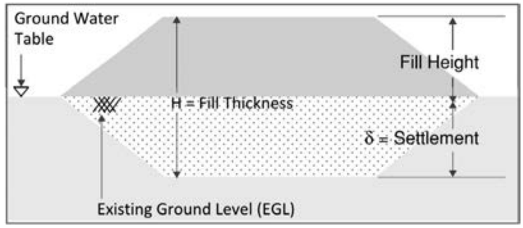

Figure 9. Definition of fill height, fill thickness and fill settlement.

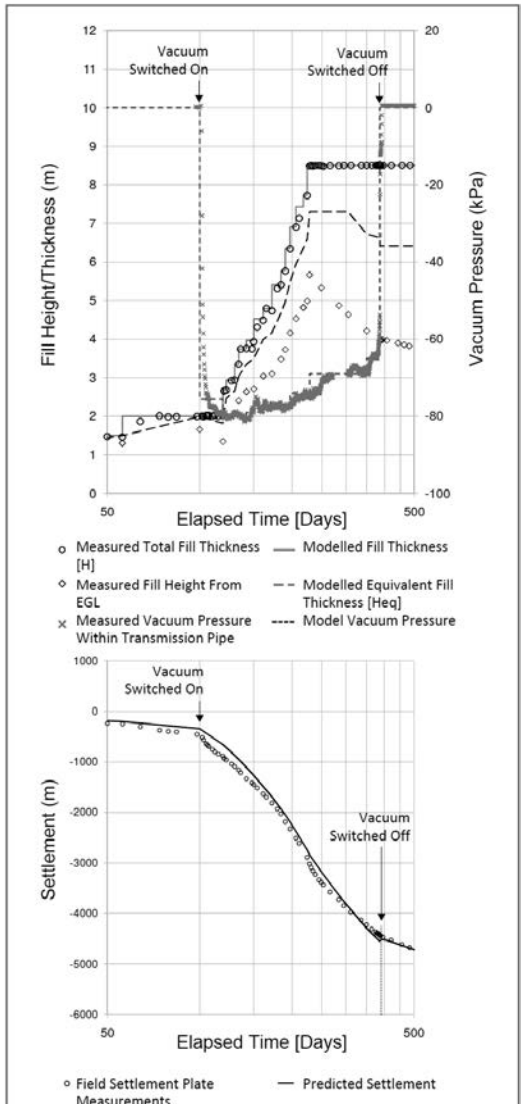

Figure 10. Comparison between predicted settlements and actual field measurements.

8.1. Settlement

The measured fill thickness and the vacuum pressure against time are shown in Figure 10. The simulated fill thickness and the vacuum pressure as summarized in Table 1 are superimposed in the same figure. As shown in Figure 10, the model loading (due to fill and vacuum pressure) agrees with the actual construction history.

The measured and predicted settlements are also shown in Figure 10. As seen in Figure 10, the predicted rate and magnitude of settlements agree well with the field measurements.

8.2. Asaoka Assessment

The total settlement inferred from the Asaoka Method at a constant time step of 28 days is 5.57m, as shown in Figure 11. With the finite element analysis, the predicted total settlement after the vacuum pressure is switched off and without additional treatment is 5.47m. The total settlement is calculated by simulating the consolidation of the ground until all the excess pore water pressure has completely dissipated. The predicted total settlement is similar to that inferred from the Asaoka Method, lending further confidence to the calibrated geotechnical model used for the prediction of long term performance.

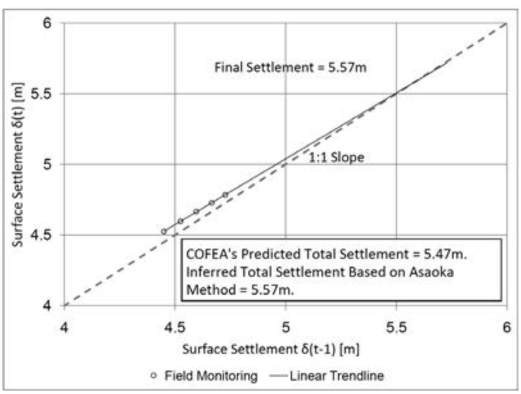

Figure 11. Total settlement predicted based on the Asaoka Method at a constant time step of 28 days.

8.3. Excess Pore Pressure

The measured vacuum pressures inside the vacuum transmission pipe are shown in Figure 12. During the vacuum preloading, the vacuum pressure gradually decreases from approximately -80kPa to -65kPa towards the end of the preloading. As the piezometer was located at about 19.3m below the ground level, it appeared that the vacuum pressure had been successfully transmitted to this depth. The measured vacuum pressures were used as the prescribed drainage boundary values in the numerical model, as discussed earlier.

During the vacuum consolidation treatment, the variations of excess pore water pressures at different depths were recorded. The measured pore water pressures at the depth of 11.8m are shown in Figure 12. The predicted excess pore water pressures at the drain-soil interface (r_p = 0.017m) and at the outer most of the equivalent soil column (r = 0.565m) are presented in the same figure. As can be seen, the predicted excess pore pressures at the outer edge of the soil cylinder due to fill construction, agree reasonably well with the field monitoring results. At the edge of the drain, the predicted pore water pressures correspond to the applied vacuum pressures.

9. CONCLUSION

This paper presents the ground response associated with the vacuum consolidation treatment. A fully coupled numerical method taking into account the interaction between pore water pressure and soil deformation has been employed. The measured settlements and pore water pressures at various embankment and vacuum loading stages were back-analyzed. The variations of the measured suctions throughout the depth of the soft soils were considered in the finite element analysis. The geotechnical model representing the site conditions was calibrated against the field measurements and performance. The numerical results show that the predicted rate and magnitude of settlements and the response of pore water pressures agree well with the field measurements.

10. ACKNOWLEDGEMENT

The authors would like to thank the Roads and Traffic Authority (NSW) and Ballina Bypass Alliance for providing the relevant project data and information and granting their permission for the publication of this paper.

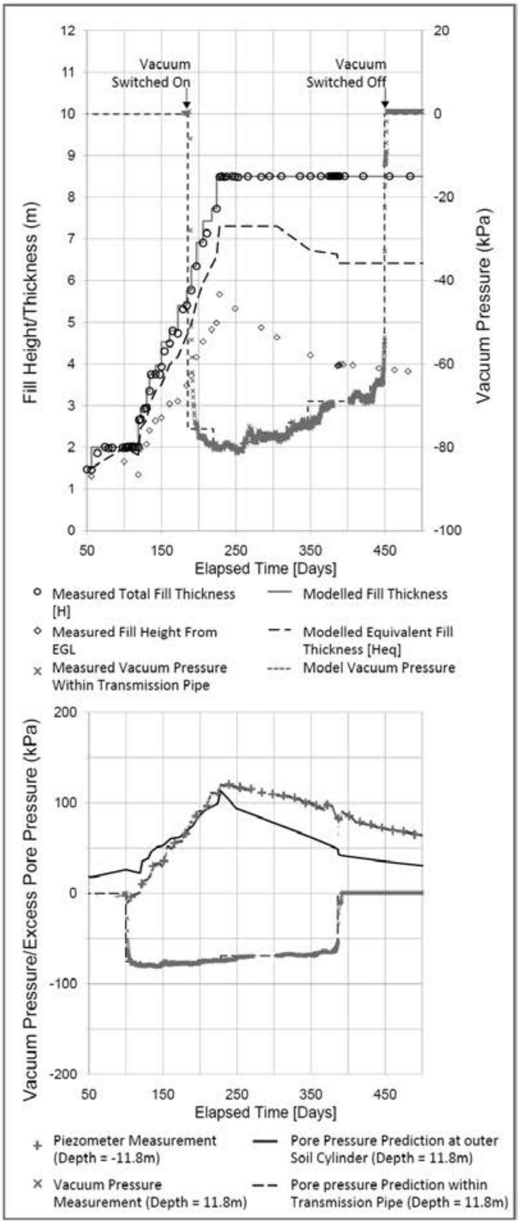

Figure 12. Comparison between predicted excess pore pressures and actual field measurements.

11. REFERENCES

Asaoka, A (1978), Observational procedure of settlement prediction, *Soils and Foundations*, Vol. 18, No. 4, Japanese Society of Soil Mechanics and Foundation Engineering, pp. 87-101.

Chu, J., Yan, S.W. & Yang, H. (2000), Soil improvement by the vacuum preloading method for an oil storage station, *Géotechnique*, 50, pp. 625-632.

Hsi, J.P. (1992), Analysis of excavation involving drawdown of the water table, PhD Thesis, *The University of Sydney*, Australia.

Hsi, J.P. & Small, J.C. (1992a), Simulation of Excavation in a poro-elastic material, *International Journal for Numerical and Analytical Methods in Geomechanics*, Vol. 16, pp. 25-43.

Hsi, J.P. & Small, J.C. (1992b), Analysis of excavation in an elasto-plastic soil involving drawdown of the water table, *Computers and Geotechnics*, Vol. 13, pp. 1-19.

Hsi, J.P. (2000), Fully coupled finite element analysis of soil deformation and groundwater flow, *Australian Geomechanics Society Mini-Symposium, Computer Methods and Software, Sydney, Australia*, 9 August 2000 pp. 1-22.

Ihm, C.W. & Masse, F. (2002), Successful application of Menard Vacuum Consolidation Method to Nakdong River soft clay in Kimhae, South Korea, *Proc. 4th International Conference on Ground Improvement Techniques*, Kuala Lumpur.

Indraratna, B., Bamunawita, C. & Khabbaz, H (2004). Numerical modelling of vacuum preloading and field applications. *Canadian Geotechnical Journal*, Vol. 41, pp. 1098-1110.

Kjellman, W. (1952), Consolidation of clayey soils by means of atmospheric pressure, in *Proc of a Conf. on Soil Stabilization, Massachusetts Institute of Technology, Cambridge, MA*. pp. 258-263.

Mayne, P.W. & Kulhawy, F.H. (1982), K_0- OCR relationship in soil, *Journal of the Geotechnical Engineering Division, ASCE*, Vol. 108, No. GT6, June 1982, pp. 851-872.

Mohamedelhassan, E. & Shang, J.Q. (2002), Vacuum and surcharge combined one-dimensional consolidation of clay soils, *Canadian Geotechnical Journal*, Vol. 39, pp. 1126-1139.

RTA (2006), Cumbalum interchange initial works, Ballina Bypass, *Initial works display material, May 2006*.

Terzaghi, K. (1943). Theoretical soil mechanics, *John Wiley & Sons*, New York.

Wood, D.M. (1990), Soil Behaviour and Critical State Soil Mechanics, *Cambridge University Press*, *Cambridge.*

Investigations on shear strength of silty sand reinforced with 3D inclusions

M. Khalaj
Civil Engineering Department, Imam Khomeini International University, Qazvin, Iran

S.A. Naeini
Civil Engineering Department, Imam Khomeini International University, Qazvin, Iran

ABSTRACT: A series of large direct shear tests (30 × 30 × 15 cm) were systematically conducted to evaluate the interface shear strength properties of reconstituted samples of silty sand with different percent of fine content. Various contents of silt (0 – 45 %) by weight mixed with sand to study the behavior of sand and silty sand in terms of shear strength for unreinforced and also reinforced samples. Comparison is made between shear strength of the reinforced and unreinforced specimens. The results of the tests indicated that as the silt content increases up to 35%, the shear strength decreases. With further increase in silt content, the shear strengths are increased. The results also showed an increase in the shearing strength of the sand and silty sand with 3D reinforcing elements.

1. INTRODUCTION

The use of soil reinforcement has shown a major increase in geotechnical engineering applications such as construction of buildings and roads, railway, embankments, stabilization of slopes and improvement of soft ground. Improvement of certain desired properties like bearing capacity, shear strength (C and φ) and permeability characteristics of soil can be undertaken by a variety of improvement techniques. One of the most common techniques is to reinforce the soil with geosynthetics. The use of geosynthetics has unique advantages over other soil strengthening techniques, due to their low mass per unit area, strength, and stiffness characteristics. The effect of reinforcement on strength improvement of geosynthetic-reinforced soil has been the subject of numerous experimental investigations.

Broms (1977) tested a dry fine sand reinforced with geotextile in a triaxial apparatus and proposed an equation for calculating the ultimate load in a reinforced soil. Gray and Ohashi (1983) studied the behavior of dry sand reinforced with different types of fibers, including natural and synthetic as well as metal fibers, through series of direct shear tests. Rajagopal et al. (1999) carried out a large number of triaxial tests on granular soil encased in single and multiple geocells to study the influence of geocell confinement on the strength and stiffness behavior of granular soils. Yang and Wang (1999) proposed a new reinforced soil structure composed of horizontal reinforced concrete grids. Lei (2001) analyzed the strength characteristics of a reinforced soil structure with reinforced concrete blocks placed in series as reinforcements. Xie (2003) presented a new type of reinforcement, reinforcing ring, whose mechanical function is to turn lateral earth pressure to stress within the reinforcing ring.

Current research works mainly emphasize on the strength, mechanism and bearing capacity of the reinforced soil with conventional horizontal inclusions (Ingold 1983, Haeri et al. 2000, Michalowski 2004, Moraci and Recalcat 2006, Latha and Murthy 2007, Naeini et al. 2009).

Meanwhile, the shape and arrangement of reinforcement on the strength of reinforced soil has been investigated. Smith and Brigilson (1979) and Xing and Zhang (1992) used model tests to study the strength and bearing capacity of earth retaining walls reinforced with inclined reinforcements. Lawton et al. (1993) presented a method for reinforcing soils using multi-oriented geosynthetics inclusions within or upon compacted soils. They carried out a series of triaxial, CBR and permeability tests and compared the effectiveness of the multi-oriented elements with fibers. Yetimoglu and Salbas (2003) investigated the shear strength of sands reinforced with randomly distributed discrete fibers by direct shear tests. The results indicated that peak shear strength and initial stiffness of the sand were not affected significantly by the fiber reinforcement. Some new configurations of inclusions were developed by Zhang et al. (2006). They proposed a new concept of soil reinforced with three-dimensional (3D) elements and carried out a series of triaxial tests to study the behavior of sand reinforced with a single-layer 3D inclusion. The results show that 3D reinforcement not only gives an apparent cohesion to the sand, but it also increases the angle of internal friction significantly.

In this paper, the soil reinforcement with a special type of geonet is studied. A fundamental difference between this sheet formed cogged geonet in this paper and other forms of 3D inclusions as well as fiber-reinforced soil is that in the presented 3D reinforced soil , the soil enclosed within the geonet cells will provide passive resistance against shearing that will increase the strength and stability of the reinforced soil. The experimental program included 36 series of large direct shear tests (LDST) on sand and silty sand reinforced with 3D geonet and the results are presented and discussed. The stress-strain behavior and shear strength of sand and silty sand reinforced with 3D inclusions are studied. Comparison is made between shear strength of sand and silty sand with different FCs before and after reinforcing.

2. EXPERIMENTAL PROCEDURE

2.1. Test Materials

High density polyethylene (HDPE) geonets (CE161 – produced by Meshiran Co. in Iran) were used as reinforcement , as shown in Fig 1. Some of their specifications and strength properties , provided by the manufacturer, are : mesh aperture = 10 x 10 (mm) , minimum mesh thickness = 3.2 mm , minimum specific weight = 0.9 g/cm^3 , maximum load at yield point = 7.6 KN/m , tensile strength at break = 290 min (ASTM D 638) , typical application = Protection of oil, Gas and water steel pipes against mechanical damage to the pipe line during the positioning and trench back-filling operations.

A clean oven-dried, sub-angular sand was used in the tests. The sand was sieved through ASTM 3/8” (d = 9.5 mm) and washed through ASTM 200 (d = 0.075 mm) and dried in oven , then mixed with 10% , 20% , 30% , 35% and 45% silt (sieved ASTM 200) by weight. The

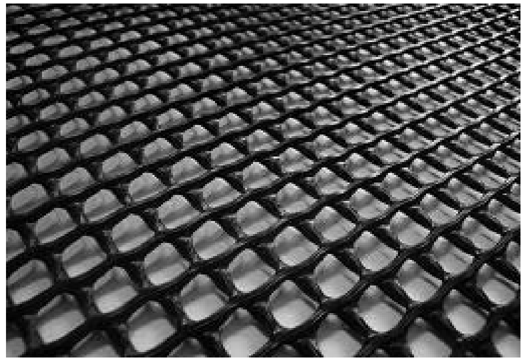

Figure 1. Geonet CE161 used in this study

clean sand is well graded in unified soil classification system (USCS) with coefficients of uniformity (C_u) and curvature (C_c) of 7.85 and 2.44 respectively. All the specimens of sand with different percent of silt were prepared in dry condition at a unit weight of 17 KN/m^3.

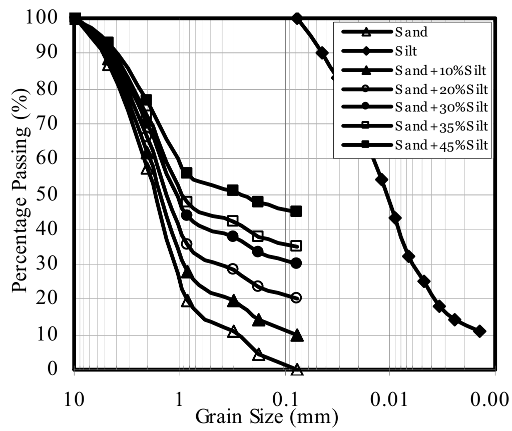

Figure 2. Particle size distribution curve

Some properties of the sand are given in Table 1. Since there was no moisture, the interparticle attraction or cohesion C was negligible and assumed zero. The particle size distribution curves for tested soils are shown in Fig. 2.

Table 1. Soil properties

FC,%	G_s	C_u	C_c	D_{50},mm	Soil Name (USCS)
0	2.661	7.9	2.44	1.75	SW
10	2.667	25.1	6.13	1.60	SP-SM
20	2.670	141.7	7.84	1.43	SM
30	2.674	238.5	0.56	1.22	SM
35	2.676	250.0	0.19	0.95	SM
45	2.681	275.0	0.06	0.26	SM

2.2. Test procedure

A series of direct shear tests on reinforced and unreinforced materials was carried out in a large direct shear box having dimensions of 30 I 30 I 15 cm. Large size shear tests offer a less expensive alternative for testing geosynthetic reinforced soils in a relatively representative environment (Bakeer et al. 1998) as opposed to large scale triaxial tests or full scale field tests. The tests were conducted at the vertical normal stresses of σ_n = 100,200,300 kPa for each soil. The materials were compacted in the box in three layers using a 100 mm square metal hammer. The dimensions of the geonets used in this study were almost 30 I 30 cm and located exactly at the shearing surface (middle of the box). Figure 3 shows the arrangement of the 3D geonets in the compacted material. The shearing rate was 1 mm/min in the tests. During shearing the shear displacement, vertical displacement and the shear load applied to the sample were carefully recorded. Using this information the required stress-strain parameters were calculated.

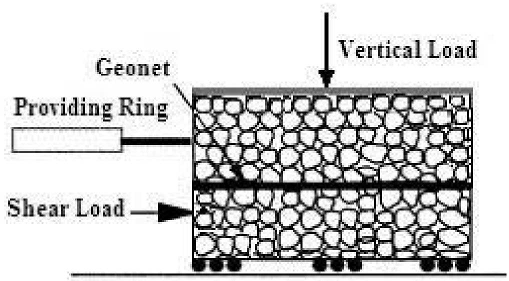

Figure 3. Geonet arrangement in the large direct shear apparatus.

3. RESULTS AND DISCUSSIONS

The effect of fine content and three-dimensional reinforcement on the soil strength properties are shown in Figures 4 to 6. As the results indicates, it is clear that for the sand without reinforcement, as the silt content increases up to about 35%, the soil strength is decreased (Fig. 4 and 6). With further increase in fine content, the soil strength is increased. This means that the soil becomes weakened with an increase in the silt content up to 35% and then strengthened again, but the clean sand is stronger than the silty sand. This event is explained by the fact that up to 35% silt content, the fine grains of silt positioned around and among the sand grains, act as filling as well as lubricant, and therefore reduces the shear strength of the soil. However, with more increase in the silt content above 35%, the soil samples show an increase in shear strength. In other words, after some threshold of silt content is reached, contacts between the sand grains totally disappear and sand grains start acting as intrusions in the silt matrix (Naeini et al. 2004).

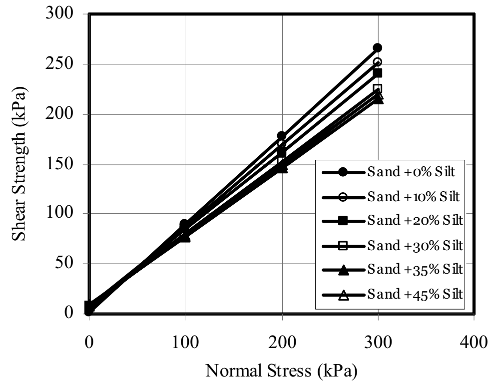

Figure 4. Large direct shear tests results on sand with different amounts of FC.

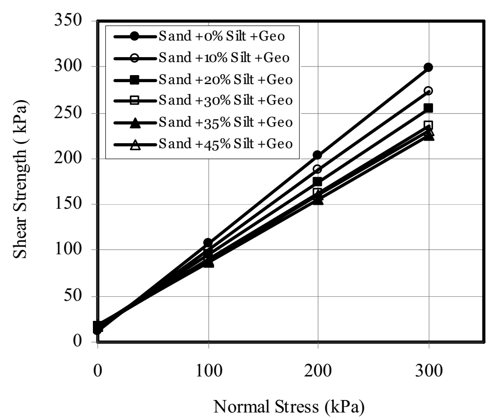

Figure 5. Large direct shear tests results on sand with different amounts of FC reinforced with 3D inclusions.

The influence of reinforcement on the shear strength of the soil is shown in Figure 5. It can be seen that the reinforced specimens have an increase in the shear strength. Figure 6 present the comparison between shear strength of the reinforced and unreinforced soils. This Figure indicate that a similar behavior occurred in reinforced soil. The existent of 35% silt content yielded lowest strength, but in compare with the soil without reinforcement, the shear strength increased.

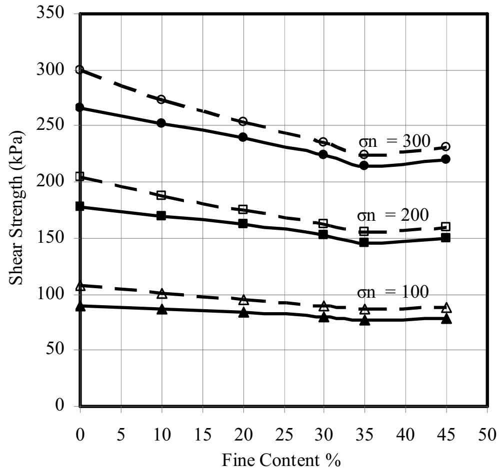

Figure 6. Unreinforced and reinforced soils shear strength comparison.

The effect of fine content on normalized shear strength for tested soils are shown in Figure 7. The experimental results indicate that, reinforcement has more effect in clean sand and as the silt content increases, the reinforcement has the lower effect. This increase in shear strength due to reinforcement at normal stress of 100 kPa is from 89.4 to 108.1 kPa, about 21% for clean sand and from 77.5 to 87.0 kPa, about 12.3% for silty sand with 35% fine content.

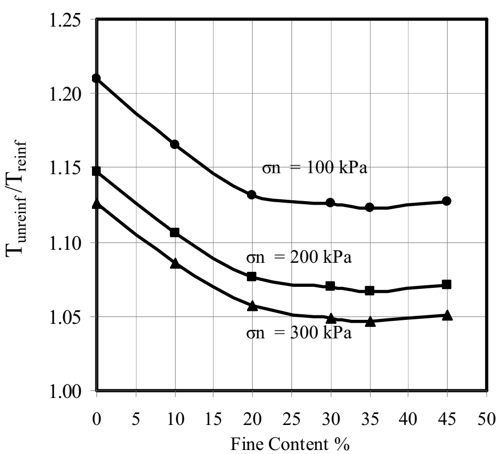

Figure 7. The effect of fine content on normalized shear strength.

The normalized shear strength parameter (C and φ) of the reinforced and unreinforced sand and silty sands determined from the experimental results are shown in Figure 8. For sand reinforced with 3D inclusions, the friction angle and apparent cohesion have increased. It can be seen that the increase in apparent cohesion and friction angle of reinforced sand was greater than reinforced silty sands. Therefore, reinforcement has more effect in clean sand and as the silt content increases, the reinforcement has the lower effect. At 35% silt content the reinforced soil specimens have a slight increase in apparent cohesion while the difference in friction angle is negligible.

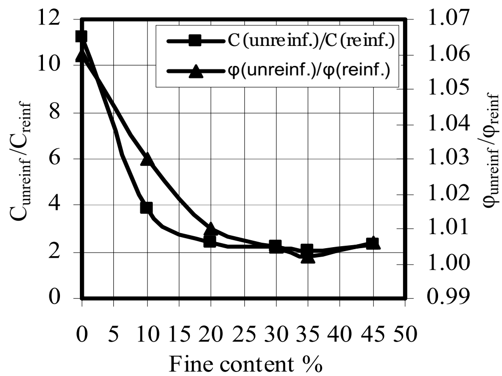

Figure 8. The effect of fine content on normalized angle of internal friction and cohesion

4. CONCLUSIONS

In this paper, a new concept of soil reinforced with 3D reinforcement has been proposed. A series of large direct shear tests was carried out on samples of dry sand and silty sand unreinforced and reinforced 3D reinforcing elements, in order to study the behavior of reinforced silty sand with different percent of fine content. The following conclusions can be drowning from the results of this study:

1) The shear strength of a soil is sensitive to the silt content. As the silt content increases up to 35%, the shear strength decreases. With further increase in silt content, the shear strength is increased.
2) The shear strength for silty sand reinforced with 3D inclusion was smaller than that of reinforced sand. From this observation, it can be concluded that reinforcement has more effect in clean sand and as the silt content increases, the reinforcement has the lower effect.

3) Three-dimensional reinforcement not only gives an apparent cohesion to the sand, it also increases the angle of internal friction.
4) The increase in apparent cohesion and friction angle of reinforced sand was greater than reinforced silty sands. As the silt content increases up to 35%, the apparent cohesion and friction angle decreased. With further increase in fine content the friction angle and apparent cohesion increased again.

5. REFERENCES

Broms B.B. 1977, Triaxial test with fabric-reinforced soil. *Proceedings of the international conference on the use of fabric in geotechniques*, vol. 3, Paris, pp. 129-134.

Baker R., Abdel-Rahman A.H., Napolitano P.J., 1998. Geotextile friction mobilization during field pullout test. *Geotextiles and Geomembranes*, 16, 73-85.

Chen Q., He C., 2000. The prototype measurement of retaining wall reinforced by a new type of wedgy tied-reinforcement. *Chinese Journal of Geotechnical Engineering*, 22(3), 289-293.

Gray D.H., Ohashi, H. 1983, Mechanics of fiber reinforcement in sand. *Journal Of Geotechnical Engineering*, *ASCE* 109(3), 335-353.

Haeri S.M., Nourzad R., Oskrouch A.M. 2000, Effect of geotextile reinforcement on the mechanical behavior of sands. *Geotextiles and Geomembranes* 18(6), 385-402.

Ingold T.S. 1983, Reinforced clay subjected undrained triaxial loading. *Journal of the Geotechnical Engineering Division, ASCE* 109(5), 738-743.

Lawton E.C., Khire M.V., Fox N.S., 1993. Reinforced of soil by multi-oriented geosynthetic inclusions. *Journal of Geotechnical Engineering*, 119(2), 257-275.

Lei S. 2001. Analysis on the strength property of reinforced earth retaining structure (wall) in the V-shaped gully. *Journal Chongqing Jiaotong University*, 20(1), 65-68.

Latha M.G., Murthy V.S., 2007. Effects of reinforcement form on the behavior of geosynthetic reinforced sand. *Geotextiles and Geomembranes*, 25(1), 23-32.

Michalowski R.L., 2004. Limit loads on reinforced foundation soils. *Journal of Geotechnical and Geoenvironmental Engineering*, 130(4), 381-390.

Moraci N., Recalcati P., 2006. Factors affecting the pullout behavior of extruded geogrids embedded in a compacted granular soil. *Geotextiles and Geomembranes*, 24(4), 220-242.

Naeini S.A., Baziar M.H., 2004. Effect of fine content on steady state strength of mixed and layered samples of a sand. *Journal of Soil Dynamics and Earthquake Engineering*, 24, 181-187.

Naeini S.A., Ziaei-Moayed R., 2009. Effect of plasticity index and reinforcement on the CBR value of soft clay. *International Journal of Civil Enginnering*, vol. 7, No. 2, 124-130

Rajagopal K., Krishnaswamy N.R., Madhavi L.G., 1999. Behavior of sand confined with single and multiple geocells. *Geotextiles and Geomembranes*, 17(3), 171-184.

Smith G.N., Brigilson G.I. 1979. Inclined stripes in reinforced soil walls. *Civil Engineering, ICE* 54(6), 60-61.

Xiong Z., Zhang M.X., 1992. Basic study on the best inclination of stripes in the reinforced retaining wall. *Journal of Lanzhou Railway University*, 11(2), 26-35.

Yetimoglu T., Salbas O., 2003. A study on shear strength of sands reinforced with randomly distributed discrete fibers. *Geotextiles and Geomembranes*, 21(2), 103-110.

Zhang M.X., Javadi A.A., Min X., 2006. Triaxial tests of sand reinforced with 3D inclusions. *Geotextiles and Geomembranes*, 24(4), 201-209.

The peculiarities of soil large area cushions erection of overburden rock

Y.L. Vynnykov, M.O. Kharchenko
National Technical University, Poltava, Ukraine

ABSTRACT: The experience of using overburden rock and its mixtures for erection of massive artificial base in this article is generalized. The results of laboratory and field investigations of their physical and mechanical characteristics in compacted state are presented. Using these data the statistical laws of physical and mechanical characteristics distribution and influence of their heterogeneity on soil cushion properties were determined. The study of processes occurring during fill and their influence on soil physical and mechanical properties were performed.

INTRODUCTION

During erection of modern building projects the over flooded territories which are made of poor-bearing soils are often used.

For such circumstances, foundation engineering practice constantly replenishes the positive experience of filled earth massif erection with improved soil physical and mechanical properties.

There are more than 100 artificial islands, thousands massive soil cushions, different earth made structures. The most famous of them are the Kansai International Airport, Chubu, Kitackusi islands & Port Island in Japan, The Palm Island having more than 134 mln. m^2, The World (55 mln. m^2), hydro alluvial region in Dubai, The Al Raha Beach (5 mln. m^2) and The Al Marjan island (5 mln. m^2) in United Arab Emirates, The Lulu Island (6 mln. m^2) in Bahrain, Perl-Qatar island (4 mln. m^2) in Qatar etc.

The Olympic base of equestrian sport Stipple-Chase Circle in Moscow (Russia), stadium “Dynamo” in Minsk (Byelorussia) etc., were erected on filled soils. Buildings of Volgodonsk atomic power station (APS) in Russia were erected on sand & gravel cushion with 10 m thickness. The base of foundations frames of APS in Kozlodui (Bulgaria) is soil cushion with 9 m thickness.

1. PURPOSES OF STUDY

Irrespective to rich experience there are a lot of unsolved problems of erection massive soil cushions, such as:

1) correlation between soil physical and mechanical properties of compacted soils obtained in laboratory and in-situ conditions;

2) possibility of using homogeneous overburden rock and their mixtures with clayey soils as a material for cushions;

3) determination of statistical distribution laws of values of physical and mechanical properties of compacted soils;

4) influence of compaction mechanism parameters on soil characteristics;

5) processes occurring with time in fill and their influence on soil physical and mechanical properties;

6) possibility of soil compaction by its own dead weight and also by vibration of mechanisms on fill surface;

7) evaluation of heterogeneity of physical and mechanical properties of compacted soil and its influence on characteristics of artificial base.

2. OBJECT OF STUDY

The large deposits of iron ore in Poltava region (Ukraine) were explored. These deposits are continuation of Kryvyi Rig iron field. Magneto quartzite fields (Gorishno-Plavninskoe, Lavrikovskoe, Eristovskoe, Belanovskoe, Vasilevskoe, Kharchenkovskoe, Manuilovskoe, Brovarskoe) spreading 45 km in length contain ore reserves of about 4 – 4,5 milliard tons. Their bedding depth is more than 500 m. In the result of field earth excavation the overburden rock dumps from open pit appear (fig. 1).

Figure 1. Lavrikovsk open pit

The problems of their utilization become more actual every year. One of the effective methods of its solving is using overburden rocks as a material for soil cushions, fills and so on. That's why a decision was taken to study the possibility of utilization them as material for massive soil cushion in designing stage of new MIDREX DRI plant "Vorskla Steel" for production of 3 MTPY slabs near Komsomolsk town.

The erection of fill with 4 – 5 m thickness and area of more than 1,9 mln. m^2 is the first plant construction stage. The steel smelting is planned on the base of Kremenchuck magnetic anomaly of ores. The plant building provides technological and ecological safety of natural resources using the technology of Austrian enterprise "Voest Alpine Industrieanlagenbau" (VAI).

3. SITE DESCRIPTION

The construction site (fig. 2) belongs to Dneprovsko-Donetsk cavity in geomorphic regard. It consists of sedimentary rocks.

Deposits of quaternary alluvial loamy sands, loams & sands lay on the surface. Typical for this territory soil profile is presented in fig. 3.

Figure 2. Over flooded territory of steel plant site

The site belongs to Dnipro & Psel left terrace. It is situated on 12 km from mouth of fairway. The construction site is over flooded and locality is swamped (fig. 2). It was ascertained that in this region there will not be hydraulic blow or failure. Ground water table will not reached 3 m of present level.

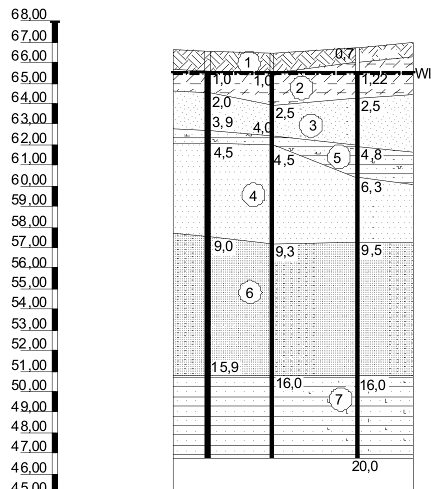

Number of hole	1	2	3
Absolute elevation of wellhead (m)	66,55	66,45	66,75
Distance between holes (m)	35	35	
Groundwater table (m)	65,55	65,45	65,53

Figure 3. Typical site soil profile: 1 – vegetable soil; 2 – plastic loamy sand; 3 – silty saturated sand, medium density; 4 – fine saturated sand, medium density; 5 – silting soft clay; 6 – fine saturated solid sand; 7 – solid and semisolid clay

4. LABORATORY TESTS OF OVERBURDEN ROCK COMPACTION PARAMETERS

Experts of Poltava National Technical University (PNTU) and research enterprise "EKFA" carry out works on scientific and technical support of erection of artificial base since 2006. At the first stage of it there were laboratory identification tests of optimum indexes of compaction of Eristov & Lavricov fields overburden rock. Test holes and sampling selection for laboratory investigations were made. Sieve analysis showed that overburden rock was presented by medium grained sand, fine sand, silty sand, loamy sand & loam.

For identification of optimum indexes of low cohesive deposits the standard modification Proctor's test in laboratory conditions was used. Rock samples were prepared of different moisture content with 2 % gradation. 2 cm of rocks were put into Proctor's matrix. Standard rings of compression and shear apparatus were installed. In these rings the soil up to initial height 10 cm was put and then soil samples were compacted by 25 blows of load weight of 25 N. Height of load fall was 30 cm (Proctor tests) and 45 cm (modification Proctor tests). After compaction the forms were dismantled, samples were prepared and maximum dry density of soil and their optimum moisture content was determined.

Using these data the mechanical properties of compacted soils in compression and shear apparatuses were determined.

5. SIMULATION OF EMBANKMENT BUILDING STAGES

Next stage of scientific and technical support is to take technical decision of site preparation under plant construction using results of laboratory investigations and simulation of fill tensely-deformed state by software "Concord" (Klovanich, 2009) and PLAXIS.

For this idea, 8 analytical schemes accounting construction stages and different improvement variants of subsoil in these schemes were taken. It was found that fill should result in settlement of subsoil on S_{max}= 64 mm without strengthening and S_{min}= 43 mm with strengthening by vertical soil cement elements to 4th engineering geological unit.

6. EMBANKMENT PROJECT

Using these data, PNTU, "EKFA", "UKRGIPROMEZ" (Ukraine), VAI, ATKINS, "Strohhausel & Partner" (Austria) decided to erect the soil cushion of 4 – 5 m thickness with necessary subsoil improvement by trenches filled with gravel 1 m wide at each 3 m step. During construction the dewatering is planned up to 2 m down of present water table. Filling material is from Eristov & Lavricov fields overburden rock which should be installed in layers of 30 cm. Each layer should be compacted to 101 % of standard Proctor's tests.

The erection of this artificial base began in autumn 2007. After implementation of drainage trenches (fig. 4, *a, b, c*) the overburden rock was delivered from open pit and put in layers of 30 cm (fig. 5, *a*). Mean value t and variation coefficient v of first layer thickness were t = 0,55 m, v = 0,282. For other layer $v \approx 0,15$ with $t \approx 0,4$ m (amount of choice is more than 100 values).

a)

b)

c)

Figure 4. The implementation of drainage trenches

Then fill was compacted by vibrorollers (weight 14 – 16 tons, frequency 30/1,95 – 40/0,9 hertz/mm) and by pneumatic rollers (weight 22 tons) carrying out 4 – 8 passages on one track (fig. 5, *b, c*).

a)

b)

c)

Figure 5. The technology of compaction of soil cushion: *a* – delivery and distinguishing of overburden rock; *b, c* – overburden rock compaction by vibro rollers

Site was broken up into 58 hooks having 13000 – 20000 m^2 and 6 – 16 layers each. There were made geotechnical quality control tests of overburden rock and their mixtures compaction.

Rational technology of carrying out operations for accelerated receiving design value of dry density of little cohesive overburden rock was experimentally grounded. First roller passage is carried out in vibratory mode by slight frequency, amplitude and low speed (2 – 3 km/h). Next two passages were carried out with vibration having higher frequency and amplitude.

Then soil moistening increases to its optimum value. Technological interval for uniform moisture distribution by soil mass is carried out. Further compaction is possible in vibrating mode with frequency 30/1,95 – 40/0,9 hertz/mm making two passages, and pneumatic mode making 2 – 4 passages on one track.

About 90 % of this artificial base was carried until present.

7. RESEARCH METHODICS OF EXCAVATED DEPOSITS PHISICAL AND MECHANICAL PROPERTIES IN COMPATION STATE

Compaction quality control of each layer of fill was studied by three samplings from each controlling point in rings having 40 cm^2 area and 140 cm^3 volume. For each hook nearly 10 point were made. Locality compaction quality control was made by pitting. For more efficient compaction quality control it is recommended to use authors' field penetrometer (Vynnykov, 2009).

Selected samples were delivered to laboratory for determination of physical and mechanical characteristics of compacted soils. The compression and shear apparatuses and laboratory penetrometer were used.

Carrying out field geotechnical control, the types of compaction mechanism, number passages on one track, mode (with or without vibration), overburden grain-size, admixture percentage, layer thickness, weather conditions and other factors were controlled.

8. RESULTS OF LABORATORY AND FIELD INVESTIGATIONS

Comparison of laboratory and field investigation results of characteristics of compacted low cohesive deposit are presented in table 1.

Table 1 shows that correlation between results of standard laboratory tests and in-situ study of characteristics of compacted soils does not exist, especially using compaction mechanism with vibration mode. That's why it is more effective to carry out experimental compaction in-situ or for laboratory tests to use impact impulse in conformity with used mechanisms.

Table 1. Physical and mechanical characteristics of compacted overburden rock

Characteristic name	Value of overburden characteristics			
	fine sand	silty sand	medium grained sand	loamy sand
Maximum water-holding capacity, %	9,04-12,13	7,92-14,35	7,16-11,55	13,36-14,6
Maximum dry density of soil, ρ_d g/cm^3, by standard & modification Proctor tests	1,704 / 1,772	1,704 / 1,772	1,741 / 1,790	1,690 / 1,728
In-situ soil dry density, ρ_d, g/cm^3	1,698-1,803	1,657-1,770	1,701-1,850	1,665-1,721
Angle of internal friction, φ, ^{0}	29-37 / 18-36	28-34 / 34-38	30-38 / 34-39	25-34 / 20-30
Unit cohesion, c, kPa	1…7 / 20,6…50	2…9 / 35,3…55,4	0…4 / 10…15	2,5…8,2 / 2…10
Deformation modulus, E,MPa	14-22 / 8,5-23,5	15-23 / 12,6-25,5	19-27 / 15,2-22	18-36,2 / 14-27,5

Note: in numerator - the results of laboratory compaction; in denominator - the results of field compaction

Experience and study results show that homogeneous low cohesive overburden rock and their mixtures with clayey soils may be used as a material for artificial base. Amount of admixtures of loamy sand and loam fluctuated within the limits of 5 – 30 % of overburden rock volume.

9. STATISTICAL STUDY OF EXPERIMENTAL DATA

The problems of determination of statistical distribution laws for values of physical and mechanical characteristics of compacted soils and evaluation of their heterogeneity were studied too. For these purposes, data of in-situ investigations were grouped according to technological compaction parameters and fill material.

Amount of the choice for physical properties (moisture and dry density) fluctuated within the limits of 100 – 200 values, and for modulus of deformation – 72 – 108. For its analysis the values received in compression apparatus by pressure σ = 0,05 – 0,30 MPa were used. Under lower pressure the received values were equal to soil structural strength. Today, general number of single determination of physical characteristics is approximately 3000 and of mechanical is more than 200.

For physical characteristics in compacted state it is more correct Gauss normal distribution law of variability values (fig. 6, *a, b*), for modulus of deformation is exponential distribution law (fig. 7, *a, b*). For badly mixed mixtures experimental diagram of values of soil dry density has three extremes and two of them are maximum (fig. 6, *c*).

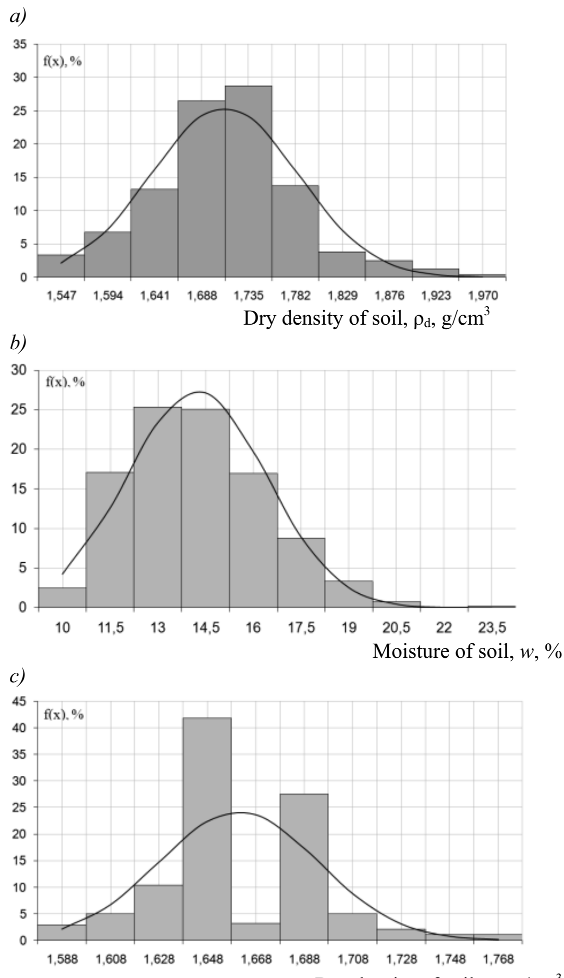

Figure 6. Experimental and theoretical distribution diagrams of variability values of physical characteristics of compacted overburden ($\leq$ 5 % admixtures) and their mixtures with loamy sand ($\approx$30 % admixtures): *a, b* – dry density and moisture of homogeneous overburden; *c* – dry density of badly mixed mixtures

a)

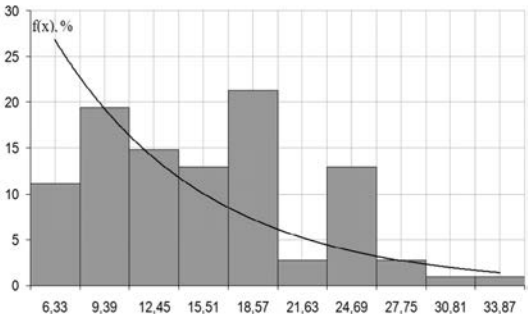

Soil modulus of deformation, E, MPa

b)

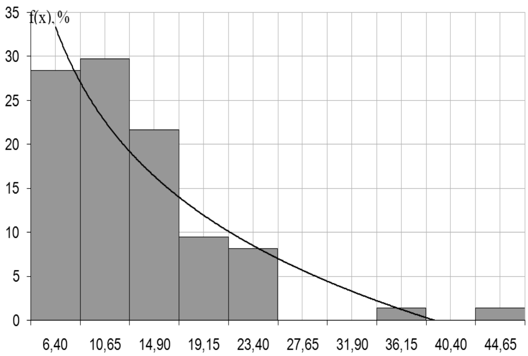

Soil modulus of deformation, E, MPa

Figure 7. Experimental and theoretical distribution diagrams of variability values of modulus of deformation of compacted overburden (*a)* and their mixtures with loamy sand (*b)* in intervals of pressure 0,05 – 0,3 MPa

Physical and mechanical characteristics of compacted heterogeneity overburden (70 % overburden and 30 % plastic loamy sand) – not so well as homogeneous overburden but variation coefficient of these characteristics increases. Statistical indexes of properties of overburden and their mixtures in compacted state are presented in table 2.

So, correlation between statistical indexes of compacted mixtures properties and homogeneity of their content and mixing quality exist.

Table 2. Statistical indexes of properties of overburden and their mixtures in compacted state

Characteristic	Mean value, x_{cp}	Dispersion, σ	Variation coefficient, *v*, %	Asymmetry, A	Excess, E
Dry density of soil, ρ_d, g/cm³, of homogeneous overburden	1,711	0,07	4,3	0,25	0,70
Dry density of soil, ρ_d, g/cm³, mixture	1,701	0,07	5,2	0,2	0,4
Moisture content, *w*, %	9,93	3,51	35	0,49	0,12
Modulus of deformation, *E*, MPa, of homogeneous overburden	15,51	6,44	42	-	-
Modulus of deformation, *E*, MPa, of mixture	13	6,92	53	-	-

Note: homogeneous overburden – 5 % of clayey particle; mixture – 30 % of clayey particle

10. INFLUENCE OF DIFERENT FACTORS ON COMPACTED OVERBURDEN ROCK PROPERTIES

Variability of technological parameters by compacting soil of massive fills is essential. These parameters are: weight of compaction mechanisms, number of passages on one track, mode, actual thickness of layer, moisture and grain-size distribution of soil, weather conditions and so on. For determination of quantitative and qualitative influence of their variability on properties of compacted soil and variation coefficient the experimental and statistical simulation and mathematical evaluation of results using modern software are used.

For in-situ study three-way analysis of variance where number of tests was 17 were used. Influence factors are soil type and content in them of admixtures (X1), number of passages on one track and mode of compacting mechanism (X2), thickness of layer (X3). Geometrical interpretation of influence of variability of technical parameters on mean value of soil dry density and limits of their variable are presented in fig. 8.

Analysis of simulation results shows that the most influence on mean value of dry density of compacted overburden has soil type and content in them of admixtures; second factor is number of passages on one track and mode of mechanisms; the least influence has thickness of layer before compaction.

a)

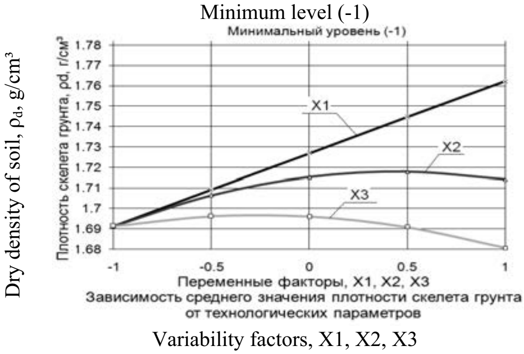

b)

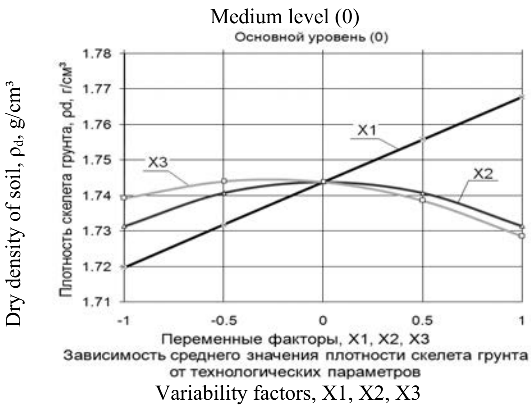

c)

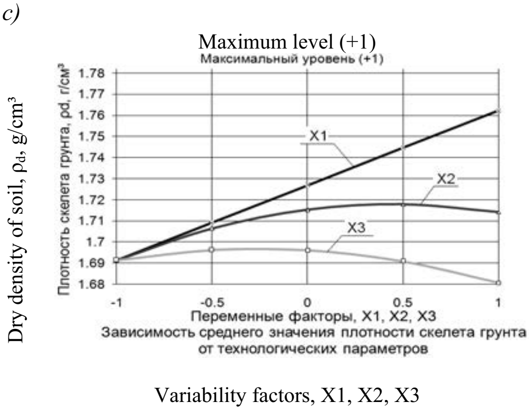

Figure 8. Influence of variability of technical parameters on mean value of dry density of soil: X1 – soil type and content in them of admixtures; X2 – number of passages on one track and mode of mechanisms; X3 – thickness of layer

Carrying out experiment, it was determined that a low cohesive rocks better compact using rollers in vibration mode. The results of comparison of compaction of fill material in vibration and static modes of rollers are shown in fig. 9.

There, one can see that dry density of soil corresponds to design values carrying out fill layers by 30 – 40 cm using as static as vibration modes. If layer thickness is more than 40 cm static mode does not provide compaction soil to design value in whole layer depth.

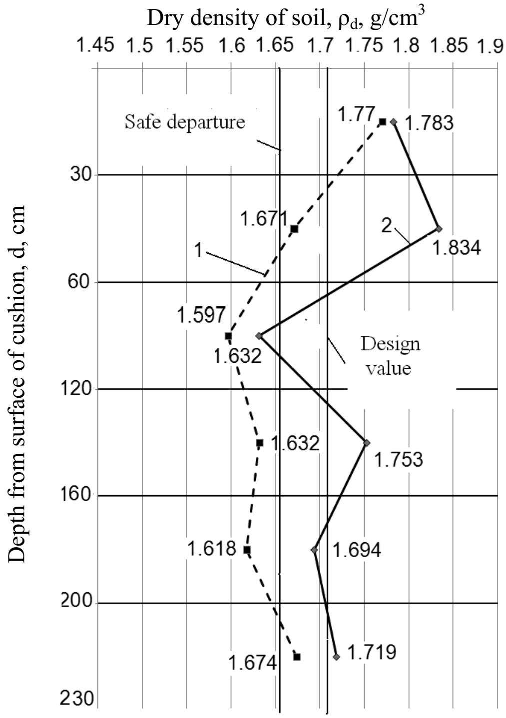

Figure 9. Change of dry density of soil by depth of compaction cushion (layers thickness are 30 – 60 cm) by roller in vibrate and static modes by 8 passages on one track: 1 – in static mode; 2 – in vibration mode

Compaction, consolidation and as well as deconsolidation always take place in filled soil (Krutov, 1988, Zotsenko, 2005, Kazarnovsciy, 2002). These processes in time depend on different factors: soil type; their state and grading; method of fill and compaction; change in time hydro geological mode in fill and so on. In sandy soil quartz particles due to silica can stick together and under certain conditions can consolidate rocks in time.

The most consolidation intensity in sandy soil takes place during 2 – 3 years and in clayey soil this process continues during 5 – 10 years.

Then intensity gradually fades.

These peculiarities were also studied by erection of soil cushion. Today, its age is about 2 years. Carrying out repeated geotechnical control after 1 – 1,5 year, it was determined that bottom fill layers had additional compaction due to weight of upper layers. In this case soil moisture content fluctuated within the limits of 6 – 25 %.

The intensity of compaction depends from value of weight of upper layers. That's why after 2 years of same pressure the values of dry density of soil were 6 % higher (from 1,62 to 1,65 g/cm^3) having 20 – 25 % moisture content of overburden.

CONCLUSIONS

Formed by recovery minerals and their mixtures with clayey soils overburden may be used as material for artificial base. For these purposes it is necessary to carry out laboratory and field investigations of their physical and mechanical properties in compacted state. Providing the properties homogeneity of overburden mixtures needs thorough mix.

The maximum dry density of soil by Proctor's laboratory tests is less than values received in-situ by modern mechanisms especially with using vibration mode of rollers. It is more effective to use values of modified Proctor's tests or to use impact impulses in conformity using mechanisms.

For physical characteristics of compacted overburden it is more correct normal distribution law, for values of modulus of deformation is exponential distribution law.

The highest influence on mean value of dry density of compacted overburden has soil type and content in them of admixtures; second factor is number of passages on one track and mode of mechanisms; the least influence has thickness of layer before compaction.

After compaction a low cohesive overburden has 1 – 10 % higher values of dry density of soil using vibration mode of rollers.

In bottom fill layers during 1 – 1,5 year there was additional soil compaction due to upper fill layers. The higher intensity of this process takes place in higher moisture content of soil (after 2 years of same pressure the values of dry density of soil were 6 % more in 20 – 25 % moisture content of overburden).

REFERENCES

Al Hamdan, W., Azzam, R., Aachan, R. 2003. Statistical methods to determine the number of field tests required for a given accuracy as implemented on broun fields of former open-pit mining sites. *Proc. of the XIIIth European Conf. on Soil Mechanics and Geotechnical Engineering*. Prague, 2003, pp. 527-533.

Chirkov, V.P. 2006. Applied methods of reliability theory in structural analysis. Moscow, 2006. 620 p.

Ermolaev, M.N., Miheev, V.V. 1976. Reliability of base and foundations. Leningrad, 1976. 152 pp.

Goldshtejn, M.N. 1971-1979. Mechanical soil properties. Moscow, V. I, 1971. 368 pp., V. II, 1973. 375 pp., V. III, 1979. 304 p.

Kazarnovsciy, V.D., Latelund, I.V., Miroshkin, A.K. 2002. Basis of design code making procedures and ensuring of necessary degree of compaction of soil highway linen. Moscow, 2002. 33 p.

Klovanich, S.F. 2009. Methods of ultimate elements in non-linear problems of structural mechanical, Zaporigja, 400 p.

Krutov, V.I. 1988. Bases and foundations on filled soil. Moscow, 1988. 244 p.

Neher, H.P., Vogler, U., Peschl, G.M. etc. 2003. Deformation of soft tailings – Probabilistic analesis. *Proc. of the XIIIth European Conf. on Soil Mechanics and Geotechnical Engineering,* Prague, 2003, pp. 173-179.

Raizer, V.D. 1995. Analysis of structural safety and design code making procedures, Moscow, 1995. 352 p.

Timofeeva, L.M. 1978. About statistical methods for strength valuation of compacted lossial soils. *Bases and foundations*. Perm, 1978, pp. 78–83.

Van Impe, W., Verastegui, R. 2007. Underwater embankments on soft soil: a case history. – London: Taylor&Francis Group. 140 p.

Vynnykov, Yu.L., Kharchenko, M.O. etc. 2009. Patent. 41209 (E02D 1/00) Penetrometer.

Zotsenko, M.L. 2005. Utilization of Poltava's MCC tailings for erection of earthworks. *Svit geotehniky*, 2005. № 4, pp. 7-11.

Geological risks in urban planning

Geological and Geotechnical Considerations for the Planning, Design and Construction of Underground Metro System in Kuwait

Waleed Abdullah
Civil Engineering Department, College of Engineering and Petroleum, Kuwait University, Kuwait

Hussain Al Sayegh
Kuwait United Development Co., Kuwait

Ananth Ramasamy
Geotechnical & Materials Department, Gulf Inspection International Co., Kuwait

ABSTRACT: The state of Kuwait is embarking in a mega project, which involves the planning, design and construction of a National Rail Network and a Rapid Transit System (Metro). During planning stage of the project, which was carried out from June 2006 till May 2008, the work included Economic, Legal, and Financial Feasibility Studies, as well as Geologic and Geotechnical Studies. A master plan was then produced delineating the national rail lines and the potential routes of four metro lines. The national railway system, which was designed to link the Saudi border in the south with the Iraqi border in the north, besides linking the east and west points in the state, was estimated to be 518 km long. The Metro, which was designed to cover the state's main residential areas, was estimated to be 171 km long. Taking into consideration the results of the geological and geotechnical study, which included literature review, site and laboratory testing of the soil profiles, as well as real estate and space availability analysis, about 65 percent of the metro lines was designed above ground on an elevated track while the remaining 35 percent to be underground. This paper discusses the engineering and geological properties of the soil profiles along the proposed Metro routes and highlights the geological and geotechnical measures recommended to be used during the design and construction of the above ground and below ground metro lines.

1. BACKGROUND

State of Kuwait plans to spend around $11.4 billion to build two main transportation systems; The National Railway Network System (NRNS) and The Kuwait Rapid Transit System (METRO).

NRNS, which was designed to link the Saudi border in the south with the Iraqi border in the north, besides linking the east and west points in the state, was estimated to be 518 km long. METRO, which was designed to cover the state's main residential areas, was estimated to be 171 km long.

Project included Economic, Legal, and Financial Feasibility studies, as well as Geologic and Geotechnical studies. The master plan produced delineated NRNS lines and METRO potential route shown in Figures 1 and 2 above.

This paper discusses the results of the investigations conducted and highlights the geological/geotechnical measures recommended for the proposed METRO construction.

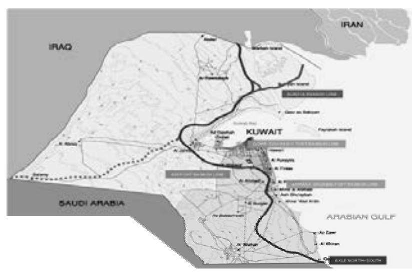

Figure 1. National Rail Network System.

Figure 2. METRO.

2. GEOLOGICAL ASSESSMENT

2.1. Project location

The state of Kuwait is situated at the North Western corner of the Arabian Gulf between latitudes 28^{o} and 30^{o} North and longitudes 46^{o} and 48^{o} East. It covers an area of approximately 17820km^{2}. It is bordered by Iraq to the north and west, Saudi Arabia to the south and the Arabian Gulf to the east.

2.2. Surface and Topography

The surface topography of Kuwait, as described by Mukhopadhyay et al. 1996**,** "is a rather monotonously flat to gently rolling desert plain broken by occasional low hills, scarps, valleys of ephemeral streams and shallow, wide inland depressions. The ground slopes gently from about 270 m above sea level in extreme southwestern corner of the country towards the northeaster corner.

2.3. General Climate

The climate of Kuwait is characterized by a typical desert environment and prolonged dry summers with extremely high temperatures and high evaporation rates. Temperature variation ranges between 3 ^{o}and 15 ^{o}C in winter and between 35 and 45 ^{o}C in summer with extreme temperatures of -3 ^{o}C in winter and 53 ^{o}C in summer **(**Al-Sanad and Shaqour, 1990). The annual precipitation is scanty with a mean of 115 mm/yr occurring between the months of November and March, with variation in intensity, duration and geographic distribution.

2.4. Geological Profile

The sub-surface condition consists of two main formations, the Dammam Formation, overlaid by the Kuwait Group.

The Dammam Formation is formed of dense dolomitic and nummulitie limestone at the base grading upwards into chalky limestone with big irregular dark chert nodules (Parsons Corporation, 1963). It crops out in Saudi Arabia and dips gently towards the North and Northeast, with some structural and erosional undulations as shown in **Figure 3**. The thickness of Kuwait Group increases with the general dip of Dammam Formation reaching over 350 m in the Northwestern part of the country. Dammam limestone was subjected to extensive erosion and karstification, and there is a sharp unconformity between it and the overlying Kuwait Group (Burdon and Al-Sharhan, 1968).

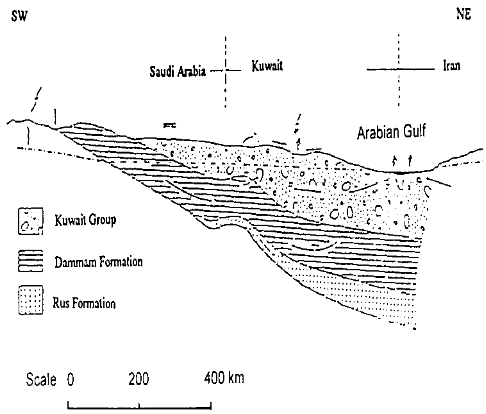

Figure 3. Geological cross-section showing the extension of Dammam limestone from Saudi Arabia.

Salman (1979) described the formations of Kuwait Group a complex of undifferentiated sequence in southern Kuwait, but can be subdivided into three formations in northern Kuwait, starting from the bottom as follows: Ghar, Lower Fars and Dibdibba as shown in Figure 4.

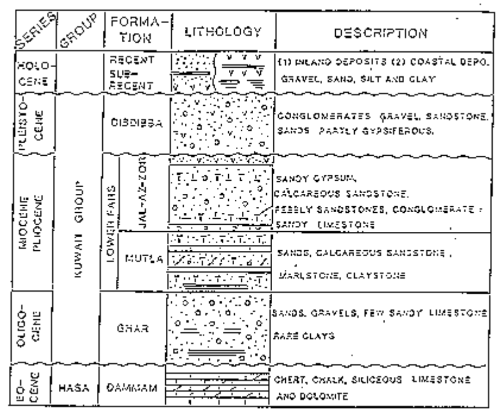

Figure 4. Kuwait Group Profile.

The Ghar Formation, the deepest of the three formations, consists mainly of sands and gravels with occasional bedding and clay intercalation. It is generally highly porous and forms a good aquifer, which is confined locally by the semi-permeable to impermeable, evaporates of the overlying Lower Fars deposits

The Lower Fars Formation is mainly compromised of anhydrite, gypsum clays, and intercalation of shallow-water limestone of Miocene-Pliocene age. Where present in thick deposits in the north, the Lower Fars Formation forms an aquitard, which separates the two aquifers of the underlying Ghar and overlying Dibdiba Formations.

The Dibdiba Formation forms the upper part of the Kuwait Group, and its occurrence is restricted to the northern part of Kuwait where its thickness reaches 200 m. It consists of cross-bedded fluviatile sands and gravels locally cemented with carbonates and sulphates with intercalation of sandy clays. These sediments were deposited in the form of sheet flood deposits and fan-shaped accumulations to varying thickness during a pluvial period of the Pleictone.

The Recent and Sub-Recent deposits provide most of the surface cover of Kuwait and owe their occurrence to particular physiographic and climatic conditions. These deposits are divided into the following six classes: eoloian deposits; residual gravel and duricusts; playa deposits; desert plain deposits; slope deposits; and coastal deposits.

2.5. Hydrological conditions

Sayed et al., 1992, revealed that Kuwait Group is a multilayered aquifer system with three main hydrostratigraphic units and several subunits. The main units being the upper aquifer, lower aquifer and intermediate aquitard. Their study further contended that all of the hydrostratigraphic units of the Kuwait Group are hydraulically connected to variable degrees dictated by the subsoil's composition, which, in general, comprises non-plastic, permeable quartz sand.

A notable feature that is observed in shallow excavations in Kuwait City and its suburbs, is an intercalation of calcareous, plastic, often cemented and almost impermeable silty, clayey sand which is having the colloquial name of "Gatch**",** (Mollah and Sayed, 1995). The presence of Gatch is significant in that it affects the hydraulic conductivity of the soil.

2.6. Morphologic features of study area

The terrain which included proposed alignment varied in ground elevation between +44m near Kuwait international airport to +4m near coastal area (Salmiya).

3. GEOTECHNICAL INVESTIGATIONS

3.1. Field works

A comprehensive geotechnical field investigation campaign was carried out for the Kuwait Rapid Transit System, from 16th December 2007 to 15th January 2008.

The field investigations consisted of fourteen boreholes, each 25 meter deep, along with in-situ testing and sampling. Boreholes locations are shown in Figure 5.

Figure 5. Boreholes locations.

Field testing included Standard Penetration Tests (SPT) as per ASTM D1586 as well as groundwater level monitoring.

In-Situ sampling included split spoon sampling, thick wall ring sampling (Dames and Moore) and one-meter long Sedi drill triple core barrel sampling runs. SPT were carried out in between the 1-m run cores throughout the depth of executed fourteen boreholes.

In addition, pressure meter test results and geophysical test results of previous studies carried out nearby the boreholes were utilized for evaluation of site conditions.

3.2. Laboratory works

All Laboratory tests were performed on selected samples recovered during the field investigation campaign, so as to verify field classifications. All tests were conducted in general accordance with applicable ASTM procedures.

4. RESULTS AND ANALYSIS

Results and analysis are based on the available soil information, all measured values from the executed geotechnical investigations and authors involvement in previous other projects in the vicinity of same borehole locations.

4.1. Identified main soil unit

The main soil unit identified is Kuwait Group deposit, which represents competent soil strata in the whole study area. The Kuwait Group consists generally of dense and very dense sandy, calcareous, uncemented to slightly cemented material, locally known as Gatch, with excellent strength and deformation properties. Stiff to very stiff imbedded clay/silt layers have also been identified within the sand deposits.

4.2. Classification

Gradation analysis, mainly to determine the percent fines content, were based on testing of 250 out of 300 split spoon samples obtained from the boreholes. About 95% of the total samples showed limited fines content, less than 30%, and more than 50 percent samples showed fines content in between 10 and 20%.

About 5 percent, only 13 samples out of 250, showed fines content over 30%. This would mean that only a few silt-clay layers are present in a predominant sandy soil in the top 25m depth below ground level. The variation of fines content verses depth is shown in Figure 6.

Gravels were only present in 71 samples or in 28percent of the total samples. Out of those, only 14 samples showed a higher content than 5%, five of which showed more than 10% and 3 greater than 20%, reaching a maximum gravel content of 27%.

Atterberg's limits tests were carried out on the SPT samples which showed relatively high fines content. Twenty four samples have shown plasticity which appeared to be high, as shown in the Casagrande plasticity chart (Figure 7).

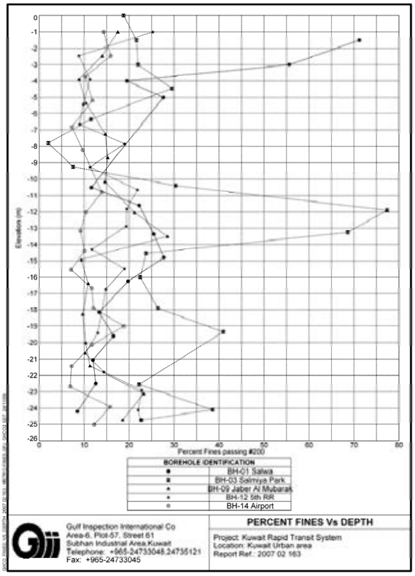

Figure 6. Percent fines versus depth.

Most of the samples show a fines fraction with Liquid Limit (LL) ranging below the 50% line, except for four near-surface samples from borehole 6, where LL is quite higher than that value.

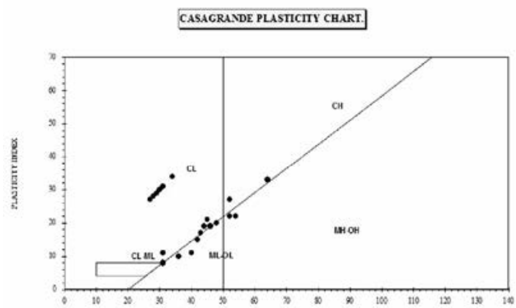

Figure 7. Casagrande plasticity chart.

Classifications tests, shown in Table 1 below, were done on 252 samples recovered in the 14 boreholes, of which 28 samples have shown plasticity. It is evident that almost all the samples belong to the sand group, poorly graded without excess percentage of fines. Most of the analyzed samples have demonstrated little or no plasticity. The average percentage of fine that passes through the sieve number 200 (0.074 mm) of all the tried samples is of 16.6%, and the part retained in the sieve number 4 (4.76 mm) is 2.1%. Both facts confirm that the soil is in general silty sands (SM) or poorly/well graded sand with silt (SP-SM or SW-SM).

Table 1. Classification tests.

Classification	Symbol	No. of samples
Sandy silt low plasticity	ML	4
Silty sand	SM	131
Poorly graded sand with silt	SP-SM	33
Well graded sand with silt	SW-SM	58
Clayey Sand	SC	3
Clay of low plasticity	CL	4
Poorly graded Sand	SP	6
Well graded Sand	SW	9

4.3. Chemical tests

The test results of pH and sulphates in the soil and chlorides in the water samples obtained from boreholes are listed in Table 2 below.

The distribution of sulphate content and calcium carbonate content in soil with depth are shown in Figure 8 and 9. The carbonate content in Kuwait group sand is slightly high in the top ten to fifteen meters. The trend is falling carbonate content with depth.

The chemical tests carried out on soil and water samples have shown moderate potential for sulphate and chloride attack on concrete according to ACI-318-08, Table 4.2.1 (Class S1 and C1). Assessment of the results as per BRE-special digest-1-2005 (3rd Edn) indicates Designate Sulfate class for location: DS-3 in combination with ACEC Class AC-2s.

Table 2. Chemical tests on ground water.

Value	pH	Sulphates (ppm)	Chloride (ppm)
Mín.	6,75	52	107
Max.	7,24	666	340
Ave.	6,98	188	165
Nº of Samples	14		14

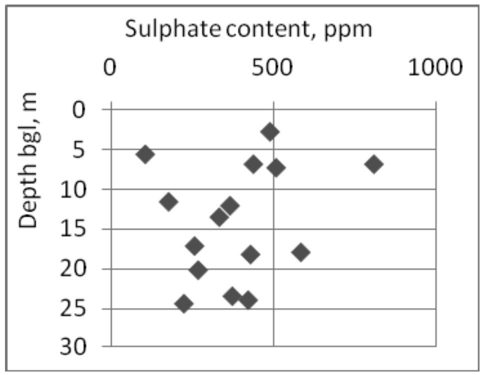

Figure 8. Variation of sulphate content with depth.

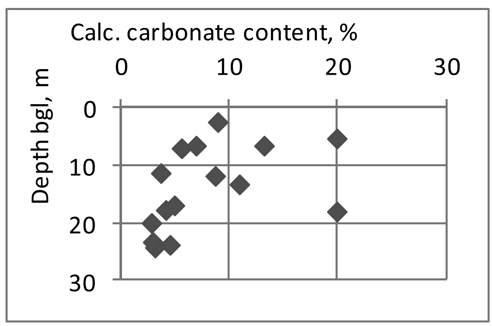

Figure 9. Variation of carbonate content with depth.

4.4. Field Strength testing

SPT N-values show the relative density of the top 1~3m consist of medium dense followed by dense to very dense in the Kuwait Group Sand. The variation of SPT-N values with respect to depth is shown in Figure 10.

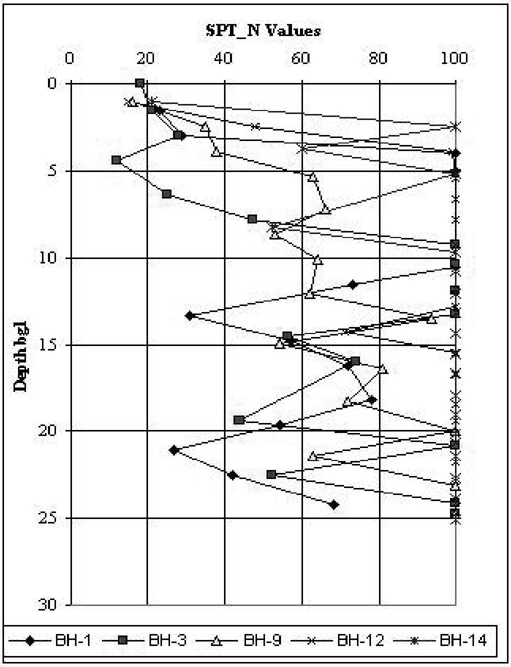

Figure10. Variation if SPT-N values with depth.

The bulk density of gatch varies between 2.0-2.1 g/cm^3 and the dry density between 1.7-1.8 g/cm^3.

Analysis of three pressure meter tests (ASTM D4719-94) and Downhole seismic tests (ASTM D7400-07) that were carried out in the vicinity of BH08, 09 and 14 in other projects were also utilized to evaluate the site characteristics. Results are listed in Tables 3 and 4 below.

Table 3. Pressure meter tests.

Near BH#	1st test depth, m bgl	Last test depth, m bgl	No. of tests
BH-8	12	70	22
BH-9	3.5	42.5	15
BH-14	3	39	13

Table 4. Downhole seismic tests.

Near BH#	1st test depth, m bgl	Last test depth, m bgl
BH-8	5	70
BH-9	2	49

Menard Pressuremeter tests results (Figure 11) indicated the variation of average modulus between 10-20Mpa in the top 10m followed by 20-35Mpa up to 25m. Then the values increased to over 70Mpa up to 40m.

Three Downhole Seismic tests indicated relatively uniform compression wave velocities of approximately 1500m/s from 15m to 40m and then a rapid increase in velocity to over 2000m/s between 40m and 45m. Beyond 50m the velocity is again uniform at approximately 1700m/s - 1800m/s.

Results of Shear Wave Velocity profiles indicated an overall increase in shear wave velocity with depth (Figure 12). Velocities range from 200m/s - 300m/s near surface to over 500m/s below 25 -30m, the highest velocities of up to 800m/s being observed in boreholes below approximately 40m.

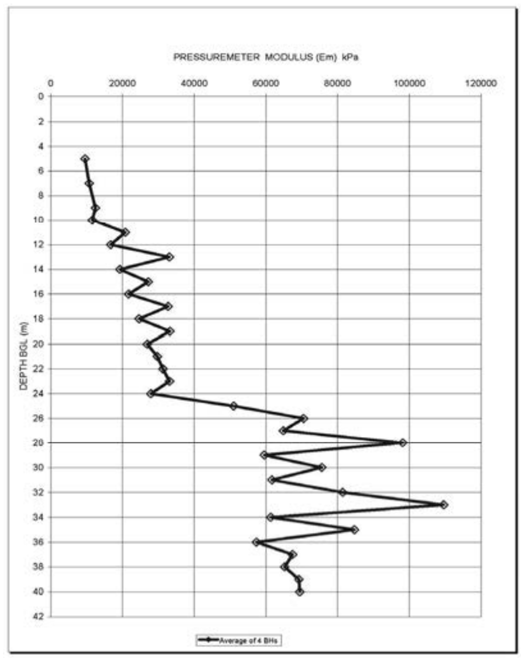

Figure 11. Variation of pressure-meter modulus with depth from 4 boreholes.

4.5. Laboratory Strength testing

About 17 direct shear tests conducted on remolded samples, showed the results of cohesion as 0.20 kg/cm^2 and 36.8º as the friction angle.

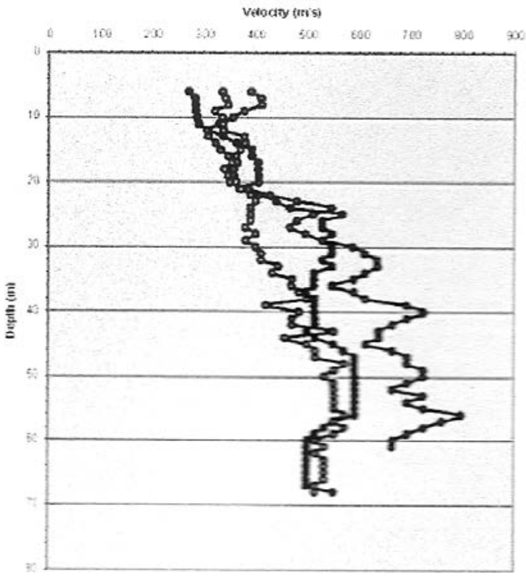

Figure 12. Variation of shear wave velocity with depth.

Fourteen Unconsolidated-Undrained three-dimensional tests (triaxial) were conducted. The angle of average friction was 34.6^o, and the average cohesion was 0.57 kg/cm^2. Results of nine Consolidated-Undrained triaxial tests reported an average cohesion of 0.031 kg/cm^2 and average friction angle of 38.2^o.

The overall strength parameters that could be considered for the calculation in the lithology unit "Kuwait Group" is therefore: Cohesion = 0.2 kg/cm^2, Friction angle = 34.6^o

5. CONSTRUCTION METHOD

Using the results of the geotechnical investigations as well as real estate allowance, about 65 percent of the metro lines were designed above ground on an elevated track while the remaining 35 percent to be underground.

Investigation indicated that, given the characteristics of the underground lines and their location within the urban area, the most suitable method for tunnel construction for all the underground sections of the proposed lines is by means of a Tunnel Boring Machine. The use of a boring machine requires that the turning radius is always over 250m. The overburden has to be in any case over 1.5 times diameter.

Conventional tunnel construction technique using piled wall/slurry wall/sheet pile wall are recommended for the remaining sections, which have length restrictions that limit the use of a tunnel-boring machine. For the surface sections, special considerations should be given for slope stability and preparation of sub-grades.

6. GEOLOGICAL AND GEOTHECNICAL HAZARDS

The following paragraphs highlight some of the major geological and geotechnical hazards that might be faced during construction of the rails systems in Kuwait, especially the underground lines.

Sinkholes: Several sinkholes were experienced between 1988 and 1989 in the Al Dahar area, 20 Km south-east of Kuwait City. The cause of these sinkholes_were attributed to the existence of Karst cavities in Kuwait (Abdulllah and Kamal, 2005)

Geological/geotechnical investigations at Al Dhahar area indicated that is located at the top of a structural high of the Dammam limestone. Dammam formation would underlie approximately 40meter thick Kuwait Group.

The occurrence of this phenomenon in Kuwait has not been reported north of Al Dhahar, where the Kuwait Group reaches a maximum of 300m in thickness. However, similar geological profile and several sinkholes incidents have been reported south of Al Dhahar and along the western coastline of the Arabian Gulf. The phenomenon needs to be taken into account as a potential hazard for infrastructure projects.

Earthquakes: Kuwait is placed in the East area of the Arabian Gulf and a significant risk of earthquakes is not reported in this area. None of the historic earthquake catalogues include events occurring in the present-day Kuwait, due to its sparse population. Only two recent earthquakes are nevertheless reported in 1993 and 1997, of 4.7 and 3.9 magnitude in southwest part of the country, related to the up-warping of the anticlinal structure of the Minagish oil field, and may be related to oil production.

Ground Water Table: The rapid increase in urban development, with the increase use of irrigation water during the last 40 years, and the random shallow presence of Gatch has considerably influenced the hydrological regime in the suburban area. The Gatch soil layer, due to its low permeability, will create an impervious layer upon which all surface water accumulates, leading to what is known as Perched water aquifer. This shallow water table has affected the construction practices in Kuwait especially for underground construction, where dewatering is always required.

7. CONCLUSION

Most of the project line extensions correspond to sensibly flat terrain, where surface is constituted of Quaternary sandy sedimentary deposits, and an anthropoid city related covering of concrete, asphalt, and others.

Almost all the tested soil samples from the study area belong to the sand group, or poorly graded, without excessive percentage of fines. The average percentage of fine that passé through sieve number 200 (0.074 mm) is of 16.6%, and the average retained on sieve number 4 (4.76 mm) is 2.1%. Soil was classified as (SM) or poorly/well graded sand with silt (SP-SM or SW-SM).

Given to the characteristics of the lines of MRTS and their location in urban zone the construction of tunnel by means of Tunnel Boring Machine is suitable for all the underground sections.

The construction by means of conventional method using piled walls/slurry walls/sheet pile wall is recommended for transition zone and in the rest of the sections whose length does not allow the use of Tunnel Boring Machine.

Considerations should be given to specific geological/geotechnical hazards that might affect the construction and sustainability of the metro lines. These hazards are Sinkholes, Earthquakes, and shallow perched water tables.

ACKNOWLEDGMENT

The work described in this paper forms part of the project that was carried out by Kuwait Metro Company for the preparation of the Master Plan for the National Rail Network System and Metro System. The authors gratefully acknowledge Metro Company for granting permission to use the data in this paper.

REFERENCES

Abdullah. W, and Kamal, H., 2005 Characterization of Desert Karst Terrain in Kuwait And The Eastern Coastline of The Arabian Peninsula, Proceedings of the Tenth Multidisciplinary Conference on Sinkholes and the Engineering and Environmental Impacts of Karst, September 24-28, 2005, San Antonio, TX

Al-Sanad, H. and Shaqour, F. 1990. Effect of groundwater level changes on the engineering properties of desert sands in Kuwait. Research Unit No. EV030, Kuwait University., Kuwait.

Burdon, D. G., and Al Sharhan, A. 1968. The problem of paleokarstic Dammam limestone aquifer in Kuwait." Journal of Hydrology, 6, 385-404.

Mollah and Sayed, 1995. Mollah, M.A. and S.A.S. Sayed. 1995. Assessment of in situ permeability with emphasis on Packer testing in Kuwait. Engineering Geology. 39: 217-231.

Mukhopadhyaya, A., Al-Sulaimi, J., Al-Awadi, E., and Al-Ruwaih, F. 1996. An overview 0f the tertiary geology and hydrology of the northern part of the Arabian Gulf region with special reference to Kuwait. Earth Science Review, 40, 259-295.

Parsons Corporation. 1963. Groundwater resources of Kuwait." V. I & II., Los Angeles (unpublished).

Salman A.S. 1979. Geology of the Jal-AZ-Zoor, Al-Liyah area, Kuwait. M.Sc. thesis, Kuwait University, Kuwait (unpublished).

Sayed, S. A. S., Saeedy, H. S. and Szekely, F. 1992. Hydraulic parameters of a multilayered aquifer system in Kuwait City. Journal of Hydrology, Amsterdam, 130, 49-70.

Study of shear strength of a reconstituted soil conductive to landslides

O. Boudlal, B. Melbouci
Geotechnical laboratory (L.G.E.A), Department of civil engineering; University Mouloud Mammeri of Tizi Ouzou, Algeria

ABSTRACT: Landslides are often catastrophic and they are more catastrophic in the case of megacities like that of September 11, 2009 in Mumbai, India. Landslides are caused when the stability of a slope changes from a stable to an unstable condition. A change in the stability of slope can be caused by a number of factors (groundwater, soil structure, erosion, earthquakes, earthwork and heavy loads due to high buildings…) acting together or alone. The landslides caused by the rain in the unsaturated soils can occur in some cases quickly under undrained conditions. The aim of this work is to study the influence of fine content, water content and confining pressure on the slip resistance using the triaxial tests.

1. INTRODUCTION

The problems of land instability frequently occur in the roads, tunnels, and dams constructions. They constitute an important field in the materials mechanics. Sometimes, some natural slopes are or may become unstable even it does not requested by these works. Researchers (Sassa 2005, 2007), (Bromhead, 2005), (Duncun 2005), are increasingly interested in studying these problems by analyzing the various factors causing instability of the land whose consequences are often catastrophic and result many dead and material damages particularly in megacities with big constructions like Tokyo, Seoul, Mexico, Mumbai, Moscow…

This experimental work is to study the influence of three essential parameters on the sliding of clayey soils.

- The sandy fines content ;
- The degree of saturation ;
- The confining stress.

Based on triaxial apparatus, the unconsolidated undrained shear tests (UU) were performed on mixtures of clay with varying, proportions of sandy fines (5%, 8%, 10%, 20% and 30%), degree of saturation (Sw = 30%, Sw = 60% and Sw = 90%), and confining stress (100 kPa, 200 kPa, 300 kPa and 400 kPa).

Finally, the test results are presented as curves (deviator stress – axial strain) and (pore pressure – axial strain) based on different parameters listed above.

2. SOME STATISTICS OF LANDSLIDES IN MEGACITIES

Megacities	Landslide date	Damages
Seoul	July 27, 1987	Heavy loss of human life as well as property damage
Mexico city	Sept 16, 2009	3 died and serious damages
India	11th and 17th August 1998	380 people were killed
Mumbai (India)	2005	78 people were killed and many others seriously injured
Sao Paulo	2009	At least 15 people were killed
Beijing	2009	7 people were killed and 65 missing
Dhaka	August 2009	About 200 families have been displaced and their homes, properties and livelihood destroyed.
Buenos Aires	9 February 2009	Two deaths and approximately twelve people are missing and 10,000 people have lost their homes,

3. IDENTIFICATION TESTS

Two types of materials have been used for the preparation of samples: clay and sandy fines.

The used clay is taken from a site near the University Mouloud Mammeri of Tizi-Ouzou, (Algeria).

The Atterberg limits determined in the laboratory by standard NF P 94 051 are presented as follows:

- Liquid limit $w_L = 43{,}5$
- Plastic Limit $w_P = 20{,}15$
- Plasticity Index $I_P = 23{,}35$

It is "plastic clay".

The used sandy fines are from the 0.1 mm sieve, collected in sand sifting, original Oued Sébaou in Tizi-Ouzou (Algeria).

4. EXPERIMENTAL APPARATUS AND PROCEDURE

4.1. Apparatus

The used apparatus is shown in figure 1. It is a monotonic triaxial apparatus by numerical command, (Digital Tritest 100), equipped with various sensors, measuring the axial displacement, force, confining pressure, back pressure and volume change or pore pressure depending drained or undrained test.

The confining pressure and back pressure are generated by the air-water system.

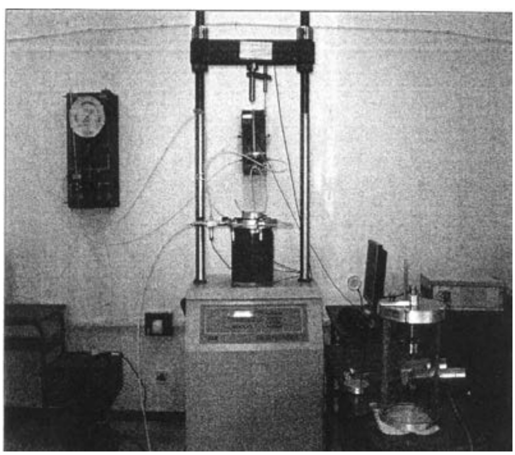

Figure 1. Triaxial apparatus.

The data are then acquired by an Acquisition Data Unit (ADU) and processed by a software data processing "DS7" (Data System 7). Finally, the results are grouped in a report in tables and curves.

4.2. Samples preparation

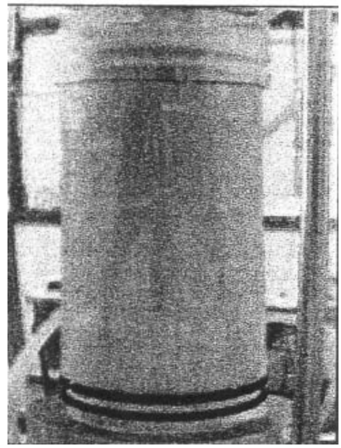

Figure 2. Samples prepared.

The clay is homogenized with different proportions of sandy fines (5%, 8%, 10%, 20% and 30%), then care-fully compacted in layers (Kenji, 2003), (Jefferies, 2006).

The samples are cylindrical in shape, with a diameter 70 mm and height 140 mm (see figure 2), they are at different degrees of saturation (30%, 60% and 90%), thus approaching the real case of saturation of natural lands.

The samples are then tested for unconsolidated undrained shear tests (UU), under different confining stress (100, 200, 300 and 400 kPa) with a shear velocity of 2.5 mm / min, it is a relatively fast speed, "fast load", that can develop very large pore pressures in the unsaturated case, this is the real case of shearing of soil in the landslides caused by rapid loading such as volcanoes, earthquakes, explosions ...).

This type of loading leading to sudden and fast failures were found frequently in recent years in several countries around the world. On May 18th, 1980 the Mount St. Helens in south-west Washington state, awoke violently exploded, causes slip of all its northern flank, which generates 57 deaths, destroys 47 bridges, 24km of railway and 300 km of roads.

In 2001 the January 13 earthquake in El Salvador has triggered more than 500 slope movements, two of them alone have killed more than 500 people and caused extensive damage to buildings and road improvements. In 2009 the explosion of career Diaoxiyan, the city of Yichang in China caused a landslide causing four deaths, many missing and enormous material damage.

5. PRESENTATION OF RESULTS

The results are presented as curves of stress-strain and pore pressure-strain, according to the confining stress (100, 200, 300 and 400 kPa), sandy fines content (5%, 8% , 10%, 20% and 30%) and degree of saturation (30%, 60% and 90%).

5.1. *Influence of confining stress on the development of deviator stress and pore pressure for clay samples.*

The figures 3 and 4 show the evolution of stress-strain and pore pressures-strain curves, within the confining stress (100, 200, 300 and 400 kPa) for the clay samples (without sandy fines) at Sw = 90%.

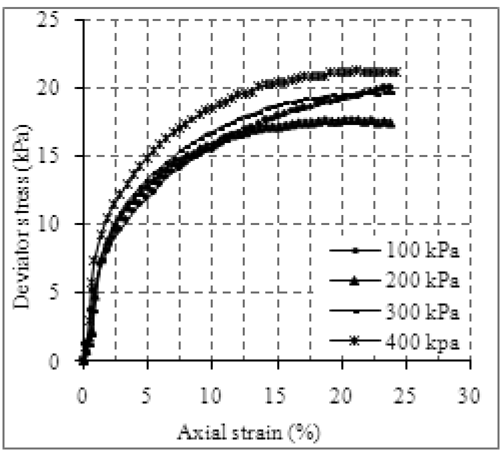

Figure 3. Evolution of deviator stress within the confining stress (Sw = 90%).

The deviator stress for a soil nearly saturated (Sw = 90%) is almost constant and does not depend on the confining stress applied. The curves are almost combined.

When there is no drainage, the water remains imprisoned in the pores. Since water is incompressible, it prevents the particles get closer when it occupies all the empty land.

Under such conditions, when the confining stress increases, the shear resistance does not change. Only the pore pressure increase. Whatever the confining stress applied, the resistance to shearing of soil remains constant. (robitaille, 1997), (Murthy, 2003), (Braja, 2006).

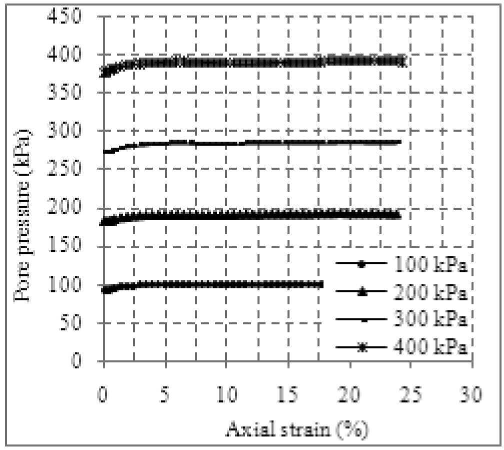

Figure 4. Evolution of pore pressure within the confining stress (Sw = 90%).

The pore pressures developed are directly proportional to the confining stress applied. After the application of all-round pressure the effective stresses in the specimen remain unchanged because, for a fully saturated soil under undrained conditions, any increase in all-round pressure results in an equal increase in pore water pressure, (US, 2003), (Craig 2004).

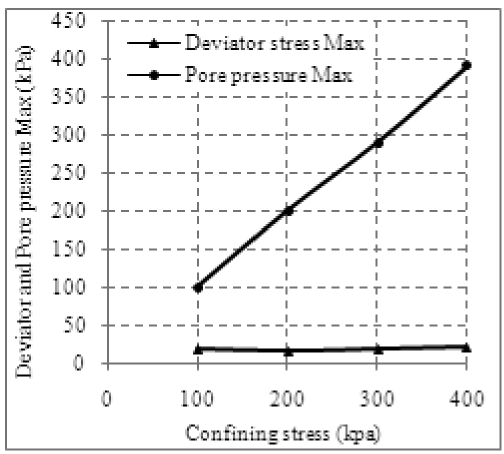

Figure 5. Evolution of the deviator stress Max the pore pressure Max within the confining stress.

The figure 5 shows clearly that the deviator stress remains constant as a function of applied confining stress, while the pore pressure increase in the same value as that of containment.

5.2. Influence of content of sandy fines on the deviator stress and pore pressures.

The figures 6 and 7 show the evolution of stress-strain and pore pressure-strain curves based on the content sandy fines (5%, 8%, 10%, 20% and 30%) under a confining stress of 100 kPa.

The addition of 8% of sandy fines seems appropriate to give the mixture a better shear resistance, and develop the weakest pore pressures.

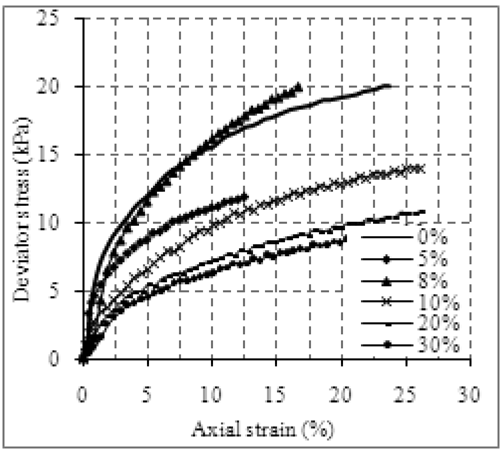

Figure 6. Evolution of the deviator stress as a function of the sandy fines content, (Sw = 90%).

The deviator stress is improving more and more with increasing of sandy fines content, but beyond 8% of sandy fines, the deviator stress begins to decrease continuously as a function of the fines content to achieve the lowest values with the addition of 30% of sandy fines.

While, the pore pressure is minimal with the addition of 8% of sandy fines. Then it increase to fluctuate between 87 kPa to 95 kPa for the other mixtures.

The pore pressure increases at the beginning of the test (between 3% and 5% of axial strain), then it evolves according to a range up to the end of the test.

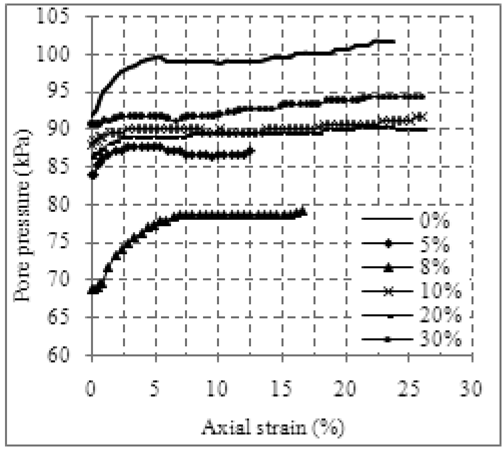

Figure 7. Evolution of the pore pressure as a function of the sandy fines content, (Sw = 90%).

5.3 Influence of degree of saturation on the deviator stress and pore pressure.

The figure 8 shows the evolution of the deviator stress and pore pressure as a function of the degree of saturation.

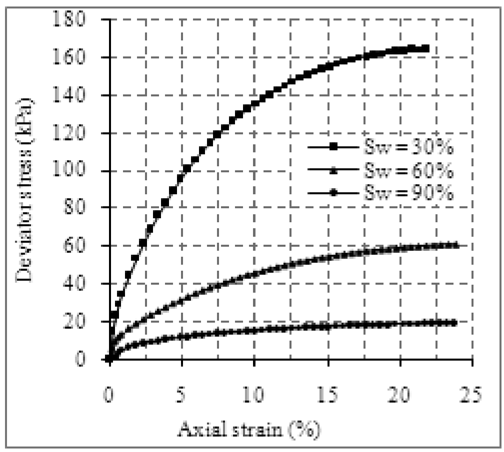

Figure 8. Evolution of the deviator stress as a function of the degree of saturation.

The shear strength decreases more with increasing degree of saturation, water weakens the grain and supports their movement against each other and thus decreases the resistance of mixtures. For cons, the pore pressure increase with increasing water content and are generally higher for samples saturated to 90%.

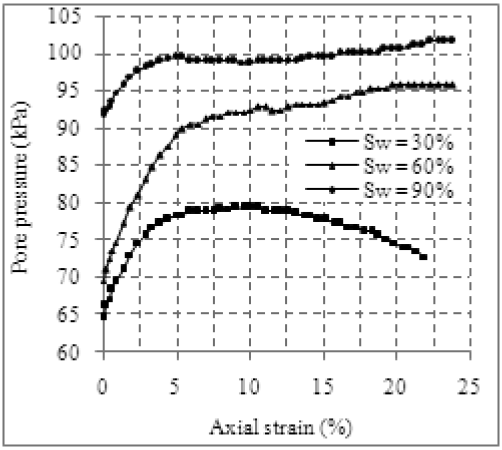

Figure 9. Evolution of the pore pressure as a function of the degree of saturation.

The figure 10 shows the evolution of deviator stress Max and pore pressure Max depending on the degree of saturation.

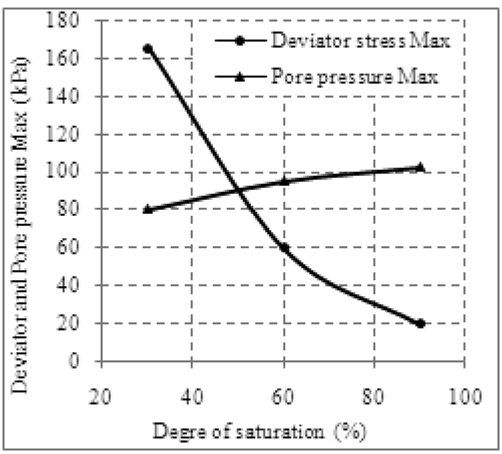

Figure 10. Evolution of deviator stress and pore pressure as a function of the degree of saturation.

We note that the deviator stress Max decrease sharply with increasing of the degree of saturation and the pore pressure increase.

6. CONCLUSION

This work includes an experimental study on reconstituted clay samples containing different proportions of sandy fines (5, 8, 10, 20 and 30%), saturated with (Sw = 30%, Sw = 60% and Sw = 90), then subjected to shear under unconsolidated undrained triaxial tests with different confining pressures (100, 200, 300 and 400 kPa). The obtained results showed that:

- The behavior of unsaturated clays depends directly on the confining stress. While it is independent of this stress in the case of clays near saturation.
- The Sw = 90% reduce significantly the resistance of the mixtures, and develop very large pore pressures.
- The containing of 5% to 8% of sandy fines improves the shear strength of mixtures and reduces the pore pressure.

This study thus allowed us to analyze, from the perspective shear strength and pore pressure, the influence of different parameters mentioned above, the behavior of clay soils (frequently encountered in the building areas of our region), and who often have significant instability, including slope and in the presence of water.

7. REFERENCES

Braja, M. 2006. Principles of Geotechnical Engineering, Canada, Nelson.

Bromhead, E.N. 2005. The Stability of Slopes, Taylor & Francis e-Library edition, London.

Craig, R.F. 2004. Craig's soil mecanics (seventh edition) UK.

Duncun, j. M. 2005. Wright S. G, "Soil Strength and Slope Stability", Canada.

Jefferies, M. & Been, K. 2006. Soil Liquefaction. *A critical state approach,* Great Britain.

Kenji, I. 2003. Soil Behaviour in Earthquake Geotechnics, Great Britain.

Kyoji. S. & al. 2007. Progress in Landslide Science, Springer-Verlag Berlin Heidelberg.

Murthy, V.N.S. 2003. Geotechnical Engineering, *principles and practices of soil mechanics and foundations engineering*, New York, Marcel Dekker Ink.

Norme NF P 94 051,. Sols : reconnaissance et essais, determination des limites d'Atterberg. Limite de liquidité à la coupelle-Limite de plasticité au rouleau.

Robitaille, V. & Tremblay, D. 1997. Mecanique des sols, *Theorie et pratique*, Modulo editeur, Quebec.

US, Army Corps. 2003. Engineering and Design, Slope stability, Manual N° 1110-2-1902, Washington, DC 20314-1000.

Building in the urban area of Constantza city (Romania) acting as a high cliff stabilization structure

R. Ciortan
SC IPTANA-SA Bucharest

S. Manea
Technical University of Civil Engineering of Bucharest

ABSTRACT: On the high cliff of Constantza, it shall be carried out a commercial center with many levels. The cliff is between level +38.00 and level +24.00, showing a virtual slope as 1:2. The center's foundation raft is at level +10.50, involving therefore excavations with depths of about 28 m at the top side and about 14.0 m at the bottom side of the slope. In time, the cliff has been consolidated in the area both by re-sloping and drainage works.

The paper shows the constructive solutions in order to support the work enclosure contour and to found the new construction co-operating with for restarting the drainage systems and requirements. During the execution time, there are stipulated monitoring works therein.

The group of all the designed solutions ensures stability for the area of the new construction supporting the ground, thus taking part to its consolidation.

1. INTRODUCTION

On the high cliff of Constantza City, a commercial centre will be built on a land surface about 400 m long and about 50 m wide, on the flank located between Traian Blvd. (levels +37 ÷+38.00 Black Sea level) and Marinarilor St. (levels +20 ÷+24,00 Black Sea level). The works will be carried out in two stages, the first stage being already in progress, as it started in June 2007 (fig.1). The typical sections of the work (fig. 2 and 3) have revealed that a foundation level of +10.5 BSl is necessary, due to the presence of multi-level basements. The maximal height of the building is of approx. 70 m and the minimal one is of approx. 40 m.

The geotechnical design constitutes a complex problem, mainly due to the fact that the building with basements is located on a flank, and ground water is present at a certain level.

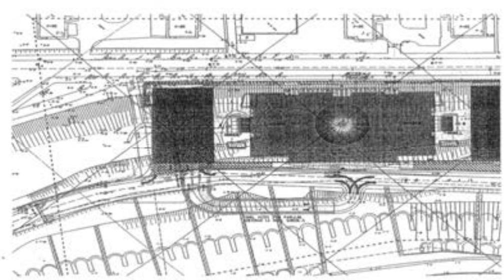

Fig.1. Plan view

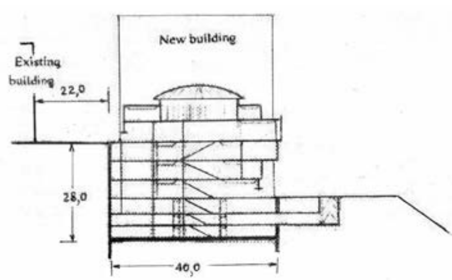

Fig.2. Cross-section

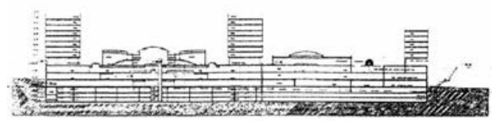

Fig.3. Longitudinal section

After considering various solutions, the concept of "building – retaining wall" has been selected, so that the new structure, in co-operation with the retaining works necessary during the construction period, would take over the loads during the operation period, therefore ensuring the cliff stability in time. The modality of supporting the work enclosure was derived from this solution, taking into account the built-up neighbouring areas.

There are some old drainage works on the cliff and the designed solution that is currently under construction provides keeping these works functional, in order to maintain the existing hydraulic regime.

2. STUDIES AND INVESTIGATIONS PERFORMED

Given the complexity of the general layout issues of the work and in accordance with the national technical norms, the following types of studies have been mainly provided: topographical, geotechnical and hydro-geological studies, expert appraisals of the existing constructions, investigations of the existing drainage and protection system.

3. SITE DESCRIPTION

3.1. Topographical, geotechnical and hydro-geological conditions

The site has an average slope of about 1 : 2.

The site is bordered by Traian Blvd. to the west, on the long side. Beyond this boulevard, at more than 20 m distance from the property boundary, there are several buildings with different heights: 5 apartment buildings with 9 storeys, a two-storey dwelling house and a restaurant – ground floor.

On the other long side, to the East, there is Marinarilor St., providing road access to the site, and the incline of the port enclosure.

The conclusions of the observations and calculations for checking the sliding stability under static conditions and under earthquake conditions, were that, in the present configuration and with the related works (partially functional drainage works, protection works), the site is generally stable.

At the time when the investigations were performed, there were signs of small local subsidence’s, and also of deterioration of the adjacent areas, such as longitudinal cracks and dishevelment’s in the carriageway.

Based on the 20 new boreholes with depths up to 50 m, on the 11 geological boreholes, on the specific laboratory tests as well as on the data supplied by 10 older boreholes kept in the records, the structure of the sub grade on the site was determined to be as follows (fig.4):

- heterogeneous fillings with thicknesses of 1 to 3 m (locally 8 m), consisting of waste of building materials at the surface, and, in depth, cohesive soils mixed with coarse materials (boulders and limestone blocks). The characteristic geotechnical parameters are: γ = 20 KN/m3, E = 10000 kPa, ϕ = 20o – 40o, c = 25 ÷ 2 kPa.

Outside the borders of the site, in the area of the apartment buildings, at the same levels, there is a loess layer which is insensible to moisture;

- a package with thicknesses of 40 m at the top side of the slope and about 25 m at the bottom side, consisting of cohesive soils as silty clays, and medium compressible clays.

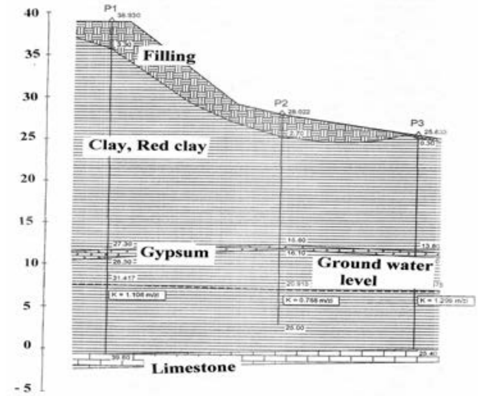

Fig.4. Soil lithology

Within this package, there can be distinguished the red and grey structured clays that are specific to the Dobrogean area, with thicknesses of around 8 to 14 m, and, in depth, the grey-greenish clays.

Slickensides were encountered within this cohesive package, at levels +23 ÷ +16 BSl and +16 ÷ +14 BSl. Also, around the levels +10.00 ÷ + 14.5 BSl, within the clay layer, there were detected continuous gypsiferous bands with thicknesses of 2 to 3 m. These findings have led to the premise that slip planes are likely to occur in these areas.

The red and grey clays that are located above the gypsum have high plasticity, are stiff-to-hard and have a specific behaviour in relation to water, the shearing strength parameters decreasing rapidly when in contact with water or air.

The geotechnical parameters determined on natural samples are: γ = 18.5 ÷ 21 KN/m3, E = 12.500 kPa, ϕ = 16o – 18o, c = 70 ÷ 90 kPa. The shearing strength parameters determined on saturated samples are ϕ = 8o – 10o, c = 40 ÷ 50 kPa. For the grey-greenish clays that are plastically stiff-to-hard, located under the gypsum layer, and featuring inclusions of degraded limestone, the resulting values were: E = 12.000÷15.200÷20.000 KPa, ϕ = 10o–18o and c = 8 ÷ 210 kPa.

- the bedrock, encountered under the levels -2 ÷ –6 BSl, consists of Sarmatian, oolitic, whitish-reddish limestone that is degraded when in contact with the clay, and which, below the levels of -8 ÷ –10 BSl, becomes compact, with a compressive strength of σrc = 15.000 ÷ 20.000 kPa.

In the Southern area of the site, there is an aquifer of average depth, at levels +6.8 ÷ + 7.57 BSl, having a flow direction from N-V to S-E, with an average slope of 1.2 %.

In the central and northern area, a shallow aquifer was formed from rainfalls and possibly leakage from the town water supply network. This aquifer is quartered in the silty clays with limestone concretions, the hydrostatic level being at +29.8 ÷ +29.3 BSl. There is a free flow of water from N-V toward S-E, with a slope of 14 %, discharging on the slope through a spring located at level +22 BSl. In this area, the average depth aquifer is located at level +7.2 ÷ +13 BSl, having a flowing direction from NN-V to SS-E and a slope of 8.4 %.

3.2. Existing protection and drainage system

In time, the cliff has been consolidated by re-sloping, surface protection and drainage vaults. Along with the construction in 1957 of a series of apartment buildings of GF+8Floors, a drainage system was executed (fig.5), consisting of:

- a longitudinal gallery on Traian Blvd, having a ovoid cross-section of 1.8 m on height and 1.40 m on widths, located at the depth of +26.0 ÷ +27.0 m, which collects and carries the water along the cliff, up to the slot galleries;
- four inspection manholes on the main gallery route;
- two transverse galleries carrying the water from the main gallery to the ditches; intermediary inspection pits of 8.0 ÷ 15.7 m on depth are located along these galleries;
- tubes ϕ 300 mm carrying the water from the manholes of the main gallery to other intermediary pits;
- connections between the pits and the water discharge ditch consisting of drains gutters.

The longitudinal gallery is located at the bottom of the loess package, above the clay layer. Hence, the water collected by the main gallery flows towards the port through gallery-type drains and transverse pipes along which inspection manholes are present. From the manholes, the water flows by gravity through pipes and ditches to the longitudinal collecting gutter located at level +6.0 m, with longitudinal slope, which discharges the water into the sea. The water discharge is about 10 l/sec., varying in relation to the period of the year and the maintenance status of the urban public networks.

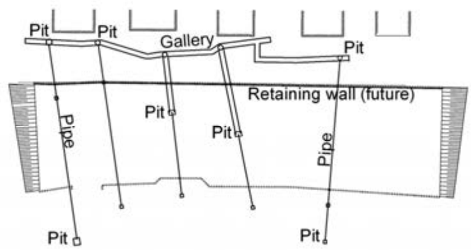

Fig. 5. Existing drainage system

4. DESIGNED WORKS

4.1. General Principles. Possible Solutions

Given the necessity to have the foundation level of the building at about +10.5 BSl, the required excavations will have depths of 28 m at the upper side of the slope (Traian Blvd. side) and 14 m at the bottom side of the slope (Marinarilor St. side). This implies execution of retaining walls on the outline of the working enclosure, in order to support the ground and reduce the surfaces affected by the construction works. The building location requires keeping and ensuring the land stability over the entire operating period of the building, considering the presence of certain constructions on the adjacent platform. In regard to these requirements, two conceptually different solutions have been analysed:

- provision of a final retaining wall at the upper side of the site, under shelter of which the works would be carried out, and which would ensure the stability of the land, without having a compound effect with the building.

- provision of a temporary retaining wall, which is necessary during the execution period for securing the necessary space for carrying out the construction works and which would have a compound effect together with the building during its operation period, ensuring the general stability of the site, the building being designed to this effect.

The first solution implies a massive, heavy retaining structure occupying a large surface of the site or a suppler structure definitively anchored in the limestone layer, requiring anchors with lengths of 80.0 ÷ 90.0 m. The provision of shorter anchors, ending in the structured clay layers, does not ensure a controllable behaviour due to clay characteristics changing over time and to the variable level of ground water. Concurrently, the definitively anchored wall requires the provision of a certain space for inspection, control and intervention at the anchoring system, which results in reduction of the build able surface. As the building is executed independently from the retaining wall, it could be directly founded on the layer of grey-greenish clay, the deformations being practically independent.

The second solution allows full usage of the build able area. In this case, the building has to be checked for sliding, in order to ensure that the load due to earth and water thrust would be taken over, including in case of earthquake occurrence. The vertical retaining wall that borders the building and the building itself form a compound effect together. Hence, there should be taken into account the fact that the thrust is applied to the building wall, without mobilizing passive resistance on the opposite side, which would imply greater strains that the building could not bear.

After comparing the two solutions, the second one has been adopted and it is applied in the designs of the working enclosure, the final drainage system and the building itself.

4.2. Excavation Solution

On the long sides of the enclosure, there was provided a retaining wall consisting of a screen of reinforced concrete anchored piles of 80 cm on diameter, disposed at a distance of 1.20m between axes (fig. 6 and 7). The piles have variable lengths; on the Traian Blvd. side, they are 32.45 m long, starting at level +38.00 (5 m embedment), and on the Marinarilor St. side, they are 16.45 m long, starting at +24.00 (3 m embedment). The excavation level is +10.50 BSl. The piles are interlocked at the top by means of a reinforced concrete beam (100 x 40 cm^2) and at the anchoring level also by means of reinforced concrete beams (30 x 80 cm). The anchors, pre-tensioned at 480 kN, have gradients of 15^o, lengths varying from 50 m to 13 m, and 8 m anchor bulbs.

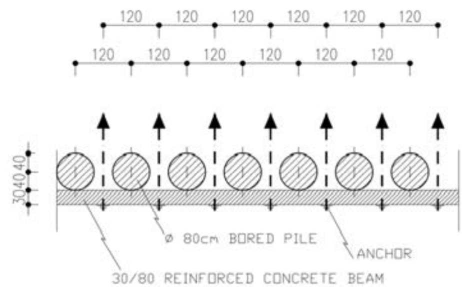

Fig.6. Anchored drilled piles screen

The solution providing spaced piles has been selected so as not to disturb the hydrodynamic regime in the site and its adjoining areas (fig. 6). The screen and the temporary retaining walls are designed considering the loads generated by the earth massif and the ground water, including the case of earthquake occurrence, so as to ensure structural safety and to limit horizontal slips in order to prevent any negative impacts on the adjacent built-up areas. The drilled pile screen is a final structure being an integral part of the final construction. For the calculation of the screen elements there have been taken into account the geotechnical characteristics of the various materials in the massif, as well as their behaviour in time, the minimal parameters being considered.

Under the shelter of the pile screens, the excavations are executed in stages, after mounting and pre-tensioning the anchors intended for each level. This faster method for carrying out the excavations has decided the manner in which the screens are to be sustained on the outside (temporary anchors) and not on the inside (props). Works for controlled collection and discharge of ground and rain water are provided in the excavated areas (pipes, slopes, gutters, ditches), taking good care to avoid moisturizing of the macro-structured red and grey clays.

4.3. Construction Solution

The architectural structure of the commercial centre provides execution of about 6 underground levels and 8 levels above ground, practically a vertical development from level +10.50 BSl up to level +80 BSl. The strength structure consists of reinforced concrete up to level +38.00 BSl and, from this level upwards, it is a metallic one.

In the case of direct foundation, in the most unfavourable scenario, this structure together with the screen wall, with no anchors, will not be able to take over the loads generated by the earth massif thrust, the ground water pressure and the earthquake additional loads during operation. The conclusions of these checks have led to the provision of piles with diameter of 120 cm and lengths up to 20.0 m under the foundation raft (fig. 7).

Taking onto consideration the screen, the mobilization of the shearing strength (cohesion) on the contact surfaces between the raft and the clayey soil and piles' capacity to take over horizontal forces, the taking over of horizontal loads during the operation period is ensured. The pile foundation solution permitted reduction of the raft thickness to 0.5 m and consequently reduction of the excavation level.

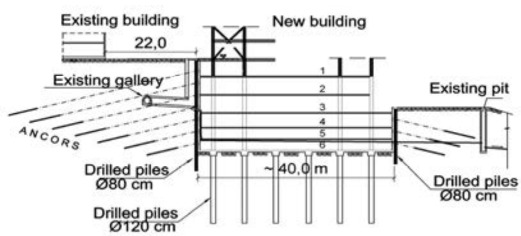

Fig.7. Solution of the building

4.4. Water Drainage

The drainage system is formed so as to ensure water collection and free flow. Practically, it was intended not to change the water flow regime, and to control the strains transmitted to the new structure, increasing the safety degree of the works.

The longitudinal drainage gallery remains outside the limit of the future building, towards the town, at distances varying from 10.0 m and 14.0 m. The lay-out of the pile screen intersects the transverse galleries. When the excavation reaches their level, the necessary set-up works will be carried out so as to ensure that the collected water is discharged downstream. To this effect, vertical tubes with diameter of 200 mm are provided. The connection area will be set-up as a manhole for routine checks.

The solution adopted with regard to water discharge includes (fig. 7):

- control manholes next to the new building, at the intersection with the existing transverse galleries; setting-up of the transverse galleries in the area of the new building so that the collected water could be taken over by the vertical pipes adjacent to the new building wall; channel along the wall at the penultimate underground level; transverse pipes to be connected to the existing downstream manholes.

In order to prevent the possible water infiltrations into the ground leading to overstraining the building, a vertical drain connected to the above-mentioned channel has been designed. The vertical drain bottom is located at level 13.95 BSl, 40 cm above the floor of the penultimate underground level. The water collected by the vertical drain will be discharged in the longitudinal collecting channel through transverse pipes with ϕ 100 mm, placed at intervals of 1.2 m, having a gradient of 1 % towards the channel.

4.5. Monitoring Works

In order to determine the behaviour of the adjacent buildings and that of the ground, measuring works have been provided in connection with: the vertical deformations (settlements) of the buildings, the road and the enclosure screen; the ground water level outside the enclosure, in front of the apartment buildings; the horizontal deformations of the land by the buildings and into the screen; the variation in width of the existing joints between the block sections; the water discharges and chemical analysis of some water samples (fig.8).

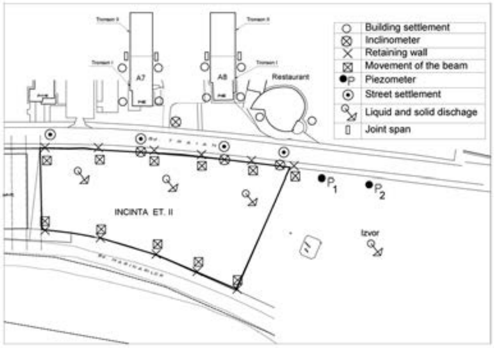

Fig. 8. Monitoring

The values measured up to date, over a period of about 24 months, with excavations up to depths of approx. 28.0 m, reveal the effectiveness of the measures taken for limiting the impact of the new works on the existing structures.

5. CONCLUSIONS

Based on some detailed geotechnical and hydro-geological studies performed on the high cliff of Constantza City, a commercial centre has been designed and is now under construction. Owing to the constructive solution that provides it would have a compound effect together with the excavation retaining system, this building plays an important part in the stabilization of the cliff in that area.

The specific site conditions, the existing local drainage and retaining works have been considered during the design of the constructive solutions. The draining system designed to collect and discharge ground water and infiltrations is connected to the existing one. Hence, the existing local conditions would not be changed, nor would the adjacent buildings be affected.

Over the entire execution period, the works will be associated with monitoring activities focusing on the behaviour of the adjacent areas, so as to be able to take timely remedial measures if necessity arises.

The concept of civil works for urban areas that would act as cliff stabilization structures should be considered for other locations as well, as it results in a more effective use of the build able areas and shorter execution periods.

6. REFERENCES

Chang-Yu Ou, 2006. Deep Excavation. London, Taylor&Francis Group.

NP 120-2006, Specification for designed and execution for deep excavation in urban area. Bucharest.

Differential classification at boundaries of soil and rock

EL- Sohby, M.A.
Faculty of Engineering, Al- Azhar University, Nasr City, Cairo Egypt

Mazen, S.O.
Housing& Building Research Center, Dokki, Cairo, Egypt

Aboushook, M.I.
Faculy of Engineering, King Abdulaziz University, Jeddah, Saudi Arabia

ABSTRACT: Nearly all naturally occurring soil formations are being created from rock by weathering or are being turned back into rock by the process of lithification.The nature of lithification determines a material that may range between those of soil and rock. The literature have been directed to categorizing this transitional border line material into soil-like and rock-like types. Many of these types are unsaturated with a certain degree of lithification and associated with geotechnical problems. These problems are due to their tendency to volume change and mobilization of swelling or collapse.

The present research aims at integrating the behavior of the material into the framework of unsaturated soil mechanics. Based on testing of 72 samples representing a wide range of soil properties, prediction charts were constructed. The proposed charts were investigated by testing 29 undisturbed samples representing a variety of transitional border line deposits and their deformations were measured. A very good agreement was found between measured and predicted values.

1. INTRODUCTION

Naturally occurring unsaturated deposits that lie on or close to the boundary between soil and rock are difficult to describe in unambiguous terms. A big range of these deposits have engineering properties transitionally between those of soils and rocks. Many weak rocks may behave as soils and conversely some stiff or hard soils may behave as rocks. The range of this overlap of performance is difficult to define.

Recently, this problem has become of common concern among geotechnical engineers and engineering geologists. As a results, international meetings were organized by either specialization to discuss the subject. The first was a session entitled "Mechanical properties of weak material" which was included in the fifth Pan- American conference on soil mechanics and foundation engineering held in Buenos Aires in 1975. This was followed by successive conferences. The most well known of them: international symposium on weak rocks held in Tokyo in 1981; a session on engineering geological problems related to formations and excavations in weak rocks included in the fifth international congress of IAEG held in Buenos Aires in 1986; Leeds conference of the engineering group of the Geological Society of London on weak rocks held in 1990; Geotechnical engineering of hard soils- soft rocks held in Athens in 1993; Geotechnics of hard soils- soft rocks held in Naples in 1998; International Conference on Problematic Soils in 2005, Famagusta, Cyprus (Aboushook et al., 2005) and International Conference on Advanced Experimental Unsaturated Soil Mechanics, in 2005, Teronto, Italy (El-Sohby et al., 2005).

In these conferences, much has been written about engineering and geological classification of soil/ rock border line deposits. However, we feel that there is, still, a considerable room for the improvement of the framework of our knowledge in that field.

Therefore, the present paper primarily presents fundamental review of the boundary between soil and rock. Then it presents a new approach for classifying and predicting the behavior of naturally occurring deposited unsaturated soil and rock by integrating their properties and behavior into the frame work of soil mechanics.

2. FORMATION OF SOIL/ ROCK BORDER LINE DEPOSITS

Nearly all naturally occurring unsaturated soil formations are being created from rock by the process of weathering or are being turned back into rock by the process of lithification. Lithification in the result of reduction of pore size, re- orientation of particles and cementation. The natural and degree of lithification determine a material that range between those of soil and rock (Bartonet al., 1993; Vaughan, 1997 and Marions, 1997.

There is a great variety of this border line material. Mudrock is a general term used that has gained increasing acceptance in the literatures as the preferred group name.

According to BS, 1981, the general term mudrock is used for lithified homogeneous argillaceous rocks. If the constituents are laminated or the rock is fissile on the bedding plane, the term shale is used.

According to De Freitas, 1993, mudrock is used to encompass argillaceous engineering rocks as opposed to clay soil. As such, it would be equivalent to the lithologies, mudstone, shale, siltstone and claystone. Attewell, 1997 gave an explanation and description of this material based on its formation and constituents as indicated in the following table 1:

3. INTEGGRATING SOIL/ROCK BORDER LINE DEPOSITS INTO THE FRAM WORK OF SOIL MECHANICS

Table 1. Basic Terms

Un-lithtified	Lithified/ Non-fissile	Litified/ Fissile	Approx. Proportions (grain size)
Silt	Siltstone	Silty Shale	2/3 silt size (2-60 micron)
Mud	Mudstone	Shale	Silt& Clay size (< 60 micron)
Clay	Claystone	Clay Shale	2/3 clay size (< 2 micron)

Soil/ rock border line material occurring in Egypt and elsewhere are mostly desert formations developed from argillaceous rocks. They are mainly unsaturated clayey soil deposits that have a certain degree of lithification. The effect of lithification often develop on the engineering properties. The extent of lithification can be measured from parameters determined from tests on intact samples relevant to mass behavior.

Lithified unsaturated soil material consists of four basic components. Clay mineral, non-clay mineral, interparticles bonds and a pore space occupied by air and water. The structure and degree of this material is determined by the nature and degree of lithification. This structure becomes compact due to the interparticle bonding that occupied part of the pore space that was then present. The extent of lithification is, therefore, a function of the density of soil material and the water content. More interparticle bonds will be present in samples of higher density and lower water content.

At high dry density and high clay content, the structure of soil will be dense and mainly composed of clay matrix and particles containing chain of sand and silt grains. Such structure tends to swell upon wetting giving rise to volume increase.

At low dry density and low clay content, the texture of soil will be mainly composed of an open structure of sand and silt which tends to collapse upon wetting giving rise to volume decrease.

Furthermore, in both cases (swell or collapse), the soil is characterized by having relatively high strength at their natural moisture content and a drastic decrease in strength upon wetting.

Therefore, these types of deposits are associated with engineering problems as a result of related volume change that give rise to ground movements and decrease in bearing capacity that may result in damage to structures.

Accordingly, from the engineering point of view, it is more convenient to consider unsaturated lithified deposits that lie on the border line between soil and rock on basis of their behavior rather than being restricted to categorizing it into soil- like and rock- like types.

4. PROBLEMATIC BEHAVIOR OF SOIL/ROCK BORDER LINE DEPOSITS

4.1 Swelling behavior

Swelling of expansive clayey soils was subjected to the study of numerous research workers, among them are: (Gillott, 1988; Tissot& Aboushook, 1983; Chen, 1988; El-Sohby et al., 988 and Taylor, 1988). Their studies may be summarized as that:

The swelling behavior is the result of interaction between the interparticle bonding and the induced swelling pressure. When the induced swelling pressure exceeds the capacity of bonding, failure in tension occur. Therefore, highly cemented clayey soils often have a high resistance to deformation and may be able to absorb significant amount of swelling pressure.

When swelling clay minerals are present and water is available, the minerals take water into their lattice structure. In less dense clayey soils, they tend to expand initially into zones of loose soil before volume increase occurs. In densely packed clayey soil with low void space, the soil mass has to swell more or less immediately to accommodate volume change.

Furthermore, where weak interaction of the cations with the surface of unit layers occur in the clay mineral as with sodium, separation of exchangeable cations from the montmorillonite surface results in double layer repulsion between platelets, tending to separate the platelets as far as possible in the water available until they are dispersed into individual platelets in water.

4.2 Collapse behavior

Collapsible soils were subject to the study of various research workers, among them are: (Feda, 1988 and Houston et al., 1988). Their studies may be summarized in the following:

Soils which are liable to collapse possess porous textures with high void ratios and relatively low densities. The micro - structures of collapsible soils takes the form of a loose skelton built of coarse grained material (sand and silt) and fine grained material (clay). The sand and silt sized particles are separate from each other and are connected by bonds and bridges. These bridges are made of clay sized material. As grains are not in contact, mechanical behavior is governed by the structure and quality of bonds and bridges. Therefore, at their natural low moisture content, these soils possess high apparent strength but they are susceptible to large reductions in void ratio upon wetting. In other words the structure collapses as bonds between the grains break down when the soil is wetted.

5. PREDICTION OF VOLUME CHANGE BEHAVIOR

As previously mentioned, the main problem associated with partially saturated lithified deposits that lie on the border line between soil and rock is their volume change in the presence of water and the mobilization of swelling pressure or collapse potential. Therefore, the main concern of design engineer is to understand the behavior of such soil and to make quantitative estimates of the anticipated volume change upon wetting. This was subject to study by various research workers and numerous relationships were established to predict volume change of unsaturated soils. However, most of the efforts was directed towards investigating either swelling characteristics or collapsibility characteristics.

In attempt to investigate the problem of these formations on one general basis, El-Sohby, 1994 initiated a comprehensive research work using experimental data from tests carried out on 72 samples of soils representing a wide range of soil properties. These soil samples were divided into two main groups each composed of 36 samples. The first group constituted sand- clay mixes with different proportions and the second constituted silt clay mixes.

In this study, the dry unit weight (γ_d) and the type of coarse grained fraction were used to express the micro - structures of soil, and the clay content to express the matrix of internal structure. Both sand and silt were mixed with different percentages of clay 0,10,20,30,40,50,60,80,90 per cent .Thus the two groups of sand-clay and silt-clay mixtures were divided into 18 groups, giving a total of 18 different soils. For each soil ,four specimens with dry densities 14.0,15.5,17, and 18.0 kN/m3 were tested. This gives the data for 72 soil specimens. All specimens were unsaturated and of 8% initial water content. The specimens were tested in the oedometer apparatus. After the specimen had reached equilibrium under 200 kN/m2, it was flooded with water and allowed to swell. The swelling per cent (axial strain) was that measured under 200kN/m2 after inundation.

The test results obtained were tabulated and used to construct charts relating the dry unit weight and clay content to predict quantitatively the swell or collapse potential of soil. This is indicated on table 2 and figures 1&2.

Table 2. Measured and predicted values of axial strain of 29 undisturbed samples

Soil No.	Measured physical properties						Axial strain	
	mo	γ_d	S_r	Clay	Silt	Sand	Measured	Predicted
	(%)	(kN/m3)	(%)	(%)	(%)	(%)	(%)	(%)
1	2.0	13.0	5.0	17	56	27	- 12.5	- 14.0
2	1.5	20.0	11.6	5	10	85	+ 5.0	+ 0.5
3	8.0	18.5	47.0	52	35	13	+ 12.5	+ 12.5
4	7.5	18.6	44.8	54	40	6	+ 13.6	+ 13.30
5	10.0	19.0	61.5	28	22	50	- 4.5	+ 1.50
6	6.0	19.6	54.6	59	37	4	+ 14.0	+ 15.0
7	15.0	16.5	61.9	45	40	15	- 0.5	+ 6.0
8	17.0	17.0	75.7	50	20	30	+ 5.0	+ 5.0
9	5.5	14.6	31.5	18	64	18	- 0.3	- 5.0
10	6.0	19.0	38.5	52	38	10	+ 8.5	+ 14.0
11	2.0	18.0	10.8	13	27	60	- 1.0	00
12	1.5	17.0	6.9	7	27	76	- 5.0	- 0.8
13	5.5	18.5	32.3	48	29	23	+ 8.9	+ 11.0
14	2.0	17.5	9.9	9	3	88	- 1.0	- 0.5
15	5.0	19.5	35.0	50	30	20	+ 15.0	+ 15.0
16	2.0	16.5	8.5	10	25	65	+ 5.0	- 0.9
17	2.0	16.5	8.5	8	5	87	- 7.5	- 0.9
18	9.5	18.0	51.0	52	30	18	+ 14.0	+ 11.5
19	5.4	16.0	21.2	7	18	75	- 3.5	- 1.2
20	8.5	18.5	50.0	48	35	17	+ 15.0	+ 12.0
21	6.5	19.0	41.7	50	33	17	+ 18.5	+ 13.0
22	8.0	19.0	37.0	92	8	00	+ 20.0	+ 25.0
23	4.5	19.0	26.0	60	30	10	+ 18.5	+ 14.0
24	2.0	15.0	6.8	15	45	40	- 6.5	- 3.0
25	3.6	19.5	25.3	53	32	15	+ 12.5	+ 13.0
26	4.0	18.5	23.5	10	31	59	- 2.5	00
27	11.0	17.5	53.0	45	35	20	+ 7.5	+ 7.5
28	3.5	18.0	18.0	48	32	20	+ 8.0	+ 10.0
29	4.0	21.0	33.0	50	35	15	+ 15.0	+ 15.0

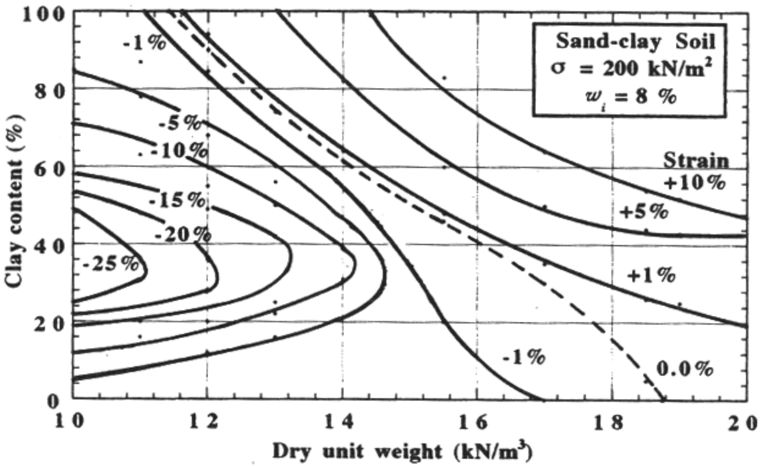

Fig. 1 Axial strain versus dry unit weight and clay content for sandy clayey soils

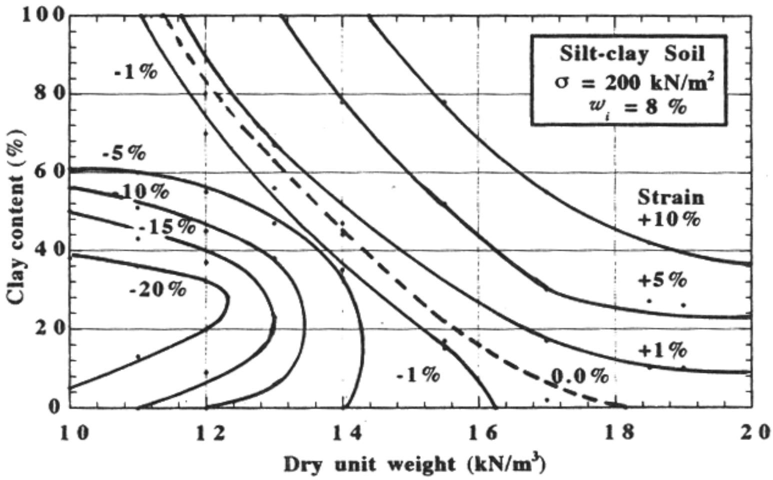

Fig. 2 Axial strain versus dry unit weight and clay content for silty clayey soils

6. TESTING THE VALDITY OF THE PROPOSED CHARTS

A previous work by Aboushook, 1988 included data of 29 undisturbed samples taken from different locations and covering a wide range of geographical areas was used. The axial strain was measured for specimens of size 35 mm in diameter and 50 mm in height. This was used to test the validity of the proposed charts.

Utilizing the proposed charts in terms of the physical properties of the 29 samples, the axial strain of each soil (predicted value) was determined. This was compared with the measured values given by Aboushook, 1994 and tabulated.

7. CONCLUSIONS

- Nearly all naturally occurring soil formations are being created from rocks by the process of weathering or are being turned back into rocks by the process of lithification.
- The nature and degree of lithification determine a material that may range between those of soil and rock.
- Soil/ rock border line deposits are mainly unsaturated formations developed from argillaceous rocks.
- Mudrock is the term used to encompass argillaceous lithified rocks. As such it would be equivalent to the lithologies mudstone, siltstone, claystone and shale.

- This type of deposits have certain degree of lithification. The effect of lithification often develop on the engineering properties. The extent of lithification can be measured from parameters determined from tests on intact samples relevant to mass behavior such as dry density, water content and clay contents.
- Unsaturated lithified deposits are characterized by associated engineering problems. This is due to their tendency to volume change upon wetting and the mobilization of swelling pressure or collapse potential.
- From the engineering point of view, it is more convenient to consider unsaturated lithified deposits that lie on the border line between soil and rock on basis of their behavior rather that being restricted to categorizing it into soil- like and rock- like types.
- To integrate soil/ rock border line deposits into the frame work of soil mechanics, a comprehensive research work was done using experimental data from tests carried out on 72 samples of soils representing a wide range of soil properties. The test results obtained were tabulated and used to construct charts relating the dry unit weight, clay content and water content to predict quantitatively the swell or collapse potential of soil.
- To test the validity of the proposed charts, the axial strains of other 29 undisturbed samples taken from different locations were determined in the laboratory and compared with predicted values using the proposed charts. Almost a complete agreement was found between the measured and the predicted values.
- The proposed charts can be used to predict qualitatively and quantitatively volume change behaviour of unsaturated lithified soil/ rock border line deposits.

8. REFERENCES

Aboushook, M.I; Mazen, S.O. and El- Sohby, M.A. (2005). Correlating predictions for problematic soils with field measurements, International Conference on Problematic Soils, Famagusta, Cyprus.

Aboushook MI (1994) Engineering geological classification of weak argillaceous rocks in some Egyptian deserts.7th Int. IAEG Congress, Lisboa, Portugal, Balkema, Rotterdam,421-427.

Attewell PB (1997) Tunneling and site investigations. Geotechnical Engineering of Hard Soils- Soft Rocks, Balkema, Rotterdam, 1767-1790.

Barton ME, Mockett LD, Palmer SN (1993) An engineering geological classification of the soil/ rock borderline materials between sands and sandstone. The Engineering Geology of Weak Rock, Balkema, Rotterdam, 125-138.

British Standard Institution 5930 (1981) Code of Practice for site investigation

Chen EN (1988) Foundation on expansive soils, Elsevier, Amsterdam, 465pp.

De Freitas M.H (1993) Weak arenaceous materials. The Engineering Geology of Weak Rock, Balkema, Rotterdam, 115-123.

El-Sohby, M.A.; Mazen, S.O. and Aboushook, M.I. (2005). Advancement in oedometer testing of unsaturated soils, International Conference on Advanced Experimental Unsaturated Soil Mechanics, EXPERUS 2005, Teronto, Italy.

El-Sohby Ma (1994) Swelling and collapsing behavior of arid soils Symposium on development in Geotechnical Engineering, Bankok 193-200.

El-Sohby MA, Mazen SO, Elleboudy AM (1988) Comparative study of problematic soils in two areas around Cairo. Proc. Symp. On Environmental Geotechnics and Problematic Soils and Rocks. Asian Insitute of Technology, Bankok, 515-526.

Feda J (1988) Collapse of soil on wetting, Engineering Geology, 25:265-267.

Gillott JE (1988) Clay in engineering geology Elsevier, Amsterdam, 226 pp.

Houston JL, Houston WL, Spadala DJ (1988) Prediction of field collapse of soils due to wetting, Proc. Of ASCE, J. of Geotechnical Engineering Division, 114:40-58.

Marions PG (1997) Hard soil- Soft rocks: Geological features, Geotechnical Engineering of Hard Soils- Soft Rocks. Balkema, Rotterdam, 1807-1818.

Taylor Rk (1988) Coal measures mudrocks, Q. J. Engineering Geology, London, 21:85-99.

Tisot JP, Aboushook MI (1983) Triaxial study of the swelling characteristics, Proc.of the Asian Regional Conference on Soil Mechanics and Foundation Engineering, Haifa,1:94-97.

Vaughan PR (1997) Engineering behavior of weak rocks. Geotechnical Engineering of Hard Soils- Soft Rocks. Balkema, Rotterdam, 1741-1748.

Seismic Microzonation of Tehran City

M. R. Ghayamghamian
International Institute of Earthquake Engineering and Seismology (IIEES), Tehran, Iran

A. Komak panah, R. Behroo
Department of Civil Engineering, University of Tarbiat Modares, Tehran, Iran

ABSTRACT: In this paper, the site effects were estimated using available geotechnical and geophysical data in Tehran city, the capital of Iran. The series of geologic, geotechnical and geophysical information were gathered and processed to characterize different soil units and their distribution in the study area. Based on this information, a GIS database was developed for Tehran city (with 614 km^2 area) divided into 2400 grids with 500 m * 500 m size. These data were employed to estimate local site effects for the grids. Then, the maps showing the distribution of site dominant frequency and soil amplification factor were developed to predict the effects of the soil layers on seismic ground motion at the bedrock.
KEYWORD: Seismic microzonation, Site effects, Tehran city, GIS soil database

1. INTRODUCTION

When an earthquake occurs, seismic waves radiate away from the source and reach the ground surface on which waves produce shaking. Ground shaking and its associated damage mostly is affected by characteristics of the input motion, surface and sub-surface geological and topographical conditions, these effects are known as “local site effects” (Kamalian et al, 2008). The nature of local site effects can be estimated in several ways: by simple, theoretical ground response analysis using geotechnical and geophysical information; by empirical methods using measurements of the actual surface and subsurface ground motions at the same site; and by measurements of ground surface motions or microtremors from site with different subsurface conditions.

Tehran, the capital of Iran, is located in a high seismic zone at the foot of the Alborz Mountains. The distribution of historical earthquakes (Figure 1) around Tehran shows that the region has been experiencing large destructive earthquakes with magnitude greater than 7 (Ambraseys and Melville, 1982). The last large historical event was the 1830 earthquake with magnitude 7.1, which occurred approximately 100 km from the Tehran city. The closest historical event to the city was a 855 earthquake with magnitude 7.1. The most important recent instrumental earthquakes, which occurred in the region, were the 2002 Changureh-Avaj earthquake (Mw=6.5), Firozabad – Kojour (2004) earthquake (Mw=6.2) and the 2007 Kahak-Qom earthquake (Mw=5.7).

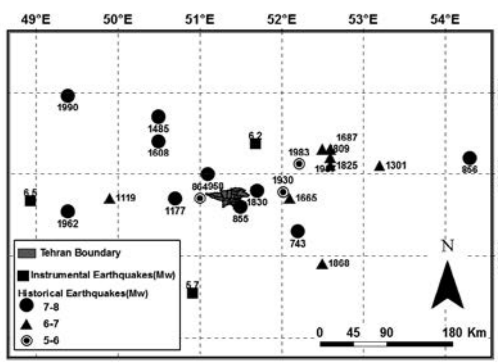

Figure 1. Distribution of historical and instrumental earthquakes around Tehran city.

Different investigations have been carried out for the seismic microzonation of Tehran city (e.g., Jafari et al., 1997, 1998, 2002; JICA, 2000; Haghshenas, 2005; Ghayamghamian, 2008). In last study, Ghayamghamian (2008) analyzed data from 34 acceleration stations belonging to the Building and Housing Research Center (BHRC). Recorded earthquake data from these acceleration stations provide unique opportunity for site effect estimation and earthquake hazard mitigation in mega city like Tehran. They analyzed acceleration data in the range 10-40 cm/s^2 from Changureh-Avaj (2002), Firozabad-Kojour (2004) and Kahak-

Qom (2007) earthquakes, which recently occurred near to the Tehran. They evaluated site amplification characteristics using empirical methods. Standard site / reference and H/V spectral ratios (HVSR) were employed to evaluate the site characteristics. The results revealed a large contribution of site effects on ground motion at the majority of the studied sites.

In this study, the recent geologic, geotechnical and geophysical information in Tehran were gathered. Based on this information, the soil condition in Tehran was categorized into 15 soil models. Then, the site response was analytically estimated. These results were implemented with the results of empirical techniques using recorded earthquake data (Ghayamghamian, 2008). Finally, the seismic microzonation maps for site dominant frequency and soil amplification factor are generated at Tehran city.

2. GEOLOGICAL SETTING

Tehran which is situated in the north-central part of Iran extended on 51°04′ - 51°36′ E and 35°34′ - 35°50′ N. Northern region of the city is a part of Alborz Mountains with height of about 3000 m, while southern part is located in plain like low lands (Figure 2). Geologically, four major types of alluvial formations with different geotechnical and geological properties covered the Tehran city (Rieben, 1955).

“A” or Hezardarreh formation, is the oldest formation and considered to be of the Pliocene-Pleistocene. This formation, which covers northeast and east parts of city, essentially includes conglomerates with lenses of sandstone, siltstone and mudstone.

“B” formation covers “A” formation and includes two facieses: “Bn” (North Tehran inhomogeneous alluvial formation) which Consist of conglomeratic mixture of gravel, pebble, and clastic size cobble and “Bs” (South Tehran clayey silt or Kahrizak formation) composed of reddish brown and beige-colored silt with some clayey component.

“C” or Tehran alluvial formation includes homogenous conglomerates, composed of gray to brown colored gravel with mixture of silt and sand.

“D” formation (Recent Alluvium) is the youngest stratigraphic unit within the Tehran region and is present as alluvial and fluvial deposits. This formation is subdivided into two different stratigraphic units, “D1” unit, as a veneer, covers the “Bs” formation in the south and is composed of line silt with a grayish cream and gray color; “D2” unit is composed of silty gravel, clastic size pebble, and covered “C” formation in north. Figure 3 shows the geologic map and distribution of various geological units covered Tehran city.

Figure 2. Physiographical position of Tehran city.

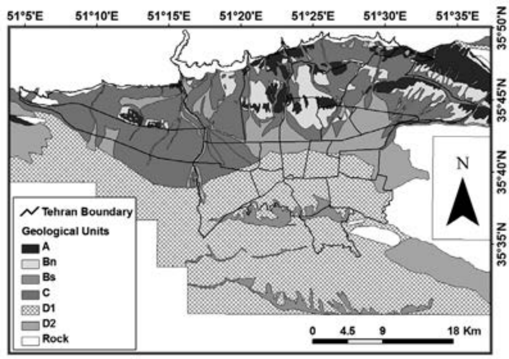

Figure 3. Geologic map of Tehran city.

3. GEOTECHNICAL AND GEOPHYSICAL INFORMATION

To complete the required database, besides of available and pre-existing data, new series of geotechnical and geophysical information including 163 boring investigations and 55 downhole tests were gathered. The collected new data conducted by national and local governments as well as public and private corporations. Then, results of the new series of geotechnical and geophysical data were compiled along with previous data in a GIS database. The distribution of the gathered geotechnical and geophysical data is shown in Figure 4.

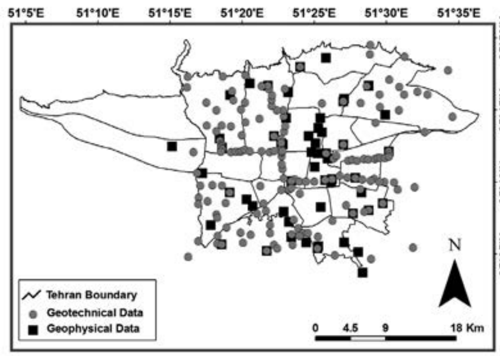

Figure 4. The distribution of gathered geotechnical and geophysical data in Tehran City.

4. ANALYTICAL ESTIMATION OF SITE EFFECTS IN STUDY AREA

According to the boring data and soil types, layer thickness, SPT-N values and shear wave velocities the soil condition were categorized into 15 geotechnical models. In Figure 5, the distribution of the soil models in Tehran is shown, furthermore the detailed information about each model are presented in Table 1 and 2. The site response analysis was performed using assumed soil models and their shear wave velocity profiles. The one-dimensional ground response analysis was conducted using free EERA (Equivalent-linear Earthquake site Response Analysis) computer program.

The depth to seismic bedrock for each representative geotechnical model was determined from downhole data. Seismic bedrock is defined to be a rock-like media with shear wave velocities in the range of 700–800 m/s (Ishihara and Ansal, 1982; ICBO, 1997, 2003; BSSC, 2003; BHRC, 2005). The study area was divided into equal grids with 500 m * 500 m size, and then the site characteristics at each grid were computed by subjecting their representative models to the defined bedrock input motions. The soil dominant frequency and amplification factor at each grid were estimated. Next, microzonation maps of the city were created showing the distribution of amplification factor and site dominant frequency throughout the study area. Figures 6 and 7 illustrate the site dominant frequency and soil amplification factor in Tehran, respectively. Due to lack of the geophysical data in western and eastern ends of the study area, and to reduce error, these regions were excluded in generation site dominant frequency and amplification factor maps. As expected, soil amplification of southern part of city is greater than that of northern part (mountain area) in general. Furthermore, the amplification factor shows large values in south and south-west of the city.

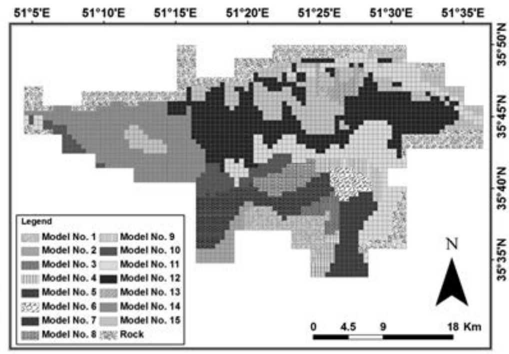

Figure 5. The distribution Geotechnical soil models for grid of 0.5*0.5 km in Tehran.

Table 1. Geotechnical and geophysical characteristics of soil models

M[1]	Depth(m)										$V_{S(30)}$ (m/s)
	5	10	15	20	25	30	35	40	45	50	
1	C1	C1	C1	C1	C1	C1	CS3	CS3	CS3	CS3	357
2	C1	C1	C2	C2	C2	C2	CS3	CS3	CS3	CS3	300
3	C1	C1	C2	C2	C2	C2	CS2	CS2	CS2	CS2	307
4	C2	C2	CS2	CS2	CS2	CS2	C3	C3	C3	C3	424
5	CS1	CS1	C2	C2	C2	C2	CS3	CS3	CS3	CS3	488
6	G2	G2	CS1	CS1	CS1	CS1	G3	G3	G3	G3	548
7	CS2	CS2	C3	C3	C3	C3	CS3	CS3	CS3	CS3	484
8	CS2	CS2	CS2	CS2	CS2	CS2	S.B[2]				601
9	G2	G2	CS3	CS3	G3	G3	S.B				453
10	C2	C2	G3	G3	G3	S.B					550
11	S3	S3	S3	S3	S3	S.B					510
12	G3	G3	G3	G3	S.B						681
13	C1	C1	C1	S.B							602
14	G3	G3	S.B								655
15	Pre-Miocene										615

[1]Model number.
[2]Seismic bedrock.

Table 2. Soil name, symbol and N_{SPT} value used in soil models

Clay	C1	C2	C3
Ave. N_{SPT} Value	15	35	75
Clay and Sand	CS1	CS2	CS3
Ave. N_{SPT} Value	15	35	75
Sand	S1	S2	S3
Ave. N_{SPT} Value	15	35	75
Gravel	G1	G2	G3
Ave. N_{SPT} Value	15	35	75

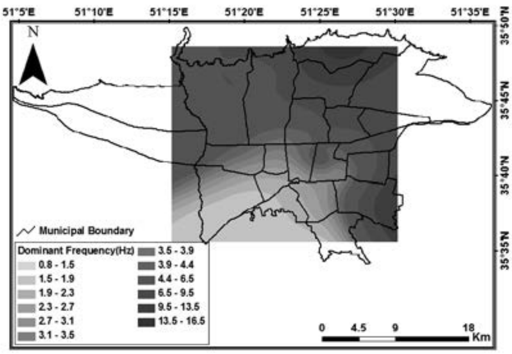

Figure 6. The distribution of site dominant frequency in Tehran city using analytical method.

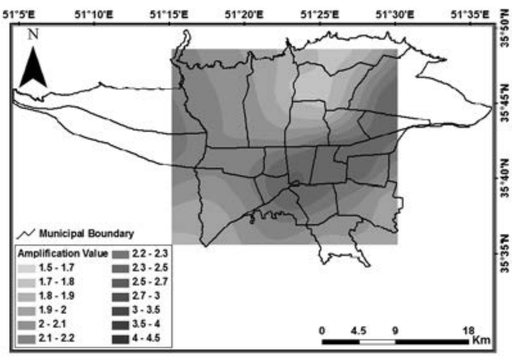

Figure 7. The distribution of soil amplification factor in Tehran city using analytical method.

5. EMPRICAL ESTIMATION OF SITE EFFECT IN STUDY AREA

To compare and verify the theoretical analyses, results of empirical techniques were also employed. To this end, the results of empirical analysis using both standard site/reference and HVSR techniques by Ghayamghamian (2008) were utilized. Figure 8 shows the location of BHRC acceleration stations in Tehran city, which are used in empirical analysis. The distribution of site dominant frequency and amplification factor based on empirical analyses are shown in Figures 9 and 10, respectively.

The comparison of the results from empirical and analytical analyses (figures 6, 7, 9 and 10) reveals the same trends, which verify the reliability of the outcome.

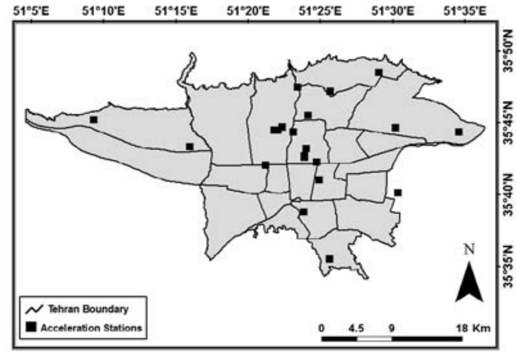

Figure 8. The location of BHRC acceleration stations in Tehran city.

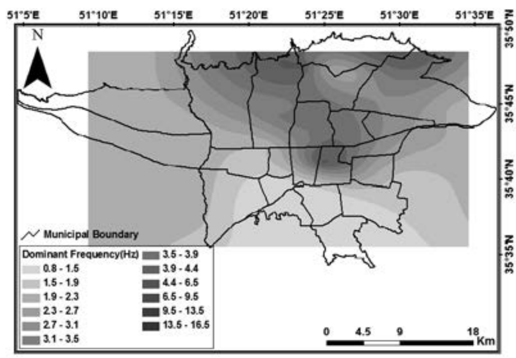

Figure 9. The distribution map of site dominant frequency based on empirical method.

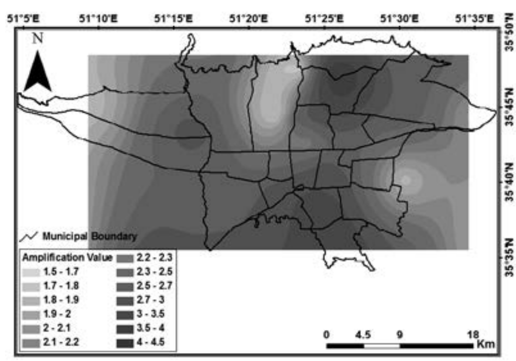

Figure 10. The distribution map of soil amplification factor based on empirical method.

6. SEISMIC MICROZONATION MAP IN STUDY AREA

The identified soil amplification characteristics from both analytical and empirical methods was compared and complied at each grid. Then, the representative dominant frequency and amplification factor of the site were selected for each grid. Figures 11 and 12 show the seismic microzonation maps for the site dominant frequency and soil amplification by combining both analytical and empirical results as well as geologic data.

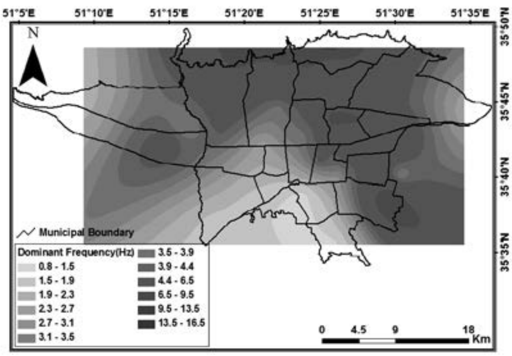

Figure 11. The zoning map of site dominant frequency by combining the analytical and empirical results.

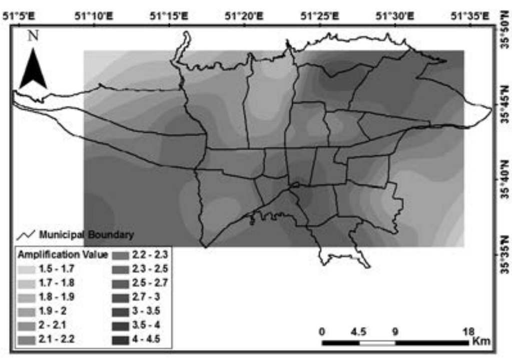

Figure 12. The zoning map of soil amplification factor by combining the analytical and empirical results.

7. CONCLUSIONS

This paper presents the most important features of seismic microzonation studies in Tehran. First, the 15 representative soil models were introduced using gathered geological, geotechnical and geophysical information at Tehran city. Second, the effect of site condition on ground motion characteristic estimated using one-dimensional analytical method. The dominant frequency shows low values in south with high amplification factor. Meanwhile the northern part of the city demonstrates high values for dominant frequency with small amplification factor values. These trends are found to be similar with those from empirical analyses, which used to verify the reliability of the outcome. The final microzonation maps for Tehran city were developed as shown in Figures 11 and 12. The values of site dominant frequency and amplification factor vary in the range of 0.8-16.5 Hz and 1.5-4.5, respectively. These maps can be applied in land-use planning in consideration of population density, building height and building importance.

It is obvious that more accurate evaluations of ground motion characteristics in the future require more geotechnical and geophysical data as well as consideration of the 3D site effects for the topography effects of surrounding mountains and subsurface geologic conditions. It should be also noted that the microzonation maps are not intended to replace site-specific investigations for structures such as hospitals and fire departments, which have critical roles in the aftermath of an earthquake.

8. ACKNOWLEDGMENTS

The authors are grateful to the Building and Housing Research Center (BHRC) for providing acceleration data.

9. REFERENCES

Ambraseys, N.N. Melville, C.P. 1982. A History of Persian Earthquakes. Cambridge University Press, UK.

Building and Housing Research Center. 2005. Iranian Code of Practice for Seismic Resistant Design of Buildings. Standard No.2800, 3rd ed.

Building Seismic Safety Council. 2003. NEHRP Recommended Provisions for Seismic Regulations for New Buildings and Other Structures. Part 1: Provisions (FEMA 368).

Ghayamghamian, M.R. 2005. Segmental cross-spectrum as a new technique in site response estimation using spectral ratio analysis. Journal of Earthquake Engineering, Vol. 9, No.2, pp. 247-264.

Ghayamghamian, M.R. 2008. Evidence for shear wave coupling due to small-scale lateral irregularities and its influence on site response estimation. Bulletin Seismological Society of America (BSSA), Vol. 98, No. 3, pp. 1429-1446.

Ghayamghamian, M.R. Nojavan, A.R. 2008. A new site classification system based on strong motion analysis in Iran. Geosupport, GSP NO.181, ASCE, Reston/VA: 1-12.

Haghshenas E. 2005. Conditions Géotechniques et Aléa Sismique Local à Téhéran 2005. PhD Thesis Joseph Fourier University (Grenoble I), Grenoble France.

Hamzehloo, H. Vaccari, F. Panza, G.F. 2007. To-

wards a reliable seismic microzonation in Tehran, Iran. Journal of Engineering Geology, No. 93, No. 1-2, pp. 1–16.
International Council of Building Officials. 1997. Uniform Building Code.
International Council of Building Officials. 2003. International Building Code.
Ishihara, K. Ansal, A.M. 1982. Dynamic behavior of soil, soil amplification and soil structure interaction. Final Report for Working Group D, UNDP/UNESCO Project on Earthquake Risk Reduction in the Balkan Region.
Jafari, M.K. Asghari, A. 1997. Seismic Geotechnical Microzonation for Southwest of Tehran. International Institute of Earthquake Engineering and Seismology, Tehran, Iran (in Persian).
Jafari, M.K. Kamalian, M. Pourazin, K. 1998. Seismic Geotechnical Microzonation for Southeast of Tehran. International Institute of Earthquake Engineering and Seismology, Tehran, Iran (in Persian).
Jafari, M.K. Razmkhah, A. Sohrabi, A. Keshavarz, M. Pourazin, K. 2002. Complementary Seismic Microzonation Studies for South of Tehran. International Institute of Earthquake Engineering and Seismology, Tehran, Iran (in Persian).
Jafari, M.K. Razmkhah, A. Pourazin, K. Sohrabi, A. Keshavarz, M. 2002. Seismic Microzonation Studies for North of Tehran. International Institute of Earthquake Engineering and Seismology, Tehran, Iran (in Persian).
Jafari, M.K. Ghayamghamian, M.R. Davoodi, M. Kamalian, M. Sohrabi, S. 2006. Site effects of the 2003 Bam, Iran, earthquake. Journal of Earthquake Spectra (EERI), Vol. 21, pp. 125-136.
Japan International Cooperation Agency (JICA). 2000. The Study on Seismic Microzonation of the Greater Tehran Area in the Islamic Republic of Iran, Final Report.
Kamalian, M. Jafari, M.K. Ghayamghamian, M.R. Shafiee, A. Hamzehloo, H. Haghshenas E. Sohrabi-bidar, A. 2008. Site effect microzonation of Qom, Iran. Journal of Engineering Geology, Vol. 97, No. 1-2, pp. 63-79.
Rieben, E.H. 1955. The geology of the Tehran plain. Am. J. Sci. 253, 617-639.

Application of sounding penetration test with the first type of penetrometers developed by "Fundamentproekt" to predicting pile load tests results.

Igor Goldfeld, Ekaterina Smirnova
OJSC "Fundamentproekt", Moscow, Russia

ABSTRACT: Based on the statistical analysis of data obtained from concurrent pile loading test and sounding penetration performed with the first type of penetrometers, the measured total shaft resistance of the cone is employed for plotting the "load–settlement" curve within the full range of loading. The curve plotting assumes two-phase behavior of the pile, feasibility to linearize the curve using the angle of slope of load increments with horizontal, and estimation of the phase characteristics of the curve from the penetration data including the proportional limit, pile bearing capacity and the elasticity modulus adjusted to the pile-soil conditions. The conversion factors used to convert between cone and pile consider the shaft resistance of cone and type of the phase pile load.

The rapid growth of mega cities leads to urban densification that causes multiplying high-rise buildings construction, deepening of foundations and underground structures. Such tendency requires advanced technique for soil investigations with sampling from greater depth, performing in-situ tests with larger loads. The problem is to conduct quick-time field and laboratory tests using methods for determining the specific behavior of foundations to be designed.

In-situ pile loading tests have been the most accurate and direct method for estimating the interaction between subsoil and foundation [GOST 5686-94]. Being the most reliable, pile load tests are rather difficult to be organized. The tests usually take place during geotechnical investigations of sites and require initial preparation such as delivery of piles and drop hammers, previous estimation of pile units in order to select optimum pile driving system and determine load increment value and pile size.

It is more convenient to conduct pile load tests on the previously developed pile field but the piles can be installed only after the soil investigations have been completed. Consequently, when conducting soil investigations, geotechnical engineers use different methods to predict pile capacity such as test on pile models, dynamic sounding, and static sounding [GOST 19912-2001]. However, test on pile models requires installation of additional equipment and applying of relatively large test loads. Test on pile model is time-consuming and, besides, a reliable method to transform the results from pile model to in-situ test pile is desired.

The penetration sounding is the most common and preferred test for pile load prediction. Two types of penetrometers are usually used. Penetrometers of the first type measure cone resistance and shaft resistance; penetrometers of the second type measure cone resistance and friction sleeve. The former are used for predicting pile load at a settlement of S=8 mm, the latter are used for predicting ultimate load capacity of a pile. The settlement of S=8mm is commonly taken as 20 % of allowable average ultimate settlement of the majority of buildings and it increases up to S=40mm during their lifetime. Tests performed with the second type of penetrometers predict pile load at failure but they are not suitable for settlement analysis.

The second type of penetrometers is considered the most applicable for soil properties estimation and when sounding with stabilization the ultimate bearing capacity of pile can be determined. Despite the conservative opinion of a number of design-engineers, "Fundamentproekt" regards penetrating with the first type of penetrometers similar to pile driving.

The effectively improved methods of structural analysis in association with foundations and their subsoil afford to specify adjustable ultimate settlement. To predict the load that causes the ultimate settlement a plot "settlement-load" within the full range of applied load is required.

This study presents a method for "settlement-load" plotting based on data obtained from penetrometers of the first type.

I. In the first place, the method provides an unequivocal fixing of characteristic values of "load – settlement" curve. To achieve that, the "load – settlement" curve is most often represented by two soil resistance phases – compacting (soil linear behavior) and shear (progressive behavior) (Fig.1) [Goldfeld, 1973]. The boundaries of the phases are obtained when angels of slope of each load increment with horizontal are linearly approximated and their meanings are plotted against the load increment values. The received points are connected with two lines. Each line corresponds to one of the phases. Their crossing point stipulates the end of the compacting phase – load of the proportional limit N_p and its inclination φ_p with horizontal. The crossing point of the second line with ordinate – $\varphi_f = 90^\circ$ stipulates the end of the shear phase – ultimate bearing capacity N_f or "pile failure".

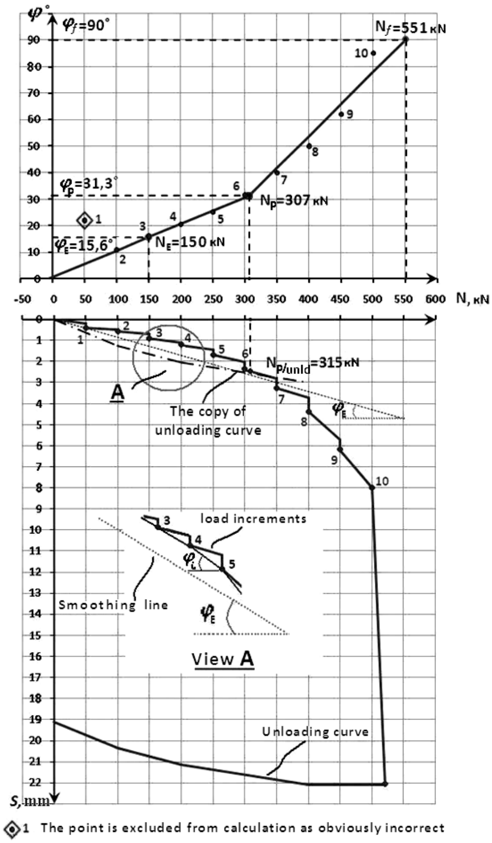

Fig.1. The results of the pile load test data proceeding.

It should be noted that elastic modulus E does not posses a "pure" meaning for piles. Its value depends on the properties of layers piles are driven into. Besides, the soil inside the pile is fully compacted and its properties vary along the embedment depth of the pile. Thus, to determine "pile-soil" behavior it is reasonable to accept the average value – φ_E, i.e. adjusted value of elastic modulus for piles – E_{pr}. As the result, two-step plot for pile testing is completely expressed by three characteristic meanings for each phase (phase meanings) – proportional limit N_p, bearing capacity N_f, and adjusted modulus E_{pr}.

The characteristic phase meanings N_p and N_f for each phase can be determined from standard penetration test data by the equation similar to the equation for pile load with the settlement of S=8mm [SP-50]:

$$N = \alpha_8\, q\, F + \beta_8\, f\, U\, L, \qquad (1)$$

where α_8, β_8 – conversion factors used to convert unit cone tip resistance and unit skin friction of the penetrometers of the first type to the unit base and shaft resistance of the driving pile respectively; q, f – average unit cone tip resistance and unit skin friction of the penetrometers respectively (kPa); F – area of cone tip (0,001 m^2); U, L – perimeter and embedment depth of pile (m).

According to the equation (1) pile load is composed of the load under the pile tip and the load along the pile shaft. When calculating characteristic phase meanings N_p and N_f the conversion factors α and β vary only. Their meanings are determined using the statistical analysis of data obtained from concurrently conducted in-situ pile test and penetration test with the first type of penetrometers. For the statistical analysis, a computer program SVAN Goldfeld et al. (1973) was used. The SVAN algorithm involves both twofold stepwise approximation of the test data and results calculated by the equation (1). To evaluate the accuracy of the analysis the calculation of pile load with prescribed settlement of S=8mm was performed and the results were compared with SP method (2004). The in-situ pile test took place on the site with 160 precast piles driven into sand, silt and firm clay. The piles were 0,25…0,35m in width, with the embedment length of 2…12m and 'rest period' of 5...60 days.

Fig. 2 presents the curves of α and β factors calculated by SVAN for three different load values and curves of α_8 and β_8 calculated according to (SP-50) and Trofimenkov (1973). settlement possesses the value close to 8mm and the ultimate shear stress corresponds to the value of settlement more than 8mm.

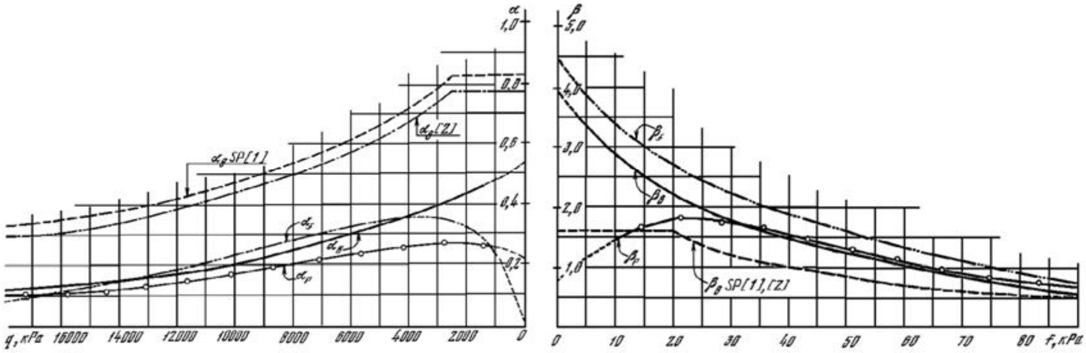

Fig.2. Comparison of α=φ(q) and β=r(f) estimated by SVAN Goldfeld et al. (1973), SP-50 and Trofimenkov (1973)

The meanings of α_8 computed by SVAN are 2÷2,5 times less then those calculated according to SP-50 method, i.e. the share of pile tip in SP-50 is overestimated. The β_8 value exceeds the corresponding values calculated with SP-50 method in 1, 5 times, i.e. the share of pile shaft is underestimated.

The comparison of α and β factors in relation to the load values shows that the meaning of α_8 is within $\alpha_p < \alpha_8 < \alpha_f$ to most soils which means that the proportional limit under the pile tip $N_{p/t}$ can reach the value when the settlement is less than 8mm. In this case, the soil under the pile tip collapses when the settlement is more then 8mm. The proportional limit of soils along the pile shaft reaches the value $N_{p/s}$ when the

Fig. 3 shows show better agreement of loads N_8 computed by SVAN with the loads obtained from pile test or determined from penetration than the loads calculated by SP-50 method. The conclusion is confirmed with the following results – the correlation index r is well over (0,94>0,76), the regression line starts at origin and coincides with absolute convergence line (tg δ=tg 45°=1), the scatter is smaller (mean square deviation is twice as little). According to SP-50 method the slope of the regression line with $N_{p/sp}$ axes (tg δ =0,51≠1) indicates that the loads estimated from penetration test exceed the loads determined from pile load test.

In accordance to the calculations, it was also determined that the share of pile tip depends on

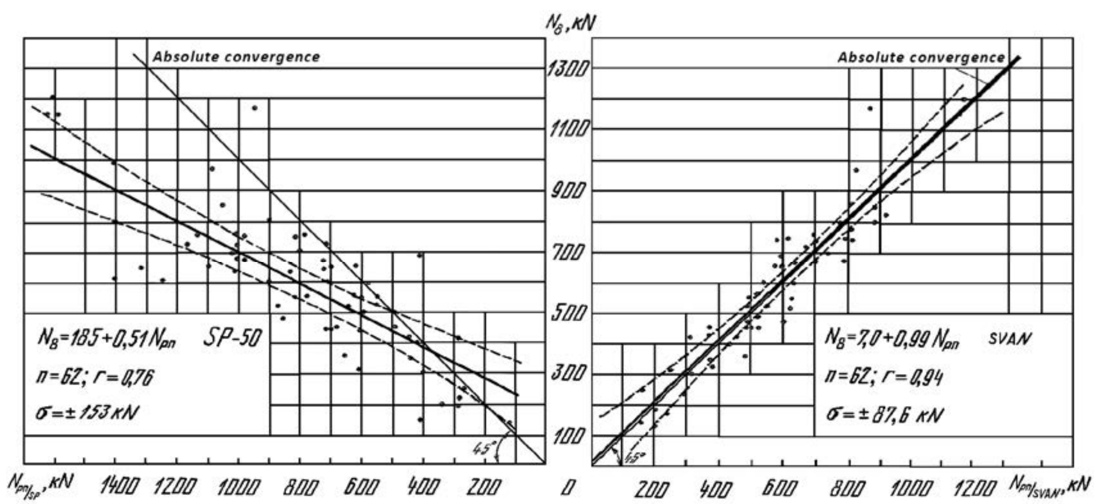

Fig.3. Comparison of N_8 obtained from pile load test and penetration test and estimated by SP-50 (left) and SVAN (right)

the embedment length of the pile. Thus, it is 40-60% for piles of 3÷6m long and reduces to 20-25% for piles of 10÷12m long.

Consequently, in order to reduce labor and material cost the embedment length of piles can be predicted and optimized.

Fig.4 presents the comparison of N_p and N_f determined from pile load test and penetration test. The results show good agreement and confirm the tendency of reducing the fraction of the load under the pile tip in the quasi-homogeneous soil.

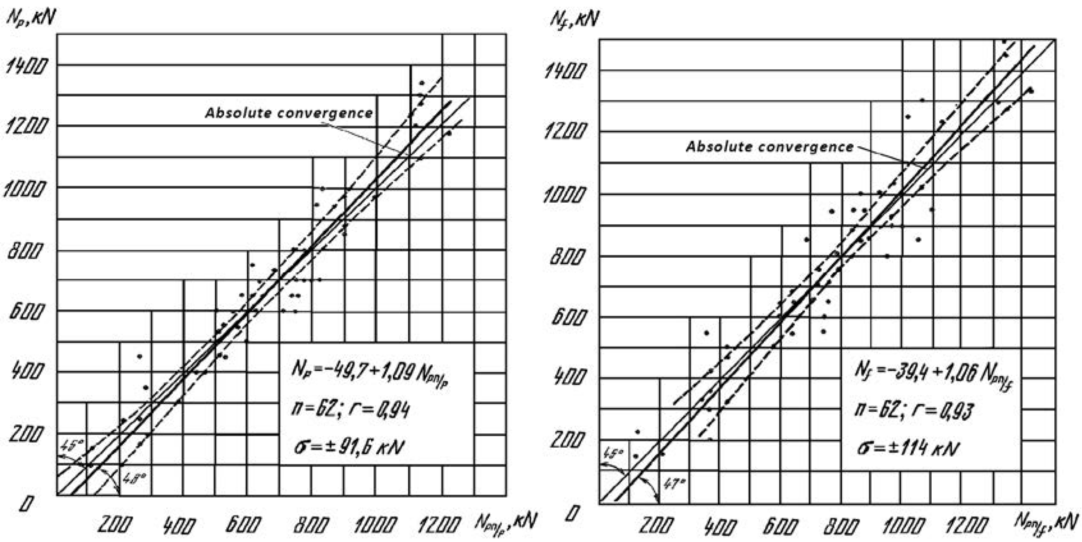

Fig.4. Comparison of N_p and N_f obtained from pile load test and penetration test

The calculation of foundation settlement is based on the elastic modulus E. The E meaning is usually estimated from field load test [GOST 20276-99] by the following equation:

$$E = (1 - \mu^2)\omega D \frac{\Delta N}{S}, \qquad (2)$$

where μ – coefficient of soil lateral expansion; ω – coefficient of load plate (0,79 for round plate); D – diameter of plate (m); ΔN, S – unit load under the plate (kPA) and corresponding settlement.

By analogy with field load test the compressibility of soil-pile base can be estimated using such characteristics as adjusted elastic modulus E_{pr} and "simulated foundation". The "simulated foundation" is composed of soil compacted by driven pile (Fig.5).

Assuming the unit load ΔN as a ratio of total load to the area of the "simulated foundation" base

$$D = \frac{8d}{15} L = 0{,}53dL \ \ (\text{м}),$$

and taking into account the laniary approximated curve of pile test, the equation (2) for E_{pr} may then be written:

$$E_{pr} = (1 - \mu^2)\omega D \frac{4N}{\pi D^2 S} = \frac{1-\mu^2}{D}\frac{N}{S} \qquad (3)$$

Or

$$E_{pr} = A \text{ ctg } \varphi_E, \qquad (4)$$

where φ_E – angle of slope of smoothing line with load axis N on the simplified load-settlement curve S=f(N); $A=1-\mu^2/D$ – a coefficient, constant for the soil base and the pile; $ctg\varphi_E = N/S$ is factor, depending on the ratio of scales accordingly to the reference frame of S=f(N).

The equation (4) allows one to estimate adjusted elastic modulus E_{pr} using both the initial part of the linearized function $\varphi=\varphi(N)$ and smoothing line at an angle φ_E with horizontal at the initial part of the curve S=f(N).

$$\varphi_E = \gamma \frac{Q}{Ld}, \qquad (7)$$

where φ_i – an angle of slope of a load increment with horizontal on the S=F(N) curve within the boundaries of compacting phase; k – a number of load increments within the boundaries of compacting phase.

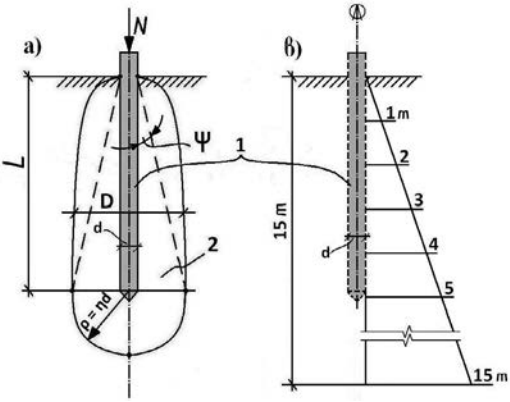

Fig.5. The scheme of pile-soil base: a) soil compacted by driven pile: ψ – angle of stress distribution; 1- driven pile; 2- simulated foundation; b) the area of "simulated foundation" base D=2p

The angle of slope of the last load increment that corresponds to the end of compacting phase (the proportional limit) can be estimated as following:

$$\varphi_p = 2\ \varphi_E \tag{6}$$

To make the estimating of E_{pr} from penetration data easier it is convenient to use the angle of slope φ_E of smoothing line of S=f(N) curve with horizontal. The value of φ_E can be estimated from the following empirical equation:

$$\varphi_E = \gamma \frac{Q}{Ld}, \tag{7}$$

where Q – total cone shaft resistance (kN); γ – empirical factor (Fig.6); L – embedment depth of pile (m); d – width of pile (m).

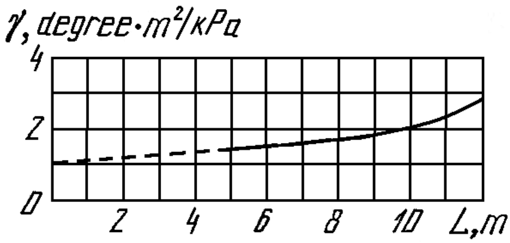

Fig.6. Correlation between γ and the embedment length of pile L (m) of the "simulated foundation"

Table 1 shows the meanings of E estimated for semi stiff clay loam and E_{pr} estimated for the soil-pile base of "simulated foundation". The comparison of E and E_{pr} meanings shows that deformation of natural soil caused by pile driving is 8…10 times less. If the results are confirmed with more data, the method can be applied to single piles.

Table 1

Material	**Elastic modulus, MPa**	**Ratio of E_{pr} to E=1**
Natural soil (E)	$(0{,}000035\ldots 0{,}00004)\cdot 10^6$	1,0
Pile compacted soil (E_{pr})	$0{,}00035\cdot 10^6$	7…10,0

Since in this study φ_E is measured in degrees, the S=f(N) and φ=φ(N) are plotted in a specific scale – the load of 50 kN, the settlement of 1 mm and angle of 10° correspond to 1sm plotted along the reference axes. The interpretation of the curves conducts when the load increment of 50kN is taken. The curve S=f(N) can be estimated by using $\varphi_p(\varphi_E)$ angles. In a number of countries the ratio tg φ=ΔS/ΔN is applied for the curve S=f(N) estimation, which is similar. Thus, according to the Standards of The Department of Public Works of California the prescribed pile load is usually taken twice as less than the load under which the total settlement does not exceed 0,25mm when the load increment of 10kN is taken. Taking into account the aforementioned scale and the size of piles (0,3m in width, 6-8m in length), the loads correspond to φ=70° and to the load which is twice as less than the ultimate bearing capacity of the piles N_f (failure load).

According to SP, the ultimate bearing capacity of pile is a load the application of which in the increment of 20kN causes the increment of settlement of 1mm. Considering the scale and the pile size this criteria agree with φ=30° and the load which is more than proportional limit and less than the pile failure load.

The accuracy of S=f(N) plotting depends on the agreement between the values of N_p, N_f and φ_p obtained from penetration sounding and from pile load test respectively. Therefore, the value of the conversion factors α and β depends on the equipment unit, "rest" of the pile and soil conditions. The method for S=f(N) plotting remains unchangeable.

The Fig.7 shows the S=f(N) curves corresponded to the three pile load tests (dashed lines) and to the three penetration tests (heavy lines). The table 2 presents the respective data.

The prediction accuracy entirely corresponds to the requirements of civil engineering. Hence, just as tests on pile models and in-situ pile load tests, so the penetration sounding with the first type of penetrometers constructed by "Fundamentproekt" may be used to perform the pile analysis within the full range of loads.

In recent years, the standard penetration tests are becoming the preferred test for pile analysis. The test is simple, fast, relatively economical, supplies continuous records with depth. In addition, because of similarities between the cone penetrometers and a pile, the penetrometers can be considered as a model pile. However, the tests on pile models have significant advantages over the penetration sounding. Using the test data, geotechnical engineers can analyze the influence of pile installation process and "rest" period of pile on the state of the construction site and the influence of lateral and moment loads on piles behavior.

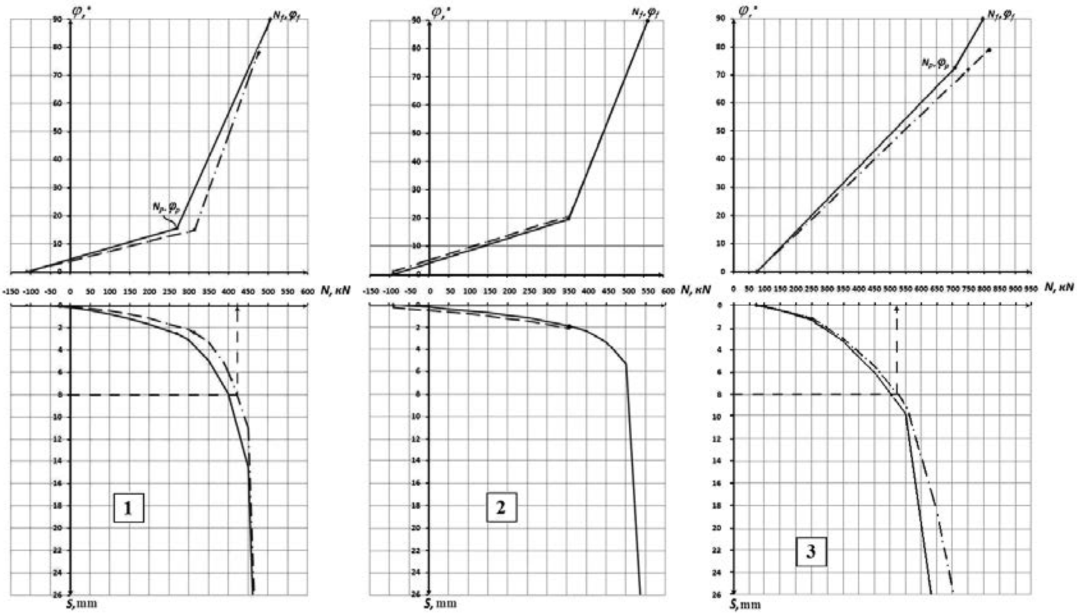

Fig.7. Standard S=f(N) and linearized φ=φ(N) curves of pile load test

Table 2

Test pile (Pt), cone penetration (Cp), distance (l, m), date	Embedment length of pile and cone		Penetration data		Loads (Characteristic meanings of plots)				
	Cross-section size / pile length	Type / d, cone length	q,кN/m² / R, кN	f,кN/m² / Q, кN	Method for evaluating	N_p, кN	N_8, кN	N_f, кN	$φ_p$, °
1. Site I (set. Yakovlevo, Podolsky District, Moscow Region), report №22814									
Pt–176; Cp–1; l=37,5; 15.03.2005	0,3x0,3 / 7,6	Type I / 0,036; 10,0	4630 / 4,6	12,1 / 10,4	Pile load test	314	420	470	14,8
					Method by SVAN	270	440	506	15,5
					Method by SP-50	—	630	—	—
2. Site II (set. Yakovlevo, Podolsky District, Moscow Region), report №22814									
Pt–179; Cp–1; l=4,4; 12.03.2005	0,3x0,3 / 7,6	Type I / 0,036; 10,0	5450 / 5,5	15,8 / 13,6	Pile load test	≥350	—	—	≥19,6
					Method by SVAN	358	505	561	20,2
					Method by SP-50	—	660	—	—
3. Site of the Palace of Soviets (Moscow), report №8341									
Pt–87; Cp–16; l=4,0; 13.12.1962	0,3x0,3 / 6,5	Type I / 0,036; 6,6	5000 / 5,1	59 / 44	Pile load test	—	670	815	—
					Method by SVAN	700	630	809	71,2
					Method by SP-50	—	760	—	—

REFERENCES

Goldfeld I.Z. 1973. Interpretation of the load-settlement curves from base resistance phases, *Transport construction.* Moscow, No. 7, pp.45-47.

Goldfeld I.Z., Pyrchenko V.A., Panyukova I.M., 1981. *The computer program "Prediction of pile bearing capacity from penetration sounding data" (SVAN)*, VNTICentr, P004968, MOFAN CNIIProekt, I-H-196, Moscow.

GOST 19912-2001. *Soils. Field test method by static and dynamic sounding*, Moscow (In Russian)

GOST 20276-99*. Soils. Field methods for determining the strength and strain characteristics*. Moscow (In Russian)

GOST 5686-94. *Soils. Field test methods by piles*, Moscow (In Russian)

Sanglerat G., 1965. *Le Pénétromètre et la Reconnaissance des Soils*. Paris, 230 p.

SP-50-102-2003. *Design and construction of pile foundations*. Moscow, pp. 25-26. (In Russian)

Trofimenkov J.G., Maryupolsky L.G., 1975. About determination of skin friction by static sounding, *Soil Mechanics and Foundation Engineering.* Moscow, No.1, pp 27-28.

Trofimenkov J.G. 1973. Updating methods for pile bearing capacity determining, *Proc., 8th Int. Soil Mechanics and Foundation Engineering, pp. 150-161.*

Tsytovich N.A. 1959. *Soils and Foundation* Moscow. pp. 207-212.

Study of bio-potential associated with deep routed trees for prediction of earthquakes

Vinod Kumar Kushwah
Department of Physics, Hindustan College of Science & Technology, Farah, INDIA

M.S.Gaur
Department of Physics, Hindustan College of Science & Technology, Farah, INDIA

R.K. Tiwari
Department of Physics, Hindustan College of Science & Technology, Farah, INDIA

ABSTRACT: Seismo-electromagnetic emissions are recently recognized as one of the most promising candidate for short term earthquake prediction. Results of bio-potential analysis of seismic electric signals (SES) are registered at Sapporo Observatory, Japan). On the basis of survey of deep routed trees in our area, we found some trees are of scientific interest to use seismologic point of view. The infrasonic waves are transverse in nature produces signals like a.c. signals in terms of electromagnetic radiation; consequently the bio-potential associated with deep roots varies significantly. We have observed potential with deep roots of banyan tree which subjected various lower frequencies at different temperature and pressure, we found very interesting results which ma helpful to monitor seismic signals and prediction of earthquakes in suspected area.

INTRODUCTION

Numerous observation and surveys have been conducted in seismic active zones for many years in order to follow the crust movements, seismicity, geomagnetism, ground water, geochemical changes and so on. However, the problem of the forecasting of strong earthquake is still far from its solution. It has been found that non-stationary areas of enhanced infrared (IR) emission linked to impending (Gornyi et al., 1988; Qiang et al., 1991; Qiang et al., 1990; Srivastav et al., 1977) with apparent land surface, temperature variation of the order of 2^0C-40^0C. The effect has become known as "thermal anomalies". The rapidity of the temperature variations rules out a flow of increasing the heat form deep below. Several alternative process have been involved: Rising wells water levels and changing moisture contents in the soil: near –ground air ionization due to radon emissions leading to the condensation of water vapor and the release of latent heat; emanation of warm gases (Gornyi et al., 1988) like Co_2 (Quing et al., 1991; Tronin, 1999; 2002). Several researchers have reported earthquake precursors from ground based observation of ultra Low Frequency (ULF) electromagnetic emissions (f=0.01-10Hz) in past years (Fraser-Smith et al., 1990, 1994; Kopytenko et al., 1990; Molchanov et al., 1992; Hayakawa et al., 1996; Hayakawa et al., 2000). The ground based observation are taken by use of transmitter signals (Gokhberg et al., 1989; Gufeld et al., 1994; Hayakawa et al., 1996b; Molchanov and Hayakawa, 1998) and the satellite observation also (Galperin et al., 1996; Parrot et al., 1999). It has been found that the emissions at ULF band can produce more convincing precursors of earthquakes in comparison to higher frequency bands because of less contamination, large skin depth and low attenuation (Park et al;., 1993; Hayakawa et al., 1998; Kopytenlo et al., 2001; Kushwah and Singh 2004; Kushwah et al., 2005; 2009). Further, the ULF emissions can penetrate the crust and propagate through the ionosphere and magnetosphere (Molchanov et al., 1995). Many researchers have been monitoring and studying the physiology of deep rooted trees. They used deep rooted tree with long ages (Ulmus Keaki tree, Japan) as a live sensor for monitoring bio-potential round O' clock, interesting results are found (Toriyama 1994; Okamoto, 1994; Toriyama and Kawaguchi, 1987). Keeping in view the potential application of seismo-electromagnetic technique for earthquake prediction studies. We have been started the studies based on this new technique at Hindustan College of Science & Technology, Farah, Mathura (India) (Geograph. Lat. 29.05^0N, Long.75.26^0E) since last year. In the present paper, we analyses the offline recoding of cutting green piece of deep rooted tree (Banyan Tree) at different pressure and different atmospheric condition and found very interesting results is discussed. The authors wish to insist that attention must be paid to the tree as a whole including the root system as a live sensor for earthquake precursors.

EXPERIMENTAL SETUP

The block diagram system used to measure the bioelectric potential of cutted green root pieces of different length of Banyan tree and the complete experimental setup (Power supply, Pressure measurement cell, and Potential meter and Frequency generator) is shown in Fig.1. The observations are taken at different pressure and different atmospheric conditions.

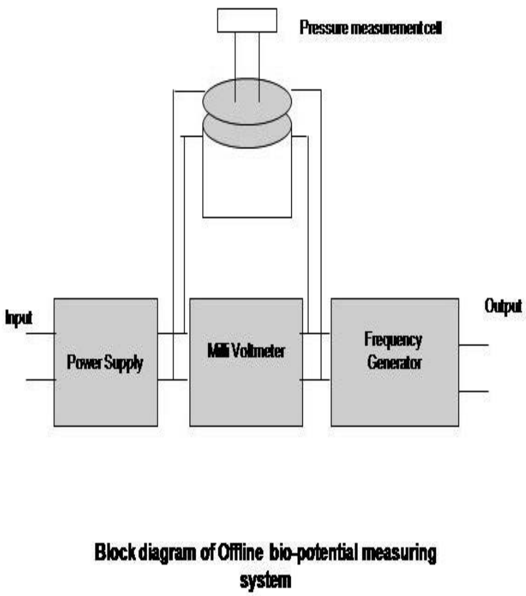

Figure 1. Block diagram of offline bio-potential measuring system

RESULT AND DISCUSSIONS:

We have recorded offline observation of bio-electric potential from green cut pieces of banyan trees root. A banyan tree which had been growing and reached the age of 70 years the concentration of xylem and phloem are gradually increases time to time. The long age banyan tree root goes into the earth around 80-90 feet so we have chosen the tree root as a live sensor for our research. We have started offline experiment in Research Laboratory, Hindustan College of Science & Technology, Farah, Mathura and for online observation we will choose a rural site near our college campus (i.e. Farah village around 15km away from college campus). If we monitor regularly the Xylem and phloem concentration ratio and observe bio-potential of banyan tree round O' clock. The xylem and phloem ratio abruptly change and bio-potential is increasing abruptly before the occurrence of earthquake under ground which will concern some online bio-potential results before occurring the large magnitude earth-quakes. In this paper we present some offline result of different length of green cut piece of banyan tree root. We have taken the different lengths of green piece (7.4 cm, 12.0cm and 17.5cm) and apply different pressures (551.70 torr, 662.0 torr, 809.11 torr, and 1029.78 torr) with 15 minutes and measuring the potential difference. The bio-potential increase due to flow of water conducting tissues i.e. xylem, some xylem tissues are divided two parts; first, Primary xylem i.e. Pro-Meristem which is produced by secondary xylem Cambiyam. Primary xylem is divided into two part Proto-xylem and Meta-xylem, Proto-xylem is outer part of the root and Meta-xylem is center part of the root which transport water from soil and many minerals to deliver the stem and branches (Okamato, 1996; Dr. Ashok Bendre and Dr. Ashok Kumar, Reference book: Introductory Botany) when we apply pressure on cutted root pieces, the internal contents i.e. meta-xylem is transport very fast, that the potential difference of this root increasing gradually which is easily seen in Fig.2. This artificial condition is similar to online parametric condition which is generate when the earthquake process under the ground and the mechanism of root cells is similar to Human blood cells (Gaur et al., 2007).

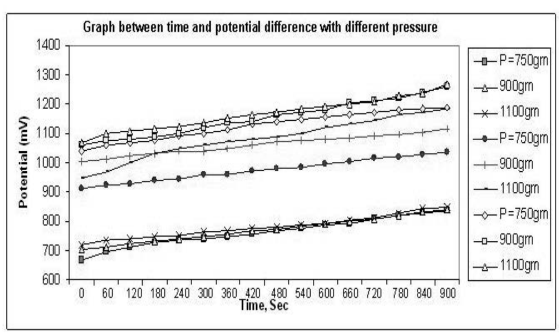

Figure2. The graph between time and potential difference with different pressure

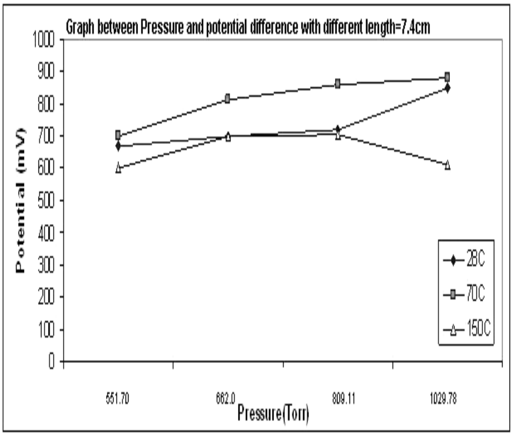

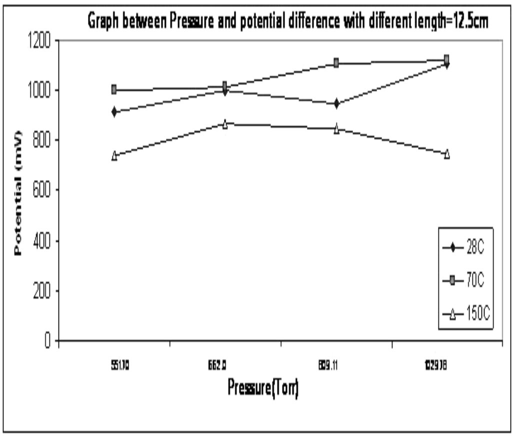

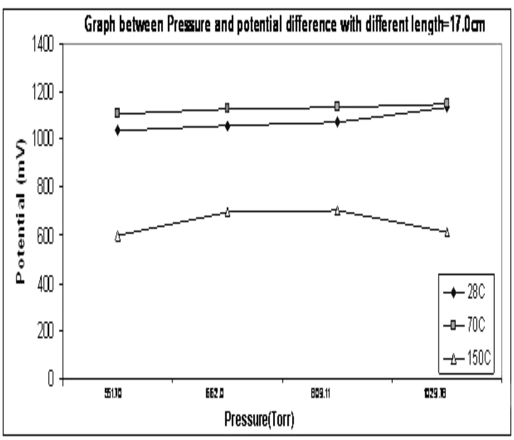

Figure 3. Graph between pressure and potential difference with different length from up to down (Section A Length=7.4cm, Section B-length=12.5cm and Section C-length=17.0cm) with different temperature

In Fig.3, the different temperature (28^0C, 70^0C, and 150^0C) conditions on various length of cutted green root piece are considered in our study. The different length of root pieces putting in the heating chamber up to 45 minutes and again apply different pressure and measure the potential difference, we found that the potential difference has increased gradually within the internal element of roots sustain the temperature like as 28^0C and 70^0C, if we apply the temperature on 150^0C during 45 minutes then we find that the potential difference is abruptly change and going to decrease because the live elements in the root are dry and destroyed the strength so this mechanism is correlate with the generation mechanism of forthcoming high magnitude earthquakes. This activity is similar to that when any unusual things (i.e. seismic activity) occurred in the ground, where the internal particle collaborate each other so the pressure and temperature increases under the earth and the time of earthquake ($M \geq 5.0$) a huge amount of energy released around 0.08×10^8 ergs. The offline experimental results are justified and compared by the online result of any further seismic activity.

CONCLUSIONS

The bio-potential study is informative for various parameters concerning to Xylem cells. Present study reveals very important results for identification of online results of bio-potential (Seismic Electric Signals, SES) configuration of root system. The banyan roots are particularly extended very deeply into the ground vertically, and also spread like a network in three dimensions. In general, one of the characteristics of a course "living root system, hydrate soil, hydrated cracks of rocks" sustains a chain of electric conductivity. It would make possible for the living tree to receive consist of geoelectrical, geoelectromagnetical and geochemical factors which represents precursory phenomena of earthquakes.

ACKNOWLEDGEMENTS

The authors are thankful to Prof. Birbal Singh, Emeritus Scientist CSIR for giving valuable suggestions. We are thankful to Director of Hindustan College of Science & Technology for supporting the research activities and also thanks for our research department for cooperate the research work.

REFERENCES

Bendre, A., and Kumar, A., 1992. *Reference book: Introductory Botany* published by Rastogi Publication, Shivaji Road Meerut.

Fraser-Smith, A.C., Bernardi, A., Mc. Gill, P.R., Ladd, M.E., Helliwell, R.A., Villard Jr., A.D., 1990. Low-Frequency magnetic field measurements near the epicenter of the Ms= 7.1 Loma Pretia earthquake, *Geophys. Res. Lettr*., 17, 1465-1468.

Fraser-Smith, A.C., Mc Gill, P.R., Helliwell, R.A., Villard (Jr) O.G., 1994. Ultra Low Frequency magnetic field measurements in southern California during the Northridge earthquake of 17 January 1994, *Geophys. Res. Lettr (USA),* 21, 2195.

Gaur, M.S., Tiwari, R.K., Shukla, P., Saxena, P., Gaur, K., and Tiwari, U., 2007. Thermally stimulated current analysis in human blood trends biometer. *Artif. Organs.* 21 (1) 8-13.

Gokhberg M.B., Gufeld, I.L., Rozhnoy, A.A., Marenko, V.F., Yampolsky, V.S., and Ponomarev, E.A., 1989. Study of seismic influence on the ionosphere by super long wave probing of the earth-ionosphere waveguide, *Phys. Earth Planet Inter. (Netherland),* 57, 64.

Gornyi, V.I., Salman, A.G., Tronin, A.A., and Shilin B.B., 1988. The Earth's outgoing IR radiation as an indicato of seismic activity. *Proc. Acad. Sci., USSR,* 301, 67-69.

Hayakawa, M., Itoh, T., Hattori, K., and Yumoto, K., 2000. ULF electromagnetic precursors for an earthquake at Biak, Indonesia on February 17, 1996, *Geophys. Res. Lettr.,* 27, 1531-1534.

Hayakawa, M., Kawate, R., Molchanov, O.A., Yumoto, K., 1996. Results of Ultra-low frequency magnetic field measurement during the Guam earthquake of 8 August, 1993. *Geophys. Res. Lettr.* 23, 241-244.

Kopytenko, Y., Ismagilov, V., Hayakawa, M., Smirnova, N., Troyan, V., Peterson, T., 2001. Investigation of the ULF electromagnetic phenomena relates to earthquake: contemporary achievements and the perspective. *Annali di Geophysica,* 44, 325-334.

Kopytenko, Yu. A., Matiasvily, T.G., Voronov, P.M., Kopytenko, E. A., Molchanov, O.A., 1990. Discovering of Ultra-Low Frequency emissions connected with spitak earthquakes and his aftershock activity on data of geomagnetic pulsations observation at Dusheti and Vardzia, Moscow, *IZMIRAN*, 888 (3), 27, Preprint.

Kushwah, V., Singh, V., and Singh B., 2009. Ultra Low Frequency (ULF) amplitude anomalies observed at Agra (India) and their association with regional earthquakes. *Phys Chem. of the Earth,* 34, 367-372.

Kushwah, V., Singh, V., Singh, B., and Hayakawa, M., 2005. Ultra Low Frequency (ULF) magnetic field anomalies observed at Agra and their relation to moderate seismic activities in Indian region. *J. Atmos. Solar. Terres. Phys.,* 67, 992-1001.

Kushwah, V.K., and Singh, B., 2004. Initial results of ultra low frequency magnetic field observations at Agra and their relation with seismic activities. *Current Sci.,* 87 (3) , 332-339.

Molchanov, O.A., and Hayakawa, M., 1995. Generation of ULF electromagnetic emissions by microfracturing. *Geophys. Res. Lettr.,* 22, 3091-3094.

Molchanov, O.A., and Hayakawa, M., 1998. On the generation mechanism of ULF seismogenic electromagnetic emissions, *Phys. Earth Planet Inter.,* 105, 201-210.

Molchanov, O.A., Kopytenko, Yu. A., Vornov, P.M., Kopytenko, E.A., Matiashvilli, T.G., Fraser Smith, A.C., Bernardi, A, 1992. Result of ULF magnetic field measurements near the epicenters of the Spitak (Ms=6.9) and Loma Prieta (Ms=7.1) earthquakes: Comparative analysis. *Geophys. Res. Lettr.* 19, 1495-1498.

Okamoto, H., 1996. A brief notes on growth physiology of plants, *J. Planet Res.,* 109, 69-74.

Park, S.K., Johnson, M.J.S., Madden, T.R., Morgan, F.D., Morison, H. F., 1993. Electromagnetic precursors to earthquakes in ULF band: A review of observations and mechanism. *Rev. Geophys.,* 31, 117-132.

Qiang, Z. J., Xu, X. D., and Dian, C.D., 1990. Abnormal infrared thermal of satellite-forewarning of earthquakes. *Chinese Sci. Bull.,* 35, 1324-1327.

Quing, Z., Xiu. Deng. X., and Chang- Gong, D., 1991. Thermal infrared anomaly-precursory of impending earthquakes, *Chinese Sci Bulletin,* 36, 319-323.

Srivastava, S.K., Dangwal, M., Bhattacharya, A., and Reddy, P.R., 1997. Satellite data reveals pre-earthquake thermal anomalies in Killari area, Maharastra, *Current Science,* 72, 880-884.

Toriyama, H., 1994. Possibility of earthquake by measurement of tree potential electromagnetic phenomena related to earthquake prediction (Ed.) by M. Hayakawa and Y. Fujinawa, *Terra Sci. Publ. (TERRAPUB), Tokyo*, pp.103-104.

Toriyama, H., and Kawaguchi, M., 1987. Anomalous bioelectric potential of silk tree prior to the 1983 Japan sea earthquake, *Science Reports of Tokyo Women's Christan University,* Nos. 76-79.

Tronin, A. A., 1999 (Ed.): Satellite thermal survey application for earthquake prediction, *Terra Sci Pub., Tokyo, Japan*, 717-746.

Tronin, A.A., 2002. Atmosphere-Lithosphere coupling: Thermal anomalies on the earth surface in seismic process, *in Seismo-Electromagnetics: Lithosphere- Atmosphere- Ionosphere coupling, edited by: M. Hayakawa and O.A. Molchanov, Terra Sci. Publ. Tokyo,* pp.173-176.

Geotechnical risks in urban planning: a few examples in a fast growing Brazilian Metropolitan Area

N.A. Nascimento
Federal University of Paraná State, Brazil

R.F.K. Puppi
Federal Technological University of Paraná State, Brazil

ABSTRACT: Geotechnical challenges in urban areas may be represented by several interventions, to which risks are associated. Deep excavations, constructions on soft ground, dewatering systems, dams, hazardous materials, presence of pressurized gas lines and other situations are just a few examples.

This paper presents and discusses four projects in Curitiba, Southern Brazil, emphasizing geotechnical activities and related risks. Foundation of hydraulic structures on organic soft soils, retaining structures for cut slopes nearby gas lines and small dams for rivers discharge control are mentioned, in a metropolitan area of about three million inhabitants. The cases presented intend to give a general view of the geotechnical challenges and risks, and show some circumstances under which the projects were designed and constructed recently.

1. INTRODUCTION

Paraná is one of the three southern States of Brazil, located south of São Paulo State and east of Paraguai and Argentina. Its development is rather recent, and a real boom started a few decades ago, pushed by wood exploration, cattle raising and huge crop areas, starting with coffee in the fifties and sixties and shifting slowly to other grains such as soy beans, wheat and corn. The state produces nowadays about one fourth of the Brazilian agricultural goods.

More recently, around 1970, the state economic trend started to change and Paraná has increased drastically its industrial production. Today, besides keeping the leadership in the nation's grain amount, the state also plays an important role in paper, vegetable oil, packed meat, foods in general, petroleum by products, ceramics, plywood, vehicles and machinery production, among other items.

Curitiba, the state's capital city, is located 25°25' latitude South, about 900 meters above mean sea level and 80 km west from the Atlantic Ocean. Along with a few other surrounding cities, defining its metro area, a population of almost three million people live and produce in this region.

Certainly, with such a quick growth in the past four or five decades mostly, infrastructure for the cities became a big problem. One of the main worries for the public authorities has always been mass transportation. The population enjoys still today a unique and well planned system, based on huge buses running on exclusive tracks, system that has increased in the whole metro area as demand requires. Although the rate of population growth goes always faster than the ability of politicians to supply the needs, most of the users seem to be satisfied with its operation.

Along with public transportation, housing, water supply and sewage treatment are as important as, or even more important needs, to be emphasized here. The authors find that a few examples of recent and very important interventions in the city justify their description, from the design stage to the job site, and may occasionally contribute to a better understanding of geotechnical challenges in big cities.

A set of four engineering works was chosen, encompassing a large housing subdivision of about six thousand lots, a sewage treatment plant built on soft soil, a water treatment plant constructed on a former lake bed and a by-pass system of two small concrete dams to control eventual hazardous materials that may reach the water streams. The first case may be of interest because there are oil and gas pipelines crossing the area, that rests on very soft soil, and specific conditions directed this project. Each case is herein presented and analyzed, attempting to give an overview of the geotechnical problems and the solutions found.

2. THE RIO BONITO HOUSING DEVELOPMENT

The Barigui River is a tributary of the main water course in the Curitiba Metropolitan Area, that is Iguaçu River (heading West and reaching Paraná River, Brasil/Paraguai border, around 700 km from Curitiba). In the flood plain of the Barigui River final stretch, a few kilometers from its delta at the Iguaçu, very soft organic clay deposits are found. The region had suffered until some years ago predatory exploration of both clay and sand, for construction purposes, and degradation was the result of it (lack of vegetation, excavation open pits and random materials dump areas).

Along with that, several engineering activities have been done as well, among which the Petrobrás Oil Refinery (right bank), Santa Rita Rural Subdivision, CIC Sewage Treatment Plant, Bolivia-Brasil Gas Line (Gasbol) and Rio Bonito Housing Development (left bank). It should be pointed out that the flood area is mainly located on the river left bank, approximately 500 m wide by 1000 m long, here under consideration.

It was observed that the local organic clay deposits are extremely weak and compressible, even if compared to well known problematic soils. The main features in the area are:

Right bank:

Petrobrás Oil Refinery (about 28 years old – higher elevation – better subsoil condition).

Left bank:

Santa Rita Rural Subdivision (about 12 years old – lots of 5.000 m2 each to accommodate one house and area for a family own agricultural production – very poor subsoil condition for civil engineering).

CIC Sewage Treatment Plant (about 7 years old – one big lake, several treatment tanks and other structures – same problematic soil).

Gas and Oil Pipeline (about 17 years old, for oil, and more recent, for gas piping – Gasbol and Ospar – TBG/Transpetro – strip land area of about 60 m wide protected by specific federal law in Brasil limiting access, crossing and constructing along the strip – several hundred kilometers in the country).

Rio Bonito Housing Development (private subdivision investment for thousands of lots, on both sides of the gas & oil lines).

As a summary of the local geotechnics, a brief description of the subsoil condition is given on Table 1.

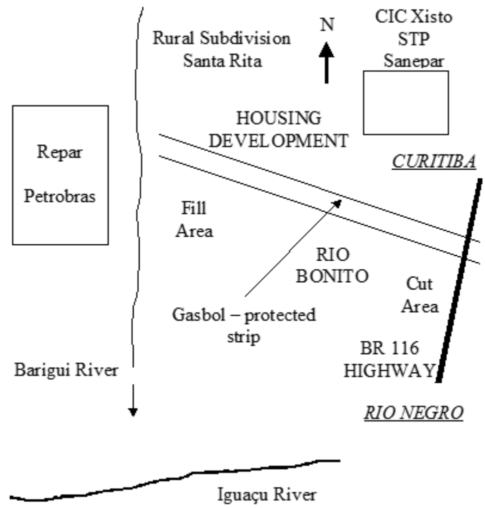

Figure 1. Approximate location of the mentioned features (not to scale).

Table 1. Some local geotechnical parameters

Job site	Description and geotechnical parameters
Vila Rural Santa Rita(initial phase: 1995)	Very soft, organic clay soil, saturated (~ 3 m); flat popular houses (Cohapar) with mat superficial foundation and streets over geossynthetic reinforced soil; no geotechnical parametrization; (*)
CIC-Xisto STP (Sanepar – 2000)	Black, soft organic soil, with sand; depth from 0,6 to 2,0 m: natural density: 1,61 to 1,89 dry density: 1,05 to 1,45 natural void ratio: 1,65 to 0,87 specific gravity: 2,62 to 2,66 compression index: 0,39 to 0,25 (**)
Repar – Petrobrás Oil Refinery (right bank of the Barigui River; over 27 years of age)	Soil predominantly from the Guabirotuba Formation (silty clay / clayey silt) of high consistency, occasionally with sand and localized organic spots; little similarity with what is found on the left bank, where the non consolidated deposits over this formation or the deeper embedment predominate; (***)

(*) observation by the authors
(**) Solum Geologia Ltda, 2000
(***) ABMS – UFPR, 1999

As far as the subdivision engineering work is concerned, one draw back was the land strip for the pipelines. According to the federal regulations for this particular case, there are severe limitations regarding its use, summarized in a booklet printed and distributed nationwide by the pipelines operator, TBG/Transpetro – it is considered INCORRECT to be done on the strip, according to the Brazilian Federal Law 6766-79:

- to harm the signalization off-sets;
- to plant any tree or vegetation other than grass;
- to use plows, graders or any agricultural machine – before any excavation needed, check by calling a 0800 phone number;
- to cause any kind of fire on the strip or close by;
- to use explosives;
- to make any kind of construction;
- to cross the strip with any vehicle weighing 10 t or more;
- to use trucks or tractors.

When the earth moving activity for the subdivision started, about six years ago, in the local higher terrain elevation, a cut slope was created with maximum height of 6 meters, 60° inclination with the horizontal and about 130 meters long, very close to the pressurized gas and oil lines. Geotechnical analysis was then required by the owner to check the slope stability and minimize possible horizontal movements of the pipelines.

The analysis determined, after soil parametrization, modeling and judgment by the consulting engineers, contractor and owners, the construction of:

- gabion type retaining wall and precast concrete piles at the toe of the slope;
- anchor-ties (passive) line at the mid-height of the slope;
- drainage and vegetation.

The schematic stabilization solution is given on Figure 2. It was found extremely important that, due to the limited amount of deformation allowed for the pipelines, very specially for the high pressure gas line, the slope had to be stable and protected against lateral movements; for these reasons, not just toe support provided by the driven piles but middle height passive tie rods were designed, including the highly draining gabion wall, that also provides weight and helps stabilizing the slope. The factor of safety for the project was taken as 1.5, according to Brazilian Standards.

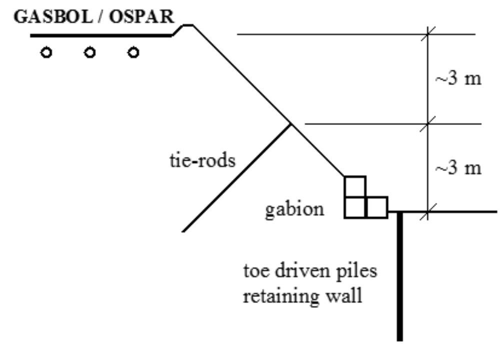

Figure 2. Stabilizing schematic solution for the cut slope (not to scale).

Both design and construction of the retaining structures were done some years ago, and the end result seemed appropriate because no problems were caused so far in the area, by the way heavy populated nowadays. Figure 3 shows the designed solution right after its implementation.

Figure 3. View of the slope after the stabilization work was completed.

3. THE CIC-XISTO STP - SEWAGE TREATMENT PLANT

This structure receives and treats the domestic sewage collected in the whole Barigui River valley, operating at a maximum capacity of about 0,5 m^3/sec. It contains four reactors, for the initial part of the treatment, placed in two rather big structures (Figure 4), that after some time send the pre-selected material (free of solids) to a sedimentation lake. The local subsoil is basically made of soft clay, mostly organic, saturated and slightly overconsolidated. This specific condition along with some excavation provided for the correct positioning of the tanks, gave origin to a direct foundation solution (mat), also adopted because it was known that the local soil profile is variable. With such a procedure, both bearing capacity and settlements were apparently verified (Brazilian Standard NBR6122-1996).

The structural design, however, defined a transversal joint that was supposed to be just in the walls, as shown on Figure 4, but was placed down to the foundation slab and caused differential behavior. As a result, there was a lot of concern as soon as the hydraulic test ended. Immediately after, a repair was provided with reinforcing steel bars in the affected area, attempting to stiffen a strip of the concrete mat along the joint. Apparently this service was successful, but the settlements kept occurring and for the efficient operation of the tanks, dependant on gravitational flow, an intervention will probably be done soon.

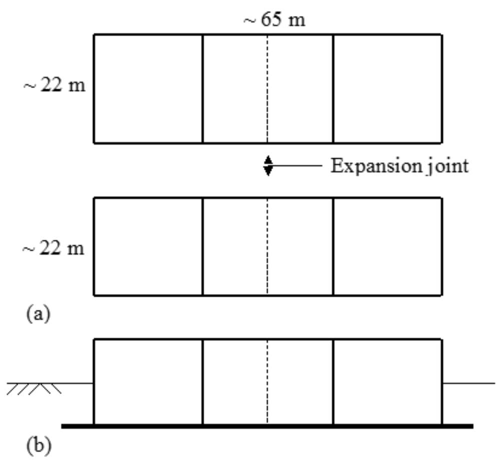

Figure 4. Plan view (a) and longitudinal cross-section (b) of the sewage tanks (not to scale).

Just as one more indication of the importance of the problem, topographical measurements of the structural deformation taken in different times (immediately after the end of construction and some years after operation, for example), indicated the order of magnitude of several centimeters, having reached about 15 cm. Although this number may seem exaggerated, there are a few indications that it can be accepted, both geotechnical and structurally speaking (The Institution of Structural Engineers, London, apud Velloso and Lopes, 1996). It should also be mentioned that the structural behavior of this tank has been very good, with no evidence of problems so far.

4. THE IRAÍ WATER TREATMENT PLANT

Another example is the Irai system, that treats water taken from two small rivers in the metro area and provides about 4 m^3/sec of potable water for the population. The area where this plant was built, about ten years ago, is flat, usually flooded and contains a lot of natural soft organic clay deposits on top of more competent material (Figure 5). An old lake was drained and direct foundation constructed over controlled fill material for the treatment tanks, each one measuring 34,5 meters by 24 meters with a height of about 6 meters .

A very careful soil parameters determination program was designed and done, including SPT wash borings, CPT soundings, undisturbed soil sampling and laboratory tests (soils characterization, compaction, strength and compressibility). As the fill work proceeded, other control values were obtained, such as compaction data, plate load tests and new SPT borings.

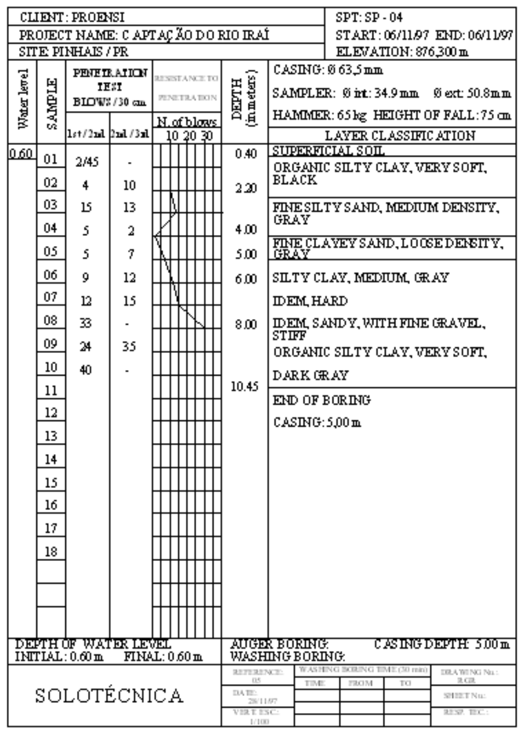

Figure 5. Standard Penetration Test.

As soon as the field work started, the contractor suggested that the geotechnical design was at least questionable, and probably wrong, giving another foundation solution for the tanks in terms of injection piles (Nascimento and Puppi, 2002). This design modification, allegedly for the sake of smaller settlements, would cost a lot more for the project, including not just the piles themselves but also a drastic structural change to concentrate loads that originally are uniformly distributed, and a longer construction time.

The authors were then called to give their opinion and strongly opposed themselves to this radical change in concept. Some more soil parameters determinations were agreed upon, obtained and basically confirmed the original design. The new procedures and later discussion took about one month, while the work site was kept on stand by, waiting for the final decision. Soon after, the normality was re-established and the work done as desired.

This kind of situation occurs rather frequently in civil engineering. Sometimes other opinions about a specific project may differ drastically, other times there may be some interest for certain engineering solution, economically more attractive for the contractor. In the present example the authors, also responsible for the geotechnical design, were surprised with the intense effort done by the builder towards the mentioned change, that could eventually be technically justifiable, but this was not the case. The original design was then maintained and the plant has now been producing normally for about seven years with no problems at all, both because there are no evidences for that and also due to the good numbers taken from the settlements measurements along time.

Again, the expression geotechnical risk can be brought to discussion: should a second opinion, during the construction phase of the project, be considered? How good, or perhaps how bad, was the original plan for such a proposed great change? There is always a risk involved, for sure. What we have to do is to minimize it. The certainty is still too far from any geotechnical solution, as settlements in any construction will always occur. The Irai water treatment tanks could be today supported by lots of piles, with less structural settlements very likely, but also at a tremendous higher cost.

5. THE PIRAQUARA-IRAÍ RIVERS BY-PASS PROJECT

This is the case of two small rivers, both being used as water supply to be treated and distributed to the local people, for which control flow hydraulic structures were designed. According to the Brazilian environmental law, whenever there is a contamination risk for water source, there must be a plan and a set of counter measurements ready to be activated. A road crossing rivers is the example for this case. The two rivers that feed the Irai Water Treatment Plant (Piraquara and Irai), had to be blocked and control flow structures devised for an occasional emergency situation, by-passing the hazardous material that otherwise could reach the water distribution system.

The by-pass system, called this way by the owner (Water and Sewage Company of Paraná – Sanepar), is located just a few kilometers away from Curitiba's downtown, in the middle of an old sand borrow area. The remains of the extensive excavations, carried out during many years, gave birth to the actual set of small lakes downstream from the intersection of the Irai and Piraquara rivers – this particular point is about 3,000 meters away from the intake channel of the water treatment plant, as shown in Figure 6.

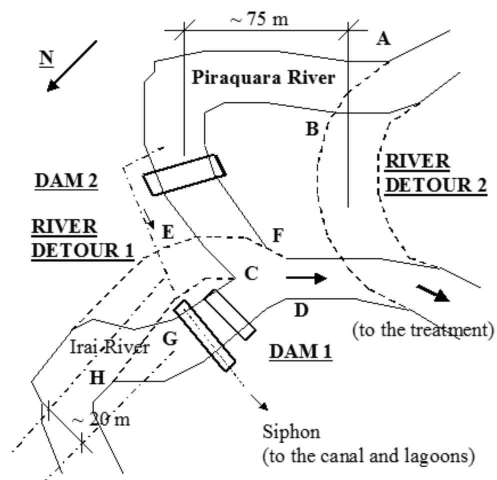

Figure 6. Plan view of the rivers intersection (not to scale).

As a result of the by-pass, both rivers can now be blocked by small dams with sluice-gates, the lakes are interconnected and an alternative water course does exist, to avoid occasionally contaminated river water to reach the treatment system.

In this area, two typical geological packages are well defined: a deeper layer of sedimentary silty and sandy clay, generally of high consistency, over-consolidated, some meters thick known as Guabirotuba Formation (ABMS-UFPR, 1999) and the superficial unconsolidated river deposits of organic clay and sand, reaching normally from a few meters to several meters in thickness. Representative results from Standard Penetration Test – SPT (NBR 6484, 2001) soil profile is given in Figure 7. The water table level is typically close to the ground level, specially in the vicinity of the rivers, although the deeper clay layers are often highly impervious, making the determination doubtful.

For the authors, an adequate balance considering risks and costs may be the answer. This design was done under Brazilian Specifications (ABNT, 1996), now under revision, based on deterministic values (global factor of safety equal to 3 for direct foundations); probably in a near future we will have to think and to work statistically, taking into account the probability of rupture or excessive settlements for geotechnical design. Meanwhile, let us be prepared to separate what is reasonable from what may be exaggerated, both technically and economically speaking.

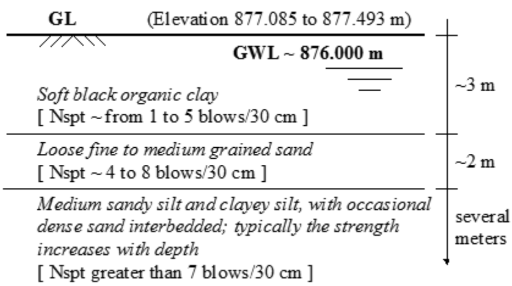

Figure 7. Typical representative soil profile of the area.

As an additional justification for that, both a reasonably high over-consolidation pressure detected from consolidation tests (NBR 3336/ABNT 1990) and occasional laboratory determinations of shear strength (unconfined compression, direct shear) or plate load tests so indicate. Again, extensive in situ and laboratorial geotechnical program of soil parameters determination, carried out for the aforementioned plant and many others in similar soils and loading conditions, showed such situation (Nascimento and Puppi 2002).

The hydraulic design determined one barrier on each river, both located close by and near the intersection point. Considering the lack of adequate and available natural materials in the surroundings, especially clay, solution using reinforced concrete was devised. Smaller sections and faster construction methods, less dependent on the weather conditions, may also justify this choice.

A typical geometry of the two dams is shown on Figures 8 and 9.Three main verifications were done, namely support, settlements and water flow through the foundation soil profile. In order to avoid possible future problems with time related deformations (consolidation of the clay layer, specially), root piles deep foundation was the preferred solution. By this means, when the cement paste is injected in the drilled and cased holes, somehow higher pressures may be used to decrease the permeability and avoid excessive water percolation as well, mainly through the sandy soil in the local profile.

This type of foundation has already been used successively in the area to support horizontal loads for highly pressurized water pipe curves. The kind and size of equipment needed to execute root piles is also another reason in their favour, comparatively to several other foundation machinery, bigger, heavier and more difficult to operate. The piles were then designed considering both compression and tension loads, basically dead weight and uplift water pressure, respectively, as well as the horizontal resultant of hydraulic pressure (Figures 8 and 9). The latter can be taken as the main reason for this kind of foundation, because the only stability check that failed before using piles was sliding (Table II).

Table II. Stability verification for the dams

	Stability check	**Factor of safety**
Foundation	Overturning moments	1,5
	– superficial	3,0
	– deep	> 3,0
Sliding	– without root piles	< 1,0
	– with root piles	> 1,5

The basic ideas for this part of the project were to speed up the field work, to concentrate it in the dry period of the year (around April to August) and to avoid as much as possible to bring soil from outside.

According to the design elevations established, the more superficial soft clay had to be removed down to the foundation level (foot slab), and the excavated material then used for the temporary rivers blocking. During the shortest possible length of time, while the material was placed in areas AB - EF and HG - CD (Figure 7), with the minimum discharge in the rivers, water was pumped continuously from the resulting intermediate holes, allowing for regular working conditions. Dewatering installations estimated in 30 m³/hour (six pre-cast concrete cased wells with one pump for a maximum discharge of 5 m³/hour each) were provided for by the contractor, considered one set at each dam. This detail was of particular importance because the fill material for the temporary dams was expected to be poor in quality, heterogeneous and permeable, making the dewatering for the construction period a fundamental activity towards general stability of the excavated area.

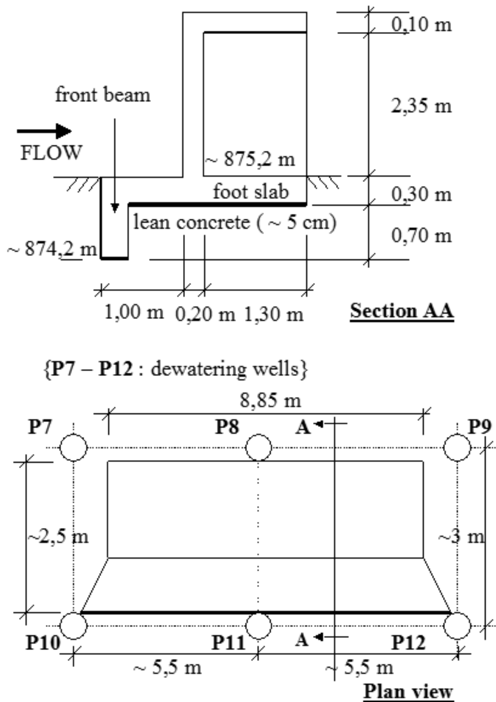

Figure 8. Piraquara and Irai Dams – cross section and plan view (not to scale)

Good quality natural materials, compaction control, impervious fill and other usual requirements in dam construction were not really achieved in this case. Although desirable and most of the times needed, the particular conditions of the present project did not contemplate such items, due to lack of materials and also to the tight budget approved (Earth Manual, 1974). Therefore, additional care had to be taken to overcome a scenario such as this.

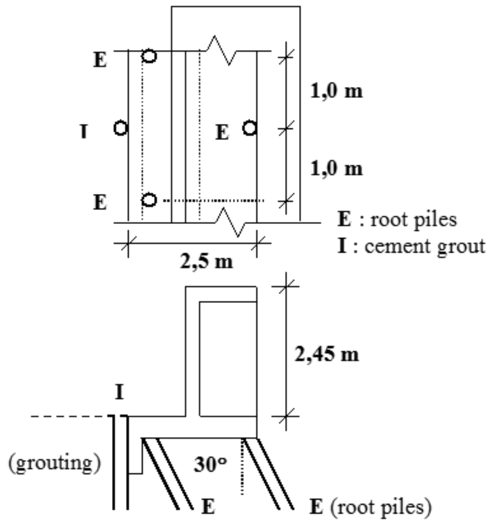

Figure 9. Plan view and cross section – dam foundation root piles and cement grouting (not to scale)

Nonetheless, the detours for both rivers were planned and executed as planned, by means of excavating the superficial sandy clay and dumping it as blocking fills, exclusively until the concrete dams were ready to operate. Construction ended a few years ago and the by-pass system is ready to be put into practice whenever it is necessary.

From the strict geotechnical point of view, the project shows a few particular features that the authors consider important. Facts such as bringing the least possible amount of materials from outside the area, using foundation root piles (also to decrease the subsoil permeability) and providing local poor quality excavated soil along with water pumping for the rivers detours, are details not commonly specified for this kind of engineering activity.

6. DISCUSSION

The four cases chosen to exemplify geotechnical works and the risks involved in designing and constructing structures in urban areas, intended to give an overview of local experiences in a fast growing area.

The subdivision showed how to deal with a stretch of pressurized gas, protected by specific law in Brazil, that was threatened by lateral and rather high excavation. The main concern was the eventual excessive movements, both vertical and horizontal, solved with a toe driven piles retaining wall, plus a three section gabion gravity wall and tie rods at mid height. Construction ended a few years ago.

The sewage treatment plant showed undesirable performance since the beginning, having the initial settlements caused worry towards the future behaviour of the structure. A monitoring with topographic readings was then established and, after about five years since regular operation started, there is a project now under consideration for the tank levelling, in the area of higher soil deformation. Nonetheless, the structure is nowadays operating and treating the incoming sewage. Although several actions were done during the soil parameters program, including SPT and CPT penetration tests, undisturbed soil sampling and laboratory testing, the end result indicated a very heterogeneous natural material and a poorer performance than the expected one. This fact may well represent the risk of constructing on difficult soils, even after what was considered a reasonably good geotechnical program of parameters determination, used for the final design. Maybe a better interaction between the geotechnical and structural designers could have avoided such a problem, as well as perhaps a more intense in situ monitoring could have also helped.

A far as the two other examples, one could be considered a unique solution for the water treatment plant, as the location of the tanks was on an old lake bed, also with soft organic soil, partly removed and filled with adequate material after having drained the area. The doubts raised by the contractor, at the early stage of the project implementation, caused a one month delay in the construction time. During this period, more in situ and laboratory tests were performed, until the final decision was taken by the geotechnical designers and the owner, and the work site was reactivated. This situation could also be considered unusual due to the fact that other interests, such as economical, eventually may have been put in practice to force a more expensive, and certainly more attractive solution for the contractor. Occasionally, this could be considered another kind of "geotechnical risk" in the project, having to do much more with the contractor's bidding interpretation than with geotechnics.

Finally, the by-pass project was also included in the report because of its importance as an ecologically correct preventive measure, in accordance with the legislation. The necessary protection of the two rivers involved, that feed the treatment plant, diverges the water to be treated nearby, in case of contamination, and avoids what could eventually be a big disaster to the local population. The geotechnical part of the problem also focused risks to find adequate natural materials, scarce in the surroundings, rather complicate subsoil conditions and access problems, especially for heavy equipment, besides construction time, low budget and uncertain weather conditions.

7. CONCLUSIONS

From what was herein presented and discussed, a few concluding remarks can be drawn, as follows:

. geotechnical risks are always present in designing and constructing civil engineering structures; a quick comparison could be made with settlements that, regardless the subsoil profile, will always happen, changing obviously the expected order of magnitude;

. some situations are particularly critical, specially foundations on soft soils, excavations nearby problematic structures and constructions under strict limitations (access, borrow materials, environmental regulations);

. although the risk does exist, geotechnical activities are of foremost importance always and the geotechnical engineer must be aware of it, taking all precautions with the objective of minimizing the inevitable risk involved.

8. REFERENCES

ABMS-UFPR (1999). "Geotechnical Characteristics of the Guabirotuba Formation." Proceedings of the Workshop ABMS-PRSC-UFPR, Curitiba, Brasil (in Portuguese).

ABNT-NBR6122. (1996). "Projeto e Execução de Fundações - Foundations." Associação Brasileira de Normas Técnicas, Rio de Janeiro, Brazil (in Portuguese).

Institution of Structural Engineers-ISE (1989) "Soil Structure Interaction: The Real Behaviour of Structures", London.

Nascimento, N. A., and Puppi, R. F. K. (2002). "ETA Irai – the geotechnical issue in a great sanitary work at the Curitiba Sedimentary Basin." Proc. I Congresso Luso-Brasileiro de Geotecnia, S. Paulo, Brazil, 425-435, (in Portuguese).

Nascimento, N. A., and Puppi, R. F. K. (2003). "Geotechnical modelling in engineering decision-making – two cases of foundations for structures." Proc. 24th CILAMCE, Ouro Preto, Brazil.

Investigating uncertainty in rock model selection using Random Set Finite Element Method

A. Nasekhian, H.F. Schweiger
Computational Geotechnics Group, Institute for Soil Mechanics and Foundation Engineering, Graz University of Technology, Austria

T. Marcher
ILF Consulting Engineers, Austria

ABSTRACT: From a practical point of view, Random Set Finite Element Method (RSFEM) has been found suitable and interesting in the context of uncertainty analysis, especially at the start of a project in which input parameters are available in form of ranges from different sources of information. Here, an attempt is made to demonstrate the capability of the framework in considering the uncertainty involved in choosing the material constitutive model. For this purpose, a real tunnelling project was chosen and two random set analyses were accomplished in which the Hoek-Brown and Mohr-Coulomb criteria have been used as the constitutive model. Discrepancies between the results are discussed and compared to the measurements. Finally, the combination of the results obtained from different random set analyses is illustrated using evidence aggregation methods.

1. INTRODUCTION

The objective of the present paper is to assess the uncertainty reflected in the results of a geotechnical problem due to the change of the rock model used in the numerical analysis within a probabilistic framework of the so-called Random Set Finite Element Method. The question is 'how far apart would the results be, when two different failure criteria, namely Hoek-Brown (HB) and Mohr-Coulomb, are adopted?'.

Random set theory is appealing in the context of geotechnical analysis, because information tends to be sparse and may only be available in the form of ranges or vague declarations of experts. When information is available from several sources, their combination can be thought of as a random set. Published values of geotechnical parameters, as well as specifications from experts conventionally appear as intervals, with no information about the probability distribution across the interval. In practical geotechnical engineering, subjective assumptions about probability density function of parameters are often made because in many cases the results of geotechnical investigations are set valued rather than being precise and point valued. The basic concepts of Random Set Theory (RST) and Random Set Finite Element Method (RSFEM) procedure have been presented in the literature (e.g. Tonon & Mammino 1996, Schweiger & Peschl 2005) and are not repeated here.

This paper argues about the capability of such a probabilistic framework in capturing the uncertainty involved in selecting the constitutive model used in the numerical model. By using the existing method of combining different sources of information the results of two separate RSFEM analyses are merged to come up with the bounds which takes into account the uncertainty in model selection. Moreover, it is shown that with a relatively small number of finite element runs the boundaries of the system responses can be calculated, which is a significant advantage as compared to full probabilistic methods, such as random field finite element analysis (Griffiths and Fenton, 2004), where a large number of realizations is required to get an accurate and smooth distribution.

2. MATERIAL MODEL SELECTION

At the beginning of a numerical analysis, a decision has to be made about the constitutive material model employed. There are many factors that are involved in model selection. For instance, some practitioners choose a model like Mohr-Coulomb (MC) for simplicity because it requires fewer input parameters in comparison to an advanced soil model. Also it may be difficult to derive the parameters for an advanced soil model due to time limitations, unreliable sources of information, or absence of proper test results. In this paper, the RSFEM was employed as an appropriate method to allow for a model variation in a numerical analysis. To demonstrate the applicability of the aforementioned method in considering model uncertainty in a reliability analysis, two simple rock/soil models, namely Hoek-Brown (HB) and Mohr-Coulomb (MC) are used, which are readily comparable and good enough for characterizing the problem under investigation.

2.1. Hoek-Brown criteria and equivalent Mohr-Coulomb parameters

Both MC and HB constitutive models are very common in practice because there are a number of empirical correlations, experience by practitioners as well as tables and graphs, which provide values for rock mass parameters according to rock type and quality, providing they don't exhibit significant anisotropy in strength and deformability (e.g. rock mass that contains a single dominant joint direction). Moreover, it is possible to calculate the equivalent MC parameters from HB ones (and vice versa) over a certain stress range. Both MC and HB models are classified as elasto-perfectly plastic constitutive models with different failure criteria. Mohr-Coulomb failure criterion relates the major and minor principal stresses linearly. However, the strength of the rock mass is usually better expressed by a parabolic function which may comply more appropriately with the real behaviour of rock (e.g. Brown 1970).

At failure, the generalized HB criterion (Hoek et al. 2002) relates the maximum effective stress σ_1 to the minimum effective stress σ_3 through the equation:

$$\sigma_1 = \sigma_3 + \sigma_{ci}\left(m_b \frac{\sigma_3}{\sigma_{ci}} + s\right)^a \tag{1}$$

where σ_{ci} is the uniaxial compressive strength of the intact rock, and *s* and *a* are model constants. The relationships between m_b/m_i, s, *a*, and the geological strength index (*GSI*) are as follows:

$$m_b = m_i \exp\left(\frac{GSI - 100}{28 - 14D}\right) \tag{2}$$

$$s = \exp\left(\frac{GSI - 100}{9 - 3D}\right) \tag{3}$$

$$a = \frac{1}{2} + \frac{1}{6}\left(e^{-GSI/15} - e^{-20/3}\right) \tag{4}$$

The Geological Strength Index (*GSI*), introduced by Hoek and Brown (1998) provides a system for estimating the reduction in rock mass strength under different geological conditions. The *GSI* takes the geometrical shape of intact rock fragments as well as the condition of joint faces into account. Finally, *D* is a factor that quantifies the disturbance of rock masses. It varies from 0 (undisturbed) to 1 (disturbed) depending on the amount of stress relief, weathering and blast damage as a result of adjacent excavations.

Only by estimating equivalent model parameters a valid comparison can be made between Hoek-Brown and Mohr-Coulomb results. The choice of the method for determining equivalent cohesion and friction angle is largely a matter of experience (Merifield et al., 2006). In general, there are two options to derive equivalent cohesion and friction angle from HB parameters. First, by fitting the MC failure line to the HB failure curve tangentially at a specific minor principal stress or normal stress, which in an elastic analysis yields similar results for a small stress variation. Second, a regression method can be applied over a dominant stress range of the problem, to obtain average values of MC strength parameters. However, this may lead to an underestimate of the strength for low stresses and an overestimate for high stresses. Nevertheless, the latter is the most frequently used method and is typically performed by fitting a linear relationship to the curve generated by Equation (1) for a range of minor principal stress values defined in Equation (5) given by Hoek et al. (2002):

$$\frac{\sigma'_{3\max}}{\sigma'_{cm}} = 0.47\left(\frac{\sigma'_{cm}}{\gamma H}\right)^{-0.94} \tag{5}$$

where σ'_{cm} is the rock mass strength and a function of HB parameters, γ is the unit weight of the rock mass, and H is the tunnel depth below the surface.

This fitting procedure results in the following equations for the equivalent MC strength parameters:

$$\varphi' = \sin^{-1}\left[\frac{6am_b(s + m_b\sigma'_{3n})^{a-1}}{2(1+a)(2+a) + 6am_b(s + m_b\sigma'_{3n})^{a-1}}\right] \tag{6}$$

$$c' = \frac{\sigma_{ci}\left[(1+2a)s + (1-a)m_b\sigma'_{3n}\right](s + m_b\sigma'_{3n})^{a-1}}{(1+a)(2+a)\sqrt{1 + \left(6am_b(s + m_b\sigma'_{3n})^{a-1}\right)/((1+a)(2+a))}} \tag{7}$$

where $\sigma_{3n} = \sigma'_{3\max} / \sigma_{ci}$

It is noted that $\sigma'_{3\max}$ should be determined for each individual case; the stresses are likely to vary within the rock mass, which makes it more difficult to select a representative value of σ'_{3max} (Merifield et al., 2006). Here the suggestion given by Hoek et al. (2002) was adopted (see Equation 5).

3. PROBLEM DESCRIPTION AND MATERIAL PARAMETERS

To illustrate the discrepancies in the outcomes of a numerical analysis resulting from selecting the two abovementioned material models, a tunnel example in rock was chosen. The layout of the tunnel geometry and the relevant finite element mesh (using approximately 900 15-noded triangle elements) are shown in Figure 1. No water table is present and consequently all calculations have been performed under drained conditions. The 460 m long tunnel with the typical horse-shoe shaped section is located in a homogeneous weathered and loosened sedimentary rock mass and its construction sequences have been designed according to the principles of the New Austrian Tunnelling Method (NATM), which involves three main excavation stages: top-heading, bench and invert. The finite element code Plaxis® (Brinkgreve et al. 2008) version 9.0 has been used for all calculations.

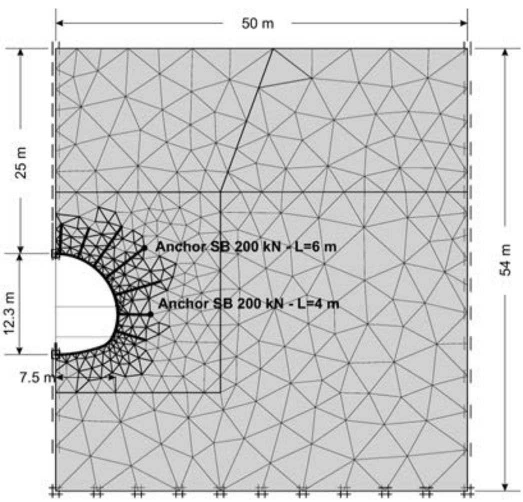

Figure 1. Deterministic finite element mesh used in RS-FEM.

3.1. *Input sets for deformability and strength parameters*

With reference to the site investigation report, it can be concluded that the tunnel lies within a homogeneous sedimentary rock mass that can be characterised by the parameters of generalized Hoek-Brown criterion listed in Table (1).

In order to attain useful results by means of the random set analysis, at least two sets of parameters for two random variables are required. It is described further, how these input set parameters for random set analysis are derived from different sources of available information.

Table 1. Hoek-Brown model parameters of the rock mass derived from site investigation report.

γ	E_i	GSI	σ_{ci}	m_i
kN/m^3	GPa	-	MPa	-
24	19-25	30-40	10-50	15-25

*Index i denotes parameters relating to intact rock.

- Deformability parameters:

The model input values for deformability properties for both models are Poisson‘s ratio (n) and deformation modulus of the rock mass (E_m). A Poisson’ ratio of 0.35, extracted from the site investigation report, was kept constant for all calculations. The in-situ deformation modulus was estimated from the following equation, which is applicable for rock masses with rock pieces having a compressive strength lower than 100 MPa (Hoek and Brown 1997):

$$E_m = \sqrt{\frac{\sigma_{ci}}{100}} 10^{(GSI-10)/40} \tag{8}$$

Table 2. Input random sets of elastic modulus of rock mass.

Set No.	*Probability assignment*	σ_{ci}	GSI	E_m
		MPa	-	MPa
1	0.5	10	30-40	1000-1770
2	0.5	50	30-40	2230-3970

*Index m denotes parameters relating to rock mass.

Considering the ranges of *GSI* and σ_{ci} presented in Table (1), one is able to infer two sets of parameters for the elasticity modulus of the rock mass, assuming that the lower value of UCS combined with the range of *GSI* makes up the first set; similarly the upper value of UCS forms the second set. Consequently, in this manner two random sets for the elastic modulus of rock mass with identical probability of

Table 4. Input random sets of both MC and HB models.

		HB Parameters				MC Parameters		Deformation modulus	Relaxation Factor		
Set	P*	m_i	σ_{ci}	D	GSI	φ	C	E_m	T.H.	Bench	Invert
-	-	-	MPa	-	-	degree	kPa	MPa	-	-	-
1	0.5	15	10	0-0.5	30-40	37-47	80-130	1300-2300	0.4-0.6	0.3-0.5	0.2-0.4
2	0.5	25	50	0-0.5	30-40	53-60	160-280	1900-3400	0.3-0.5	0.2-0.4	0.1-0.3

* Probability assignment

assignment (i.e. each with 50% likelihood of occurrence) using Equation (8) are derived and given in Table (2).

- Strength parameters:

Similar to the elastic modulus, it is possible to obtain two sets of parameters for equivalent MC parameters using the information in Table (1) and Equations (5-7) assuming that for set (1), which represents worse ground condition than set (2), lower values of m_i and σ_{ci} are used and likewise higher values are taken for the second set.

Table 3. Input random sets of the MC equivalent strength parameters.

Set No.	Probability assignment	σ_{ci}	m_i	GSI	φ	c
		MPa	-	-	o	kPa
1	0.5	10	15	30-40	37-47	80-130
2	0.5	50	25	30-40	53-60	160-280

In addition it is assumed that the disturbance factor might change between undisturbed (D=0) to firmly disturbed (D=0.5), which are considered corresponding to the lower and higher values of GSI respectively, i.e. the set of disturbance factor is dependent on GSI values. Input sets of the MC strength parameters corresponding to the HB failure criterion parameters are listed in Table (3).

4. RANDOM SET FINITE ELEMENT ANALYSIS

4.1. Input parameters

According to the Random Set Theory the input parameters are required to be set-valued rather than single values. As it has been provided in the previous section, some deformability and strength parameters are chosen as uncertain basic variables involved in random set analysis. In addition, a relaxation factor R_f (Vogt et al. 1998) is employed to account for 3D effects in a 2D tunnel analysis in an approximate manner. By experience, two sets are selected for this variable, they are given in Table (4). It is noted that the values for different construction stages are correlated to each other, i.e. in any realisation the left or right extreme of R_f for top-heading, bench and invert are used together. The values used in Table (4) for elastic modulus of rock mass are slightly different with those given in Table (2) due to applying the variance reduction technique accounting for spatial variability of soils, which has been elaborated by Vanmarcke 1983 and applied in Random Set Analysis by Schweiger and Peschl (2005).

Thereby, two sets of parameters have been obtained from the combination of two information sources. First, from current knowledge regarding the site exploration; and second, from correlation relationships, which in fact indicate the experience gained from similar ground conditions in other projects. The set-based values of four basic variables involved in RSFEM calculations for both HB and MC constitutive models are presented in Table (4). Figure (2) and (3) depicts the basic variables in terms of cumulative probability for Hoek-Brown and Mohr-Coulomb constitutive models respectively. Except *GSI* and *D* which only have a simple interval, the rest have two sets with equal likelihood of occurrence (50%).

4.2. Determinist finite element calculations

The actual excavation sequence according to NATM principles leads to 7 calculation phases as follows:

1. Initial stresses
2. Pre-relaxation phase of top heading excavation

3. Installation of anchors and primary lining in top heading
4. Pre-relaxation phase of bench excavation
5. Installation of anchors and primary lining in bench
6. Pre-relaxation phase of invert excavation
7. Completion of primary lining and anchors

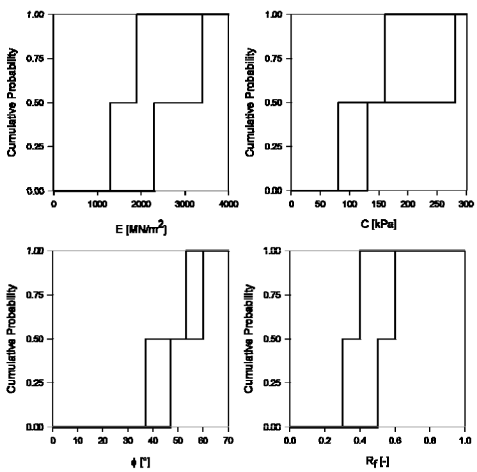

Figure 2. Set-based input random variables of MC model used in RS-FEM.

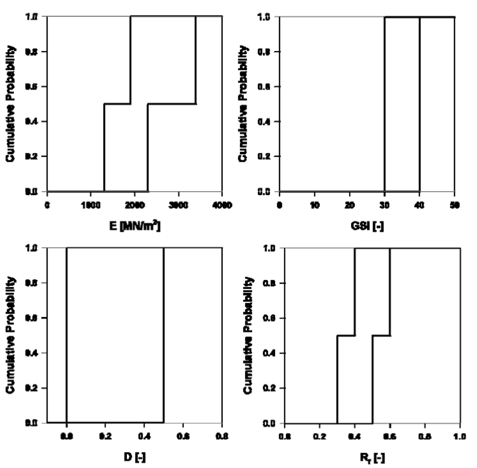

Figure 3. Set-based input random variables of HB model used in RS-FEM.

According to the random set model, a number of deterministic finite element calculations have to be performed. The results such as stresses, strains, displacements and internal forces in structural elements are obtained in terms of lower and upper bounds as discrete cumulative probability distribution (CDF), which may be compared with measured data. Any kind of system response of the model that may be extracted from FE calculations can be expressed in terms of lower and upper CDF bounds. Based on random set input variables presented in the foregoing section all the finite element calculations required for RSFEM have been carried out. For more details about the procedure of RSFEM in a geomechanical problem, it is referred to Nasekhian and Schweiger (2010). It should be noted that the random variables have been assumed stochastically independent, which generally speaking is not correct; but for simplicity and from a practical point of view this is admissible. For each constitutive model the RSFEM procedure is applied separately. The number of realisations required to accomplish the RSFEM in which the HB and the MC model have been used are 64 and 256 FE calculations respectively, based on Equation (9) given by Schweiger and Peschl (2005):

$$n_c = 2^N \prod_{i=1}^{N} n_i \tag{9}$$

where N is the number of basic variables and n_i the number of information sources available for each variable.

Figure (4) plots the probability box (p-box) of displacement of the tunnel crown as well as maximum moment of the lining for both HB and MC constitutive models along with the in-situ measurements. This indicates that the results of the calculated bounds are in good agreement with the measurements and thus it maintains the general capability of the RSFEM in capturing the uncertainties involved in the basic random variables. Since the measurements of only two sections of the tunnel with similar conditions to the model were available, the measurement values are illustrated in the plot with two steps in form of a discrete cumulative distribution. As depicted in Figure (4-a) the most likely values for crown displacement are in the range of [1.5, 4.3] and [1.5, 5.2] mm obtained by MC and HB model respectively.

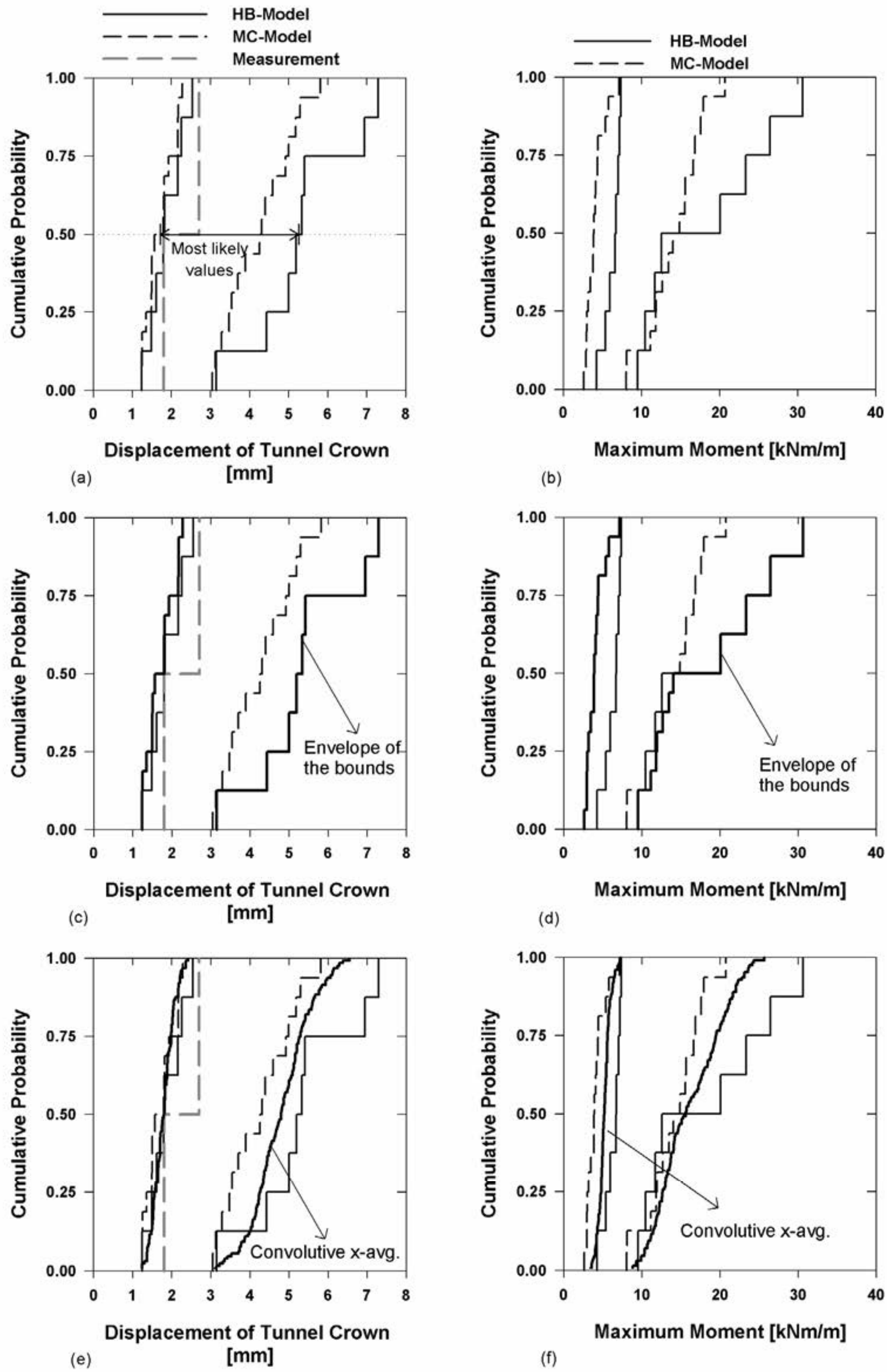

Figure 4. RSFEM results of the crown displacement and the maximum lining moment a) resulting bounds of both HB and MC models along with in-situ measurements b) envelope of bounds c) Convolutive bounds by aggregating the lower and upper bounds of both models.

Generally, the most likely values are defined as values with the highest probability of occurrence, where the slope of the corresponding cumulative distribution function is steepest. For purpose of illustration, it is assumed that the most likely values have a probability of 50% as shown in Figure (4-a). It can be seen that random set results encompass the measurements within the range of most likely values, although the displacements are small in the sense of absolute values. Despite the fact there was not a possibility to measure maximum moment of the lining, it is anticipated that like the crown displacement, actual moments in the lining fall inside the range shown in Figure (4-b).

If one wishes to consider the uncertainty involved in the material model used in numerical analysis it can be carried out using the notion of aggregating evidence, which has been presented by several authors. Here we aggregate the results of two separate Random Set analyses (i.e. one with HB and the other with MC model) to come up with the final bounds enclosing the uncertainty in material model selection. In fact, the random set analysis result of each material model is considered as one source. In this study, two methods of aggregating evidence are employed to merge these sources, namely Envelope and Convolutive x-averaging (Sentz and Ferson, 2002). The bounds made up by these methods have been shown in Figure (4-c to 4-f) for the results of crown displacement and maximum moment of the tunnel lining. As it can be seen, the envelope of the bounds results in a conservative solution whereas the convolutive x-averaging yields a compromise between the bounds obtained by both constitutive models. The convolutive x-averaging provides a joint cumulative distribution function of the system results produced from two different numerical models. The upper bounds of the marginals are averaged to obtain the upper bound on the joint distribution. The same process is repeated for the lower bound. The probability assignments of the joint distribution are the product of the marginal's masses. There are several other combination rules for aggregating different so-called Dempster-Shafer structures reviewed by Sentz and Ferson (2002) which would be equally applicable.

The differences between HB and MC results originate from two main reasons. First, despite of the suitable fitting procedure, there is a difference between the two failure criteria, which results in different numbers of failure points in each model, leading to different plastic strains and consequently internal forces in the lining. Secondly, a different flow rule is adopted for the two models, which has some influence in particular for low stress levels and tensile stress.

5. RELIABILITY ANALYSIS USING RANDOM SET RESULTS

Next, the serviceability limit state of the shotcrete lining at the final stage will be assessed. On the basis of the results obtained from the original design calculation a shotcrete thickness of about 30 cm is required for top-heading and bench. This amount is decreased to 20 cm for the invert. Following the formula of Schikora and Ostermeier (1988) the limit state function can be written as:

$$g(\mathbf{x}) = N_{\lim} - N \tag{10}$$

with

$$N_{\lim} = \frac{f_c d}{F_s}\left(1 - 2\frac{e(\mathbf{x}) + e_a}{F_s d}\right) \tag{11}$$

where f_c – uniaxial strength of shotcrete; e_a – imperfection; d – thickness of lining; $e(\mathbf{x})$ – eccentricity M/N; M – bending moment; N – axial force; F_s – factor of safety.

The serviceability limit state of the shotcrete lining is defined by exceeding the admissible stress which is based on the potential for damage of the lining due to cracking when the tensile capacity of the material is exceeded. The following assumptions were made regarding other variables involved in Eq. (11), i.e. for the shotcrete an uniaxial strength of about 17.5MPa is used, and to cover imperfections an eccentricity of e_a = 2.0cm, and for the serviceability limit state a safety factor of F_s = 2.1 is considered. Figure (5) depicts the range of the evaluated limit state function using REFEM results. Beta distribution has been fitted to all the discrete CDF of g(x). The lower and upper values of probability of exceeding the admissible normal force in the lining, $N>N_{lim}$, where cracking takes place, corresponding to lower and upper CDF of g(x) for both HB and MC models are approximately zero. The values of probability of failure indicate that the shotcrete satisfies the serviceability criterion and it is expected that major cracking will not occur in the lining.

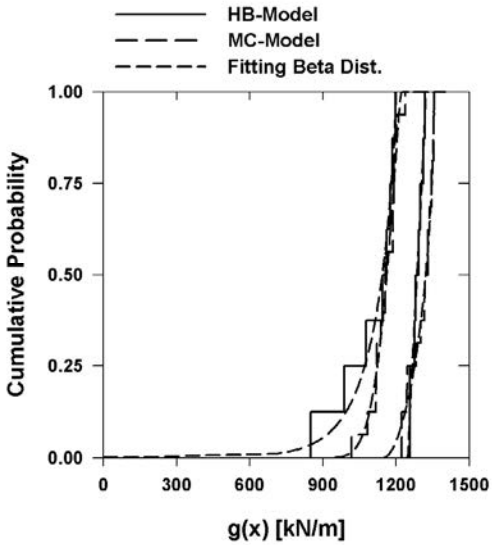

Figure 5. Bounds of the random set results of shotcrete serviceability limit state function

6. CONCLUSION

In this study an extension of RSFEM was presented that enables the Random Set model to consider uncertainty of the constitutive model used in numerical analysis by using evidence aggregation methods. Two separate Random Set Finite Element Analyses were performed in which common constitutive models, namely the Hoek-Brown and the Mohr-Coulomb model were employed. The range of predicted results of tunnel crown displacement was compared to the measurements available in the project and good agreement could be observed. The HB criterion requires less finite element realisations as compared to the MC model, which can be seen as an advantage from a practical point of view.

Acknowledgment

The authors would like to acknowledge the support of the Austrian Society for Geomechanics (ÖGG) for this work.

7. REFERENCES

Brown, E.T. 1970. Strength of models of rock with intermittent joints. *J. Soil Mech. Found. Div.*, ASCE 96, SM6, 1935-1949.

Brinkgreve, R.B.J. Broere, W. & Waterman, D. 2008. *PLAXIS, Finite element code for soil and rock analyses*, users manual. The Netherlands.

Griffiths, D.V. & Fenton, G.A. 2004. Probabilistic slope stability analysis by finite elements. *J Geotech Geoenv Eng*, ASCE, 130(5): 507–518.

Hoek, E. & Brown, E.T. 1988. The Hoek-Brown failure criterion - a 1988 update. *Proc. 15th Canadian Rock Mech. Symp.* J.C. Curran (ed.), Toronto, Dept. Civil Engineering, University of Toronto, 31-38.

Hoek, E. & Brown, ET. 1997. Practical estimates of rock mass strength. *Int J Rock Mech Min Sci*; 34(8): 1165–86.

Hoek, E. Carranza-Torres, C. & Corkum B. 2002. Hoek–Brown failure criterion—2002 edition. *Proceedings of the North American Rock.* Mechanics Society Meeting, Toronto.

Merifield, R.S. Lyamin, A.V. & Sloan, S.W. 2006. Limit analysis solutions for the bearing capacity of rock masses using the generalised Hoek–Brown yield criterion. *Int J Rock Mech Min Sci*; 43:920–937.

Nasekhian, A. & Schweiger, H.F. 2010. Random Set Finite Element Method ‐ application to tunnelling. The 4th International Workshop on Reliable Engineering Computing , Singapore (in print).

Schikora, K. & Ostermeier, B. 1988. Temporäre Sicherung von Tunneln mit Spritzbeton - Tragwirkung und Bemessung. *Bauingenieur*, 63: 399-403 (in German).

Schweiger, H.F. & Peschl, G.M. 2005. Reliability analysis in geotechnics with the random set finite element method. *Computers and Geotechnics* 32, 422–435.

Sentz, K. & Ferson, S. 2002. *Combination of Evidence in Dempster-Shafer Theory.* SAND2002-0835 Technical Report. Sandia National Laboratories, Albuquerque,New Mexico.

Tonon, F. & Mammino, A. 1996. A random set approach to the uncertainties in rock engineering and tunnel lining design. *Proc. ISRM International Symposium on Prediction and Performance in Rock Mechanics and Rock Engineering (EUROCK '96)*, Vol. 2, Barla (ed.). Torino, Italy: Rotterdam, A.A. Balkema, 861-868.

Vanmarcke, E.H. 1983. *Random fields – analysis and synthesis*. Cambridge, MA: MIT-Press.

Vogt, C. Bonnier, P. & Vermeer, P.A. 1998. Analyses of NATM-Tunnels with 2-D and 3-D Finite Element Method. *Proc. of the Fourth European Conference on Numerical Methods in Geotechnical Engineering (NUMGE98)*, Cividini (ed.), Springer, 211-219.

Geotechnical Parameters of a Coral Deposit under a building foundation from Metropolitan Area of Recife - Brazil

J.T.R. Oliveira
Catholic University of Pernambuco, Recife, Pernambuco, Brazil

T.M. Silva
Catholic University of Pernambuco, Recife, Pernambuco, Brazil

ABSTRACT: This paper presents the geotechnical parameters of a deposit of corals, located in the City of Jaboatão dos Guararapes, Metropolitan Area of Recife - PE. The studied layer occurs between 7 and 13 meters of depth. These parameters had been obtained from the interpretation of SPT and CPT tests, carried through in the geotechnical investigation executed with the purpose to supply subsidies the project of the foundations of a building of 20 floors. The relative density, the Bulk modulus and the friction angle of the studied material had been estimated, from existing correlations in international literature, considering the material as being similar to one soil granular sandy. From the gotten results it was observed that the band of variation of the parameters is great, concluding itself that the material is sufficiently heterogeneous, with relation to its geotechnical properties.

1. INTRODUCTION

In the geological history of the subsoil of the Region Metropolitan of Recife, geodynamic processes are diverse that had contributed in the formation of the different deposits. Amongst these processes, the successive sea-level rise and regressions in the Quaternary had been responsible for the formation of deposits with different geotechnical properties. Faced with increasing real estate expansion and valuation of coastal lands, exists a trend in the market to the increase of the constructions, what it results in a bigger shipment in the foundations you seat on the different deposits found in Recife, between which is gifts layers of corals.

This paper presents the geotechnical parameters of a deposit of corals, located in the City of Jaboatão dos Guararapes, Region Metropolitan of Recife - PE. These parameters had been esteem from the interpretation of SPT and CPT tests, carried through in the geotechnical investigation executed with the purpose to supply subsidies the project of the foundations of a building of 20 floors. The relative density, the modulus of elasticity and the friction angle of the studied material had been gotten, from existing correlations in international literature, considering the material as being similar to one soil granular sandy. The values of relation K had been gotten still enter the resistance of tip of CPT test and the number of blows of sounding SPT.

2. DEPOSIT OF CORALS

The corals, according to Gusmão Filho and Amorim Jr. (1998), they are secretions of zoofits, that they are animals that if seem plants, notables for its capacity to construct structures of calcium massive carbonate skeletons. These animals occur in hot water oceans and coastal lands next to these situated seas in regions to tropical climate.

According to Dominguez et al. (1990) the great majority of reefs of coral to the long one of the coast of the State of Pernambuco is constituted of prolongated and discontinuous bodies, with the parallel axe biggest to the axle of the coast. The individual dimensions of these reefs bodies vary between 1 and 4 km length. The authors still comment who, the localization and the general morphology of these reefs of coral, suggests a narrow relation with the sandstone banks that they are associates. These sandstone banks of the coast northeastern present age between 6,000 and 6,500 years, while the corals have dating between 2,800 and 3,800 years.

Laborel (1969), cited for Dominguez et al. (1990), it affirms that of the 18 species of described corals for Brazilian reefs, only 9 occur in reefs of the coast of the Pernambuco State.

3. GEOTECHNICAL INVESTIGATION

The deposit studied in the present paper is located in a land to the side-sea in the quarter of Candeias, in the City of Jaboatão of the Guararapes, situated in the South zone of the Region Metropolitan of Recife. 3 bore-hole of SPT test and 4 bore-hole of the CPT test had been carried through. It's important to register that a mechanical cone was used, pertaining to the Institute of Technology of Pernambuco (ITEP). Figures 1 and 2 present the geotechnical profile of the subsoil with results of SPT and CPT tests.

The soundings initially show composed subsoil for a fine sand layer, loose, with average thickness of 3 meters. A fine sand layer is followed, very dense medium dense, with thickness of 4 meters. One follows a layer of corals and shells, with fine sand. It can still be noticed that the layer of studied coral occurs between 7 and 13 meters of depth. This layer presents a lesser resistance to the penetration.
the column with no indentation. Equation numbers should be placed in parenthesis at the end of the line to the right of the column.In this site projected and a composed building for a structure of reinforced concrete with 20 (twenty) floors, 23 (twenty and three) columns. The foundations of the building are shallow foundations with footings supported directly in the compact sand layer (Oliveira et al., 2002).

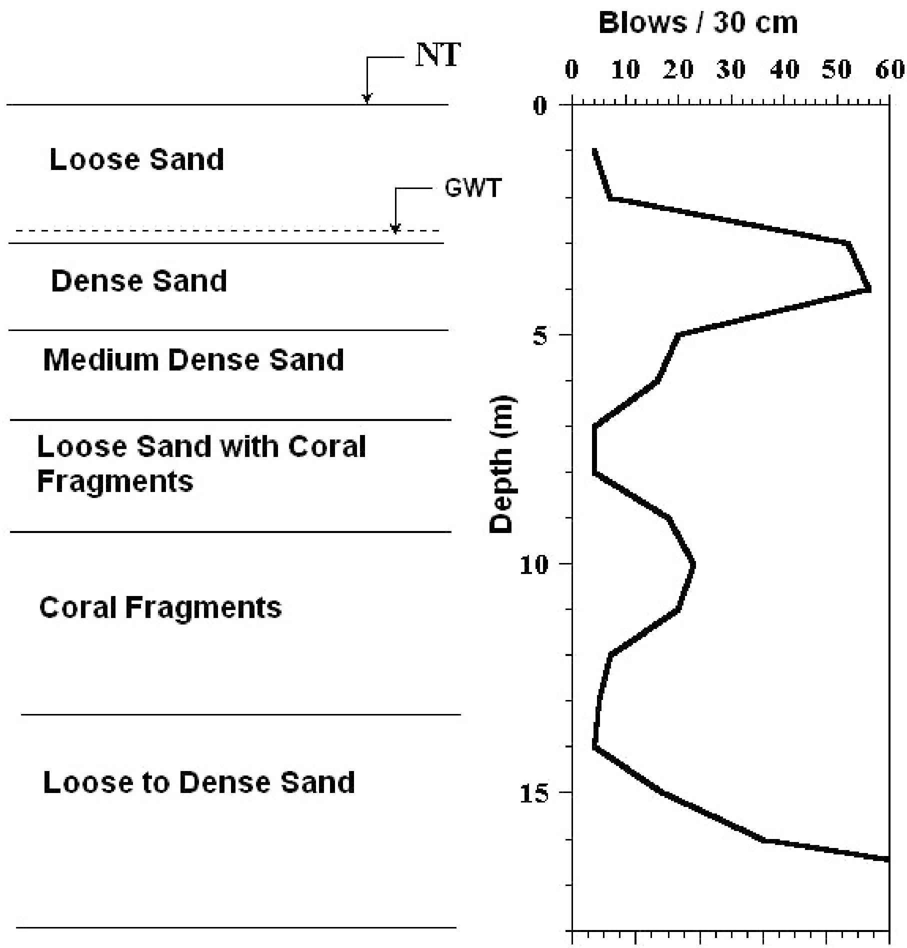

Figure 1 - Geotechnical profile of subsoil – SPT test

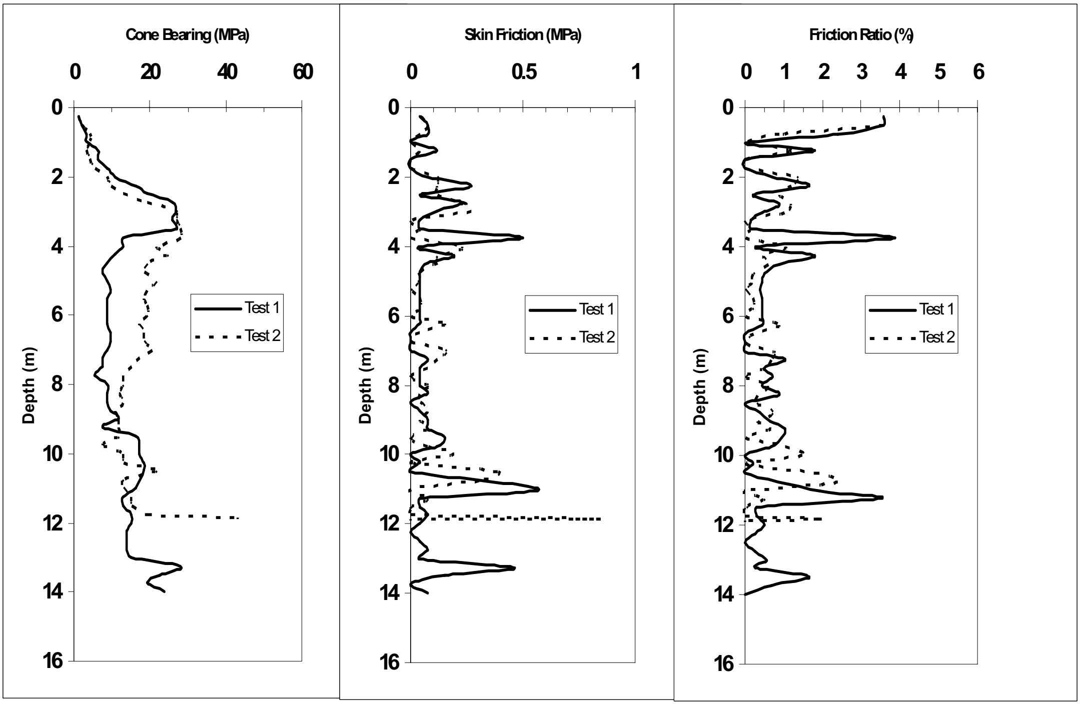

Figure 2 – Results of cone penetration test

4. GEOTECHNICAL PARAMETERS

4.1. Soil classification

Adopting the chart of Robertson and Campanella (1983), to classify the material studied in the present paper, it is concluded that the layer of fragments of corals can be classified as an sandy material, therefore presents high values of tip resistance (between 7 and 23 MPa), associates the values of inferior friction ratio 2%.

4.2. Relative density

Considering the ground as an sandy material, since the fragments of corals appear mixed the sand on the basis of and the classification of the previous item, the relative density was esteem using the proposals of Gibbs and Holtz (1957) (Equation 1) and Skempton (1986) (Equation 2), based in the N-SPT. The used formulas are the following ones:

$$Dr = (N/(0{,}28\sigma'_{vo} + 16))^{0,5} \quad (1)$$
$$Dr = (N/(0{,}28\sigma'_{vo} + 27))^{0,5} \quad (2)$$

Dr = Relative density, N = Number of blows SPT test and σ'_{vo} = vertical effective stress.

Values between 18 and 72% had been found. Of this form the layer of fragments of corals can be compared with sand loose to medium compacts. As a great variation in the values of the N exists, the band of variation of the relative density also is wide. The relative density was also esteem on the basis of the results of CPT test, from the correlation of Lancellota (1985), cited for Schnaid (2000). The expression is the following one:

$$Dr = -98+66\log (qc/(\sigma'_{vo}{}^{0,5})) \quad (3)$$

Dr = Relative density,, qc = cone resistance e σ'_{vo} = vertical effective stress.

Values between 61 and 83% had been gotten. These values are superior to the found ones from SPT test, as well as present a lesser dispersion.

4.3.Internal friction angle

The angle of internal friction of the material was obtained from the expression of Meyerhof (1956), cited for Gusmão Filho (1998), in function of the relative density. This expression is the following one:

$$\phi = 28° + 0,15Dr \quad (4)$$

Dr = relative density,
ϕ = Internal friction angle.

Values between 31 and 39º for the layer of fragments of corals had been found, with base in the relative density gotten to break do SPT. The average value of the attrition angle is approximately 34. On the basis of the estimated results of relative density from the CPT test, had been found values superior, varying between 37 and 41º. The average value is in the band of 39º. These values are inside of the described band in literature for sands of the plain of Recife (Costa, 1960; Gusmão Filho, 1998; Gusmão et al., 2002). Figure 3 presents the variation of the friction angle with the depth.

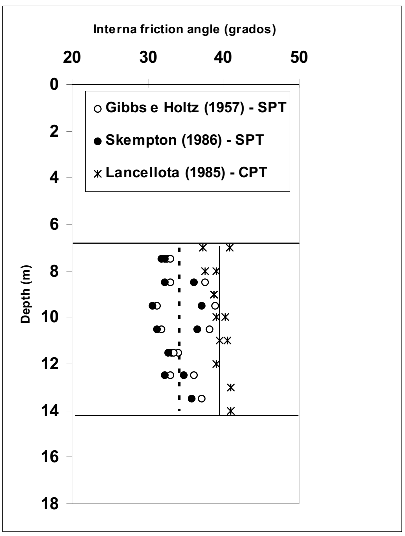

Figure 3 - Variation of the friction angle with the depth - Correlation of Meyerhof (1956) in function of the relative density

4.4 Bulk modulus

Values of the bulk modulus of the layer of fragments of corals had been gotten from the correlations of Décourt (1995) and Baldi et al. (1986), in function of N and qc, respectively. The used expressions had been the following ones:

$$E = 3,5N \quad (5)$$
$$E_{25} = 1,5qc \quad (6)$$

Where:
E = Bulk modulus,
N = Number of blows SPT test
E_{25} = Bulk modulus 25% of failure stress
qc = Cone resistance

The results gotten from the suggestion of Décourt (1995) vary between 14 and 80 MPa. The values gotten from the expression of Baldi et al. (1986) they are situated between 11 and 35 MPa. On the other hand, values of measurement of stress carried through in the constructed building had presented deformations between 43 and 75 mm (Oliveira et al., 2002). Considering that the compressible layer of the subsoil is practically the layer of fragments of corals and that stresses it is imminently elastic, being valid the Hooke´s Law, can be found modulus of elasticity varying between 9 and 16 MPa. These values are situated in the lower limit of the band of results found from correlations with the field tests. Gusmão Filho (1998) presents values of the modulus of elasticity of sands of the plain of Recife, gotten from direct load tests, using the theory of the elasticity. The gotten values had varied between 13 and 38 MPa for natural sands, and between 31 and 75 MPa for compact sands with sand and gravel columns. The values presented for Gusmão Filho (1998) for natural sands are very next to the gotten ones in the present article, from the CPT. Table 1 summarizes these comparisons.

Table 1. Values of Bulk modulus

Reference	Soil	E (MPa)
Gusmão Filho (1998)	Natural sand of Recife Plain	13 a 38
Gusmão Filho (1998)	compact sands with sand and gravel columns of Recife Plain	31 a 75
Present paper SPT (Décourt,1995)	Fragments of corals	14 a 80
Present paper CPT (Baldi et al.,1986)	Fragments of corals	11 a 35
Present paper settlement measurement	Fragments of corals	9 a 16

4.5 CPT x SPT correlation

With the objective to contribute with the experience in CPT test (dutch cone), a study on the correlation of the results of this test with SPT test was carried through. This correlation makes possible the transposition of information between the two types of soundings, what it can be interesting in projects of deep foundation. This transposition, however, must be made with care due to dispersion of the values. They had been gotten, for the relation qc/N, values between 0,65 and 6,5 MPa. The band of values for sandy material of literature varies between 0,4 and 1,2 MPa (Aoki and Velloso, 1975; Alonso, 1980; Danziger and Velloso, 1986; Robertson et al., 1983). Of this form the superior limit of the band of results gotten for the layer of fragments of corals is above of the described values in literature.

A trend proven internationally exists, of the relation qc/N to increase with the increase of the diameter of the grains of the soil, represented for the average diameter D50 (Robertson et al., 1983; Robertson and Campanella, 1983). Considering that the layer of fragments of corals can present very superior particles of size to traditional ground, the increase in the relation qc/N, can of certain form be waited. Robertson et al.(1983) presents a correlation between qc/N and the average diameter of the ground (D50). The expression is the following one:

$$(qc/pa)/N = 5{,}44\ D_{50}^{\ 0{,}26} \tag{7}$$

Where:
Pa = atmospheric pressure

Robertson et al. (1983) they present values of the relation qc/N varying up to 12, with variation of the average diameter up to 10 mm. Becoming a extrapolation of Equation 7 for bigger values of average diameter, can be found superior values to the presented ones in literature, for ground of conventional grain size distribution. Figure 4 illustrates this commentary, also indicating the band of values gotten for the layer of fragments of corals, object of study of the present paper. It’s important to register that, Schnaid (2000) comments the data of Robertson et al. (1983) they are not corrected, to take in account relative effect to the energy of driving, pore-pressure, etc., the dispersion in the results is great. Bigger studies, however, are still necessary on the correlation qc/N, in deposits of fragments of corals.

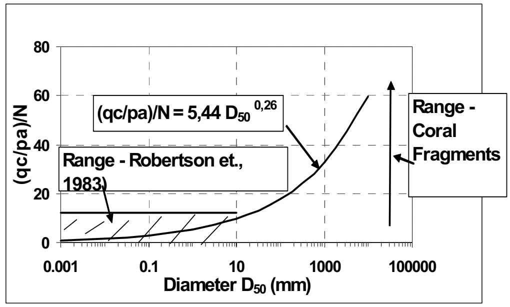

Figure 4 – Variation of qc/N with diameter of grain (modify by Robertson et al., 1983)

5. CONCLUSIONS

The present paper presented the geotechnical parameters of a deposit of fragments of corals, gotten in situ tests. The following one can be concluded:

- The layer of fragments of corals can be classified as an sandy material, from the abacus of Robertson and Campanella (1983);
- The gotten values of the relative density from correlations with SPT and CPT, indicate that the studied material can medium be fit as similar to a loose sand;
- The values of the gotten angle of friction from correlation used had been situated between 31 and 41 degrees. The values gotten from assay CPT had been slightly superior to the gotten ones from sounding SPT. These values are inside of the described band in literature for sands of the plain of Recife;
- The results for the modulus of elasticity gotten from the suggestion of Décourt (1995) vary between 14 and 80 MPa. The values gotten from the expression of Baldi et al. (1986) they are situated between 11 and 35 MPa. These results had been compared with values of literature and with results of backward-analysis of measurements of it stresses;
- They had been gotten, for the relation qc/N, values between 0,65 and 6,5 MPa. Of this form the superior limit of the band of results gotten for the layer of fragments of corals is very above of the described values in literature.

6. REFERENCES

Alonso, U. R. (1980). Correlações entre resultados de ensaios de penetração estática e dinâmica para a cidade de São Paulo, *Revista Solos e Rochas*, Vol.3, No.3: 19-25;

Aoki, N., Velloso, D. A. (1975). An aproximate method to estimate the bearing capacity of piles, Proceedings 5th Pan. Conf. on Soil Mech. and Found. Engineering, Buenos Aires;

Baldi, G., Bellotti, R., Ghionna, V., Jamiolkowski, M., Pasqualini, E. (1986). Interpretation of CPTs and CPTUs: Drained Penetration of Sands, International Geotechnical Seminar, Cingapura;

Costa, A.J. (1960). O Subsolo do Recife, Boletim Técnico da Secretaria de Viação e Obras Públicas, Recife, Vol. LVIII a LXI;

Danziger, B.R., Velloso, D.A. (1986). Correlações entre SPT e os Resultados dos Ensaios de Penetração Contínua, VIII COBRAMSEG, Vol.1: 103-113;

Décourt, L. (1995). Prediction of load Settlement Relationships for Foundation on the Basis on the SPT-T, Ciclo de Conferências Internacionais Leonard Zeevart: 87-104, México;

Dominguez, J.M.L., Bittencourt, A.C.S., Leão, Z.M.A.N., Azevedo, A.E.G. (1990). Geologia do Quaternário Costeiro do Estado de Pernambuco, *Revista Braileira de Geociências,* 20 (1-4):208-215;

Gibbs, H.J., Holtz, W.G. (1957). Research on Determining the Density of Sands by Spoon Penetration Testing, 4th ICOSOMEF, 1,35-39, Londres;

Gusmão, A.D., Pacheco, J.L., Gusmão Filho, J.A. (2002). Caracterização Tecnológica de Estacas de Compactação para Fins de Melhoramento de Terrenos, XII COBRAMSEG, São Paulo;

Gusmão Filho, J.A. (1998). *Fundações: do Conhecimento Geológico à Prática da Engenharia*, Editora da UFPE, Recife;

Gusmão Filho, J. A., Amorim Junior, W. M. (1998). Propriedades de Depósitos de Conchas para Fins de Fundações - Anais do XI COBRAMSEG, Brasília, V.3, p.1367-1374;

Laborel, J.L. (1969). Madreporaires et hidrocoralliaires recifaux dês cotes brésiliennes. Systematíque, ecologie, repartition verticale et geographic. *Ann. Inst. Oceanogr.* 47:171 -226.

Meyerhof, G.G. (1956). Penetration Tests and Bearing Capacity of Cohesionless Soils, *Journal of Soil Mechanics and Foundation Engineering Division*, ASCE, 82 (1): 1-19;

Oliveira, J. T. R., Gusmão , A. D., Araújo, A. G. (2002). Comportamento Tensão-Deformação Das Fundações De Três Edifícios Monitorados, XII COBRAMSEG;

Robertson, P., Campanella, R. (1983). Interpretation of cone penetrometer test, Part I: Sand, *Canadian Geot. Journal*, 20(4), 718-733;

Robertson, P., Campanella, R., Wightman, A. (1983). SPT-CPT Correlations, *Journal of Geot. Eng.* 109(11), 1449-1459, New York: ASCE;

Schnaid, F. (2000). *Ensaios de Campo e suas Aplicações à Engenharia de Fundações*, Editora Oficina de Textos, São Paulo;

Skempton, A.W. (1986). Standard Penetration Test: Procedures and the Effects in Sands of Overburden Pressure, Relative Density, Particle Size, Ageing and Overconsolidation, *Géotechnique*, 36 (3): 425-447.

Tunnelling Through a Highly Slide Prone Area at Meghalaya, India

S.S. Porowal, VSM
Border Roads Organisation, India

A.K. Dey
NIT Silchar, Assam, India

ABSTRACT: Landslide at Sonapur (latitude $25^0 6'30''$ N and longitude $92^0 21' 51''$) in the state of Meghalaya in India became active in 1988 after Cachar earthquake in 1987. Since then the landslide was a regular phenomenon during monsoon period and the road communication of the southern part to the mainland used to be cut off completely. The only way to tackle the problem was to remove the debris by deploying bulldozers. An innovative approach in the form of a cut and cover tunnel through the slide prone area was tried for the first time in India to find a permanent solution of the problem. This paper deals with the design methodology and problems associated with the construction of the tunnel.

1. INTRODUCTION

The state of Meghalaya is situated in the north eastern region of India. This region is little backward comparing to other part of the country because of its geographical location, dense forest, numerous hills, heavy rains etc. Communication in this region is also very poor. One National Highway passes through this state connecting the southern part of this region. Some places along the highway are unstable during monsoon in the month of June and July. Moreover, an active seismic fault namely Dauki fault lies on the southern part of the Meghalaya state due to which the entire state falls under seismic zone V, the highest seismicity zone in India. Frequent earthquakes of magnitude 5.0 and above are very common in this state. For an example 12 numbers of earthquakes of magnitude 4.9 to 6.3 occurred from September to December, 2009. Sonapur (latitude $25^0 6'30''$ N and longitude $92^0 21' 51''$) is one of the most slide prone areas along this highway. The area was dormant for a long time and became active in 1988 after 1987 Cachar earthquake. Since then the road gets blocked every year during monsoon period due to heavy flow of muck. The flow is so rapid that it pushes everything on its way down to a hilly stream, namely the river Lova.. In 1999 one express bus with 35 passengers was slide down by this flowing muck at night and three people died and several injured. Several measures like, geotextile treatment, wire crate wall, ground anchorage to the slope, flattening of the slope with proper benching etc. were under taken in this part to control the slide but nothing proved fruitful. An alternative route through the hill was also suggested but could not be materialized because of high cost.

To overcome the problem many alternatives of tunneling were considered and finally one Cut & Cover type tunnel was found to be the most appropriate in that area because of the easy, economic and rapid construction technique. The tunnel was constructed within nine months and performed very well during the last two monsoons. There was not a single day road blockade since operation of the tunnel.

The paper deals with different Geological aspects of the area, design methodology, problem encountered during execution of tunnel and present performance of tunnel based on data recorded through various instruments.

2. GEOLOGICAL INVESTIGATION

The crustal materials of Meghalaya mainly consist of Pre-Gondwana landmass outcrop which slopes down into basinal depressions in many part of the region. The rock consists mainly of granite gneiss, hornblende-biotitic gneiss and biotic-cordierite gneiss of early Proterozoic age. The metamorphic rocks are overlain uncomfortably in a number of places by younger Proterozoic sediments called Shillong series. The muck matrix consists of roughly 60% silty clayey sand and 40% boulder of size medium to very large. The muck matrix in water is very soft and behaves like a thick fluid without any shear strength. One person was buried alive in this matrix. The soil in dry condition is quite stable and possesses both cohesion and angle of internal friction.

Figure 1 shows the geological map of the Sonapur landslide area. The seismotectonic maps of the area (Plate) depict that the locality lies near the epicenter of a number of past earthquakes. The area consist of Archean-Proterozoic cratonic elements overlain by cretaceous of recent platform sediments and lies between the E-W trending Himalayas and N-S trending Arakan-yoma tertiary mobile belts developed as consequence of collision between Indian and Eurasian plates towards north and subduction of Indian plate below Burmese plate, in the east respectively. As a result of these earth movements the plateau has come to be sandwiched between important regional structural elements. Of these, the most important structural element which controls the southern boundary of the plateau is the Dauki fault.

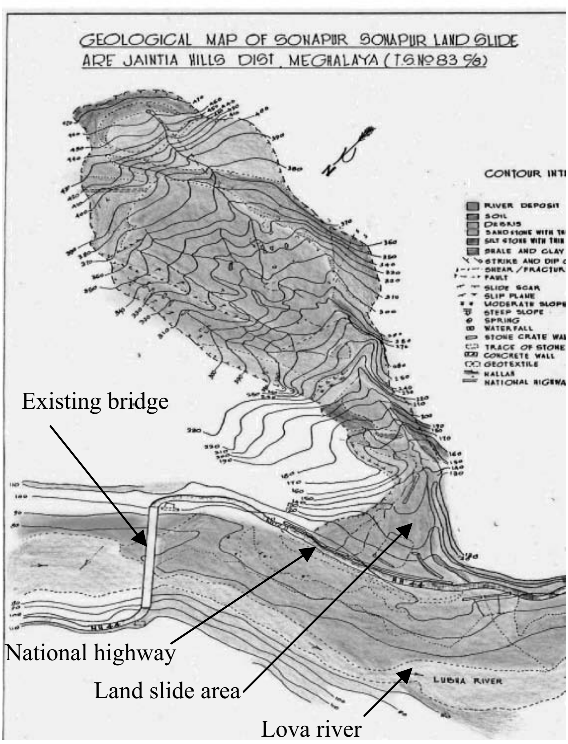

Figure 1. Geological Map of Sonapur landslide area

2.1. *Landslide zone*

The length of the slide zone is 120 m and height of the sliding hill is 370 m above the road level. The slide zone is drained by a spring channel with a natural drainage network developed over the years in this zone. The slide zone is characterized by a dendrite drainage pattern of medium intensity. The spring channel is almost a straight course with deep undercutting. Seepage points are observed at RL 320 m and RL 270 m above the road level. The deep gorges have been formed between RL 160 m and 210 m due to deep under cutting. At RL 190 m the drainage channel is blocked by two huge rock masses and incising deep cut at lower portion. The debris was composed of heterogeneous material of shale, Silt stone and stone of varying sizes ranging from clay to boulder. In the region above RL 280 m the debris was mainly composed of clay and earth except a few blocks of a sand stone. From bottleneck portion of 190 m down to the riverbed the debris accumulation was more and the composition of debris was 60% earth and 40% boulders.

3 CAUSES OF LANDSLIDE

The main causes of Sonapur land slide are weak geological formation, slope instability, discontinuous pattern of joints, fractures and faults, steep slope of the hill and very heavy rainfall. The first time this slide got activated in 1988 monsoon after 1987 Cachar earthquake. The sliding zone was increased in size because of prolonged and heavy rainfall in the subsequent years. The rain water along the faults in rocks aggravated the situation by inducing rock slides coupled with sliding of overlying soil. Intermittent shale layers were the other sources of instability, since the shale is very hard in dry condition but flows like a fluid in submerged condition. Thus, rainfall intensity and cumulative rainfall are the most relevant factors for inducing landslide problem at Sonapur. A detailed study/analysis reveals that rainfall in excess of 1000 mm in a particular month triggers the landslide. The cumulative annual rainfall at the landslide varies between 4000 to 6000 mm. Table 1 shows the rainfall data over the last seven years (Rao, 2008).

Table 1. Record of past rainfall

Year	Total Rainfall in mm	Highest Rainfall in a particular month during monsoon in mm
2002	6564	1531
2003	5000	1273
2004	7490	2458
2005	4974	969
2006	4188	1519
2007	4860	1027
2008	4487	1312

Figure 2 shows a picture on clearance of debris after a landslide. Figure 3 shows the size of a stone rolled down from the hill top.

Figure 2 Clearance the debris flow at land slide

Figure 3. Clearing a massive stone from the land slide area

4. MANAGEMENT OF THE PROBLEM

For the last 20 years, the only method to tackle the problem was to deploy Bulldozer/ Excavator during every monsoon, to keep the line of communication through. A task force used to be deployed at the site to meet the eventualities. It is estimated that around Rs 2.00 crores ($ 0.40 million) was the national loss for the road blockage per day in addition to immeasurable human sufferings. In one occasion, the road was blocked for nearly thirty days because of a huge landslide.

5. SOLUTION TO THE PROBLEM

The solution to the problem should meet two criteria – (1) to overcome the problem and (2) to maintain the traffic flow. The option for an alternate route or a tunnel through the hills was rejected because of high cost. Construction of a cut and cover tunnel appeared to be the most promising one. However, the concept of the cut and cover tunnel is totally new in the road construction industry in India particularly in an area of heavy rainfall and high seismic risk. However, the first author of this paper took a bold step to initialize the implementation of the concept. An outline of the tunnel was framed out and the proposed dimensions are shown in table 2. A typical cross section of the finished structure is also shown in figure 4.

Table 2 Dimension of the proposed tunnel

Length	123 m
Width	8 m
Height	9 m
Thickness of all members	0.80 m

It was also proposed to provide an earth cushion of 5.0 m at the crown of the tunnel to absorb the impact of sliding boulders.

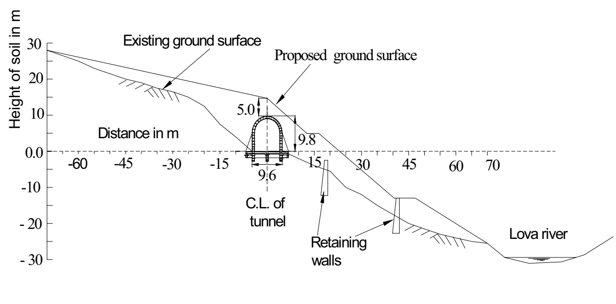

Figure 4. Typical cross section of the proposed structure

6. DESIGN METHODOLOGY

The structure of a cut and cover tunnel consists of four elements for a satisfactory design (Koveri and Tisa, 1998)

1. The original ground
2. The tunnel arch
3. The lateral backfill and
4. The backfill above the tunnel roof.

The geotechnical investigation of the site was conducted to ascertain the properties of soil. The geotechnical study is immensely important as, it evaluates the fundamental inputs for the all relevant data/in formations needed to design the structure. Based upon in-situ and laboratory tests, it was observed that the finer portion of the top soil has the following properties :

$c = 20$ kPa , $\phi = 8^0$, $\gamma = 15$ kN/m^3

% of sand = 10, % of silt = 40 and % of clay = 50;

The tunnel was designed against a lateral load due to backfill given by Eq. (1)

$$p_h = \gamma\, h \cot^2\alpha - 2c \cot\alpha \qquad (1)$$

where, γ, unit weight of soil, h, height of the soil column and $\alpha = 45^0 + \phi/2$.

The height h was increased step wise with an increment of 1.0 m and the earth pressure was calculated for each height. The structure as a whole was checked against sliding. However, to be on the safer side, three number of shear keys were provided below the tunnel bed and two numbers below the counterforts. 80 cm thick counterforts at 5.0 m c/c were constructed along the length of the tunnel to increase the resistance of the structure against flexure.

An overburden due to the backfill above the roof was considered in the design of the structure. The dead loads for static analysis consisted of weight of structure, earth cushion weight, live load with impact, additional loads on account of hydrostatic pressure, falling boulders from slide and earthquakes.. Calculation of stresses on the structure is performed by means of special finite element modeling allowing for full loading considerations at the full operation stages with worst combination of loads. The deformation pattern of the structure as obtained from the finite element analysis is shown in Figure 5. The maximum pressure intensity at the base was found to be around 170 kN/m^2. It was proposed that the top back fill would be placed in layers with light compaction so that the shear strength of the backfill will be more than the values of the debris. It was assumed that the improved properties of the lightly compacted backfill will be as follows :

$c = 50$ kPa , $\phi = 30^0$, $\gamma = 18$ kN/m^3 .

With the above values the stability of the final slope as shown in Figure 4 was checked and found O.K.

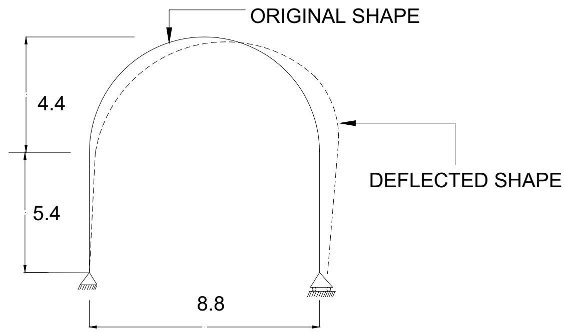

Figure 5. Deformation pattern of the tunnel section

In this the slope stability was checked against potential failure and required support measure designed, in order to satisfy two criteria for any successful open cut stability i.e. adequate factor of safety and controlled creep deformation. Lateral yield would cause ground movement around the cut and would evidently increase the sliding risk The analysis was carried out in plain strain conditions.

It can be seen that the structure is not a standard one, because of site requirements. During the design work it was also kept in mind that the working period in the said site is only six to seven months, because of long monsoon period in Meghalaya state. For construction of the arch roof a proper gantry was designed on rail sections. With the above studies, deliberation and site specific requirements the final section is shown in Figure 6 and the salient features were given in table - 2.

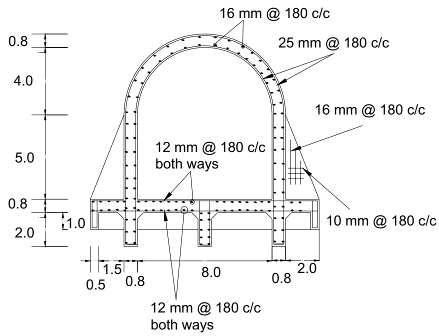

Figure 6. Typical cross section of the proposed cut and cover tunnel

It was decided to keep 5 m earth cushion above the crown of the tunnel for absorbing the impact of falling boulders.

7. CONSTRUCTION PHASE AND PROBLEMS FACED

The Administrative approval from Government received in Dec 2006 for a sum of Rs 11.80 Crores ($ 2.5 million) for construction of this tunnel and allied structures. The work was commenced in the first week of January 2008 by creating space by cutting the hill side. A traffic diversion was first created in the down-stream side of the proposed site to pass the existing traffic. During laying of the foundation it was observed that the foundation soil consisted of fully saturated very soft muck. The thickness of this muck was found to be around 1.0m. Since the foundation could not be laid over this very soft muck, two alternatives were considered (1) to replace the muck with good soil (2) to construct piles. The first alternative was found to be cheap and workable and was adopted. The entire muck strata of 20 m wide and 3 m depth was thereby removed and the excavation was filled with granular river bed materials. Compaction of the fill-up materials was carried out in layers with a vibratory road roller. After the compaction, the bearing capacity was checked with a plate load test and found to be more than 200 kN/m^2 . A layer of 25 – 30 cm size boulder soling was laid over the finished surface over which 200 mm thick lean concrete was laid. This treatment was found to be quite effective in other areas of road construction. The five number shear keys were then constructed and the same were connected laterally with a diaphragm at 10 m centre to centre to improve the structural rigidity of the base further. Thickness of the base slab was 80 cm and haunches were provided below the 80 cm thick vertical wall. Additional longitudinal reinforcements were provided at junctions between the base slab and wall and between the wall and the top arch.

For constructing the arch, one gantry of 5.0 m long was fabricated at the site. When one gantry was found to be effective, one more gantry was fabricated so that the construction activity was started from the two ends. This expedited the construction activity and the entire arch was completed by one working season i.e. within three months. In order to discharge water from the spring channel a multi cell box cell culvert of 6 m X 6m with 3 No of cells constructed. The size of 6 m was adopted as at times, the muck flow also come along with water and in order clear debris sufficient size of cell is most suitable. In order to have a proper riding quality either side of tunnel the rigid pavement of 100 m on were provided near the entry and exit ends of the tunnel. Sufficient number of weep holes were provided in the vertical portion of the tunnel wall to drain out the water trapped in the earth fill in the up-stream side of the tunnel.
The schematic drawing of 5 m wide gantry is given in Figures 7 and 8..

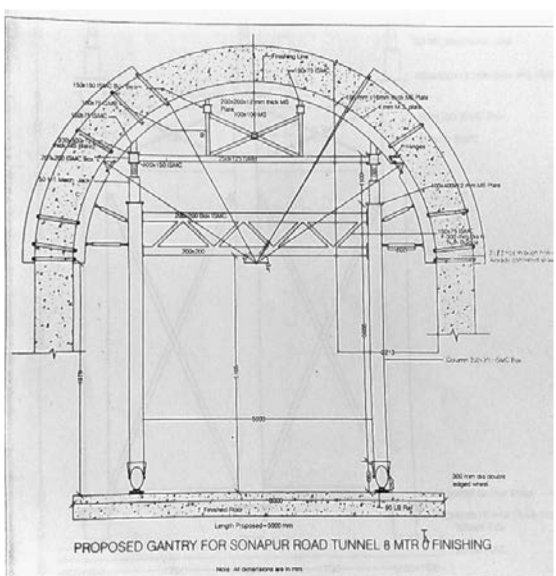

Figure 7. Details of the gantry

Figure 8. Photograph of the gantry

Once the gantry was erected the casting of segment started in April second week with both the gantries. From May to August 2008 the roof segments were completed and in the month of September 2008 both the portals were also completed. Meanwhile the monsoon also began in month of May 2008, and the completed structure became vulnerable to the active land slide. An open space about 15 m wide was created between the structure and the hill so that the falling boulders do not directly hit the tunnel structure. The idea worked very well and the whole of muck and debris evolved during the monsoon period got deposited in the space. The main tunnel structure completed in Sept 2008 and same got inaugurated and tunnel was opened for the traffic on 29 Sept 2008 (Fig -9).

Figure 9 Complete view of the tunnel

Figure 10 shows the front view of the tunnel.

Figure 10 Front view of the tunnel.

8. PRESENT PERFORMANCE

The use of instrumentation is an essential part of any construction activity now a days. Geotechnical instrumentation is different from any other type of instrumentation in that it needs a comprehensive and complete inter action between the designer, the user and the instrument supplier. Proper installation of the geotechnical instrument is also important because once the instrument is embedded, it cannot be taken out. If an instrument has failed after installation, it cannot be replaced. In order to carry out a proper study on the post construction behavior of a tunnel structure, monitoring of the instruments is also necessary. . Some of the instruments are precise levelling (PLP) arrays, combined inclinometer/extensometer, Probe extensometer, Strain gauges, etc.

In the present work the instrumentation part could not be completed till reporting of this paper. However one settlement gauge was installed at the base of the tunnel near the hill side at the middle of the length. Figure 11 shows the settlement of the foundation. The details of the instrumentations and their data records will be published in near future.

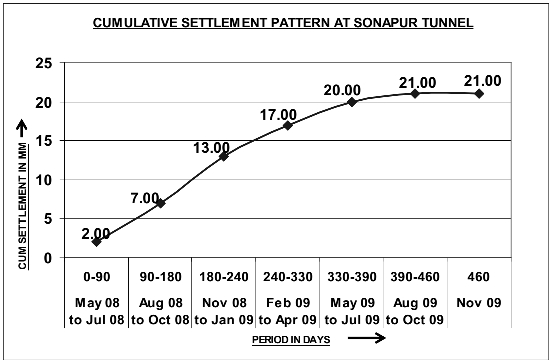

Figure 11 Settlement of the foundation

9. CONCLUSIONS

The economic tunneling with RCC cut & cover structure constructed across an active land slide has permanently solved one of the major trouble spots on very important highway and provided a great relief to 15 million populations to a developing country like India. The completion cost of the tunnel with other allied structure was Rs 14 Crores ($ 2.9Millon). This innovative approach has led the way to solve the hundreds of such active landslides in Indian Himalayas where stable base is available. This approach will go in a long way for sustainable development of underdeveloped hilly region in the Northeast part of India.

10.. REFERENCES

Kovari, K. & Tisa, A. 1998. Computatiional model and charts for cut and cover tunnels. *International Association for bridge and structural engineering Colloquium Tunnel Structures.* June 4–6 Stockholm, Sweden

Rao, K. S. 2008. Interim Report on site specific studies of Sonapur landslide Jaintia hill District ,Meghalaya (T.S. NO.83 C/8).

Remediation of Man-Induced Hillside Slide

Z. Smiljkovic, PE PM ASCE, V. Dubljevic, PE, A. Balatov, PE
IK Consulting Engineers, Belgrade, Serbia,

ABSTRACT: Reljici Pumping Plant construction complex was faced with sliding of hillside stretch extending uphill from the open cut dug for structures foundation. The landslide escalated in autumn of 2008 and lengthened throughout the winter of 2008/09. The Consultant had to design the remedial measures and to back those with appropriate design models, emulating the landslide mechanism and the effects of retaining structure. That was an endeavor of the Consultant to cope with an issue associated with unknowns and variables overwhelming the available design inputs. Contractors' determination to be more prudent while cutting and protecting the hill slopes in similar project conditions is one of the main messages of the article. The benefits are being, the dispute avoidance and improvement of risk sharing mechanism between the parties concerned, both contributing to smooth projects implementation.

1. INTRODUCTION

Reljici Pumping Plant is one of the key components of Montenegro Domestic Water Supply System. The 7000 cum reservoir of treated water, the pumping station and finally the control building were designed to be the main operation units of the Plant. The two outgoing uphill steel pipes, 800mm in dia each, are conveying the treated water up to the balancing reservoir, wherefrom the water supply of Montenegro on shore cities is achieved by gravity. Construction of the Plant commenced in 2008 and is still on. By October 2008, the treated water reservoir was completed, while the remaining two units remained still to be constructed.

An open cut 40.0 m x 40.0 m covering the area of the Plant's Units structures was excavated in 2008. Under the effects of 2008/2009 winter precipitations, a stretch of uphill side of circa 32 m by 30 m subsided then collapsed, escalating to suite of succeeding slides towards the treated water reservoir. The *Figure 1* hereafter illustrates schematic presentation of the Plant's structures, the landslide extension inclusive.

2. GEOLOGICAL BACKGROUND

Here, the Consultant's approach to establish phenomenological factors affecting hillside triggering process, was governing. To this effect, additional field and laboratory exploratory works were programmed aiming to define the soil properties, the phreatic surface fluctuation and the potential landslide pattern. Land survey of unstable hillside zone was considered as well. The exploratory works were completed towards the end of summer of 2009.

Field investigations were optimized to three exploratory boreholes, 10m in depth each, including core recovery and geological mapping of core samples. The boreholes were located in the area of the landslide toe, at its crest and midspan of hillside sliding mass. Towards the groundwater monitoring, the boreholes were assigned the piezometric role too. Besides, the selected samples were subjected to lab tests, comprising – volumetric weight and moisture content, then modulus of deformability, Poisson ratio, shear strength parameters, grain composition and plasticity index.

The additional exploratory works featured four geological horizons, all moderately dipping towards the hillside bottom, and which were characterized to be: (i) sub-surface stratum of clayey debris, to the depth of 1.8 to 3.6 m, (ii) the weathered flysch stratum underlying the clay debris, 1.5 to 2.4 m in thickness, (iii) the saturated brown clay, and finally (iv) the compact flysch which extends therefrom downward. In regard the strata composition and their mechanical properties, those were characterized to be of homogenous structure and of isotropic behavior at their depths.

The table 1 illustrates full *'as evaluated'* characterization of soil and rock mass parameters.

In summary, the soils and rock masses building up the hillside geotechnical structure were appraised to be medium plastic, low-permeable, then poorly to fairly structured media, strength wise. Under the implications adopted herein before and after, the clayey debris and saturated clay were deemed to be the '*soil-like'* rock mass while flysch formation was defined to be the '*rock mass'*.

Groundwater table monitoring had proved the phreatic surface being fluctuating. The fluctuations ranged from of 2.5 to 6.35 m in depth and from 0.65 to 8.0 m, referring to the crest and to the toe of landslide, respectively. The vadose zone fluctuated correspondingly, ranging from a shallow to relatively deep one, always succeeding the alternation of dry and wet annual seasons.

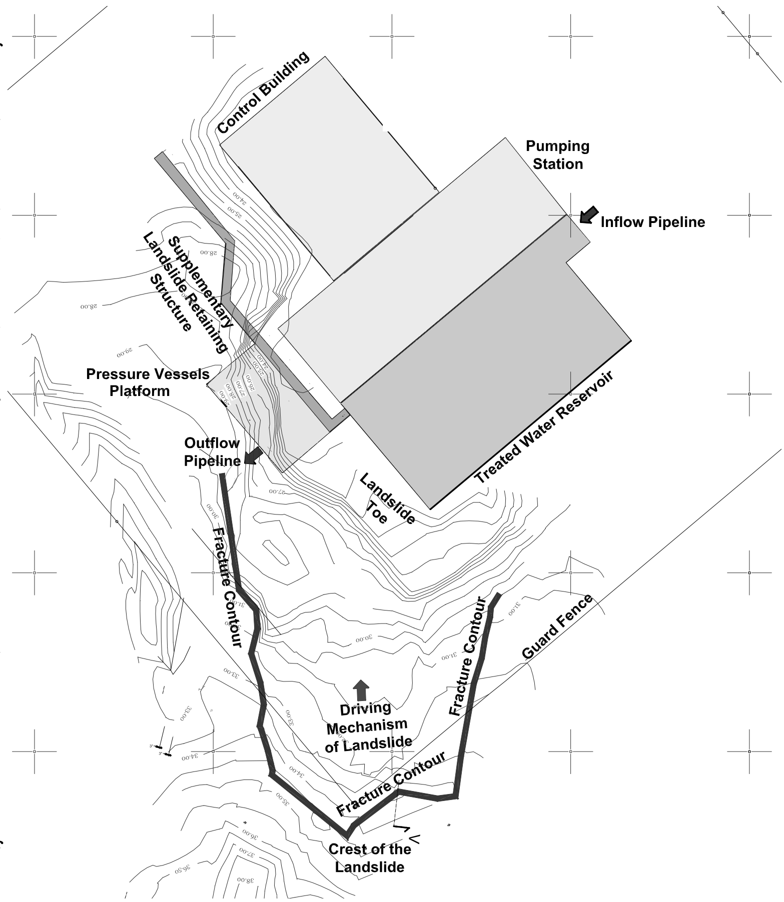

Figure 1*: Schematic presentation of Plant's structures and landslide expanse*

Description	I Clayey Debris	II Weathered Flysch	III Saturated Clay	IV Compact Flysch
Plasticity Index	Medium-Plasticity Soil PI =30-50	Not applicable, it is classified to be rock mass	Medium-Plasticity Soil PI =30-50	Not applicable, it is classified to be rock mass
Grains Distribution	Silty fractions predominantly, followed by sandy and clayey fractions. Concluded on soil grins classification, which goes:: Clay < 0.002 mm, Silt 0.002 – 0.06 mm, Sand 0.06 – 2.0 mm			
Volumetric Weight (kN/m^3)	20.5	18.0	22.0	23.0
Modulus of Deformability (MPa)	10.0	7.5	8.0	420.0
Poisson Ratio	0.40	0.37	0.40	0.34
Cohesion (kN/m^2), Peak/Residual	27.0/10.0	30.0/12.0	13.0/5.0	100.0/70.0
Angle of Internal Friction, Peak/Residual	25/20 Degrees	20/17 Degrees	27/22 Degrees	45/40 Degrees
Hydraulic Conductivity (m/s)	$4x10^{-7}$ Soil of low permeability	$4x10^{-8}$ Rock Mass of very low permeability	$3x10^{-7}$ Soil of low permeability	10^{-8} Rock Mass of very low permeability

Table 1: Soils characterization along the stratification column of the hillside deposits and rock mass

It was concluded that the ground water generation was originated by the rainfalls intruding downward through the soil fissures or by recharging the permeable slacks of mountain side extending above the landslide crest. The groundwater oozing downhill throughout low permeable medium with variable boundary alias phreatic surface was termed to be a shallow unconfined flow domain. Under *in situ* original ground conditions preceding construction of the Plant, the foregoing closely corresponds to steady underground flow regime, which promoted the piezometric lines to be the fundamental inputs for design models of the landslide remedial measures.

3. EVOLUTION OF FAILURE MECHANISM AFFECTING HILLSIDE INSTABILITY

While by its induction, the landslide discussed herein can be termed as the '*man induced*', by its nature, the slide was derived to be an exogenetic process. Here it is worth highlighting, the landslide genesis which had been originated during construction stage of the Plant, following the abstraction of a volume of rock mass in order to accommodate the Plant's structures. To this effect, four stages of hillside behavior appeared to be distinctive in view of evolution of its failure mechanism.

Stage A**: **Original Slope Conditions

The succeeding draft (*Figure 3*) illustrates the fundamental geological and geomorphological features of a section of hillside, the bottom part of which was acquired for Plant's construction. Yet, pre-tender site reconnaissance and field investigations of the Plant's area, did not foreshadow the potentials of hillside instabilities, the groundwater induced erosive processes, or whatsoever. Owing to that, the Plant's site was found suitable for construction purposes.

Stage B: Excavation of open cut for construction of the Plant

Once the hillside was undercut, the *in situ* stress conditions had been disturbed. While passing from primary to secondary stress states, i.e. from *in situ* to an engineered hill slope state, the normal and shear componential stresses along the cut perimetric zones take the decreasing and increasing trends, respectively. In geotechnical engineering, such slope stress conditions are often aligned with so called '*stress release*' phenomenon. In case of Reljici open cut slope, the $\boldsymbol{\sigma_1}$ exhibited a change from 140 kPa to 3 kPa, the $\boldsymbol{\sigma_3}$ from 60 kPa to – 93 kPa, and $\boldsymbol{\tau}_{xy}$ from 0.0 kPa to 45 kPa, always referring to *in situ* and engineered slope conditions respectively.

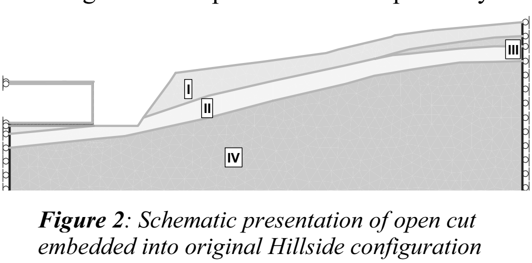

***Figure 2**: Schematic presentation of open cut embedded into original Hillside configuration*

The cracking of clay debris and weathered strata, both remaining to zones of stress release was the ending outcome of the secondary stress conditions of hillside section affected by open cut. The reduction of shear strength and modulus of deformability of the soil material had occurred as concomitant effects as well.

Stage C: Precipitation Impacts

Once the rainfall season of 2008/09 had come forth, the hillside area being subjected to secondary porosity induced by *in situ* stress release, had increased its absorbing potential. Then, the consequential augmenting of water ingress had diminished vadose zone and simultaneously had amplified the seepage pressures. Initial seepage pattern of affected hillside area had been thereby considerably changed, causing thus weakening of soil intergranular forces and declining in effective stresses.

Stage D: Fracturing of Soil and Hillside Slope Collapsing

Once the balance of slide driving force and slide resisting force has been changed in favour of the former one, the slide process became triggered. Whilst the increased seepage pressure exhibiting throughout rainy season had intrinsically challenged driving force to pyramid, the softening of clayey debris stratum and partially the weathered flysch due to water ingress had aggravated the shear strength potential of the strata. In consequence of the latter, the hillside resisting force decreased. Such a landslide kinematics had additionally been favoured by moistening the transition layer in between the clayey debris and weathered flysch, which then became slipping, exercising the role similar to that of slickenside in a fault plane. On balance, the transition layer in between the two strata was suspected to coincide to sliding surface. The first hillside instability occurred towards the end of October 2008, while a number of slide momentums ensued thereupon, all succeeding the heavy rainfalls in the area.

4. CONCEPT OF LANDSLIDE REMEDIATION MECHANISM

Remediation mechanism embraced substantially the measures, (i) restoring the hillside resisting force closely to its original magnitude, and (ii) these, demobilizing the slide driving force to value which is well inferior to that of resisting one. In order to achieve those, the measures permanently stabilizing the unstable slope, were extended to: (i) control of surface water influx to the slide such that to cut off its infiltration to crumbled soil mass, (ii) underground water, i.e.

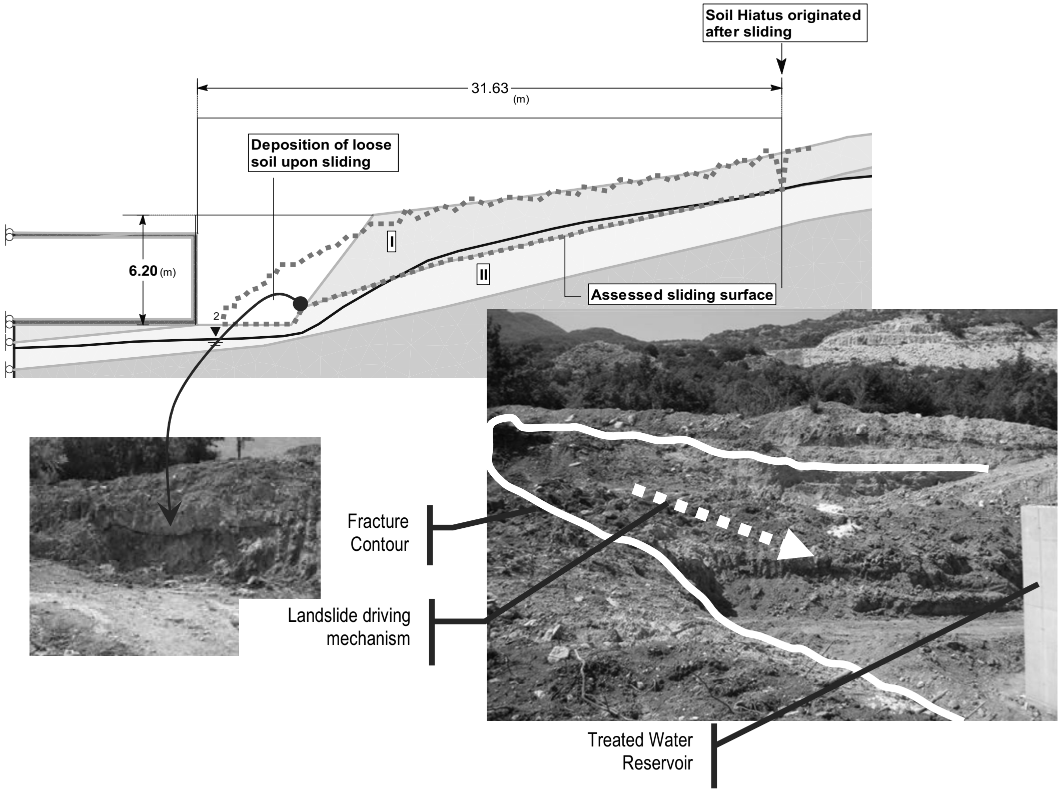

***Figure 3**: Stage D- Illustration of Landslide Failure Pattern*

its phreatic surface control, (iii) provision of suitable structural retention aiming to receive the residual pressures of sliding mass, and (iv) surface flattening and forestation covering the slide area, its fringe towards stable soil inclusive.

A perimetric drainage ditch encompassing sliding body beyond its fracture line has been intended to intercept the downhill precipitation loads and to convey those to nearby brook. The depths of the ditch extended down to clayey debris stratum but up to the elevations under-topping the uppermost phreatic surface. The ditch drainage structure consisted of: polyethylene sheet installed at its downhill wall; the geotextile, lining the overall excavation contour of the ditch; and the gravelly filter infill. Figure 4 herein is self explanatory to the effect. The surface water runoff into sliding body had thereby been considerably alleviated, which in turn inhibited building up of seepage forces and softening of clayey strength. While the polyethylene membrane was assigned the seepage barrier role, the geotextile sheet was intended

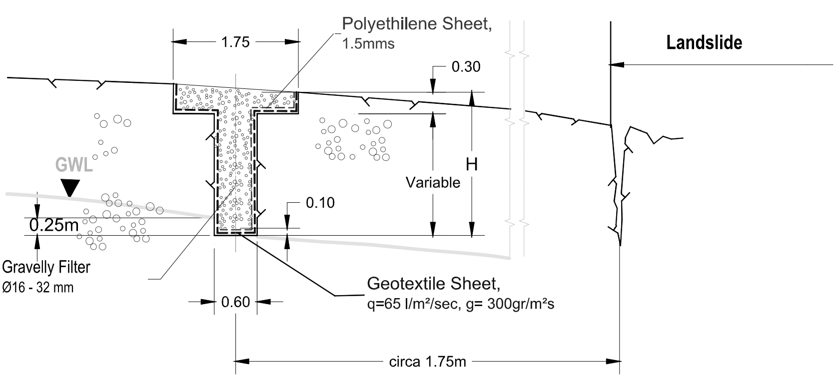

***Figure 4**: Perimetric drainage ditch encompassing sliding body*

to mitigate the soil erosion and to hinder plugging of filter's infill. Besides, a surface rainfall water gutter topping the backfill deposition and facing the retaining structures was foreseen, too.

extending towards the pumping station, beyond the reservoir width, an additional reinforced concrete retaining wall was found as a reasonable solution. Besides its retaining function, the use of the wall extended to accommodation of the platform for pressure vessels, the facilities that were to be installed to damping the potential surge pressures expected to occur incidentally at the pumping main of the water supply system.

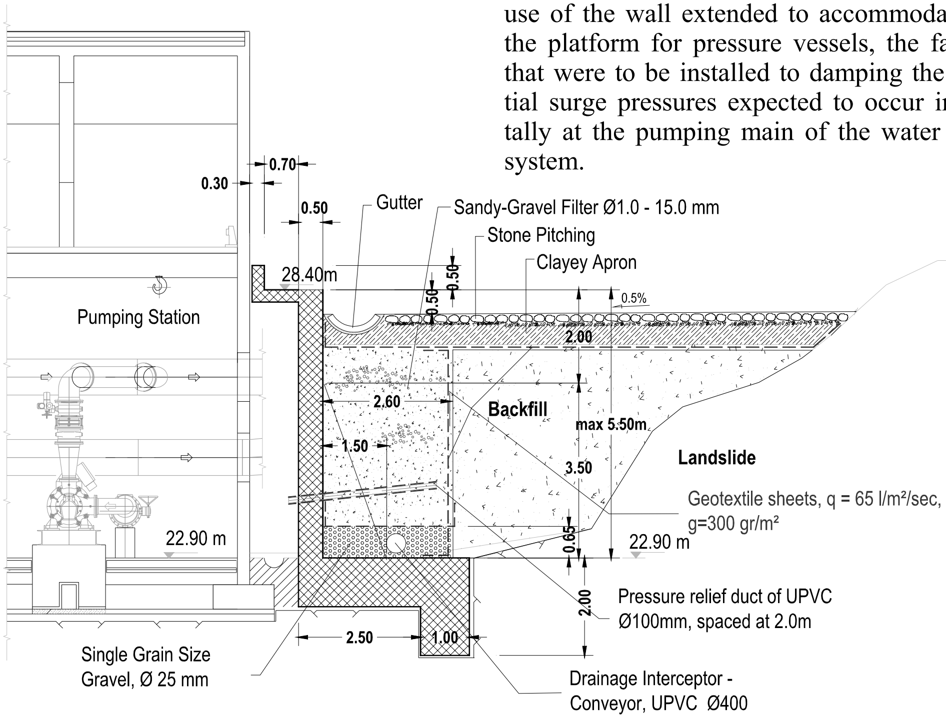

Figure 5:*RC Gravity Retaining Wall with counterforts spaced at circa 5.0m*

The toe drainage interceptor in conjunction with perimetric drainage ditch served the groundwater seepage control, and specifically, the control of saturated zone fluctuation, the upper boundary of which should not enter the suspected sliding surface. The clayey debris stratum and partially that of weathered flysch, should thereby be freed from strength weakening and the building up of pore pressures. Increase of resisting force of the hillside was to be the ending contribution of the toe drainage collector. The UPVC perforated drain Φ400mm the surrounding single grain size gravelly infill of 25mm, then both over-lined with sandy - gravel filter of Φ 1.0 -15.0 mm, the hydraulic conductivity of which considerably overcomes the surrounding backfill, served as gravity groundwater collector and the conveyor. By their controlling of water table, they relieve the retaining structures from high hydrostatic pressures, which in turn contribute to cost effectiveness of the structures.

While considering the landslide retention option, it was found viable to use the existing reservoir of treated water. For the landslide toe

The adopted retaining options coupled with backfill seating behind should have secured gravity support for potential post-construction slide pressures. The landslide resisting force had to be further reinforced thereby. The project design studies have proved the existing reservoir to be suitable framework for sustaining post-remediation slide pressures.

Planting of surface layer of clayey debris was intended to strengthen its structure against desiccation following fissures expansion. This directly led to reduction of water ingress and to barring the development of seepage pressures. Forestation of hillside area with aspen tree was ultimately adopted as a suitable solution.

5. DESIGN MODEL OF LANDSLIDE REMEDIAL MECHANISM

A 2-D plain strain model merged with that of 2-D shallow unconfined flow domain was used to simulate numerically the state of the hillside at which the landslide process triggers. By a general code of practice, the approach had to quantify the state after which the hillside did not longer perform its presumed function and had commenced to slide. The latter is defined to be the ultimate limit state of the hillside which was undercut for construction of the Plant. Besides, the RocScience, Phase 2/V6 software package supported by Coulomb-Mohr failure criterion, was employed to perform strain-stress analysis of hillside section affected by instabilities, and following the remedial measures, the analysis of retaining structure – rock foundation- sliding mass, compound system. The latter was also defined to be the coupled computation model. As for the constitutive behaviour of the system, the analysis extended to elasticity and plasticity domains, by contemporaneous considering as homogenous and isotropic the strata of geological horizons I, II, III and IV.

That was eventually taken as '*maximum design earthquake*' generally pursuant to ICOLD Guidelines for large dams (1989).

Pseudo-static earthquake loading featured through method of Seismic Coefficient was utilized for stability analysis of Retention – Rock – Landslide compound system. There, the additional horizontal body force alias inertial mass force, assignable to each material element of the coupled model was applied.

5.1. Emulation of Landslide triggering process

Given unfaulty structure of hillside strata, the rock mass medium was modeled as continuous assemblage of the strata resulting to continuous element model method. The model was found

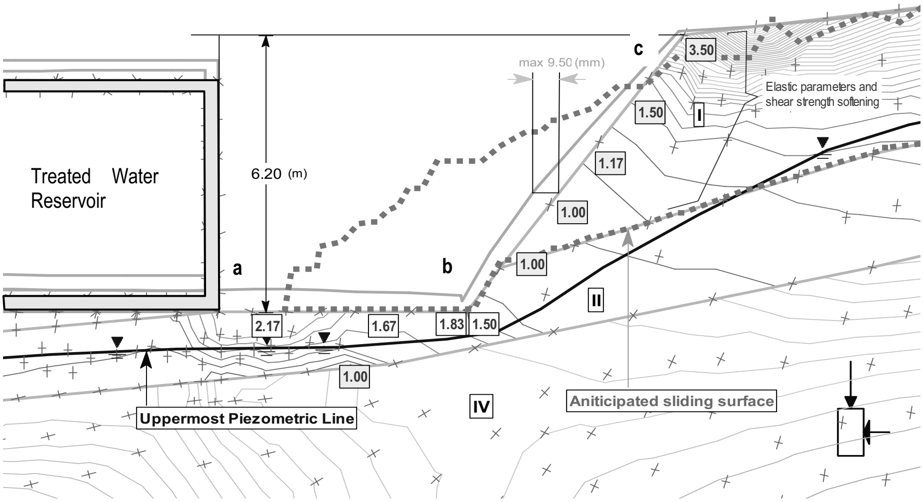

Figure 6*: Strength factors, deformation line and total secondary field stress featuring static conditions of toe area of landslide, while softening of material parameters of horizon I to 65% of their initial values*

A predefined free flow surface inputted as piezometric line was implemented as boundary condition too.

The gravity field stress with ratio of 0.5 of horizontal to vertical stress component was adopted to feature *in situ* stress conditions, governing across the strata depths. In addition, the seismic map of Republic of Montenegro was taken as a basis for seismic risk assessment the compound system could be exposed to. A conclusion was inferred therefrom, the system may undergo the seismic hazard of intensity 9 according to MMI, the probability of which extends to 500 years return period. Besides, the event specific earthquake effects gauged whilst 1970 earthquake impacting Montenegro Region, had foreshadowed the susceptibility of Reljici Plant site to peak ground acceleration of 0.2g.

suitable to emulate the hillside bahaviour beginning at its virgin state, through the state of undercutting, until the state of collapse. Yet, its applicability appeared appropriate for analysis of interactive process generation in the Retention – Rock – Sliding Mass compound model. Among the Gravity Load amplification and the Material Strength Reduction methods for slope stability analysis, the authors inclined to the latter one. The preference prevailed due to the fact of seepage induced weakening of the clayey debris strength, the stratum which eventually collapsed *in situ*. There, the shear strength parameters and the elastic parameters of stratum **I** were gradually downgraded until the model has become numerically unstable. No-convergence of the model was taken as suitable indicator of the slope failure i.e. the slide process triggering.

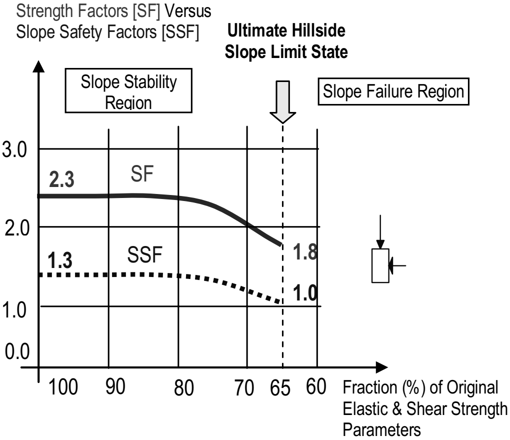

Figure** 7: Strength Factors versus Slope Stability Factors across the region of strength softening of stratum **I

The initial, interim and limit states of undercut hillside behaviour were observed by means of the strength factor magnitudes [SF] featuring each particular stress-strains increment of material reduction process. There, the model fringe designated along the a-b-c perimeter (*Figure 6*), was particularly distinctive whereas, the associated strength factors decreasing trend, had indicated the state of numerical instability of the model, which was concurrently aligned with failure kick-off of *in situ* slope physical model. Hence, the related set of strength factors trending to unity, has lined off the region of the element model which then became relevant for observing its numerical tendency.

Whilst subjected to field **I** strength softening, the SF set mean values of the model fringe a-b-c exhibited the variation from 2.36 to 1.80, corresponding to 100% and the 65% of original rock mass parameters respectively. There, the point of SF_{mv} = 1.80 (*Figure 7*), has defined the boundary whereupon the landslide triggering process is to be expected, i.e. the boundary of the two regions of model behaviour.

From geotechnical point of view, the point of SF_{mv} = 1.80 was assigned the meaning of ultimate hillside slope limit state. Figure 7 herein is self-explanatory to the effect. Coincidentally, the undercut Slope Safety Factor (SSF) was reaching the value of 1.30, which was appraised to be satisfactory, under proviso of having installed the appropriate slope protection measures in the first instance.

5.2. Stability Analysis of Retention-Rock Foundation- Sliding Mass Compound System

Unlike the conventional approach based on safety factors mechanism (sliding, overturning, floatation), a coupled '*soil-structure*' interaction model was taken as a medium for examination of stability of unique system. Its global stability is basically grounded on the ratios of rock strength and the induced stress, theoretically defined as strength factors. In case of plasticity domains, the instability of coupled model is taking place once the strength factors ($S_{max} \geq 1.0$) are approaching to unity. In principle, (i) the model exhibiting equilibrium at each distinct point of its domain, and (ii) the tolerable Retention deformation keeping Retention function serviceable, were two basic criteria for reckoning on whether the compound structure is considered stable or not.

Concretely, the strength factors output remaining both to static-unsoftening (*Figure 8*) and pseudo -static-softening conditions (*Figure 9*), has substantiated the stability of compound structural system. The latter being coincident with ultimate limit state of unprotected hillside slope, whereupon the landslide process starts triggering, meaning that the retaining wall has

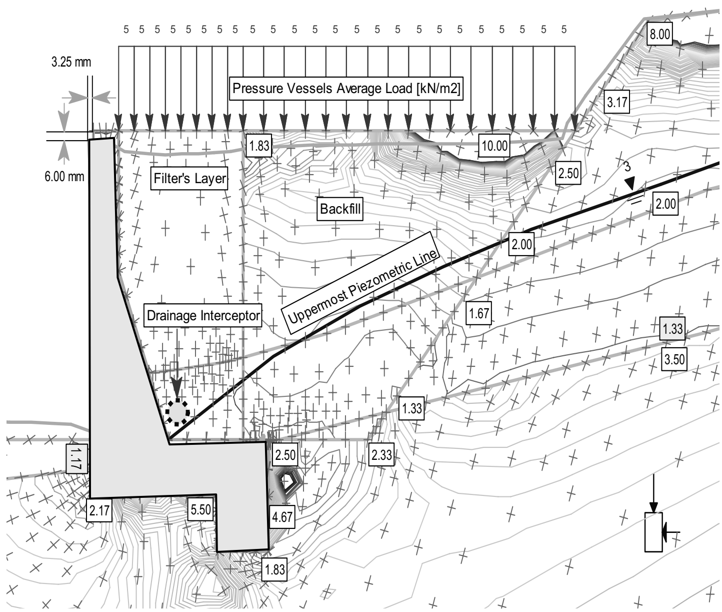

***Figure** 8: SFactors, deformation line and total stress field characterizing the static conditions and original strength parameters of coupled model* exercised its supporting role. There, the minimum values of strength factors ranged from 1.33 to 1.17. Yet, the convergence of coupled model warranted the stability of *in situ* physical structure. It goes without saying, that the concrete component became irrelevant in view of promoting the strength failure mechanism there through.

Serviceability of retaining wall wise, the maximum horizontal displacement of its crest, extended from 3.25mm (*Figure 8* – static unsoftening conditions) to 22.5mm (*Figure 9* – pseudo-static earthquake conditions softened for 35%). Here it is worth noting the earthquake-softening conditions (*Figure 9*), which imposed circa 7 times higher peak displacement comparing to that of static ones.

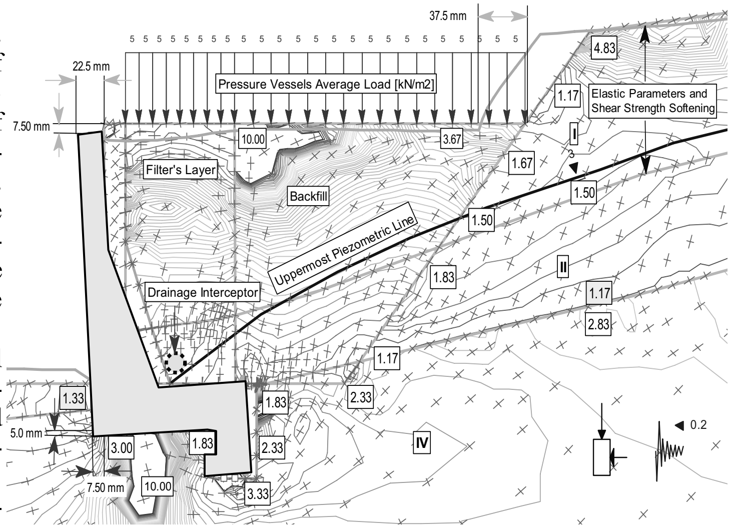

Figure 9*: SFactors, deformation line and total stress field characterizing the pseudo-static earthquake conditions and the reduced for 35% the strength parameters of coupled model*

Again, in relation to wall height (H=6.6 m), the displacements were taking the fractions of 1/2030 of H and 1/290 of H respectively, which was estimated to be still serviceable as regard the structure's purpose.

In conclusion, both geotechnical and serviceability aspects of coupled model, have proved the compound structure being serviceable to the purpose of reinforcing the landslide resisting force.

5.3. Proportioning of Concrete Retaining Wall – ASD versus LSD

Once the '*soil-structure*' interaction model was applied, the Limit State Design (LSD) appropriated nowadays to concrete structures analysis, became of limited effect. Under the specific circumstances, that was because of the interacting status of design loads which used to accommodate to each particular strain increment. Hence, the concrete wall loads factorization appeared to be impractical. In addition, the failure or limit state mechanism used to propagate through rock mass but not across the concrete medium. And lastly, the point arose as to which factorization level the strengths of rock mass-concrete composite are to be associated with, then. All these have promoted the Allowable Stress Design (ASD) to take precedence over the Limit State Design (LSD) of Retaining Wall.

6. CONCLUSION

The article put in emphasis the compilation of seepage control and retention mechanisms, as a suitable framework for remediation of Reljici hillside slide pattern. In addition, it was demonstrated that '*solid-seepage*' and '*soil-structure*' coupled modeling of landslide triggering process and landslide retention mechanism could better feature their behaviour *in situ* in comparison to conventional approaches.

7. REFERENCES

Fu Hua Chen, P.E. Honorary Member ASCE, 1999. Soil Engineering. Testing, Design and Remediation. CRC Press. Boca Raton London New York Washington, D.C.

W. F. Chen, Editor in Chief, Purdue University, West Lafayette, Indiana, 1995. The Civil Engineering Handbook, CRC Press, Boca Raton New York London Tokyo.

Dennis E. Becker, *Eighteenth Canadian Geotechnical Colloquium:* Limit states design for foundations, Part I. An overview of the foundation design process.

Evert Hoek, Geotechnical Considerations in Tunnel Design and Contract Preparation. Tunneling '82 Symposium, Brighton, England.

Evert Hoek, Professor of Rock Mechanics, Imperial College, London & P. Londe, Technical Director, Coyone & Bellier, Paris. General Report for Third Congress of the International Society for Rock Mechanics. Denver, September 1974.

Tony Waltham BsC DIC PhD, Civil Engineering Department Nottingham Trent University City. SPON PRESS, London and New York. Foundations of Engineering Geology.

Respects regarding the analysis of the grounds setting stability by means of the Mohr-Coulomb egression criteria

Dan ZAROJANU
University of Suceava, ROMANIA

ABSTRACT: The paper takes into account the fact that the total of the points in limit equilibrium, limits a prism of unstable ground. There is considered the case of the distributed loads operating in a half-plan and the determination of the points is done by the help of the egression criterion „Mohr – Coulomb".

Results: The contour of the breaking surface could be a circular curve; The sight angle, because the ground characteristics, may have, sometimes, several values; that means there are several curves describing the contour of the breaking surface. In this situation the Mohr-Coulomb criterion is not enough. It must be completed with peculiar earth characteristics.

1. INTRODUCTION

The research presented has been done within research project DEGRATER – „The creation of a georeferenced database in Suceava plateau by monitoring the damaged soils on digital images, as a decision base in ecological improvement", within the PNCDI II program – Partnerships in Priortary Domains (no. 31047/2007).

Supposing that the points in ultimate equilibrium, in a ground charged by a distributed force describes the contour of the breaking surface, the problem consists in finding out these points using the Mohr-Coulomb criterion. That means to build the Mohr circle with the unit principal stresses as well as the Coulomb straight-line with the ground cohesion and the ground internal friction values. The next step is to impose the contingence of the Mohr circle and the Coulomb straight line.

In practical conditions, this is a common situation, mainly of the roads structures loaded by wheels charges, which can be simulated as a half-plane charged by a distributed load (*Fig.1*).

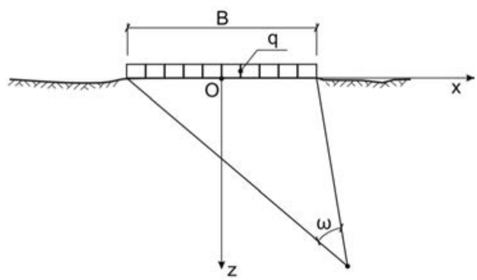

Figure 1. Half-plane charged by a distributed load

2. THE DETERMINATION OF THE UNIT PRINCIPAL STRESSES AND THE SIGHT ANGLE. THE ULTIMATE EQUILIBRIUM CONDITION

The form of principal unit stresses, is already known in case of a distributed charge on a half-plane (*Fig.1*):

$$\sigma_{1,2} = \frac{q}{\pi} \cdot (\omega \pm \sin \omega), \tag{1}$$

where $\sigma_{1,2}$ are the principal unit stresses, q is the distributed load and ω is the sight angle.

The ultimate Mohr–Coulomb equilibrium condition consists in the contingence between the Coulomb straight-line and the Mohr circle built with the stresses produced by the considered case charge (*Fig. 2*).

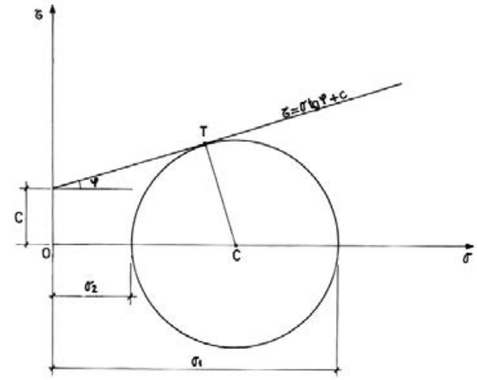

Figure 2. The Mohr – Coulomb ultimate equilibrium condition

In *Fig. 2* there are the folowing significations: φ - the internal friction angle of the ground; c – the cohesion of the ground; σ, τ - the unit compression stress and the unit shearing stress; Analytically, the contingence condition becomes:

$$\sin\omega\cdot\cos\varphi-\omega\cdot(1-\sin\omega)\cdot tg\varphi=\frac{c\cdot\pi}{q} \qquad (2)$$

The result of the equation (2) is the sight angle:

(cπ/q+cosφ)/[(1-sinφ)tgφ ≤ ω ≤ (cosφ-cπ/q)/[(1-sinφ)tgφ] (3)

There are presented two numerical examples of earth specific features and specific loads:

Example 1:
$c=0{,}6daN/cm^2$; $\varphi=25^0$; q= 100daN/m
There are 3 solutions:
ω = - 691,678 rad; ω = - 688,482 rad;
ω = -693,099 (Fig.3)

Example 2:
$c=0{,}5daN/cm^2$; $\varphi=33^0$; q=200daN/m
There is only a solution:
ω = - 260,439 rad

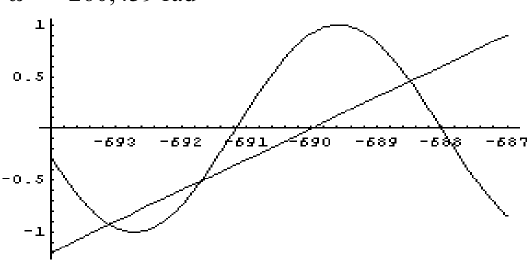

Figure 3. Example 1 case

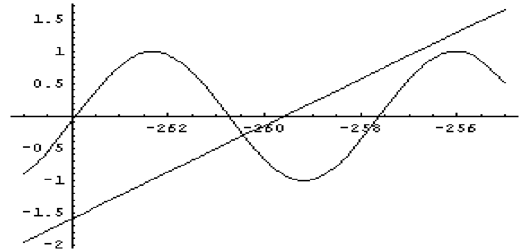

Figure 4. Example 2 case

In order to find out the breaking surface condition, one has to proceed as it follows:

It is already known that in case of a half-plane charged by a distributed load, the principal unit stresses paths (the isostatical curves) have the folowing shapes (Fig.5):

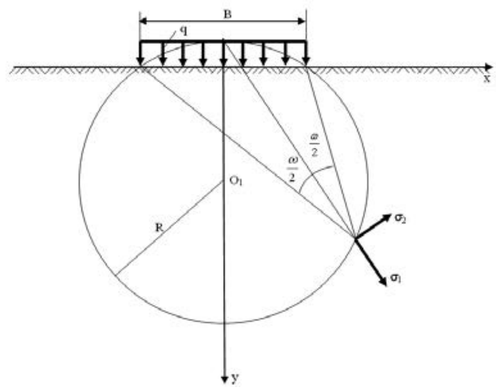

Figure 5. The isostatical curve of the unit principal stresses

That means that the principal stresses pairs that verify the Mohr-Coulomb criterion are on an isostatical curve, that is a circle whose radius must be found out.

The length *B* of the distributed charge is known, as well as the sight angle.

From the *Fig.*5 it could write:

$$\sin\omega=\frac{B}{2R} \qquad (4)$$

Because of (Eq. 2), it can obtain R – the radius of the curve that describes the contour of the breaking surface (the radius of the isostatical curve, where the values σ_1, σ_2 verify the Mohr – Coulomb criterion) and the sight angle being already found out as it was shown upon.

From (Eq. 2):

$$R=\frac{B}{2\omega(1-\sin\varphi)\cdot\frac{\sin\varphi}{\cos^{2}\varphi}+\frac{2c\cdot\pi}{q\cdot\cos\varphi}} \qquad (5)$$

3. CONCLUSIONS

The contour of the breaking surface could be a circular curve.

The sight angle, because the ground characteristics may have, sometimes, several values; that means there are several curves describing the contour of the breaking surface. In this situation the Mohr-Coulomb criterion is not enough. It must be completed with peculiar earth characteristics.

REFFERENCES

Răileanu,P. et al. 1986. *Geologie, geotehnică, fundații*, vol. I,II,III, I.P.Iaşi.

Stanciu A. Lungu I. 2006. *Fundații*, Ed. Tehnică, Bucureşti.

Zarojanu, D. 2008. Graphical method of breaking surface determination in an earth massif by using the condition of ultimate equilibrium , *Journal of Physics*, vol 53, pg.417-421.

Session 3b

Preservation of hydrogeological situation

Geoecological problems

Geotechnical sustainability

Preservation of hydrogeological situation

PRB – nanotechnology useful for protection of groundwater underneath landfill

J. Fronczyk, K. Garbulewski
Department of Geotechnical Engineering, WULS, Warsaw, Poland

ABSTRACT: One of the newly developed technologies to prevent the migration of pollutants to groundwater is imposing the flow of polluted water through a sorbent material filling a permeable reactive barrier (PRB). The PRB in configuration of a continuous reactive wall or a funnel-and-gate system is typically filled with nanoscale zero-valent iron (nZVI), activated carbon, silica, zeolite and other suitable materials. This paper concentrates on examination of the zeolite and zeolite-sand mixture as reactive materials to immobilize the contaminants from landfills. Investigations including batch tests have been performed on zeolite samples mined in Slovakia (Niżny Hrabovec deposit) and zeolite-sand mixture containing 80% of zeolite. Based on the test results the general conclusions and design recommendation were drawn. It was concluded that PRB with material tested is promising nanotechnology to protect the groundwater environment beneath landfill.

1. INTRODUCTION

In recent years, nanotechnology (shortened to "nanotech") has been included for environmental remediation as nontoxic, abundant and potentially least costly method (Joo and Cheng, 2006). Generally nanotechnology deals with structures and particles of the size 100 nanometers or smaller and involves developing materials within that size as a nanoscale zero-valent iron (ZVI). Nanoscale ZVI is effective for among others dechlorination of chlorinated solvents in contaminated groundwater, reduction of nitrate to atmospheric N_2, immobilization of numerous inorganic and organic cations and anions, including agrochemicals (herbicides, pesticides and insecticides) (Roehl et al., 2005). Zhang et al (1998) found that the reactivity due to an surface area of ZVI (average of 33.5 m^2/g) is higher up to 100 times in comparison to reactivity on a surface area normalized basis. The most common methods of the ZVI installation in the ground involve constructing a continuous wall (Fig.1) or funnel-and-gate systems situated across the flow paths of polluted groundwater, injection or grouting (Roehl et al., 2001). Due to this, it is possible to remove the pollutants without extracting the contaminated soils and water to the ground surface. After passing the polluted groundwater through a barrier filled with a reactive medium, the contaminants are transformed into less hazardous or are attached to the medium through physical or chemical sorption (Gavaskar et al., 2002). Therefore, it is important to find a cost-effective adsorbent for universal application in the PRB. Developing materials at the nano scale can also include natural zeolites, a minerals with a group of aluminosilicate with a porous structure (Fig. 2) consist of a threedimensional framework, having a negatively charged lattice. Zeolite can accommodate a wide variety of cations, such as Na^+, K^+, Ca^{2+}, Mg^{2+} and others. These positive ions are rather loosely held and can readily be exchanged for others in a contact solution. The ability to selectively sort molecules based primarily on a size exclusion process. The maximum size of the molecular or ionic species that can enter the pores of a zeolite is controlled by the dimensions of the channels ranging

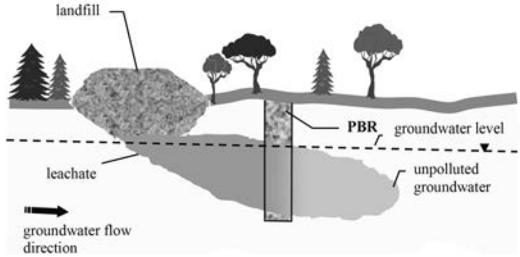

Figure 1. The concept of permeabe reactive barriers.

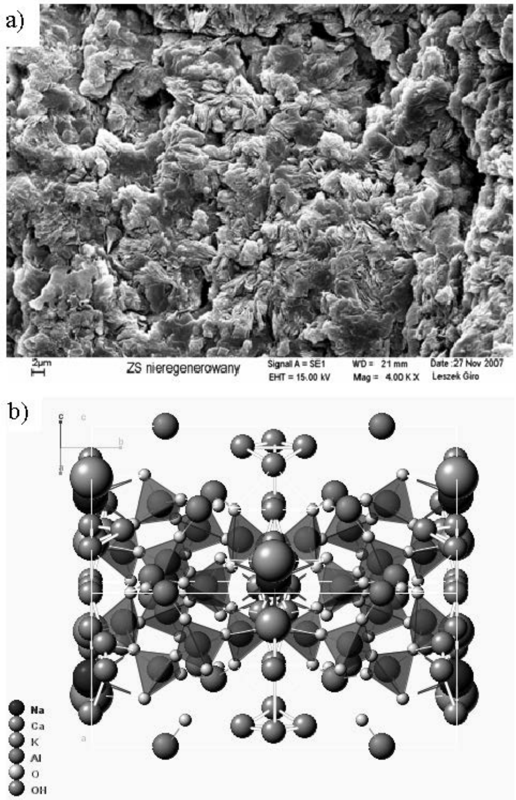

Figure 2. Scanning electron micrograph of zeolite(a) and model structure of sodium clinoptilolite (http://webmineral.com) (b).

from 0.40 to 0.72 nm (Czurda, Haus 2002, Upmeier, 1996).In addition to ion exchange, on the surface or within the structure of the zeolite may also be held chemicals. However, these processes take place less intensively than ion exchange.

The advantage of the zeolite group of minerals is their strong chemical and thermal stability and high ability to modify their surface properties (Ciciszwili et al., 1990). The mineral formula of zeolite is:

$$(K_2,Na_2,Ca,Mg)_4Al_8Si_{40}O_{96}\cdot 24H_2O \qquad (1)$$

Recently, in order to prove the advantages of using the PRB with zeolite or zeolite-sand mixtures for protecting the contaminated groundwater underneath landfill comprehensive laboratory investigations including the batch technique were undertaken.
The zeolite used as ion exchanger in the experiments was obtained from Slovakia. The chemical composition of the zeolite used

Table 1. Average chemical composition of Slovak zeolite (percentage by weight).

Component	Slovak zeolite	
	Upmeier 1996	Zeocem
SiO_2	71.6	65-71.3
Al_2O_3	12.46	11.5-13.1
Fe_2O_3	1.52	0.7-1.9
TiO_2	0.16	0.1-0.3
CaO	3.19	2.7-5.2
MgO	0.72	0.6-1.2
Na_2O	0.62	0.2-1.3
K_2O	3.27	2.2-3.4
MnO	0.03	-
P_2O_5	0.03	-
The residue after ignition at 1000 º C	7.94	-

in the study is shown in table 1. This paper concentrates on examination of the zeolite-sand mixture as reactive material to immobilize the contaminants from landfills. The first stage of investigations included the selection of chemical compounds, the influence of which on the sorbent properties was checked in laboratory conditions. The selection of pollutants was performed based on results of the chemical composition analyses of leachates gathered from municipal waste disposal sites in Warsaw. Investigation have been performed on Vistula sand (medium sand) mixture with Slovak zeolite (ZS), which fulfil the required hydraulic and sorption properties. The analyses of the sorption properties of the mixtures have been carried out using two methods: batch and column tests (Fronczyk, 2008). The batch tests, results of which are presented in this paper, were performed for inorganic (Cu^{2+}, Nh_4^{+}) and organic (methylene blue, hyamine) contaminants.

2. BATCH TESTS

2.1. Test method

For inorganic compounds specimens consisting of 2 g dry tested material and of 100 ml of solution were placed in 250 ml flasks. For organic compounds weight of the test materials varied in the range of 0.1-0.8 g and the volume of solution and concentration of organic compounds were constant. Heavy metal and ammonium ion solutions of different concentrations were prepared from their pure salts ($CuCl_2$, NH_4Cl) and organic compound solutions from their analytical solutions ($C_{16}H_{18}ClN_3S$, $C_{27}H_{42}ClNO_2$). Initial concentration of heavy metal (Cu) ranged from 5 to 300 mg/l, of ammonium ranged from 5 to 360 mg/l in one-component solution and the initial concentration of hyamina and methylene blue was 0.2g/l and 20g/l, respectively. Initial pH and electrical conductivity values ranged from 2,5 to 7,1 and from 13 to 3570 μS/cm, respectively.

The specimens were shaken vigorously for 24 h and centrifuged. The solutions were analyzed for equilibrium concentrations. The experiments were performed in duplex at laboratory temperature of 21-22ºC. The measured liquid phase concentrations were used to calculate the sorption capacity of the sorbent. The solid phase compositions were calculated from the differences between initial and equilibrium compositions of the liquid phase, according to the equation (1):

$$\frac{x}{m} = \frac{V}{M}(C_0 - C_R), \qquad (2)$$

where C_0 and C_R are the initial and equilibrium concentration of tracer in the liquid phase, x/m - the zeolite-sand mixture phase concentration, V - the volume of solution and M - the mass of dry zeolite-sand mixture.

2.2. Discussion of test results

Copper, ammonium, methylene blue and hyamine adsorption isotherms on ZS and ZS80 from the batch experiments are shown in Figure 3. The sorption data were described using the Langmuir isotherm. The results of these analyses, using linear regression procedures, are shown in Tables 2. Fitting of observed data to the Langmuir's sorption isotherm resulted in a maximal sorption capacity ($C_{a,max}$) of chosen substances of zeolite and zeolite-sand mixtures. The constant K_L may be related to the energy of adsorption and can be regarded as an "affinity parameter" between the exchanging cation and zeolite for a given system (EPA, 1992). It was found that the Langmuir isotherm fitted the data best. In order to compare results

Table 2. Langmuir constants

Copper				
Parameter	ZS	ZS80	ZS50	ZS20
C_{amax}, mg/g	8.394	7.920	6.059	3.064
K_L, l/mg	0.622	0.140	0.323	0.268
R^2	0.99	0.94	0.99	0.99
Ammonium				
C_{amax}, mg/g	15.061	14.406	5.699	2.020
K_L, l/mg	29.450	21.514	3.30	0.630
R^2	0.99	0.98	0.99	0.93
Methylene blue				
C_{amax}, mg/g	0.639	0.568	-	-
K_L, l/mg	0.176	0.129	-	-
R^2	0.71	0.85	-	-
Hyamine				
C_{amax}, mg/g	0.177	0.301	0.064	-
K_L, l/mg	1.606	0.337	5.464	-
R^2	0.66	0.73	0.74	-

obtained for copper and ammonium with results given in the literature, Figure 3 presents the results of Wojnarski et al. (2003), Petrus and Warchoł (2003), Wang et al. (2007) and Jorgensen and Weatherley (2003). In all cases, tests were carried out on Na-form of zeolite. On this basis, it can be concluded that the results for the zeolite does not differ from the results given in literature. The studies show that clinoptilolite, which in 95 percent is part of the Slovak zeolite, characterize a high sorption capacity of ammonium. This is proved by value of exchange capacity C_{amax} for ammonium in comparison with the values of this parameter for copper.

3. DESIGN CONSIDERATIONS

The method of PBR with zeolite or zeolite-sand mixtures has a number of advantages, but also limitations resulting from the properties of reactive materials and contaminants as well as processes occurring between pollutants and materials. Results of laboratory tests indicate that the use of PBR with zeolite and zeolite-sand mixtures (ZS80) for groundwater protection in the neighborhood of landfills is justified in the following cases:

- location of particularly disadvantageous conditions or improperly protected landfill

- damage of composite liners of landfills (e.g. geomembrane).

The main limitation in the application of ZS80 to PBR near landfills is the limited sorption capacity and selectivity of this material. Among the leachate compounds heavy metals (Cu^{2+}, Pb^{2+}, Cr^{3+}) and NH_4^+, K^+ and Fe^{2+} / Fe^{3+} ions are retained, whereas others do not react with the material, or the intensity or duration of these processes are not sufficient to achieve the required concentrations in groundwater (Fig. 4) (Fronczyk 2008, Katzenbach et al. 2008).

Selection of the reactive material requires analysis of the investigations carried out in accordance with the diagram shown in Figure 4. The design of PRB should provided a general framework for: - identification of the geometrical parameters, - qualification and selection of reactive material to guarantee the optimal conditions for barrier functioning by established period of time. PRB design involves the following steps: investigation tests which include site and contaminants characterization, qualification tests during which reactive material is selected and verification tests, which are necessary for modeling and engineering design.

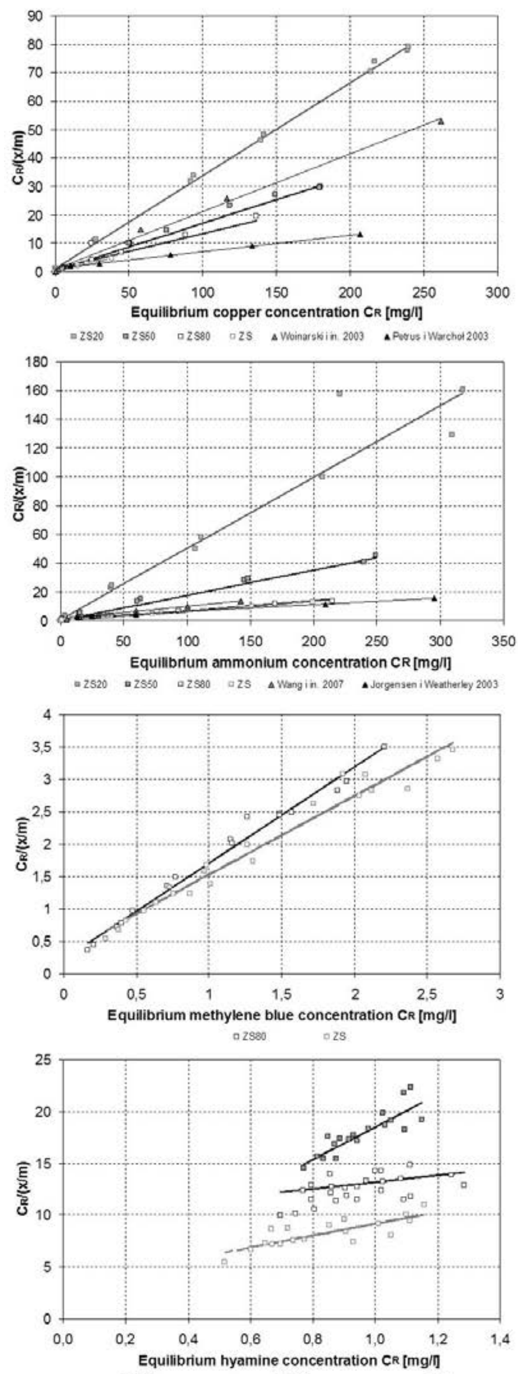

Figure 3. Langmuir adsorption isotherms for copper, ammonium, methylene blue and hyamine.

4. FINAL REMARKS AND CONCLUSIONS

Based on the laboratory test results the general conclusions related to the ability of the use sand-zeolite mixtures as materials in the permeable reactive barriers were drawn. Zeolite-sand mixtures have several properties, which make its use in PRBs promising. These are materials, that selectively retardate pollution occurring in municipal landfill leachate. The most intensive ion-exchange-sorption processes on the surface of studied materials occur for inorganic cationic substances (Cu^{2+}, NH^{4+}, Pb^{2+}), with lower intensity organic compound dissociated to cations (eg. methylene blue). Organic compounds non-dissociated or dissociated to anions (eg. phthalic acid, benzene) are not retained by ZS and ZS80 (80% content of zeolite) regenerated to sodium form. Finally, according to the test results obtained it was concluded that PRB is promising nanotechnology to protect the groundwater environment beneath landfill.

The main limitation of PRB application with ZS and ZS80 is the inability to retain the entire spectrum of contaminants that may potentially be present in the landfill. Specific questions arise when considering

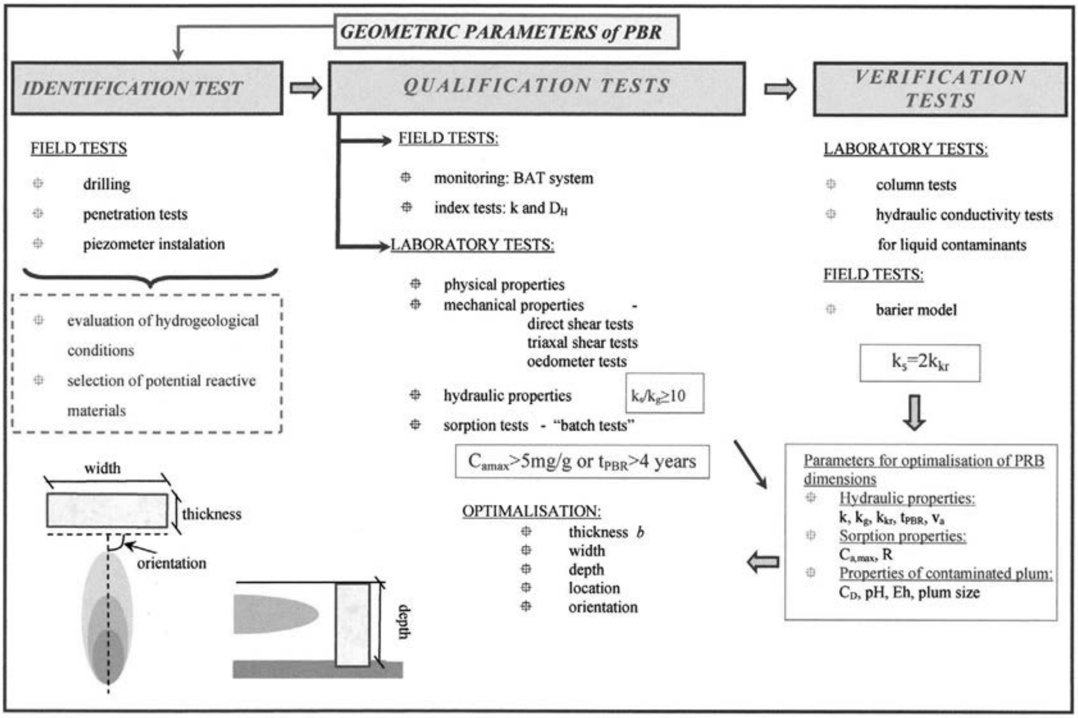

Figure 4. Diagram for determining the geometrical parameters of PRB

the retention of pollutants such as organic compounds and anionic substances.

PRB is an inexpensive method and does not convey technological difficulties. The effectiveness of the method depends on the properties of reactive materials. In the case of zeolites and zeolite-sand mixtures the method should apply the principles given in this study.

Acknowledgments: This research was supported by Grant no. 2P04G 088 29 from the Ministry of Science and Higher Education, Warsaw, Poland.

5. REFERENCES

Ciciszwili, G.W., Andronikaszwili, T.G., Kirow, G.N., Filizowa L.D. 1990. *Natural zeolites*. Warszawa: Wydawnictwa Naukowo-Techniczne (in Polish).

Czurda, K.A. & Haus P. 2002. Reactive barriers with fly ash zeolites for in situ ground water remediation. *Applied Clay Science,* Vol. 21, pp. 13-20.

EPA 1992. Batch-type procedures for estimating soil adsorption of chemicals. *EPA/530SW87006F*.

Fronczyk, J. 2008. Zeolite-sand mixtures in permeable reactive barriers in the landfill surroundings. PhD thesis, Faculty of Engineering and Environmental Science WULS (in Polish).

Gavascar, A., Gupta, N., Sass, B., Janosy, R. & Hicks, J. 2002. *Design guidance for application of permeable reactive barriers for groundwater remediation*. Ohio: Battelle Press.

Joo, S.-H., & Cheng, I.F. 2006. *Nanotechnology for environmental remediation*. NY: Springer.

Jorgensen, T.C., & Weatherley, L.R. 2003. Ammonia removal from wastewater by ion exchange in the presence of organic contaminants. *Water Research*, **37**: 1723-1728.

Katzenbach, R., Fronczyk, J. & Garbulewski, K. 2008. Evaluation of zeolite-sand mixtures as a reactive material towards landfill leachate. In Z. Młynarek, Z. Sikora & E. Dembicki (eds), *Geotechnics in Maritime Engineering*. Gdansk: Polisg Committee on Geotechnics & Gdansk University of Technology, pp. 875-882.

Petrus, R. & Warchoł, J. 2003. Ion exchange equilibria between clinoptilolite and aqueus solution of Na^+/Cu^{2+}, Na^+/Cd^{2+}, Na^+/Pb^{2+}. *Microporous and Mesoporous Materials*, Vol. 61, pp. 137-146.

Roehl, K.E., Huttenloch, P. Petrus, R. & Czurda K. 2001. Permeable sorption barriers for in-situ remediation of polluted groundwater – reactive materials and reaction mechanisms. In Green 3, *The Exploitation of Natural Re-*

sources and the Consequences, London, 2001, pp. 466-473. Thomas Telford Publishing.

Roehl, K.E., Meggyes, T., Simon, F.-G. & Stewart D.I. 2005. *Long-term performance of permeable reactive barriers*. Amsterdam: Elsevier B.V.

Upmeier, M. 1996. Optimierung mineralischer Deponieabdichtungen durch natürliche Zeolithe und Aktivkohle. *Angewandte Geologie* Karlsruhe, Vol. 42 (in German).

Wang, Y.-F., Lin, F. & Pang W.-Q. 2007. Ammonium exchange in aqueous solution using Chinese natural clinoptilolite and modified zeolite. *Journal of Hazardous Materials*, Vol. 142, pp. 160-164.

Wojnarski, A.Z., Stevens, G.W. & Snape I. 2006. A natural zeolite permeable reactive barrier to treat heavy-metal contaminated waters in Antarctica: kinetic and fixed-bed studies. *Process Safety and Environmental Protection*, Vol. 84(B2), pp. 109-116.

Zhang, W.-X., Wang, C.-B. & Lien H.-L. 1998. Treatment of chlorinated organic contaminants with nanoscale bimetallic particles. *Catalysis Today*, Vol. 40, No. 4, pp. 387 – 395.

www.zeocem.sk

http://webmineral.com

Iron-based biogrout for soil improvement in Singapore

V. Ivanov, J. Chu, V. Stabnikov, J. He, M. Naeimi

School of Civil and Environmental Engineering, Nanyang Technological University, Singapore

ABSTRACT: Chemical grouts have often been used in various geotechnical applications. However, they are usually expensive and may be harmful to urban environment. A new type of grout, the so-called biogrout, which is based on the cheap ferrous/ferric salts, has been developed using microbial technology. The time taken for the biogrout to take effect and the distance of biogrout can penetrate in soil depended on the concentration and activity of specific bacteria in the biogrout. The reaction time can vary from several minutes to several days. Several compositions of iron-based biogrouts for different geotechnical applications have been developed and tested. The testing results showed that ferrous/ferric-based biogrouts are most applicable for construction of reservoirs, ponds, dams, and land reclamation through formation of grout curtains. The biogrout also increases the strength of soil at the same time while decreasing the permeability of the soil.

1. INTRODUCTION

Chemical grouting is a common technique adopted in geotechnical engineering to improve the mechanical properties of soil (Karol, 2003). In adopting this method, grout is injected into the voids of soil to increase the strength or reduce the permeability of soil. However, chemical grouting can be expensive and toxic for environment.

An alternative approach is to use biogrout (Ianov and Chu, 2008; Mitchell and Santamarina, 2005). Biogrouting is to fill the voids, channels or fissions in soil or rock through microbial activity or by the microbial products. Due to small size of bacterial cells, 1-3 μm, biogrouts can be applied to soils with permeability below 10^{-6} m/s. It can decrease the permeability to 10^{-10} m/s. This effect is similar to the effect of chemical grouts (Sarsby, 2000; Indraratna and Chu, 2005). However, cement grout is applicable for soils with permeability below 10^{-4} m/s and can decrease permeability up to 10^{-6} m/s (Sarsby, 2000).

The use of microbial technology into geotechnica engineering has been called Microbial geotechnology. It is a branch of geotechnical engineering aiming to improve the mechanical properties of soil so that it will be more suitable for construction and environmental purposes (Ivanov and Chu, 2008). There are several mechanisms that are suitable for biogrouting into soil or rock: 1) filling of the voids and channels in soil with inorganic compounds settled due to activity of microorganisms; 2) filling in the pores and channels with microbial biomass and polysaccharides; 3) cementation (binding) of the particles with inorganic compounds, which is mediated by microorganisms; 4) biocementation (binding) of the particles with microbial biomass and polysaccharides; 5) formation of salt bridges between the soil particles and colloids mediated by microorganisms; 6) microbial formation of gas bubbles and desaturation of soil for prevention of liquefaction.

The major advantages of biogrouts over chemical grouts are lower cost and low or even zero harmful effects on urban environment (Ivanov and Chu, 2008). However, application of the biogrout is more complicated than chemical grout because biogrout includes both microbial and chemical components and its geotechnical application is site-specific. An advantage of biogrout in comparison with the conventional cement is that the solution of biogrout has low viscosity and can penetrate into the porous soil by gravity.

Potential geotechnical applications of the biogrouts are as follows: 1) to form grout curtains to reduce the migration of pollutants after accidental spill or leakage of toxic pollutant into permeable soil; 2) to prevent piping and to enhance stability of earth dams and dikes; 3) to construct the reservoirs and ponds; 4) seepage control; 5) to control erosion of the banks or coastal area; 6) to increase slope and excavation stability; 7) to reduce the liquefaction potential of soil; 8) to enhance the stability of dams; 9) to increase the bearing capacity of foundations; 10) to fix leakages of ground water in underground constructions; 11) soil settlement control; 12) decrease soil expansion potential; and 13) reduce corrosion of the pipelines.

Geotechnical applications of biogrouts that are relevant to the construction of megacities include land reclamation, stabilization of the roads and pipelines, the sealing of the drippings in the tunnels, and the reduction of the liquefaction potential of soil. One aim of our research was to develop biogrout that is suitable for urban geotechnical applications.

2. RESULTS

Settling of biogrouts

The following biogrouts have been tested to strengthen soil and to decrease permeability of the sandy soil: 1) conventional biogrout containing calcium chloride, urea, and urease-producing bacteria. The conventional biogrout has been used as control; and 2) iron-based biogrout, which was ferrous/ferric-containing solution produced by iron-reducing bacteria from iron ore and organic waste, with an addition of urea and urease-producing bacteria to increase pH.

The major chemical reactions in conventional biogrout are as follows:

$$(NH_2)_2CO + 3H_2O \rightarrow CO_2 + 2NH_4^+ + 2OH^- \quad (1)$$

which is performed by urease-producing bacteria, and

$$Ca^{2+} + CO_2 + 2\,OH^- \rightarrow CaCO_3\downarrow + H_2O \quad (2)$$

The major chemical reactions in innovative biogrout are as follows:

$$1.5\,(NH_2)_2CO + 4.5H_2O \rightarrow 1.5CO_2 + 3NH_4^+ + 3OH^- \quad (3)$$

which is performed by urease-producing bacteria, and

$$(HCOO)_3\,Fe + 3OH^- + 3NH_4^+ \rightarrow Fe(OH)_3\downarrow + 3\,HCOONH_4 \quad (2)$$

Production of hydroxide ions can be performed also by denitrifying bacteria using organic substances as electron donor:

$$NO_3^- + 2.5\,CH_2O \rightarrow N_2 + 2.5CO_2 + 1.5H_2O + 2OH^- \quad (3)$$

or sulphate-reducing bacteria:

$$SO_4^{2-} + 2CH_2O \rightarrow H_2S + 2CO_2 + 2\,OH^- \quad (4)$$

Typical pH that can be created by these processes is from 8.3 to 9.5 as shown in Fig. 1.

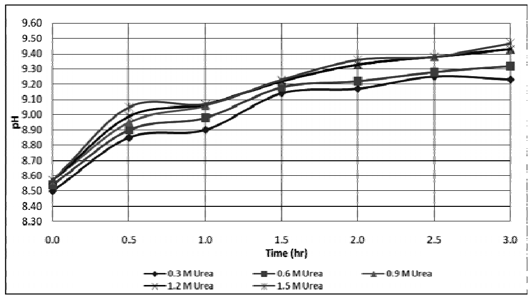

Fig. 1. Increase of pH during hydrolysis of urea in the biogrouting process.

Ferric formate and lactate but not ferric citrate are suitable for the precipitation at pH above 8.5 (Fig. 2). It means that ferric salts of organic acids produced by fermenting bacteria are suitable as the components of biogrouting mixture.

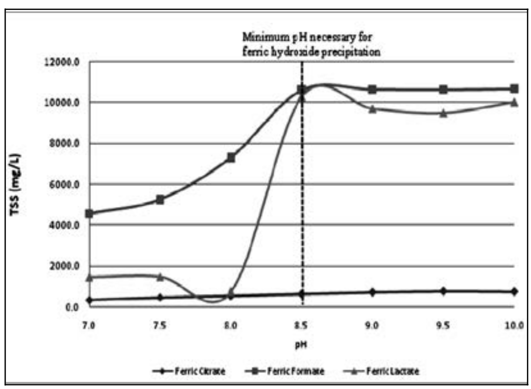

Fig.2. Precipitation of ferric hydroxide (TSS) depending on pH in the biogrouting process.

Depending on activity of urease-producing bacteria or urease the rate of precipitation could be faster. For example, calcium-based grout can form precipitate after 10 minutes. This precipitation can continue for several hours as shown in Fig. 3.

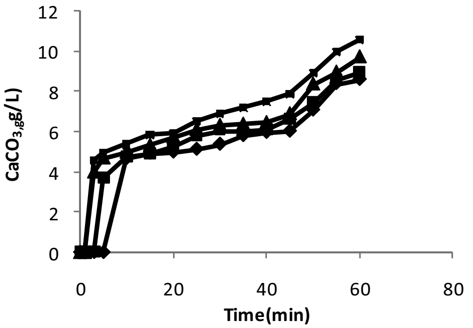

Fig. 3. Precipitation of $CaCO_3$ from the mixture of $CaCl_2$ and urea with different concentrations of urease.

Sandy soil treated with biogrouts

Constant head permeability tests in a triaxial cell and unconsolidated undrained triaxial tests were carried out to measure the change in the soil properties of the treated soil. The geotechnical parameters of microbial soil biocementation depend on the mass ratio of biogrout and soil particles as well as a number of the treatments in the series of the repeating treatment, see Figs. 4 and 5.

The compressive strength for the air dried samples increased gradually with the number of the treatments using iron-based biogrout and were in the range from 11 kPa to 18 kPa. Whereas, the compressive strength increased from 19 kPa to 56 kPa just for two treatments of the oven dried samples, to 79 kPa, 106 kPa and 149 kPa after the 3rd, 4th and 5th treatment, respectively (Fig. 4). The permeability of the soil was reduced from $1.1x10^{-4}$ m/s for untreated sample to $5.9x10^{-5}$ m/s for sand sample after 5 treatments (Fig. 5).

Conventional microbial grout based on calcium salt has decreased the permeability of sandy soil up to $2.5x10^{-9}$ m/s and increased the unconfined compressive strength (UCS) for dry samples to 1600 kPa. For the wet samples, the maximum UCS was 800 kPa (Fig. 6).

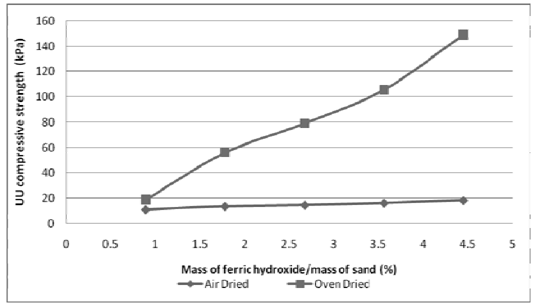

Fig. 4. The unconsolidated undrained (UU) compressive strength triaxial test results of both the oven dried and air dried sand samples biotreated using iron-based grout. Points show the values in the sequence from 1 to 5 treatments of the sample.

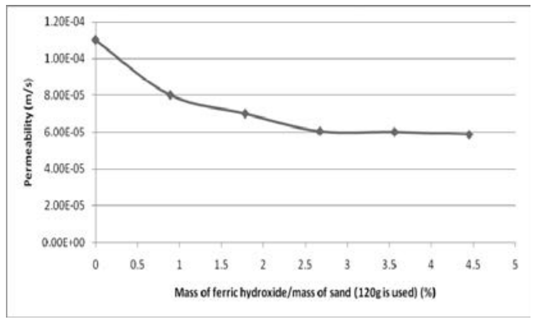

Fig. 5. Permeability of biocemented sand samples.

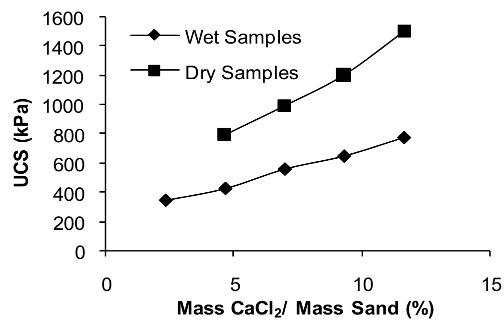

Fig. 6.The uncomfined compressive strength (UCS) results of both the wet and air dried sand samples biotreated using calcium-basd biogrout.

3. MECHANISMS OF BIOGROUT

The scanning electron micrograph (SEM) of untreated and biotreated sand samples are shown in Figs. 7 to 9. A comparison of Fig. 7 and Fig. 8 shows that the sand particles are bound together after it is treated by the iron-based biogrout in Fig. 8 and by calcium-based biogrout in Fig. 9. It can also been seen that the pores are also filled by biogrout. This explains the mechanisms of biogrout.

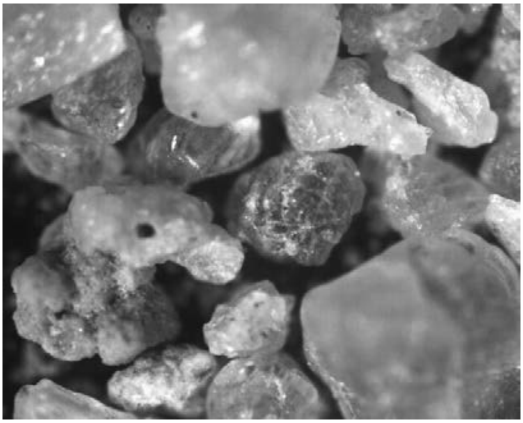

Fig. 7. Untreated sand

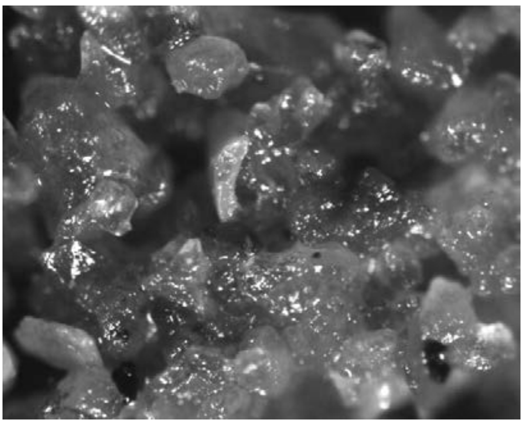

Fig. 8. Sand treated with the iron-based biogrout

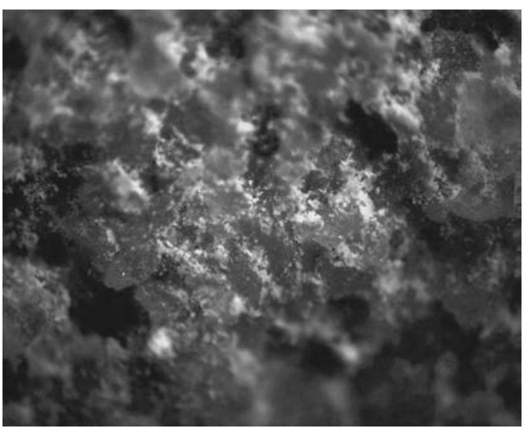

Fig. 9. Sand treated with the calcium-based biogrout

4. CONCLUSIONS

Because of lower cost of iron-based grout and not significant increase of strength of wet samples, the potential geotechnical applications of the iron-based biogrouts include large-scale reduction of permeability, which is not required significant increase of mechanical strength of soil. These urban geotechnical applications could be as follows: 1) to form grout curtains to reduce the migration of pollutants after accidental spill or leakage of toxic pollutant into permeable soil; 2) to diminish piping of earth dams and dikes; 3) to construct the reservoirs and ponds; 4) seepage control; 5) to fix leakages of ground water in underground constructions; 6) reduce corrosion of the pipelines; 7) land reclamation; 8) the sealing of the drippings in the tunnels; 9) the reduction of the liquefaction potential of soil.

5. REFERENCES

Ivanov V. and Chu J. 2008. Applications of microorganisms to geotechnical engineering for bioclogging and biocementation of soil *in situ. Reviews in Environ. Sci. and Biotechnol.*, Vol.7, pp. 139-153.

Indraratna B. and Chu J. (Eds) 2005. Ground Improvement – Case Histories. Oxford, UK, Elsevier.

Karol R.H. 2003. Chemical Grouting and Soil Stabilization, 3rd ed. New York, M. Dekker. Mitchell J.K. and Santamarina J.C. 2005. Biological considerations in geotechnical engineering. *J. Geotech. Geoenvir. Eng.*, Vol.131, pp. 1222-1233.

Sarsby R. W. 2000. Environmental Geotechnics. Thomas Telford Publishing, 584 p.

Quality assurance of a secant pile wall using three different non-destructive test methods

E. Niederleithinger
BAM Federal Institute for Materials Research and Testing, Berlin, Germany

O. Klingmüller, M. Schallert
GSP mbH, Mannheim, Germany

A. Bobbe
Landestalsperrenverwaltung Sachsen, Pirna, Germany

ABSTRACT: Pile secant walls are used as foundations, hydraulic barriers or for securing excavations. Especially on sites with complex geology or complicated constructions much effort has to be spent on quality assurance. Most non-destructive testing methods, which are applied on a regular basis on single piles, can't be used directly on pile walls.

Measurements at a construction site of a flood protection barrier in Grimma, Saxony/Germany have shown the potential of low strain pile integrity measurements, ultrasonic crosshole logging and parallel seismics. If applied in an unconventional manner and combined properly they can give valuable data on pile length, soil type below the piles, and construction quality.

1. INTRODUCTION

As a result of the events in 1998 and 2002, when several cities where flooded, the German states spent major efforts on enhancing their flood protection constructions. In city areas, where limited space prohibits the erection of earthen embankments, wall-type constructions have to be built.

In the city of Grimma (near Leipzig, Saxony) it was decided to use a pile secant wall as foundation, due to the potential high water levels (and thus high loads) expected in major events. At the same time the foundation serves as a hydraulic barrier to prevent water movements below the barrier. The subsurface soil structures are complex. The narrow valley is filled with holocene river sediments (silt, sand, gravel). The piles have to reach the low permeable degradated porphyry rock underneath.

Additional complications arise from the layout of the existing buildings, which are partly under cultural heritage protection. In case of the section discussed here, the pile secant wall has to follow the geometry of a 19^{th} century administration building (Figure 1).

As usual the secant pile wall was constructed by drilling unreinforced primary piles (90 cm diameter, gap width 54 cm) and later on reinforced secondary piles (90 cm diameter as well) in between by cutting away a part of the primary ones. Pile length is 10 to 13 m in most cases.

Several non-destructive testing methods are used on a regular basis for the quality assurance of bored piles. In many countries they are included in standards (ASTM, AF-NOR), regulations or widely accepted recommendations (e.g. DGGT, 2007). The experiences in using these methods without adoption on pile secant walls are mixed. Thus so far no standards for the non-destructive test of pile secant walls exist.

Figure 1: Construction site in Grimma, Saxony.

2. METHODS

We have chosen three established testing methods and tried to adopt them to the needs for quality assurance in the described case.

2.1. Low strain pile integrity testing (PIT)

The low strain pile integrity testing method (PIT) is the most used and at the same time most simple method in pile quality assurance. A hammer stroke is applied to the pile top, a geophone or accelerometer on the pile “listens” for echoes from the stress wave traveling down the pile at the toe or major defects (Figure 2, Figure 3). The method is described in detail e.g. in Turner, 1998 and DGGT, 2007. The length L of a pile or the depth of a defect is calculated from the wave velocity c_p and the time difference between impulse and echo Δt by the simple equation:

$$L = \frac{c_p \cdot \Delta t}{2}, \qquad (1)$$

The major drawback is, that c_p is not known without calibration by an independent method, leading to errors margins of up to 10%. But in the case described here the parallel seismic method could be used as reference.

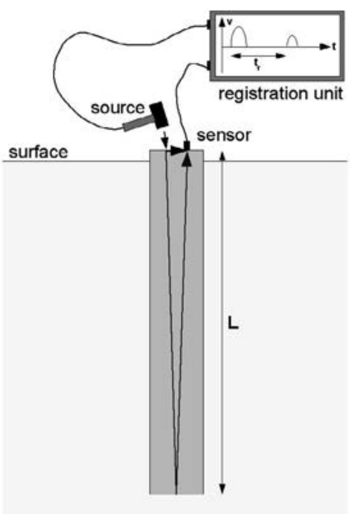

Figure 2: Principle of low strain pile integrity testing

The method is currently not much used (nor recommended, Klingmüller & Kirsch, 2004) for quality assurance of pile secant walls. When used on pile secant walls the wave energy dissipates to the neighbored piles resulting in lower amplitude toe reflections and much less resolution of defects in a particular pile. In addition side reflections may appear which are difficult to interpret.

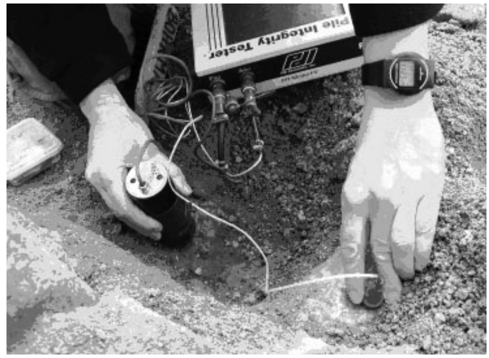

Figure 3: Pile integrity testing in Grimma

2.2. Parallel Seismics (PS)

The parallel seismic method (PS) was invented in the early 1970s in France and was used quite frequently in the USA since the late 1980s. A hammer stroke is applied on top of the pile. Sensors (e. g. hydrophones) are placed in a nearby borehole, recording mainly the first arrivals (Figure 4).

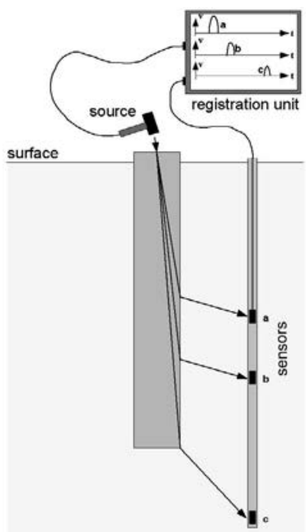

Figure 4: Principle of the parallel seismic method

A change in the slope of the travel time curve (time of first arrival vs. sensor depth) marks approximately the pile toe. Method details and the developments of the more accurate interpretation method used here are described in Niederleithinger et al., 2005. The wave velocities of pile and soil can be determined from the travel time curve without calibration. The accuracy in terms of pile length of the method is about 1 - 5% depending on pile-borehole distance and other parameters. Major drawbacks are the need of a borehole (which prohibits the test of more than a few piles on each site) and the lack of defect detection capability.

Figure 5: PS test in Grimma. Impact on top of pile secant wall (background), sensors in front tube.

2.3. Crosshole SonicLogging (CSL)

The Crosshole Sonic Logging (CSL) method checks piles internally for quality problems. Several pipes are fixed to the reinforcement cage before casting. The tubes are filled with water before testing. An ultrasonic transmitter and a corresponding receiver are lowered in separated pipes (Figure 7, Figure 6). Time of flight, amplitude and/or B-Scans of the transmitted waves are recorded. The method is described in detail in Turner, 1998 or DGGT, 2007.

Figure 6: CSL measurements in Grimma

Normally the test is done between tubes within one pile. But as the placement of tubes in primary piles is not feasible, the quality assurance of these piles and most important, of the contact zones between piles is not possible.

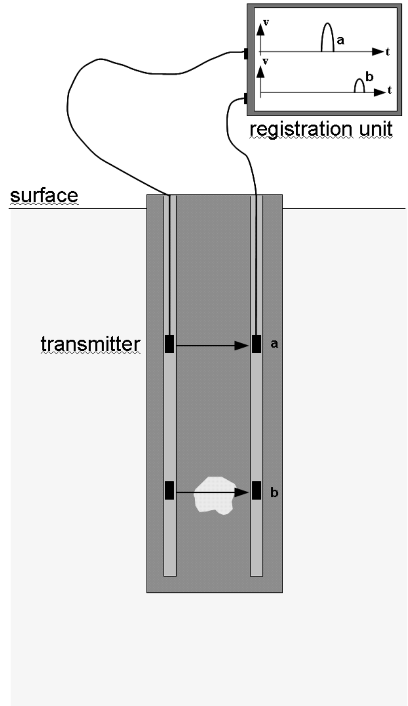

Figure 7: Principle of the crosshole sonic logging method (CSL).

A promising solution is to place the transmitter in one secondary pile and the receiver in the next one to assess the primary pile in between. To the knowledge of the authors this has not been tried (or at least not been published) before. By using several tube combinations in theory the most part of the primary piles is covered (Figure 8). Number and position of raypaths is dependent on number and position of tubes.

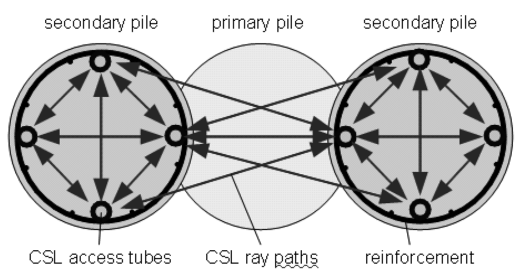

Figure 8: CSL ray coverage inside and across piles of a pile secant wall.

3. RESULTS

3.1. Low strain pile integrity testing (PIT)

Only a few piles at the Gimma site could be tested with PIT. The reason was that most piles were not accessible after removing the weak top concrete and before construction of the pile cap.

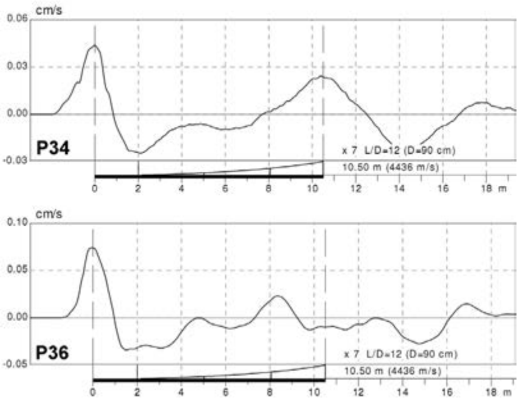

Figure 9: PIT results on two sound piles of a pile secant wall: P34 (top) shows toe signal, P36 (bottom) not.

Figure 9 shows examples of Pit records measured on two piles known to be 10.5 m long. Both piles were investigated by CSL and did not show any flaws. The signal from pile No. 34 (top of Figure 9) shows a broad, but nevertheless clearly visible toe signal. The calculated velocity of about 4400 m/s is rather high, which is probably due to the fact that these piles were several months old at the time of measurement. Pile No. 36 (bottom), which is only 1.4 m apart and was made by the same crew at the same time with the same type of concrete shows a completely different PIT signal. The reasons are not exactly known, but can be related to signal energy propagating to other piles leading to side reflections and a weaker toe response. The acoustic coupling conditions between piles vary a lot (see next section), so that some piles may show these effects, some not.

3.2. Parallel Seismics (PS)

Parallel seismic measurements were taken at several positions of the pile secant wall to check the length of the piles and to provide calibration data for integrity testing.

Example data for pile 137 are shown in Figure 10. There is some drift in the signal, but first arrival of wave trains can clearly be identified.

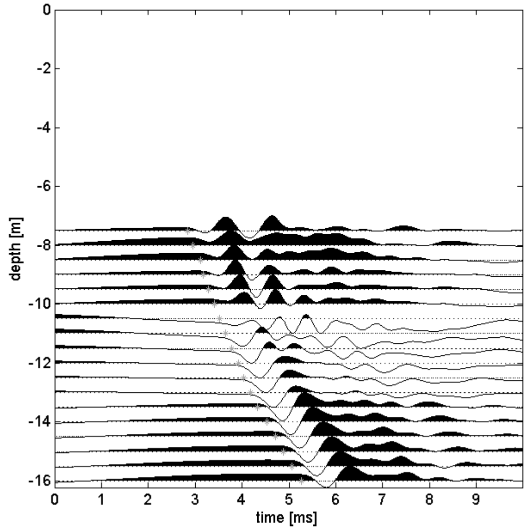

Figure 10: Parallel Seismic data from pile 137. First arrivals marked *.

These traveltimes have been interpreted by automated curve fitting using formulas from Niederleithinger et al. , 2005.

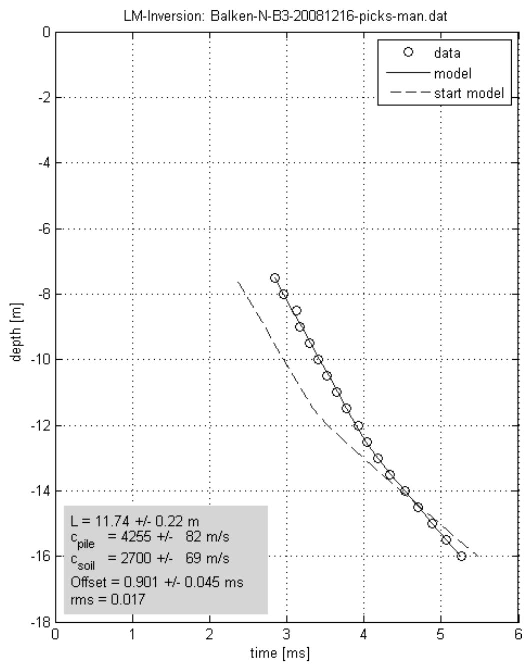

Figure 11: Interpretation of PS first arrivals by curve fitting.

The calculated pile length of 11.74 +/- 0,22 m has to be corrected by -0.5 m to 11.24 m as the sensor tube top was above the pile head. The result is in good correspondence to the designed pile length of 11.5 m.

3.3. Crosshole Sonic Logging (CSL)

The tests with transmitter and receiver both in the same pile did not give any hints for quality problems. Time of flight and amplitude are almost constant over the entire length of the piles. A sample result is given in Figure 12.

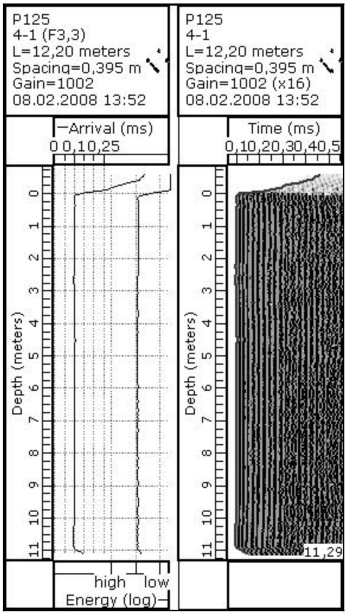

Figure 12: Typical CSL result of a pile internal tube pair.

Most of the records taken across primary piles showed feature as in the left part of Figure 13. The amplitudes are much lower compared to single pile records and sow some variation vs. depth. But as the time of flight is almost constant, these signatures are probably due to to varying conditions at the pile to pile interfaces.

A few records showed features as visible in the right part of Figure 14. Time of flight as well as amplitudes show major variation and even lack of signal in some parts. There are several possible causes: lack of contact between piles, flaws in the interior of the primary piles or problems with the CSL access tube. In the particular cases discussed here, the reason for the inhomogeneities is probably the latter one, as the features of Figure 14 are similar to the ones seen in a test specimen with a delaminated access tube (Niederleithinger et al, 2010). But as some of the features are near surface, visible inspection was recommended. Anyway is was planned from the beginning to cut away the topmost 1.5 m, so that flaws in this section are of no importance.

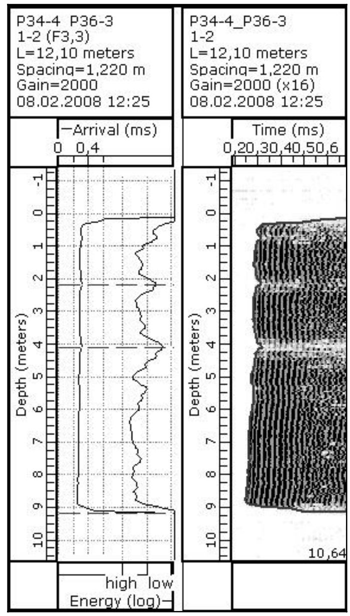

Figure 13: Pile-to-pile CSL result with minor anomalies.

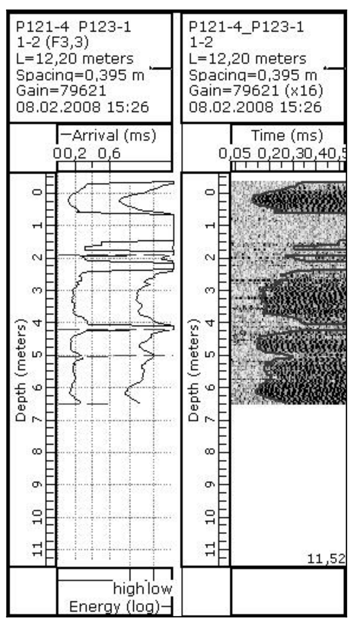

Figure 14: Pile-to-pile CSL result with major anomalies.

4. CONCLUSION AND OUTLOOK

The methods tested at a pile secant wall in Grimma, Saxony have shown their potential for a regular use for quality assurance.

Low strain pile integrity testing is only of limited use on pile secant walls, especially when used as the only method for quality assurance. Results and interpretation should be handled with care. New developments as multichannel testing may lead to better results.

The use of parallel seismics is recommended to provide calibration data for integrity testing. This way, the error margin for pile length can be reduced by a significant amount. In addition, the wave velocity determined for the material below the piles gives hints whether the piles have reached the deteriorated rock layer.

Crosshole sonic logging has shown potential to detect flaws or cracks in or between piles. But the results are sometimes difficult to interpret and need validation and calibration.

5. REFERENCES

DGGT AK 2.1: Empfehlungen des Arbeitskreises „Pfähle“ (EA Pfähle). Ernst& Sohn, Berlin, 2007.

Klingmüller, O., & Kirsch, F., 2004: A quality and safety issue for cast-in-place piles 25 years of experience with low-strain integrity testing in Germany: From scientific peculiarity to day-to-day practice. *Current Practice and Future Trends in Deep Foundations*, American Society of Civil Engineers, Geotechnical Special Publication No. 125, 2004, S. 202-221

Niederleithinger, E., Taffe, A., & Fechner, T.: Improved Parallel Seismic Technique for Foundation Assessment. *Proceedings of SAGEEP 2005*, Atlanta, USA.

Niederleithinger, E., Amir, J., & Hübner, M., 2010: Qualitätssicherung von Pfahlwänden mit der Ultraschallmethode - eine Machbarkeitstudie. *Proceedings of Bauwerksdiagnose 2010*, Berlin.

Turner, M. J: Integrity testing in piling practice. *Ciria Report 144*, London, 1997.

Geoecological problems

Eco-friendly Jute Geotextiles for Environment Protection

P K Choudhury[1], D N Goswami[2] and T Sanyal[3]

ABSTRACT: Global environment is governed by three main basic elements viz., soil, water and air. Natural environment is progressively transformed by indiscriminate deforestation, ever-expanding urbanization / mega-cities, building large industrial projects, setting up nuclear plants etc.

Restoration of environmental eco-system through application of bio-engineering measures is a proven method. Scientists have developed number of new eco-compatible and bio-degradable products for environment protection. In this respect jute geotextile, made out of 100 % natural fibres of jute, has been found to be highly effective for protection of surface soil erosion, stabilization of earthen slopes & overburden dumps including afforestation in arid zones in conjunction with civil engineering structures. It is one of the low cost technologies for protection of environment. Method of application of Jute Geotextiles and its impact on environment has been discussed in this paper.

1. INSTRUCTION

Food and Agriculture Organization (FAO) of UNO has declared year 2009 as the International Year of NATURAL FIBRES. Jute is an important natural fibre and has a wide range of effective applications in different fields. Its application as Jute Geotextile (JGT) has beneficial environmental uses. Most importantly, JGT facilitates bio-engineering measures far by improving geotechnical performance. Bio-engineering is being increasingly favoured all over the world. It is cheap and effective. Bioengineering approach combines engineering interaction with natural vegetation. Open weave JGT having a 3-D structure is capable of holding soil particles due to precipitation by reducing the velocity of surface run off, till vegetation grows and its root system anchor the soil as a permanent reinforcement. The vegetative cover when grown up over the eroding surface protects environment and improves ecology. Through this technology environment can be protected by increasing greeneries. Indian Jute Industries' Research Association (IJIRA) had conducted number of field trials with the support of Jute Manufactures Development Council (JMDC) and in collaboration with a number of Government Organizations in different states of India with open weave jute geotextile for erosion control on hill slopes, highway embankments, river banks, mine spoils and land slide areas. Results were found to be highly encouraging. The paper highlights the function, properties and method of installation of open weave jute geotextile along with the effect of its applications.

2. EROSION CONTROL SYSTEM BY OPEN WEAVE JUTE GEOTEXTILE

Soil erosion is a phenomenon of dislodgement of soil particles caused by natural actions like rain and wind or human activities like urbanization and mining etc. Such erosion may be controlled by reducing the erosivity co-efficient of the soil by some extraneous applications of engineering products. Open weave JGT, with 3-D structure, is commonly used to control surface soil erosion. It has two important properties viz high drapability and good water absorbing capacity that makes it quite capable to take the shape of the contours of the soil configuration and can remain in intimate contact there with absorption of moisture. It can absorb water as high as five times of its own dry weight and releases the moisture during dry spell leading to create a congenial atmosphere for quick growth of vegetation. It has been observed by several R & D organizations in India and abroad that for permanent protection of land from erosion, the best covering material is vege-

[1] P K Choudhury, In-Charge Geotech Cell, Indian Jute Industries' Research Association.
[2] D N Goswami, Civil Engineer, Indian Jute Industries' Research Association & Jute Manufactures Development Council.
[3] T Sanyal, Geotechnical Advisor, Jute Manufactures Development Council, Kolkata, India.

tation in the form of grass, bush, legumes and trees which increases shear strength of soil due to root penetration as high as 4.17 kN / m^2 for a soil depth up to 50 cm (5) . This force is enough to arrest the dislodgement of soil particles from the surface soil. Role of JGT here is to check erosion of soil at the initial stage and to foster growth of vegetation. After vegetation comes up the intended function of JGT virtually ceases. JGT bio-degrades naturally and forms humus that add nutrient to the soil.

Another important aspect of JGT is its capacity to prevent surficial soil loss and thus reducing surface soil erosion to a minimum level. Studies carried out by Ingold and Thomson (1990) indicates that JGT installed in sandy loam soil on 1:2 slope reduced the soil loss to about 1.3 g mm^{-1} compared to 8.8 g mm^{-1} in control. With growth of dense vegetative cover JGT can protect 99.0 to 99.9 percent soil loss with a crop factor of .001 to 0.01 (Ingold and Thomson, 1990). Fifield et al (1988) reported a crop factor (ratio of soil loss from soil covered by an erosion control system to soil loss from bare soil) of as high as 0.3, whereas after about one year with the establishment of good grass cover a value of 0.01 was recommended. Tests carried out by Ingold and Thomson further confirmed that JGT can significantly reduce the rain splash detachment of surficial soil. JGT checks soil erosion by absorbing the impact of kinetic energy of falling rain drops, arresting the downward flow of the dislodged soil particles with its 3 D structure and thus reducing surface run-off.

Various kinds of products made from natural and synthetic origin are available as erosion control material. IJIRA developed four types of open weave jute geotextiles namely T_1 (500 g/m^2) and T_2 (400 g/m^2), T_3 (300 g/m^2) & T_4 (730 g/m^2) as erosion control material which are shown in Table 1. The performance of JGT to control soil loss, maintaining humid soil temperature for the growth of vegetation have also been studied by Silsoe College, U. K. and the results are shown graphically in Figure 1,2 & 3.

3. FUNCTIONS OF OPEN WEAVE JUTE GEOTEXTILES

(i) Soil below the threads of the fabric is protected from direct impact of falling rain drops.
(ii) Dislodged soil particles are entrapped by the warp and weft threads of JGT in contact with the soil and prevented from moving downward.
(iii) Reduces velocity of surface runoff by forming mini-check dams with the threads of the fabric laid across the slope of the land.
(iv) Helps foster growth of vegetation which ultimately controls erosion.

4. APPLICATION AREAS

(i) Landscape engineering.
(ii) Protection of slopes either natural or man made.
(iii) Stabilization of sand dune in sea beach against shifting by wind.
(iv) Damage repair after mining activities and loss of soil for natural calamities.
(v) Stabilization of Fly Ash (PFA) dumps generated by Power Plants.
(vi) Development of forestry in semi-arid zones.

Table 1. Properties of Different Types of Open Weave Jute Geotextile

Physical Characteristics	Woven			
	T_1	T_2	T_3	T_4
Weight (g/m^2)	500	400	300	730
Threads/m (MD X CD)	65 x 45	340 x 150	110 x 120	70 x 70
Length (m)	70	100	100	100
Width (cm)	122	122	122	122
Thickness at 2 kPa (mm)	5	4	3	6
Coverage (%)	50	45	40	40
Tensile Strength (kN/m) (MD X CD)	10.0 x 7.5	12 x 10	10 x 10	12 x 12
Stain at Break (%) (MD X CD)	11 x 15	10 x 12	12 x12	13 x 13
Water Absorption Capacity (%)	500	500	400	500

(vii) Mulch in nursery bed of horticulture/agriculture for quick germination.

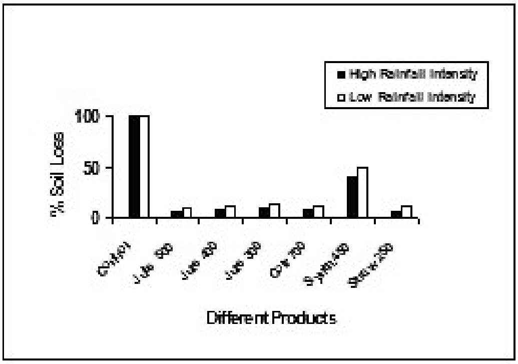

Figure 1. Control of Soil Loss with Different Types of Agrotextiles
(SILSOE COLLEGE, UK)

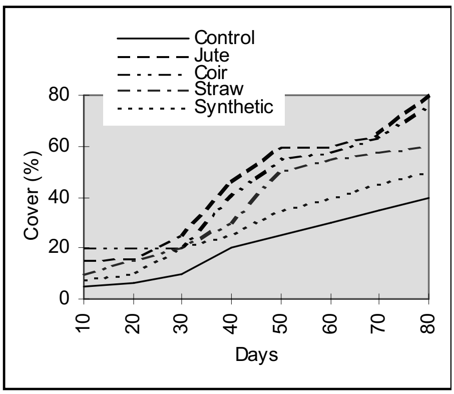

Figure 2. Vegetation Cover % with Time
(SILSOE COLLEGE, UK)

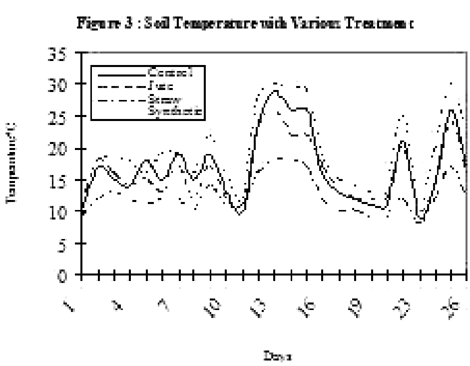

Figure 3. Soil temperature with various treatments
(SILSOE COLLEGE, UK)

5. METHOD OF INSTALLATION

Installation of JGT is as under-

(i) Preparation of land by leveling, dressing and cleaning.

(ii) Digging trenches of size 150 mm X 150 mm at top and bottom for anchoring the JGT and refilling the trench with gravel or suitable aggregates after laying JGT.

(iii) JGT should be laid from the top of slope to the bottom along the direction of surface run-off.

(iv) Overlapping the sides of JGT by 100 mm and 150 mm at the ends.

(v) Anchoring of JGT by wooden pegs or U-shaped iron nails of 11 gauge 15 cm long and at an interval of 1000 mm on all directions.

(vi) Spreading seeds of suitable grass, bush/legumes etc. or by planting suitable saplings/cuttings in equal spacing.

Post-installation care should be taken on the treated land till vegetation is established.

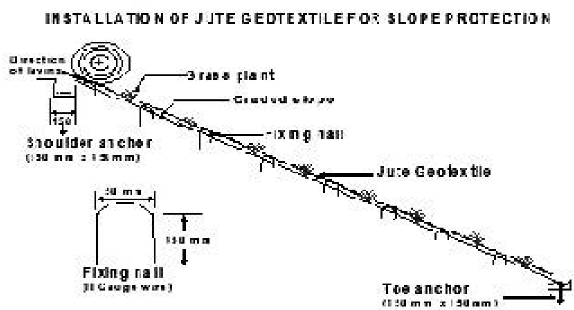

Figure 4. Method of JGT Installation

6. APPLICATION OF JGT FOR SLOPE STABILIZATION TOWARDS ENVIRONMENT PROTECTION:

A good number of applications of JGT have been undertaken for stabilization of different types of slope to protect environment. A list of such trials with JGT in India with encouraging results is given in the annexure.

A case study has also been discussed for a slope stabilization measures taken up with the use of JGT at Hydroelectric Power Project, Kullu, Himachal Pradesh, India.

7. A case study for slope stabilization at Parbati Hydroelectric Power Project, Himachal Pradesh, India under National Hydroelectric Power Corporation Ltd -

7.1. LOCATION:

The affected hill slope area is situated at Behali of Parbati Hydroelectric Power Project (Stage – III), Himachal Pradesh, India under National Hydro-electric Power Corporation Ltd. The hill slope along the approach road to the power plant was damaged severely during monsoon with erosion of surface soil and dislocation of stones and boulders affecting the environment nearby. The hill slope along the approach road is considerably steep, the slope angle varying from 46 □ to 65 □.

The area wears a verdant look. Construction of the project has affected the greeneries around. Excavations and frequent movement of trucks and automobiles has caused air pollution. Site has assumed a somewhat rugged look when the slope-remedial measures were taken up.

7.2. GEOTECHNICAL CHARACTERISTICS OF SOIL AND AMBIENCE:

The rock type in this area is mainly slate with dolomitic limestone and brands of metabasics or chlorite schist at few places. The hill slope is not within the fault zone and the surface run-off area is governed by precipitation. There is no indication of underground water and perennial springs in the hill slope area. However, water seepage is seen in places during monsoon. The soil is predominantly gravel-mixed inorganic soil. Average annual rainfall in the area was recorded to be 798 mm to 1858mm.

7.3. REMEDIAL MEASURES UNDERTAKEN:

The affected hill area was shaped to proper slope by removal of excess stone boulders, grits and debris and by filling in large voids. The slope irregularities were corrected and eased. Geotechnical corrections were made by construction of rubble masonry revetment walls and breast walls at different levels.

7.4. SLOPE COVERED WITH JGT:

730 gsm open weave JGT was placed from the top of the slope after excavating anchoring trenches at the top. The fabric was anchored within the trench and was rolled down to cover the whole slope area of approximately 25,000 sq m. Over lapping of 100 mm at the sides and 300 mm at the end was provided. Inverted 'U' shaped staples and wooden pegs were fixed on the JGT on slope at suitable intervals. The anchoring trench was filled up with stones, grits and sand particles after laying JGT.

Before laying JGT on the slope, 100 mm thick layer of manure-mixed soil with admixture of seeds of Ailanthus Sp. was placed on the slope and the surface was leveled. The top soil surface was kept moist for two to three weeks

Table 2. Soil parameters of the area treated with JGT:

SL. NO.	TEST	UNIT	RESULT	REQUIREMENTS	
1.	Grain Size Analysis		% Retained	% Cumulative Retained	Passing
	4.75	mm	58.3	58.3	41.7
	2.0	mm	8.3	66.6	33.4
	1.0	mm	10.8	77.4	22.6
	425	micron	5.0	82.4	17.6
	300	micron	2.9	85.3	14.7
	150	micron	2.1	87.4	12.6
	75	micron	1.7	89.1	10.9
2.	Soil Classification		GM		
3.	Cohesion (C)		0		
4.	Angle of internal friction (□)		38 □		
5.	Permeability	cm/s	2×10^{-4}		

till sprouting of vegetation started. The slope was fully covered with vegetation within three months after laying of JGT. The roots of the plants took care of the slope soil on bio-degradation of JGT after about a season cycle. The area was fully stabilized after one year of laying JGT.

7.5. CONCLUSION:

Open weave JGT laid on the slope helped retain the top soil and prevented its detachment. Growth of vegetation ensured stabilization of the surface soil on the slope after bio-degradation of JGT, a biodegradable natural environment-friendly geotextile. At the same time JGT facilitated faster growth of vegetation through its capacity to create a congenial micro-climate around.

National Hydro-electric Power Corporation Ltd may consider restoring the virginity of the denuded portions of the site by applying JGT with appropriate vegetation after the project is completed. JGT even when laid on plains is effective in arresting soil detachment and consequent denudation and is an effective material for watershed management as well. Manure and additional soil layer on top had to be used because of the character of the exposed surface which had no good soil where vegetation could thrive. Otherwise in areas with top soil in place there is no need to have either soil or manure for vegetative growth.

7.6. ACKNOWLEDGEMENT:

The authors are grateful to the authorities of Parbati Hydro-electric Project in preparing the paper. They are thankful to Col. Amitava Poddar, Acting Director, IJIRA and Sri Atri Bhattacharya, Secretary, JMDC for their kind permission to publish this paper.

Annexure I. List of field trials carried out in India with JGT for erosion control and slope protection measures.

Sl No	Site/ Location	Year of Application and User Organization	Particulars of work done	Results
1	Sahashradhara Dehradun, Uttarkhand	1987, Central Soil & Water Conservation Research & Training Institute.	Mine Spoil stabilization With open weave JGT- 6.5 x 4.5 - 500 g/m^2 Area covered:10000 m^2	By 1990 erosion checked, water pollution decreased, slope covered with vegetation.
2	Arcuttipur, T.E. Cachar, Assam	1995, Tea Research Association	Control of top soil erosion With open weave JGT- 34 x 15 - 400 g/m^2 Area covered: 5000 m^2	Soil loss reduced by 97%
3	Kaliasour, UP	1996, CRRI & PWD of U.P. Govt.	Land slide management With open weave JGT- 6.5 x 4.5 - 500 g/m^2 Area covered: 5000 m^2	Land slide checked, covered with vegetation.
4	Bilaspur, Chhattishgarh	2001, Western Coal Fields Ltd.	Mine spoil stabilization With open weave JGT- 7 x 7 -730 g/m^2 Area covered: 40,000 m^2	Spoil stabilized, slope covered with vegetation
5	Western Coal Field, Maharshtra	2001, Western Coal Fields Ltd.	Mine spoil stabilization With open weave JGT 7 x 7 – 730 g/m^2 - Area covered: 44,000 m^2	Slope covered with vegetation, spoil heap stabilized

6	Sonapur, Assam	2003, Border Roads Organization	Land Slide Management With open weave JGT- 12 x 12 -292 g/m^2 Area covered :30,000 m^2	Landslide controlled, slope was stabilized with full vegetative cover.
7	Ramby Project, TLDP – III, Sikkim	2004, National Hydro-electric Power Corpora-tion TLDP - III	Land Slide Management & Steep slope stabilization With open weave JGT- 7 x 7 – 730 g/m^2 Area covered: 5,400 m^2	Land slide checked and slope was stabilized.
8	NHPC, Assam	2005, National Hydro-electric Power Corpora-tion	Slope stabilization with Open weave JGT- 7 x 7 – 730 g/m^2 Area covered :24,000 m^2	Slope stabilized and covered with vegetation.
9	Barmana, Koldam Project, HP	2005, NTPC Limited	Slope stabilization with Open weave JGT- 7 x 7 – 730 g/m^2 Area covered: 4,800 m^2	Slope stabilized and covered with vegetation.
10	Mundeswari Bridge approach, Arambag, WB	2005, Public Works Depart-ment, Govt. of West Bengal	Embankment Slope stabili-zation with Open weave JGT- 6.5x4.5-500 g/m^2 Area covered: 3,500 m^2	Bridge approach stabilized, embankment slope covered with vegetation.
11	Kullu Parvati, -Stage I, HP	2007, National Hydroelectric Power Corpora-tion	Slope stabilization with Open weave JGT- 6.5x4.5- 500 g/m^2 Area covered: 18,000 m^2	Slope stabilized and covered with vegetation.
12	Port Blair, A & N Island	2007, Border Road Tusk Force (GREF)	Slope stabilization with Open weave JGT- 6.5x4.5-500 g/m^2	Slope stabilized, vegetation established.
13	Allahabad bypass, UP	2007, NHAI	Slope stabilization with Open weave JGT- 6.5x4.5 -500 g/m^2 Area covered: 4,80,000m^2	Erosion checked, slope stabilized with vegetative cover.
14	Nagaland	2008, Border Road Organiza-tion	Slope protection of road embankment With open weave JGT- 12 x 12 -292 g/m^2	Embankment is in good shape and slope stabilized.

8. REFERENCES

Choudhury, P. K. 2002. Jute Agrotextile in Agriculture, Horticulture & Forestry; Proc. *All India Seminar on advanced Technology for optimum Agricultural productivity org. by IE (I), Chennai.*

Juyal, G. P. and Dadhwal, K.S. 1996. Geojute for erosion control with special reference to Mine spoil rehabilitation, *Publication Indian Journal of Soil conversation,* Vol. 24, No.3.

Juyal, G. P. Katiyar, V.S. Sastry, G. Singh, G. Joshie, P. and Arya, R. K. 1991. Geojute for rehabilitation of steep mine soil areas – *Publication C.S.W.C.R. & T Institute, Dehradun.*

Louis, S. 1996. Conservation Grass Wins Monsanto's *"John Franz Sustainability Award"* , Vetiver Newsletter- Newsletter of the Vetiver Network, No. 16.

Sanyal, T. 2006. Jute Geotextile in erosion control & strengthening of Sub-grade – Two Case Studies proc. *IGS-CBIP*, New Delhi, Publication No.298.

Engineering Characteristics of the Sand and Pond Ash Mixture Compaction Pile

Jong-Nam Do, Dong-Chan Choi
Dept. Civil of & Environmental Engineering, Hanyang University

Kyung-Min Kim
Geotechnical Engineering & Tunneling Research Division, KICT

Byung-Sik Chun
Dept. Civil of & Environmental Engineering, Hanyang University

ABSTRACT: In this study, choosing the pond ash which has similar engineering characteristics with sands, it was performed clogging test and large direct shear test changing the mixture ratio for studying permeability characteristics and strength characteristics of sands and bottom ash mixture compaction pile.

In the result of large direct shear test, 100% of sand's internal friction angle was 1.18 times larger than 100% of bottom ash's value. Shear strength was increased as bottom ash ratio was more and more because a particle of bottom ash's shear strength characteristics was reflected. In the result of clogging test, a change of permeability was small according to the sands and bottom ash mixture ratio, but as time passes by, hydraulic conductivity was excellent that mixture compaction pile using larger ratio of bottom ash.

1. INTRODUCTION

In recent years Korean economy is growing rapidly due to the influence of industrialization. In particular, investments in large-scale residential complexes, industrial complexes, roads, ports, railroads and airports are continuously made. Accordingly, considering the fact that 70% of the country is mountains in Korea, the necessity of efficient and economical soft ground improvement is gradually increasing.

Accordingly, in Korea, vertical drain methods have been used frequently as large-scale soft ground improvement methods. Among them, the most basic sand drain (SD) method, the most economical Plastic Board Drain (PBD) method, the vacuum consolidation method, and the sand compaction pile (SCP) method have been used according to ground conditions and environment.

In particular, the sand compaction pile (SCP) method installs sand compaction piles in the soft ground with a certain interval(Datye et. al.,1975; Mitchell et. al., 1985). However, sand is short supply in recent years, and has to be imported, and sand collection results in destruction of nature(Madhav et. al., 1978 ; R.D. Barksdale et. al., 1983). So alternative methods are urgently needed.

Accordingly, in this study, pond ash(bottom ash), a substitute for sand used in the sand compaction pile method, which has similar engineering properties, was selected, and the engineering properties were identified through the large-scale direct shear test and the clogging test as a basic research on the compaction pile mixing bottom ash and sand.

2. ENGINEERING PROPERTIES OF BOTTOM ASH

2.1. Basic physical properties

The material used in this study is the bottom ash collected on January 16, 2009 from Yeongheung Thermoelectric Power Plant. To understand the properties of the target bottom ash before the test, the size distribution test, the atterberg limit test for measuring the consistency of bottom ash, and the specific gravity test were conducted. The basic physical properties are shown in Table 1. In general, the bottom ash produced in thermoelectric power plants across the country is classified in most cases as sand, such as SW, SP or SP-SM according to the Unified Soil Classification System, and belongs to the A-1-b group according to the AASHTO classification system (Byung-sik Chun et. al., 2000. The bottom ash used in this study came from Yeongheung Thermoelectric Power Plant, and the result of size distribution analysis showed that it is SW according to the Unified Soil Classification System. The result of the Atterberg limit test showed that it is non-sintering (N.P.).

Table 1. Properties of Bottom ash

Properties	Properties of Bottom ash
USCS	SW
Gravity, G_s	2.27
WL(%)	N.P
IP(%)	N.P
No.4 (%)	99.37
No.200 (%)	2.86
Coefficient of uniformity, C_u	8.0
C_c	2.0

2.2. Characteristics of compaction

Compaction test was conducted for the bottom ash collected from Yeongheung Thermoelectric Power Plant on January 16, 2009 according to the A compaction and D compaction test method. The compaction test is illustrated in Fig 1 and the test result is shown in Fig 2. As for A compaction, the maximum dry unit weight was 1.312t/m3, and the optimal water content was 23.30%, while as for D compaction, the maximum dry unit weight was 1.483t/m3, and the optimal water content was 16.30%. Like general earth and sand, as the compaction energy increased, the maximum dry density increased, and the optimal water content decreased.

Figure 1. Compation test of Bottom ash from Yeongheung thermoelectric Power Plant

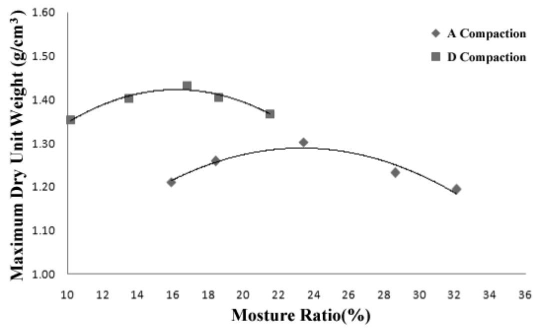

Figure 2. Result of the compaction test of bottom ash from Yeongheung thermoelectric Power Plant

3. INDOOR TEST

3.1. Outline

In this study, to identify the engineering properties of the compaction pile mixing bottom ash and sand, the large-scale direct shear test and the clogging test were conducted while the mixing ratio was varied

3.2. Large-scale direct shear test

The large-scale direct shear test is not clearly defined, but it is generally conducted according to the direct shear test method. In this study, to understand the shear properties of the compaction pile mixing bottom ash and sand, the large-scale direct shear test was conducted while the bottom ash:sand mixing ratio was varied, i.e. 100:0, 80:20, 60:40, 50:50, 40:60, 20:80 and 0:100. In this test the test was conducted at the shear rate of 1mm/hr while the vertical load was varied, i.e. 100, 200 and 300kPa. The dimensions of the large-scale direct shear tester are shown in Table 2.

Table 2. Dimensions of large scale direct shear test

Equipment size	2100mm(L) × 1700mm(W) × 1850mm(H)	
Maximum loading weight	Horizontal	50ton
	Vertical	20ton
Oil pressure valve & control equipment	1~100mm/min	
Oil pressure pump equipment	250kg/cm^2	
Displacement meter	Horizon-tal	200mm
	Vertical	100mm
Shear box size	d=300mm	h=350mm

3.3. Clogging test

In this test, a model tank for simulating the clogging phenomenon, which causes the deterioration of the long-term drainage capacity during the installation of the compaction pile mixing bottom ash and sand in the soft ground, was made, and clay ground was created in the model tank, and the compaction pile mixing bottom ash and sand was installed to measure the drainage capacity of the pile according to the increase of lateral pressure. The shape and configuration of the clogging tester is shown in Fig 3 and 4. If the pressure of the compressor is increased, the clay ground in the model tank will receive water pressure and be consolidated, and the interstitial water in the clay is discharged through the pile with a large coefficient of permeability. □h in Fig. 3 was measured according to the increase of time and lateral pressure, and drainage capacity was evaluated.

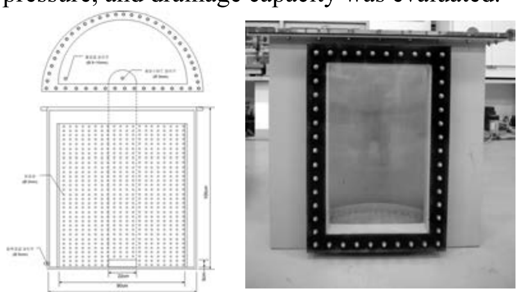

Figure 3. Clogging tester

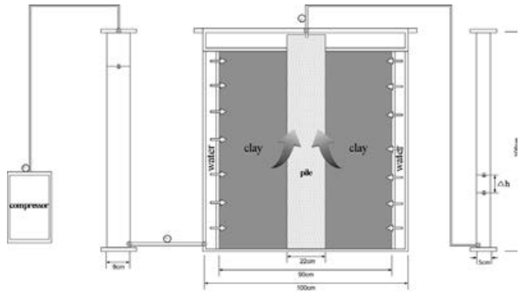

Figure 4. Structure of the clogging tester

4. RESULT OF THE INDOOR TEST

4.1. Result of the large-scale direct shear test

In the coarse-grained compaction pile the fact with the greatest impact on the bearing capacity is the angle of internal friction (Lee Dae-Soo et al., 2005). Accordingly, the cohesion(c) and the angle of internal friction(Φ) was calculated through the large-scale direct shear test while varying the bottom ash:sand mixing ratio, i.e. 100:0, 80:20, 60:40, 50:50, 40:60, 20:80 and 0:100. The result is shown in Fig 5 and Table 3. The result showed that the Φvalue of the 100% bottom ash compaction pile was about 1.18 times greater than that of the 100% sand compaction pile, and that as the mixing ratio of the bottom ash increased, the shear strength parameter increased as well though the difference was very small. As the mixing ratio of the bottom ash increased, it is believed, more of the shear properties of the bottom ash particles were reflected shear.

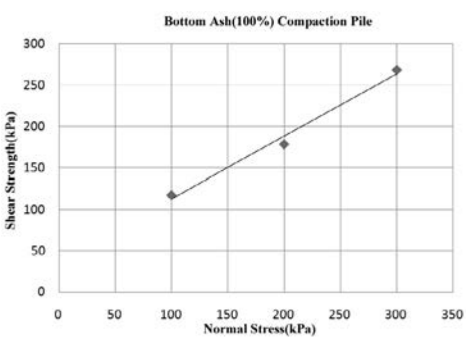

(a) Bottom ash:Sand(100:0)

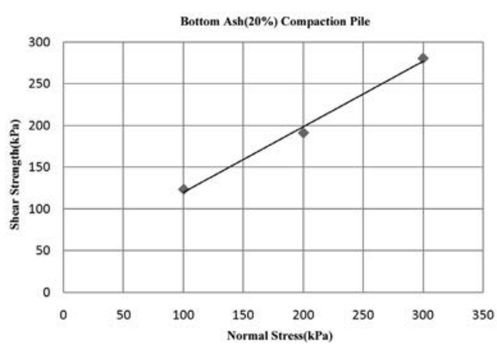

(b) Bottom ash:Sand (20:80)

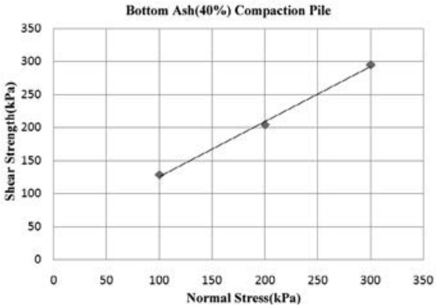

(c) Bottom ash:Sand (40:60)

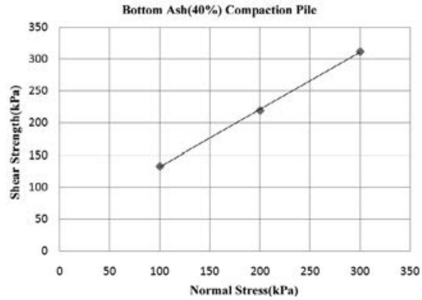

(d) Bottom ash:Sand (50:50)

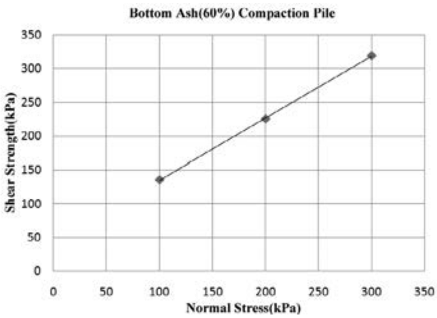

(e) Bottom ash:Sand (60:40)

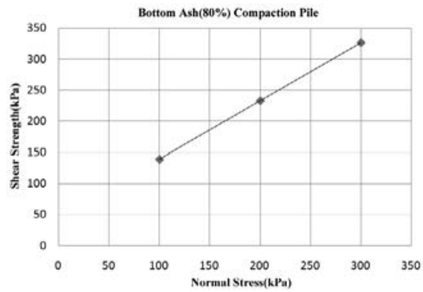

(f) Bottom ash:Sand (80:20)

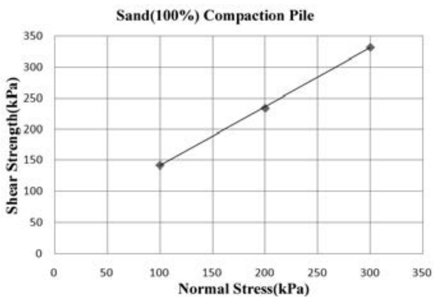

(e) Bottom ash:Sand (100:0)

Figure 5. Result of the large scale direct shear test

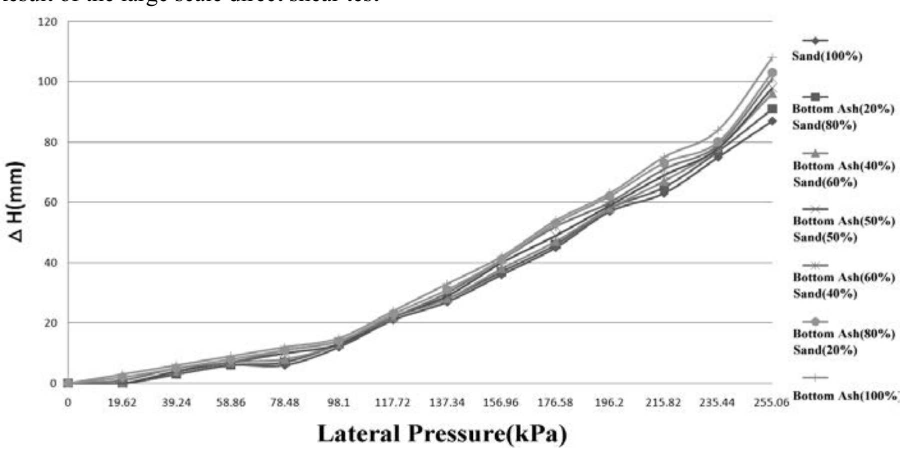

Figure 6. Result of the clogging test

Table 3. Result of the large scale direct shear test

Bottom Ash contents	0	20	40	50	60	80	100
c(kPa)	37.05	41.05	43.01	43.06	42.01	45.76	46.22
Φ	36.86	37.95	39.78	41.75	42.53	43.07	43.53

4.2. Result of the clogging test

The result of the clogging test is shown in Fig 6, and the change in permeability according to the mixing ratio between bottom ash and sand was very small, but as time passed, the drainage capacity of the mixed compaction pile with a large bottom ash mixing ratio was excellent, and thus advantageous to promoting the consolidation of soft ground.

5. RESULT OF THE INDOOR TEST

In this study, bottom ash, a substitute for sand used in the sand compaction pile method, which has similar engineering properties, was selected, and the engineering properties were identified through the large-scale direct shear test and the clogging test as a basic research on the compaction pile mixing bottom ash and sand. The results are summarized as follows.:

(1) The compaction test of the bottom ash collected on January 16, 2009 from Yeongheung Thermoelectric Power Plant was conducted, and the result showed that, for A compaction, the maximum dry unit weight was 1.312t/m3, and the optimal water content was 23.30%, while for D compaction the maximum dry unit weight was 1.483t/m3, and the optimal water content was 16.30%. Like general earth and sand, as the compaction energy increased, the maximum dry density increased, and the optimal water content decreased.

(2) The result of the large-scale direct shear test showed that the Φvalue of the 100% bottom ash compaction pile was 1.18 times greater than that of the 100% sand compaction pile, and as the mixing ratio of bottom ash increased, the shear strength parameter increased as well though the difference was very small. As the mixing ratio of the bottom ash increased, it is believed, more of the shear properties of the bottom ash particles were reflected shear.

(3) The result of the clogging test showed that the change in permeability according to the mixing ratio between bottom ash and sand was very small, but as time passed, the drainage capacity of the mixed compaction pile with a large bottom ash mixing ratio was excellent, and thus advantageous to promoting the consolidation of soft ground.

6. REFERENCES

Byung-Sik Chum, Yoo-Hyeon Yeoh, Baek-Yung Kim, Jin-Suk Yang. 2000. Bearing capacity of Gravel Pile in the Soft Ground, *Proceedings of Fourteenth Southeast Asian Geotechnical Conference*, Hong King, pp.124~131.

Datye, K. R., and Nagaraju, S. S. 1975. Installation and Testing of Rammed Stone Columns, *Proceedings of 5th Asian Regional Conference on Soil Mechanics and Foundation Engineering*, pp. 101~104.

Madhav, M. R. and Vitkar, P.P. 1978. Strip Footing on Weak Clay Stabilized with a Granular Trench of Pile, *Canadian Geotechnical Journal*. Vol. 15. No. 4, pp.605~608.

Mitchell, J.K. and Huber, T.R. 1985. Performance of a Stone Column Foundation, J. Geotech. Eng. ASCE, Vol.111, No.2, pp.205~223.

R. D. Barksdale and R.C. Bachus. 1983. Design and Construction of Stone Columns Vol. I, Turner-Fairbank Highway Research Center, pp. 1~11, pp. 117~118.

Noise control with multifunctional geosynthetics

I. Duzic
Colbond GmbH & Co. KG, Obernburg, Germany

S. Shchukin
Moscow State University Of Civil Engineering MGSU, Moscow, Russia

ABSTRACT: This report deals with sound-insulating geosynthetics. It describes their structure and effectiveness by two practical examples that have been validated by measurements. The project examples refer to applications between residential areas and railway tracks.

1. INTRODUCTION

The increasing building density in large cities requires careful planning of buildings near acoustic sources e.g. railways or machinery which can affect the quality of life. This requires the absorption of vibration that can enter the buildings. However sound-absorbing elements used in building foundations are exposed to moisture, which could negatively influence their sound-absorbing capability as sound propagation in water is faster than in air. (The speed of sound in water is approx. four times higher than in air for boundary temperature of 0°C and a pressure of 1013 hPa). Therefore it would be reasonable to link the "sound absorption" and "drainage" functions. This can be achieved by using special geosynthetic mattings.

Figure 1. Construction at high density of building.

Adequate specification of suitable materials requires not only technical knowledge of the product properties regarding vibration characteristics but also practical experience.

2. SOUND-ABSORBING ELEMENT

The effectiveness of damping structure-borne sounds by using geosynthetic mattings can be explained by the physical model of a Mass-Spring-Damper System (Fig. 2).

2.1. Physical model: Mass-Spring-Damper System (Hering et al. 1995)

The vibrations in the ground are represented by the exciter force F_E. The intensity of this force is reduced by the elastic and damping properties of the geosynthetic mattings.

The elastic support of an exciter mass creates an oscillatory system. If the resonant frequency of the system is lower than the excitation frequency, the oscillation amplitude of the introduced force F_L will be lower than the excitation amplitude. This would lead to a sound insulation.

It can be compared to a floating screed which has an elastic interlayer between it and the reinforced concrete floor to absorb impact noise.

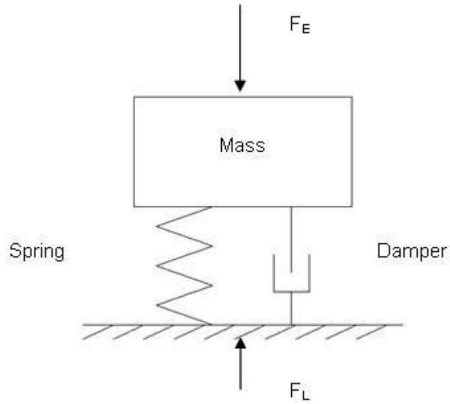

Figure 2. Mass-Spring-Damper System.

The intensity of the sound absorption is described by the insulation efficiency η:

$$\eta = 1 - F'_L / F'_E , \tag{1}$$

F'_L: Amplitude of the introduced force

F'_E: Amplitude of the exciting force

2.2. Geosynthetic mattings

The following geosynthetic mattings shown in figure 3 exhibit spring-damper behaviour.

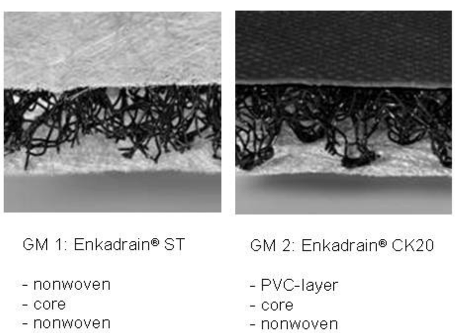

Figure 3. Geosynthetics for drainage and sound insulation.

GM 1 is made of a core of polyamide monofilaments covered on both sides with a nonwoven layer. GM 2 is a variation of GM 1 in which one of the nonwoven layers is replaced by a PVC layer. GM 2 is used for cast-in-situ concrete where the PVC layer prevents seepage of cement laitance. Both products are made of the same core.

The core structure can be described as a Mass-Spring-Damper System. Therefore it can be used as a sound insulating element. One of the most important properties of an insulating element is the dynamic stiffness, which can be measured according to „DIN EN ISO 10846-2“ (2008). The measurements on GM 2 show a very low dynamic stiffness (Siegmann et al. 2009). The lower the dynamic stiffness, the higher the vibration insulation.

In addition to the laboratory test the following project examples show the effectiveness.

3. PROJECT EXAMPLES AND MEASUREMENTS

3.1. Building near railway tracks (Schwab et al. 2005)

In Bern (Switzerland), a new railway switch was installed (Fig. 4). Soon after, a high level of vibration pollution was experienced by people living in buildings close to the switch (approx. 5 metres). The railway was heavily used by approx. 100 trains per day. This required urgent remedial measures to reduce the noise pollution.

Figure 4. Buildings near railway.

A trench was dug between the buildings and the railway. Two layers of GM 1 were installed in the trench and the spaces around filled with gravel concrete.

Measurement 1 – before and after installation of the trench:

Vibration measuring points were defined at the foundation, in the living room and in the garden. The measured variable was the vibration speed. The comparison of 'before' and 'after' measurements revealed a decrease in vibration by a factor of between 2 to 7 after the remedial work (Fig. 5).

Measurement 2 – vibration propagation along the trench (Fig. 6):

Additional measurements along the trench with sensors on both sides should directly show the effect of the trench. Five measuring points were installed on each side. The highest insulation was found at measuring point three. This is located directly at the track-switch and revealed a vibration drop from 6.6 mm/s to 0.8mm/s (Fig. 7).

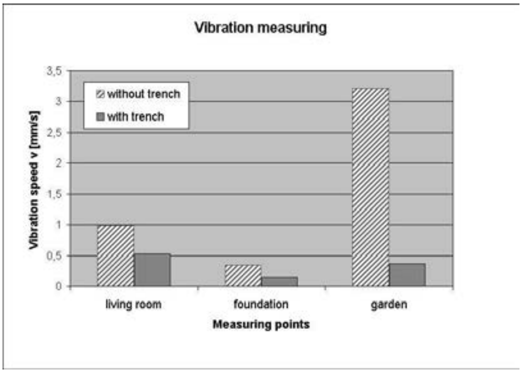

Figure 5. Vibration speed before and after installation of the trench with GM 1.

The trench has significantly decreased the vibrations below the requirements specified in "DIN 4150-2" (1999). Interviews with the residents confirmed the results, which were above expectations.

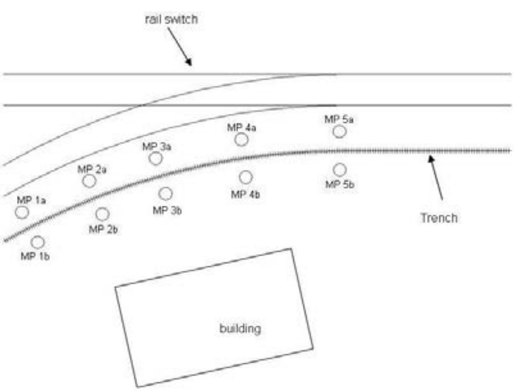

Figure 6. Measuring points in front of and behind trench.

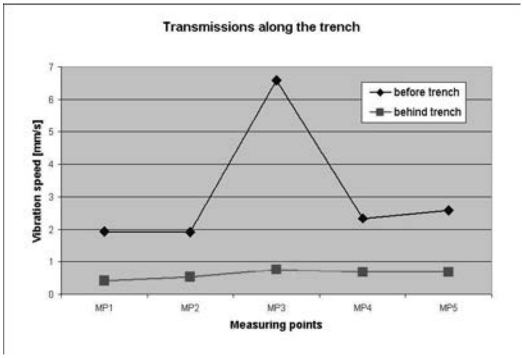

Figure 7. Measuring data in front of and behind trench.

3.2. Building near railway tunnel (Bertschinger 2001)

The new residential area in Grand-Parc, Brunnen is located very close to the railway tunnel of the Gotthard line in Switzerland. Trains that use the tunnel cause vibrations in the ground. The transmission of the vibrations to the nearby buildings had to be prevented.

The living space is decoupled from the vibrations by an elastic layer between the slab and the lower part of the garage area. Thus vibrations caused by trains and introduced to the garage area are decoupled from the living space.

As the building is on a hillside, some walls of the living space had to be backfilled with soil (Fig. 8). To decouple the soil and living space, two layers of GM 1 were installed on the walls to reduce vibration transmission. To evaluate the effectiveness of the GM 1 sound insulation, measurements on the floor were taken at two different times:

Situation A: no backfill
Situation B: walls of living quarters backfilled and GM 1 installed

Both measurements were taken on two busy weekdays.

The results show that the vibration impact is low with only 1dBA increase at situation B compared to situation A. To the human ear a difference of 1 dBA is insignificant. Furthermore a deviation of 1 dBA is within measurement accuracy. The results show that vibrations can completely be absorbed by the GM 1.

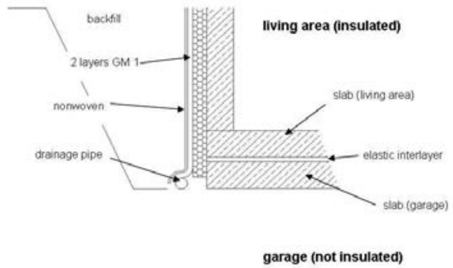

Figure 8. Building near railway tunnel, living space (upper part), garage (lower part).

4. CONCLUSION

The GM 1 and GM 2 geosynthetic blankets combine the functions of drainage and sound insulation. For intra-urban applications between living areas and railways, sound emissions can be reduced and the quality of life increased. Switzerland has a high building density and a lot of experience in the use of geosynthetic materials for vibration reduction. The use of GM 1 and GM 2 is not limited to railway applications; it can also be used for decoupling buildings from each other.

5. REFERENCES

DIN 4150-2: 1999. Erschütterungen im Bauwesen Teil 2: Einwirkungen auf Menschen in Gebäuden. Deutsches Institut für Normung e.V., Berlin, Germany

DIN EN ISO 10846-2: 2008. Akustik und Schwingungstechnik – Laborverfahren zur Messung der vibro-akustischen Transfereigenschaften elastischer Elemente – Teil 2: Direktes Verfahren zur Ermittlung der dynamischen Steifigkeit elastischer Stützelemente bei Anregung in translatorischer Richtung. Deutsches Institut für Normung e.V., Berlin, Germany

Hering E., Martin R. and Stohrer M. (1995). Physik für Ingenieure, 5.Auflage, VDI Verlag GmbH, Düsseldorf, Germany

Bertschinger, H.P. (2001). Grand-Parc Brunnen Vergleichsmessungen, Stauffer Engineering GmbH, Ottenbach, Schweiz

Schwab, M and Gloor, D. (2005). BLS Doppelspurausbau Fischermätteli-Weissenbühl: Bodenschlitz als Abschirmung gegen Erschütterungen, Erfahrungsbericht, Gartenmann Engineering AG, Bern, Schweiz

Siegmann J., Waßmann R. and Dinh T. T. (2009). Bericht Nr. 208/09 über die Ermittlung der dynamischen Bettungsziffern einer Multifunktionsmatte Enkadrain CK20, TU Berlin, Schienenfahrwege und Bahnbetrieb, Berlin, Germany

Use of Jute Geotextiles in MSW land fills

Tapobrata Sanyal
Geotechnical Advisor, Jute Manufactures Development Council, Kolkata, India

ABSTRACT: Disposal of municipal solid wastes (MSW) is a matter of concern all over the globe. The problem is more acute in developing countries in Asia due to unbridled population growth. Though engineered sanitary land fills are one of the preferred modes of disposal of MSW, there are cases of failure of MSW dumps in Asia.

The main reason behind such failures is heterogeneous composition of MSW with varying and sometimes unpredictable settlement behavior. Settlement-more aptly consolidation–is a protracted process. The entrapped moisture/water within MSW fills triggers the process of destabilization of dumps.

Extraction of water from inside MSW fills can be quickly and conveniently done by inserting pre-fabricated vertical jute drains (PVJD). Capping of dumps can also be done conveniently by covering the top of dumps by non-woven jute geotextiles. The advantage is that jute is eco-concordant, highly water-absorbent and bio-degradable and can also create a congenial micro-climate conducive to vegetation.

INTRODUCTION

Disposal of municipal solid wastes (MSW) is a matter of great environmental concern all over the globe. The problem is more acute in developing countries in Asia which accommodate about 60.5% of the global population with a high degree of density. Engineered sanitary land-filling is one of the preferred modes of disposal of MSW in urban conglomerates in China and India (around 90%) principally because of its cost-competitiveness with other modes and comparative operational ease. But there still remains a hiatus between the professed standards and quality of implementation. There are several instances of massive failure of MSW dumps in Asia.

The failures are pointers to adopt geo-environmental interventions in regard to MSW landfills. Besides water, leachate flow and harmful gas generation, aspects of settlement of landfills, instability of MSW dumps and contaminant transport require remediation.

The existing system of stabilizing, capping, anti-settlement methods may be conveniently replaced by use of appropriately designed Jute Geotextiles (JGT) that can act as separator, filter and drainage facilitator. JGT are eco-compatible, highly hygroscopic, get integrated with MSW/soil on bio-degradation enhancing the hydraulic conductivity of MSW fill and facilitate growth of vegetation when exposed by acting as mulch. Extraction of water from within MSW fills can be effectively done by insertion of pre-fabricated vertical jute drains (PVJD).

The paper presents a concept on prospective use of JGT in MSW landfills with distinct cost- and technical advantages.

COMPOSITION OF MSW

Municipal solid wastes are heterogeneous in character. Kitchen & garden wastes, metal, glass, waste paper, plastics, remnants of textiles, rubber, wood and the like are typical constituents of MSW in varying proportions. Evidently their degradability, compressibility, hygroscopic property, hydraulic conductivity and shear strength are at wide variance. Proportion of the constituent waste materials also varies from place to place depending largely on the life style of the residents.

Significant studies have been conducted on the nature of MSW composition in China, India, Korea, Singapore, U K, USA and other countries (Chen et al 2007). MSW in India and China have a larger share of kitchen and garden wastes (about 40%-50%) than other countries. Time taken by the organic waste conglomerates to bio-degrade in a MSW dump plays a significant role in its stability. No MSW classification system based on geotechnical characteristics is available at present presumably because of lack of authentic data.

SALIENT CHARACTERISTICS OF MSW

To ensure stability of MSW dumps it is important to ascertain the hygroscopic property of such dumps. It has been found (Koerner & Soong-2000) that entrapped moisture within MSW dumps triggers the process of destabilization of MSW fills. Water-retention characteristics of MSW dumps also determine the rate of leachate generation.

Pore water pressure held by osmotic and capillary pressures when in excess destabilize a waste dump. Retention of water within a fill is also caused as a result of hydrophilic materials such as plastics. Pore water pressure usually develops in organic wastes bio-degradation of which may result in release the entrapped pore water. Water retention of MSW depends also on the degree of compaction of the wastes and overburden pressure, besides the degree of organic bio-degradation.

Quite a few researchers have studied hydraulic conductivity of MSW by performing permeability tests or leachate pumping tests. It has been found that the value of hydraulic conductivity of MSW is usually in the range of 10^{-6} to 10^{-4} m/s which suggests that the overall hydraulic conductivity of MSW is similar to fine sand and silty sand (Chen et al 2007). In China it has been found that hydraulic conductivity of waste fills depend on overburden pressures up to 300 kPa (Chen et al 2005).

Degree of saturation of MSW also affects its hydraulic conductivity. Clogging of pores within a waste dump is another factor to reckon with in this respect. It is relevant to point out that cohesion values of MSW vary from 0 to 67 kPa while angle of internal friction ranges from 10^o to 53^o.

CAUSES OF FAILURE/SETTLEMENT OF MSW DUMPS/FILLS

Settlement of MSW landfills is influenced by a number of factors. Composition of MSW being heterogeneous in character, its settlement behavior is apt to vary. Waste dumps as already indicated are usually highly compressible and bio-degradable. Settlement of MSW is a protracted process and could reach to the extent of 30% to 40% of the initial fill height. Moreover landfill expansion has become common, necessitating installation of a separator between the existing and the extended waste dumps. Differential settlement upsetting the leachate drainage system of MSW landfills has also been reported.

The other reason could be imprecise assessment of the angle of internal friction of MSW mass. The angle varies between 10° to 53° while cohesion hovers between 0 to 67 kPa (Machado et al 2002).

By far the most critical factor triggering instability of MSW dumps and settlement of MSW landfill is entrapment of water within (Koerner & Soong 2000). Dumps are often raised to a height of 50 meters without any semblance of compaction. In land-fills organic and inorganic wastes are seldom segregated leaving chances for differential settlement in land-fills. Entrained water squeezes out to some extent due to mechanical compaction. Prediction of settlement of landfills built with MSW has in fact remained elusive because of the wide range of heterogeneity of MSW.

Three mechanisms of compression in MSW have been recognized (Chen et al 2007) e.g. instantaneous compression & compression due to applied load (primary compression), compression due to waste decomposition and mechanical creep (secondary compression). The situation assumes complexity when there is layered settlement due to variation of share in organic wastes. Compression due to such decomposition is reported to be between 18% and 24% of the waste thickness (Coduto & Huitric-1990). The process of settlement due to decomposition may continue for years.

JUTE GEOTEXTILES (JGT)

Geotextiles made of jute fibres may control both settlement and rotational slides in high MSW dumps and settlement in MSW landfills. Jute fibres are ligno-cellulosic in character with inherent properties suitable for manufacturing tailor-made geotextiles. The first jute mill was set up near Calcutta (now Kolkata) in West Bengal, India way back in 1855. Today the number of jute mills in India is 77. Jute is abundantly grown in the eastern region of the Indian sub-continent (includes Bangladesh) and jute industry happens to be one of the oldest surviving agro-industries in the world.

ADVANTAGES OF JGT

Technical advantages of JGT are several. These are –

- High initial strength
- Low elongation at break

- Being highly water-absorbent (about 5 times its dry weight), effects better on-land storage than any other geotextile. An excellent drainage medium.
- Its 3-D construction helps reduce the velocity of overland flow and entrap detached soil particles thus facilitating control over surface soil erosion
- Leads all other natural fibres in respect of spinnability
- Its drapability is the best of all geotextiles — man-made and natural
- Environment-friendly. Acts as mulch. On biodegradation it becomes immiscible with soil and improves its hydraulic conductivity.

Besides, JGT has the following commercial advantages. These are –

- Easy availability
- Can be tailor-made to comply with the specifications of the end-users
- Cost-competitive compared to man-made geotextiles.

SUGGESTED REMEDIAL MEASURES WITH JGT

As already indicated in the preceding, the major cause of settlement of solid waste dumps/fills is entrapment of water within. One of the possible ways to overcome the problem is to use eco-compatible Pre-fabricated Vertical Jute Drain (PVJD) [Figure 1]. It is well known that riddance of water from compressible soil mass hastens its natural consolidation. The time for consolidation depends upon the square of the distance the water takes to pass out of the soil. The installation of PVJD and other band drains shortens drainage paths for the water and therefore quickens the process of consolidation.

PVJD consists of an outer sheath made of jute within which there are coir or jute wicks. The sheath is normally of plain weave (FIBRE drain as developed by S L Lee et al) or braided (BRECO drain as developed by P K Banerjee et al). The indicative features of PVJD are shown in Table 1.

PVJDs can be pre-inserted at the site of solid waste dumping with the help of bamboo poles or similar rigid uprights. The height of dumps should be pre-fixed. A network of wider PVJDs may be installed on the top surface for lateral drainage of water that comes up due to capillary action. Wider PVJDs would be less expensive and would ensure better and quicker drainage. Wider PVJDs can be laid at suitable levels if the height of dump is more than 6 meters high. It needs to be studied the extent of effectiveness of the proposed PVJD-system against primary and secondary compression and associated long-term settlement of solid waste dumps.

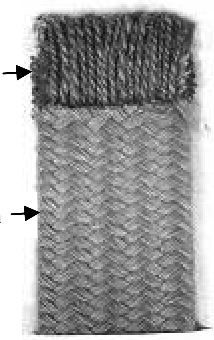

Figure 1. Pre-fabricated braided vertical jute drain

Conventional design of man-made band drains stresses on two aspects –

-- prevention of piping
-- adoption of a sheath having AOS larger than that of the surrounding soil.

For prevention of piping, US Army Corp of Engineers follows the following empirical relation

$$O_{85}/d_{85} \leq 1, \quad (1)$$

Regarding the second criterion hydraulic conductivity of the sheath should at least be 10^{-4} m/s in view of the fact that the usual soil-surrounds have hydraulic conductivity of the order of 10^{-6} m/s or less.

The other important aspect of band drain design is to determine the equivalent drain diameter D_e and equivalent zone of influence Z_e. According to Kjellman, band drain efficiency is dependent more on its circumference than its cross-section. He has suggested the following relation –

$$D_e = 2(B + t)/\pi \approx 2B/\pi(m), \quad (2)$$

where B stands for breadth of the band drain (strip) and t for its thickness.

Table 2 highlights the properties of typical nonwoven geotextile.

Table 1. Indicative features of PVJD

Sl	PROPERTIES	FIBRE Drain	BRECO Drain
1	Width (mm)	Bet. 90 & 100	Bet. 90 & 100
2	Thickness at 20 kPa (mm)	Bet 8 & 10	Close to 10
3	Strength (kN)	4.5	2.4
4	Elongation (%)	4 to 5	5 to 6
5	EOS-O_{95} of sheath (mm)	0.6	> 0.3
6	Permeability at 50 mm head at 2 kPa (mm/sec)	0.41	0.54
7	Discharge capacity at 50 kPa at unit hydraulic gradient (ml/sec)	13.1 (with 4 coir wicks)	22 (with 16 coir wicks)

The number of PVJD would depend on the covered area of a dumping site. Based on the analysis of Kjellman the equivalent zone of influence (Z_e) is 1.05 L for triangular grids and 1.13 L for square grids of vertical drains where L stands for spacing of vertical drains may be adopted. Each drain is supposed to cover a vertical cylinder of soil of depth equal to the band drain length. It is also assumed that (i) horizontal sections remain equal (despite unequal degree of consolidation), (ii) the drain functions as an ideal well without any through-flow resistance and (iii) Darcy's Law will be applicable to the ground water flow.

It may be mentioned that non-woven JGT (usually 500 gsm variety) can be used as daily cover over dumps to check air pollution and infestation by rats and vermin. Daily covers with non-woven JGT can drain off surface water that comes up from inside the dumps and that falls on surface as precipitation at intermediate stages. Non-woven JGT is cheaper than the woven variety of JGT, more permeable and better water-absorbent and drainage facilitator.

COST

The usual width of PVJD is 100 mm though drains having a width of 85 mm can be manufactured complying with end-user requirements. The strength and porometry of the jute sheath can also be tailor-made. Usually a PVJD of 100 mm width with a strength of 45 kN/100 mm and pore-sizes of 300 microns costs US $0.25 per linermeter (ex-factory in India).

CLOSURE

Use of Jute-made vertical band drains and/or non-woven JGT may be useful for stabilizing MSW heaps if there is no arrangement for recycling MSW otherwise. Environmentally concordant greenery can be developed on such heaps aided by jute's mulching action and ability to create congenial micro-climate that facilitates growth of vegetation.

While accepting the effectiveness of PVJD, it is however felt that there is need to modify the Kjellmann-relations considering the characteristics of jute especially its hygroscopic character and transmissivity. Empirical relations can be established by undertaking field trials with PVJD.

Table 2. Specifications of Non-woven Jute Geotextiles

Mass per unit area (g/m^2) [ASTM D5261]	500
Thickness (mm) at 2 kPa [ASTM D5199]	4
Width (cm) [IS 1954]	150
Tensile Strength (kN/m) [MD x CD] [ASTM D4595]	4 x 5
Elongation at break (%) [MD x CD] [ASTM D4595]	20 x 25
Apparent Opening Size, O_{95} (μm) [ASTM D4751]	500
Permittivity at 50 mm constant head (s^{-1}) [ASTM D4491]	1.94

ACKNOWLEDGEMENT

The author is grateful to Mr. P. K. Chaudhury and Dr. Mahuya Ghosh of Indian Jute Industries' Research Association, Kolkata, India for furnishing relevant inputs.

BIBLIOGRAPHY

Banerjee, P.K. Rao, G.V. & Sampath Kumar, J. P. 1997. Characteristics of BRECO drain for soft soil consolidation - *Geosynthetics Asia 1997 at Bangalore, India*

Chen, Y. Ke, H. & Zhan, L. 2005. Experimental study on engineering properties of municipal solid waste in China-*Proceedings of the 2nd Germany conference on Geo-environmental Engineering*

Chen, Y. & Zhan, L. 2007. Geo-environmental Issues associated with landfills of municipal solid wastes-*Proceedings of the 13th Asian Regional Conference on Soil Mechanics & Geotechnical Engineering at Kolkata, India*

Coduto, D. P. & Huitric, R. 1990. Monitoring landfill movements through precise instruments-*Geotechnics of Waste Fills-Theory & Practice, STP 1070, ASTM*

Van Zanten, R. V. 1986. Geotextiles And Geomembranes in Civil Engineering- *Published by A A Balkema , Rotterdam/Boston*

Koerner, R.M. & Soong, T.Y. 2000. Stability assessment of ten large landfill failures-*Advances in transportational & geo-environmental system using geosynthetics- ASCE Geotechnical special Publication no 103*

Machado, S. L. Carvalho, F. M. & Vilar, O. M. 2002. Constitutive model for municipal solid waste-*Journal of Geotechnical & Geo-environmental Engineering Vol 127/No 11*

Ramaswamy, S.D. Natural fibre prefabricated drain — A case study- *Geosynthetics Asia 1997 at Bangalore, India*

The effect of oil contamination on the shear strength, settlement and compressibility of the sand

M. Jiryaei Sharahi
National Petrochemical Co. of Iran, Petrochemical Industries Development Management Co., Tehran, Iran

ABSTRACT: Onshore and offshore oil spills, contaminate soil and ground water, thus, The geotechnical properties such as shear strength, settlement and compressibility altered. In this investigation, an laboratory testing program was carried out to determine the influence of crude oil contamination on the shear strength, settlement and compressibility parameters of the sand. Testing Include basic properties, triaxial, compaction and consolidation tests on clean and contaminated sand with various oil contents. The results Indicated reduction in strength and Increase in settlement and compressibility.

1. INTRODUCTION

Every year several onshore and offshore spills occur around the world, and these oil spills ultimately contaminate the soil. The physical properties of the oil–contaminated soil will also control the stability of slopes as well as the bearing capacity of foundations and other structures.

Very few studies that deal with geotechnical properties of contaminated soils are available in the literature. Eving and Das (Evgin & Das, 1992) carried out triaxial tests on clean and contaminated sand. They found that full saturation with motor oil caused a significant reduction in the friction angle of both loose and dense sands. Meegoda and Ratnaweera (Meegoda & Ratnaweera, 1994) examined the compressibility of contaminated fine-grained soils by consolidation tests. The results revealed increased compressibility. They proposed correction factors to account for the change in the compression index caused by viscosity of the pore fluid. Results of Alsanad et al. tests (Alsanad et al., 1995) indicate a small reduction in strength and permeability and an increase in compressibility due to contamination. the results show, increased strength and stiffness due to aging and a reduction of the oil content due to evaporation of volatile compounds. Aiban (Aiban, 1997) shows the effect of moisture content and temperature on the engineering properties of oil contaminated sands by modified oedometer and triaxial setups. results of Sheen et al. laboratory tests (Sheen et al., 1999 & 2001), indicate oil contamination of the unsaturated sand reduce the bearing capacity of a surface strip foundation. In the work of Puri (Puri, 2000), hydraulic conductivity was observed to be a function of the initial viscosity and the degree of oil saturation. However it appears that further and more complete studies are necessary to quantify several parameters which are of interest to geotechnical engineers. The purpose of this paper is to determine the influence of crude oil contamination on the shear strength, settlement and compressibility parameters of the sand by triaxial, consolidation, and compaction tests.

2. SAND AND CRUDE OIL USED FOR TESTS

Babolsar sand from the north of Iran was used for the present laboratory tests. Sieve analysis tests were conducted on representative samples of the sand. Fig.1 shows the grain size distribution curve of this sand which is classified as SP or poorly graded sand, according the Unified Classification System. The sand has the specific gravity of 2.66, the maximum and minimum dry densities 1.77 g/cm^3 and 1.51 g/cm^3 in accordance with ASTM D4253 and D4254 and 1 percent natural water content.

Maroon crude oil from Iran was used as the contaminant. This crude oil had the following parameters: specific gravity of 0.858, vapor pressure = 57.3 KPa, oil content = less than 20 percent, and sulphur content = less than 1 percent.

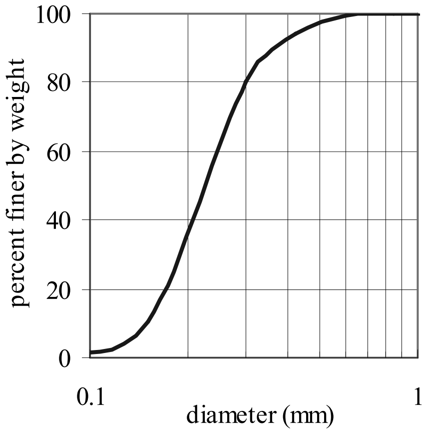

Figure 1. Sieve analysis of the used sand

All samples for triaxial, consolidation tests were remolded in the test mold with static compaction to achieve homogeneity and uniformity and the required relative density. In the case of contaminated specimens, the amount of oil was calculated as a percent by weight of the dry sand, as follows

$$w_{oil} = \frac{w_o}{w_s} \quad (1)$$

where w_{oil} , w_o and w_s are the oil content, weights of the oil and dry sand, respectively. It was then mixed with the predetermined weight of the dry sand to give the required relative density after that the specimen was mixed with required water. The triaxial test specimens were molded in a thin–walled tube, compacted from both sides to the required dimensions.

3. COMPACTION TESTS

Standard proctor compaction tests were carried out on clean sand and on the same sand after mixing it with 2, 4, 6, and 8 percent by weight of crude oil, the results are plotted in Fig.2 in the form of dry density versus water content curves. The maximum dry density for this sand is 1.7 g/cm^3 at an optimum moisture content of 12 percent. With the presence of oil up to 4 percent better compaction characteristics were achieved. For example, with 2 percent of oil additive the maximum dry density reached 1.72 g/cm^3 at a moisture content of 9 percent. With 4 percent oil the maximum dry density and optimum moisture content were 1.74 g/cm^3 and 7.7 percent, respectively. This reflects the lubricating effect caused by the presence of oil, which facilitates compaction and reduces the amount of water needed to reach maximum density. However, with further increase of the oil content to 6 percent, the compaction curve had inferior compaction characteristics. From these compaction tests, it appears that the field compaction of the oil contaminated sands will be extremely difficult if the oil content exceeds 6 percent.

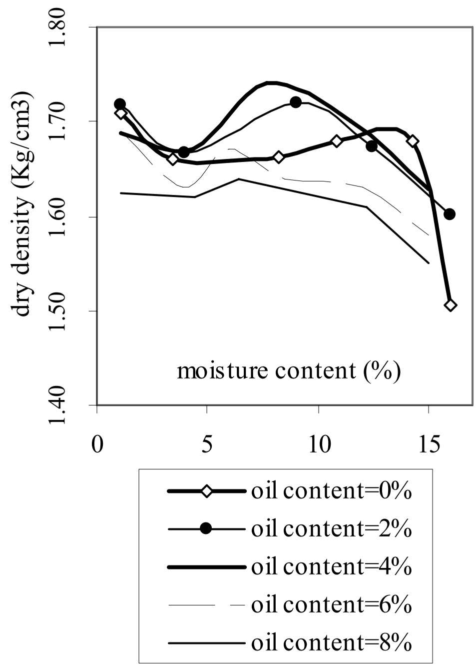

Figure 2. Compaction curves for various oil contents.

4. CONSOLIDATION TESTS

Consolidation tests were carried out on clean sand, and same sand mixed with 2, 4, 6 and 8 percent crude oil. All specimens were 75 mm diameter × 20 mm thickness and were prepared at a relative density of 60 percent and saturated with water prior to the tests. The results are plotted in Fig.3 in the form of e–logp' curves. As can be seen, the compressibility increased substantially in the presence of crude oil. The compression index, C_c, increased from 0.027 for clean sand to 0.039 with 2 percent oil content, to 0.48 with 4 percent oil content, to 0.053 with

6 percent oil content, and to 0.055 with 8 percent oil content. This compressibility, although not significant or large, more than doubled due to crude oil contamination. Mechanical factors such as viscosity facilitate the sliding of particles due to lubrication of soil particles, which will cause an increase in the compression index with an increase in viscosity.

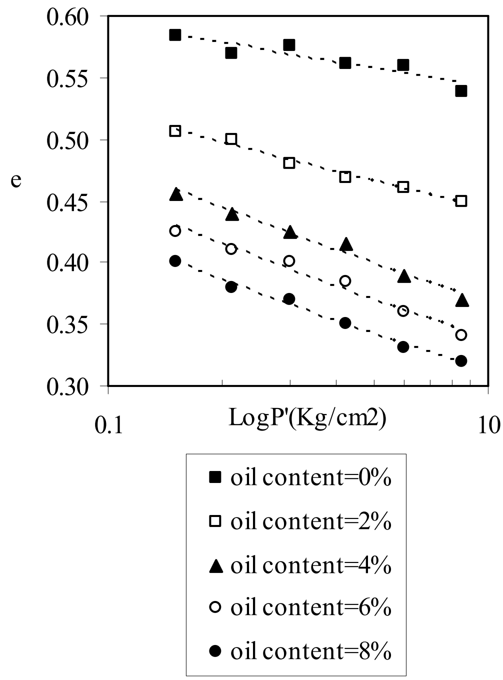

Figure 3. Normally consolidation curves for various oil contents and relative density of 60%

5. TRIAXIAL TESTS

Consolidated drained (CD) triaxial tests were conducted on clean sand and sand mixed with 2,4,6,and 8 percent of crude oil. All specimens being 38 mm diameter and 80 mm height, were perpared at relative densities of 30,60, and 90 percent and were saturated prior to the test by application of back pressure.

Consolidated undrained (CU) triaxial tests were conduct on clean sand and sand mixed with 3,5, and 7 percent of crude oil too.

Fig.4 shows the variation of the ultimate friction angle, φ_{ult} , for various relative densities and oil contents. From these figures it appears that φ_{ult} decreases with increase of the oil content. For example ultimate friction angle decreases from 32 degree to 24 degree with increase of oil content from 0 percent to 8 percent in relative density of 60 percent. However, with increase of the oil content from 3 percent, the rate of decrease of ultimate friction angle was smaller. This is probably due to the fact that the surface of the sand grains will initially become coated with oil which results in a decrease in friction when the sand grains slip and slide over each other.

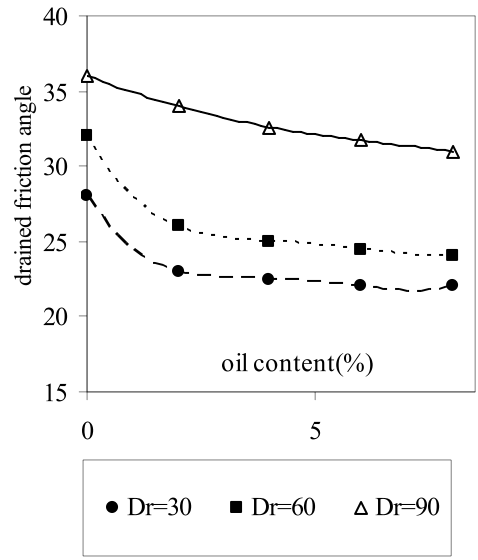

Figure 4. Drained friction angle-oil content curves resulted from CD triaxial tests.

Variation of the tangent modulus, E_i, with various oil contents and relative densities is shown in tables1-3. It appears that E_i decreases with increase of the oil content. For example for relative density of 60 percent and confined pressure 2.5 kg/cm^2 E_i decreases from 44.3 MPa for clean sand to 22.1 MPa for sand with 8 percent oil content.

Table 1. Ei values for various relative densities and oil contents (σ3=1 kg/cm2)

Oil content	Relative density (%)		
	30	60	90
0	21	30	53.6
2	16.3	21	39.6
4	14	18.6	35
6	11.7	16.3	30.3
8	11.6	16	28

Results of the CU triaxial tests are shown in Fig.5. these results are in clear agreement with the results of the CD triaxial tests.

Table 2. Ei values for various relative densities and oil contents (σ3=2.5 kg/cm2)

Oil content	Relative density (%)		
	30	60	90
0	30.3	44.3	70
2	23.3	32.6	54
4	19.8	25.6	44
6	17.5	23.3	40
8	16.3	22.1	38

Table 3. Ei values for various relative densities and oil contents (σ3=4 kg/cm2)

Oil content	Relative density (%)		
	30	60	90
0	39.6	55.9	88
2	30.3	41.9	68
4	25.6	32.6	56
6	23.3	30.3	52
8	21	28	48

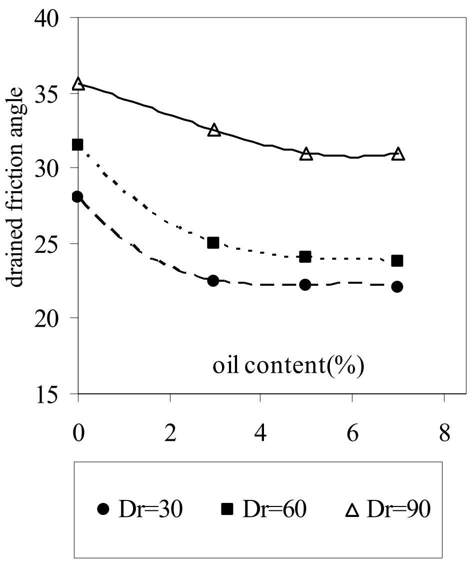

Figure 5. Drained friction angle-oil content curves resulted from CU triaxial tests.

6. CONLUTIONS

The results of triaxial tests on crude – oil contaminated sand at threee relative densities, compaction tests, and consolidation tests are presented . Based on test result the following conclusions can be drawn: i) when the crude oil content increase from zero to about 3 percent the friction angle decrease mostly and for oil content further than 3 percent the reduction in friction angle is not substantial. ii) with the increase of oil content, the compression index increases. Thus with the increase of oil content, the consolidation settlement increases. iii) compaction characteristics of sand improve with the presence of oil up to 4 percent by weight. with 6, and higher percent crude oil the maximum dry density decreased sharply.

7. REFERENCES

Aiban, A. 1998. The Effect of Temperature on the Engineering Propertios of Oil–contaminated Sand. *Journal of Environmental International*, Vol. 24, No.1/2, PP: 153-161.

AASHTO. (12th edition) 1978. *Standard Specifications for Transportation Materials and Methods of Sampling and testing*, partI Specifications (PP 828); part II, Tests (PP 998). Washington DC.

Al-Sand, H.A. & Eid, W.K. 1995. Ismail, N.F. Geotechnical Properties of Oil-contaminated Kuwaiti Sand. *Journal of Geotechnical Engineering*, ASCE, Vol. 121, No. 5, PP: 407-412.

Al –sanad, H.A. Ismael, N.F. 1997. Aging Effect on Oil- contaminated Kuwaiti Sand. *Journal of Geotechnical and Geoenvironmental Engineering*, Vol.123, No.3, PP: 290-294.

ASTM. 1991. *Annual Book for ASTM Standards*, vol. 04.08, Philadelphia.

Sheen, E.C. & Lee, J.B. & Das, B.M. 1999. Bearing Capacity of a Model Scale Footing on Crude Oil-contaminated Kuwaiti Sand. *Journal of Geotechnical And Geological Engineering*, Vol.17, PP: 123-132.

Sheen, E.C. & Lee, J.B. & Das, B.M. 2001. Bearing Capacity of Unsaturated Oil-contaminated Sand. *International Journal of Offshore and Polar Engineering*, Vol.1, No.3.

Evign, E. & Das, B.M. 1996. Geotechnical Proprties of Oil- contaminated Sand. *Proceeding of 49 th Canadian Gecotechaical Conference*,

Mohammed, L.F. 1995. Performance and Persistence of Oil Binder in Oil–Stabilized Bahraini Soil. *Proceeding of Second Regional Conference of the ASCE-Saudi Arabia Section*, Vol.I, Beirut, Lebanon, PP: 287-299.

Puri, V.K. 2000. Geotechnical Aspects of Oil-Contaminated Sands. *Soil and Sediment Contamination: An International Journal*, Vol. 9, No. 4, PP: 359-374.

Material Properties of Ductile-Fiber-Reinforced Cementitious Composite Using Pyroclastic Flow Deposits

K. Watanabe, M. Fujii
Tokai University, Japan

M. J. Arai
System Measurement Co., Ltd., Japan

ABSTRACT: Recently, ductile-fiber-reinforced cementitious composites (DFRCC) have been developed, which show performances largely superior to those of fiber-reinforced concretes so far known. DFRCCs are composites of cementitious material reinforced with fibers, which have multiple cracking characteristics and much improved toughness during bending, tension, and compression fractures.

In the present study, we have used white cement and shirasu, which is pyroclastic flow deposits obtainable in a large quantity from South Kyushu, as fine aggregate and examined material properties of white cement-shirasu mortar reinforced with PVA fibers, targeting at its use for pavement panels as a secondary product of concrete.

1. INTRODUCTION

Nowadays it becomes very important to deal with global environmental issues, and also in concrete industries, researches on concretes with recycled aggregates have extensively been carried out, in order to solve the problem of environmental destruction due to natural aggregate extraction, as well as the problem of exhaustion of natural aggregate resources.

Basing on this background, Takewaka et al. (Takewaka et al., 1987) and Kawamata et al. (Kawamata et al., 1988) have respectively made a series of investigation on the applicability of shirasu, which is pyroclastic flow deposits obtainable in a large quantity from South Kyushu, as an alternative to fine aggregate for concretes, and revealed the mix proportion and material properties such as strength of shirasu concrete. Examples of the application of shirasu concrete to pier foundations have also been reported (Takewaka, 2004). Kaku et al. have proposed a formula for estimation of concrete strength basing upon their study on concretes with shirasu as fine aggregate and lapilli as coarse aggregate (Kaku et al., 1989).

From these results, the alternative use of shirasu to fine aggregate for concretes appears promising, and shirasu concrete can be used not only for members of structures, but also for a variety of other applications.

The present authors have also investigated the mix proportion, strength and durability of white cement-shirasu mortar prepared from white cement with shirasu as fine aggregate, targeting to use this mortar as pavement panels as a secondary product of concrete (Watanabe et al., 2008). The results show that 1) the relation between the 28 day compressive strength and the cement to water ratio for white cement-shirasu mortar is linear, as is found for general cement and that 2) the 28 day compressive strength does not change significantly with the change in fine aggregate to cement ratio if the water to cement ratio is constant.

Recently, ductile-fiber-reinforced cementitious composites (DFRCC) have been developed (Naaman et al., 1996; Li, 1993; BRI et al., 2000; JCI, 2002), which show performances largely superior to those of fiber-reinforced concretes so far known. DFRCCs are composites of cementitious material reinforced with fibers, which have multiple cracking characteristics and much improved toughness during bending, tension, and compression fractures (JCI, 2002). An attempt to use them as energy absorbing devices of structures has been reported (BRI et al., 2000). It is expected that DCRCCs may contribute considerably to improvement not only in strength performance but also in durability, by applying them to secondary products of concrete.

Thus, in the present study, we have used white cement and shirasu as fine aggregate and examined material properties of white cement-shirasu mortar reinforced with PVA fibers,

Table 1. Outline of specimens.

Specimen	Cement	Fine aggre-gate	Water-cement ratio (W/C) (%)	Fine aggregate-cement ratio (S/C)	Fiber volume fraction (V_f) (%)
WHS40-VF0	WH	S	40	0.15	0
WHS40-VF2					2
WHS40-VF3					3
WHS50-VF0			50	0.40	0
WHS50-VF2					2
WHS50-VF3					3
WHS50-VF4					4
WHS60-VF0			60	0.80	0
WHS60-VF2					2
WHS60-VF3					3
OPN40-VF0	OP	N	40	0.60	0
OPN40-VF3					3
OPN50-VF0			50	0.80	0
OPN50-VF3					3
OPN60-VF0			60	1.00	0
OPN60-VF3					3

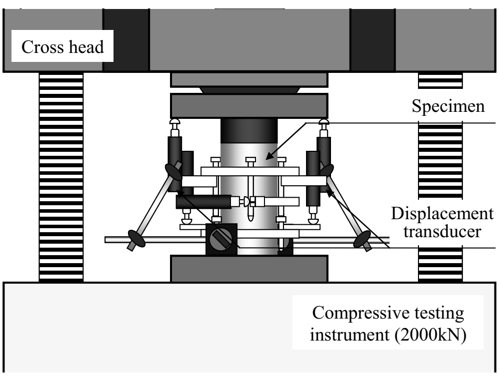

Figure 1. Compressive loading system.

targeting at its use for pavement panels as a secondary product of concrete.

2. EXPERIMENTAL METHOD

In the present study we have carried out uniaxial compression tests and notched beam 3-point bending tests for plain mortar and fiber-reinforced mortar specimens listed in Table 1. Two kinds of mortars were examined, namely white cement-shirasu mortar (WHS) with use of white cement (WH, density: 3.05g/cm^3) and shirasu (S, surface-dry density: 2.09g/cm^3, water absorption: 6.53%, fineness modulus: 1.32), and ordinary natural aggregate mortar (OPN) with use of ordinary Portland cement (OP, density: 3.16g/cm^3) and natural fine aggregate (N), which is a 7:3 mixture (mass ratio) of crushed sand (surface-dry density: 2.70g/cm^3, water absorption: 1.36%, fineness modulus: 2.94) and pit sand (surface-dry density: 2.57g/cm^3, water absorption: 2.55% ,

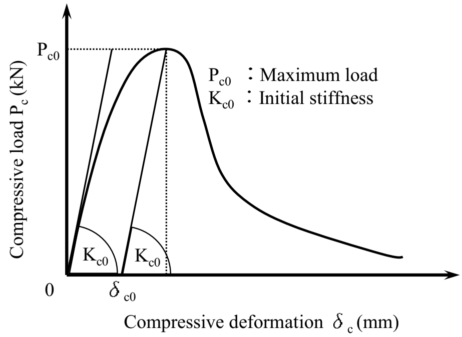

(a) Compressive load-compressive deformation relation.

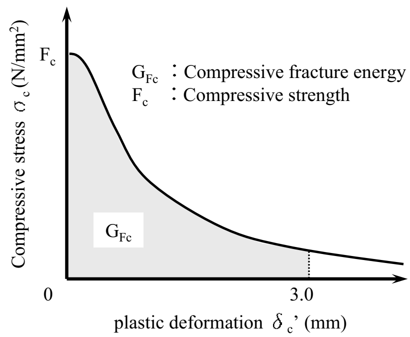

(b) Compressive stress-plastic deformation relation.

Figure 2. Estimation procedure of compression softening curve.

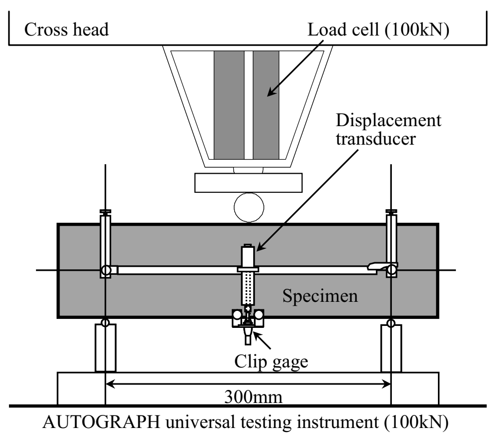

Figure 3. 3-point loading system.

fineness modulus:1.51). The water to cement ratios (W/C) were 40, 50 and 60%, and the fiber used was PVA fiber (diameter: 0.20mm, length: 24mm), the fiber volume fractions (V_f) being 0, 2 and 3% (VF0, VF2, and VF3).

2.1. Uniaxial Compression Tests

Fig. 1 shows schematically the experimental apparatus used for uniaxial compressive loading. A 2000kN compression testing instrument was used for loading. Specimens for tests were cylinders of 100φ x 200mm, and three specimens were prepared for each test. Measurement items were load, vertical and transversal strains measured at the center of specimen with a compressometer, and displacement between the loading plates. Data obtained were acquired with a data logger. Specimens were removed from the molds in one day after the placement and then cured in water in the standard way for 28 days before tests.

Fig. 2 shows the estimation procedure of compression softening. The experimentally obtained relation between the compressive load (P_c) and compressive deformation (δ_c) is first converted into the relation between the compressive stress (σ_c) and the plastic deformation (δ_c'). Then, the area up to δ_c'= 3.0mm is calculated from the σ_c-δ_c' relation. In the present study, this is referred to the compressive fracture energy (G_{Fc}). The experimental results are extrapolated to δ_c'=3.0mm, if the data are not available up to δ_c'= 3.0mm. The value of δ_c'=3.0mm in the estimation was chosen because for G_{Fc} and the σ_c -δ_c' relation the difference in patterns between plain mortar and fiber-reinforced mortar can be shown more clearly.

2.2. Notched Beam 3-Point Bending Tests

The outline of loading for notched beam 3-point bending is shown in Fig. 3. Specimens were square columns of 100 x 100 x 400mm and three specimens were prepared for each test. A notch of 5mm in depth was made at the center of specimen with a diamond saw (blade thickness: 1mm) just before loading. The span between the fulcrums was 300mm. The loading was made with a 100kN precision AUTOGRAPH universal testing instrument under controlled speeds of the crosshead. The crosshead speed was chosen so as to correspond to the lording speed of 0.2mm/min for fiber-reinforced mortar. For plain mortar, however, the loading speed was set at 0.01mm/min, in order to avoid an abrupt decrease in load after the maximum load. Measurement items are load, displacement at the center of the specimen and the displacement at the opening of the notch. The respective experimental data were acquired with a data logger. Specimens were removed from the molds in one day after the placement and cured in water in the standard way for 28 days before tests.

The flexural toughness is estimated by the following procedure (JSCE, 1999).

First, the flexural strength is obtained from the equation given below.

$$f1_b = \frac{P \cdot \ell}{b \cdot h^2} \times \frac{3}{2}, \qquad (1)$$

where $f1_b$: flexural strength (N/mm^2), P: maximum load (N), ℓ: span (mm)., b: width of the fracture section (mm), h: height of the fracture section (mm).

Then, the flexural toughness is expressed in terms of the modulus of flexural toughness and obtained using the following equation.

$$f2_b = \frac{T_b}{\delta_{tb}} \times \frac{\ell}{b \cdot h^2} \times \frac{3}{2}, \qquad (2)$$

where $f2_b$: modulus of flexural toughness (N/mm^2), T_b: area below the curve from the origin to δ_{tb} (N mm), δ_{tb}: displacement at the center of the span (mm), ℓ: span (mm), b: width of the fracture section (mm), h: height of the fracture section (mm).

3. RESULTS AND DISCUSSION

3.1. Material Properties

Table 2 shows a list of various material properties obtained experimentally for plain mortar and fiber-reinforced mortar.

(1) Young's Modulus, Compressive Strength, and Flexural Strength

Fig. 4 shows Young's modulus (E), compressive strength (F_c) and flexural strength ($f1_b$) as a function of water to cement ratio (W/C). Both for WHS and OPN, F_c and E decrease with increasing W/C, regardless of fiber mixing value. This tendency is, however, unclear for $f1_b$. F_c and f1b are practically the same for OPN and WHS in the range of W/C studied, though E for WHS is smaller than that for OPN. On the

Table 2. Material properties.

Specimen	Fresh			Hardening									
	Flow	Air	Temperature	Density	Young's modulus E	Compressive strength F_c	Compressive fracture energy G_{Fc}	Split tensile strength*1	Flexural strength $f1_b$	Number of crack*2	Crack band width*3	Flexural toughness $f2_b$*4 Displacement: 7.5mm	Flexural toughness $f2_b$*4 Displacement: 15mm
	(mm)	(%)	(℃)	(g/cm^3)	(kN/mm^2)	(N/mm^2)	(N/mm)	(N/mm^2)	(N/mm^2)	(本)	(mm)	(N/mm^2)	(N/mm^2)
WHS40-VF0	250	0.3	23.5	2.01	15.6	61.9	31.9	3.65	3.71	1.0	—	2.20	—
WHS40-VF2	203	1.2	24.0	1.98	15.2	55.4	55.6	4.15	6.45	1.3	2.93	3.95	2.45
WHS40-VF3	182	2.0	23.5	1.98	14.8	52.5	70.8	3.27	9.91	2.7	15.8	6.49	4.24
WHS50-VF0	246	1.0	22.0	1.97	13.4	42.5	30.2	3.58	3.70	1.0	—	2.40	—
WHS50-VF2	219	1.7	22.0	1.95	13.1	40.4	44.1	3.55	5.88	1.5	9.22	3.74	2.31
WHS50-VF3	168	1.6	21.5	1.93	12.7	37.0	57.3	3.23	10.8	7.2	36.6	7.90	5.64
WHS50-VF4	176	1.7	22.5	1.91	11.2	34.8	78.1	3.42	9.57	6.8	25.7	8.08	6.14
WHS60-VF0	253	0.0	20.5	1.93	12.9	31.5	33.9	3.12	3.64	1.0	—	2.29	—
WHS60-VF2	239	2.4	21.0	1.90	12.1	28.4	42.2	2.76	4.65	1.0	6.87	3.18	2.08
WHS60-VF3	181	0.9	24.0	1.87	10.1	26.7	49.7	3.01	8.81	6.7	24.8	6.16	4.14
OPN40-VF0	248	0.7	20.0	2.16	19.5	59.2	46.8	3.30	4.42	1.0	—	2.59	—
OPN40-VF3	175	1.8	20.0	2.10	17.0	50.1	67.7	3.16	12.2	2.0	7.84	6.01	3.42
OPN50-VF0	245	0.9	19.0	2.11	16.2	40.0	23.2	3.05	3.39	1.0	—	1.93	—
OPN50-VF3	180	2.4	19.5	2.06	13.9	38.9	53.1	2.73	10.0	4.5	27.6	6.39	4.13
OPN60-VF0	239	0.9	19.0	2.05	12.9	29.0	18.9	2.26	2.74	1.0	—	1.77	—
OPN60-VF3	174	2.0	19.0	2.01	12.0	29.5	57.0	2.35	9.82	6.0	28.5	7.62	5.35

*1: Initial cracking stress for fiber reinforced mortar

*2: The values indicate the number of cracks observed after the test for notched beam specimen.

*3: Measured with vernier calipers for the specimens with multiple cracking property

*4: Line in the table indicates that the flexural toughness was not obtained at displacement: 15mm.
The flexural toughness for plain mortar was obtained at maximum load.

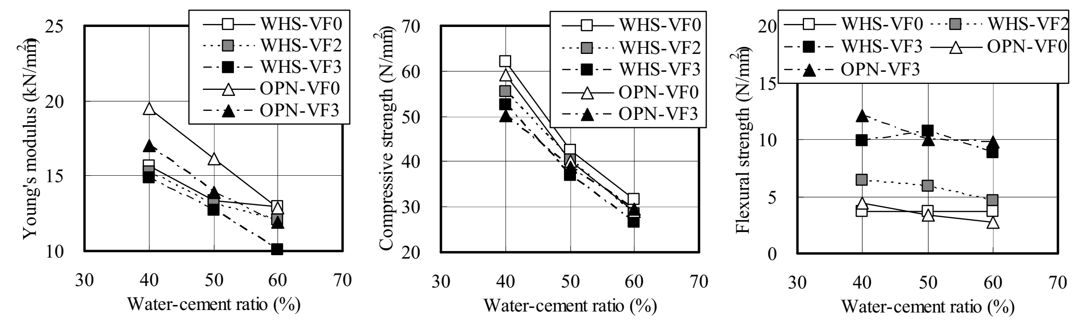

(a) Young's modulus. (b) Compressive strength. (c) Flexural strength.

Figure 4. Young's modulus, compressive strength and flexural strength.

other hand, E and F_c of fiber-reinforced mortar are smaller than those of plain mortar both for WHS and OPN, regardless of value of W/C. The values of $f1_b$ of fiber-reinforced mortar, however, tend to increase, the increase being most obvious for V_f=3%.

(2) Compressive Fracture Energy, Modulus of Flexural Toughness, and Number of Cracks

The relations of the compressive fracture energy G_{Fc}, modulus of flexural toughness $f2_b$ and number of cracks to the water/cement ratio W/C are shown in Fig. 5.

Fig. 5 (a) shows the result for G_{Fc} which has a tendency to decrease with increase in W/C up to W/C=50%, regardless of fiber mixing value. This tendency is, however, unclear at W/C=60%. For both of WHS and OPN the values of G_{Fc} for fiber-reinforced mortar are larger than those for plain mortar, regardless of W/C value. It is also seen that for WHS G_{Fc} increases with increase in V_f.

As shown in Fig. 5 (b), the values of $f2_b$ are

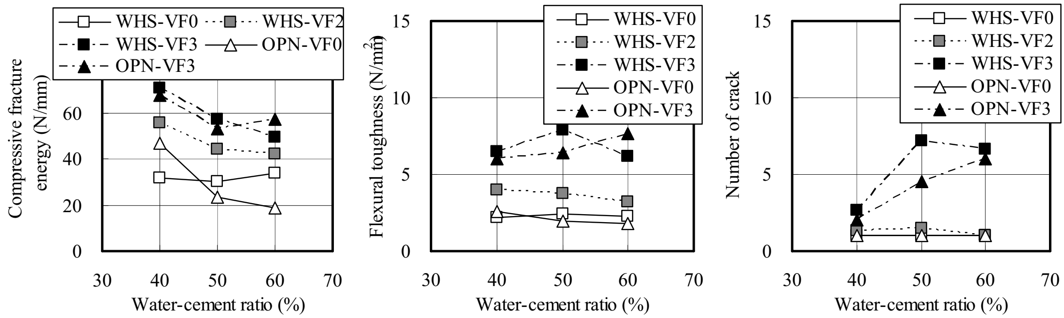

(a) Compressive fracture energy. (b) Flexural toughness. (c) Number of crack.

Figure 5. Compressive fracture energy, flexural toughness and number of crack.

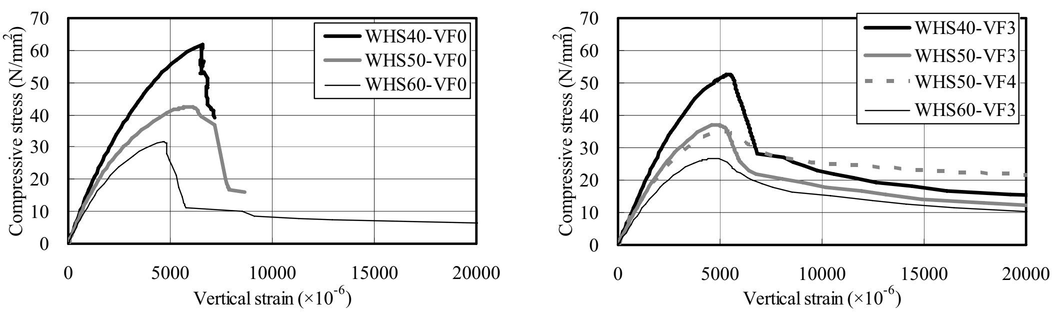

(a) WHS-VF0. (b) WHS-VF3.

Figure 6. Compressive stress – vertical strain relation (WHS).

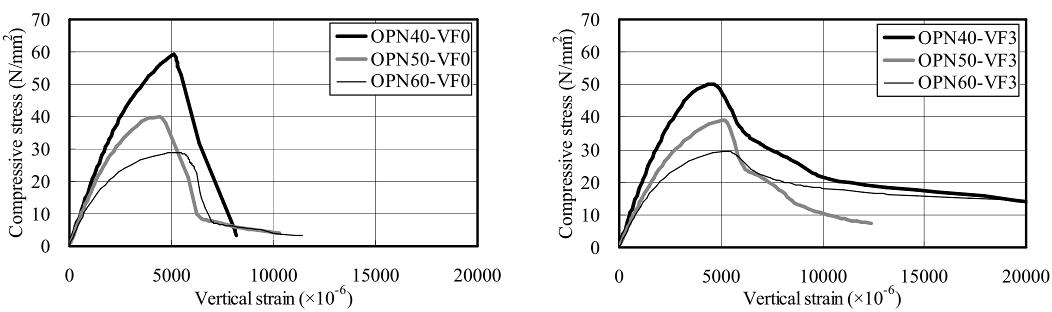

(a) OPN-VF0. (b) OPN-VF3.

Figure 7. Compressive stress – vertical strain relation (OPN).

not largely affected by W/C, regardless of fiber mixing value. . For both of WHS and OPN the values of $f2_b$ for fiber-reinforced mortar are larger than those for plain mortar, regardless of W/C value. It has also been found that for WHS the values of G_{Fc} increase with increase in V_f.

As to the number of cracks shown in Fig.5 (c), a single crack is found both for plain mortars of WHS and OPN. For mortar of WHS, the number of cracks is still one or so at V_f=2%. The number of cracks becomes 2 to 3 at V_f=3% for both of WHS and OPN with W/C=40%. In the cases of W/C=50% and 60%, however, this number becomes 5 or more, which shows that the samples with shirasu as fine aggregate have a sufficient crack dispersion property and flexural toughness and that the application to DFRCCs is quite promising.

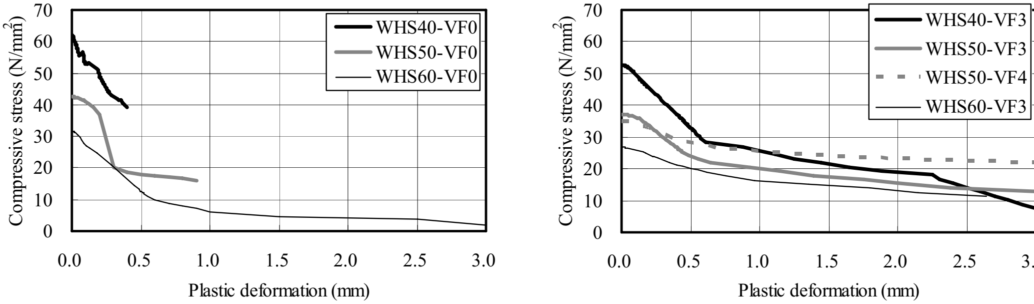

(a) WHS-VF0.

(b) WHS-VF3.

Figure 8. Compressive stress – plastic deformation relation (WHS).

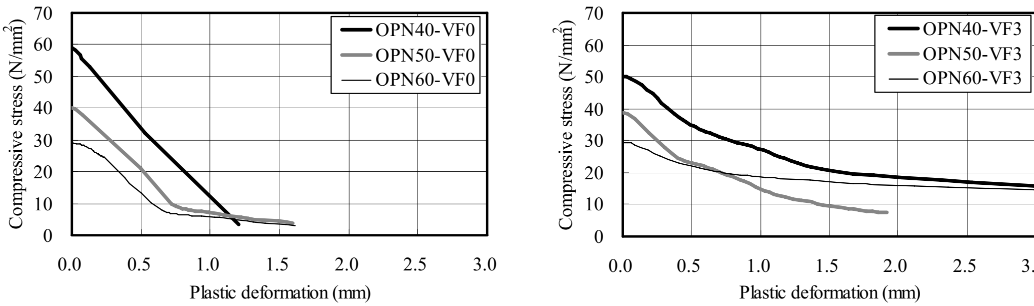

(a) OPN-VF0.

(b) OPN-VF3.

Figure 9. Compressive stress – plastic deformation relation (OPN).

3.2. Compressive Fracture Behaviors

(1) Compressive Stress-Vertical Strain Relation

Figs. 6 and 7 show the σ_c-vertical strain relation obtained from uniaxial compression tests for WHS and OPN. The vertical strain was measured with a displacement transducer set between the loading plates. Representative data are shown for the σ_c -vertical strain relation.

The result for WHS given in Fig. 6 shows an enhanced ductility beyond F_c in the σ_c-vertical strain relation due to fiber mixing, regardless of W/C value. For fiber-reinforce mortar with W/C=50%, the σ_c-vertical strain relation shows a larger enhancement of ductility beyond F_c by changing V_f from 3 to 4%. For fiber-reinforced mortar the ductility is also enhanced beyond F_c with increase in W/C, as shown in the σ_c-vertical strain relation. For plain mortar, however, this tendency is unclear, probably because stable loading is difficult due to increased strength with decreasing W/C.

As seen in Fig.7, the σ_c-vertical strain relation for OPN shows an increase in ductility beyond F_c with addition of fibers, similar to the case of WHS. For fiber-reinforced mortars, an increase in ductility beyond F_c is seen in the σ_c-vertical strain relation with increasing W/C, except for W/C=50%.

(2) Compressive Strain-Plastic Deformation Relation

Figs. 8 and 9 show the results of the σ_c-δ_c' relation obtained from uniaxial compression tests for WHS and OPN. Only representative results are shown in the figures.

As shown in Fig. 8 for WHS, the σ_c-δ_c' relation shows an increase in ductility with mixing of fibers, regardless of W/C, and for fiber-reinforced mortar with W/C=50% the σ_c-δ_c' relation shows a much more ductility with increasing V_f from 3 to 4%. These results are similar to those shown previously in Fig. 6.

The tendency shown in Fig. 9 for OPN is the same as that shown in Fig.7, which is similar to the tendency for WHS. From these

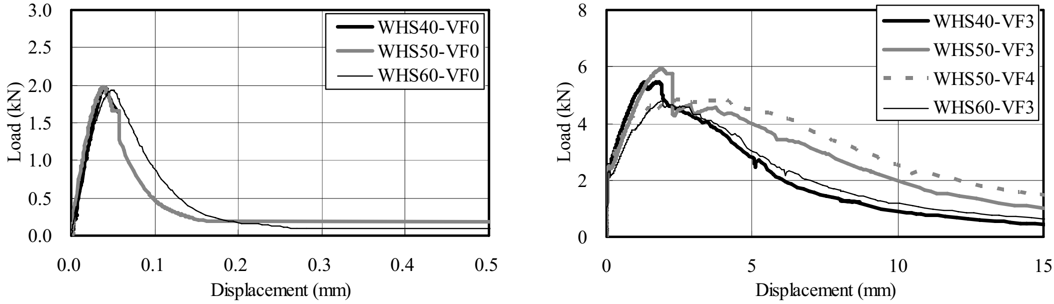

(a) WHS-VF0. (b) WHS-VF3.

Figure 10. Load – displacement relation (WHS).

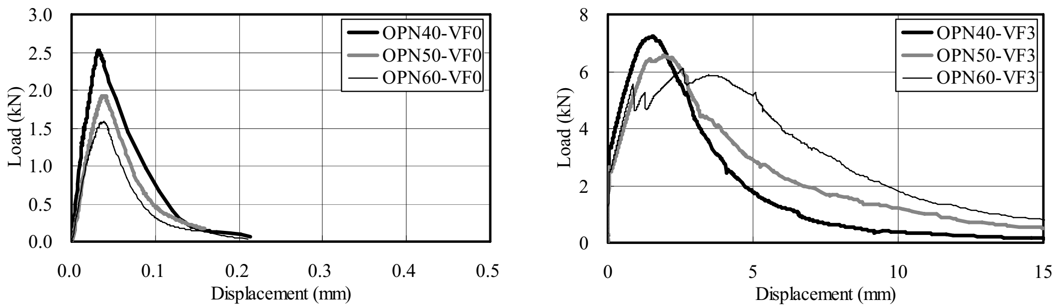

(a) OPN-VF0. (b) OPN-VF3.

Figure 11. Load – displacement relation (OPN).

results it is highly expected that the simplified σ_c-δ_c' relation can be applied to the analysis for estimation of mechanical properties of members made of WHS, in a similar way to the case of OPN (Watanabe et al., 2002).

3.3. Flexural Fracture Behaviors

Figs. 10 and 11 show the load-displacement relations obtained from 3-point bending tests for notched beams of WHS and OPN. Representative results are given for the respective load-displacement relations.

In Fig. 10, the load-displacement relation after the maximum loading shows a considerable enhancement of ductility due to mixing of fibers, regardless of W/C value. For fiber-reinforced mortars with V_f =3% the patterns of the load-displacement relation after the maximum load are similar for W/C=40 and 60%, but the load-displacement relation for W/C =50% shows an enhanced ductility after the maximum load. It has also been found that the toughness of fiber-reinforced mortars with W/C=50% is not much improved with increase in V_f from 3 to 4%.

The results for OPN given in Fig. 11 show a considerable enhancement of ductility after the maximum load in the load-displacement relation by mixing of fibers, regardless of W/C, just as the case for WHS. For fiber-reinforced mortars, the load-displacement relation shows an enhanced ductility after the maximum load with increasing W/C. These results differ from those for WHS. This is probably due to the difference in aggregates, but the details are to be investigated in future.

4. CONCLUSIONS

The results obtained in the present study are summarized as follows.

(1) Setting the water to cement ratio at 50 and 60% and the fiber volume fraction at 3%, mortars with shirasu as fine aggregate have a sufficient crack dispersion property and flexural toughness and can be used as a ductile-fiber-reinforced cementitious composite.

(2) For fiber-reinforced white cement-shirasu mortars, no significant improvement in ductility has been obtained with increase in fiber volume fraction from 3 to 4%.

5. REFERENCES

BRI. and BCJ. 2000. *U.S. − Japan Cooperative Research Program − Development of Smart Structural System −, Report in 1999*. Tokyo: Building Research Institute and the Building Center of Japan (in Japanese).

JCI. 2002. *Technical Committee on High Performance Fiber Reinforced Cementitious Composites, Committee Report on High Performance Fiber Reinforced Cementitious Composites*. Tokyo: The Japan Concrete Institute, 128 pp. (in Japanese).

JSCE. 1999. *Standard Specification for Concrete Structures 1999*. Tokyo: Japan Society of Civil Engineers, pp. 217-219 (in Japanese).

Kaku, T. and Hori, S. 1989. Strength of Concrete Using volcanic ash. *Proceedings of the Japan Concrete Institute*, Vol. 11, No. 1, pp. 59-64 (in Japanese).

Kawamata, K., Takewaka, K. and Matsumoto, S. 1988. Study on the Practical Use of SHIRASU to Fine Aggregate for Concrete. *Proceedings of the Japan Concrete Institute*, Vol. 10, No. 2, pp. 577-582 (in Japanese).

Li, V.C. 1993. From Micromechanics to Structural Engineering − The Design of Cementitious Composites for Civil Engineering Applications. *J. Struct. Mech. Earthquake Eng.*, Japan Society of Civil Engineers, Vol.10, No.2, pp. 37-48.

Naaman, A.E. and Reinhardt, H.W. 1996. Characterization of High Performance Fiber Reinforced Cement Composites − HPFRCC. *High Performance Fiber Reinforced Cement Composites 2 (HPFRCC2)*, pp. 1-23.

Takewaka, K., Matsumoto, S. and Kawamata, K. 1987. Fundamental Study on the Use of SHIRASU to Fine Aggregate for Concrete. *Proceedings of the Japan Concrete Institute*, Vol. 9, No. 1, pp. 7-12 (in Japanese).

Takewaka, K. 2004. State-of-the-Art-Report on Characteristics of SHIRASU Concrete and its Practical Use. *Concrete Journal*, Vol. 42, No. 5, pp. 38-47 (in Japanese).

Watanabe, K., Shirai, N., Oh-oka, T., Hakuto, S. and Fujita, T. 2002. Study on Elasto-plastic Behavior of Ductile Vinylon Fiber Reinforced Mortar Shear Wall. *Transactions of the Architectural Institute of Japan*, No. 559, pp. 211-218 (in Japanese).

Watanabe, K., Fujii, M. and Arai, J.M. 2008. Material Properties of White Cement Mortar Using Pyroclastic Flow Deposits. *Proceedings of the 18th International Offshore and Polar Engineering Conference*, pp. 516-520.

Geotechnical sustainability

Statistical Analysis of Some Geotechnical Properties of Najaf City

Namir K. S. Al-Saoudi
Building and Construction Eng. Dept. University of Technology Baghdad, Iraq

Mohammed Sh. M. Al-Shakerchy
College of Engineering, University of Kufa, Al Najaf, Iraq

ABSTRACT: Najaf is one of the most important provinces in Iraq with total area about 80 km2.It is located in the middle part of Iraq and rests on high plateau over sandy ground west of Euphrates River. It extends between 44˚ 15′ 23″- 44˚ 25′ 25″ longitude and 31˚ 54′ 25″–32˚ 02′ 45″ latitude and lies on the edge of the sedimentary plain of the lower Mesopotamian. Database of the geotechnical properties of different sectors of the city is set forward through the process of collecting, sorting and statistically analyzing all available data from different geotechnical investigation sources. Regression analysis revealed satisfactory correlations between different geotechnical parameters, providing rapid information and reducing cost of detailed investigation

1. INTRODUCTION

Najaf city is located in the middle of Iraq and south of Baghdad in west of the Euphrates river. The name “Najaf” in Arabic means the high land where water cannot be reached. It is located on high plateau over a sandy ground, west of the Euphrates River and looking down from northern and eastern sides

Historically, the old Najaf city is limited to few districts with total area of 2 km^2, near and surrounding the holly shrine of Imam Ali the fourth Khalifa in Islam. Gradually the city was and still extending in the east and south east directions which put the old city and the business centers in the north western parts of the city and not in the center of the great Najaf.. Its total area now is about 80 km^2. (Yousif, B. F., 2004)

Najaf is expected to have huge development programs in the coming years, where huge buildings like hotels, markets and airport are expected to be constructed. For these reasons all previous data and ongoing observations related to the geological and geotechnical information are sorted and analyzed based on SPSS-release 11.0.0 program. Representative values for different geotechnical parameters are revealed and satisfactory models including the (sand / fine ratio), gypsum content, N value from SPT and measured angle of internal friction are obtained for each sector of the city.

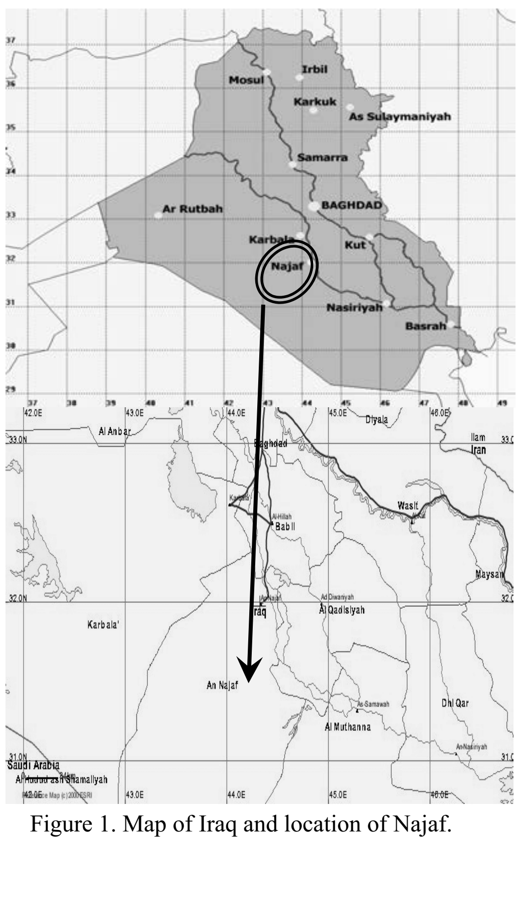

Figure 1. Map of Iraq and location of Najaf.

2. TOPOGRAPHY OF NAJAF CITY

The relief of Najaf is characterized by the differences in elevations of the topographic features, their elevations range between 15 m to 60 m. The main distinguished land forms are basically the soil in high areas known as Tar Al-Najaf and Al-Kufa, whereas soil of depression area is represented in Bahr Al-Najaf .Digital map of the Najaf region with 3-dimensional profile is produced, the data (GCPs) extracted from the topographic map is shown in Figure 2.(http://www globalsecurity.org , Maps of Al Najaf)

With such topography, there were limitations in the directions of extension of the old city. The limitations were along the west side which is the direction of Bahar Al Najaf, a depression that ends at the edge of the plateau. The second limitation was along the north western side where the public cemetery exists. Therefore the actual extension was and still taking place in the east and southern east directions, this has put the old city and the business centers in the north-western parts of the city and not in the center of the great Najaf as shown in figure (3).(Fadhil, E. 2001)

3. GEOLOGY OF NAJAF CITY

The geology of Najaf is part of the geology of Iraq. The main formations and features that are exposed in Al Najaf area are as follows :(Buday, J and Jassim, S. Z., 1984), (Barwarg, A. M. and Slewa, N. A 1995),

1. Dibdibba formation: It is pebbly sandstone developed along Tar Al-Najaf zone
2. Slope deposit: Morphologically, they form narrow, gentle slopes or the feet of the main ridges. They are composed of mixture of clay, silt and sand with rock fragments ranging in thickness between 0.5-2.0m
3. Gypcrete: The gypcrete was developed along Tar Al-Najaf zone forming a cap of rock overlaying the Dibdibba formation. Few patches were also formed below the Tar by capillary action, as a result of underground water oscillations. Secondary gypsum and sandstone are present in this formation.
4. Sabkha deposits: They are located at Bahr Al-Najaf and along both sides of Euphrates River. Generally, they contain sand with random distribution of gypsum and are covered with salty effloresances. Sabkha may be developed in any shallow depression by either evaporation of lake or underground water.
5. Depression fill deposits: They were developed due to local condition of micro relief, and filled with water perennially or periodically. They are covered with clay, sand and silt.
6. Flood plain deposits: The main lithological components are silty clays being followed by silt, sand and rock fragments.

4. LAYOUT OF AL-NAJAF MAP

As a first step for developing a map that demonstrate the location of all geotechnical activities, the boundaries of the old and new city are located according to the map prepared by the Administration of the Construction Planning in Al Najaf in 1997.

This map consists of square grid mesh with side length equal to 1000 meters. Each square element is denoted by two kinds of coordinates, with numbers 1 to 9 for vertical coordinates and letters A to P for the horizontal coordinate, as shown in Figure 4. (Shakerchy, M. Sh., 2007)

The location of all sectors and number of boreholes in addition to the elevations with reference to sea level are shown in the figure 4. Fifteen site investigation reports performed between the periods from 2002 to 2004 were collected from different projects. These projects covered several Najaf districts as follow: -

1-Old city (8 projects),
2-Al Sa'ad (1)
3-Al Qudos (1)
4-Adala District (1)
5-Wafa District (1)
6-Al-Askary District (1)
7-Al-Salam District (1)
8-Milad District (1)

After thorough investigation the collected data from each report is analyzed in accordance with the available districts. Each district is analyzed separately in the form of the expected soil profile and parameters such as sand/fine ratio, gypsum content, N-value, angle of internal friction ø are plotted against depth.

The outcome is shortcut numerical models with overall satisfactory coefficients of correlations useful for rapid evaluation

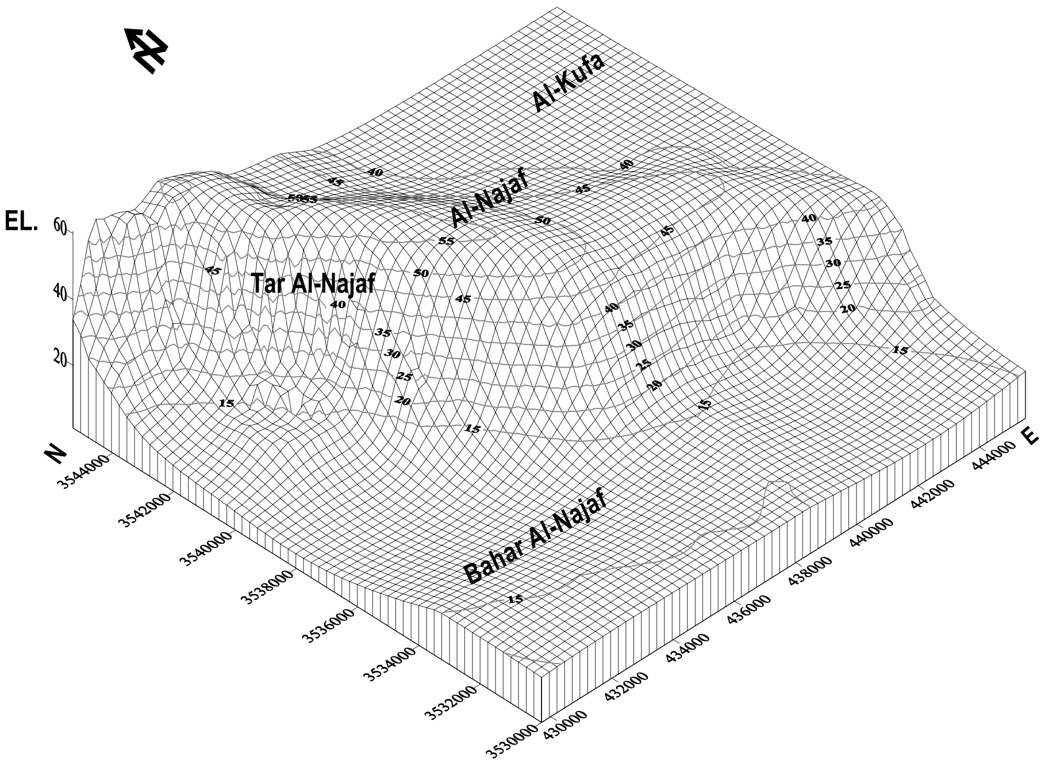

Figure 2 Topography of Najaf city

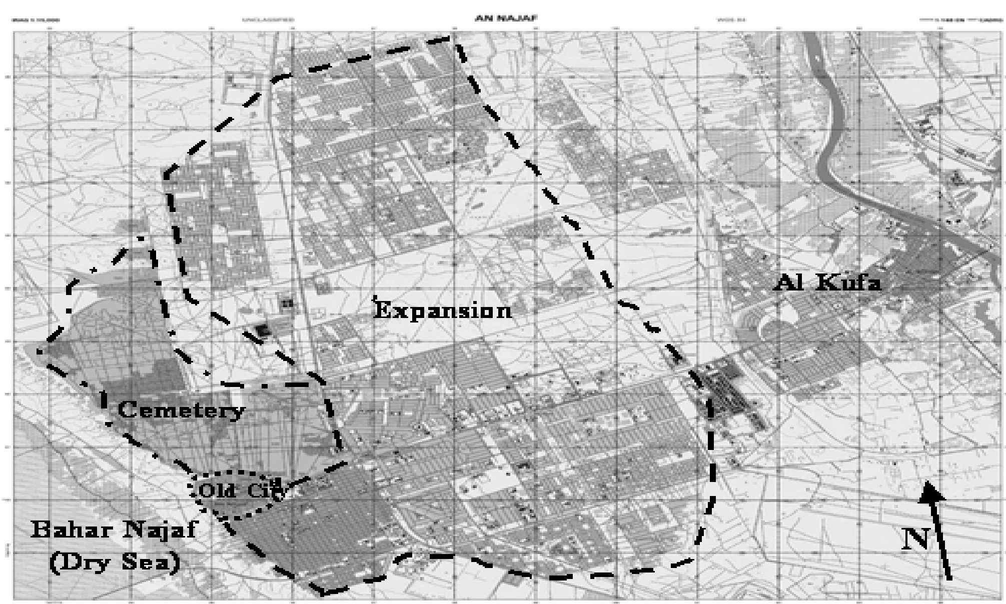

Figure 3 Layout of Najaf city

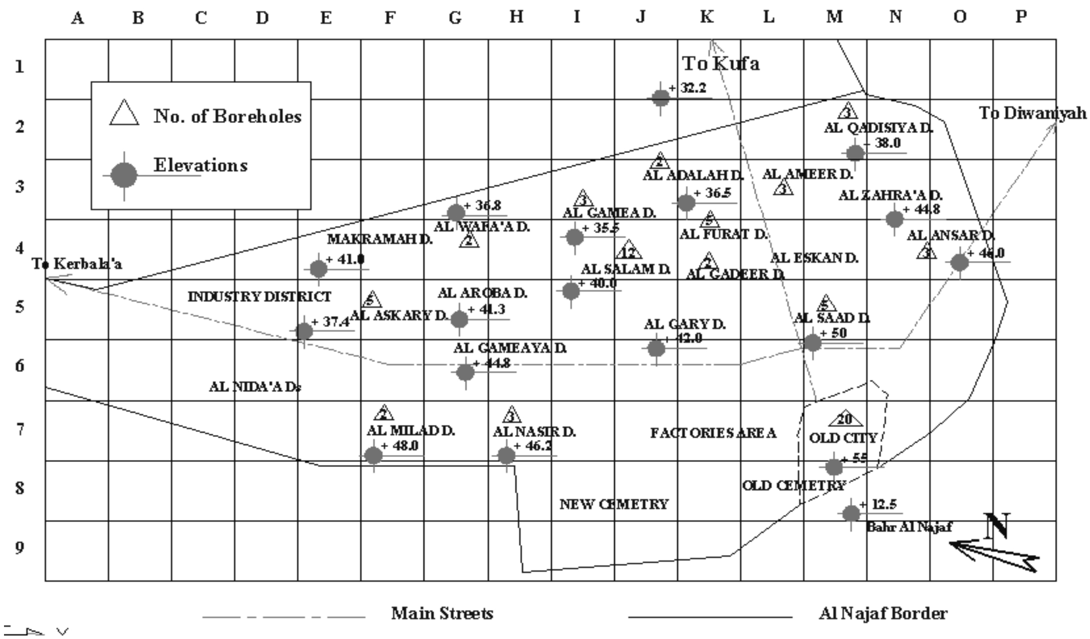

Figure 4 Grid System of Najaf Map with boreholes and elevations locations

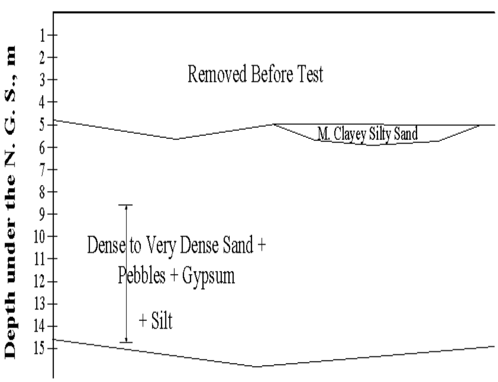

Figure 5. Typical Soil Profile of Old City.

5 PRESENTATION OF GEOTECHNICAL PROPERTIES

5.1 The Old City

The old city consists of four districts and located in squares M7, M8 and N7. Typical soil profile is shown in figure 5 indicating three distinct layers. The first is fill layer with average depth 4.5m, overlaying a second layer of thin lens of clayey silty sand with average depth of 1m. The third layer is a dense to very dense sand with pebbles, gypsum, and silt and extends to the end of boring. Table 1 illustrates the range, frequency and number of observations of the data collected from eight site investigation reports. Representative data of a typical sector of the old city are plotted versus depth in figures 6a, b, c and d respectively. The sand/ fine ratio, figure 6a indicates a fairly constant trend with depth and with average value 3.

Table 1 Data considered in the analysis – old city -

Parameter	Range	Frequency	No. of Observations
Layer of Fill Materials, m	4 – 5	13	17
Soil Type, sand percentage	> 70 %	22	34
Gypsum Content, %	< 10	15	21
N-value, blows	> 50	42	44
Φ, deg.	30 - 35	10	12

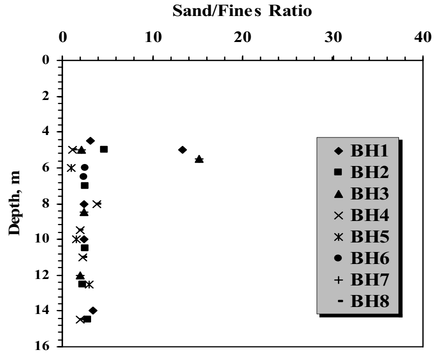

Figure 6 a sand/Fines ratio versus depth

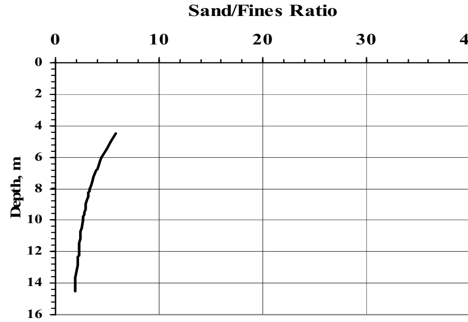

Figure7 a Best fit of data in fig 6a

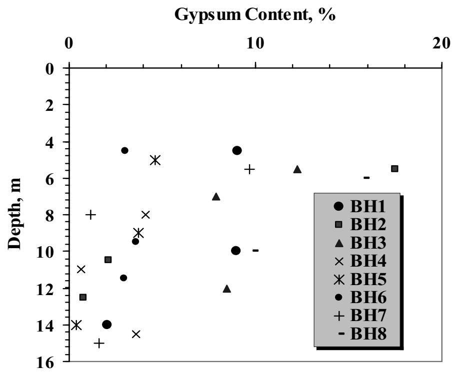

Figure 6 b Gypsum versus depth Content

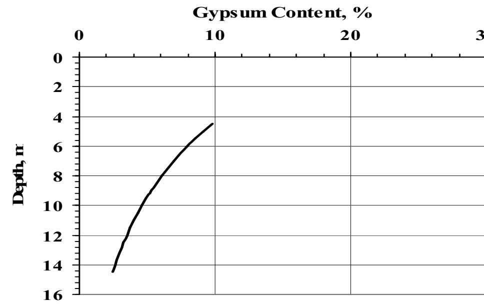

Figure7 b Best fit of data in fig 6b

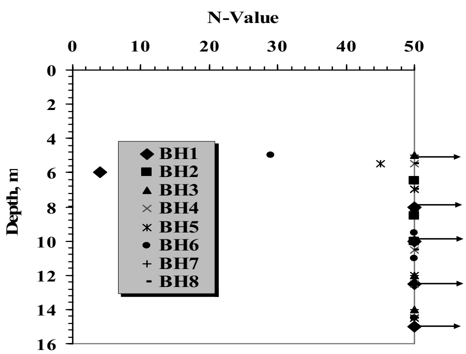

Figure 6 c SPT –N- versus depth

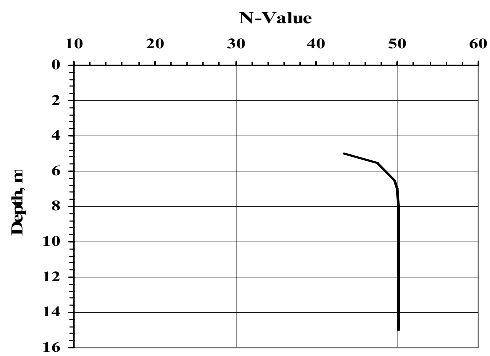

Figure 7 c Best fit of data in fig 6c

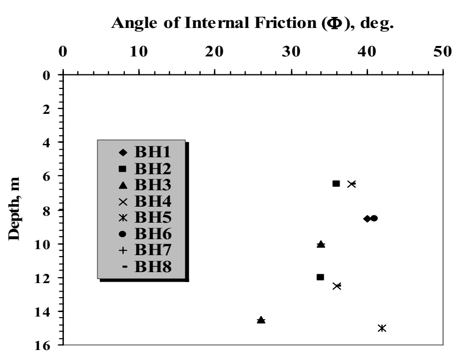

Figure 6 d Angle of Int. friction versus

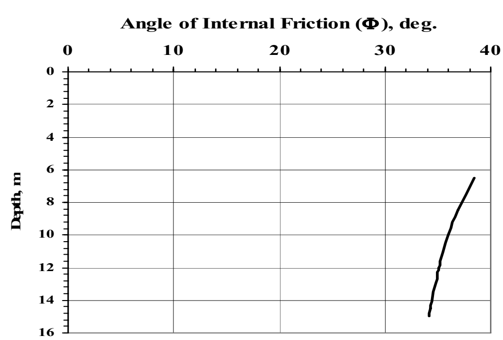

Figure 7 d Best fit of data in fig 6d

The gypsum content, figure 6b is scattered drastically with an overall decreasing trend with depth. The N values, figure 6c, are generally high ≥ 50 and the angle of internal friction Ø, figure 6d, ranges randomly with depth but with narrow limits between 35° and 40°

To formulate a mathematical model for the scattered data of the parameters shown in figure 6 and for the depth of soil layer below 4m till end of boring, curve Expert v. 1.3 was used for this purpose. It is found that the best models that fits the collected data of sand/fine ratio, gypsum content, N-value and angle of internal friction Ø versus depth are those shown in figures 7a, b, c and d respectively. The output of the analysis revealed equations 1, 2, 3 and 4. These equations are limited for the range of depth between 4 and 14 meters below natural ground level

$$Sand / Fine = 0.461 \cdot D^{(7.61/D)} \quad (1)$$

$$Gypsum = 18.0945 \cdot e^{(-0.137 \cdot D)} \quad (2)$$

$$N - value = 50.08177 - 27813.13 \cdot e^{(-1.4036 \cdot D^{1.107})} \quad (3)$$

$$\phi = 27.9837 \cdot D^{(1.1/D)} \quad (4)$$

5.2 New Extensions

The new extensions refer to the new districts out side the old city in all directions (see Fig.3). Table 2 illustrates the range, frequency and number of observations of the data collected from site investigation reports performed at different sectors within the new extension.

A typical soil profile of one sector of the new extensions of the city is shown in figure 8. The profile consists of two main layers; the first is sand with gypsum with an average depth of 4.0m, followed by clayey silty sand with gypsum with average thickness of about 5.0m. The collected data are analyzed and parameters like sand/fine ratio, gypsum content, N-value and angle of internal friction are plotted versus depth in figures 9a, b, c and d respectively.

Similar to the old city, Curve Expert v. 1.3 was used for this purpose to determine the best model that fits the collected data. It is found that the best models that fits the collected data of sand/fine ratio, gypsum content, N-value and angle of internal friction Ø versus depth are those shown in figures 10a, b, c and d respectively

Table 2 Data considered in the analysis – New extension -

Parameter	Depth, m	Range	Frequency	No. of Observations
Sand / fines percent	0 - 14	≥ 70 %	113	150
Gypsum Content, %	0.5 - 2.0	10 - 20	18	27
		20 - 30	6	7
	2.0 - 12.5	≤ 6	44	61
N-value, blows	0.5 – 2.5	20 - 30	18	31
		> 50	13	20
	2.5 – 12.5	> 50	121	169
Φ, deg.	0 - 14	35 - 40	38	58

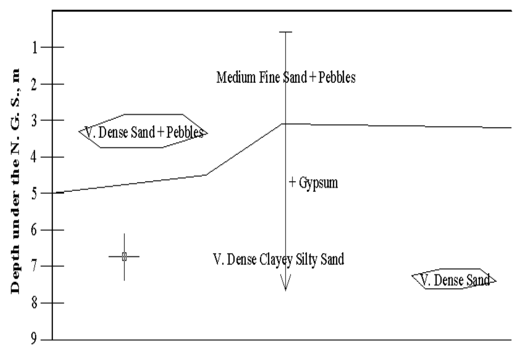

Figure 8 Typical soil profile of the new extension

The statistical analysis revealed equations 5, 6, 7, and 8. These equations are limited for the soil profile shown in figure 8, covering the depth of soil from 0.5m to 9m below natural ground level

$$Sand / Fines = 5.3134.D^{0.73465} \quad (5)$$

$$Gypsum = 13.015^{(-0.1586D)} \quad (6)$$

$$N - value = 21.1482 + 13.2.\ln D \quad (7)$$

$$\phi = 36.4336D^{(-0.131lD)} \quad (8)$$

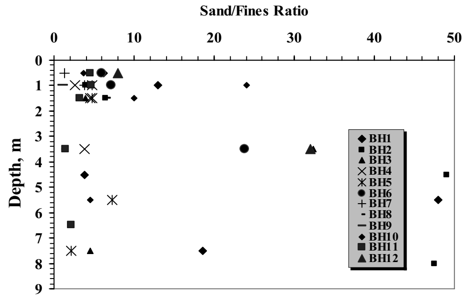

Figure 9 a sand/Fines ratio versus depth

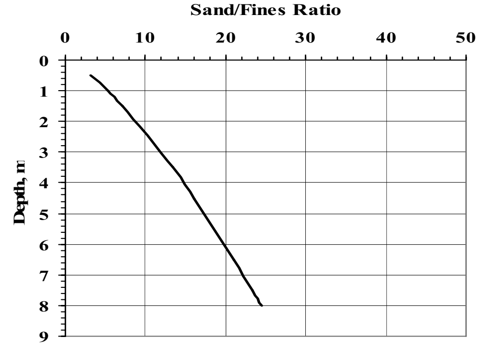

Figure 10 a Best fit of data in fig 9 a

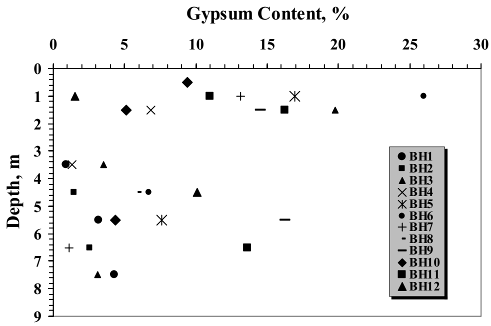

Figure 9 b Gypsum versus depth Content

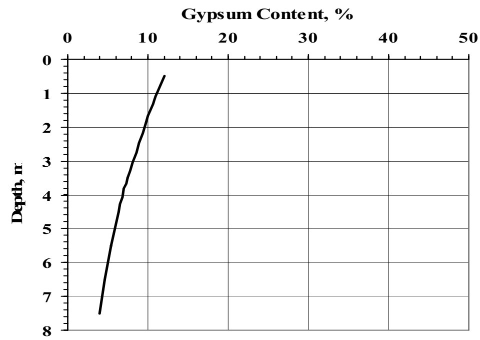

Figure 10 b Best fit of data in fig 9 b

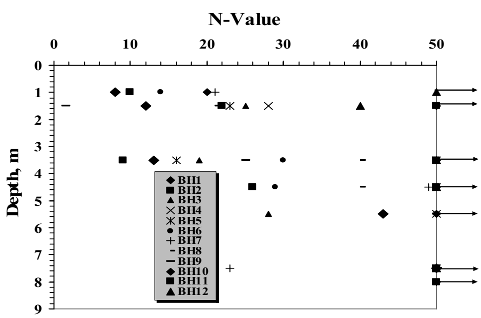

Figure 9 c SPT –N- versus depth

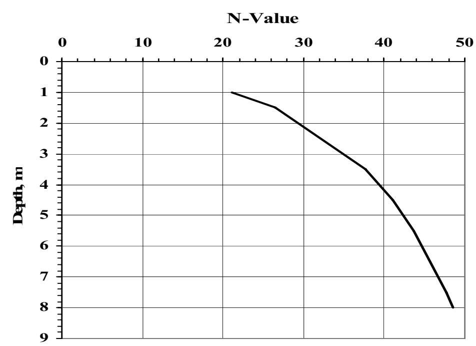

Figure 10 c Best fit of data in fig 9 c

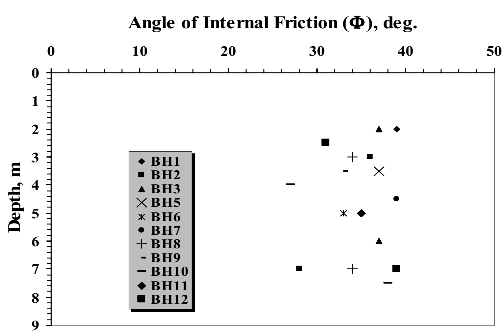

Figure 9 d Angle of Int. friction versus depth

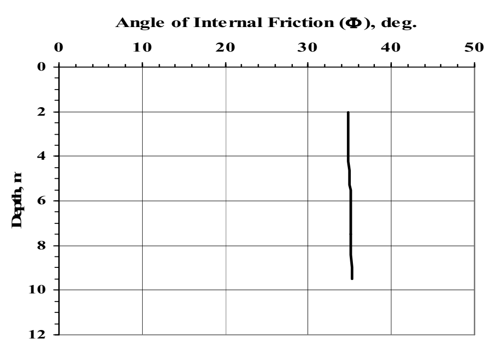

Figure 10 d Best fit of data in fig 9 d

6. CONCLUSIONS

Najaf city consists in of two parts, the old city and the new extension. The topography and the geological formations are very complex. The geotechnical data collected and analysed from several site investigations revealed representative soil profiles for each sector of each part.

In spite of the scattered data of the parameters sand / fines ratio, gypsum content, SPT- N- and Ø with depth, the developed equations 1,2,3 and 4 for typical sector of the old city and 5,6,7 and 8 for typical sector of the new extension are considered useful shortcut guidelines providing rapid estimate of the geotechnical properties.

8. REFERENCES

Al Shakerchy, M. Sh. 2007 Geotechnical Properties of Al Najaf City Soil with Emphasis on the Infiltration and Strength Characteristics, *Ph. D. Thesis, Building and Construction Dept., University of Technology, Baghdad, Iraq*.

Barwarg, A. M. and Slewa, N. A., 1995, Geological Map of Al Kerbala, *Quadrangle sheet NI-38-14, State Establishment of* Geological Survey and Mining.

Buday, J and Jassim, S. Z., 1984, Tectonic Map of Iraq*", DGGSMI*, Baghdad, Iraq.

Fadhil, E.2001.SatelliteImage Processing from GIS Application. *Phd thesis university of Baghdad*.

Yousif, B. F., 2004, The Use of Remote Sensing Techniques in the Classification of Al-Najaf Soil, *M. Sc. thesis, Building and Construction Engineering Department, University of Technology, Baghdad, Iraq*.

http://www.globalsecurity.org/military/word/iraq/an-najaf-map.htm, *Maps of Al Najaf.*

Crushed brick blends with crushed concrete as a sub-base material for pavement construction

A.Arulrajah, T.Aatheesan, B.Vuong
Swinburne University of Technology, Melbourne, Australia

M.W.Bo
DST Consulting Engineers, Ontario, Canada

ABSTRACT: Recycling and reuse of waste materials is a topic of global concern and of great international significance. Recycled concrete and crushed brick for instance are viable substitute materials for virgin natural construction materials in engineering applications such as pavement sub-base material. This paper is based on research carried out in Melbourne, Australia and investigates the blending of crushed brick with crushed concrete and examines the possible usage of these blended materials as pavement sub-base materials. Extensive laboratory tests were undertaken to determine the engineering properties of crushed brick blended with crushed concrete in different percentages. The tests indicated that the crushed brick blends were suitable for usage as a pavement sub-base material.

1. INTRODUCTION

Recycling and reuse of waste materials is a topic of global concern and of great international interest. The urgent need for recycling is driven mainly by environmental considerations, due to the increase scarcity of natural resources and the increasing cost of land fill in most countries. Construction and demolition (C&D) materials are generated by regeneration of infrastructure such as demolition activities and accounts for the major proportion of the waste materials present in landfills. Recycled crushed brick and crushed concrete are viable substitute materials for natural construction materials in engineering applications such as pavement subbase and other road construction applications. Some countries have been using recycled C&D materials in civil engineering applications but there is still scope for wider engineering applications of such recycled materials. This paper primarily focuses on the applicability of crushed brick blends with crushed concrete in pavement sub-base material.

The engineering properties of crushed brick blended with crushed concrete were investigated by means of laboratory testing. A suite of laboratory tests were conducted on blend mixes of 10%, 15%, 20%, 25% and 30% of crushed brick with crushed concrete. The resulting engineering properties were compared with the existing local authority specifications for flexible pavement sub-base material.

2. EXISTING LOCAL SPECIFICATIONS

VicRoads is a statutory authority responsible for managing the road network (roads & bridges) in Victoria, Australia. VicRoads classifies recycled crushed concrete for pavement sub-base and light duty base as Class CC2, Class CC3 and Class CC4 (VicRoads, 2006). This classification is based on the physical and mechanical properties of crushed concrete. Table 1 presents the physical properties of crushed concrete as specified by VicRoads. Table 2 presents the before compaction grading limits for 20mm Class CC3 crushed concrete. Table 3 presents the after compaction grading requirements for Class 3 crushed rock sub-base which is applicable for crushed concrete.

3. ENGINEERING PROPERTIES OF CRUSHED BRICK BLENDS

Samples of crushed brick and crushed concrete were collected from Alex Fraser Recycling site at Laverton North, Victoria as well as Delta Recycling site at Sunshine, Victoria, Australia. Alex Fraser Group and Delta Group are the leading suppliers of high quality sustainable civil construction materials in Australia supplying recycled materials such as crushed brick, crushed concrete and crushed rock in various classes. The crushed brick and crushed concrete used in this research had a maximum aggregate size of 20 mm.

Table 1: Physical properties of crushed concrete (VicRoads, 2007)

Test Value			
Test	Class CC2	Class CC3	Class CC4
Liquid Limit (%) (max)	35	35	40
Plasticity Index (max)	6	10	20
California Bearing Ratio (%) (min)	100	80	15
Los Angeles Abrasion Loss (max)	30	35	40
Flakiness Index	35	-	-

Table 2: Grading requirement for 20mm Class CC3 crushed concrete (VicRoads, 2007)

Sieve Size AS (mm)	Target Grading (% Passing)	Limit of Grading Test Value Before Compaction (% Passing)
26.5	100	100
19.0	100	95-100
13.2	85	75-95
9.50	75	60-90
4.75	59	42-76
2.36	44	28-60
0.425	19	10-28
0.075	6	2-10

Table 3: Grading requirements for Class 3 sub-base crushed rock after compaction (VicRoads, 1995)

Sieve Size (mm)	Permitted Grading After Compaction (% passing) – Nominal size 20 mm
26.5	100
19.0	95-100
13.2	75-95
9.5	60-90
4.75	42-76
2.36	28-61
0.425	14-29
0.075	6-14

Laboratory tests were undertaken on blended mixtures of 10%, 15%, 20%, 25% and 30% crushed brick with crushed concrete. The laboratory tests included modified compaction, particle density, and water absorption, California Bearing Ratio (CBR), Los Angeles abrasion, Atterberg limit, pH, organic content, and clay content. The blend mixtures were prepared by hand mixing to the required percentages by weight. Crushed brick from Alex Fraser Recycling site typically consist of 70% brick and 30% other materials such as asphalt, concrete and rock. Crushed brick from Delta Recycling site on the other hand typically comprises 40 % brick, 55 % crushed concrete and 5 % asphalt.

The laboratory tests were undertaken in accordance with Australian Standards AS 1141 (1996) & AS 1289 (1998). Particle density and water absorption tests were undertaken in both coarse (retained on 4.75 mm sieve) and fine (passing 4.75 mm sieve) material. The physical characteristics of crushed brick blends with crushed concrete obtained from the laboratory tests are summarised in Table 4. The particle size distribution results prior to compaction and after compaction for crushed brick blended with crushed concrete (Class 3) are summarised in Table 5 and Table 6.

Table 4: Engineering properties of crushed brick blended with crushed concrete (Class 3)

Sample Description		70CC3		75CC3		80CC3	85CC3	90CC3	100CC3
Brick Content (%) by weight		30		25		20	15	10	0
Material Source		AFR	DR	AFR	DR	AFR	AFR	AFR	AFR
Test Description		Test Results							
Particle density (Coarse) (t/m^3) - Series 1		2.67	2.69	3.08	2.73	2.68	2.71	2.47	2.76
Particle density (Coarse) (t/m^3) - Series 2				2.71		2.71	2.71	2.71	
Particle density (Fine) (t/m^3)				2.43		2.60	2.41	2.43	
Water absorption (Coarse) (%) - Series 1		5.56	4.84	5.23	5.44	4.95	5.36	5.69	4.66
Water absorption (Coarse) (%) - Series 2				5.4		5.7	5.5		
Water absorption (Fine) (%)				6.9		7.5	8.7		
CBR (%)	Series1	117	102	88	113	104	169	97	160
	Series2	190		141		152	132	177	118
Los Angeles abrasion				28				32	
pH		11.11		11.44		11.30	10.88	11.05	11.49
Compaction (Modified)	Max dry density (t/m^3)	1.95	1.95	1.94	1.95	1.95	1.99	1.95	1.96
	Opt. moisture content (%)	12.5	12.5	12.0	12.5	11.7	11.7	12.0	12.0
Atterberg Limit	Plastic limit	N.O		N.O		N.O	N.O	N.O	N.O
	Liquid limit	N.O		N.O		N.O	N.O	N.O	N.O
	Plasticity Index	N.P		N.P		N.P	N.P	N.P	N.P
Clay content (%)					1.20		0.40	0.50	0.50

Note: AFR – Alex Fraser Recycling; DR – Delta Recycling
70CC3 refers to 30% crushed brick content blended with 70% crushed concrete (CC3) by weight
N.O – Not obtainable; N.P – Non plastic

Particle densities of coarse aggregates (retained on 4.75 mm sieve) are higher than the fine aggregates (passing 4.75 mm) and water absorptions of coarse aggregates are lesser than the fine aggregates. The coarse aggregates of blends may contain the natural aggregates used in concrete and the fine aggregates may contain cementations mortar. This may lead to the higher particle density and lower water absorption in coarse aggregates and lower particle density and higher water absorption in finer aggregates. The pH values of all blends are over 7 and this indicates that the blends are alkaline by nature.

4. COMPARISON WITH LOCAL SPECIFICATIONS

The laboratory test results were subsequently compared with existing local specifications for pavement sub-base applications. The Los Angeles Abrasion Loss values are clearly within the maximum value of 35 normally adopted by VicRoads for Class 3 sub-base pavement materials.

As the clay content in all the blends was low, the plastic limit and liquid limit could not be obtained. This is because the Atterberg limit is directly related to clay mineralogy and as such, higher clay contents result in higher plasticity. This aspect may mean that some difficulties may occur with the workability of the crushed concrete blends as cohesion of particles and a “tight” prepared surface is usually a sought after characteristic. A field trial of the crushed concrete would best determine the degree of difficulties that may be experienced. The addition of small quantities of clayey sand or plastic crusher fines may overcome this potential issue.

The grading limits of all blends before compaction using 20mm Class CC3 crushed concrete were within VicRoads lower and upper bounds for Class CC3 crushed concrete subbase application, as shown in Figure 1.

Figure 2 presents the CBR results for the crushed brick blends. The CBR values of the tested blends were above 80% and found to satisfy the VicRoads requirement for Class CC3 material. The differences in CBR results for the Series 1 and Series 2 tests could be due to slight differences in the aggregate strengths and proportions since they were carried out on different bulk samples and several months apart.

Table 5: Particle size distribution (before compaction)

Sample Description	70CC3	75CC3	80CC3	85CC3	90CC3	100CC3
Brick Content (%) by weight	30	25	20	15	10	0
Particle size (mm)	Percentage of total passing (%)					
26.5	100.0	100.0	100.0	100.0	100.0	100.0
19	99.3	99.4	98.9	99.6	99.5	98.8
13.2	88.1	88.8	88.9	88.3	89.5	86.7
9.5	74.7	75.7	77.6	75.4	77.1	74.8
4.75	54.3	56.0	57.1	55.4	57.2	55.4
2.36	42.4	43.4	44.4	42.8	44.4	43.3
0.075	5.8	6.6	6.4	6.1	6.7	5.8

Table 6: Particle size distribution (after compaction)

Sample Description	70CC3	75CC3	80CC3	85CC3	90CC3	100CC3
Brick Content (%) by weight	30	25	20	15	10	0
Particle size (mm)	Percentage of total passing (%)					
26.5	100.0	100.0	100.0	100.0	100.0	100.0
19	99.4	100.0	99.2	99.5	99.4	98.7
13.2	85.6	85.8	87.6	83.0	88.8	82.2
9.5	74.8	77.3	78.0	70.9	81.6	73.5
4.75	56.2	58.8	59.7	47.8	67.6	55.6
2.36	45.5	47.2	48.2	36.3	55.9	44.6
0.425	25.4	25.7	24.1	16.9	28.3	22.6
0.075	9.7	9.5	7.3	4.8	8.1	6.9

5. CONCLUSIONS

The results of the laboratory tests undertaken in this research have shown overall that the incorporation of “crushed brick” into crushed concrete has “low to minimal affect” on the physical and mechanical properties of the original material. As such, the crushed brick blends with crushed concrete were demonstrated to satisfactorily meet the current VicRoads specification requirements.

The research indicates that initially up to 15% “crushed brick” could be safely added to Class 3 crushed concrete blends. The degree of breakdown occurring in the crushed brick blend is on the limit of what would be acceptable for this material. Depending on the results of field trials, it may be possible to increase the percentage of crushed brick added in the future.

The grading limits of all crushed brick blends, “before and after” compaction were also within VicRoads specified upper and lower bounds for crushed concrete (CC3) whilst some grading for the crushed brick blends were close to the specified limits.

6. ACKNOWLEDGEMENT

The authors would like to acknowledge Sustainability Victoria for funding this research project (Contract No: 3887). The authors would also like to acknowledge Alex Fraser Group and Delta Group for providing samples of crushed brick and crushed concrete as well as their technical assistance on this project. The views expressed are those of the authors and do not necessarily represent those of VicRoads.

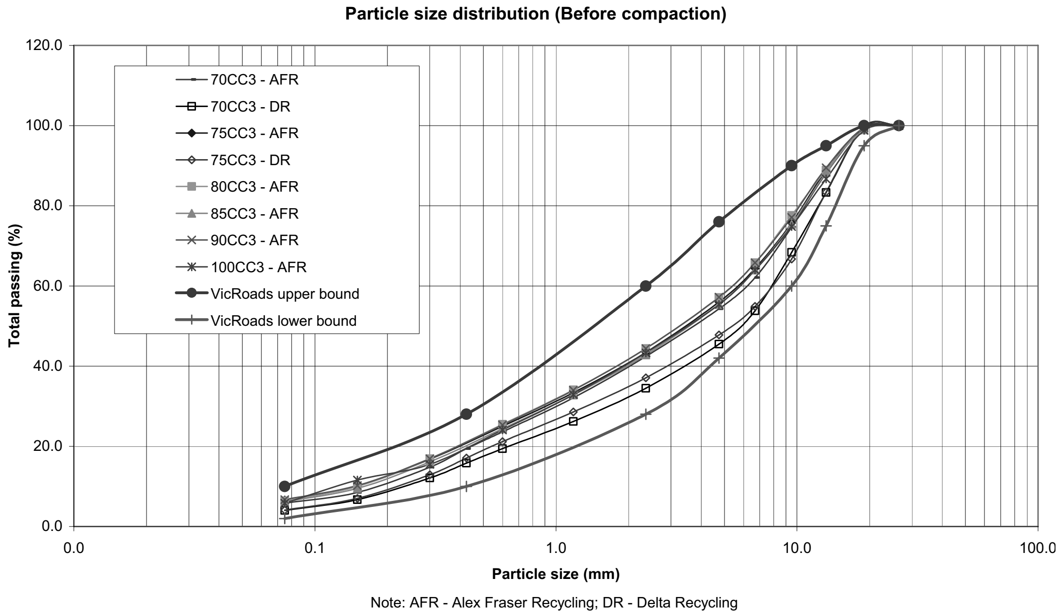

Figure 1: Particle size distribution (before compaction) of crushed brick blends

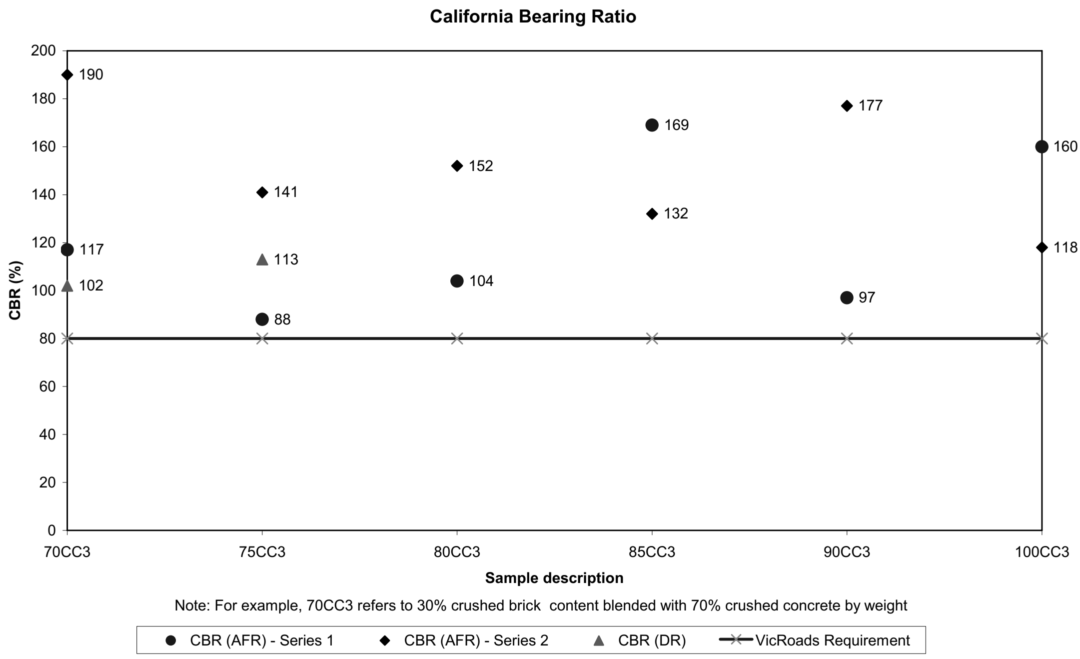

Figure 2: California Bearing Ratio of crushed brick blends

7. REFERENCES

Australian Standards AS 1141(1996) Method for sampling and testing aggregates*, Standards Australia, Standards* Association of Australia.

Lay, M.G. (1998) Handbook of road technology, Third edition, Volume 1, Gordon and breach science publishers, Netherlands.

VicRoads (2007) Standard Specifications for Road works and Bridge works, *Section 820 Recycled crushed concrete for pavement subbase and light duty base,* January.

How to calculate the impact of geotechnical condition plots of land with commercial use on market value for this type of real estate

M. Gwóźdź-Lasoń
Cracow University of Technology, Institute of Geotechnic, Cracow, Poland

ABSTRACT: This paper attempts to answer some of the following questions: What is the main selling advantage of a plot of land? Which attributes materially influence its market value the most? How calculate the influence weak subsoil on market value of plot with commercial use? This focus is not accidental, as the paper sets out to prove that the subsoil load bearing capacity, as directly inferred from the local geotechnical properties, considerably influences the market value of this type of real estate.

1. INTRODUCTION

In all Europe, in particular in Poland which is one of new entrants into the European Union and also co-organiser the football tournament EURO 2012, number of investments grow up in very height speed. In Poland it's planned that a many new sports stadiums, hotels, cinemas, schools, swimming pools, hospitals, roads, highways, parking spaces, shopping centre, railway station, and another commercial structures are to be built in very nearest future or just have been building .

Investors are trying to find and buy suitable plots of land with commercial use and start the construction processes as quickie as possible . The prices of land in big Polish city like Warsaw, Cracow, Katowice, Lodz, Gdansk have been still grow up. Now all plots of land in commercial use which have good location need a different kind of reinforced systems which increase the load bearing capacity of the subsoil because usually the natural condition of this soil can't afford to transfer the loads from building into the ground in a correct way.

There are many different soil reinforced methods and technology which depends not only on the condition, types and structure of the subsoil but values of external and internal loads which must be transmitted deep into the ground, as well. The cost of all works, materials and time which investor must spend on the strengthening systems reach even the half of all investment costs.

The concept of reinforcing soils is not new, because it come into use in the early 1970's when, first steel strips and later, geosynthetics were included in the construction of reinforced soil walls and steep slopes. The knowledge about the way of cooperation between the different kind of reinforcing systems and the weak subsoil is very important because help to chose the proper numerical model to design spacing, diameters and lengths of gravel or sand columns, piles or geosynthetic and estimate the cost of all materials, human and machines works and time corresponding to adjust load bearing capacity of subsoil to assumption circumstances.

In these paper one of the way, how to calculate the influence weak subsoil on market value of plot of land was shown. The market value of the plots of land with commercial use is directly related to the localization because the land for sale in Warsaw or Cracow will cost far more than the land for sale in, for example, Białystok. Also transport links for this type of plots of land are very important. Land in close proximity main roads and motorway will usually be valued at a far higher price than the equivalent land only accessible by winding B roads in the countryside. There are many another market attributes of plots of land, which have big influence on their market value and this kind of characteristic is rather easy to calculate used common estimate method. But there is one attribute called geotechnical parameters of subsoil which is very important distinguishing mark especially for land where commercial engineering structure used to be built. Up till now, the role of this factor has not been included or defined in any binding regulations and is not taken into account in the market valuation of this type of land in a common way. The influence of geotechnical physical and mechanical parameters of the subsoil on market value rise sharply when the condition of the subsoil become weaker. The procedure how to calculate the impact of this parameter on market value of plots of land in commercial use is shown in this papers.

This issue relate to land in big cites, especially in the center of town, when there's really small land to built some commercial construction, and new developed plots of land used to be weak subsoil with previous agricultural, anthropogenic or green space land's purpose. The cost of reinforced that subsoil to be able built some construction on it should be shown, because it have big influence on market value and at least the market price of plots of land which is really very big in big cities. Usually in good location of megacities all plots of land with good geotechnical condition has been built over, now we have plots of land usually with bad geotechnical condition, so the way of estimate the market value of that land used the information about bearing capacity of land like market attribute seems to be very important problem especially for plots of land in megacities area.

2. PRICE OF LAND – A COST ANALYSIS

Real estate appraisal, property valuation or land valuation is the practice of developing an opinion of the value of real property, usually its market value.

Market Value is the estimated amount for which a property should exchange on the date of valuation between a willing buyer and a willing seller in an arms-length transaction after proper marketing wherein the parties had each acted knowledgeably, prudently, and without compulsion.

It is important to distinguish between market value and price. A price obtained for a specific property under a specific transaction may or may not represent that property's market value.

The comparables (or comps) method is the most common one which is used to estimate market value for example of our selected plot of land with commercial use. It's real estate appraisal term referring to properties with characteristics that are similar to a subject property whose value is being sought. This can be accomplished either by a real estate valuer who attempts to establish the value of a property through market analysis or using another defined methods when the simplest one is impossible to do.

A market analysis is documented investigation of a market that is used to inform about the prices of different kind of real estates, about trends of price changes for different space of local markets or inform about types and number of market attributes which have influence on real estate market value.

All calculation which is used to estimate market value base on market analysis data and understand how the data was derived. A large number of market analysis techniques are related to sales forecasting, others are more general techniques for analyzing markets. The literature defines several areas in which market analysis is important. These include: sales forecasting, market research, and marketing strategy.

On Figure 1A was shown a diagram with a market prices of plots of land in commercial use in Cracow over a defined period of time and a trends line which show the changing level of prices using simply probability calculations. Average price of the $1m^2$ plot of land in commercial use in Cracow from the group of 125 transactions is 1.899,18 zł./m^2 that is about 460,00 euro/m^2 – on November 2009.

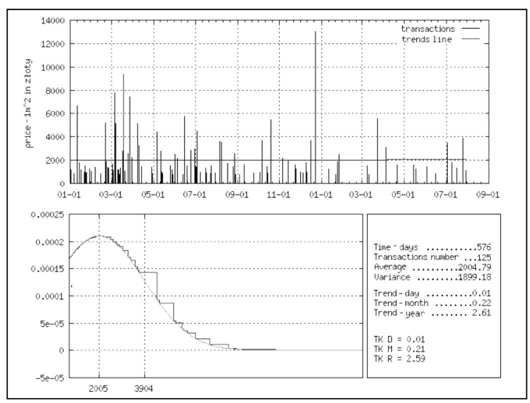

Figure 1A. Example of market analysis that forecasting the trends of changing the price of plots with commercial use in the Cracow. Data from January 2008 to September 2009.

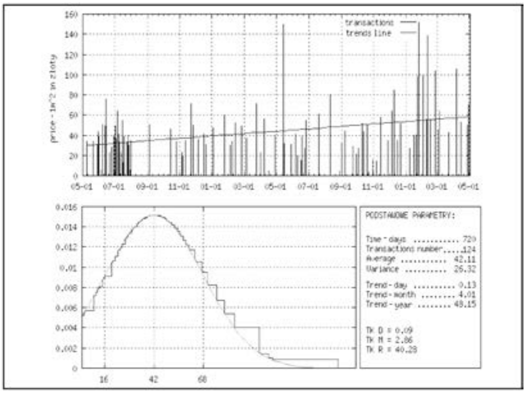

Figure 1B. Example of market analysis that forecasting the trends of changing the price of plots with commercial use on the outskirts of the Bielsko – Biała region. Data from January 2008 to September 2009.

On Figure 1B was shown the same type of diagram but with a market prices of plots of land in commercial use on the outskirts of the Bielsko – Biała region and a trends line which show the changing level of prices. Average price of the 1m^2 plot of land in commercial use in surrounding of Bielsko - Biała from the group of 124 transactions is 42,11 zł./m^2 that is about 10,00 euro/m^2.

Using this characteristic of local market we are able to estimate market value of land which depends on market attributes of real estate like location, neighbourhood, square area of plot, form factor of plot, infrastructure, profiles or designation in the local spatial development plans. But use this method and analysis there is no chance to calculate the influence of geotechnical parameters of subsoil on market value of commercial land, so another way or method must be find.

3. THE RESIDUAL METHOD FOR ESTIMATE MARKET VALUE OF LAND

Residual method allows to estimate the maximum value, which the potential investor may pay for the real estate in its present condition in connection with the investment project envisaged for implementation. When the investor want to buy a plot of commercial use it's obviously that want to built commercial engineering structure on this ground.

Residual method is implemented when determining the value of real estate which can be subject to development, expansion, modernization or other improvements. In our case real estate which is a plot of land must be reinforced to be used like subsoil under big commercial investments. The value of the property can be specified solely for the land, for the land with its components before the improvements or for the land components separately. It is used in analyzing and preparing development projects for real estates. These situations usually require determining the value of individual components of the real estate.

When the load bearing capacity of the subsoil is not strong enough to bear loads from the engineering structure – the soil must be reinforced. There are a number of specialised methods for ground with poor load capacity properties, including: prefabricated drainage pipes and dynamic consolidation, deep compacting through vibroflotation and vibro-replacement, the Solicrete jet-grounding, compaction grounding and the Solifrac method stream injnection, dry and wet deep ground mixing, CFA piling or gravel, cemented or concrete and gravel columns, ect. All of these methods and technology create costs which investor must spend when the plot of land is in bad geotechnical condition. But buying plot of land use in commercial way with perfect geotechnical parameters the investor is able to start at once rise the buildings or roads and safe many time and money.

So when we want to calculate the market value of land that is strong enough to built on it at once we can chose one of comparable method but if we want to estimate the market value depends on geotechnical condition of soil we must calculate how many money investor must spend on reinforced system and in the end subtract it from market value for land with is strong enough. The cost of reinforced system we can estimate use numerical models and make simulation for weak subsoil and for weak subsoil with reinforced system that give us answer about number of reinforced elements which are needed to obtain correct bearing capacity of our land.

4. THE NUMERICAL MODELS OF WEAK SUBSOLI

A number of computational models of reinforced ground were proposed for this representative cross-section. For these case a two-dimensional model was adopted and the operation of the reinforcement components was considered as a single row of columns or gravels that have assign "blur parameters" which are calculated like average value of reinforces system and surrounding subsoil for a guidelines grid. The numeric simulations assumed the ground and the reinforcing system of piles or columns as an elastic-plastic model applying the Drucker-Prager or Coulomb – Mohr criteria, as characterised by the same parameters (γ, E, ν, Φ, c, Ψ).

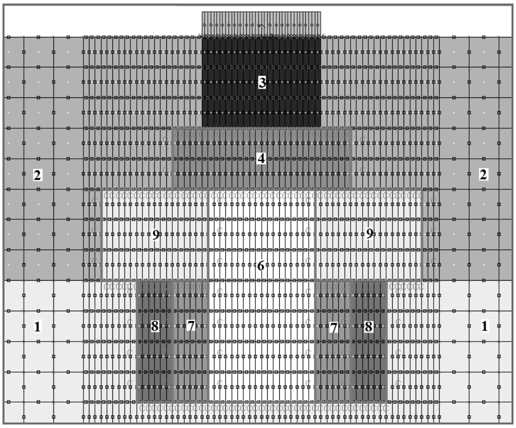

Figure 2. Example of numerical model of subsoil with reinforcement systems which is necessary to install to satisfy the required geotechnical conditions for external loads come from designed buildings. Number of FEM elements means: 1 and 2 – subsoil (S), 3 and 4 – foundation (F), 6 – reinforced system (RS), 8, 7 and 9 – interlayer of modified soil (MS)

The modelling process generating computational models take into consideration the method and technology of soil reinforced system. The earlier research which involved FEM numeric procedures and the Z_Soil package, show that this kind of simple numerical models of reinforced subsoil give information about load bearing capacity of subsoil before and after reinforced procedure which are adequate for this type of task.

Based on generally accepted principles the numerical modeling patterns of subsoil reinforced by different kind of methods and technology especially by gravel-columns made by percussive consolidation, gravel columns in geosynthetic sleeves and gravel columns made by vibroreplacement was tested.

The main assumption for the adopted numerical model was made of using continuum medium and by accepting the elasto–plastic character of materials and we accepted a plane strain model. The computer program Z_SOIL which offers an attractive alternative to traditional approaches to geotechnical problems was used to solve the one step of main task.

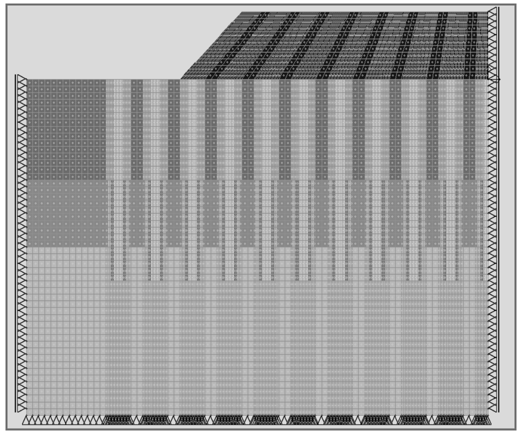

Figure 3. Example of numerical model of subsoil with reinforcement systems under embankment.

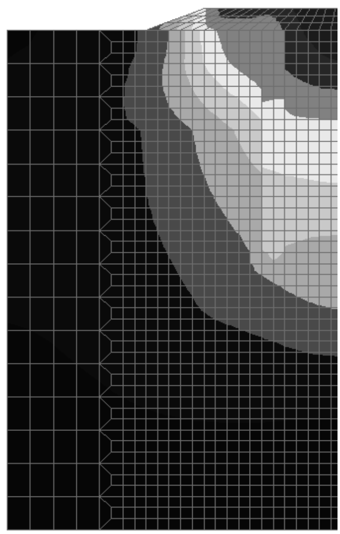

Figure 4. Example of numerical simulation result – border strain for numerical model of subsoil with reinforcement systems

5. CONCLUSIONS

The results presented in this paper give us the opportunity to solve a very important problem using simple numerical model of weak subsoil without and with reinforced system. For these type of numerical models and for obtain results come from numerical simulation in Z_Soli program cost of reinforced systems can be estimate in easy and rather short time.

On the other hand information about time and cost that investor need to start build something on the plot of land may be used for estimate real market value of plot of land with commercial use because only in the case when the cost of reinforced works is known the residual method of estimate market value can be used. So the residual method is the most appropriate tool to estimate the value of an undeveloped land real estate taking into account the influence of its load-bearing capacity on the market value

6. REFERENCES

BOULON, M. and NOVA, R. (1990) *Modelling of soil – structure interface behaviour: a comparison between elastoplastic and rate type laws*, Computers and Geotechnics, Vol. 9, 21-46.

GASZYŃSKI J. and GWÓŹDŹ-LASOŃ M., (2005) *Numerical models of reinforced soil,* Proceeding of the 16th ICSMGE International Conference on Soil Mechanics and Geotechnical Engineering, Osaka, Japan, September 12-16, 2005, pages 709-802, Millpress Science Publishers, 2005.

GASZYŃSKI J. and GWÓŹDŹ-LASOŃ M., (2006) *A numerical study of deformation and stress behavior of the subsoil reinforced by gravel columns,* Proceeding of the XIII Danube – European Conference on Geotechnical Engineering, Active Geotechnical Design in Infrastructure Development, Slovenia, Liubljana, May 29-31, 2006, page no 221-225

GASZYŃSKI J., GWÓŹDŹ-LASOŃ M., (2007) *FEM Analysis of Reinforced Subsoil Under Shopping Center* - Proceeding of the XIV European Conference on Soil Mechanics and Geotechnical Engineering. Madrid 2007, pages 335-339

GOUGHNOUR R.R. Research & Development, Vibroflotation Foundation Company, U.S.A. (1983) *Settlement of vertically loaded stone columns in soft ground*, Proceedings of The Eight European Conference on Soil Mechanics and Foundation Engineering/ Helsinki, Vol.1.,235-240

GRIFFITHS D.V., (1985) *Numerical modeling of interfaces using conventional finite elements*, Proceedings of the 5th International Conference on Numerical Methods in Geomechanics, Nagoya, Balkema / Rotterdam / Boston, Vol. 2, 837-844

GWÓŹDŹ-LASOŃ M. (2007) *Numerical models of the subsoil reinforced by different kind of methods and technology*, PhD thesis, Cracow University of Technology, 2007

GWÓŹDŹ-LASOŃ M. (2007) *Czynniki wpływających na wartość rynkową nieruchomości gruntowych o przeznaczeniu komercyjnym* – Nieruchomości C.H. BECEK wrzesień 2006 Nr 09 (97) ISSN 1506-2899, str. 35-38

GWÓŹDŹ-LASOŃ M. (2009) *Szacownie nieruchomości niezabudowanych z wykorzystaniem metody rezydualnej* – Nieruchomości C.H. BECEK październik 2009 Nr 10 (134) ISSN 1506-2899, str. 30-35

GWÓŹDŹ–LASOŃ M.: (2009) *Wykorzystanie numerycznych modeli ośrodka gruntowego i metody rezydualnej do szacowania wartości rynkowej nieruchomości gruntowych o przeznaczeniu komercyjnym* – Wybrane Zagadnienia z Dziedziny Budownictwa - Praca zbiorowa pod redakcją Andrzeja WAWRZYNKA, Wydawnictwo Politechniki Śląskiej Gliwice 2009 ISBN 978-83-7335-622-1, str. 423-431

LEWIS R.W., SCHREFLER B.A., (1998) *A finite element method in the deformation and consolidation of porous media*. 2nd ed. New York: John Wiley & Sons Ltd.

UEBERHUBER, Ch.W. (1997) *Numerical computation*, Springer Verlag, Berlin.

WALLAYS, M. Research & Geotechnics, Delapierre, J. Van den Poel, J. Franki, Belgium. (1983) *Load transfer mechanism in soils reinforced by stone or sand columns*, Proceedings of The Eight European Conference on Soil Mechanics and Foundation Engineering/ Helsinki, Vol.1., 313-317.

Z_Soil.PC 2007, (1998), *2D User Manual*, ZACE Services Ltd., Lozanna.

Strength and physical characteristics of waste tire powder – added composite geomaterial

Y.T. Kim, H.S. Kang
Dept. of Ocean Eng., Pukyong National Univ., South Korea

ABSTRACT: This paper investigates the strength and physical characteristics of waste tire powder–added composite geomaterial (WCG) in which dredged soils, waste tire powder and bottom ash are reused for recycling. The mixed soil samples were subjected to unconfined compression, 1-D compression and elastic wave tests to investigate their unconfined compressive strengths, compressibilities and small strain properties. Test results show that the unconfined compressive strength and unit weight decrease as the waste tire powder content increases, but axial strain at peak increases. The stress–strain relationship of WCG shows a ductile behavior rather than a brittle behavior. The results of elastic wave tests indicate that the higher waste tire powder content, the lower elastic wave velocity and the lower shear modulus (G).

1. INTRODUCTION

The recycling of industrial wastes and by-products for use as construction materials is an important means to achieve a sustainable environmentally friendly society. Waste tire, dredged materials, fly ash, and bottom ash are examples of commonly recycled waste materials.

The annual generation of dredged soil has been increasing due to dredging from navigation channels and construction sites of large-scale port and harbor projects such as Busan New Port, Korea. Generally, the dredged soil is simply deposited in disposal basins. This practice, however, is not environmentally sound, and societal demand to reuse the dredged soil in construction projects has increased (Kim et al., 2008).

Due to a large number of vehicles in Korea, the annual generation of waste tire has been increasing. The number of waste tires in the Korea generated is approximately 20 millions (Yoon et al., 2008). Waste tire has been used in various applications in civil engineering, for instance, for reinforcing soft soil in road construction and backfilling in retaining structures as lightweight material (Masad et al., 1996; Al-Tabbaa and Aravinthan, 1998; Lee et al., 1999; Bosscher et al., 1997; Tweedie et al., 1998; Tatlisoz et al., 1998; Cetin et al., 2006). Pierce and Backwell (2003) mixed recycled crumb rubber and Class F fly ash to produce a rubber-based flowable fill. The ranges of measured strength agree well with those typically achieved with standard flowable fill. They concluded that such material may be suitable for a lightweight fill application, such as bridge abutment fills and trench fills. Wu and Tsai (2009) presented an experimental study using recycled crumb rubber and native silty sand to produce a lightweight, soil-based, rubberized controlled low strength material(CLSM) for a bridge approach repair.

Bottom ash and fly ash are by-products of the combustion of pulverized coal in power plants. Generally, generation of bottom ash account for about 15 to 20 percent of the total ash (fly ash and bottom ash). The fly ash is widely used for cement material and pozzolanic material. But bottom ash is usually dumped in waste disposal sites at ash pond. It is estimated that several millions ton of bottom ash have been disposed in huge stockpiles across Korea.

A number of studies and applications have been conducted on reusing dredged soil as a construction material. Lightweight soil is one example of recycling dredged (Tsuchida, 1995; Tsuchida et al., 1996; Tsuchida et al., 2000; Otani et al., 2002; Tsuchida and Kang, 2002; Watabe et al., 2004; Kim et al., 2008; 2010). The unit weight of lightweight soil usually ranges 6 to 15 kN/m^3, which is a result of incorporation of lightening materials such as air foam. In the case of using air foam for lightening material, however, defoaming tends to increase when a source soil has a high organic material content. In addition, defoaming can occur during hardening process of the mixture in which the air foam defoams over curing time (Tsuchida and Egashira, 2004). In this study, waste tire powder was added to composite material as a lighting material instead of air foam. It may not only help solve defoaming problem of air foam, but also has advantage of reusing waste tire.

WCG is considered to be environmentally friendly because it provides a means to recycle dredged soil, waste tire powder and bottom ash at the same time. It can be characterized as a material with a light unit weight that results from admixtures of waste tire powder. The purpose of this study is to investigate the mechanical characteristics of WCG with various contents of waste tire powder and bottom ash. In this study, 5 groups of soil samples were prepared with varying contents of waste tire powder ranged from 0% to 100% at 25% intervals by the dredged soil weight. The mixed soil samples were subjected to unconfined compression, 1-D compression and elastic wave tests to investigate their mechanical properties and small strain properties.

2. MATERIALS AND EXPERIMENTAL PROGRAM

Dredged clayey soil was taken from the construction site of Busan New Port, Korea. The natural water content of the dredged soil is 54.7 % and its plasticity index about 20.7. The dredged soft clay is classified as low plasticity clay, CL, according to the Unified Soil Classification System (USCS). Ordinary Portland cement was used in this study as a cementing agent.

Bottom ash from Samchunpo power plant in Korea was selected for reuse in this study. The specific gravity obtained for bottom ash is 2.0. As shown in Figure 1, bottom ash used for this study was composed of particle sizes ranging from 0.075 to 4.76mm (passing US standard #4 sieve). It appears to be a poorly graded sand-like material.

Bottom ashes were analyzed for chemical composition via X ray fluorescence spectrometer. The major chemical compositions in bottom ash are SiO_2, AL_2O_3, Fe_2O_3, and CaO comprising 52.7, 19.33, 11.48, and 9.98%, respectively. According to Lea (1980), pozzolanic materials, when blended with cement, will affect the cementing properties of the cement, in particular, the later reaction of amorphous silicates with $Ca(OH)_2$ to form C-S-H and C-A-H. It is supposed that the bottom ash provides Si, which enhances the formation of C-S-H, a gel in cement responsible for strength development.

The particle size distribution and particle shapes of waste tire powder are also shown in Figures 1 and 2, respectively. Waste tire powder used for this study was composed of particle sizes ranging from 0.1 to 2.0mm. Effective sizes (D_{10}) of waste tire powder and bottom ash are approximately 0.30 and 0.93, respectively.

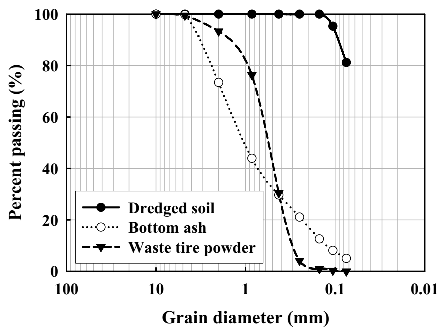

Figure 1. The grain size distribution curves of admixtures.

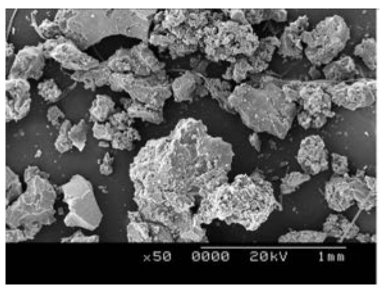

Figure 2. SEM image of waste tire powder.

As shown in Table 1, several types of specimen were prepared. The water and cement content were fixed at 140% and 20% by weight of the dry dredged soil, respectively. To evaluate the effect of waste tire powder and bottom ash on the strength of lightweight soil, various mixing ratios were selected. Test specimens were prepared at 5 different percentages of waste tire powder content (i.e. 0%, 25%, 50%, 75%, and 100% by weight of the dry dredged soil) and 3 different percentages of bottom ash content (i.e. 0%, 50%, and 100% by weight of the dry dredged soil). The specimens were stored in a curing room with temperature of 25±5° for 28 days.

The samples for unconfined compressive test were 72mm in diameter and 148mm in height. To evaluate the strength and physical characteristics of WCG, several series of unconfined compression tests, 1-D compression tests and elastic wave tests carried out. The axial strain rate of unconfined compression test was 1%/min in the test.

Table 1. Mixing ratios

Component	Mixing ratio(%[a])
Water content (Wi)	140
Cement content (Ci)	20
Bottom ash content (BAi)	0, 50, 100
Waste tire powder content (WTi)	0, 25, 50, 75, 100

a: percentage by the weight of dredged soil

3. RESULTS AND DISCUSSION

3.1. Bulk unit weight

Bulk unit weight is one of the important characteristics of lightweight soil. Figure 3 shows the bulk unit weight of WCG as a function of the percentage of waste tire powder and bottom ash. The values of bulk unit weight of the WCG with bottom ash content of 0% and 100% decrease from 14kN/m^3 to 11kN/m^3 and 15kN/m^3 to 12kN/m^3, respectively, as waste tire powder content increases. It indicates that the bulk unit weight of WCG is strongly dependent on the waste tire powder content. For a given waste tire powder content, the bulk unit weight of bottom ash content of 100% is 1kN/m^3 greater than that of bottom ash content of 0%.

3.2. Stress-strain behavior

Figure 4 (a) and (b) presents the stress-strain curves of WCG with bottom ash content of 0% and 100%, respectively. These curves were obtained from unconfined compression tests for WCG after 28 days curing. The stress-strain curves of WCG strongly depend on inclusion of bottom ash as well as waste tire powder. As shown in Figure 4 (a) and (b), the unconfined compressive strength of WCG with 100% bottom ash is much greater than that of WCG without bottom ash. For the case of WCG with 0% bottom ash in Figure 4 (a), with the exception of specimens with a relatively low waste tire powder content(i.e., 0%, 25%), the unconfined compressive stress gradually increases with strain after yielding due to elastic compression of waste tire. For the case of WCG with 100% bottom ash in Figure 4 (b), an increase of waste tire powder content contribute to decrease in peak stress. Inclusion of waste tire powder to soil mixture produces more ductile behavior as shown in Figure 4 (b).

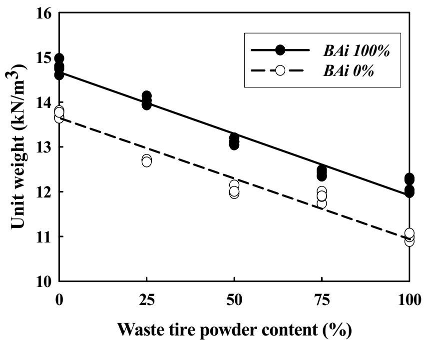

Figure 3. Variation of bulk unit weight with waste tire powder content

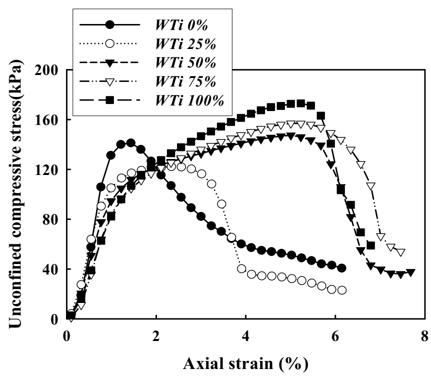

(a) BAi 0%

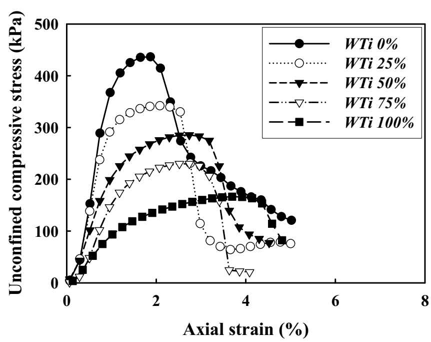

(b) BAi 100%

Figure 4. Stress-strain curves of WCG with varying waste tire powder content.

WCG with waste tire powder content 0% has typical shear failure. As the waste tire powder content increases, however, the failure shape of WCG shows bulging failure. Figure 4 indicates that the peak strain increases with increasing waste tire powder content.

3.3. Unconfined compressive strength

Figure 5 shows the variation of unconfined compressive strength of WCG with bottom ash and waste tire powder contents. It is found that the unconfined compressive strength decreases with an increase in waste tire powder content. However, in the case of WCG without bottom ash, the unconfined compressive strength slightly increases with increasing waste tire powder content. This increase in the unconfined compressive strength results from the compression characteristics of crumb rubber as shown in Figure 4(a).

In the case of the low waste tire powder content, inclusion of the bottom ash into mixture leads to an increase in strength. Kim et al. (2010) reported that the increase in shear strength is caused not only by the development of friction at the interface of the mixture components, but also by bond strength is due to the pozzolanic reaction of the bottom ash. On the other hand, as the waste tire powder content increases, the unconfined compressive strength of WCG converges to a certain value regardless of bottom ash content (i.e., about 200kPa in this mixing ratio). This result indicates that waste tire powder dominates the mechanical behavior of WCG at the waste tire powder content of 100%. The unconfined compressive strength of WCG is strongly influenced by the waste tire powder content.

3.4. Secant modulus

The relationship between the scant modulus (E_{50}) and waste tire powder content is shown in Figure 6. The secant modulus denotes the slope of the line between the origin and the point $q_u/2$ on the stress-strain curve. The E_{50} of WCG tends to decrease as the waste tire powder increases. In the case of low waste tire powder content, inclusion of bottom ash into mixtures gives higher scant modulus at given waste tire powder content. Scant modulus tends to converge to certain value with an increase in waste tire powder content. This trend is similar to that of unconfined compressive strength as shown in Figure 5.

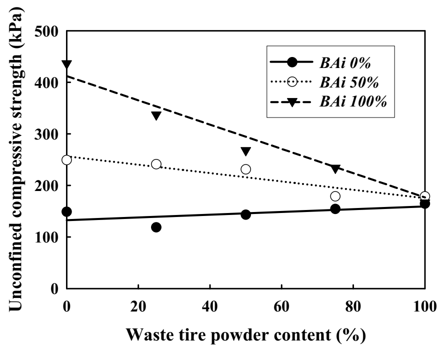

Figure 5. Variation of unconfined compressive strength with bottom ash and waste tire powder contents.

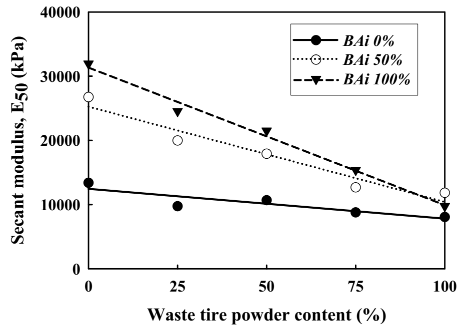

Figure 6. Variation of secant modulus with bottom ash and waste tire powder contents.

3.5. 1-dimensional compression

Figure 7 shows the effective stress-void ratio curves of WCG with varying waste tire powder content, which are measured from 1-dimensional compression tests. Test results indicate that the more waste tire powder content gives the higher compression curves, which has higher compression index and swelling index due to the elastic compression characteristic of crumb rubber.

3.6. Small strain properties

Elastic waves propagate into specimens without altering the fabric or causing permanent effects because they are transmitted under a very small strain of less than 0.001% (Dyvik and Madshus, 1985). The primary and shear waves were measured to assess the small strain stiffness of the WCGs. Ultrasonic transducers were used as both transmitters and receivers because they can convert electrical voltage to mechanical load and vice versa (Lee and Santamarina, 2005). A pair of 500-kHz P-wave transducers (A3441, Panasonic) and a pair of 50-kHz S-wave transducers (SWC75, Ultran) were selected to measure the P-and S-waves, respectively. The elastic wave velocities were calculated to consider the tip-to-tip distance between the transducers and the travel time of the measured signals through the specimen.

Figure 8 shows the P- and S-wave velocities as functions of the waste tire powder content. The results of the elastic wave tests indicate that the elastic wave velocities gradually decrease as the waste tire powder content increases. The P- and S-wave propagation velocities are approximately 820 and 420 m/s, respectively, for 0% waste tire powder content, and decrease to approximately 480 and 180 m/s for 100% waste tire powder content.

Figure 9 shows the shear modulus as functions of waste tire powder content and bottom ash content. The shear moduli of 100% bottom ash content are much greater than those of 0% bottom ash content at a given waste tire powder content. Two different mechanisms are involved in the increase of the elastic wave velocities and WCG stiffness with an increase in the bottom ash content: the fabric change and the particle bonding effect. As the bottom ash content increases, the fabric of the WCG changes from fine to coarse material, and the packing density increases, despite the specific gravity of the bottom ash being lower than that of the dredged material.

On the other hand, it is shown that the shear modulus decreases with an increase in waste tire powder content. The trends are very similar to those of the elastic wave velocities and WCG stiffness, and in agreement with the stress–strain relationship shown in Figure 4.

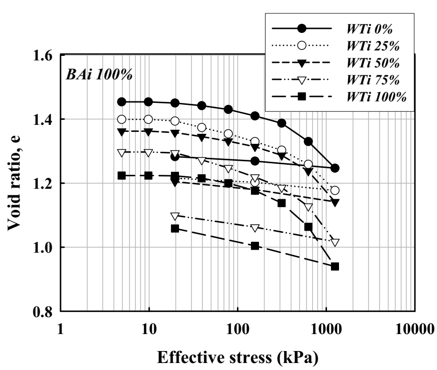

Figure 7. Effective stress-void ratio curves of WCG with varying waste tire powder content

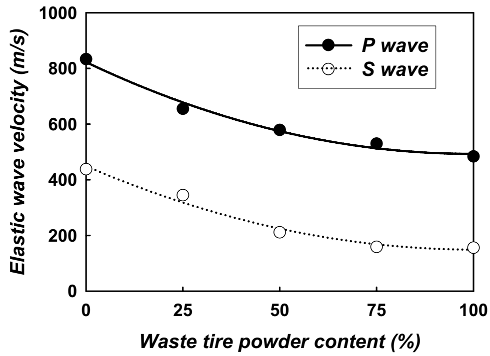

Figure 8. Variation of elastic wave velocity with waste tire powder content (100% bottom ash).

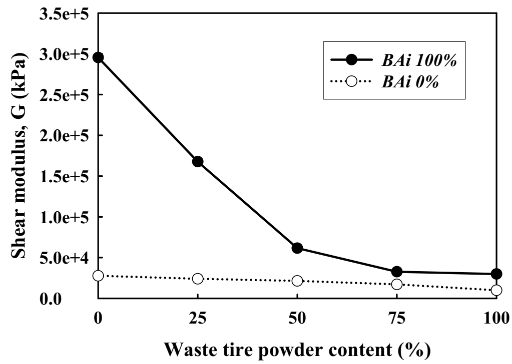

Figure 9. Variation of shear modulus with waste tire powder content.

4. CONCLUSIONS

Several series of laboratory tests were performed to evaluate the strength and physical characteristics of waste tire powder–added composite geomaterial (WCG). WCG was made of dredged clayey soil, cement, waste tire powder, and bottom ash.

The bulk unit weight of the WCG decreases as waste tire powder content increases. The bulk unit weight strongly depends on the waste tire powder content. Bottom ash inclusion improves the strength of WCG, but waste tire powder contributes to decrease the strength. As the waste tire powder content increases, the failure shape of WCG shows bulging failure. The results indicate that compression characteristics of WCG increase as the waste tire powder content increase.

The results of the elastic wave tests indicate that the elastic wave velocities gradually decrease with an increase in waste tire powder content. The shear moduli of 100% bottom ash content are much greater than those of 0%

bottom ash content at a given waste tire powder content.

5. ACKNOWLEDGMENT

This research was supported by Basic Science Research Program through the National Research Foundation of Korea (NFR) funded by the Ministry of Education, Science and Technology (2009-0086833)

6. REFERENCES

Al-Tabbaa, A., and Aravinthan, T. 1998 Natural clay-shredded tire mixtures as landfill barrier materials, *Waste Management*, 18, pp. 9-16.

Bosscher, P.J., Edil, T.B., and Kuraoka, S. 1997 Design of highway embankments using tire chips, *Journal of Geotechnical and Geoenvironmental Engineering*, ASCE, 123(4), pp. 295-304.

Cetin, H., Fener, M., and Gunaydin, O. 2006 Geotechnical properties of tire-cohesive clayey soil mixtures as a fill material, *Engineering Geology*, 88, pp. 110-120.

Dyvik, R. and Madshus, C. 1985. Lab measurements of Gmax using bender elements. *Proc. ASCE Conference on Advances in the Art of Testing Soils under Cyclic Conditions*, pp. 186–196.

Foose, G., Benson, C., and Bosscher, P. 1996 Sand reinforced with shredded waste tires, *Journal of Geotechnical Engineering*, 122(9), pp. 760-767.

Kim, Y.T., Kim, H.J., and Lee, G.H. 2008 Mechanical behavior of lightweight soil reinforced with waste fishing net, *Geotextiles and Geomembranes*, 26(6), pp. 512-518.

Kim, Y.T., Ahn, J., Han, W.J., and Gabr, M.A. 2010. Experimental evaluation of strength characteristics of stabilized dredged soil. Accepted by *J. Mat. in Civ. Engrg., ASCE.*

Lea, F.M. 1980. The chemistry of cement and concrete, *third ed. Edward Arhold*. London.

Lee, H.J., Salgado, R., Bernal, A., and Lovell, W.C. 1999 Shredded tires and rubber-sand as lightweight backfill, *Journal of Geotechnical and Geoenvironmental Engineering*, ASCE 125(2), pp. 132-141.

Lee, J.S. and Santamarina, J.C. 2005. Bender elements: performance and signal interpretation. *J. of Geotechnical and Geoenvironmental Engineering*, ASCE, 131 (9): pp. 1063–1070.

Masad, E., Taha, R., Ho, C., and Papagiannakis, T. 1996 Engineering properties of tire/soil mixtures as a lightweight fill material, *Geotechnical Testing Journal*, 19(3), pp. 297-304.

Otani, J., Mukunoki, T., and Kikuchi, Y. 2002. Visualization for engineering property of in-situ light weight soils with soils with air foams, *Soil and Foundations*, 4(3), pp. 93-105.

Pierce, C.E., and Blackwell, M.C. 2003. Potential of scrap tire rubber as lightweight aggregate in flowable fill, *Waste Management*, 23, pp. 197-208.

Tatlisoz, N., Edil, T.B. and Benson, C.H. 1998. Interaction between reinforcing geosynthetics and soil-tire chip mixtures, *J. Geotech. and Geoenvir. Engrg.*, ASCE, 124(11), pp. 1109-1119.

Tsuchida, T. 1995. Super geo-material project in costal zone. *In: Proceedings of the International Symposium on Ocean Space Utilization COSU'95*, Yokohama, pp. 22-31.

Tsuchida, T., and Egashira, K. 2004. The lightweight treated soil method, *New Geomaterials for Soft Ground Engineering in Coastal Areas*. A.A. Balkema Publisher, London.

Tsuchida, T., and Kang, M.S. 2002. Use of lightweight treated soil method in seaport and airport construction projects, *In: Proceedings of the Nakase Memorial Symposium*, Soft Ground Engineering in Coastal Areas. A.A. Balkema, Yokosuka, pp. 353-365.

Tsuchida, T., and Kang, M.S. 2003. Case studies of lightweight treated soil method in seaport and airport construction projects, *In: Proceedings of the 12th Asian Regional Conference on Soil Mechanics and Geotechnical Engineering*, Singarpore, pp. 249-252.

Tsuchida, T., Fujisaki, H., Makibuchi, M., Shinsha, H., Nagasaka, Y., and Hikosaka, K. 2000. Use of light-weight treated soils made of waste soil in airport extension project, *Journal of Construction Management and Engineering*, JSCE 644(VI-46), pp. 3-23 (in Japanese).

Tsuchida, T., Takeuchi, D., Okumura, T., and Kishida, T. 1996. Development of lightweight fill from dredgeds, *Proc.of Environmental Geotechnics*, Balkema, pp. 415-420.

Tweedie, J.J., Humphrey, D.N., and Sandford, T.C. 1998. Tire shreds as retaining wall backfill: Active Conditions, *Journal of Geotechnical and Geoenvironmental Engineering*, 124(11), pp. 1061-1070.

Watabe, Y., Itou, Y., Kang, M.S., and Tsuchida, T. 2004. One-dimensional compression of air-foam treated lightweight geo-material in microscopic point of view, *Soils and Foundations*, 44(6), pp. 53-67.

Wu, J.Y., and Tsai, M. 2009. Feasibility study of a soil-based rubberized CLSM, *Waste Management*, 29(2), pp. 636-642.

Yoon, Y.W., Heo, S.B., and Kim, K.S. 2008. Geotechnical performance of waste tires for soil reinforcement from chamber tests, *Geotextiles and Geomembranes*, 26, pp. 100-107.

Collective member of the Russian Society for Soil Mechanics, Geotechnics and Foundation Engineering

CO. Ltd. 'BALTIY'

191028, PM St. Petersburg, ul. Furshtatskaya, d. 19, pom. 35-H tel /fax: (812) 528-35-70, email: baltiy@yandex.ru

Company “Baltiy” was established on October, 1, 1991 at the beginning of Russian society reorganization when most of the buildings in the cities of central Russia were in need of restoration and reconstruction. The geography of the building sites of “Baltiy” is rich: Moscow, St Petersburg, Smolensk, Odessa, Pskov, Sochi and many other points. The firm successfully worked to the benefit of Moscow Kremlin, Central Bank of Russia, Neurosurgery Institute, hotel “Ararat” and many other organizations including buildings being part of cultural or historical heritage.

Ararat Park Hyatt Hotel - Moscow

Shcherbakovsky's Chambers - Moscow

The firm provides full range of services: geological engineering survey, design, construction (including sites of cultural heritage), examination of projects, technical inspection and scientific research. “Baltiy” may act as general designer and general contractor.The firm has fair name after successful implementation of unique works, often including nonstandard engineering solutions. “Elite of the national economy” and “Company of 2007” were awarded to “Baltiy”.

Limited liability company
SCIENTIFIC AND PRODUCTION COMPANY

FUNDAMENTSTROJPROEKT

INTEGRATED ENGINEERING, CONSTRUCTION AND RECONSTRUCTION
The firm and its leaders, members of the Russian society
of soil mechanics, geotechnics and fundament building, experts of the MGE.
The company has the license for the restoration of cultural heritage
(monuments of history and culture)

109428, Moscow, Ryazan Avenue, 59, NIIOSP k. 223, 211.
www.fsp-um.ru
tel/fax: 8-495-411-9091, 8-499-170-2828, E-mail: 1702828@rambler.ru

THE BASIC DIRECTIONS OF ACTIVITY OF THE COMPANY

- engineering, geodetic and geological surveys, survey grounds, foundations and surface buildings, testing pile dynamic and static loads;
- geotechnical monitoring safety developement environment including control movement of the structures using high-precision surveying instruments, measurement of deformations and stresses in soils and load-bearing structures and interactive design based on the results of these measurements;
- the whole complex of works zero cycle, including device zero cycles method "top-down” construction Foundation slabs, foundations, monolithic walls and ceilings;
- deepening cellars with further construction of underground premises (garages, bank storage basins, etc.) when reconstructing the buildings;
- all kinds of pile foundations of driving, drillingengravings and drillinginjection;
- strengthening the foundations of drillinginjection-pile with your slaughter;
- seal founded crushed stonei-pile using pneumatic-beat;
- strengthening established then "mikrodur", silica-injectionj and resin-injectionj ;
- device slot foundations, fencing underground facilities and ground arrays on inkjet technology "Jet- grounting".

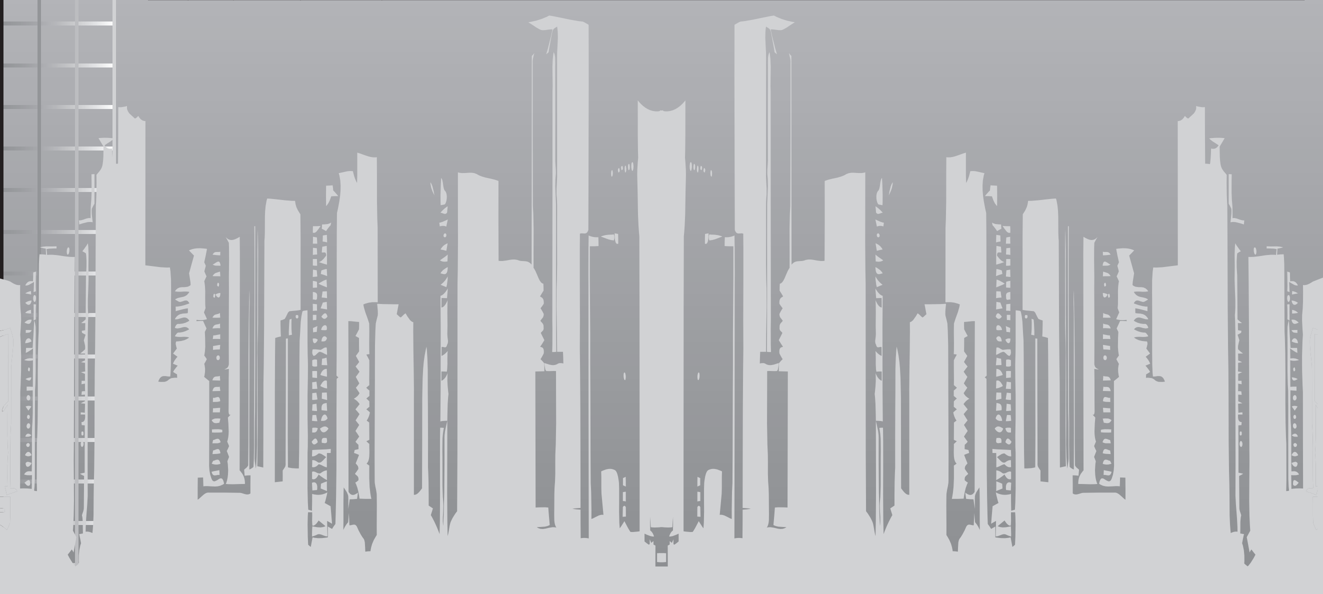

OOO «NPO «OLIMPROEKT»

SURVEYING AND DESIGNING

IN CIVIL ENGINEERING

TECHNICAL INSPECTION OF BUILDINGS
AND STRUCTURES

COMPLEX GEOTECHNICAL CALCULATIONS

DESIGN OF EXCAVATION SUPPORTS, FOUNDATIONS
AND UNDERGROUND PARTS OF BUILDINGS

GEOTECHNICAL MONITORING

NIIOSP

GERSEVANOV RESEARCH INSTITUTE OF BASES AND UNDERGROUND STRUCTURES

GRF

GEORECONSTRUCTION FUNDAMENTPROJECT

TECHNISCHE UNIVERSITÄT DARMSTADT

Разрядно Импульсные Технологии и Аппараты

BAUER ТЕХНОЛОГИЯ

BALTIY

ОЛИМ НП РОЕКТ О

ФУНДАМЕНТСТРОЙПРОЕКТ

Геостройпроект

ЗАО "ИНЖЕНЕРНО - КОНСУЛЬТАЦИОННЫЙ ЦЕНТР ПРОБЛЕМ ФУНДАМЕНТОСТРОЕНИЯ"
CENTRE FOR FOUNDATION ENGINEERING PROBLEMS

LIMITED LIABILITY COMPANY
INSTITUT KANALSTROIPROIEKT